Identification of PI3K/AKT pathway related gene mutations in triple-negative breast cancer and their association with response to PI3K inhibitors

A thesis submitted for the degree of Ph.D. by:

Grace Colley, M.Sc.

August 2026

The work in this thesis was carried out under the supervision of:

Dr. Alexander Eustace

School of Biotechnology

Dublin City University

I hereby certify that this material, which I now submit for assessment on the programme of study leading to the award of Doctor of Philosophy is entirely my own work, and that I have exercised reasonable care to ensure that the work is original and have conformed to the regulations on the use and declaration of Generative AI, and does not to the best of my knowledge breach any law of copyright, and has not been taken from the work of others save and to the extent that such work has been cited and acknowledged within the text of my work.

Signed: Grace Colley

ID No.: 21267087

Date: 07/08/2026

Tools: Clearly indicate the tool name and model (or version) you used and the date(s) of use. If you used a tool multiple times, provide the range of dates over which the tool was used and the model/versions used.	Google Gemini, 2.0-3.6 Flash, used between 01/02/2025 and 07/08/2026
Outputs: Specify what tool outputs were generated and used by you and for what purpose.	I primarily used Gemini to compile papers on topics relevant to my thesis, to summarise papers, to correct errors encountered in some of my R coding, and to improve the structure/wording of sentences that I had written.
Prompts: Provide a record of the prompts you used here or link to an appendix where the prompts used are listed.	"Find all papers about (e.g.) TP53 and PIK3CA co-mutations published within the last 5 years" "Summarise this paper" "What does this paper say about ***?" "Improve the structure of this senteance" "Reword this better" "How does X relate to Y based on this paper?" Input *Error message from R*
Iterations: Provide some commentary on the number and type of iterations. This can be linked to your report on prompts and outputs above.	I would ask it to make a sentence more concise while still retaining the information. If it gave me information on a topic from a published paper, I would give it another paper and ask it to revise the summary of the topic based on additional publication. Sometimes I would ask it to change the tone to a more formal tone. After it would produce a piece of information based on a paper, I would go and read the paper and then ask it to refine the information based on my observations of reading the paper.
Critical Reflection: If Gen AI tools have been used minimally, a very brief critical reflection on its role in the research submitted for examination can be included here. Otherwise, specify the parts of the thesis where critical reflection on the use and role of Gen AI tools is included.	Gen AI is a useful tool when used with caution. I acknowledge its shortcomings, particularly in the area of research that I am in. I made sure to always verify any summaries or information on a particular topic generated by Gen AI by going back and checking exactly what the published paper said. I have done a lot of personal research into Gen AI's flaws, seeing how its responses are shaped based on the information you feed it, biasing toward what you've primed it with. It is ultimately just a reasoning tool which can be useful for basic tasks, however, I would always verify anything produced by it in the literature. That being said, it is particularly useful for coding errors. Again, it's not perfect, but it can detect tiny errors in a line of code that may take the human eye significantly longer to catch.

Table of Contents

Acknowledgements ..... **x**
Abbreviations ..... **xii**
Abstract ..... **xvi**
1. Introduction **1**
1.1. Introduction **2**
1.2. Cancer development and progression **3**
1.2.1 Hallmarks of cancer 3
1.3. Breast cancer **5**
1.3.1. Breast cancer epidemiology 6
1.3.2. Aetiology and risk factors 7
1.3.3. Molecular subtypes of breast cancer 9
1.4. Triple-negative breast cancer **11**
1.4.1. TNBC subtypes and heterogeneity 11
1.4.2. Established and potential candidate biomarkers in TNBC 16
1.4.2.1. Protein expression biomarkers 18
1.4.2.1.1. *Receptor tyrosine kinases* 18
1.4.2.1.2. *Non-receptor tyrosine kinases* 21
1.4.2.2. DNA expression biomarkers 21
1.4.2.3. RNA expression biomarkers 24
1.4.2.4. Immunotherapy biomarkers 24
1.4.2.5. Signalling pathways 25
1.4.3. Treatment of TNBC 27
1.4.3.1. Conventional therapeutic approaches 28
1.4.3.2. Targeted therapeutic approach 32
1.4.3.2.1. *Approved targeted therapies* 33
1.5. The PI3K/AKT/mTOR signalling pathway **39**
1.5.1. The PI3K signalling pathway in cancer 43
1.5.1.1. Molecular alterations driving PI3K pathway activation in TNBC 47
1.6. Targeting the PI3K pathway **48**
1.6.1. PI3K inhibitors 48
1.6.1.1. Pan-PI3K inhibitors 49

1.6.1.2. Isoform-selective PI3K inhibitors 50
1.6.1.3. Dual PI3K/mTOR inhibitors 52
1.6.2. AKT inhibitors 53
1.6.3. mTOR inhibitors 53
1.6.4. Resistance to PI3K/AKT/mTOR inhibitors in cancer 55
1.6.5. Rationale for targeting PI3K pathway alterations in the context of *TP53* dysfunction 57
1.7. Summary 58
1.8. Study aims and objectives 59
2. Methods and materials 61
2.1. Identification and characterisation of *TP53*-PI3K^{act} TNBC 62
2.1.1. Study design overview 62
2.1.2. Cohort selection and definition of TNBC 63
2.1.2.1. METABRIC cohort 63
2.1.2.1.1. *Study background* 63
2.1.2.1.2. *TNBC definition in METABRIC* 63
2.1.2.2. TCGA cohort 64
2.1.2.2.1. *Study background* 64
2.1.2.2.2. *TNBC definition in TCGA* 64
2.1.2.3. Independent cohort analysis 64
2.1.3. Genomic alterations and definition of *TP53*-PI3K^{act} 64
2.1.3.1. Mutation and copy number data 64
2.1.3.2. Definition of *TP53*-PI3K^{act} TNBC cohort 65
2.1.4. Co-occurrence analysis 65
2.1.5. Survival analysis 66
2.1.5.1. Endpoints 66
2.1.5.2. Cox proportional hazards analysis 66
2.1.5.3. Restricted Mean Survival Time analysis 67
2.1.5.4. Interaction analysis 68
2.1.6. Clinical characterisation 68
2.1.7. Gene expression analysis 68
2.1.7.1. Differential expression analysis 68
2.1.7.1.1. *METABRIC* 69
2.1.7.1.2. *TCGA* 70

2.1.7.2. Gene set enrichment analysis 70
2.1.7.3. Single-sample GSEA 71
2.1.7.4. TNBC subtype classification 72
2.1.7.4.1. *Modified TNBCtype-6 classification* 72
2.1.7.4.2. *TNBCtype-4 reassignment* 73
2.1.7.4.3. *Statistical analysis of TNBC subtype distributions* 73
2.1.7.4.4. *Identification of intermediate or transitional TNBC subtype states* 73
2.1.8. Differential protein expression analysis 74
2.2. Differential expression analysis of MCF10A cell line RNA-seq data 74
2.2.1. Sample data background and processing 74
2.2.2. Data quality control and normalisation 74
2.2.3. Differential expression analysis 75
2.2.4. Investigation of target genes 75
2.3. Cell lines and reagents 75
2.4. Mycoplasma testing 77
2.5. STR profiling 78
2.6. Transfection and transduction 78
2.6.1. Viral transfection 78
2.6.2. Viral transduction 80
2.7. Proliferation assay 81
2.7.1. Acid phosphatase assay 83
2.8. Apoptosis assay 83
2.9. Immunoblotting 83
2.9.1. Protein extraction and quantification 83
2.9.2. Western immunoblotting 84
2.10. RPPA analysis 86
2.10.1. Protein extraction and quantification 86
2.10.2. Protein-protein interaction analysis 86
2.11. Statistical analysis 87

3. Cooperative *TP53* loss and PI3K pathway-activation define a distinct high-risk TNBC state 88
3.1. Introduction 89

3.2. Defining a high-risk *TP53*-PI3K-activated TNBC cohort 89
3.3. Characterisation of *TP53*-PI3K^{act} TNBC 92
3.3.1. Co-occurrence of *TP53* mutations and PI3K^{act} alterations in TNBC 95
3.3.2. Prognostic evaluations of *TP53*-PI3K^{act} in TNBC 96
3.3.3. Clinical characterisation of *TP53*-PI3K^{act} TNBC 99
3.3.4. Molecular characterisation of *TP53*-PI3K^{act} TNBC 104
3.3.4.1. Co-occurring genomic alterations in *TP53*-PI3K^{act} TNBC 104
3.3.4.2. TNBC subtype distribution in *TP53*-PI3K^{act} 104
3.3.4.3. Transcriptional profiling of *TP53*-PI3K^{act} TNBC 109
3.3.4.3.1. *Pathway-level enrichment and cross-cohort concordance in TP53-PI3K^{act} TNBC* 113
3.3.4.3.2. *Single-sample scoring of metabolic, immune, and cell cycle pathway activity in in TP53-PI3K^{act} TNBC* 116
3.3.4.4. Differential protein expression in *TP53*-PI3K^{act} TNBC 120
3.4. Summary 122

4. Targeting PI3K/AKT signalling in *TP53* and *PIK3CA* co-mutated TNBC: dual inhibition with alpelisib and RTK inhibitors 123
4.1. Introduction 124
4.2. Identification of *TP53*- and/or *PIK3CA*-MUT TNBC cell line models 125
4.3. Effects of single-agent targeted therapies on TNBC cell lines harbouring *TP53* and/or *PIK3CA* mutations 127
4.3.1. Reduced sensitivity to alpelisib in *TP53/PIK3CA* co-mutant TNBC 127
4.3.2. Targeting TNBC with RTK inhibitors 129
4.3.2.1. RTK targets of crizotinib are upregulated in TNBC compared to other BC subtypes 129
4.3.2.2. Differential sensitivity of TNBC cell lines to crizotinib treatment 130
4.3.2.3. Sensitivity of *TP53/PIK3CA* co-mutant TNBC cell line to ALK inhibitor and resistance to MET inhibitor 132
4.3.3. Summary 134
4.4. Effects of RTK-targeted therapies in combination with PI3K inhibitor alpelisib on TNBC cell lines harbouring *TP53* and/or *PIK3CA* mutations 135
4.4.1. Crizotinib in combination with alpelisib 135

4.4.1.1. Moderately synergistic response to alpelisib and crizotinib combination in *TP53*-MUT/*PIK3CA*-WT TNBC cell lines 136
4.4.1.2. Differential response to alpelisib and crizotinib combination in *TP53*-WT/*PIK3CA*-MUT TNBC cell lines..... 138
4.4.1.3. Synergistic response to alpelisib and crizotinib combination in *TP53/PIK3CA* co-mutant TNBC cell lines 140
4.4.2. Other RTK inhibitors in combination with alpelisib 142
4.4.3. Summary..... 144
4.5. Combined treatment with alpelisib plus crizotinib induces apoptosis in *TP53/PIK3CA* co-mutant TNBC cell lines 145
4.6. Alpelisib plus crizotinib treatment induces significant protein dysregulation in *TP53/PIK3CA* co-mutant TNBC cells..... 147
4.7. Summary..... 163

5. The role of *TP53* alterations, alone and in combination with *PIK3CA* alteration, in modulating response to alpelisib and crizotinib in isogenic MCF10A models..... 164
5.1. Introduction..... 165
5.2. Distinct *TP53* alterations influence gene expression profiles, potentially enhancing sensitivity to the PI3K inhibitor alpelisib 167
5.2.1. Alpelisib sensitivity profiling in *TP53*-altered MCF10A cell lines revealed enhanced sensitivity in G245S and R273H mutants, consistent with baseline gene expression differences..... 167
5.2.2. Analysis of the top ranked genes from the DEA of alpelisib-sensitive versus alpelisib-resistant MCF10A cell lines reveals potential drivers of alpelisib sensitivity..... 172
5.2.3. PI3K/AKT pathway KEGG analysis highlights dysregulated genes linked to alpelisib response in *TP53*-altered MCF10A cell lines 174
5.2.4. Crizotinib response profiling across *TP53*-altered MCF10A cell lines reveals mutation-specific differences in drug sensitivity..... 177
5.2.5. Summary..... 178
5.3. Investigating the impact of *TP53* alterations on alpelisib and crizotinib response in *PIK3CA*-MUT MCF10A models..... 178
5.3.1. Expansion of MCF10A cell line panel to evaluate alpelisib sensitivity across diverse *TP53* alterations 179

5.3.2. Confirmation of *PIK3CA*-WT and *PIK3CA*-MUT transduction by elevated PIK3CA protein expression in cell lines 182
5.3.3. Alpelisib sensitivity in *TP53/PIK3CA*-altered MCF10A cell lines 184
5.3.4. Crizotinib sensitivity in *TP53/PIK3CA*-altered MCF10A cell lines 186
5.3.5. Alpelisib plus crizotinib combination sensitivity in *TP53/PIK3CA*-altered MCF10A cell lines 188
5.3.6. Summary 191
6. Discussion 193
6.1. Introduction 194
6.2. *TP53*-PI3K^{act} defines a high-risk state in TNBC 195
6.2.1. Conclusion 203
6.2.2. Limitations and future work 204
6.3. Therapeutic implication of *TP53* mutations and combination strategies in *TP53/PIK3CA* co-mutant TNBC 206
6.3.1. Conclusion 213
6.3.2. Limitations and future work 215
6.4. Modelling mutation-specific therapeutic responses in isogenic cell models 217
6.4.1. Conclusion 223
6.4.2. Limitations and future work 224
6.5. Final conclusion 226
References 227

Acknowledgements

Firstly, I would like to express my deepest gratitude to my supervisor, Dr. Alex Eustace, for his constant support, guidance, patience, and understanding throughout both my Master's and PhD journey. Thank you for giving me the opportunity to undertake this research, for believing in my abilities, and for the countless hours you dedicated to discussions, feedback, and mentorship. Your encouragement has been invaluable, and I am incredibly grateful for everything you have invested in me over the years. I would also like to acknowledge the Health Research Board, whose Emerging Investigator Award funded this research. I am sincerely grateful for the financial support that made this work possible.

My sincere thanks go to my examination panel, Dr. Simon McDade and Dr. Denise Harold, for the time and care they dedicated to reviewing my thesis. Your thoughtful comments and constructive feedback challenged me to strengthen this work and ultimately helped shape it into a more thorough and impactful piece of research. I would also like to thank Dr. Damien King for chairing the viva examination process.

To everyone in the Eustace Group, thank you for making the lab such a supportive and enjoyable environment. In particular, I would like to thank Arnau, Dalal, Laura, and Anita for generously sharing their expertise, patiently teaching me new techniques, and always being willing to answer questions. Your guidance has been greatly appreciated. More broadly, I have been incredibly fortunate to complete my PhD within the Life Sciences Institute. The collaborative atmosphere and genuine willingness of people to help one another made it a wonderful place to work. Thank you to everyone who lent a hand, offered advice, or simply provided encouragement along the way.

During my PhD, I was also fortunate to spend time working in Dr. Joshua LaBaer's laboratory at Arizona State University. I am sincerely grateful to everyone in the lab for making me feel so welcome from the moment I arrived. In particular, I would like to thank Dr. Jin Park for integrating me into the group so effortlessly and for his generosity with both his time and expertise. I would also like to thank Dr. Lydia Sakala for kindly taking me under her wing during my time there.

Finally, I would like to thank my family and friends, whose support carried me through every stage of this journey. To my mam, thank you for your unwavering love, encouragement, and belief in me. You may still not know what a TP53 is, but none of this would have been possible

without you. Every achievement in these pages is built on the foundation of your support, and for that I will always be grateful. The real marathon begins in the final 10 kilometres; the same can certainly be said of a PhD. To Gabi – who joined this race for the hardest miles – thank you for your company during every late-night writing session, every packet of support jellies, and for always knowing exactly what I needed, often before I did.

It's true what they say – no one completes a PhD alone. I have been exceptionally fortunate to be surrounded by people who believed in me every step of the way. Thank you.

Abbreviations

4EBP1	Eukaryotic Translation Initiation Factor 4E-Binding Protein 1
ABCC11	ATP-Binding Cassette Subfamily C Member 11
ADC	Antibody-Drug Conjugate
adj.p	Adjusted P-Value
ADP	Adenosine Diphosphate
AKT	Protein Kinase B
ALK	Anaplastic Lymphoma Kinase
AR	Androgen Receptor
ATM	Ataxia-Telangiectasia Mutated
BAD	BCL2 Associated Agonist of Cell Death
BC	Breast Cancer
BCL2	B-Cell Lymphoma 2
BH	Benjamini-Hochberg
BL1	Basal-Like 1
BL2	Basal-Like 2
BLIA	Basal-Like Immune-Activated
BLIS	Basal-Like Immune-Suppressed
BRCA1/2	Breast Cancer Gene 1/2
c-MYC	Cellular Myelocytomatosis
Cas9	CRISPR-Associated Protein 9
CI	Confidence Interval / Combination Index
CLCA2	Chloride Channel Accessory 2
C_{max}	Maximum Plasma Concentration
CN	Copy Number
CNA	Copy Number Alteration
CNV	Copy Number Variation
CRAT	Carnitine O-Acetyltransferase
CRISPR	Clustered Regularly Interspaced Short Palindromic Repeats
DBD	DNA-Binding Domain
DDR	DNA Damage Repair
DEA	Differential Expression Analysis
DN	Dominant Negative
DRI	Dose Reduction Index
DSS	Disease-Specific Survival
ECM	Extracellular Matrix
$ED_{50/75/90}$	Effective Doses for 50/75/90% Maximal Response
EGFR	Epidermal Growth Factor Receptor
EMT	Epithelial-Mesenchymal Transition
ER	Estrogen Receptor
ERBB2	Erb-b2 RTK2

ERK	Extracellular Signal-Regulated Kinase
FC	Fold-Change
FDA	Food and Drug Administration
FDR	False Discovery Rate
FGFR	Fibroblast Growth Factor Receptor
FOXA1	Forkhead Box A1
GF	Growth Factor
GOF	Gain-of-Function
GSEA	Gene Set Enrichment Analysis
GSK3A/B	Glycogen Synthase Kinase 3 Alpha/Beta
HDM2	Human Double Minute 2
HER2	Human Epidermal Growth Factor Receptor 2
HGD	Homogentisate 1,2-Dioxygenase
HR	Hormone Receptor / Hazard Ratio
HRc	Homologous Recombination
IC_{50}	Half-Maximal Inhibitory Concentration
ICI	Immune Checkpoint Inhibitor
IHC	Immunohistochemistry
IM	Immunomodulatory
INPP4B	Inositol Polyphosphate-4-Phosphatase Type II
J	Jaccard Index
JAK	Janus Kinase
KD	Knockdown
KM	Kaplan Meier
KRT	Keratin
L2FC	Log2 Fold-Change
LAR	Luminal Androgen Receptor
lncRNA	long non-coding RNA
LOF	Loss-of-Function
M / MES	Mesenchymal
MAPK	Mitogen-Activated Protein Kinase
MDS	Multidimensional Scaling
MET	MET Proto-Oncogene
METABRIC	Molecular Taxonomy of Breast Cancer International Consortium
MSL	Mesenchymal Stem-Like
MTOR	Mammalian Target of Rapamycin Kinase
$mTORC_{1/2}$	Mechanistic Target of Rapamycin Kinase Complex 1/2
MUT	Mutant
NES	Normalised Enrichment Score
OE	Overexpression
OR	Odds Ratio
ORF	Open Reading Frame
ORR	Overall Response Rate

OS	Overall Survival
P	P-Value
PAM50	Prediction Analysis of Microarray 50
PARP	Poly(ADP-Ribose) Polymerase
PCA	Principal Component Analysis
pCR	Pathological Complete Response
PD-1	Programmed Cell Death Protein 1
PD-L1	Programmed Death-Ligand 1
PDK1	3-Phosphoinositide-Dependent Protein Kinase-1
PFS	Progression-Free Survival
PH	Proportional Hazards
PI3K	Phosphoinositide 3-Kinase
PIK3CA/B/C/D/G	Phosphatidylinositol-4,5-Bisphosphate 3-Kinase Catalytic Subunit Alpha
PIK3R1	Phosphoinositide-3-Kinase, Regulatory Subunit 1
PIP2	Phosphatidylinositol 4,5-Bisphosphate
PIP3	Phosphatidylinositol 3,4,5-Trisphosphate
PPI	Protein-Protein Interaction
PR	Progesterone Receptor
PTEN	Phosphatase and Tensin Homolog
PTM	Post-Translational Modification
RAF	Rapidly Accelerated Fibrosarcoma
RAS	Rat Sarcoma
REEP6	Receptor Accessory Protein 6
RFS	Relapse-Free Survival
RMST	Restricted Mean Survival Time
RNA-seq	RNA Sequencing
RON	Recepteur d'Origine Nantais
ROS1	ROS Proto-Oncogene 1
RPPA	Reverse-Phase Protein Array
RTK	Receptor Tyrosine Kinase
S100A8/A9	S100 Calcium Binding Protein A8/9
SD	Standard Deviation
SNP	Single Nucleotide Polymorphism
SPDEF	SAM Pointed Domain Containing ETS Transcription Factor
SPINK8	Serine Peptidase Inhibitor Kazal Type 8
ssGSEA	Single Sample Gene Set Enrichment Analysis
STAT3	Signal Transducer and Activator of Transcription 3
T-DXd	Trastuzumab Deruxtecan
TAD	Transactivation Domain
TCGA	The Cancer Genome Atlas
TET	Tetramerisation Domain
TIL	Tumour Infiltrating Lymphocyte
TME	Tumour Microenvironment

TNBC	Triple-Negative Breast Cancer
TP53 / p53	Tumour Protein p53
TP53-PI3K^{act}	TP53-mutated, PI3K-activated
TROP2	Trophoblast Cell Surface Antigen 2

Abstract

Title: Identification of PI3K/AKT pathway related gene mutations in triple-negative breast cancer and their association with response to PI3K inhibitors

Name: Grace Colley

Triple-negative breast cancer (TNBC) is the most aggressive breast cancer subtype, characterised by high recurrence rates, poor prognosis, and limited targeted therapies due to absence of hormone receptors and HER2 expression. Although TNBC frequently harbours *TP53* and *PI3K* pathway alterations, their combined functional impact as an integrated molecular phenotype remains underexplored.

This thesis defines a *TP53*-PI3K pathway-activated (*TP53*-PI3K^{act}) subgroup characterised by co-occurring *TP53* mutation and PI3K pathway activation (*PIK3CA* mutation, *AKT1* mutation, or *PTEN* loss). Using METABRIC and TCGA TNBC cohorts, integrated genomic and transcriptomic analyses assessed prevalence, survival, and molecular features. Proteomic analyses were also incorporated to refine pathway activity signatures and improve subgroup stratification across cohorts. *TP53*-PI3K^{act} tumours showed significantly poorer survival independent of clinical covariates and TNBC subtype, with enrichment of PI3K/AKT signalling, metabolic reprogramming, inflammatory signalling, and BL2/LAR transcriptional programmes.

Functional studies in TNBC cell lines demonstrated resistance to PI3K inhibitor alpelisib in *TP53/PIK3CA* co-mutant cells, which was overcome by dual PI3K and RTK inhibition, leading to synergistic anti-proliferative and pro-apoptotic effects. This combination more effectively suppressed PI3K/AKT signalling and downstream effectors, including 4E-BP1. In isogenic MCF10A models, *TP53* missense variants showed allele-specific effects on alpelisib response, with DNA-contact mutants more sensitive than structural mutants. Introduction of *PIK3CA*-H1047R reduced alpelisib sensitivity across *TP53* backgrounds, while combination therapy enhanced efficacy with context-dependent synergy.

Overall, *TP53*-PI3K^{act} defines a convergent oncogenic state characterised by signalling and metabolic reprogramming and poor outcomes, representing a distinct and targetable TNBC subset. In this context, dual PI3K and RTK inhibition may overcome adaptive resistance, although therapeutic response is strongly influenced by *TP53* variant class and PI3K pathway

genotype. These findings support integration of *TP53* and PI3K pathway status into future clinical stratification and trial design, and highlight the need for genotype-informed combination strategies to overcome heterogeneous therapeutic resistance in TNBC.

1. Introduction

1.1 Introduction

Cancer is characterised by the uncontrolled proliferation of cells in the body, with over 200 distinct types of the disease distinguished based on the tissue or organ of origin (1,2).

Breast cancer (BC) is the most commonly diagnosed form of cancer (3) and the second leading cause of cancer-related deaths in women, as reported by the American Cancer Society (4).

In Ireland, it is the most common invasive cancer in women (excluding non-melanoma skin cancer), comprising 29.8% of cases with 3,587 annual diagnoses (2020-2022 average), an age-standardised incidence rate of 157.1 per 100,000, and a lifetime risk of 1 in 7. It ranks second for cancer deaths in Irish women (16.7% of invasive cancer deaths), with 753 annual deaths (2020-2022 average) at a mortality rate of 35.1 per 100,000, though 5-year net survival reached 85.1% for 2009-2018 diagnoses (5).

Its global and national prevalence imposes a substantial burden on healthcare systems – encompassing direct costs (e.g. treatments), resource demands (e.g. beds, staff time), and indirect costs (e.g. productivity losses) – as well as broader impacts (e.g. out-of-pocket expenses, travel, family strain). In Ireland, for instance, travel for treatments claimed 35% of Irish Cancer Society grants in 2006 (€150,167 of €429,511). These burdens underscore the need for early detection and targeted therapies to curb cancer growth and alleviate clinical/socioeconomic impacts (6,7).

BC refers to a collection of distinct malignancies that primarily originate in the glandular epithelial tissue of the breast, i.e. the ductal and lobular epithelial cells, though some cases may arise in other breast tissues, such as the nipple or surrounding stromal tissue (8). This form of cancer can develop in different regions of the breast, with specific subtypes denoted based on their invasiveness with regards to the primary tumour site (9). Primary BC tumours are commonly removed via surgical resection, however, spreading of the disease, i.e. dissemination or metastasis, occurs in 20-30% of BC patients and is the leading cause of mortality across all types of cancer (10,11). Advanced-stage BC diagnoses, where the disease has spread to lymph nodes or distant organs (e.g. brain, liver), are often associated with more aggressive subtypes, leading to reduced treatment efficacy (12). Early diagnosis of BC is thus imperative to ensure better patient prognoses and higher survival rates (13).

With rapid advances in molecular biology, along with progress made in improved methods of screening, diagnosis, and treatment, the mortality rate of BC has fallen annually since 1989

(14). However, the pace of mortality decline has slowed in the past decade, potentially reflecting increased rates of incidence and decreases in mammography uptake (15). In addition to this, specific subtypes of BC are particularly difficult to therapeutically target (16) and many patients are unresponsive or acquire resistance following exposure to treatment. Further investigation is imperative to understand these mechanisms of resistance to effectively treat all BC subtypes (17).

1.1. Cancer development and progression

1.1.1. Hallmarks of cancer

Human cells, including those in breast tissue, can acquire diverse functional alterations that drive abnormal tissue growth, contributing significantly to the development and progression of cancer. In 2000, Hanahan and Weinberg proposed six characteristics as the hallmarks of cancer (18), which have since been updated and refined (19) and currently embody eight established hallmarks and two enabling attributes as demonstrated in Figure 1-1(a) and described in Table 1-1. Additional prospective hallmarks and characteristics have also been described (Figure 1-1(b); Table 1-1) but require further validation (20).

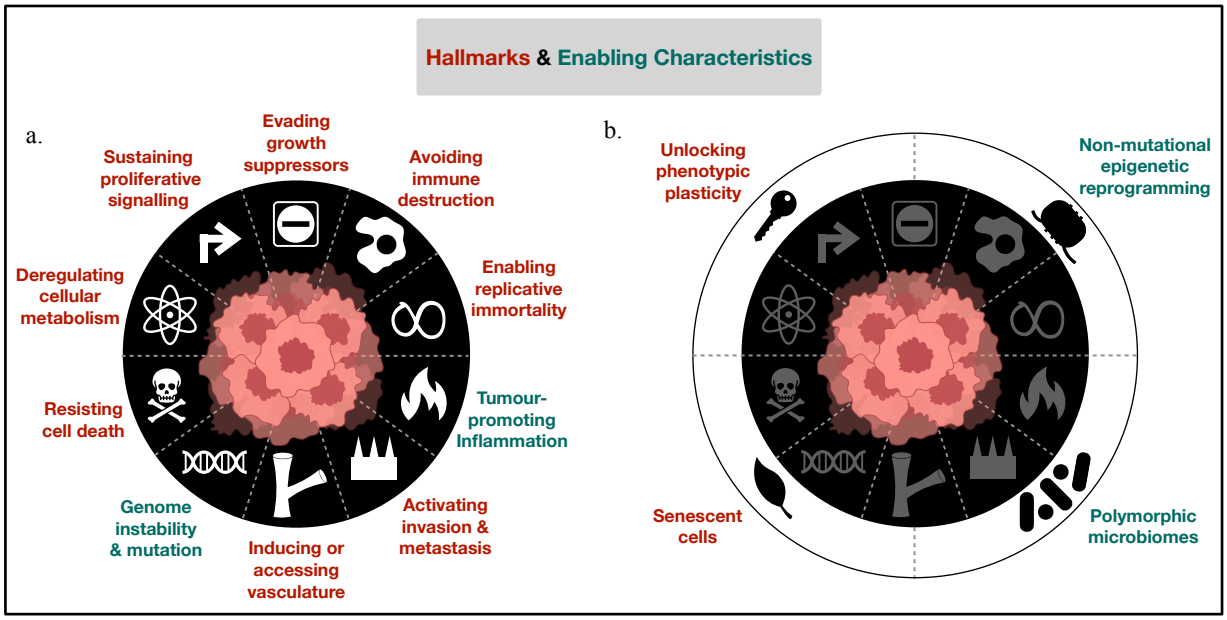


Figure 1-1: The Hallmarks and Enabling Characteristics of Cancer. (a) established hallmarks and enabling characteristics of cancer. **(b)** Emerging hallmarks and enabling characteristics of cancer. Schematic recreated by the author, adapted from Hanahan *et al.* (2022) for illustrative purposes (20).

Table 1-1: Hallmarks and enabling characteristics of cancer. Brief descriptions of the eight established hallmarks of cancer and two enabling characteristics of cancer mechanisms (indicated in green), as well as the four potential emerging hallmarks and enabling characteristics (indicated in red) (20).

Hallmark	Description
Sustaining Proliferative Signalling	Cancer cells grow and divide uncontrollably due to altered signalling pathways (21).
Evading Growth Suppressors	Cancer cells bypass growth-inhibiting signals via dysregulation of tumour suppressors like tumour protein 53 (p53), phosphatase and tensin homolog (PTEN), and retinoblastoma protein (Rb) (22).
Avoiding Immune Destruction	Tumours evade the immune system, including via immune checkpoint pathways such as programmed death protein 1 (PD-1) and the PD-1 ligand (PD-L1) (23).
Enabling Replicative Immortality	Cancer cells maintain telomere length through telomerase, avoiding senescence (24,25).
Tumour-Promoting Inflammation	Chronic inflammation in the tumour microenvironment supports growth and progression (26,27).
Activating Invasion and Metastasis	Cancer cells gain mobility and invade surrounding tissues via epithelial-mesenchymal transition (EMT) (28).
Inducing or Accessing Vasculature	Tumours promote new blood vessel formation (angiogenesis) to support growth and metastasis (29).
Genome Instability and Mutation	DNA damage and chromosomal abnormalities increase tumour heterogeneity and therapy resistance (30,31).
Resisting Cell Death	Cancer cells evade apoptosis and other forms of regulated cell death (32–34).
Deregulating Cellular Metabolism	Altered metabolism supports energy demands of rapidly proliferating cells (35).
Unlocking Phenotypic Plasticity	Cells shift between different states, enhancing heterogeneity and therapy evasion (36).
Non-Mutational Epigenetic Reprogramming	Epigenetic changes affect gene expression without altering DNA sequence, influencing growth and differentiation (37).
Polymorphic Microbiomes	Microbial diversity in the tumour microenvironment can modulate cancer progression and therapy response (38).
Senescent Cells	Senescent cells contribute to proliferation, invasion, angiogenesis, and immune suppression through senescence-associated secretory phenotype (SASP) factors (39).

Note: *For detailed descriptions and examples, see Hanahan et al., 2022 (20).*

1.2. Breast cancer

BC arises predominantly from the epithelial tissue of the breast and is characterised by uncontrolled cell growth and proliferation, primarily within the glandular and stromal tissue (40–42). The glandular tissue of the mammary gland comprises of branching ducts and secretory lobules, responsible for the production and passage of milk (43), while the stromal elements include the breast's adipose and connective tissues (44). Lymphatic tissue is also present in the breast, functioning to both maintain tissue-fluid balance via waste removal and traffic cells for immune response (45). Various types of tumours can arise within the breast, however, the majority are benign, non-cancerous alterations such as fibrocystic changes, cysts, and connective tissue scarring (46).

BC can be broadly defined as being invasive or non-invasive. Non-invasive BC refers to a cancer that has not spread beyond the lobules or ducts to the surrounding breast tissue. These types of BC are known as "*in situ*" forms of cancer, as they remain in their origin of development (47,48). Lobular carcinoma *in situ* (LCIS), accounting for just ~3% of cases, describes BC that begins in the lobules. It is considered a risk factor for invasive disease rather than a precursor as only 7-12% of patients with LCIS develop invasive BC (49). Ductal carcinoma *in situ* (DCIS) refers to BC that develops in the breast ducts, representing 20-25% of all BCs, with an estimated 20-50% of cases progressing to invasive disease (50).

When *in situ* carcinoma – most commonly DCIS – breaches the ductal or lobular basement membrane and invades the surrounding breast tissue and stroma, it is classified as invasive BC (IBC) (51). The two main histological types of IBC are invasive ductal carcinoma (IDC) and invasive lobular carcinoma (ILC) (52), named according to their cells of origin. IDC is considerably more prevalent, accounting for ~80% of invasive cases, while ILC represents around 10% (53). In some instances, invasive cancer cells can further disseminate beyond the breast and regional lymph nodes through the circulatory or lymphatic systems. This stage is referred to as metastatic BC (MBC), in which cancer cells establish secondary tumours at distant sites – most commonly in the bones, brain, liver, and lungs – in a non-random process termed metastasis organotropism (54). Despite occurring in different organs, secondary breast tumours generally retain many molecular and histopathological characteristics of the primary tumour, although organ-specific adaptations and additional mutations can lead to partial divergence (55). Figure 1-2 illustrates *in situ* and invasive breast carcinomas.

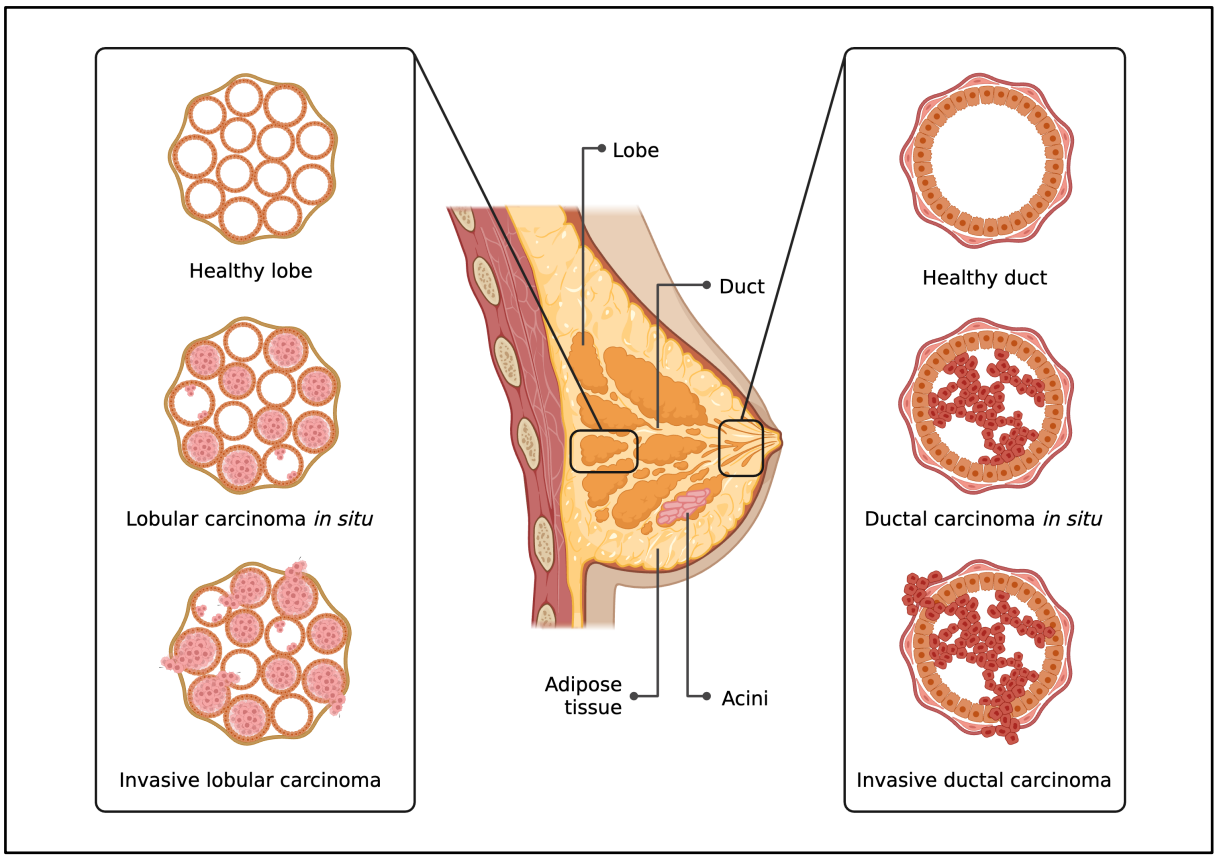


Figure 1-2: Breast anatomy and major histological subtypes of BC. Created with Biorender.com.

1.2.1. Breast cancer epidemiology

BC is consistently among the most commonly diagnosed cancers, alongside lung, prostate, and colorectal cancers (56). Estimates of BC cases and deaths in 2020 were acquired from the GLOBOCAN database . A large variation in incidence rates exists across countries and regions of the world with the highest BC incidence rates of greater than 80 per 100,000 observed in Australia/New Zealand, Western Europe, North America, and Northern Europe and the lowest rates of less than 40 per 100,000 observed in Central America, Eastern and Middle Africa, and South-Central Asia. Despite the disparity in incidence rates, there was less geographical variation in mortality, however it was observed that countries undergoing socioeconomic transition bear a disproportionate share of BC deaths; with the highest mortality rates of greater than 20 per 100,000 found in Melanesia, Western Africa, and Micronesia/Polynesia (3).

Kim *et al.* analysed global patterns and trends in BC and projected that, if current rates of diagnosis and mortality continue, there will be 3.2 million new cases and 1.1 million BC-related deaths annually by 2050. These burdens are expected to disproportionately affect countries with low human development index (HDI) (57,58).

This elevated mortality in low-HDI countries is further compounded by barriers to preventive screening, such as mammography. A systematic literature review carried out by Vieira *et al.* in 2017 indicated that BC mammography screening reduces mortality and should be performed on a large scale in women between 50 and 69-74 years of age. It was found that mammograms are not regularly performed in developing countries due to public healthcare system limitations, such as health service accessibility and cost of tests (59).

1.2.2. Aetiology and risk factors

A wide variety of non-genetic and genetic, demographic, intrinsic, and extrinsic risk factors have been identified in relation to BC development and the various subtypes of the disease. Identification of these factors have led to improvements in preventative measures, as well as the development of more targeted therapies for different BC subtypes. Table 1-2 describes some of the most well-known risk factors associated with the development of BC (60).

Table 1-2: Risk factors of BC. Brief description of the "controllable" (indicated in green) and "uncontrollable" (indicated in red) risk factors associated with BC development (60–77).

Risk Factor	Associated Risk
Controllable	
Weight	Being overweight increases BC risk, particularly post-menopause, through higher estrogen levels (61).
Diet	High intake of processed foods and saturated/trans fats increases risk; fruit, vegetables, and omega-3 fatty acids are protective (62).
Exercise	Reduced physical activity is linked to increased BC risk, mainly in post-menopausal women (63).
Alcohol	Higher consumption elevates BC risk partly by increasing endogenous estrogens (64).
Smoking	Risk rises with both duration and intensity of smoking (65).
Estrogen Exposure	Prolonged exposure to endogenous or exogenous estrogens increases BC risk (66).
Oral Contraception	Slightly increases BC risk with long-term use; risk returns to baseline a few years after stopping (67,68).
Uncontrollable	
Age	BC risk increases with age (69).
Gender	Women are at much higher risk; <1% of cases occur in men (70,71).
Familial/Genetic History	BC 1/2 (*BRCA1/2*) mutations and other genetic variants increase BC risk; prior BC diagnosis also raises risk (72,73).
Race	White women are more likely to be diagnosed with BC, but Black women have greater risk of mortality. The incidence of triple-negative BC (TNBC) in Black women is twice of that in White women (78).
Radiation Therapy	Childhood exposure to chest radiation increases later BC risk (75).
Breast Cellular Alterations	Conditions like atypical hyperplasia increase BC risk (76).
Estrogen Exposure	Early onset menstruation, late menopause, absence of childbearing, and environmental estrogen exposure (77).

1.2.3. Molecular subtypes of breast cancer

As discussed in Section 1.3., the two most common forms of invasive BC are IDC and ILC, classified as histological subtypes because they are defined by tissue or cellular architecture under the microscope (79). While histological subtyping offers valuable insights into BCs, molecular classification is generally considered more informative for personalised treatment, as it reflects the tumour's genetic profile (80).

Immunohistochemical (IHC) staining of specific molecular markers using antibodies is the primary clinical method of BC molecular subtype diagnosis. The expression of the hormone receptors (HRs) for estrogen and progesterone (ER and PR), the human epidermal growth factor (GF) receptor 2 (HER2), and the Ki67 proliferation marker proteins indicate the specific subtype (81).

Gene expression analyses have facilitated further molecular subtype classification with the messenger ribonucleic acid (mRNA) expression of 50 genes (i.e. the prediction analysis of microarray 50 (PAM50) signature) defining five main intrinsic subtypes of BC (82). PAM50 offers a more refined molecular classification and can identify BC subtypes that may be missed by IHC markers. This molecular information can help inform clinical decisions, such as selecting patients for targeted therapies or risk-adapted treatment strategies. However, its higher cost and limited accessibility compared with IHC currently restrict its routine use in standard clinical practice (83).

Knowledge of the different molecular subtypes of BC have allowed for the development of various treatment options and is crucial for patient stratification for these treatments (81). The main molecular subtypes of BC are luminal A, luminal B (HER2-positive or HER2-negative), HER2-overexpressing/positive, and triple-negative or basal (84,85). Table 1-3 summarises their key characteristics and clinical outcomes. Improvements in gene expression profiling methods have also led to the identification of less common BC subtypes, namely Claudin-low, Interferon-rich, and Molecular Apocrine (82).

Table 1-3. Characteristics of the Main Molecular Subtypes of BC.

	HR	HER2	Ki67	Outcome	Prevalence**	5-year Survival***
Luminal A	+	-	-	Good	70%	95.5%
Luminal B	+	+ or -	+	Intermediate	9%	94.1%
HER2-Overexpressing	-	+	NA	Poor*	4%	89.3%
Triple-Negative/Basal	-	-	NA	Poor	11%	83.1%

**HER2-overexpressing subtype is traditionally associated with a poor outcome, however, developments in targeted therapeutics are improving prognoses (86).*
***Prevalence measured in invasive female BCs from the SEER database in the United States between 2018 and 2022. Rates are per 100,000 patients and are age-adjusted to the 2000 US population (87).*
****5-year survival based on BC-specific survival (BCSS) rate measured in 321,958 females with operable invasive BC from the SEER database (88).*

The luminal A subtype is characterised by an ER-positive (ER+), typically PR-positive (PR+) (though some cases are PR-negative (PR-), which is linked to a less favourable prognosis (89–91)), and HER2-negative (HER2-) status, as determined by IHC staining. This subtype is also negative for Ki67, a marker for tumour cell growth and proliferation (84). Luminal A BC is associated with a better prognosis than other subtypes with therapeutically targetable HR expression (92).

Despite having the same HR status, luminal B differs from luminal A based on Ki67 and, in some cases, HER2 expression, and has a poorer outcomes partly due to decreased sensitivity to endocrine therapy (93). The luminal B subtype can be subdivided into HER2+ and HER2- categories, with the former traditionally associated with a worse outcome, however patient prognoses are improving with advances in HER2-targeting therapies (94).

The development of HER2-targeted therapeutics, such as trastuzumab, represented a major advance in the treatment of the HER2-overexpressing subtype. This subtype lacks HR expression and is characterised by aggressive tumour behaviour and historically poor prognosis; however, targeted therapies have significantly improved clinical outcomes (95).

The triple-negative or basal subtype of BC lacks HR expression and does not demonstrate HER2 overexpression or gene amplification. Consequently, it lacks the conventional therapeutic targets used in endocrine and HER2-amplified disease, and treatment has historically relied primarily on chemotherapy, contributing to its therapeutic complexity. TNBC accounts for roughly 10-15% of all BC subtypes and has the worst prognosis, with lower rates of survival and increased risk of recurrence (96).

According to the American Cancer Society's 2024 BC Facts & Figures report, Black women have a lower overall BC incidence but a 38% higher mortality rate compared to other racial/ethnic groups. This disparity is largely attributable to the 2-fold higher prevalence of the aggressive TNBC subtype in Black women (~19% vs. 9-11% in others) (97).

1.3. Triple-negative breast cancer

TNBC represents a heterogeneous subtype of BC, characterised by its aggressive nature and variable treatment responses. Lacking ER, PR, and HER2 expression, it is insensitive to endocrine and HER2-targeted therapies (98). It is commonly observed in women with a mutated *BRCA1* gene, although *BRCA1/2* germline mutations only occur in approximately 10-20% of TNBC cases, and is characterised as an aggressive form of BC with diverse treatment response (99–101).

TNBC exhibits shorter survival times than other BC subtypes due to its high mortality and recurrence rates (97). It is also highly invasive, with distant metastasis occurring in an estimated 46% of patients (98). Recognised for its limited response to targeted therapies, TNBC necessitates further biomarker validation to enhance treatment outcomes (102).

1.3.1. TNBC subtypes and heterogeneity

Despite the classification of TNBC as a single intrinsic subtype of BC, molecular profiling of the disease has uncovered a significantly high level of heterogeneity and genetic complexity (103). In 2011, Lehmann *et al.* identified six genomic subtypes of TNBC based on gene expression analysis, which are depicted in Figure 1-3; basal-like 1 (BL1), basal-like 2 (BL2), immunomodulatory (IM), mesenchymal (M), mesenchymal stem-like (MSL), and luminal androgen receptor (LAR) groups. An additional subtype which encompassed samples that could not be definitively classified due to low correlations and overlapping features with multiple subtypes was identified. They were designated as unstable (UNS) (104).

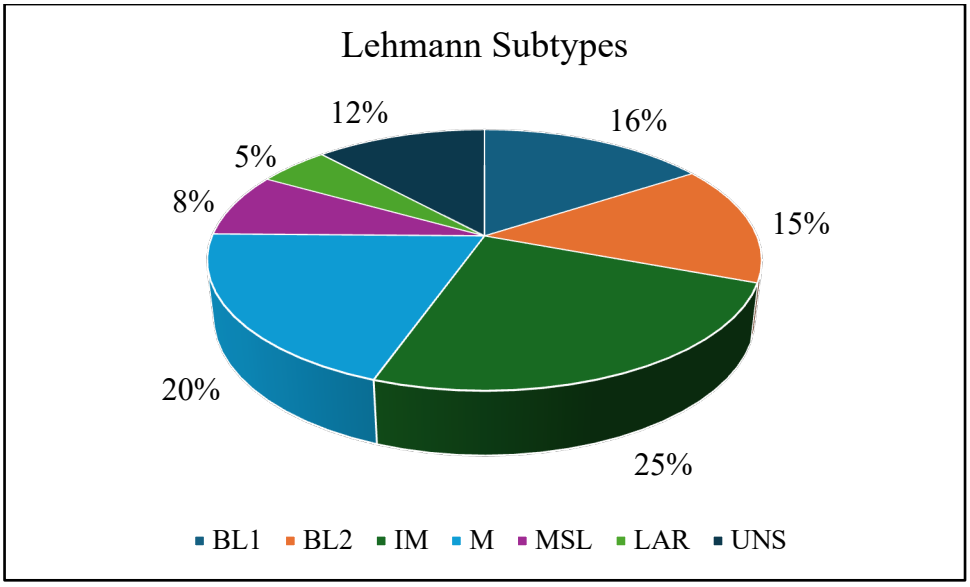


Figure 1-3: Lehmann intrinsic subtype distributions. Distribution of Lehmann subtypes adapted from the Santonja *et al.* study of a TNBC cohort (n=125) (105).

The BL subtypes (BL1 and BL2) are characterised by high proliferation and GF signalling, with cellular myelocytomatosis (*c-MYC*) amplification, epidermal GF receptor (EGFR) activation, and PI3K/AKT pathway upregulation often due to *PTEN* loss (98) in a wide range of cases depending on different studies (e.g. 17-44% (106,107)).

The BL1 subtype is dominated by cell cycle and DNA damage response genes, with *c-MYC* amplification and *BRCA1/2* mutations driving sensitivity to poly (adenosine diphosphate (ADP)-ribose) polymerase (PARP) inhibitors (e.g. olaparib) and cisplatin. Whereas, the BL2 subtype emphasises GF pathways (*EGFR,* MET proto-oncogene (*MET*), nerve growth factor (*NGF*)) and glycolysis-related gene expression, with less reliance on DNA repair defects, leading to poorer response to DNA-damaging agents but potential responsiveness to specific targeted pathway and GF inhibitors (108).

The IM subtype is defined by immune signalling, including TNF-α, interferon, and PD-1/PD-L1 pathways, driven by tumour infiltrating lymphocytes (TILs). The immune-rich profile of IM tumours make it the most immunotherapy-responsive TNBC subtype, such as the PD-L1-targeted pembrolizumab drug (98).

The M subtype features EMT driven by Src, PI3K/AKT, and transforming GF beta 1 (TGF-β) signalling, promoting invasiveness and sensitising these tumours to PI3K/mammalian target of rapamycin (mTOR) inhibitors (e.g. everolimus) and Src inhibitors (e.g. dasatinib), but resistance is common due to the activation of alternative signalling pathways (107,109,110).

MSL mirrors the M subtype's EMT and GF signalling, but also expresses stemness-related pathways like Wnt and angiogenesis. MSL also responds to PI3K/mTOR and Src inhibitors but is less responsive to chemotherapy due to stromal interactions and low proliferation rates (98).

The LAR subtype is driven by androgen receptor (AR) signalling, with low activity of *EGFR*, Src, *c-MYC*, or immune pathways, significantly distinguishing it from other TNBC subtypes. LAR tumours respond to AR antagonists (e.g. bicalutamide), but show limited sensitivity to chemotherapy (108). Moreover, enrichment of phosphatidylinositol 3-kinase (*PIK3CA*) mutations in LAR tumours sensitise this subtype to PI3K/AKT inhibition (111).

Table 1-4 is adapted from a review by Sporikova *et al.* and summarises the characteristics of TNBC subtypes, detailing their primary signalling pathways, key biomarkers, chemotherapy sensitivity, and potential targeted therapies (108).

Table 1-4: Characteristics of TNBC Subtypes (16,98,108,112–117).

Subtype	Signalling Pathways	Primary Biomarkers	Sensitivity to Chemotherapy	Potential Targeted Therapy
BL1	Cell cycle Cell division DNA damage response	*BRCA1/2, MYC, NRAS,* Ki-67	High sensitivity (most sensitive subtype)	PARP inhibitors
BL2	GF signalling (EGFR, MET, NGF) Glycolysis Glucogenesis	*EGFR, EPHA4, EPHB2, PDGFRA, PDGFRB, ROR1, MET, TP53*	Low sensitivity	PARP inhibitors GF inhibitors (e.g. MET)
IM	Immune signalling (T cell, NK cell, TNF) Cytokine signalling	TILs, PD-L1, *JAK1/2, STAT1/3, IRF1/7, TNF*	Moderate sensitivity	Immune checkpoint inhibitors (e.g. PD-L1)
M	EMT (PI3K/AKT/mTOR, TGF-β, Src) Cell motility Cell differentiation GF signalling (EGFR, PDGF, ERK 1/2)	*WNT, TGF-β, ALK, MYC,*	Moderate sensitivity	TK inhibitors Src inhibitors PI3K/AKT/mTOR inhibitors GF inhibitors (e.g. EGFR)
MSL	EMT Cell motility GF signalling Angiogenesis Low proliferation	*EGFR, PDGFR, ERK1/2 VEGFR2*	Moderate sensitivity	TK inhibitors Src inhibitors PI3K/AKT/mTOR inhibitors Anti-angiogenic therapies (e.g. anti-VEGF)
LAR	AR signalling PI3K/AKT/mTOR pathway	*AR, FOXA1, KRT18, XBP1, PIK3CA*	Low sensitivity (least sensitive subtype)	AR inhibitors PI3K inhibitors

Abbreviations: *PDGF* = platelet-derived GF; *ERK1/2* = extracellular signal-regulated kinase 1 and 2; *NRAS* = neuroblastoma RAS viral oncogene homolog; *EPHA4* = ephrin type-A receptor 4; *EPHB2* = ephrin type-B receptor 2; *PDGFRA* = PDGF receptor alpha; *PDGFRB* = PDGF receptor beta; *ROR1* = receptor tyrosine kinase-like orphan receptor 1; *JAK1/2* = janus kinase 1/2; *STAT1/3* = signal transducer and activator of transcription 1/3; *IRF1/7* = interferon regulatory factor 1; *WNT* = wingless-related integration site; *ALK* = anaplastic lymphoma kinase; *PDGFR* = PDGF receptor; *VEGF* = vascular endothelial growth factor; *VEGFR* = vascular endothelial growth factor receptor; *FOXA1* = forkhead box A1; *KRT18* = keratin 18; *XBP1* = x-box binding protein 1; *TK* = tyrosine kinase.

In 2016, Lehmann *et al.* revised this classification of TNBC, refining it to just four subtypes owing to the expression of immune-related genes being attributed to TILs and stromal cell content rather than the cancer cells (98).

Building on Lehmann's TNBC classification, Burstein *et al.* proposed a complementary refinement based on genomic profiling into four subtypes – basal-like immune-activated (BLIA), basal-like immune-suppressed (BLIS), LAR, and mesenchymal (MES) – with a focus on immune stratification within basal-like tumours for improved prognostic and therapeutic relevance (117). These classifications were validated in a cohort of over 500 Chinese TNBC cases, confirming their robustness (118).

Additionally, a Fudan University Shanghai Cancer Centre (FUSCC) study analysed transcriptomic profiles from 165 Chinese TNBC samples to develop the FUSCC classification system, integrating mRNA and long non-coding RNA (lncRNA) expression profiles to define four subtypes: IM, LAR, MES, BLIS (119).

This approach, tailored for Asian cohorts with higher LAR prevalence (23%), enhances molecular characterisation and therapeutic targeting (e.g. PD-1 inhibitors for IM, AR antagonists for LAR), however, its generalisability is limited by the Chinese-focused sample, necessitating validation in larger, more diverse populations (116).

While no standardised subtyping method exists for TNBC in clinical practice – where guidelines prioritise biomarkers like PD-L1 and *gBRCA* over full molecular profiling – major transcriptomic classifications (e.g. Lehmann, Burstein) converge on at least four main subtypes: BLIA, BLIS, LAR, and MES (116). Figure 1-4 provides a synopsis of each Lehmann and corresponding Burstein subtype according to their specific pathway enrichment.

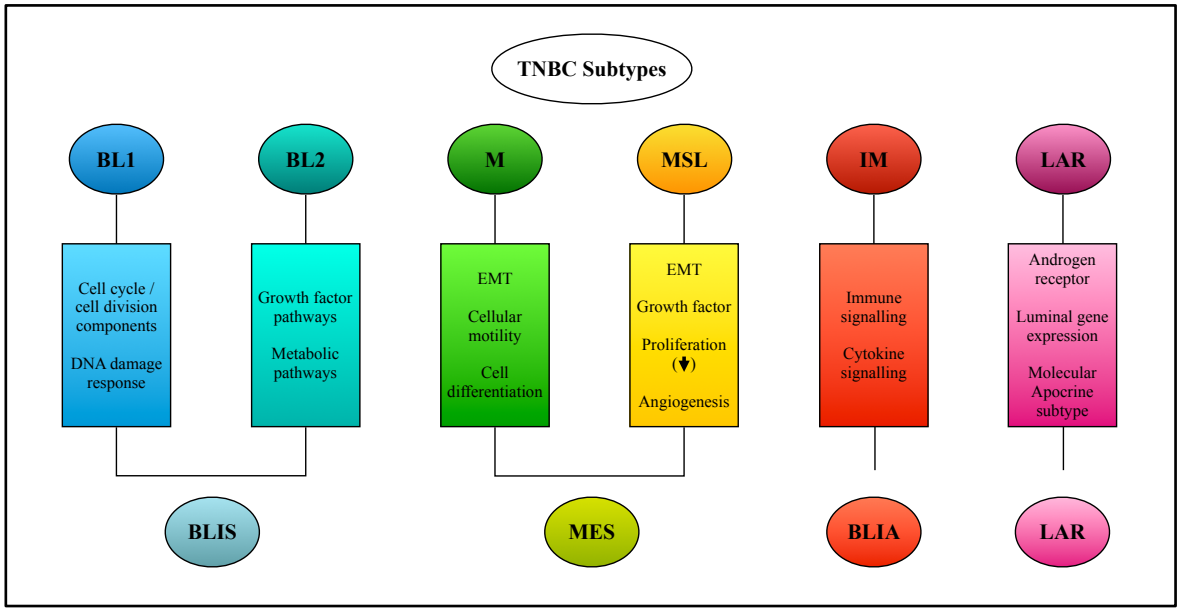


Figure 1-4: Lehmann and Burstein intrinsic subtypes of TNBC. Pathways associated with the 6 Lehmann intrinsic subtypes of TNBC and their corresponding Burstein subtypes (112,120).

1.3.2. Established and potential candidate biomarkers in TNBC

Molecular advances have defined distinct TNBC gene expression and mutation profiles, leading to biomarker-driven targeted therapies. However, few of these therapies have significantly improved TNBC patient prognosis. Current research on TNBC employs advanced techniques to identify robust prognostic and predictive biomarkers. These approaches, detailed in Table 1-5, enable comprehensive multi-omic profiling to uncover subtype-specific molecular signatures and potential therapeutic targets, facilitating personalised treatment strategies (121).

Table 1-5: Biomarker Discovery Approaches (122–151).

Approach	Techniques / Analyses	Identify / Predict / Monitor	Example Biomarker
Genomic	WGS; WES; Targeted gene panels; CGH	Mutations; CNVs; SVs	*TP53* mutation
Transcriptomic	RNA-seq; Microarray analysis; Single-cell RNA-seq	Gene expression dysregulation (e.g. pathway dysregulation)	*HORMAD1* overexpression
Proteomic	MS; RPPA; IHC	Overexpressed/activated proteins	EGFR overexpression
Epigenomic	DNA methylation arrays; ChIP-seq; ATAC-seq	DNA methylation and histone modification changes.	*BRCA1* promoter hypermethylation
Functional Genomics	CRISPR-Cas9 screens RNAi (shRNA/siRNA) screens ORF expression libraries	Essential genes; Synthetic lethal interactions	*PARP1* dependency
Metabolics and Lipidomics	NMR spectroscopy; MS-based metabolite profiling	Altered metabolism; Metabolic vulnerabilities	Glutathione levels
Immunoprofiling	Flow cytometry; CyTOF; Immune gene signatures (RNA-seq); Multiplex IHC or spatial transcriptomics	Immunotherapy biomarkers; TME	TILs
Bioinformatics and Systems Biology	Network analysis; ML for biomarker prediction; Pathway enrichment; Survival analysis	Multi-omic biomarkers/therapeutic targets; treatment response prediction	PI3K pathway activation
Patient-Derived Models	PDX; PDOs; 3D cultures and spheroids	Therapeutic response; biomarker validation	Olaparib sensitivity in *BRCA*-mutated PDXs
Liquid Biopsy	ctDNA; Exosomes; CTCs	MRD; resistance mechanisms; dynamic biomarker levels	Circulating *TP53* mutations

Abbreviations: WGS = whole genome sequencing; WES = whole exome sequencing; CGH = comparative genomic hybridisation; RNA-seq = RNA-sequencing; MS = mass spectrometry; RPPA = reverse phase protein array; ChIP-seq = chromatin immunoprecipitation sequencing; ATAC-seq = assay for transposase-accessible chromatin with high throughput sequencing; CRISPR = clustered regularly interspaced short palindromic repeats; Cas9 = CRISPR-associated protein 9; RNAi = RNA interference; shRNA = short hairpin RNA; siRNA = small interfering RNA; ORF = open reading frame; NMR = nuclear magnetic resonance; CyTOF = cytometry by time-of-flight; ML = machine learning; PDX = patient-derived xenografts; PDO = patient-derived organoid; ctDNA = circulating tumour DNA; CTC = circulating tumour cell; CNV = copy number variation; SV = structural variant; MRD = minimal residual disease; *HORMAD1* = Hop1, Rev7, Mad2 (HORMA) domain-containing-1.

1.3.2.1. Protein expression biomarkers

1.3.2.1.1. Receptor tyrosine kinases

EGFR

EGFR, a transmembrane RTK in the erythroblastic leukaemia viral oncogene (ErbB) family, drives cell proliferation and migration via PI3K/AKT and mitogen-activated protein kinase (MAPK) pathways (152). In TNBC, EGFR overexpression or amplification promotes uncontrolled tumour growth and metastasis, especially in basal-like subtypes (98,153). EGFR overexpression occurs in at least 50% and up to 78% of TNBC cases and correlates with reduced overall survival (OS) and higher metastasis risk, indicating poor prognosis (154). *EGFR* amplification is a mechanism of protein overexpression and occurs in up to 24% of TNBCs, while mutations are more rare (155), with many studies reporting no *EGFR*-activating mutations (156).

EGFR inhibitors, such as cetuximab and erlotinib, have demonstrated limited efficacy as monotherapies in EGFR-high TNBC, partly due to intrinsic resistance mechanisms including activation of alternative growth signalling pathways (e.g. PI3K/AKT, MAPK) and downstream mutations that bypass EGFR inhibition. No therapies are currently approved by the U.S. Food and Drug Administration (FDA) specifically for TNBC. Clinical trials are currently exploring combinations of EGFR inhibitors with other targeted therapies, such as PARP inhibitors, to overcome resistance (157).

VEGF

VEGF, a key angiogenic protein, stimulates blood vessel formation by promoting endothelial cell growth and migration. In TNBC, VEGF overexpression drives tumour progression by enhancing vascular supply, facilitating tumour growth and metastatic spread, and activating downstream signalling pathways such as PI3K/AKT, RAS/MAPK, and phospholipase C-gamma (PLC-γ) (158,159).

VEGF expression is detected in 30-60% of TNBC cases, with elevated levels linked to aggressive disease. High VEGF expression is associated with shorter OS and increased metastatic potential, making it an indicator of poor prognosis (160). VEGF-targeted agents such as bevacizumab yield limited monotherapy success due to resistance, with no FDA approvals for TNBC-specific use (161). Clinical trials exploring VEGF-targeted agents combined with chemotherapy or immune checkpoint inhibitors aim to improve efficacy. Limited OS benefits and safety concerns regarding side effects have led to the termination of

some studies, while others demonstrate high overall response rates and improved progression-free survival (PFS) (162–165).

FGFR

Fibroblast GF receptors (FGFRs), a family of RTKs, promote cell proliferation, survival, and angiogenesis via RAS/MAPK, PI3K/AKT, PLC-γ, and JAK/STAT pathways (166). In TNBC, FGFR amplification or overexpression drives tumour growth and metastasis by enhancing signalling cascades (167).

FGFR amplification, primarily *FGFR1* and *FGFR2*, occurs in 10-15% of TNBC cases (168), while overexpression is reported in 20-30% of tumours (167,169–171). High *FGFR* expression or amplification correlates with reduced OS and higher recurrence risk (160,168).

FGFR inhibitors like erdafitinib and lucitanib have demonstrated antitumour activity in FGFR-altered TNBC as monotherapies, although no specific FGFR inhibitor are currently approved for this indication (168,172–174). Ongoing pre-clinical studies and clinical trials are exploring FGFR inhibitors both alone and in combinations with chemotherapy or PI3K/mTOR inhibitors to overcome resistance (175–177).

HER2

HER2, an RTK in the ErbB family, promotes cell proliferation and survival through downstream signalling pathways such as MAPK, PI3K/AKT, Wnt, and JAK/STAT (178). In TNBC, defined by low HER2 expression, rare *ERBB2* (HER2) mutations or low-level expression drive tumour growth in specific subsets by enhancing signalling (179).

ERBB2 mutations occur in ~3% of TNBC cases, while low-level overexpression (HER2-low, 1+/2+ IHC score without amplification) is reported in ~34-50% of TNBC tumours (179–182). HER2 low-level expression correlates with a favourable prognosis in TNBC, with some studies reporting improved survival in HER2-low TNBC patients compared to a HER2-null group (183–186).

While no HER2-targeted therapies have specifically been approved for TNBC, the antibody-drug conjugate (ADC) Trastuzumab deruxtecan (T-DXd) was approved in January 2025 for patients with HER2-low or ultralow metastatic BC, which includes TNBC cases with this HER2 status (187).

c-Kit

c-Kit, an RTK, promotes cell survival, proliferation, and differentiation through activation of PI3K/AKT, MAPK/ERK, Src, PLC-γ, and JAK/STAT pathways upon binding to its ligand, stem cell factor (SCF) (188).

c-Kit overexpression varies widely across studies, which may be due to the use of different antibodies, staining protocols, or scoring, occurring in 15-49% of TNBC cases. While c-Kit expression alone does not consistently predict patient survival in TNBC, its co-expression with *TP53* mutations in primary tumours is an independent prognostic factor for poorer overall survival (102,189–191).

c-Kit inhibitors, especially nilotinib, show significant cytotoxic effects in TNBC cell lines, however their efficacy may depend on co-targeting other kinases. Dasatinib, a multi-kinase (including c-Kit) inhibitor, demonstrates limited efficacy in unselected TNBC, but may increase sensitivity to inhibition of other kinase targets, such as c-Met, and chemotherapies, like paclitaxel (192–194).

Cytokeratins

Cytokeratins, such as cytokeratin 5/6 (CK5/6), are basal-type intermediate filament proteins that maintain epithelial cell integrity and are involved in cell differentiation. In TNBC, CK5/6 expression is associated with basal-like features and correlates with EMT and tumour invasiveness (195–198).

CK5/6 expression prevalence in TNBC varies in studies, ranging from ~30% to over 50%, with higher rates reported in basal-like subtypes (199–202). Expression is generally correlated with shorter overall survival and poor clinical and pathological response to chemotherapy in TNBC, indicating poor prognosis (201). While CK5/6 expression is not directly targetable, it serves as a biomarker identifying the aggressive basal-like BC subtypes (196).

1.3.2.1.2. Non-receptor tyrosine kinase

AR

AR, a nuclear receptor transcription factor that is activated by binding androgen hormones (e.g. testosterone and dihydrotestosterone (DHT)), promotes cell proliferation and survival by regulating gene expression upon binding to androgens (203). In TNBC, AR overexpression drives tumour growth and metastasis by activating PI3K/AKT and MAPK pathways, particularly in the LAR subtype (204).

AR expression prevalence in TNBC is highly variable across studies, ranging from ~7-75%, likely due in part to inconsistent thresholds for positivity, variable testing protocols, and antibodies, with higher prevalence in LAR TNBCs (205,206).

AR positivity is associated with variable prognosis, often linked to better OS in LAR subtypes but poorer response to chemotherapy in some cohorts (207–210). AR inhibitors like enzalutamide and bicalutamide have demonstrated modest clinical benefit in AR-positive TNBC, supporting further exploration in combination therapies (211,212).

1.3.2.2. DNA expression biomarkers

BRCA1/2

BRCA1/2, tumour suppressor genes encoding proteins critical for homologous recombination (HRc) DNA repair, maintain genomic stability by repairing double-strand (ds) DNA breaks (213). In TNBC, *BRCA1/2* mutations – often truncating or frameshift – impair HRc repair, leading to genomic instability and tumour progression, particularly in basal-like subtypes (214).

BRCA1/2 mutations occur in 10-20% of TNBC cases, with higher prevalence in hereditary BCs (i.e. germline mutations) and younger patients (101,215). Somatic *BRCA1/2* mutations are more rare, with one study reporting mutations in 11.6% and 4.5% of TNBC patients, respectively (216).

In TNBC, *BRCA1/2* mutations do not generally correlate with poorer survival. These mutations can predict improved response to DNA-damaging chemotherapies (e.g. platinum agents), but in the absence of targeted therapy, they are also associated with an elevated risk of recurrence (217,218).

PARP inhibitors, such as olaparib and talazoparib, exploit synthetic lethality in *BRCA1/2*-mutated TNBC, particularly in *TP53* co-mutated cases, with FDA approvals for patients harbouring germline *BRCA1/2* mutations (including TNBC) (218,219). Ongoing trials are exploring combinations with immunotherapy (e.g. PD-1/PD-L1 checkpoint inhibitors) to enhance efficacy (220,221).

Homologous recombination deficiency

BRCA1/2 mutations contribute significantly to homologous recombination deficiency (HRcD) in TNBC, yet the higher prevalence of HRcD (~50-60% of cases – the highest among BC subtypes) indicates additional causes. These include other HRc pathway genes (e.g. *BRCA1/2*, partner and localiser of *BRCA2* (*PALB2*), *RAD51C/D*, ataxia-telangiectasia mutated (*ATM*), and checkpoint kinase 2 (*CHEK2*)) and epigenetic alterations. This enhances tumour mutational burden and sensitivity to DNA-damaging therapies (222–224).

TP53

TP53, a tumour suppressor gene encoding the p53 protein, regulates cell cycle arrest, DNA repair, and apoptosis in response to cellular stress. In TNBC, *TP53* mutations, predominantly missense or truncating, impair p53 function, promoting uncontrolled proliferation and genomic instability, particularly in basal-like subtypes. *TP53* mutations occur in 60-80% of TNBC cases, making them the most frequent genetic alteration in this BC subtype (225–228).

The relationship between *TP53* mutations and survival in TNBC is complex and context-dependent. *TP53* mutations are generally associated with poorer survival due to impaired p53 function, however, some studies suggest that specific DNA-binding domain (DBD) mutations, may correlate with better response to certain chemotherapies, potentially improving survival in subsets of TNBC patients. Conversely, mutations outside of the DBD are associated with poorer overall survival, increased recurrence risk, and resistance to chemotherapy (227,229,230). The heterogeneity of *TP53* mutations in TNBC, with distinct hotspot and DNA-binding alterations driving varied oncogenic or therapy-sensitising effects, highlights the need for functional classification to improve prognosis and therapeutic strategies (231).

TP53-mutated TNBC is challenging to target directly due to p53's loss of function. Ongoing studies are exploring synthetic lethality approaches, such as PARP inhibitors for co-occurring *BRCA1/2* mutations, which are already compromised by *TP53* dysfunction (232,233). Clinical trials are investigating drugs like APR-246 to restore or reactivate mutant p53 function, aiming

to enhance apoptosis and overcome chemotherapy resistance in *TP53*-mutated tumours, though no FDA-approved therapies are yet available (234).

PIK3CA

PIK3CA, an oncogene encoding the p110α catalytic subunit of PI3K, drives cell proliferation, survival, and metabolism via the PI3K/AKT/mTOR pathway (235). In TNBC, *PIK3CA* mutations, primarily hotspot mutations (e.g. H1047R, E545K), activate this pathway, promoting tumour growth and resistance to apoptosis, particularly in LAR subtypes (236).

PIK3CA mutations occur in ~10-15% of TNBC cases, representing the second most commonly altered gene after *TP53*, with higher prevalence in LAR TNBC (up to 40%), often co-occurring with *TP53* and AR alterations (109,237–239). In TNBC, *PIK3CA* mutations, enriched in luminal BCs that lose HR expression during metastasis, are associated with better survival compared to non-mutated cases, yet they promote chemotherapy resistance by activating the PI3K/AKT/mTOR pathway and suppressing apoptosis (240,241).

PI3K inhibitors (e.g. alpelisib) and AKT inhibitors (e.g. capivasertib) show promise in *PIK3CA*-mutated TNBC, particularly in combination with chemotherapy or other targeted therapies to overcome the complex feedback mechanisms observed in the PI3K/AKT pathway (242–244). Alpelisib combined with nab-paclitaxel was evaluated in the phase III EPIK-B3 trial (NCT04251533) for advanced TNBC with *PIK3CA* mutations or *PTEN* loss; however, the study was terminated due to insufficient clinical activity in TNBC patients, despite earlier phase I/II signals suggesting potential improvements in overall response rates (ORR) and PFS (245–247). AKT inhibitors ipatasertib and capivasertib, evaluated in the phase II LOTUS and PAKT trials, showed improved PFS and OS in *PIK3CA*/*AKT1*/*PTEN*-altered metastatic TNBC when added to paclitaxel, leading to them progressing to phase III trials. However, results from the phase III trials fell short of predefined efficacy thresholds (162).

Co-Occurring TP53 and PIK3CA Mutations

Co-occurring *TP53* and *PIK3CA* mutations, identified in ~7.5% of BC cases via cBioPortal analysis of the TCGA Breast Invasive Carcinoma dataset (248), amplify tumour aggressiveness beyond singular mutations by synergistically activating the PI3K/AKT/mTOR pathway and impairing p53-mediated apoptosis. Additionally, mutant *TP53* may lead to the hyperactivation of PI3K/AKT signalling via *PTEN* suppression. Unlike isolated *TP53* or *PIK3CA* mutations,

these co-mutations drive worse survival and therapeutic resistance, potentially driven by compensatory PI3K/AKT pathway activation (237,249).

1.3.2.3. RNA expression biomarkers

microRNAs & lncRNAs

MicroRNAs (miRNAs) and lncRNAs, regulatory non-coding RNAs, modulate post-transcriptional (PTM) gene expression in TNBC (250). Oncogenic miRNAs like *miR-21* and *miR-155* drive proliferation, EMT, and chemoresistance by targeting *PTEN* and suppressing apoptosis, while tumour-suppressive *miR-200* family members are downregulated, enhancing metastasis (251–254). One study by Kumar *et al.* demonstrated the high diagnostic potential (Area Under the Receiver Operating Characteristic Curve (AUC) 94.9-97.1%) of a three miRNA signature (upregulation of *miR-21* and *miR-155*, downregulation of *miRNA-205*) (255).

lncRNAs such as *HOTAIR* and *MALAT1* promote invasion and immune evasion by binding or "sponging" miRNAs, upregulating Wnt/β-catenin and PI3K/AKT pathways, often amplifying pathway effects (251,256,257).

miRNAs and lncRNAs show promise as therapeutic and diagnostic biomarkers for TNBC, but large-scale clinical trials are required to validate their targetability and diagnostic utility in this subtype (250,258).

1.3.2.4. Immunotherapy biomarkers

TILs

TILs, immune cells within the TME, modulate TNBC immunogenicity and progression (259), particularly in the IM subtype which has the highest density of TILs (260). In TNBC, high TIL levels correlate with robust anti-tumour responses, enhancing cytotoxic T-cell activity and cytokine production (259).

TILs are present in varying levels in TNBC, with a median TIL level of 15%, where 34% of cases have TIL levels above 30% and 21% have TIL levels of 50% or higher, according to a study of 1,966 early stage TNBC patients who did not receive adjuvant or neoadjuvant chemotherapy (261). Higher densities of TILs are linked to better OS and chemotherapy response (262) and may be used to predict response to immune checkpoint inhibitors (ICIs) (e.g. pembrolizumab) (263).

PD-1/PD-L1

PD-1 and its ligand PD-L1, immune checkpoint molecules, regulate TNBC tumour immune evasion by suppressing T-cell activity (264). In TNBC, PD-L1 is overexpressed in ~20-40% of cases, promoting immune escape and tumour progression (265).

High PD-L1 expression correlates with better survival and response to immunotherapy (266,267). Clinically, PD-L1 status serves as a biomarker to predict response to ICIs, with an FDA-approved companion diagnostic (PD-L1 IHC 22C3) for TNBC (268). Therapeutically, anti-PD-1/PD-L1 agents such as pembrolizumab in combination with chemotherapy improve outcomes in PD-L1-positive metastatic and early-stage TNBC, with FDA approvals based on KEYNOTE-522 and KEYNOTE-355 trials (269).

1.3.2.5. Signalling pathways

Signalling pathways critically regulate TNBCs aggressive tumour biology, driving proliferation, survival, and metastasis through interactions with genetic alterations. Dysregulated pathways amplify tumour heterogeneity and therapy resistance, with many pathways exhibiting crosstalk that further enhances TNBC's complexity, serving as prognostic and predictive biomarkers (270). Table 1-6 summarises key pathways as TNBC biomarkers. All of these pathways are associated with poorer prognosis in TNBC.

Table 1-6: Signalling pathways as biomarkers of TNBC (109,162,271–315).

Signalling Pathway	Genetic Alterations/Causes of Activation	Role in TNBC	Therapeutic Targeting
PI3K/AKT/ mTOR	*PIK3CA* mutations/amplification; *PTEN* loss/inactivation; *AKT1* mutations; GF receptor overexpression	Promotes cell proliferation, survival, metabolism, and resistance to apoptosis.	PI3K inhibitors (e.g. alpelisib, taselisib); AKT inhibitors (e.g. capivasertib, ipatasertib); mTOR inhibitors (e.g. everolimus)
MAPK/ ERK	RTK overexpression; *RAS* mutations/amplification/CNV; Raf/MEK/ERK upregulation	Drives cell proliferation, invasion, metastasis, and angiogenesis.	MEK inhibitors (e.g. trametinib, selumetinib); ERK inhibitors (e.g. ulixertinib, ravoxertinib); RAF inhibitors (e.g. dabrafenib, sorafenib)
Wnt/ β-Catenin	Wnt ligand or Frizzled receptor overexpression; APC loss/downregulation; *TP53* loss; Rare *CTNNB1* mutations	Regulates EMT, metastasis, stem cell self-renewal, and chemoresistance.	Porcupine inhibitors (e.g. LGK974, ETC-159); β-catenin/TCF interaction inhibitors (e.g. PRI-724, BC2059); Tankyrase inhibitors (e.g. XAV939)
NF-κB	Overexpression of upstream activators (e.g. TNF receptors, EGFR); Cytokine/TNF-driven expression; Notch/pAKT correlation	Involved in inflammation, immune response, cell survival, proliferation, and anti-apoptosis.	IKK inhibitors (e.g. BMS-345541, TPCA-1); Proteasome inhibitors (e.g. bortezomib, carfilzomib); NF-κB transcription inhibitors (e.g. DMF, parthenolide)
JAK/ STAT	Cytokine receptor overexpression (e.g. IL-6R); *JAK2* amplification; *STAT3* overexpression/ acetylation; *EGFR* activation	Facilitates tumorigenesis, proliferation, invasion, angiogenesis, immune evasion, and chemoresistance.	JAK inhibitors (e.g. ruxolitinib, tofacitinib) STAT3 inhibitors (e.g. stattic, S31-201) JAK2-specific inhibitors (e.g. fedratinib, pacritinib)
EGFR	Amplification; Overexpression; Rare mutations; JAK/STAT3 activation	Supports cell proliferation, invasion, differentiation, angiogenesis, and metastasis.	EGFR TKIs (e.g. erlotinib, gefitinib); EGFR mAbs (e.g. cetuximab, panitumumab); Dual EGFR/HER2 inhibitors (e.g. lapatinib, neratinib); EGFR ADCs (e.g. depatuxizumab mafodotin)
Notch	Notch receptor and ligand overexpression (e.g. Notch1, Notch4); Notch receptor mutations; NF-κB/pAKT correlation	Contributes to stem cell-like properties, differentiation, survival, and chemoresistance.	GSIs (e.g. DAPT, MK-0752); Notch receptor-specific Abs (e.g. tarextumab, brontictuzumab); Notch ligand inhibitors (e.g. demcizumab)
Hedgehog	Overexpression of Hh components (e.g. SHH, PTCH, SMO); GLI1/GLI2 overexpression; NF-κB crosstalk	Regulates stemness, angiogenesis, embryogenesis, and metastasis.	SMO inhibitors (e.g. vismodegib, sonidegib) GLI inhibitors (GANT61, ATO) Hh ligand inhibitors (e.g. robotnikinin)

Abbreviations: MEK = mitogen-activated protein kinase kinase; APC = adenomatous polyposis coli (APC); *CTNNB1* = catenin beta 1; IL-6R = interleukin 6 receptor; STAT3 = signal transducer and activator of transcription 3; Hh = hedgehog; SHH = Sonic hedgehog; PTCH = patched homolog 1; SMO = smoothened; GLI(1/2) = glioma-associated oncogene (homolog 1/2); NF-κB = nuclear factor kappa-light-chain-enhancer of activated B cells; TCF = T-cell factor/lymphoid enhancer-binding factor; IKK = inhibitor of κB kinase; DMF = dimethyl fumarate; (m)Abs = (monoclonal) antibodies.

1.3.3. Treatment of TNBC

As explored in Section 1.4.1., challenges in the treatment of TNBC arise due to the heterogenous and invasive nature of this disease subtype, contributing to poorer therapeutic outcomes compared to other BC subtypes. While conventional strategies like chemotherapy and radiotherapy remain foundational for TNBC management, their non-specific mechanisms often lead to off-target healthy cell toxicity, underscoring the need for precision approaches (316).

Recent research is driving the discovery of TNBC-specific biomarkers (as discussed in Section 1.4.2.) and, more specifically, TNBC subtype-specific biomarkers for the development of more targeted treatments for TNBC and the incorporation of these into clinical practice (121). Figure 1-5, adapted from a figure by Manjunath *et al.*, summarises the conventional and targeted therapeutic treatment strategies for TNBC (317).

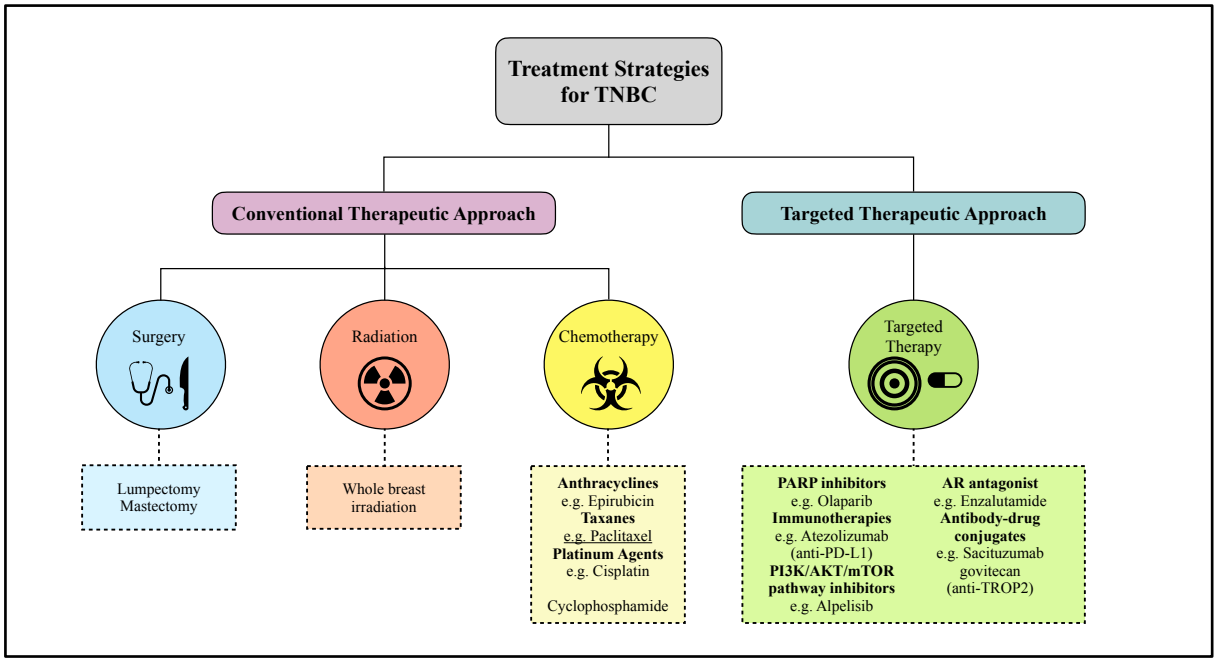


Figure 1-5: Treatment strategies for TNBC. Conventional and targeted therapeutic approaches for the treatment of TNBC (317–321).

1.4.3.1 Conventional therapeutic approaches

For TNBC, conventional therapeutic approaches encompass neoadjuvant and adjuvant therapies. Neoadjuvant therapy – typically involving chemotherapy regimens such as anthracyclines and taxanes (e.g. doxorubicin, cyclophosphamide, and paclitaxel), or radiation – is administered prior to surgery to shrink tumours and eliminate potentially metastatic cells. In contrast, adjuvant therapies are delivered post-surgery to eradicate residual disease (322,323).

Depending on the stage of cancer, surgery can be performed to remove the tumour and some of the surrounding tissue (i.e. a lumpectomy) or to remove the entire breast (i.e. a mastectomy). Surgery can improve patient survival and reduce mortality, and can be used alone or with other treatment types. Limitations associated with surgery are reduced effectiveness for advanced stages of cancer and it potential residual disease which may lead to recurrence or metastasis (318).

Radiation therapy

The use of directed X-rays or subatomic particles in the treatment of cancer is known as radiation therapy (324). Radiation therapy is an important part of the multifaceted management of BC and can be administered to the whole breast (i.e. whole breast irradiation (WBI)) or to part of the breast (i.e. partial breast irradiation (PBI)) (325).

Post-operative WBI is recommended for most TNBC patients, whereas PBI is not, as the TNBC subtype is the only independent predictor of recurrence following accelerated PBI (326,327). Some long-term side effects associated with breast radiotherapy include damage to the heart and lungs, nerve damage, chronic swelling, and second malignancies (328).

Chemotherapy

Chemotherapy functions to inhibit cell proliferation and tumour growth, and furthermore avoid invasion and metastasis, however chemotherapeutic agents target all cells and do not exhibit specific anti-tumour activity. Chemotherapeutic agents may be administered in different settings (i.e. primary, metastatic), as well as in combination with other therapeutics (329,330).

Systemic chemotherapy is the main adjuvant treatment administered to patients for the treatment of TNBC. A combination of surgery and systemic chemotherapy may be used to treat TNBC, with varying regimens dependent on the patient and stage of cancer. Chemotherapy can

be administered adjuvantly as the primary treatment, neoadjuvantly to reduce tumour size prior to surgical resection, or post-operatively to reduce the risk of patient relapse. Commonly used drugs in chemotherapy treatment regimens for TNBC include anthracyclines, taxanes, and platinum agents, as well as cyclophosphamide (see Table 1-7) (318,331,332).

Chemotherapy can be administered in combination with other chemotherapeutic agents or targeted therapies for the treatment of TNBC. Several combination therapies have been approved to improve treatment outcomes, including:

Chemotherapy Combinations (333–337)

1. Doxorubicin + cyclophosphamide (AC), followed by paclitaxel (ddAC-T)
2. Docetaxel + cyclophosphamide (TC)
3. Epirubicin + cyclophosphamide (EC)
4. Docetaxel + AC (TAC)
5. Paclitaxel + carboplatin (PC or T/Cb)
6. Docetaxel + carboplatin (DC or T/Cb)

Chemotherapy + Targeted Therapeutic Combinations (338)

1. Pembrolizumab + chemotherapy (PC, followed by AC or EC)

While Sacituzumab govitecan and T-DXd are technically single agent/monotherapy ADCs, they are both targeted antibodies that deliver a chemotherapy payload.

Table 1-7: Chemotherapeutic agents to treat TNBC (318,328,339–353).

Class	Examples	Primary Mechanism of Action	Toxicities/Limitations
Anthracyclines	Doxorubicin Epirubicin	Form a ternary complex with topoisomerase-II preventing re-ligation of double-stranded DNA breaks and thus promoting growth arrest and apoptosis.	Anthracyclines are cardiotoxic and cumulative doses administered, and potentially use with other agents, increases risks of heart failure. Other side effects include myelosuppression and hepatic failure.
Taxanes	Paclitaxel/ Nab-Paclitaxel Docetaxel	Bind to polymerised tubulins, stabilising microtubules by preventing depolymerisation or increasing polymerisation, causing subsequent arrest of the cell cycle at the mitotic phase. This leads to cell apoptosis and necrosis.	Common side effects which limit the use of taxanes include bone marrow suppression, peripheral nerve damage, and hypersensitivity reactions such as nausea, vomiting, and diarrhoea.
Platinum Agents	Carboplatin Cisplatin	Upon entering a cell, chloride ions of the platinum compound dissociate leaving the central platinum ion to cross-link DNA strands, resulting in DNA synthesis and function inhibition.	Neuropathy and myelosuppression are also associated with platinum-based agents, as well as damage to the kidneys and a number of gastrointestinal side effects.
Nitrogen Mustards	Cyclophosphamide	Undergoes conversion, metabolization, and cleavage to form phosphoramide, an active alkylating agent, which forms cross-linkages with DNA and RNA, subsequently leading to programmed cell death.	The main side effects of the nitrogen mustard cyclophosphamide are myelosuppression, urinary bladder inflammation and bleeding, gonadal disfunction, and alopecia
Antimetabolites	Capecitabine Gemcitabine	Inhibit key enzymes in DNA and RNA synthesis, such as thymidylate synthase, disrupting nucleotide production and leading to cell cycle arrest and apoptosis.	Antimetabolites cause myelosuppression, increasing risks of infection and anaemia, and may lead to gastrointestinal toxicity, including mucositis and diarrhoea.
Microtubule Inhibitors (Vinca Alkaloids)	Eribulin (Vinorelbine)	Disrupt microtubule dynamics by binding to tubulin, inhibiting spindle formation during mitosis, leading to cell cycle arrest and apoptosis.	Microtubule inhibitors cause neurotoxicity, including peripheral neuropathy, and myelosuppression, increasing risk of infection and anaemia.

Treatment Order for TNBC

The order of treatment for TNBC, per the American Society of Clinical Oncology (ASCO) guidelines, is shown in Figure 1-6.

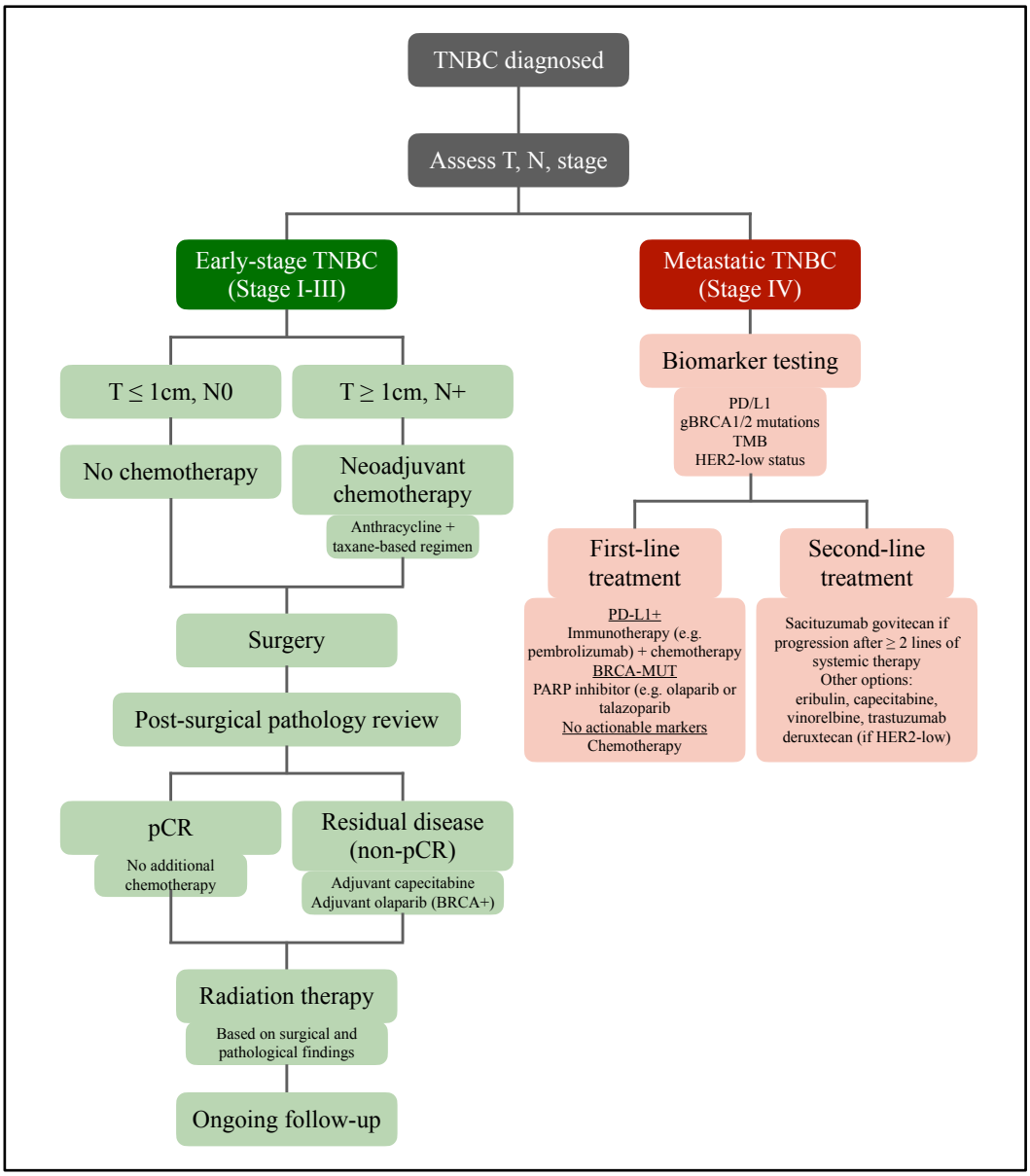


Figure 1-6: Treatment sequencing for early-stage and metastatic TNBC based on ASCO clinical practice guidelines (162,354–357)**.** Abbreviations: T = tumour; N = node; pCR = pathological complete response; MUT = mutant.

1.4.3.2 Targeted therapeutic approach

In operable TNBC, 30-40% of patients develop recurrence or metastasis within 5 years, while nearly 50% of all TNBC patients experience distant metastasis – typically within 2 years of diagnosis (median time to metastasis: 19.7-31.2 months). Post-metastasis survival averages 17-25 months, often compounded by resistance to standard systemic chemotherapy regimens, which underscores the urgent need for biomarkers and personalised treatment strategies beyond conventional therapies (358).

Biomarkers associated with TNBC and its various subtypes, as described in Sections 1.4.1. and 1.4.2., may be therapeutically targeted or they may provide prognostic or predictive information about a specific treatment. These biomarkers may be identified by a number of methods, such as tissue immunohistochemistry, histological/cytological analysis, and a variety of specific assays (as detailed in Table 1-5). Biomarkers in targeted therapy is the focal point of numerous ongoing preclinical and clinical trials (121), and several TNBC subtype-specific biomarkers have emerged as potential therapeutic targets (Figure 1-7).

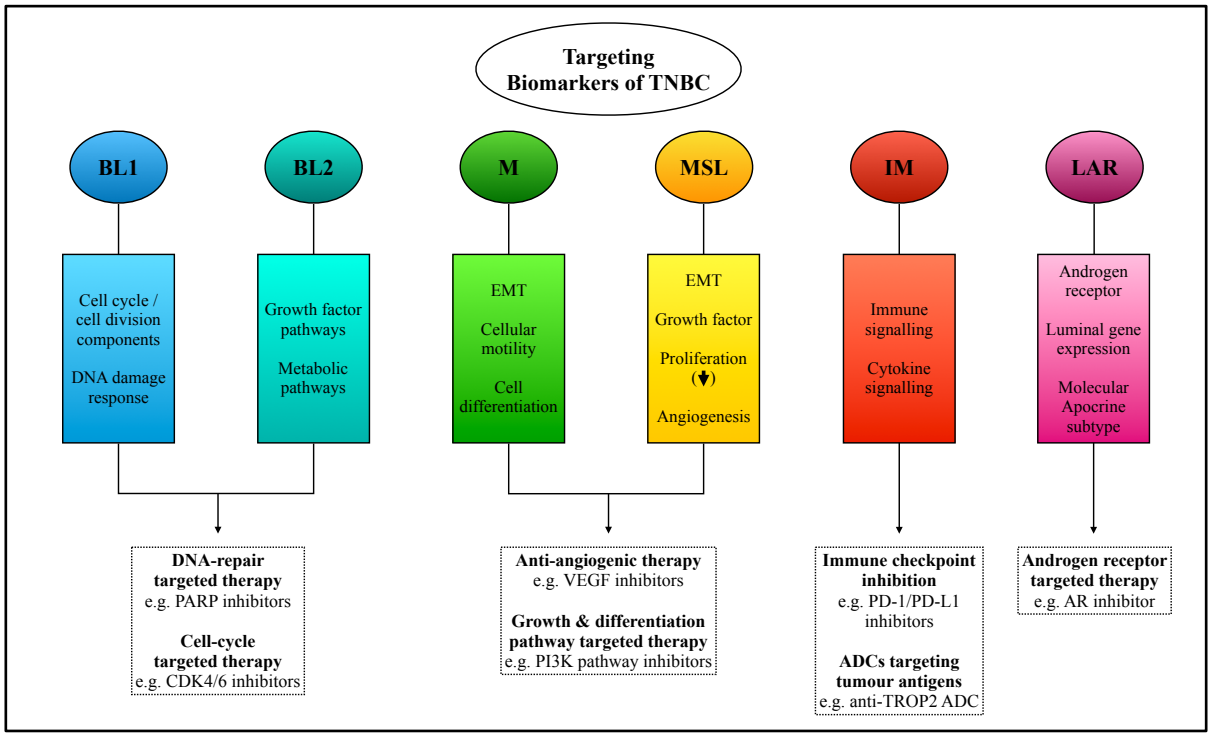


Figure 1-7: Targetable TNBC subtype biomarkers. Targeted therapeutic options based on biomarkers of specific TNBC subtypes (112,120,359). Abbreviations: TROP2 = human trophoblastic cell surface antigen 2.

1.4.3.2.1. Approved targeted therapies for TNBC

Approximately 30-40% of women with TNBC will experience disease relapse, often progressing to metastatic disease (360). Some targeted therapeutics have been approved for use in TNBC in the metastatic setting (see Figure 1-8), while others remain under investigation (361).

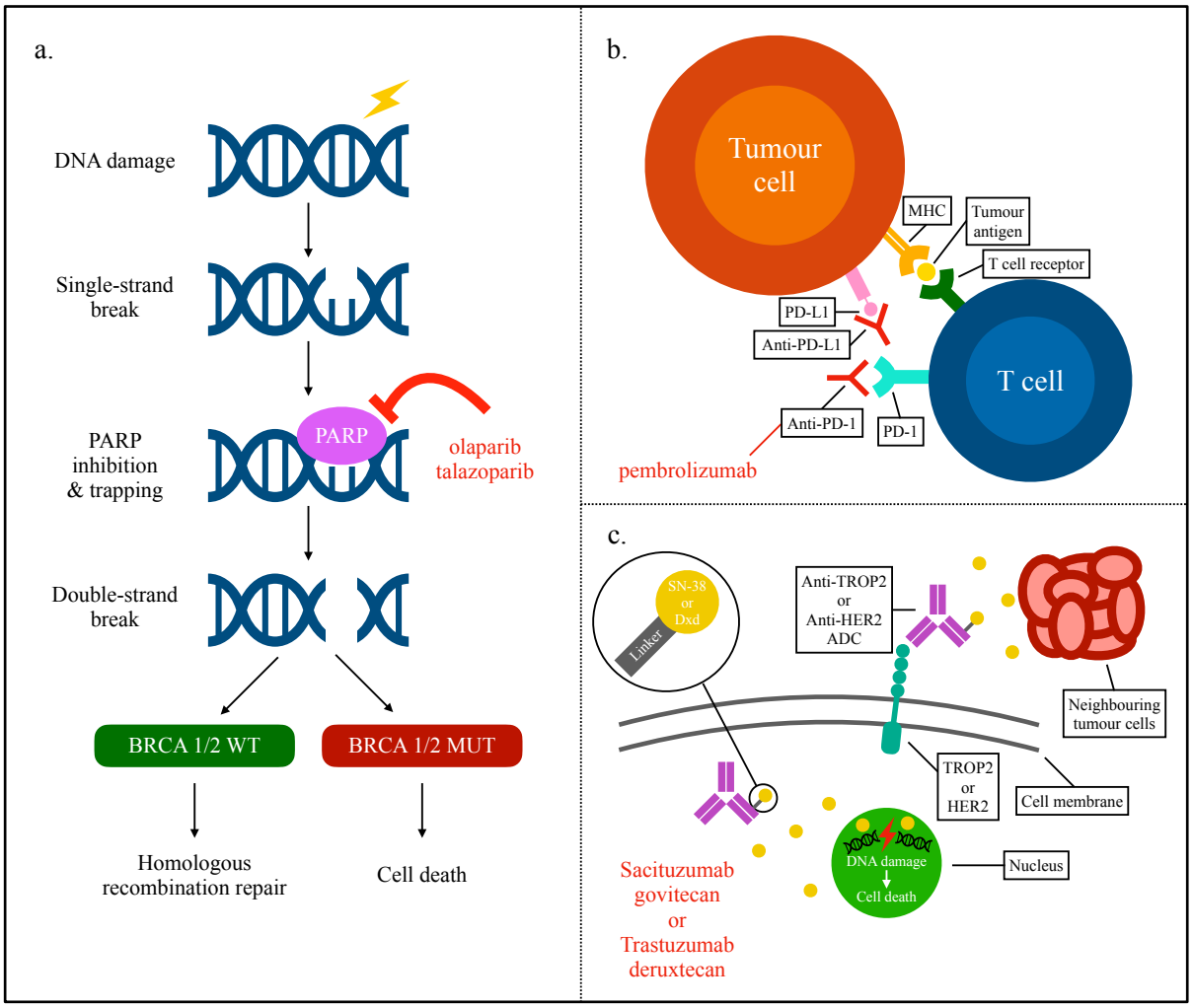


Figure 1-8: Approved TNBC targeted therapy. (a) PARP inhibition in *BRCA1/2*-mutated vs. *BRCA*-wildtype (WT) cells. **(b)** Immune checkpoint inhibition of PD-1/PD-L1. **(c)** ADC intercellular and extracellular cytotoxicity (362–367).

PARP Inhibitors

PARPs are a family of enzymes involved in DNA damage repair (DDR). PARP enzymes detect and bind to damaged DNA at the DBD, whilst also binding to nicotinamide adenine dinucleotide (NAD+) at the PARP active site, to produce ADP-ribose moieties and recruit DDR proteins. This PTM is known as polyADP-ribosylation (PARylation). PARPs catalyse the

transfer of ADP-ribose from NAD+ to target proteins to repair single-strand breaks (SSBs) via base excision repair (BER) (321,368). PARPs may also play a role in alternative DNA repair pathways, such as HRc and non-homologous end joining (NHEJ) (363).

As demonstrated in Figure 1-8(a), PARP inhibitors impede DDR of SSBs via binding of the PARP enzyme-bound NAD+, thus inhibiting PARP enzyme activity and subsequent PARylation. Inhibition can also occur by blocking PARylation of PARP itself (autoPARylation) in a process known as PARP "trapping", preventing the release of the PARP enzyme, and thus inhibiting the recruitment and binding of other DDR proteins. In the absence of repair, DNA replication stalls and causes this SSB to become a double-strand break (DSB) (369,370).

Inhibition of PARP alone is not enough to cause cell death as DSBs may still be repaired via homology-directed repair, however, in combination with HRc deficiency caused by mutations in the *BRCA1/*2 genes, synthetic lethality can occur and result in cell death (371).

Preclinical studies demonstrated that both olaparib and talazoparib PARP inhibitors effectively target BC cells, with *BRCA1/2* mutations or HRc deficiency, enhancing DNA damage and cell death (372).

The phase III OlympiAD (olaparib) and EMBRACA (talazoparib) clinical trials showed significant improvements in PFS and ORR in patients with germline *BRCA1/2*-mutated (*gBRCAm*), HER2-negative metastatic BC, including TNBC. In OlympiAD, olaparib (Lynparza) improved median PFS to 7 months from 4.2 months with standard chemotherapy (hazard ratio (HR) 0.58) and achieved an ORR of 59.9% vs. 28.8%. Similarly, in EMBRACA, talazoparib (Talzenna) demonstrated a median PFS of 8.6 months vs. 5.6 months (HR 0.54) with an ORR of 62.6% vs. 27.2%. Both agents were associated with improved quality of life compared to chemotherapy. Based on these results, both drugs received FDA approval in 2018 for treating advanced or metastatic *gBRCAm*, HER2-negative BC. In 2022, olaparib also gained approval as an adjuvant treatment for patients with high-risk, early-stage HER-negative BC with *gBRCA1/2* mutations, based on the OlympiA trial results, which showed a significant improved distant disease-free survival (DDFS) (373–379).

While no FDA approval exists for somatic *BRCA1/2* mutations in BC, the GeNeo (NCT04641676) study demonstrated olaparib's efficacy in various cancers with somatic or germline *BRCA1/2* mutations. Ongoing studies are investigating the therapeutic relevance of somatic *BRCA1/2* mutations in guiding PARP inhibitor treatment (380,381).

Anti-PD-1/PD-L1 Immune Checkpoint Inhibitors

PD-1 receptors are expressed at the cell surface of activated immune cells (T cells, natural killer (NK) cells, B cells, macrophages, and some dendritic cells (DCs). PD-1 expression in T-cells is induced by T-cell receptor (TCR) activation (382).

Ligation of PD-1 to its ligands PD-L1 and PD-L2, normally expressed on antigen-presenting cells (APCs), mesenchymal stem cells (MSCs), and bone-marrow derived mast cells (BMMCs), hinders this TCR signalling (382,383), inhibiting the function of effector T-cells and TIL, while simultaneously increasing immunosuppressive regulatory T cell (Treg) function. This ultimately prevents excessive stimulation of the immune response, protecting against autoimmunity and maintaining immune tolerance, giving the basis for PD-1's "immune checkpoint" categorisation (384).

As mentioned in Section 1.4.2.4., PD-L1 is frequently upregulated in tumour cells, allowing them to hijack the PD-1/PD-L1 inhibitory pathway to evade host immune response (371). Therapeutic targeting of this pathway using ICIs to block PD-1/PD-L1 interactions, as demonstrated in Figure 1-8(b), promotes anti-tumour activity (385).

Preclinical studies have demonstrated that PD-1/PD-L1 blockade restores anti-tumour immunity and synergises with chemotherapy in TNBC models (386). The phase III KEYNOTE-522 trial showed that the PD-1 inhibitor pembrolizumab (Keytruda) plus chemotherapy significantly improved pCR (64.8% vs. 51.2%) and event-free survival (HR 0.63) in early-stage TNBC. In metastatic TNBC, KEYNOTE-355 reported improved PFS in PD-L1 combined positive score (CPS) $\geq$ 10 patients (9.7 vs. 5.6 months, HR 0.65). Pembrolizumab received FDA approval in 2021 for high-risk early-stage and PD-L1-positive metastatic TNBC (338,387–394).

Atezolizumab (Tecentriq), a PD-L1 inhibitor, initially gained accelerated approval in 2019 based on IMpassion130 (PFS 7.5 vs. 5.0 months, HR 0.62), but this was withdrawn in 2021 after IMpassion131 failed to confirm the PFS benefit (395,396).

Anti-TROP2 ADC

ADCs comprise three fundamental components: a mAb, a cytotoxic drug, and a chemical linker connecting the aforementioned parts. The mAb is constructed to be specific for a certain tumour cell-surface antigen and, as demonstrated in Figure 1-8(c), upon binding of the antigen, the ADC can be internalised into the cell and the cytotoxic payload is released into the cytoplasm

which causes tumour cell death. The linked drug may also be released extracellularly if the ADC is not internalised, leading to the death of neighbouring tumour cells (bystander effect). In addition, the antibody itself can contribute to tumour cell killing via immune effector mechanisms: the Fc portion of the mAb can recruit natural killer cells, macrophages, and other immune cells to mediate antibody-dependent cellular cytotoxicity (ADCC) or phagocytosis (ADCP), and can also activate the complement cascade (CDC), further enhancing antitumour activity (367,397).

TROP2, encoded by the tumour associated signal transducer (*TACSTD2*) gene (398), is a transmembrane glycoprotein that is highly expressed on the surface of epithelial cells across various cancer types. TROP2 is normally expressed at a low level and is involved in embryonic development, formation of placental tissue, and stem cell proliferation. When overexpressed, *TACSTD2* functions as an oncogene with the TROP2 protein promoting tumour development and progression in multiple epithelial cancers, including BC, and occurring most prevalently in the TNBC subtype (399).

Preclinical studies have demonstrated that Sacituzumab govitecan, an ADC targeting TROP2 and delivering the topoisomerase I inhibitor SN-38, exhibits potent cytotoxic activity against TNBC cell lines and xenograft models, including tumours resistant to conventional chemotherapy (400).

In the phase III ASCENT trial, Sacituzumab govitecan (Trodelvy) significantly improved outcomes in patients with metastatic TNBC who had received at least two prior therapies, with a median PFS of 4.8 vs. 1.7 months (HR 0.41) and an ORR of 35% vs. 5% compared to standard chemotherapy. The drug also improved OS (11.8 vs. 6.9 months, HR 0.51) and demonstrated a manageable safety profile. Based on these results, Sacituzumab govitecan received FDA approval in 2020 for patients with metastatic TNBC previously treated with two or more systemic regimens (401,402).

Anti-HER2 ADC

While TNBC is defined by a lack of ER, PR, and HER2 expression, emerging evidence indicates that a subset of TNBC tumours expresses low levels of HER2, making them responsive to HER2-targeted ADCs which can exploit even low-level HER2 expression to deliver cytotoxic payloads selectively to tumour cells (179).

Fam-T-DXd-nxki (Enhertu) is an ADC composed of a mAb linked to the topoisomerase I inhibitor DXd. T-DXd targets the HER2 receptor (as shown in Figure 1-8(c)) (403).

Preclinical studies have demonstrated that T-DXd exhibits potent anti-tumour activity in HER2-expressing BC models, including tumours with low HER2 expression (404).

In the phase III DESTINY-Breast04 trial, T-DXd significantly improved outcomes in patients with HER2-low metastatic BC, including TNBC, compared to standard chemotherapy. Specifically, T-DXd achieved a median PFS of 9.9 vs. 5.1 months and a median OS of 23.4 vs. 16.8 months, with improvements being both statistically significant and clinically meaningful. Based on these results, T-DXd received regulatory approval in August 2022 for the treatment of HER2-low metastatic BC, including patients with metastatic TNBC (179,405).

Emerging Targeted Therapies in TNBC

In addition to currently approved agents, a growing number of novel targeted strategies are undergoing clinical evaluation in TNBC, reflecting a shift toward biomarker-informed and combination-based therapeutic approaches.

Next-generation ADCs continue to build on the clinical success of earlier agents. Datopotamab deruxtecan, a TROP2-directed ADC with a topoisomerase I inhibitor payload, is being evaluated in the phase III TROPION-Breast02/03/04 trials in metastatic and early TNBC, with emerging data suggesting meaningful anti-tumour activity in heavily pretreated populations. These studies aim to determine whether earlier-line use or rational combinations can further improve outcomes (406).

Targeted kinase inhibition remains an area of active investigation. Anti-angiogenic strategies such as apatinib, including combinations with the PD-1 inhibitor camrelizumab, are being explored to disrupt tumour vascular signalling and enhance immune response. Multi-targeted tyrosine kinase inhibitors such as lucitanib and pathway-directed combinations, including GSK2141795 with trametinib, aim to simultaneously suppress parallel oncogenic signalling pathways that contribute to therapeutic resistance (114).

Immunotherapeutic strategies are also evolving beyond PD-1/PD-L1 blockade. Dual immune checkpoint inhibition approaches include PD-1/LAG-3 combinations such as spartalizumab plus ieramilimab (407), and PD-L1/CTLA-4 combinations such as durvalumab with tremelimumab (408). Additional strategies incorporate immune-modulating agents such as the indoleamine 2,3-dioxygenase 1 (IDO1) inhibitor epacadostat or the histone deacetylase

(HDAC) inhibitor entinostat to enhance tumour immunogenicity and overcome immune resistance (409,410).

For molecularly defined subtypes, AR-targeted therapy is being evaluated in the LAR subtype of TNBC. The AR inhibitor enzalutamide, in combination with the PI3K inhibitor Taselisib, represents an example of subtype-specific targeting currently under early-phase clinical investigation (114).

Collectively, these emerging strategies emphasise rational combination therapy as a central theme in TNBC management, aiming to address tumour heterogeneity, bypass adaptive resistance mechanisms, and improve the durability of clinical responses beyond what has been achieved with single-agent targeted therapies (411).

Resistance to Targeted Therapy in TNBC

Resistance to targeted therapies in TNBC remains a critical barrier, driven by the disease's molecular heterogeneity and adaptive mechanisms. Upregulation of alternative signalling pathways, such as PI3K/AKT/mTOR or MAPK, often bypasses targeted inhibition, with studies showing pathway reactivation in patients treated with single-agent kinase inhibitors (214,412–414).

Efflux pumps and altered drug metabolism reduce intracellular drug concentrations, notably in ADCs like Sacituzumab govitecan, where multidrug resistance 1 (*MDR1*) and multidrug resistance-associated protein 1 (MRP1) overexpression correlates with resistance (415,416).

Immunotherapy resistance, observed in TNBC patients treated with anti-PD-1/PD-L1 agents like pembrolizumab, stems from low TILs, immune-suppressive microenvironments, or LAG-3/CTLA-4 upregulation (417–419).

Epigenetic modifications, including histone deacetylation and DNA methylation, further contribute to resistance by silencing tumour suppressor genes, conferring resistance on PARP inhibitor-treated patients (e.g. olaparib) (420,421).

These mechanisms underscore the shift toward combination strategies in TNBC, such as pairing kinase inhibitors with immunotherapies or epigenetic modulators, to overcome resistance and improve therapeutic efficacy (422,423).

1.5. The PI3K/AKT/mTOR signalling pathway

The PI3K signalling pathway plays a crucial role in normal cellular processes, including insulin signalling, glucose homeostasis, cell growth, proliferation, and survival (see Figure 1-9). However, its aberrant activation – often driven by mutations in pathway components or upstream regulators like RTKs – occurs in many cancer types, contributing to tumour development and progression. Knowledge of the genes and proteins involved in the PI3K signalling pathway, as well as its upstream mediators and downstream targets, is imperative for understanding its physiological functions and fully elucidating its dysregulated role in cancer (424,425).

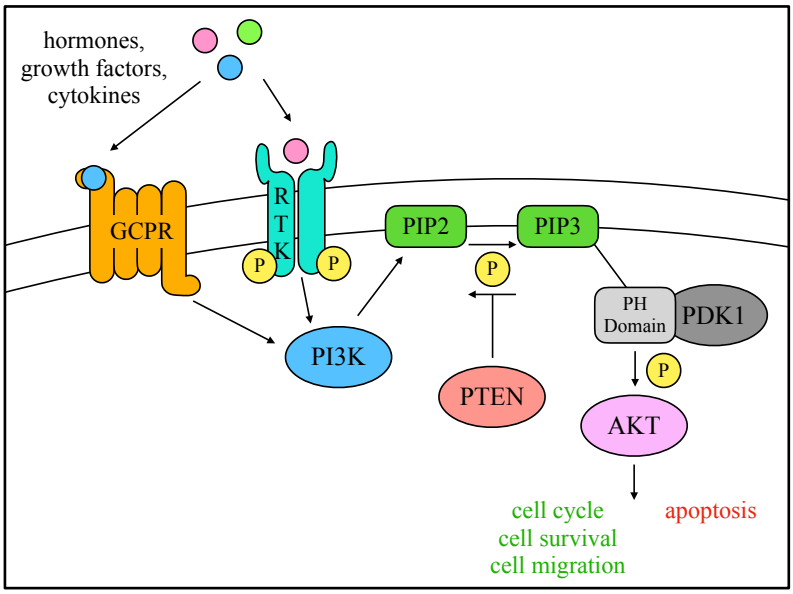


Figure 1-9: PI3K/AKT signalling. Activation of RTKs and GCPRs leads to recruitment of PI3K and phosphorylation of PIP2 to PIP3. PIP3 can bind to the PH-domain of PDK1 leading to AKT phosphorylation and activation. PTEN dephosphorylates PIP3 to PIP2, inhibiting AKT activation (426).

There are three different classes of the PI3K heterodimer – classes I, II, and III. Class I constitutes class IA and class IB PI3Ks. Class IA PI3K has the greatest implications in human cancer (427) and consists of the catalytic and regulatory subunits, p110 and p85, with three different types of the former (110α, 110β, and 110δ, encoded by the phosphatidylinositol-4,5-bisphosphate 3-kinase catalytic subunit alpha/beta/delta genes (*PIK3CA/B/D*), and five different isoforms of the latter (p85α, p55α, p50α, p85β, p55γ) (428). The catalytic subunit of class IB PI3Ks consists solely of p110γ, encoded by PI3KC gamma (*PIK3CG*), which binds to the p101 and p87 regulatory subunits (429). Binding with the regulatory subunits stabilises the catalytic proteins inhibiting PI3K pathway activation (427).

The PI3K pathway can be initiated by various molecules (see Figure 1-10), including GFs, hormones, and cytokines, which activate upstream regulators such as RTKs and G protein-coupled receptors (GPCRs) (424). Binding of ligands to the transmembrane region of an RTK can result in autophosphorylation of the cytoplasmic region tyrosine residues, leading to the recruitment of p110 to RTKs and subsequent PI3K activation (426). GPCRs similarly trigger PI3K via ligand-induced conformational changes, enabling direct binding of their Gβγ subunits to the p110β or p110γ isoforms (430).

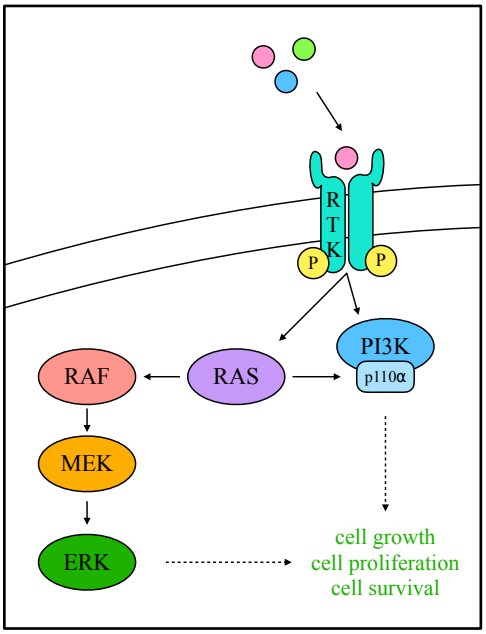


Figure 1-10: Role of RAS in PI3K pathway activation and cell cycle. Following activation and autophosphorylation, RTK binds to RAS which can lead to both PI3K and RAS/RAF/MEK/ERK pathway activation (431).

Other activating molecules include small GTPases, such as RAS (432). Activated RTKs can bind to RAS, which can lead to both PI3K pathway activation via binding of RAS to the p110α subunit and activation of the RAS/rapidly accelerated fibrosarcoma (RAF)/MEK/extracellular signal-regulated kinase (ERK) pathway, both of which promote cell growth, proliferation and survival (433).

Following activation, PI3K catalyses the phosphorylation of the 3'-hydroxyl group of the inositol ring of phosphatidylinositol-4,5-biphosphate (PtdIns (4,5) P2 or PIP_2) to produce phosphatidylinositol-3,4,5-triphsophate (PtdIns (3,4,5) P3 or PIP_3) (see Figure 1-11). *PTEN* normally functions as a negative regulator of PI3K counteracting pathway activation via dephosphorylation of PIP_3 to PIP_2, thus affecting downstream signalling. This leads to cell growth inhibition and the enhancement of cell sensitivity to apoptosis, thereby functioning as a tumour suppressor (434).

PIP_3 can bind to a variety of cytosolic proteins that contain pleckstrin homology domains and functions as a lipid second messenger to promote pathway activation. 3-phosphoinositide-dependent protein kinase-1 (PDK1) is a Pleckstrin homology domain-containing kinase dependent on PI3K which activates protein kinase B (AKT) and other AGC kinases sensitive to GFs via phosphorylation of the activation loops and hydrophobic motifs (435). The pleckstrin homology domain of PDK1 allows for localisation of it and AKT at the plasma membrane as well as phosphorylation of the AKT activation loop following activation of PI3K (436).

Mammalian target of rapamycin (mTOR) protein kinase activity occurs both upstream and downstream of AKT and is achieved through the mTOR complexes ($mTORC_1$ and $mTORC_2$). PRAS40 usually functions to inhibit autophosphorylation of $mTORC_1$ and prevent binding of downstream S6K and $_4EBP_1$ proteins. Phosphorylation of PRAS40 by phosphorylated AKT (p-AKT) leads to dissociation of PRAS40 from the $mTORC_1$ complex and subsequent mTOR signalling (437,438). mTOR activates S6k and inactivates $_4EBP_1$ resulting in protein translation and cell growth (439). In addition to this, AKT can regulate the tumour suppressor complex subunit 1-tumour suppressor complex subunit 2 (TSC1-TSC2) tumour-suppressor complex via phosphorylation of TSC2 which prevents RHEB inhibition, allowing for mTOR activation (440). ERK is also an upstream regulator of $mTORC_1$, demonstrating some of the complex crosstalk between pathways (441). $mTORC_2$ is an established activator of AKT, with the ability to phosphorylate its Ser473 residue, and thus a promotor of cell proliferation and survival (442).

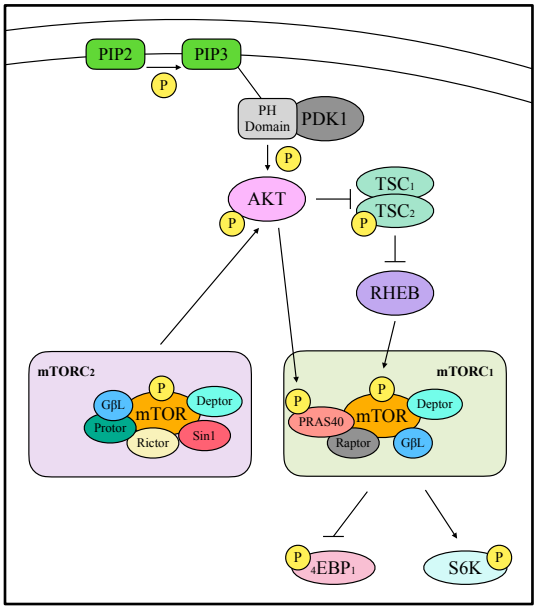


Figure 1-11: AKT/mTOR signalling. The $mTORC_2$ complex regulates AKT via phosphorylation. AKT regulates $mTORC_1$ via phosphorylation of the PRAS40 subunit. AKT also inhibits the TSC1-TSC2 tumour-suppressor complex blocking RHEB inhibition of downstream $mTORC_1$ signalling. $mTORC_1$ inhibits $_4EBP_1$ and activates S6K via phosphorylation (437,438).

AKT plays a role in cell survival regulation via inhibition of pro-apoptotic transcription factors (see Figure 1-12), such as forkhead box O (FOXO) and Bcl-2 associated agonist of cell death (BAD). FOXOs function to activate target gene transcription to promote cell death, cell cycle arrest, and maintenance of metabolic stability via cellular oxidative stress. BAD is a pro-apoptotic protein in the Bcl-2 family that regulates programmed cell death. Phosphorylation of FOXO and BAD by AKT results in suppression of apoptosis and promotion of cell survival (443), while phosphorylation of human double minute 2 (HDM2) by AKT enhances its nuclear translocation (from the cytoplasm) and stability. HDM2 can then bind and regulate p53, marking it for proteasomal degradation and export to the cytoplasm (444).

Glycogen synthase kinase-3 (GSK3) is another downstream target of AKT, whereby AKT inactivates this protein via phosphorylation leading to reduced phosphorylation of GS, allowing glycogen synthesis to proceed (445,446). Other GSK3 substrates such as c-Myc and β-catenin are stabilised upon GSK3 inactivation, promoting cell growth, survival, and proliferation (447).

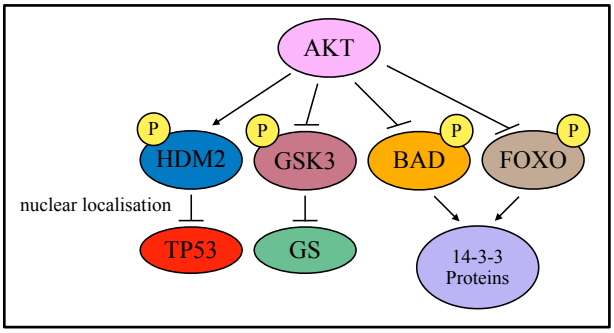


Figure 1-12: AKT downstream phosphorylation targets. Phosphorylation of HDM2 enhances nuclear localisation leading to p53 degradation. BAD phosphorylation leads to suppressed apoptosis and binding to 14-3-3 proteins. 14-3-3 proteins also bind to FOXO following phosphorylation causing cytoplasmic retention and inhibition of transcriptional activity. AKT inactivates GSK3 via phosphorylation, resulting in reduced glycogen synthase (GS) (444,445,448,449).

1.5.1. The PI3K signalling pathway in cancer

The PI3K signalling pathway (illustrated in Figure 1-13) is frequently altered in human cancer and one of the most commonly dysregulated pathways in BC, and is significant in driving tumour initiation and progression (435). Mutations occurring in PI3K pathway gene members, as well as those upstream of the pathway, are implicated in PI3K pathway activation and downstream oncogenic signalling and could potentially be therapeutically targeted (450).

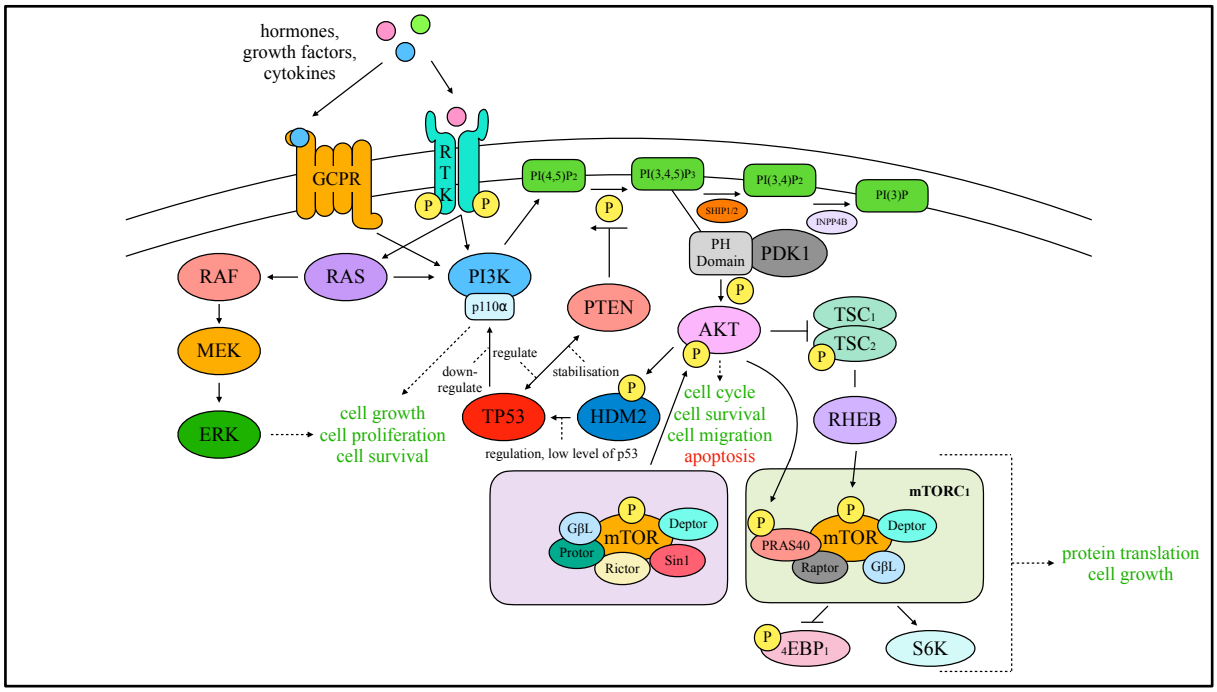


Figure 1-13: PI3K signalling in cancer. PI3K signalling promotes cancer cell growth, proliferation, survival, and metastasis, and inhibits apoptosis. Mutations in pathway genes promote tumorigenesis and cancer progression.

Aberrant activation of cell surface receptors, i.e. RTKs and GCPRs, can occur as a result of gain-of-function (GOF) mutations, gene amplification, chromosomal rearrangement, or self-sustaining autocrine signalling (451). PI3K alterations can activate and enhance PI3K signalling (449).

Mutations and amplifications in *PIK3CA*, which encodes p110α, are most commonly observed in BC, with a prevalence of up to 40% in primary BC, varying by subtype. These mutations have been well-established as activators of the PI3K signalling pathway which has led to the development and FDA-approval of the PI3Kα inhibitor alpelisib. *PIK3CA* "hot spots" are home to the majority of the gene's somatic mutations: E542K or E545K in exon 9 (located in the helical domain of p110α), and H1047R or H1047L in exon 20 (located in the kinase domain near the activation loop) (452–454), leading to increased PI3K signalling and stimulation of downstream AKT signalling (455).

The prevalence of *PIK3CA* alterations in BC render them attractive targets for targeted therapies (456). For instance, alpelisib – a selective PI3Kα inhibitor – has demonstrated improved PFS in patients with *PIK3CA*-mutated disease, leading to its FDA approval for HR-positive, HER2-negative advanced BC in combination with fulvestrant. However, *PIK3CA* mutation status is not a perfect biomarker for predicting response to alpelisib. This was demonstrated primarily in clinical trials for ER+/HER2- advanced BC, such as the phase 3 SOLAR-1 trial, which showed variable outcomes with some *PIK3CA*-mutated tumours exhibiting resistance despite overall PFS benefits (457,458). Limited early-phase studies in TNBC, including a phase II alpelisib monotherapy trial in PI3K-altered, pretreated cases and a phase Ib alpelisib and olaparib combination study, have similarly demonstrated mixed efficacy signals with no approvals to date (459,460).

This variability may arise from rare co-occurring mutations in genes such as *PTEN* or *AKT1* (which are usually mutually exclusive with *PIK3CA* alterations, limiting significant overlap), which can independently activate the PI3K/AKT pathway or bypass PI3Kα inhibition (461). Feedback loops within the pathway can reactivate downstream signalling – for example, mTORC1 upregulation can impair autophagy – while alternative routes such as RTK signalling or compensatory cascades (e.g. MAPK/MEK or IL-6-STAT3) may sustain tumour growth despite *PIK3CA* inhibition. Additionally, tumour heterogeneity and selection of resistant subclones further complicate response prediction (462,463).

PTEN and inositol polyphosphate-4-phosphatase type II (*INPP4B*) are tumour suppressors, which both suppress PI3K pathway activity. The former dephosphorylates PIP_3 to PIP_2, whilst the latter dephosphorylates $PIP(3,4)P_2$ to PIP(3)P following SH2-containing inositol phosphatase 1/2 (SHIP 1/2) dephosphorylation of PIP_3 to $PIP(3,4)P_2$ (464,465). Mutations in both of these genes can inhibit their normal functions, leading to downstream AKT activation (466,467), however, *INPP4B* also demonstrates oncogenic activity in certain cancers with increased expression driving therapeutic resistance (468–470).

PTEN mutations have been reported in approximately 5% of BC cases, however, epigenetic regulation and/or loss of heterozygosity (LOH) is responsible for gene inactivation in approximately 30% of sporadic BCs. Inactivation of *PTEN* results in PI3K/AKT signalling deregulation and subsequent cancer activation and progression (471).

INPP4B alterations vary based on BC subtypes, with increases observed in 14-40% of HR-positive BCs, where estrogen signalling can upregulate its expression. In this context, *INPP4B* can act as an oncogene, stabilising AKT signalling, leading to increased cell proliferation and resistance to apoptosis (468). Conversely, loss of *INPP4B*, commonly observed in TNBC, can lead to increased PI3K/AKT pathway activation via accumulation of $PtdIns(3,4)P_2$, which enhances AKT phosphorylation and downstream signalling (472).

AKT mutations have been observed in a number of cancer types including BC, e.g. the E17K somatic mutation in the PH-domain of *AKT1*. *AKT1* mutations are most prevalent in ER-positive, HER2-negative BC (6.0%). These mutations can lead to greater binding affinity between kinases and phosphatidylinositol phosphorylated lipids, as well as increased membrane localisation relative to WT *AKT*. This in turn may lead to tumour progression (461,471,473). Capivaseritb, an AKT inhibitor, was approved in 2023 for adults with HR-positive, HER2-negative locally advanced or metastatic BC with one or more *PIK3CA*, *AKT1*, or *PTEN* alterations, used in combination with fulvestrant (474).

p53 is a tumour suppressor protein encoded by the *TP53* gene. The p53 protein responds to cellular stresses to regulate target gene expression and induce cell cycle arrest, apoptosis, DNA repair, metabolism changes, and senescence (475). Aberrations in the *TP53* gene are common across all types of cancer, many of which are inactivating missense mutations, and are known to play a significant role in tumorigenesis. The p53 protein has three primary domains – transactivation domain (TAD), DBD, and tetramerisation domain (TET) – with the majority of

genetic alterations in human cancer occurring in the DBD, preventing binding of downstream targets (476).

p53 is negatively regulated by the HDM2 protein via physical binding and p53 degradation, resulting in low levels of p53 in normal cells (477). Studies have demonstrated the regulatory effects of p53 on the *PTEN* tumour suppressor gene via the functional p53 binding site present within the *PTEN* promotor region (478). Evidence suggests that *PTEN* may protect p53 from both loss-of-function (LOF) via negative transcription of *HDM2* and degradation by way of physical association with the protein, indicating a positive feedback loop between *PTEN* and p53 (479,480). Despite these stabilising functions, deletion of *PTEN* and subsequent activation of the PI3K pathway has been shown to activate p53, with significantly increased p53 expression present in PTEN-/- cells (249,481).

p53 has also been shown to regulate cell survival via inhibition of *PIK3CA*, and furthermore, the PI3K/AKT pathway, independent of *PTEN*. This transcriptional down-regulation of *PIK3CA* via p53 has been demonstrated in head and neck cancer cell lines, where the PTEN protein was not detected and induction of p53 resulted in decreased *PIK3CA* expression and reduced AKT phosphorylation, indicating the transcriptional regulatory effects of p53 on *PIK3CA* (482). *TP53* mutations are prevalent in 30% of BC patients, leading to loss of tumour suppressor function and enhanced tumour aggressiveness (226,483).

A study, which investiged the mechanisms involved in the regulation of *PIK3CA* transcription via p53 in ovarian cancer, described two promotors present on the *PIK3CA* gene that have been shown to directly bind to p53 resulting in transcriptional inhibition. It was found that suppression of p53 resulted in increased levels of p110α transcripts, proteins, and PI3K signalling pathway activity, while overexpression of p53 resulted in decreased levels of p110α protein (484). However, an Expression of Concern was subsequently issued for this study owing to concerns regarding the reliability of several western blot images, although an external expert consulted by the journal considered the study's overall conclusions to be potentially supported by subsequent independent reports (485). LOF mutations in *TP53* have been shown to correlate with hyperactivation of *PIK3CA* and the PI3K pathway, resulting in worse prognoses for head and neck squamous cell carcinoma patients (486). Co-occurring *TP53* and *PIK3CA* mutations are observed in ~7.5% of BCs (248). These mutations synergistically dysregulate the PI3K/AKT signalling pathway, driving oncogenesis (237,487,488).

1.5.1.1. Molecular alterations driving PI3K pathway activation in TNBC

Dysregulation of PI3K signalling is one of the most frequently occurring oncogenic abnormalities observed in TNBC and has been associated with therapeutic resistance (489). PI3K pathway mutations characterise a significant TNBC subgroup. The occurrence of mutations in single genes are rare, however, a certain combination of activating and inactivating mutations are prevalent in approximately 25-30% of advanced TNBC (109). Table 1-8 shows the frequency of key PI3K pathway mutations in TNBC.

Table 1-8: Key PI3K pathway mutations in TNBC (107,109,239,240,472,482,484,490–495)**.**

Gene (alteration)	TNBC %	Effect on PI3K/AKT/mTOR signalling in TNBC
PIK3CA (activating mutations)	~10-15%	*PIK3CA* mutations activate the PI3K pathway by increasing PIP_3 production, leading to constitutive AKT/mTOR signalling that promotes survival, proliferation, and therapy resistance.
TP53 (loss/mutation)	~60-80%	*TP53* mutations increase genomic instability and can enhance PI3K pathway activation by disrupting its regulatory control over genes such as *PTEN*.
PTEN (loss/deletion/ low expression)	~35-57% (varying due to detection methods)	*PTEN* loss removes the PIP_3 to PIP_2 brake, resulting in PIP_3 accumulation and subsequent AKT/mTOR activation.
INPP4B (loss/inactivation)	~70-80%	*INPP4B* loss or inactivation results in disruption of its tumour suppressor function leading to increased levels of $PI(3,4)P_2$, prolonging activation of both PI3K and ERK pathways, and delaying degradation of RTKs like EGFR and MET.
AKT (activating mutations)	<5%	*AKT* activating mutations directly hyperactivate AKT and downstream mTOR signalling. AKT activation by *AKT* mutations is rare in TNBC, more often occurring as a result of *PIK3CA/PTEN/INPP4B* alterations.
PIK3R1 (regulatory subunit mutations /loss)	~6%	Mutations or loss of *PIK3R1* (the p85α regulatory subunit of p110α) leads to impaired negative regulation of p110α and increased PI3K signalling.
AKT3 (amplification)	~14%	*AKT3* amplification in TNBC drives aggressive tumour growth and proliferation primarily by suppressing p27 and hyperactivating the PI3K/AKT/mTOR signalling pathway.
MTOR (activating mutations)	~1.8%	Although *MTOR* mutations are rare in TNBC, they drive hyperactivation of the mTOR pathway to promote tumour cell proliferation and survival. *PTEN* loss represents a more prevalent mechanism of mTOR signalling activation.

Abbreviations: *PIK3R1* = phosphoinositide-3-kinase, regulatory subunit 1.

1.6. Targeting the PI3K pathway

Inhibitors targeting different elements of the PI3K/AKT/mTOR pathway have been developed in an attempt to impede signalling and ultimately prevent the growth and spread of cancer (423).

1.6.1. PI3K inhibitors

PI3K inhibitors fall under three categories dependent on their target(s); pan, isoform-selective, and dual inhibitors. Some of these inhibitors have received FDA approval for various indications (see Figure 1-14) whilst others are still under preclinical and clinical investigation (496).This section will focus primarily on FDA-approved PI3K inhibitors, with brief mention of inhibitors that have been or are currently being tested in phase III trials, but have not yet received regulatory approval.

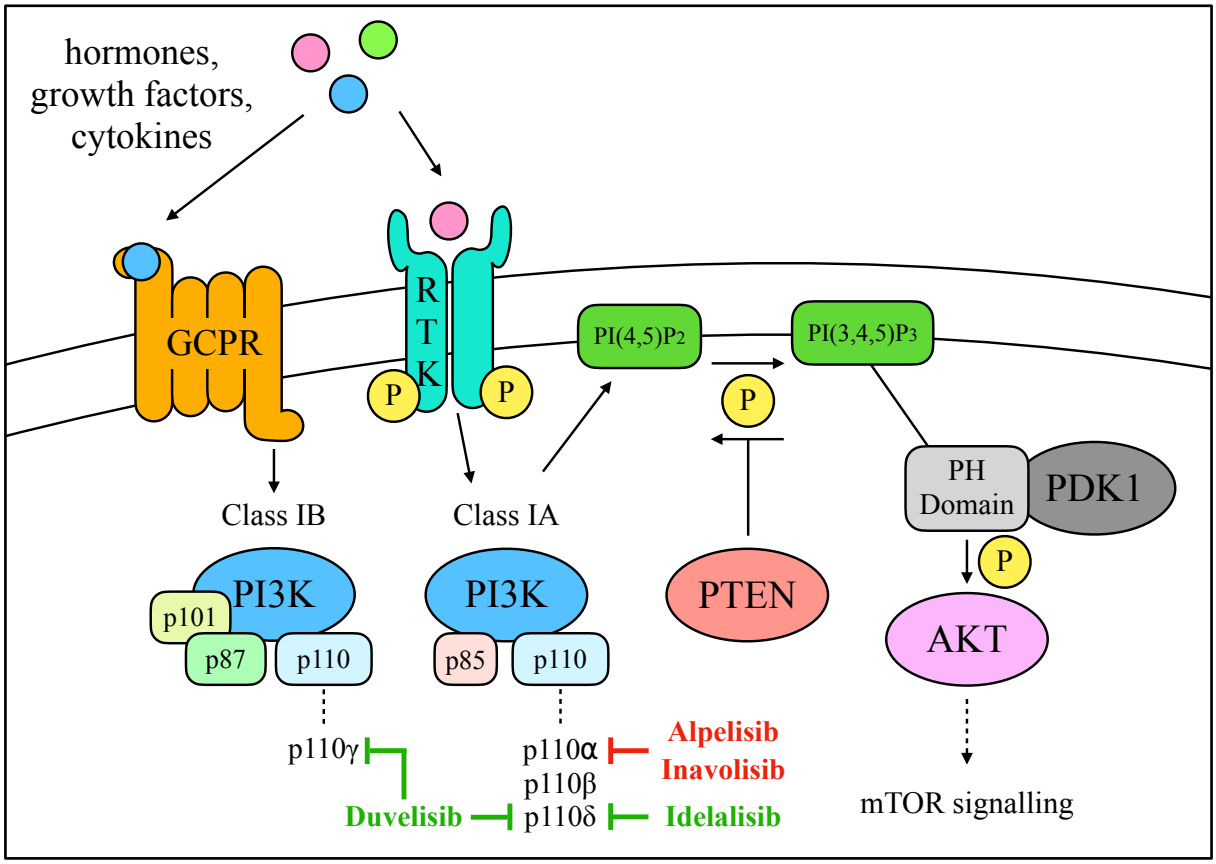


Figure 1-14: Approved PI3K inhibitors. Isoform-selective PI3K inhibitors include alpelisib, idelalisib, and duvelisib. Duvelisib is specific for both the p110δ and p110γ isoforms. Approved in BC shown in red; approved in other solid tumours shown in green (496–499).

1.6.1.1.Pan-PI3K inhibitors

Pan-PI3K inhibitors are named with such prefix as they target all isoforms of the class-I PI3K catalytic subunit (p110-α, -β, -δ, and -γ) (500). During the early stages of PI3K-targeted drug investigations, when the structure of the PI3K protein had not yet been fully elucidated, inhibitors targeting all four isoforms were primarily developed. Different p110 isoforms are frequently associated with varying functions, such as glucose metabolism, and targeting them all can therefore lead to increased safety risks, specifically adverse events related to glucose metabolism, e.g. hyperglycaemia (496).

Copanlisib

Copanlisib (Aliqopa) is an intravenous pan-class I PI3K inhibitor with selectivity for the α and δ isoforms. It was initially approved by the FDA in 2017 for relapsed follicular lymphoma based on the CHRONOS-1 trial but has since been withdrawn from the U.S. market following the failure of the confirmatory phase III CHRONOS-4 trial to demonstrate a significant improvement in PFS (501,502).

In BC, copanlisib has been evaluated in several clinical trials. A phase Ib trial (NCT02705859) combining copanlisib with trastuzumab in heavily pretreated HER2-positive BC patients showed preliminary evidence of tumour stability (503). A phase II study of copanlisib in patients with *PIK3CA*-mutated tumours reported an ORR of 16% and clinical benefit rate of 36% (504). Additionally, a phase Ib/II trial assessing the combination of copanlisib with eribulin in metastatic TNBC demonstrated enhanced tumour growth inhibition and apoptosis induction, irrespective of PI3K pathway alterations (505).

Despite these promising findings, copanlisib is not approved for BC, and ongoing trials continue to explore its efficacy and safety in combination therapies for both HER2-positive and TNBC subtypes (506).

Buparlisib

Buparlisib (BKM120) is an oral, pan-class I PI3K inhibitor developed by Novartis for the treatment of various cancers, including BC. In clinical trials, buparlisib has been evaluated in other therapies. The BELLE-2 trial assessed buparlisib plus fulvestrant in patients with HR-positive, HER2-negative BC who had progressed on prior endocrine therapy. While the combination showed a significant improvement in PFS compared to fulvestrant alone, it was associated with increased toxicity, leading to the discontinuation of the study (507).

Similarly, the BELLE-3 trial, which included patients who had progressed on mTOR inhibitors, was terminated due to excessive side effects. The BELLE-4 trial, evaluating buparlisib plus paclitaxel in HER2-negative BC, did not meet its primary endpoint of improved PFS and was stopped (508,509). Additionally, a phase II study (NCT01790932) of buparlisib in metastatic TNBC reported a clinical benefit rate of 12%, with no confirmed objective responses. Despite its preclinical promise, buparlisib has not been approved for BC treatment, and Novartis has decided not to pursue further development of buparlisib for BC (510).

1.6.1.2.Isoform-selective PI3K inhibitors

Isoform-selective PI3K inhibitors target specific isoforms of PI3K, unlike pan-PI3K inhibitors, which broadly inhibit multiple isoforms. These selective inhibitors were developed to allow higher dosing while minimising adverse events associated with pan-PI3K inhibitors, such as hyperglycaemia, diarrhoea, and immune suppression. By reducing off-target effects, isoform-selective inhibitors offer a safer therapeutic profile. However, their narrower selection criteria mean they are suitable only for patients with tumour or diseases driven by the specific PI3K isoform targeted (498,511).

Idelalisib

Idelalisib (Zydelig) is an oral, selective inhibitor of the PI3Kδ isoform, developed by Gilead Sciences. It was FDA-approved in 2014 for the treatment of relapsed chronic lymphocytic leukaemia (CLL), small lymphocytic lymphoma (SLL), and follicular lymphoma (FL) in patients who had received at least two prior systemic therapies (512).

A phase Ib study (NCT02044822) assessed its combination with rituximab in previously untreated CLL patients with a 17p deletion, however, the study was terminated due to an observed rate of serious adverse events and deaths (512). There are currently no clinical trials assessing idelalisib in BC or TNBC.

Duvelisib

Duvelisib (Copiktra), a dual inhibitor of PI3K δ and γ isoforms, has been extensively evaluated in clinical trials for hematologic malignancies, demonstrating efficacy in B-cell disorders. The pivotal phase III DUO trial (NCT02004522) compared duvelisib monotherapy to ofatumumab in 319 patients with CLL or SLL, yielding a median PFS of 13.3 months vs. 9.9 months (HR 0.52) and an ORR of 74% vs. 45% (513,514). Based on these results, duvelisib received FDA approval in 2018 for relapsed/refractory CLL/SLL after at least two prior systemic therapies.

Duvelisib also received accelerated approval for FL based on results from the DYNAMO trial (NCT01882803), however, approvals were voluntarily withdrawn for this indication due to logistics and costs, not safety or efficacy (515,516).

The phase III TERZO trial (NCT06522737) is currently recruiting patients to evaluate duvelisib versus standard gemcitabine or bendamustine in patients with T-cell lymphoma with T follicular helper (TFH) phenotype (nTFHL), including angioimmunoblastic T-cell lymphoma (AITL). This study aims to confirm PFS superiority based on the phase II PRIMO trial's (NCT03372057) 48% ORR (517,518). There are currently no clinical trials assessing idelalisib in BC or TNBC.

Alpelisib

Alpelisib (Piqray/BYL719), a selective PI3Kα inhibitor, has been clinically evaluated primarily for HR-positive, HER2-negative advanced BC with *PIK3CA* mutations. Significant outcomes were reported in the phase III SOLAR-1 trial (NCT02437318), which demonstrated median PFS of 11.0 months for alpelisib plus fulvestrant versus 5.7 months for placebo plus fulvestrant (HR 0.65) in patients with *PIK3CA*-mutated advanced BC. These results led to alpelisib's FDA approval in 2019 for this indication. The trial reported an ORR of 26.6% vs. 12.8% in the placebo arm, with common adverse events including hyperglycaemia and diarrhoea (454,458).

The phase III EPIK-B3 trial (NCT04251533) is ongoing, assessing alpelisib with nab-paclitaxel in advanced TNBC with *PIK3CA* mutations or *PTEN* loss, but results are not yet published. A phase II trial (NCT04216472) is also currently evaluating the same combination as neoadjuvant treatment for anthracycline-refractory early-stage TNBC with *PIK3CA* or *PTEN* alterations (246,519).

Inavolisib

Inavolisib (also known as GDC-0077 / Itovebi) is an investigational, oral, highly selective PI3Kα inhibitor designed to target tumours with *PIK3CA* mutations. It has a dual mechanism of action: in addition to inhibiting the catalytic activity of mutant p110α, it facilitates degradation of the mutated protein (520). In the Phase III INAVO120 trial (NCT04191499), inavolisib in combination with palbociclib and fulvestrant more than doubled PFS compared to palbociclib + fulvestrant alone (15.0 vs. 7.3 months; HR = 0.43). The regimen was generally

well tolerated, with no new safety signals beyond those expected from the individual drugs (521,522).

In October 2024, the FDA approved inavolisib in combination with palbociclib and fulvestrant for adults with endocrine-resistant, *PIK3CA*-mutated HR-positive, HER2-negative, locally advanced or metastatic BC, as detected by an FDA-approved test, following recurrence on or after adjuvant endocrine therapy (523).

Taselisib

Taselisib (GDC-0032), a potent, selective PI3K inhibitor targeting the α, β, and γ isoforms with enhanced activity against *PIK3CA*-mutated tumours, has been investigated primarily in HR-positive, HER2-negative advanced BC. The phase III SANDPIPER trial (NCT02340221) demonstrated a modest improvement in median PFS of 7.4 months with taselisib plus fulvestrant vs. 5.4 months with placebo plus fulvestrant (HR 0.7) in patients with *PIK3CA*-mutated advanced BC, achieving an ORR of 28% vs. 11.9%. Despite these results, taselisib's development was halted due to limited clinical utility and significant toxicities and it has not received FDA approval for any indication (524).

Taselisib was evaluated in HER2-negative BC in early phase trials (e.g. NCT01862081) combining taselisib with anti-PD-L1 therapies, but significant efficacy was not reported (525).

1.6.1.3.Dual PI3K/mTOR inhibitors

Both the PI3K and mTOR proteins are critical members of the PI3K/AKT/mTOR pathway, which has led to the recent development of inhibitors targeting both enzymes. This dual targeting allows for both the inhibition of cell proliferation and promotion of apoptosis. As of yet, there are no approved dual PI3K/mTOR inhibitors, however a variety of inhibitors of this kind have been or are currently being pre-clinically and clinically investigated (526).

Gedatolisib

Gedatolisib, a pan-PI3K/mTOR inhibitor, has shown significant efficacy in HR-positive/HER2-negative advanced BC. The phase III VIKTORIA-1 trial (NCT05501886) reported a 76% reduction in progression risk (median PFS 9.3 vs. 2.0 months, HR 0.24) for the triplet regimen of gedatolisib, palbociclib, and fulvestrant, and a 67% reduction (median PFS 7.4 months, HR 0.33) for the doublet gedatolisib and fulvestrant in *PIK3CA*-WT patients,

versus fulvestrant alone (527). These results have led to a New Drug Application which was accepted by the FDA in August 2025 (528).

1.6.2. AKT inhibitors

AKT inhibitors are a class of targeted therapeutics designed to block the activity of AKT with the aim of disrupting aberrant PI3K/AKT signalling. AKT inhibitors can be used alone or in combination with other therapies to enhance efficacy while addressing resistance mechanisms. There is currently only one approved AKT inhibitor (424).

Capivaseritb

Capivasertib (Truqap), is a first-in-class, orally bioavailable AKT inhibitor targeting all three AKT isoforms (*AKT1/2/3*) in the PI3K/AKT signalling pathway. Approved by the FDA in 2023, it is used in combination with fulvestrant to treat HR-positive, HER2-negative, locally advanced or metastatic BC with *PIK3CA*, *AKT1*, or *PTEN* alterations, following progression on endocrine therapy. The phase III CAPItello-291 trial (NCT04305496) demonstrated that capivasertib plus fulvestrant doubled PFS (7.3 vs. 3.1 months, HR 0.50) compared to placebo plus fulvestrant in patients with these alterations (474).

The phase III CAPItello-290 trial (NCT03997123) evaluated capivasertib combined with paclitaxel as first-line treatment for locally advanced or metastatic TNBC. However, it did not meet its primary endpoints of improving OS in either the overall population or patients with *PIK3CA/AKT1/PTEN* alterations, though PFS showed improvement in the latter group (7.5 vs. 5.6 months, HR 0.70) (529).

1.6.3. mTOR inhibitors

mTOR inhibitors block the mTOR protein kinase downstream of PI3K and AKT, disrupting aberrant signalling pathways, slowing tumour progression, and overcoming treatment resistance. Often combined with chemotherapy or other targeted therapies, they enhance outcomes in advanced or metastatic BC cases (530).

Everolimus

Everolimus, an mTOR inhibitor, was approved by the FDA in 2012 for use in combination with exemestane in postmenopausal women with advanced HR-positive, HER2-negative BC following progression on aromatase inhibitors. This approval was based on the phase III BOLERO-2 trial (NCT00863655), which demonstrated improved PFS (7.8 vs. 3.2 months, HR

0.45) but no OS benefit (531). The subsequent phase III BOLERO-3 trial (NCT01007942) demonstrated modest PFS improvements (7.0 vs. 5.8 months, HR 0.78) in HER2-positive disease when combined with trastuzumab and vinorelbine, while BOLERO-1 (NCT00876395) found no overall PFS benefit in first-line HER2-positive settings (532).

In the 2022 SWOG S1207 phase III adjuvant trial (NCT01674140) for high-risk HR-positive, HER2-negative BC, everolimus added to endocrine therapy yielded no significant invasive disease-free survival (iDFS) or OS benefits overall, though premenopausal patients improved (533). The 2025 ELEVATE phase Ib/II trial (NCT05563220) reported promising results for elacestrant plus everolimus in ER-positive/HER2-negative metastatic BC post-CDK4/6 inhibitor treatment, with a median PFS of 8.3 months and a 25% ORR (534).

In TNBC, a phase II neoadjuvant trial of cisplatin and paclitaxel with or without everolimus showed no pCR improvements and increased adverse events (535).

Temsirolimus

Temsirolimus, an mTOR inhibitor approved by the FDA in 2007 for advanced renal cell carcinoma, showed modest activity (ORR 9.2%, median time to tumour progression (MTT) 12 weeks) in a phase II trial of 109 pretreated metastatic BC patients at 75 mg weekly IV, but higher toxicity at 250 mg (536).

The phase III HORIZON trial (NCT00083993) of temsirolimus plus letrozole versus placebo in first-line HR-positive advanced BC found no overall improvement in PFS or OS (537). A phase I/II trial (NCT01111825) with neratinib in trastuzumab-refractory settings showed limited efficacy in heavily pretreated TNBC (538). Similarly, a phase II neoadjuvant doxorubicin, bevacizumab, temsirolimus/everolimus (DAT) trial in mesenchymal/metaplastic subtypes post-anthracycline yielded no pCR and grade 3 neutropenia/mucositis in 18% each (539).

Sirolimus

Sirolimus (Rapamycin), an mTOR inhibitor approved by the FDA in 1999 for renal transplant rejection prevention, showed clinical activity in a phase II trial (NCT00411788) of 6 mg daily oral sirolimus plus trastuzumab in trastuzumab-refractory HER2-positive metastatic BC. In 9 evaluable patients, it achieved an ORR of 11% and a clinical benefit rate (CBR) of 44%, and was well tolerated with grade 3 toxicities including pneumonitis and myelosuppression (540). In HR-positive advanced BC, a retrospective study of 36 patients on sirolimus (2 mg/day) plus

endocrine therapy reported a median PFS of 4.9 months with tolerable toxicity (mostly grade 1-2, lipid disorders common (69.4%)) (541).

In preclinical TNBC models sirolimus and cyclophosphamide showed synergy in suppressing tumour growth and metastasis, but no dedicated clinical trials have been reported (542).

1.6.4. Resistance to PI3K/AKT/mTOR inhibitors in cancer

Despite recent advances in the development of inhibitors that target the PI3K/AKT/mTOR pathway, patients often eventually develop resistance to these drugs. This occurs as a result of adaptive responses or compensatory mechanisms, which lead to pathway reactivation or other resistance mechanisms, and thus limit the effectiveness of PI3K/AKT/mTOR inhibitors (463). Mechanisms of resistance to these inhibitors are summarised in Table 1-9.

Table 1-9: PI3K/AKT/mTOR inhibitor resistance mechanisms (412,451,543–558).

Mechanism	Subcategory	Effect
Genetic Alterations*	*PIK3CA* mutations	Hyperactivates PI3K, reduces inhibitor sensitivity.
	PTEN loss	Upregulates PI3K/AKT, causes PI3K/mTOR inhibitor resistance.
	AKT1 mutations	Enhances survival, lowers inhibitor efficacy.
	RAS/BRAF mutations	Activates MAPK, bypasses pathway inhibition.
Feedback Loops	Hyperinsulinemia	Reactivates PI3K/AKT via insulin signalling.
	RTK reactivation	Upregulates PI3K/MAPK via EGFR, HER2, MET, etc.
	$mTORC_1$ feedback	Reinstates PI3K/AKT, reduces mTOR inhibitor effect.
	SGK activation	Compensates AKT loss, sustains $mTORC_1$ activity.
Parallel Pathways	MAPK/ERK activation	Compensates via ERK, weakens pathway inhibition.
	RAS/RAF/MEK/ERK	Activates alternative pathways, reduces efficacy.
	Wnt/β-catenin	Promotes tumour growth, contributes to resistance.
Secondary Mutations	*PIK3CB* mutations	Increases p110β activity, resists PI3K inhibitors.
	MTOR mutations	Sustains mTOR signalling, bypasses inhibition.
	AKT overexpression	Elevates AKT, reduces inhibitor potency.
Metabolic Adaptations	Autophagy upregulation	Promotes survival under PI3K/mTOR inhibition.
	Metabolic rewiring	Sustains growth via alternate energy pathways.
Microenvironment	Stromal signalling	Reinstates pathway via cytokine/GFs.
	Isoform compensation	p110β/δ compensates for p110α inhibition.

**While genetic alterations of the PI3K/AKT/mTOR pathway can sensitise cells to pathway inhibitors, some may cause pathway reactivation and co-occurring alterations can lead to inhibitor resistance.*

Progress made in the identification and development of inhibitors selectively targeting the PI3K/AKT/mTOR pathway was initially thought to be a promising approach to the treatment of various cancer types, including BC. However, results from clinical trials have not lived up to this initial enthusiasm with a majority of PI3K inhibitors not advancing past pre-clinical studies or early-phase trials. Limitations associated with these inhibitors include poor patient selection and toxicities related to necessary therapeutic doses. Adaptive responses following exposure to PI3K inhibitors may contribute to the requirement for these increased therapeutic doses and further drug resistance may be acquired via mechanisms such as those described in Table 1-9. These mechanisms provide considerable justification for the use of specific drug combinations to overcome resistance (463,551).

1.6.5. Rationale for targeting PI3K pathway alterations in the context of *TP53* dysfunction

Although individual genomic alterations contribute to TNBC pathogenesis, their clinical impact may be amplified when they converge on complementary oncogenic processes. In particular, the high prevalence of *TP53* mutations in TNBC, together with frequent activation of the PI3K/AKT/mTOR pathway, suggests biologically relevant cooperation with therapeutic implications .

As previously outlined, *TP53* mutations are present in approximately 60-80% of TNBC cases and disrupt cell cycle arrest, DNA damage responses, and apoptosis, enabling survival of genomically unstable tumour cells (559). In this context, pro-survival signalling pathways such as PI3K/AKT/mTOR may become critical for tumour maintenance (412). Mutant p53 has been shown to enhance PI3K pathway activity through mechanisms including *PTEN* suppression (560) and modulation of upstream receptor signalling, supporting functional crosstalk between these pathways (561,562).

While *PIK3CA* mutations occur at a lower frequency (~10-15% of TNBC) (563,564), PI3K pathway activation extends beyond mutational events and may arise through *PTEN* loss, *AKT* activation, or RTK signalling (565,566). Importantly, co-occurring *TP53* and *PIK3CA* alterations have been associated with worse survival and increased therapeutic resistance compared to either alteration alone, suggesting the existence of a biologically aggressive subset characterised by impaired apoptotic control and sustained proliferative signalling (237).

Despite substantial clinical investigation, PI3K/AKT/mTOR inhibitors have demonstrated limited efficacy as monotherapy in TNBC, likely due to adaptive resistance and pathway redundancy. These observations underscore the need for improved molecular stratification and for rational combination strategies targeting survival dependencies in genomically defined TNBC subsets (567).

The interaction between *TP53* dysfunction and PI3K pathway activation therefore provides a strong biological and clinical rationale for further characterisation of this co-altered population and for exploration of targeted therapeutic approaches.

1.7. Summary

Resistance to conventional therapeutic approaches is commonly observed in TNBC, providing rationale for the identification of targeted therapeutic options. Recent years have seen the development of such therapies, however there are only a few which have been granted approval for the treatment of TNBC. The PI3K pathway is frequently dysregulated in TNBC, however no PI3K inhibitors have been approved for use in this specific subtype. In addition to this, results from clinical trials of PI3K inhibitors have demonstrated suboptimal patient response due to poor patient selection and mechanisms of resistance, although this may be overcome with the use of specific drug combinations.

Given the high prevalence of *TP53* mutation in TNBC, this study explored the mechanisms driving resistance to PI3K inhibition within this genetic background and assessed rational combination strategies incorporating PI3K inhibitors and repurposed clinically approved drugs to enhance treatment response.

1.8. Study aims and objectives

Hypothesis: Concurrent *TP53* dysfunction and PI3K pathway activation define a biologically distinct and clinically aggressive subgroup of TNBC characterised by poor prognosis, altered molecular signalling, and reduced sensitivity to PI3K-targeted therapy. Furthermore, *TP53* mutation status – including specific *TP53* variants – modulates response to PI3K inhibition, and combination strategies targeting compensatory pathways can overcome resistance and reveal therapeutically actionable vulnerabilities.

Overall Aim: The overarching aim of my PhD project is to investigate the biological, clinical, and therapeutic significance of concurrent *TP53* mutation and PI3K pathway activation in TNBC, and to determine whether this co-altered state defines a distinct high-risk disease subgroup with unique molecular characteristics and therapeutic vulnerabilities. Through integrated analyses of patient cohorts, TNBC cell lines, and isogenic models, this project characterises the impact of *TP53*-PI3K pathway interactions on tumour biology, prognosis, and treatment response, while identifying mutation-specific mechanisms of drug sensitivity and resistance to inform precision medicine strategies for TNBC patients.

Specific Objectives:

1. **To determine whether concurrent *TP53* mutation and PI3K pathway activation define a distinct high-risk subgroup of TNBC.** This objective aimed to establish the clinical and biological significance of *TP53*-PI3K pathway co-alteration in TNBC. Using the METABRIC and TCGA cohorts, I assessed the prevalence of *TP53*-PI3K^{act} tumours, their association with patient outcomes, and their clinicopathological, genomic, and transcriptomic characteristics. The goal was to determine whether *TP53*-PI3K^{act} represents a biologically distinct disease state beyond existing TNBC classification systems.
2. **To investigate the impact of *TP53* mutations on sensitivity to PI3K-targeted therapy in TNBC.** This objective examined whether *TP53* dysfunction contributes to the limited efficacy of PI3K inhibitors observed in TNBC. Using mutation-stratified TNBC cell lines, I evaluated responses to the PI3Kα inhibitor alpelisib and compared sensitivity across *TP53*-mutant (MUT), *PIK3CA*-MUT, and *TP53/PIK3CA* co-mutant models. This allowed assessment of *TP53* mutations as potential biomarkers of resistance to PI3K inhibition.

3. **To evaluate whether combined PI3K and RTK inhibition can overcome resistance in *TP53/PIK3CA* co-mutant TNBC.** This objective tested the hypothesis that adaptive RTK signalling contributes to resistance following PI3K inhibition. Through drug combination studies involving alpelisib and RTK inhibitors, particularly crizotinib, I assessed antiproliferative and apoptotic responses in TNBC models and investigated the molecular mechanisms underlying therapeutic synergy using proteomic and signalling analyses.
4. **To determine how distinct *TP53* mutation classes influence therapeutic response and PI3K pathway dependence.** This objective addressed the functional heterogeneity of *TP53* mutations using a panel of isogenic MCF10A models harbouring different *TP53* alterations alone or in combination with a *PIK3CA* alteration. By comparing responses to alpelisib, crizotinib, and combination treatment, I investigated how specific *TP53* variants shape signalling networks, drug sensitivity, and resistance mechanisms, with the aim of identifying mutation-specific therapeutic vulnerabilities.

Collectively, these objectives sought to improve our understanding of *TP53*-PI3K-driven TNBC biology and inform the development of more effective targeted therapies.

2.Methods and materials

2.1. Identification and characterisation of *TP53*-PI3K^{act} TNBC

2.1.1. Study design overview

This study was designed to define and comprehensively characterise a biologically and clinically high-risk subgroup of TNBC defined by co-occurring *TP53* mutation and PI3K pathway activation (hereafter referred to as *TP53*-PI3K^{act}). Two independent, publicly available BC cohorts were used in this study: the Molecular Taxonomy of Breast Cancer International Consortium (METABRIC) cohort and the Cancer Genome Atlas (TCGA) Breast Invasive Carcinoma cohort. These cohorts were selected due to the availability of comprehensive genomic, transcriptomic, clinical, and survival data.

The study followed a structured, multi-stage analytical framework:

1. **Definition of a *TP53*-PI3K^{act} subgroup:** We first evaluated the survival impact of *TP53-PIK3CA* co-mutation in TNBC relative to *TP53*-only mutant and subsequently tested additional PI3K-pathway alterations to determine which events were associated with comparable adverse prognosis. Based on these analyses, a survival-associated definition of PI3K pathway activation (PI3K^{act}) was established.

2. **Cross-cohort validation and survival modelling:** The prevalence, co-occurrence, and prognostic impact of *TP53*-PI3K^{act} were assessed independently in METABRIC and TCGA. Survival analyses included univariable and multivariable modelling, proportional hazards (PH) testing, and alternative survival metrics where PH assumptions were violated.

3. **Clinical and molecular characterisation:** Clinical features, intrinsic molecular subtype distributions, and co-occurring genomic alterations were compared between mutation-defined subgroups (*TP53*-PI3K^{act}, *TP53*-only, PI3K^{act}-only, and non-altered) to determine whether *TP53*-PI3K^{act} tumours represent a distinct clinicopathological entity.

4. **Transcriptomic and pathway-level profiling:** Differential gene expression and gene set enrichment analyses (GSEAs) were conducted to identify biological programmes associated with *TP53*-PI3K^{act}. Single-sample GSEA (ssGSEA) scores were generated to quantify pathway activity at the tumour level."

5. **Protein-level validation:** RPPA data from TCGA were analysed to determine whether transcriptional differences were reflected at the protein and phospho-protein level.

All analyses were performed separately in each cohort to account for differences in clinical annotation, TNBC definition, molecular profiling platform, and sample composition. Reproducible patterns observed across both datasets were interpreted as robust features of the *TP53*-PI3K^{act} subgroup.

2.1.2. Cohort selection and definition of TNBC

2.1.2.1. METABRIC cohort

2.1.2.1.1. Study background

The METABRIC study is a large-scale BC genomics project that profiled over 2,000 primary breast tumours with long-term clinical follow-up. Tumours were analysed using targeted sequencing for somatic mutations and high-resolution single nucleotide polymorphism (SNP) arrays for copy number alterations (CNAs) alongside gene expression profiling using Illumina microarrays. Clinical data include tumour size, nodal status, histologic grade, intrinsic molecular subtype classification, treatment information, and long-term survival outcomes, including OS and relapse-free survival (RFS). The depth of clinical annotation and extended follow-up made METABRIC particularly suitable for survival modelling and multivariable prognostic analyses (568,569).

All METABRIC data were accessed through cBioPortal. Only primary tumour samples with available mutation, copy number (CN), survival, and mRNA expression data were retained for downstream analyses.

2.1.2.1.2. TNBC definition in METABRIC

TNBC samples in METABRIC were defined using the clinical receptor-status annotations for ER-, PR-, and HER2-negative. ER and HER2 status were predominantly measured by IHC when available, while PR status was not consistently assessed by IHC and was derived from clinical pathology reports. Samples negative for ER, PR, and HER2 were classified as TNBC (570). After applying these criteria, n = 320 TNBC patients were identified in METABRIC, of which n = 299 had available mutation and CNA data.

2.1.2.2. TCGA cohort

2.1.2.2.1. Study background

The TCGA-BRCA cohort is a comprehensive multi-omics dataset encompassing genomic, transcriptomic, and clinical data from over 1,000 BC patients. The cohort includes extensive clinical annotations, histopathology, and molecular profiling, allowing for integrative analyses of BC subtypes. Data were accessed through cBioPortal (TCGA, PanCancer Atlas dataset), which provides harmonised clinical and molecular data for consistent downstream analyses (571).

2.1.2.2.2. TNBC definition in TCGA

In TCGA, TNBC samples were defined based on the basal PAM50 molecular subtype, rather than directly using ER, PR, or HER2 receptor status. While IHC-based receptor status is available in the older Firehose Legacy dataset, these measurements are not fully harmonised or standardised across samples. The PanCancer TCGA dataset provides harmonised clinical and molecular data, but it does not include IHC receptor status. Using the basal PAM50 subtype therefore allows for a consistent, transcriptomics-based definition of TNBC that aligns with its molecular characteristics and ensures comparability across samples (571). A total of n = 171 basal PAM50 TNBC patients were identified in TCGA, all of whom had mutation and CNA data available.

2.1.2.3. Independent cohort analysis

Analyses were carried out independently for each cohort (METABRIC and TCGA) to avoid introducing biases from cross-cohort harmonisation. Each dataset was processed and analysed using its respective TNBC definitions – clinical receptor status in METABRIC and basal PAM50 subtype in TCGA – allowing results to be compared across cohorts while preserving cohort-specific data characteristics. This approach also accounts for potential differences in measurement platforms and TNBC definitions between the two studies.

2.1.3. Genomic alterations and definition of *TP53*-PI3K^{act}

2.1.3.1. Mutation and copy number data

Somatic mutations and CNAs were obtained from cBioPortal. In METABRIC, mutations were measured using targeted gene panel sequencing and CNAs were derived from Affymetrix SNP 6.0 arrays (569). In TCGA, mutations were measured by WES, and CNAs were also derived from SNP 6.0 arrays (571,572).

Somatic mutation and CNA data were extracted for genes involved in *TP53* and PI3K pathway signalling, including *TP53*, *PIK3CA*, *AKT1*, *PTEN*, *PIK3R1*, and *AKT3*. All non-synonymous coding variants were included in analyses, without restriction by variant class due to limited sample sizes; however, the majority of identified variants were annotated as putative drivers in the respective cohort databases. *PTEN* deletion was defined as a homozygous deletion, and gene amplifications were defined according to cohort-specific CNA thresholds reported in the METABRIC and TCGA datasets (568,571).

2.1.3.2. Definition of *TP53*-PI3K^{act} TNBC cohort

To identify PI3K-pathway alterations associated with adverse survival in *TP53*-MUT TNBC, Cox PH models were fitted in the METABRIC cohort comparing *TP53*-MUT tumours carrying each individual PI3K-related alteration versus *TP53*-only tumours (see Section 3.5. for additional details on the survival analysis). The alterations evaluated included *PIK3CA* mutation, *AKT1* mutation, *PTEN* deletion, *PIK3R1* mutation, *AKT3* amplification, *PIK3CA* amplification, and *PTEN* mutation. Notably, within the METABRIC TNBC cohort there was only a single *AKT2*-mutant tumour and no *AKT3* mutations detected; therefore, these were excluded due to insufficient sample size. Based on their survival impact, PI3K^{act} was defined as the presence of *PIK3CA* mutation, *AKT1* mutation, or *PTEN* homozygous deletion. The *TP53*-PI3K^{act} subgroup was subsequently defined as tumours harbouring a *TP53* mutation together with at least one PI3K^{act} alteration. For downstream analyses, four mutation-defined groups were considered:

- *TP53*-PI3K^{act}
- *TP53*-only
- PI3K^{act}-only
- Non-altered tumours (WT for *TP53*, *PIK3CA*, and *AKT1*, with no *PTEN* deletion)

2.1.4. Co-occurrence analysis

Co-occurrence of *TP53* mutations and PI3K^{act} alterations in TNBC was assessed independently in the METABRIC and TCGA cohorts. For each cohort, the observed number of tumours harbouring both *TP53* mutations and ≥1 PI3K^{act} alteration (*TP53*-PI3K^{act}) was compared to the expected number under the assumption of independent events, calculated as:

$$\text{Expected } \textit{TP53}\text{-PI3K}^{act} = \frac{\textit{TP53}\text{-MUT x PI3K}^{act}}{\text{Total TNBC patients}}$$

To test for statistical association, a two-sided Fisher's exact test was applied using a 2x2 contingency table of *TP53* mutation status (mutant vs. WT) and PI3K status (activated vs. non-activated) (573). Odds ratios (ORs) and 95% confidence intervals (CIs) were calculated for each cohort. Additionally, permutation analysis was performed by randomly shuffling mutation labels across patients 10,000 times to generate an empirical null distribution of *TP53*-PI3K^{act} counts. A two-sided permutation p-value was calculated as the proportion of iterations in which the simulated co-occurrence was equal to or exceeded the observed value (574). Fisher's exact tests and permutation testing were performed in R (version 4.5.0). All analyses were conducted separately in METABRIC and TCGA to account for potential cohort-specific differences in mutation frequencies and cohort sizes.

To further characterise the molecular context of *TP53*-PI3K^{act} TNBC, additional analyses were performed to assess enrichment of recurrent somatic mutations, structural variants, and CNAs relative to *TP53*-only tumours using cBioPortal. Multiple-testing correction using the Benjamini-Hochberg (BH) method was applied to control the false discovery rate (FDR) while maintaining statistical power across the large number of genomic features tested (575). These analyses were conducted separately in METABRIC and TCGA to account for differences in cohort-specific genomic backgrounds.

2.1.5. Survival analysis

2.1.5.1. Endpoints

Survival endpoints were defined according to cohort-specific data availability (obtained through cBioPortal):

- **METABRIC:** OS and RFS
- **TCGA:** OS and disease-specific survival (DSS)

Survival time was measured from the date of diagnosis to the occurrence of the event of interest (death or relapse) or censoring at last follow-up.

2.1.5.2. Cox proportional hazards models

Cox PH regression was used to estimate HRs with 95% CIs for survival outcomes across mutation-defined TNBC subgroups. For univariate analyses, HRs were calculated relative to the *TP53*-PI3K^{act} subgroup to directly assess differences in survival compared with this high-risk group. For multivariable models, HRs were reported relative to *TP53*-only tumours, allowing evaluation of the independent prognostic impact of *TP53*-PI3K^{act} after adjustment for

clinical covariates. Clinical covariates included age at diagnosis, tumour size, nodal status, and neoplasm histologic grade in METABRIC, and age, nodal status, and tumour stage in TCGA. PH assumptions were assessed using Schoenfeld residuals, and where violations were detected:

- Univariate analyses: Restricted mean survival time (RMST) analysis was performed (see Section 3.5.3.).
- Multivariable models: models were stratified or incorporated time-dependent covariates.

In METABRIC, for OS, the global PH assumption was violated, indicating that the effects of one or more covariates on the hazard of death changed over time rather than remaining constant (576); the model was stratified by nodal status and histologic grade, and age at diagnosis was included as a time-dependent covariate. For RFS, a minor violation was observed for histologic grade, but the global test was not significant and no stratification was applied. In TCGA, the global PH was violated for the univariate analysis and therefore RMST analysis was performed (see Section 3.5.3). PH assumptions were generally satisfied for the multivariable analysis, although minor violation was observed for the *TP53*-PI3K^{act} group, and results were interpreted with caution. In addition, to assess whether the adverse prognosis of *TP53*-PI3K^{act} tumours was independent of intrinsic TNBC transcriptional subtype, multivariable Cox models in METABRIC were stratified by TNBC subtype with *TP53*-PI3K^{act} set as the reference group, while adjusting for standard clinical covariates.

All Cox models were implemented in R using the survival package (version 3.8-6), with HRs reported as described for univariate and multivariable analyses. Survival distributions were visualised using Kaplan Meier (KM) curves with accompanying risk tables, generated using the ggplot2 package (version 4.0.1) in R.

2.1.5.3. Restricted Mean Survival Time analysis

For the TCGA cohort, PH assumptions were not satisfied. Therefore, survival was also evaluated using Restricted Mean Survival Time **(**RMST) analysis, which estimates the average survival time up to a prespecified truncation point (here, 48 months), providing an alternative measure of survival that does not rely on PH assumptions (577). Differences in RMST between *TP53*-PI3K^{act} and *TP53*-only were calculated (578). Analyses were performed in R using the suvRM2 package (version 1.0-4), with RMST differences and corresponding p-values calculated within the package.

2.1.5.4. Interaction analysis

To evaluate potential synergistic effects between *TP53* mutation and PI3K pathway activation on survival, interaction terms were included in Cox PH models for OS and RFS in the METABRIC cohort. Specifically, models incorporated main effects for *TP53* mutation status, PI3K^{act} status, and the interaction term *TP53* x PI3K^{act}. HRs and 95% CIs for the interaction term were estimated, and statistical significance was assessed using Wald tests.

2.1.6. Clinical characterisation

Clinical variables and tumour annotations for TNBC patients were extracted from cBioPortal for the METABRIC and TCGA cohorts. Analyses focused primarily on comparisons between *TP53*-PI3K^{act} and *TP53*-only tumours, as *TP53*-only represents the largest reference group within TNBC and allows assessment of the incremental clinical impact of PI3K pathway activation. To provide broader context, categorical and continuous variables were also evaluated across all four mutation-defined subgroups (*TP53*-PI3K^{act}, *TP53*-only, PI3K^{act}-only, and non-altered).

Categorical variables were compared using chi-square (χ^2) tests, while continuous variables were evaluated using Wilcoxon rank-sum tests or Kruskal-Wallis (KW) tests for multi-group comparisons. FDR adjustment of p-values was performed using the BH method. Clinical features analysed included patient demographics (age, menopausal status, vital status), tumour histology, surgical treatment type, and molecular features (e.g. PAM50 and integrative cluster classification, HER2 CN status). For TCGA, a combined hypoxia score was calculated as the mean of three published signatures (Ragnum, Winter, Buffa), and comparisons across mutation-defined subgroups were performed using the same non-parametric approach. All statistical analyses were performed in R.

2.1.7. Gene expression analysis

2.1.7.1. Differential expression analysis

Differential expression analysis (DEA) was performed to identify transcriptional differences between *TP53*-PI3K^{act} and *TP53*-only TNBC tumours in the METABRIC and TCGA cohorts. Analyses were conducted independently for each cohort due to differences in gene expression profiling platforms and data preprocessing methods. Statistical modelling and visualisation were implemented in R. When duplicate gene symbols were present in the expression matrix,

rows were collapsed by calculating the mean expression value across duplicated entries to generate a single expression value per gene.

Genes were considered significantly differentially expressed if they satisfied both of the following criteria:

- $|\log_2$ fold change (L2FC)$| \geq 0.585$ (equivalent to ≥1.5-fold change)
- FDR-adjusted p-value (adj.p) ≤ 0.05 (BH correction)

Significant genes were classified as upregulated (positive L2FC; i.e. higher expression) or downregulated (negative L2FC; i.e. lower expression) in *TP53*-PI3K^{act} tumours relative to *TP53*-only tumours.

Volcano plots were generated to visualise differential expression results by plotting L2FC against $-\log_{10}$(adj.p). Genes meeting significance thresholds were highlighted according to direction of change, and the most significant genes were annotated on the plot.

To visualise gene expression patterns across tumours, heatmaps were generated using the pheatmap package (version 1.0.13) for the top-ranked differentially expressed genes based on adj.p. Expression values were z-score scaled across samples to emphasise relative expression differences, and hierarchical clustering was applied to both genes and samples. Tumour samples were annotated according to mutation-defined subgroup to facilitate visual comparison of transcriptional patterns.

2.1.7.1.1. METABRIC

Gene expression data for the METABRIC cohort were obtained from cBioPortal. Expression measurements were generated using the Illumina HumanHT-12 v3 microarray platform and provided as $\log_2$-transformed probe intensity values representing continuous mRNA expression levels. Expression data were imported into R and subset to ensure that only the TNBC patients were retained in the study. METABRIC expression values were batch-corrected to remove cohort-specific effects while preserving biological differences between mutation-defined groups. Principal component analysis (PCA) showed that major components were initially driven by cohort, and batch correction reduced this effect without altering group structure. DEA was conducted using the limma R package (version 3.64.3). This method fits linear models for each gene and applies empirical Bayes moderation to improve variance estimation (579), allowing robust identification of genes with altered expression between *TP53*-PI3K^{act} and *TP53*-only tumours.

2.1.7.1.2. TCGA

Gene expression data for the TCGA cohort were obtained from the TCGA PanCancer Atlas dataset in cBioPortal. Expression measurements were derived from RNA sequencing performed on the Illumina HiSeq platform and quantified as batch-normalised RNA-Seq by Expectation Maximisation (RSEM) expression values. Expression matrices were subset to include only the basal-like TNBC samples retained for analysis. Where genes lacked an official Hugo symbol, missing symbols were filled by mapping the Entrez ID to the corresponding gene symbol using the org.Hs.eg.db annotation database. Differential expression between *TP53*-PI3K^{act} and *TP53*-only TNBC was assessed using the limma package with voom-transformed expression values. Voom converts count data to log_2-expression values with associated precision weights, allowing linear modelling analogous to that applied to the METABRIC microarray dataset, thereby enabling cross-cohort comparability (579).

2.1.7.2. Gene set enrichment analysis

To investigate whether transcriptional differences between *TP53*-PI3K^{act} and *TP53*-only TNBC tumours were associated with specific biological pathways, gene set enrichment analysis (GSEA) was performed independently for each cohort. Genes were ranked according to a composite score combining direction and significance of differential expression, calculated as the product of L2FC and -log_{10}(adj.p). Small deterministic offsets were added to break ties, and genes were sorted in descending order to generate a ranked gene list suitable for GSEA. Pathway-level analyses were conducted using the fgsea R package (version 1.34.2), which implements a fast pre-ranked GSEA algorithm (580). Two collections of gene sets were evaluated:

- Hallmark gene sets, representing curated biological processes,
- Reactome gene sets, representing canonical signalling and metabolic pathways.

For each pathway, normalised enrichment scores (NES) and adj.p were calculated. Pathways with an FDR ≤ 0.05 were considered significantly enriched. Leading-edge genes driving the enrichment signal were extracted for downstream interpretation. Results were visualised using dot plots, with NES on the x-axis, pathways on the y-axis, point size reflecting -log_{10}(adj.p), and colour indicating gene set collection (Hallmark or Reactome).

To assess cross-cohort concordance at the level of pathway-driving genes, overlap of leading-edge gene sets was quantified for pathways that achieved at least nominal significance (p ≤

0.05) in both METABRIC and TCGA. Leading-edge genes, defined as the subset of genes contributing most strongly to the enrichment signal in each pathway (581), were extracted from the GSEA results and used as a refined representation of pathway activity. Concordance between cohorts was measured using the Jaccard index (J), defined as the size of the intersection divided by the size of the union of leading-edge gene sets for each corresponding pathway:

$$J = \frac{\text{Shared leading-edge genes}}{\text{Total unique leading-edge genes}}$$

Jaccard indices were calculated independently for all overlapping significant pathways, enabling quantitative comparison of gene-level consistency underlying shared pathway enrichment signals. This approach allowed assessment of whether similar biological processes were driven by conserved or divergent gene subsets across datasets, beyond pathway-level enrichment statistics alone (582).

2.1.7.3. Single-sample GSEA

To assess pathway activity at the individual tumour level, single-sample GSEA (ssGSEA) was performed using the GSVA R package. Unlike conventional GSEA, which evaluates enrichment between predefined groups, ssGSEA calculates an enrichment score for each gene set within each individual sample, enabling assessment of tumour-level pathway activity and heterogeneity.

Pathways selected for ssGSEA were derived from the GSEA results. Gene sets were obtained from the Hallmark and Reactome collections in the MSigDB database using the msigdbr R package. ssGSEA enrichment scores were calculated independently for the METABRIC and TCGA expression datasets. Individual pathway scores were subsequently grouped into broader biological programmes (metabolic, immune, and cell cycle), and mean programme scores were calculated for each tumour. This enabled comparison of overall programme activity across the four mutation-defined subgroups (*TP53*-PI3K^{act}, *TP53*-only, PI3K^{act}-only, and non-altered).

Statistical comparisons of both programme-level and individual pathway-level scores between mutation-defined subgroups were performed using pairwise Wilcoxon rank-sum tests with BH correction for multiple testing. Results were visualised using boxplots overlaid with individual tumour-level data points. All analyses were conducted independently in the METABRIC and

TCGA cohorts using R. For visualisation, programme scores were standardised using z-score transformation.

2.1.7.4. TNBC subtype classification

Intrinsic transcriptional subtype classification was performed independently in the METABRIC and TCGA TNBC cohorts using the TNBCtype classifier tool (https://cbc.app.vumc.org/tnbc/index.php). TNBCtype analysis was run on batch-corrected METABRIC mRNA data and TCGA mRNA data. Prior to subtype assignment, duplicate gene entries in METABRIC were consolidated by selecting the probe with the highest variance. Samples flagged by TNBCtype for potential ER expression (METABRIC: n = 4; TCGA: n = 13) were excluded from downstream analyses.

The TNBCtype tool classifies TNBCs into Lehmann's six molecular subtypes – BL1, BL2, IM, M, MSL, and LAR (see Section 1.4.1.) – based on correlation of each tumour's gene expression profile to predefined subtype centroid signatures (104,583,584). Under the original TNBCtype-6 methodology, subtype assignment is determined by the highest correlation coefficient between a tumour and the six subtype centroids. Samples are classified as unclassified (UNC) if (i) the maximum correlation coefficient is < 0.1 or not statistically significant ($p > 0.05$), or (ii) the difference between the two highest correlation coefficients is < 0.05, indicating ambiguity between subtypes (583).

2.1.7.4.1. Modified TNBCtype-6 classification

In this study, a modified "best-hit" implementation of TNBCtype-6 was applied. The minimum correlation threshold (correlation coefficient ≥ 0.1 and $p \leq 0.05$) was retained to ensure biologically meaningful assignment. However, the ambiguity filter based on a < 0.05 difference between the two highest correlation coefficients was not applied. Instead, tumours meeting the correlation and significance thresholds were assigned to the subtype with the highest correlation coefficient, regardless of the magnitude of difference between the top two subtype correlations. Tumours failing to meet the ≥ 0.1 and significance criteria were classified as UNC, reducing the risk of assigning tumours with weak or non-specific subtype associations to a potentially unreliable TNBC subtype (581).

2.1.7.4.2. TNBCtype-4 reassignment

Following TNBCtype-6 classification, TNBCtype-4 reassignment was performed to reduce the influence of immune- and stromal-derived transcriptional signals. This approach aims to better capture tumour-intrinsic biological subtypes by minimising classification driven by non-tumour components of the TME (584). Under the TNBCtype-4 framework, tumours initially classified as IM or MSL are reassigned to their second-highest correlated intrinsic subtype (BL1, BL2, M, or LAR). In this study, reassignment was performed if the second-highest correlation coefficient met the ≥ 0.1 threshold and statistical significance criterion ($p \leq 0.05$). If these criteria were not met, the tumour was designated UNC. As with the TNBCtype-6 implementation, no minimum difference threshold between correlation coefficients was imposed during reassignment.

2.1.7.4.3. Statistical analysis of TNBC subtype distributions

Differences in TNBC subtype composition across mutation-defined subgroups were assessed using Pearson's χ^2 tests with p-values obtained by simulation (10,000 replicates) to account for small expected counts and potential violation of χ^2 assumptions. Standardised residuals were calculated to identify subtypes that were over- or under-represented relative to expectations under independence. Pairwise comparisons between *TP53*-PI3K^{act} and *TP53*-only tumours were also performed using Fisher's exact tests to confirm the significance of subtype shifts, with p-values reported.

2.1.7.4.4. Identification of intermediate or transitional TNBC subtype states

To account for omission of the original ambiguity filter (difference < 0.05 between the two highest subtype correlations), additional annotation was performed within the *TP53*-PI3K^{act} subgroup. Tumours whose two highest subtype correlation coefficients were within 0.05 of each other were flagged as intermediate or potentially mixed transcriptional states. This secondary classification allowed identification of tumours lying near subtype boundaries or exhibiting transitional phenotypes, while retaining a primary best-hit subtype assignment.

All subtype assignments and downstream comparisons were conducted separately in METABRIC and TCGA to account for differences in expression platforms and TNBC cohort definitions.

2.1.8. Differential protein expression analysis

Protein-level differences between *TP53*-PI3K^{act} and *TP53*-only TNBC were assessed using TCGA RPPA data (571). Only subgroups (i.e. *TP53*-PI3K^{act}, *TP53*-only, PI3K^{act}-only, non-altered) with sufficient numbers of patients were included in statistical testing. Expression values were batch-corrected to remove technical variation across RPPA runs while preserving biological differences between mutation-defined subgroups. Differential expression was evaluated using linear modelling with empirical Bayes moderation as implemented in the limma R package. Significance thresholds were set at $|L2FC| \geq 0.263$ and BH-adj.p ≤ 0.05. Significant proteins were visualised using boxplots and heatmaps to illustrate subgroup-level expression patterns. All analyses and visualisations were conducted in R.

2.2. Differential expression analysis of MCF10A cell line RNA-seq data

2.2.1. Sample data background and processing

MCF10A cell lines transduced with *TP53* mutations (G245S, R273H, R175H, Y163C), *TP53* WT-overexpressed (p53OE), and WT-knockdown (p53KD), along with the parental *TP53*-WT (p53WT) MCF10A cell line were generated by the LaBaer laboratory at the BioDesign Institute, Arizona State University (ASU) (585). RNA was extracted from these samples and RNA-seq was performed by the LaBaer group. Assembled read counts and sample metadata were provided to me for my analysis.

2.2.2. Data quality control and normalisation

Raw read counts were converted to counts per million (CPM) using the edgeR package (version 4.6.3) in R (version 4.5.0) to account for library size differences. Quality control involved filtering genes to reduce noise and enhance statistical power. Mitochondrial genes and Cas9-related genes were removed. Low-expression genes with CPM ≤ 1 in three or more samples were also excluded. Library sizes were assessed before and after filtering to confirm data integrity. The trimmed mean of M-values (TMM) normalisation method, implemented in edgeR, was applied using the calcNormFactors function to adjust for differences in sequencing depth and RNA composition across samples. Multidimensional scaling (MDS) plots were generated using the plotMDS function to visualise sample relationships. Normalised TMM counts were $\log_2$-transformed for downstream analysis.

2.2.3. Differential expression analysis

DEA was conducted using the edgeR package on filtered MCF10A RNA-seq data. A design matrix was created from sample group annotations (e.g. sensitive vs. resistant). Dispersions were estimated with the estimateGLMCommonDisp, estimateGLMTrendedDisp, and estimateGLMTagwiseDisp functions. A quasi-likelihood generalised model was fitted using the glmQLFit function. Pairwise comparisons were performed with the glmQLFTest function, using contrasts defined by a custom function. P- values were adjusted with the BH method (FDR ≤ 0.05). Genes with FDR ≤ 0.05 and $|L2FC| \geq 0.585$ were considered significantly differentially expressed. Volcano plots and heatmaps were generated using the ggplot2 and pheatmap functions. Normalised gene counts for DEGs were extracted and converted to z-scores to facilitate visualisation of relative expression differences.

2.2.4. Investigation of target genes

GSEA was conducted as per Section 2.1.7.2.. KEGG pathway visualisations were generated using the pathview package (version 1.48.0) in R for the PI3K/AKT pathway (hsa04151) with gene data mapped (586).

2.3. Cell lines and reagents

This project utilised six TNBC cell lines (see Table 2-1): HDQ-P1 and CAL-51 from the German Collection of Microorganisms and Cell Cultures (DSMZ, Braunschweig, Germany); MDA-MB-453, MDA-MB-468, MFM-223, and BT-20 from the American Type Culture Collection (ATCC, Manassas, VA, USA). The cell lines HDQ-P1, MDA-MB-453, and MDA-MB-468 were cultured in Roswell Park Memorial Institute-1640 medium (RPMI-1640) (Sigma-Aldrich) supplemented with 10% foetal bovine serum (FBS) (Gibco). The MFM-223 and BT-20 cell lines were grown in Eagle's Minimum Essential Medium (EMEM) (Sigma-Aldrich) with 10% FBS and 2 mM L-glutamine. The CAL-51 cell line was maintained in Dulbecco's Modified Eagle's Medium (DMEM) with high glucose and supplemented with 10% FBS. The HEK-293T cell line, which was grown in DMEM with high glucose and supplemented with 10% FBS, was also used for viral transfection. Cell culture media were changed every 2-3 days, and the cells were sub-cultured with trypsin (0.25% Trypsin (Gibco) + 0.02% ethylenediaminetetraacetic acid (EDTA) (Sigma-Aldrich)) upon reaching 70% confluency, with a maximum passage limit of 10. All cell culture procedures were conducted following the guidelines established in the NICB standards of practice (SOP) [SOP-007].

Table 2-1: Cell lines used in this project and the relevant culture medium, type, and conditions required for growth.

Cell Line	Culture Medium	Culture Type	Culture Conditions
BT-20	EMEM + 10% FBS + 2mM L-glutamine	Adherent	37°C, 5% CO_2
CAL-51	DMEM + 10% FBS	Adherent	37°C, 5% CO_2
HDQ-P1	RPMI-1640 + 10% FBS	Adherent	37°C, 5% CO_2
MDA-MB-453	RPMI-1640 + 10% FBS	Adherent	37°C, 5% CO_2
MDA-MB-468	RPMI-1640 + 10% FBS	Adherent	37°C, 5% CO_2
MFM-223	EMEM + 10% FBS + 2mM L-glutamine	Adherent	37°C, 5% CO_2
HEK-293T	DMEM + 10% FBS	Adherent	37°C, 5% CO_2

The MCF10A cell lines (ATCC, CRL-10317) stably expressing WT, KD, and missense mutant p53 proteins (see Table 2-2), which were developed by the LaBaer group at the Biodesign Institute at Arizona State University (ASU), were utilised for this project. These mutant p53 proteins are expressed on top of the endogenous WT *TP53*. Detailed information regarding the MCF10A altered cell lines used in this study can be found in the publication by Pal *et al.* (585). The mutations expressed are the most prevalent *TP53* mutations found in BC patients and all occur in the DBD of *TP53*. They are categorised based on whether they occur at residues that contact DNA (DNA contact mutants) or affect the overall structure of the *TP53* protein (structural mutants). The MCF10A cells were developed using Gateway plasmids sourced from the DNASU plasmid repository (dnasu.org). The *TP53* gene segments containing missense mutations were cloned into either the pLX304 vector for WT p53 (Addgene) or the pLenti4/V5-DEST vector for missense mutants (ThermoFisher Scientific). Stable cell lines were generated through lentiviral transduction.

The MCF10A cells were maintained in DMEM-F12 media which was supplemented with 5% horse serum (ThermoFisher), 10 ng/mL human epidermal GF (hEGF) (ThermoFisher), 0.5 µg/mL hydrocortisone (Sigma), 100 ng/mL cholera toxin (Sigma), and 10 µg/mL insulin (Sigma). The MCF10A cells were adherent and routinely passaged with trypsin at 80-90% confluence.

Table 2-2: The WT or missense *TP53* DBD alterations expressed in MCF10A cells used in this project.

TP53	Mutation Type / Control
p53WT	Control
p53OE	Control
p53KD	Control
G245S	Structural
Y163C	Structural
Y220C	Structural
H179R	Structural
Y234C	Structural
R175H	Structural
R273H	Contact
R248W	Contact
R273C	Contact
R248Q	Contact

The drug compounds used in this project are described in Table 2-3, including their primary molecular targets.

Table 2-3: Compounds used in this project and the relevant suppliers, stock concentrations, and storage conditions.

Compound	Supplier	Stock Concentration	Storage Conditions	Primary Target(s)
Alpelisib	MedChemExpress	10mM in DMSO	-20°C	PI3Kα
Crizotinib	MedChemExpress	10mM in DMSO	-20°C	ALK/c-MET/ ROS1/RON
Ceritinib	MedChemExpress	10mM in DMSO	-20°C	ALK
Capmatinib	MedChemExpress	10mM in DMSO	-20°C	c-MET

2.4. Mycoplasma testing

Cell lines were routinely screened for mycoplasma contamination. Following a minimum of three passages after thawing and a 72-hour incubation period post media change, cell culture supernatants from each of the cell lines were collected and centrifuged at 1000 RPM for 5 minutes to eliminate cellular debris. The resulting supernatants were stored at -20°C until further analysis.

Mycoplasma presence was assessed using the Hoechst DNA staining method, employing the normal rat kidney fibroblast (NRK) cell line as an indicator. NRK cells were cultured on coverslips in duplicate, to which the cell line supernatants were added and incubated at 37°C

with 5% CO_2 until they reached approximately 50% confluency. Subsequently, the supernatant and NRK medium were discarded, and the NRK cells were fixed on the coverslips using Carnoy's Fixative (1:2 glacial acetic acid:methanol) for 20 minutes on ice, then allowed to air dry. Following fixation, NRK cells were stained with the fluorescent dye Hoechst 33258 (Sigma) for 10 minutes, which selectively binds to DNA, illuminating the nuclei of cells and any extra-nuclear DNA, including that from mycoplasma. Each coverslip was washed twice with ultra-high purity water and examined under a fluorescent microscope at an excitation wavelength of 400 nm.

2.5. STR profiling

Cell line authentication and interspecies contamination testing were conducted using IDEXX BioAnalytics CellCheck^{TM} service, specifically CellCheck 9 – human (9 marker STR profile and Interspecies Contamination Test). Following a minimum of three passages after thawing and a 72-hour incubation period post media change, cells were trypsinised and counted. $1x10^6$ cells were centrifuged at 1000 RPM for 5 minutes and stored at -20°C before being sent for STR profiling. Genomic DNA was extracted from cell line samples and multiplex PCR assays amplified species-specific STR markers with validated primers, followed by capillary electrophoresis to determine fragment sizes and generate unique STR profiles. Electropherograms were analysed using automated software to assign allele calls, and profiles were compared against reference databases (e.g. NCBI BioSample Database) to confirm cell line identity, with an identity matching score over 80% indicating consistency with the cell line of origin. Interspecies contamination was assessed for human, mouse, rat, Chinese hamster, and African green monkey DNA.

2.6. Transfection and transduction

2.6.1. Viral transfection

For the transfection process, HEK-293T cells were plated in 25 cm^2 flasks at a density of 2×10^6 cells per flask and allowed to culture overnight until they reached 70-80% confluence. Transfection reagents were combined with the packaging plasmids – PAX2 (Figure 2-2(a)), gifted by Malin Parmer (587), and pCMV-VSV-G (Figure 2-2(b)), gifted by Bob Weinberg (588) – along with either of the viral plasmids of interest – pHAGE-*PIK3CA* (Figure 2-2(c)) or pHAGE-*PIK3CA*-H1047R (Figure 2-2(d)), both gifted by Gordon Mills & Kenneth Scott (589)

– as outlined in Table 2-4. The mixture was gently pipetted up and down at least ten times and incubated for 30 minutes to facilitate complex formation.

Three distinct plasmid combinations were prepared:

1. pCMV-VSV-G + PAX2 + pHAGE-*PIK3CA*,

2. pCMV-VSV-G + PAX2 + pHAGE-*PIK3CA*-H1047R, and

3. pCMV-VSV-G + PAX2 (serving as a negative control for transfection).

Table 2-4: Transfection reagents and viral plasmids used for transfection.

Reagent/Plasmid	Supplier	Category no.	Quantity
PAX2 plasmid	Addgene	35002	3 μg
p-CMV-VSV-G plasmid	Addgene	8454	2 μg
pHAGE-*PIK3CA* plasmid	Addgene	116771	4 μg
pHAGE-*PIK3CA*-H1047R plasmid	Addgene	116500	4 μg
Opti-MEM™ Reduced Serum Medium	Gibco	15392402	500 μL
PEI MAX®	Polysciences	24765	27 μL

After removing the old media from the HEK-293T cells, fresh media was added. Following the incubation period, the transfection reagents and plasmid mixture were added dropwise to the cells to enhance the formation of liquid droplets containing the plasmids. The day after transfection, the media from the HEK-293T cells, which contained the produced virus, was collected and stored at 4°C, after which fresh media was replenished in the cells. On the subsequent day, the media containing the virus was again collected from the HEK-293T cells and combined with the previously collected media. The combined media was then filtered using a 0.45-micron filter, aliquoted into single-use 1 mL portions, and stored at -80°C for future use.

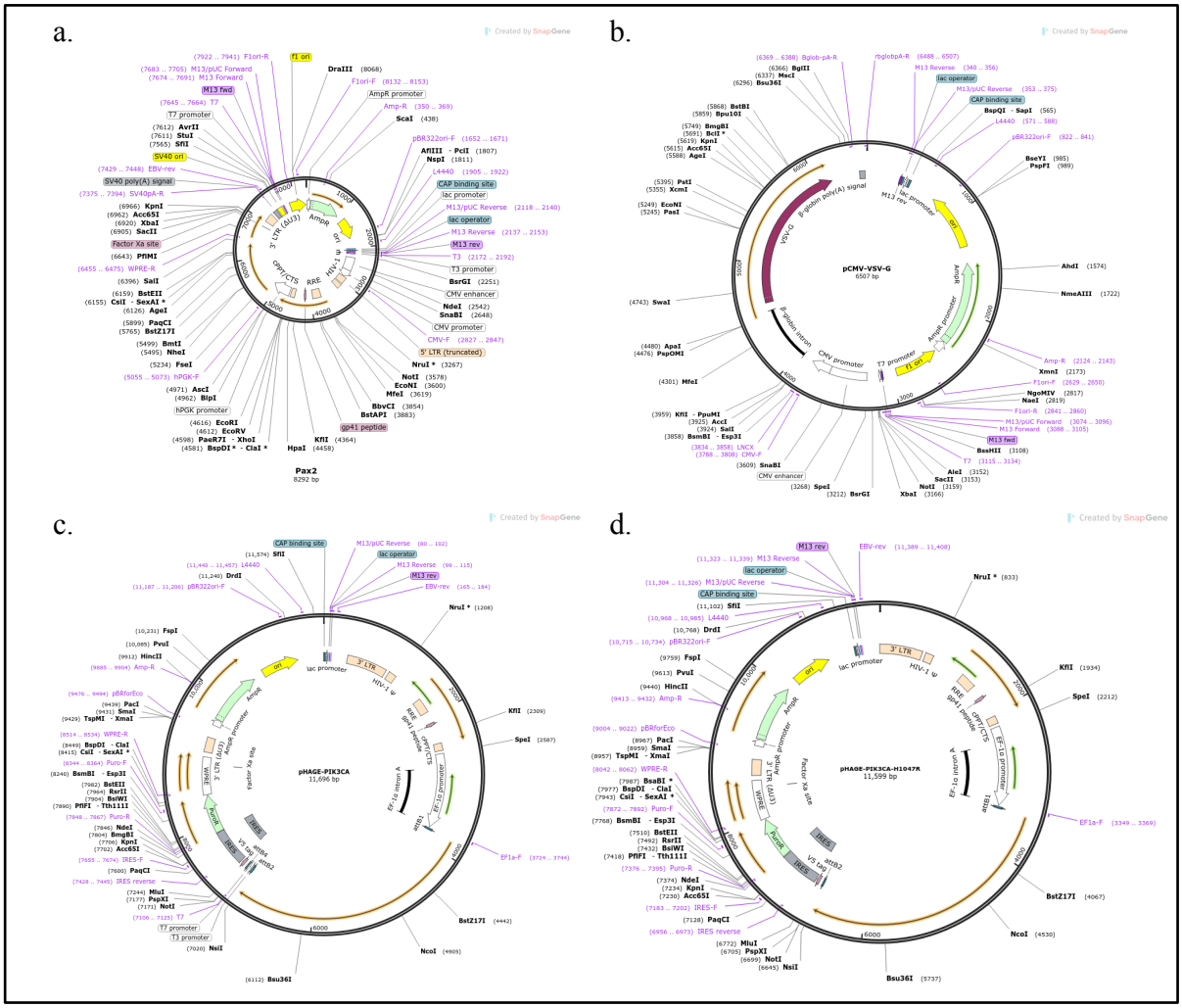


Figure 2-2: Map of the (a) PAX2, (b) pCMV-VSV-G, (c) pHAGE-*PIK3CA*, and (d) pHAGE-*PIK3CA*-H1047R plasmids, exhibiting the different genes and restriction enzyme sites present on the plasmids. The images were obtained from Addgene (www.addgene.org).

2.6.2. Viral transduction

Select MCF10A cell lines (p53WT, p53OE, p53KD, Y234C, R273C, and R248Q) were chosen for transduction and seeded at a density of 8 x 10^4 cells per well in a 6-well plate (see Figure 2-3 for plate layout). The following day, the media was removed, and each well received 1 mL of virus along with 1 µL of the transfection reagent polybrene. The plates were incubated for 2 hours to facilitate transduction. After this incubation, the viral solution and polybrene were removed, and 1 mL of fresh media, 1 mL of virus, and 2 µL of polybrene were added to each well, followed by overnight incubation. The subsequent day, the media was again removed, and fresh media was added to the cells. On the next day, the media was replaced with fresh media containing the selection agent puromycin at a concentration of 2.5 µg/mL. The selection agent was maintained until all cells in the control well (containing no virus) were dead, which

took approximately 2-3 days. The selected cells were grown in the selection compound for a minimum of 14 days before being utilised for experimental procedures.

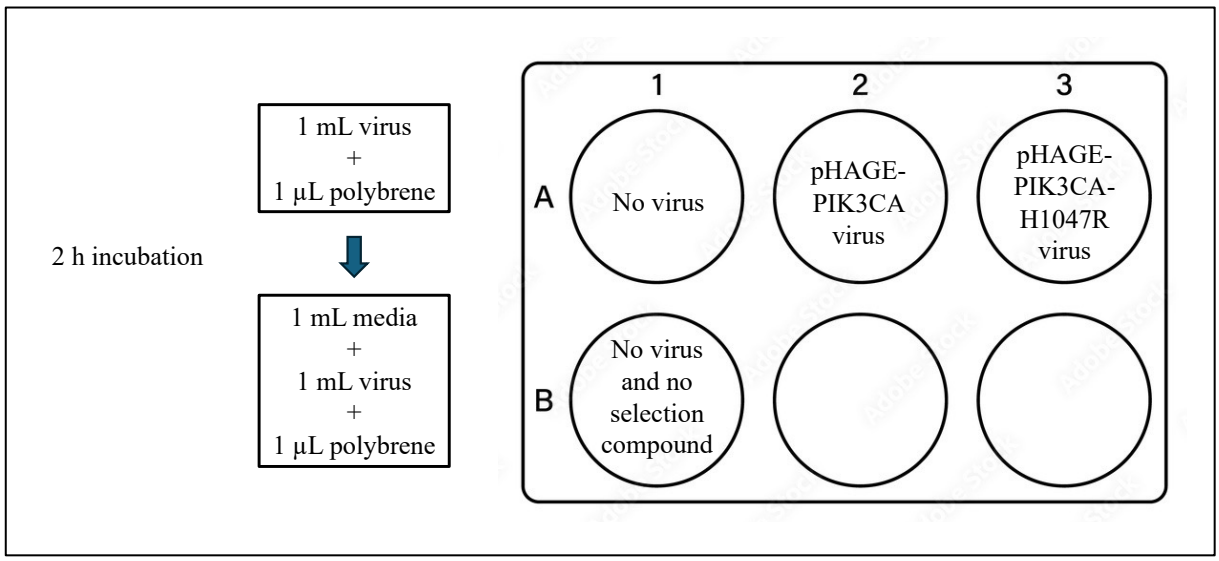


Figure 2-3: Plate layout for viral transduction.

2.7. Proliferation assay

Cell lines were plated in 96-well plates at varying densities ranging from 2000 to 5000 cells per well (cpw) (refer to Table 2-5), with each well containing 100 µL of culture medium.

Table 2-5: Seeding density for each cell line per well of a 96-well plate, i.e. cpw.

Cell Line	Seeding Density
BT-20	3000
CAL-51	3000
HDQ-P1	3000
MDA-MB-453	3000
MDA-MB-468	2000
MFM-223	5000
MCF10A (all)	2000

After a 24-hour incubation, the cells were treated with either a single drug or a combination of drugs (see Table 2-6) in an additional 100 µL of medium.

Table 2-6: Concentration ranges of alpelisib and RTK inhibitors for combination proliferation assays. Cells were treated with five serial concentrations of each drug.

		Conc. (μM)			
Cell Line	***TP53/PIK3CA***	**Alpelisib†**	**Crizotinib**	**Ceritinib**	**Capmatinib†**
MDA-MB-468	MUT/WT	0.31 – 5.00	0.16 – 2.50	-	-
HDQ-P1	MUT/WT	0.16 – 2.50	0.31 – 5.00	-	-
BT-20	MUT/MUT	0.08 – 1.25	0.16 – 2.50	-	-
MFM-223	MUT/MUT	0.08 – 1.25†	0.31 – 5.00	0.31 – 5.00	0.31 – 5.00
MDA-MB-453	WT/MUT	0.08 – 1.25	0.31 – 5.00	-	-
CAL-51	WT/MUT	0.04 – 0.63	0.08 – 1.25	-	-
MCF10A (all)	-	0.16 – 2.50	0.16 – 2.50	-	-

†Alpelisib was used at 0.16-2.50 μM in the MFM-223 alpelisib plus capmatinib combination experiments.

The cells were then incubated for five days, after which cell proliferation was assessed using the acid phosphatase assay designed for adherent cell lines. The half-maximal inhibitory concentration (IC_{50}) values were calculated using CalcuSyn software, and the combination index (CI) values at the effective doses for 50%, 75%, and 90% maximal response (ED_{50}, ED_{75}, ED_{90}) were determined to evaluate whether the drug combinations exhibited antagonism, additivity, or synergism. The CI is a quantitative measure derived from the Chou-Talalay method that provides a definition for drug interactions (590,591). This evaluation was used to assess whether the drug combinations exhibited antagonism, additivity, or synergism, with classifications of synergism or antagonism adhering to the established guidelines detailed in Tables 2-7. To determine if the observed synergy was achievable within therapeutic ranges (i.e. below maximum peak plasma concentrations, for clinical relevance), we presented dose reduction index (DRI) values – calculated using Calcusyn software – at ED_{50}, where DRI measures the fold-reduction in doses needed for the combination versus monotherapy to reach equivalent effects.

Table 2-7: CI value ranges defining synergism or antagonism in drug combination studies (590,591).

Range of CI	Symbol	Description
< 0.10	+++++	Very strong synergism
0.10-0.30	++++	Strong synergism
0.31-0.70	+++	Synergism
0.71-0.85	++	Moderate synergism
0.86-0.90	+	Slight synergism
0.91-1.10	±	Nearly additive
1.11-1.20	–	Slight antagonism
1.21-1.45	– –	Moderate antagonism
1.45-3.30	– – –	Antagonism
3.30-10.00	– – – –	Strong antagonism
> 10.00	– – – – –	Very strong antagonism

2.7.1. Acid phosphatase assay

The medium was removed from the 96-well plates, and the cells were washed three times with phosphate-buffered saline (PBS). Subsequently, 100 µL of acid phosphatase substrate (10 mM p-nitrophenol phosphate) (Sigma) in 0.1 M sodium acetate (Sigma) containing 0.1% Triton X-100 (BDH, pH 5.5) was added to each well, and the plates were incubated at 37°C for 1 to 2 hours. After incubation, 50 µL of 0.1 M sodium hydroxide (NaOH) was added to each well to halt the hydrolysis of p-nitrophenyl phosphate. The absorbance was then measured using a microplate reader (BioTek) with Gen4 software at 405 nm and 620 nm as a reference. The percentage growth of cells was calculated relative to an untreated control, and the background control containing sodium acetate and NaOH was recorded and subtracted from each measurement prior to calculating the percentage growth. All IC_{50} and combination assays were conducted in triplicate at a minimum. While some single-agent IC_{50} assays were initially performed in duplicate, the IC_{50} determinations were repeated for the combination assays, ensuring a minimum of triplicate measurements overall.

2.8. Apoptosis assay

Cells were seeded in a 96-well plate and incubated overnight to allow adherence. The following day, cells were treated with single agents or combinations along with the Incucyte Caspase-3/7 Green Dye for Apoptosis (Sartorius). Plates were placed in the Incucyte S3 live-cell analysis system and cell confluence was monitored over 4-120 h using phase contrast imaging and normalised to the confluence at the 0 h timepoint. Apoptosis was evaluated by quantifying Caspase 3/7 activity, visualised as green fluorescent objects and analysed via image-based quantification with Incucyte integrated analysis software, with values normalised to cell confluence. Relative Caspase 3/7 activity was further normalised to the untreated control across the 4-64 h timeframe.

2.9. Immunoblotting

2.9.1. Protein extraction and quantification

Cells were plated in 6-well or 100mm plates and grown to ~70% confluence. Cells were then serum-starved overnight and subsequently supplemented with 5% serum the following day. Cells underwent a 24-hour treatment with either a single drug or a combination of drugs of interest in the 5% serum media. Cells being analysed for baseline protein expression were maintained in 5% serum media without the drug treatment. The cells were then washed three

times with cold PBS while on ice. Subsequently, 120 µL of RIPA buffer (Sigma), supplemented with a 1X Protease Inhibitor (PI) cocktail (Sigma), 2 mM phenylmethylsulfonyl fluoride (PMSF) (Thermo Scientific), and 1 mM sodium orthovanadate (NaOV) (Sigma), was added to each well, and the cells were incubated on ice for 20 minutes. The cells were then scraped, and the lysis buffer was collected. To ensure thorough cell lysis, the lysates were subjected to shearing by pipetting up and down and then centrifuged at 14,000 rpm for 10 minutes at 4°C. The supernatant was carefully collected and stored at -80°C. The protein concentration in the lysates was quantified using the Pierce™ bicinchoninic acid (BCA) Protein Assay kit (Thermo Scientific), following the manufacturer's protocol.

2.9.2. Western immunoblotting

Different amounts of protein (5-40 µg) were separated using precast Bolt 4-12% Bis-Tris Plus Mini Protein Gels (Invitrogen) via electrophoresis in a Mini Gel Tank (Invitrogen) with 1X running buffer, prepared by diluting 50 mL of 20X Bolt MOPS SDS Running Buffer (Invitrogen) in 950 mL of reverse osmosis water (RO.H_2O). Following electrophoresis, proteins were transferred from the gels to a nitrocellulose membrane using the iBlot 2 Gel Transfer Device and Transfer Stacks (Invitrogen). The transfer was verified using Ponceau S bioreagent (Sigma), after which the membrane was washed three times with ultra-high purity (UHP) water to eliminate the stain. To block non-specific binding, the membranes were incubated for 1 hour at room temperature with 1X sodium chloride (**N**aCl), ethylenediaminetetraacetic acid (**E**DTA), tris(hydroxymethyl)aminomethane (**T**ris) / Triton (**NET**) buffer (refer to Table 2-8 for the preparation of 10X NET buffer), containing gelatin.

Table 2-8: Volumes and concentrations of compounds used for 10X NET buffer.

Compound	Stock Concentration	Volume (mL)	Final Concentration
NaCl	5 M	1500	1.5 M
EDTA	0.5 M	500	0.05 M
Tris pH 7.8	1 M	2500	0.5 M
Triton X-100	100%	25	0.5%
H_2O	100%	475	-

Primary and secondary antibodies were diluted in NET buffer according to the specifications outlined in Table 2-9. The membrane was incubated with the primary antibody at 4°C overnight. Following this incubation, membranes were washed three times for 10 minutes each with PBS. Subsequently, the membranes were incubated with the secondary antibody at room temperature for 1 hour, followed by another round of washing with PBS. Western blotting was

visualised using the Licor Odyssey system with Odyssey V3 software, and densitometric analysis was conducted using Image J software. Relative density values were calculated by normalising against a housekeeping protein.

Table 2-9: Primary and secondary antibodies

Antibody	PTM	Supplier	Dilution	Secondary antibody	Category no.
Anti-rabbit secondary (800CW)	-	LiCor	1:5000	-	926-3211
Anti-rabbit secondary (680RD)	-	LiCor	1:5000	-	926-68071
Anti-β-actin	-	Cell Signalling Technology	1:1000	Anti-Rabbit	4970
Anti-GAPDH	-	Cell Signalling Technology	1:1000	Anti-Rabbit	5174
Anti-AKT	-	Cell Signalling Technology	1:1000	Anti-Rabbit	9272
Anti-phospho-AKT	Ser473 phosphorylation	Cell Signalling Technology	1:500	Anti-Rabbit	9271
Anti-phospho-AKT	Thr308 phosphorylation	Cell Signalling Technology	1:500	Anti-Rabbit	9275
Anti-4E-BP1	-	Cell Signalling Technology	1:1000	Anti-Rabbit	9644
Anti-phospho-4E-BP1	Thr37/46 phosphorylation	Cell Signalling Technology	1:500	Anti-Rabbit	2855
Anti-PI3Kα	-	Cell Signalling Technology	1:1000	Anti-Rabbit	4129

2.10. RPPA analysis

2.10.1. Protein extraction and quantification

Cells were seeded and treated according to the protocol outlined in Section 2.8.1. Following treatment, the cells were washed three times with cold PBS on ice. A total of 150 µL of lysis buffer, consisting of 1% Triton X-100, 50 mM HEPES (pH 7.4), 150 mM NaCl, 1.5 mM MgCl2, 1 mM EGTA, 100 mM NaF, 10 mM sodium pyrophosphate, 1 mM sodium vanadate, 10% glycerol, along with protease and phosphatase inhibitors (Roche Applied Science Cat. # 05056489001 and 0490683700), was added to each well. The plates were incubated on ice for 20 minutes, with gentle shaking every 5 minutes. The lysates were then collected, and protein concentrations were quantified as described in Section 2.1.1. The protein concentrations were adjusted to 1.0 µg/µL using lysis buffer for dilution. Cell lysates were combined with 4X sodium dodecyl sulfate (SDS) sample buffer (comprising 40% glycerol, 8% SDS, 0.25 M Tris-HCl at pH 6.8, and beta-mercaptoethanol at 1/10 the volume) in a 3:1 ratio of lysate to sample buffer. The samples were boiled for 5 minutes and subsequently stored at -80°C until submission for analysis. A volume of 80 µL from each sample was submitted for RPPA analysis by the Functional Proteomics RPPA Core Facility at The University of Texas MD Anderson Cancer Centre. This facility employs a high-throughput antibody-based RPPA platform to quantify protein expression and phosphorylation in signalling networks, analysing approximately 500 validated antibodies per cell line sample via serial dilution, nitrocellulose printing, automated immunostaining, and laser-based signal detection. Detailed procedures and antibody validation protocols are available on their website (https://www.mdanderson.org/research/research-resources/core-facilities/functional-proteomics-rppa-core.html), with the current expanded antibody list accessible via their education resources (https://www.mdanderson.org/research/research-resources/core-facilities/functional-proteomics-rppa-core/education-and-references.html).

2.10.2. Protein-protein interaction analysis

The STRING Database (https://string-db.org) provides a comprehensive and user-friendly platform for analysing and visualising protein interactions through integration of various sources of biological data. STRING was utilised to explore the protein-protein interaction (PPI) networks associated with the differentially expressed proteins from the RPPA analysis. STRING generates interaction scores that indicate the confidence level of these protein interactions, reflecting the likelihood that an interaction is valid. Scores range from 0 to 1, with

a score of 1 indicating maximum confidence. These scores can be classified as 'normal' or 'transferred'; 'normal' scores are derived from data originally observed in the organism of interest, while 'transferred' scores are based on data from other organisms and are inferred through homology or orthology.

2.11. Statistical analysis

The two-tailed Student's t-test with unequal variance was employed to determine p-values for the proliferation assays, Western blot, and RPPA results, analysing biological replicates with a significance threshold set at p-value ≤ 0.05. In instances of multiple testing, the BH correction method was applied to yield adj.p values, with adj.p ≤ 0.05 deemed significant for analyses. Statistical significance is denoted as follows: * $p \leq 0.05$, ** $p \leq 0.01$, *** $p \leq 0.001$.

3.Cooperative *TP53* loss and PI3K pathway-activation define a distinct high-risk TNBC state

3.1. Introduction

Co-occurring alterations affecting *TP53* and the PI3K signalling pathway have been associated with adverse clinical outcomes in BC, suggesting that disruption of TP53's tumour suppressor function alongside activation of PI3K pro-survival signalling may define a biologically aggressive tumour subset (592). While *TP53* mutations are present in the majority of TNBC cases (~80%) (227), PI3K pathway activation occurs through multiple mechanisms, including *PIK3CA* mutations (~10-15%) (239), as well as alterations affecting other pathway regulators such as *PTEN* loss (35-57%) (107,593) or *AKT* activation (<5%) (412).

Despite the high prevalence of *TP53* mutations in TNBC and the frequent dysregulation of the PI3K/AKT/mTOR pathway described in Section 1.5.1.1., the combined clinical and molecular impact of co-occurring *TP53* dysfunction and PI3K pathway activation remains incompletely defined. While previous studies have reported associations between these alterations and adverse clinical outcomes (237,594), integrated analyses incorporating transcriptomic, proteomic, and survival data within this subgroup are lacking.

In this chapter, a *TP53*-PI3K pathway-activated (*TP53*-PI3K^{act}) TNBC subgroup is defined based on the presence of a *TP53* mutation together with genomic alterations predicted to activate PI3K signalling. The impact of incorporating multiple PI3K pathway alterations into this definition is first assessed by comparing survival outcomes relative to *TP53*-only tumours, which represent the predominant genetic background in TNBC. The resulting *TP53*-PI3K^{act} subgroup is then characterised across two independent BC cohorts, METABRIC and TCGA, evaluating alteration co-occurrence, clinical characteristics, survival outcomes, and multi-omic features. Through this cross-cohort analysis, the aim is to identify reproducible molecular and clinical attributes of a potentially high-risk TNBC subgroup that may have implications for prognostic stratification and therapeutic targeting.

3.2. Defining a high-risk *TP53*-PI3K-activated TNBC cohort

Analyses were first performed in the METABRIC TNBC cohort (n = 299), which is well annotated with long-term survival follow-up data (median follow-up: 186.6 months for OS and 165.4 months for RFS). *TP53-PIK3CA* co-mutant TNBC tumours were analysed first to assess the association between co-occurring *TP53* mutation and PI3K pathway activation and survival. Additional PI3K-activating alterations were then incorporated to evaluate whether

these tumours exhibited comparable or greater survival risk in the context of *TP53* mutation. OS and RFS were assessed using Cox PH regression.

TP53-PIK3CA co-mutant TNBC tumours showed significantly poorer survival compared with *TP53*-only tumours, with increased risk observed for both OS (HR = 1.93, p = 3.09×10^{-03}) and RFS (HR = 1.96, p = 5.20×10^{-03}). Incorporation of additional PI3K-activating alterations demonstrated that this adverse prognostic association was maintained when *AKT1* mutations or *PTEN* deletions were included, with comparable or higher HRs observed for both OS and RFS. In contrast, inclusion of other PI3K-related alterations, including *PIK3R1* mutations, *PTEN* mutations, *AKT3* amplification, or *PIK3CA* amplification, was not consistently associated with poorer survival outcomes (Table 3-1). Notably, the METABRIC TNBC cohort contained only one *AKT2*-MUT tumour and no detected *AKT3* mutations; consequently, these alterations were not included in this analysis.

Based on these results, *TP53*-MUT tumours harbouring a *PIK3CA* mutation, *AKT1* mutation, or *PTEN* deletion were defined as *TP53*-PI3K-activated (*TP53*-PI3K^{act}). This *TP53*-PI3K^{act} subgroup, highlighted in yellow in Table 3-1, exhibited significantly poorer survival compared with *TP53*-only TNBC, with increased risk of death (OS: HR = 2.02, p = 2.55×10^{-04}) and relapse (RFS: HR = 1.94, p = 1.80×10^{-03}). Compared with the smaller *TP53-PIK3CA* mutant group, the *TP53*-PI3K^{act} group captures additional high-risk tumours, while maintaining or slightly increasing the observed survival risk.

Table 3-1: Survival impact of *TP53*-MUT tumours harbouring *PIK3CA* or other co-occurring PI3K-pathway alterations in METABRIC TNBC.

		OS			RFS		
***TP53*-MUT (n = 238) +**	**vs. *TP53*-only (n)**	**HR**	**95% CI**	**p-value**	**HR**	**95% CI**	**p-value**
***PIK3CA*-MUT (n = 53)**	37 vs. 201	1.93	1.25-2.97	**$3.09x10^{-03}$**	1.96	1.22-3.15	**$5.20x10^{-03}$**
***PIK3CA*-MUT or *AKT1*-MUT (n = 10)**	46 vs. 192	1.94	1.31-2.87	**$9.70x10^{-04}$**	1.84	1.18-2.86	**$6.88x10^{-03}$**
***PIK3CA*-MUT or *PTEN-del* (n = 15)**	47 vs. 191	2.00	1.34-2.98	**$7.25x10^{-04}$**	1.96	1.27-3.04	**$2.54x10^{-03}$**
***PIK3CA*-MUT or *PIK3R1*-MUT (n = 8)**	43 vs. 195	1.71	1.14-2.59	**0.010**	1.49	0.93-2.39	0.099
***PIK3CA*-MUT or *AKT3*-amp (n = 55)**	75 vs. 163	1.61	1.12-2.32	**$9.45x10^{-03}$**	1.48	0.98-2.22	0.060
***PIK3CA*-MUT or *PTEN*-MUT (n = 18)**	51 vs. 187	1.30	0.86-1.96	0.217	1.35	0.86-2.11	0.199
***PIK3CA*-MUT or *PIK3CA*-amp (n = 34)**	58 vs. 180	1.27	0.83-1.94	0.234	1.31	0.82-2.09	0.224
***PIK3CA*-MUT or *AKT1*-MUT or *PTEN*-del**	55 vs. 183	2.02	1.38-2.93	**$2.55x10^{-04}$**	1.94	1.28-2.95	**$1.80x10^{-03}$**

*The first row (TP53-mut + PIK3CA-mut) serves as the reference group for comparison against TP53-only patients. Subsequent rows test TP53-MUT tumours harbouring the listed PI3K-pathway alteration or PIK3CA mutation. HRs are highlighted in green scale, where darker green indicates a higher HR. Significant p-values are indicated in **bold**. The TP53-PI3K^{act} subgroup is highlighted in yellow. All Cox PH models satisfied the PH assumption ($p \geq 0.05$).*

To further explore whether the survival effect observed in *TP53*-PI3K^{act} tumours reflected a potential interaction between *TP53* mutation and PI3K pathway activation, an interaction term (*TP53* x PI3K^{act}) was incorporated into Cox PH models for OS and RFS. This analysis tests whether the combined presence of *TP53* mutation and PI3K pathway activation is associated with a greater survival risk than would be expected from the individual effects of each alteration alone.

The interaction terms showed a trend toward increased risk (OS: HR = 1.76; RFS: HR = 1.60); however, these effects did not reach statistical significance (p = 0.165 and 0.342, respectively). Given the lack of statistical significance, these results are not presented in a dedicated table or figure. This likely reflects the small number of tumours harbouring PI3K pathway activation in the absence of *TP53* mutation (n = 20), which limited statistical power to detect independent or interaction effects. Consequently, while the results suggest a possible cooperative effect between *TP53* mutation and PI3K pathway activation, larger cohorts would be required to formally evaluate this interaction.

In summary, these analyses identify *TP53*-PI3K^{act} as a biologically and clinically high-risk TNBC subgroup. Expanding the definition beyond *TP53-PIK3CA* co-mutation to include *AKT1* mutations and *PTEN* deletions captures additional alterations that activate PI3K/AKT signalling. Including these additional alterations not only maintains, but slightly increases, the observed survival risk compared with *TP53*-only TNBC. Together, these findings justify further analyses to better characterise the molecular and clinical features underpinning its aggressive behaviour.

3.3. Characterisation of *TP53*-PI3K^{act} TNBC

Following the definition of *TP53*-PI3K^{act} as a high-risk TNBC subgroup, we next sought to perform a comprehensive characterisation of these tumours. This analysis used two independent TNBC cohorts with available mutation, survival, clinical, and mRNA data: METABRIC, where TNBC was defined based on ER, PR, and HER2 negativity, and TCGA, where TNBC was defined using the basal PAM50 subtype due to missing receptor status for many patients. Although these classification approaches differ, there is substantial overlap between clinically defined TNBC and the basal PAM50 subtype (595). Analysing the cohorts independently therefore allows assessment of whether *TP53*-PI3K^{act}-associated molecular and clinical features are reproducible across datasets, despite differences in TNBC definition and molecular profiling platforms.

The prevalence of *TP53* and PI3K^{act} alterations, along with the number of tumours in each subgroup, is summarised in Table 3-2. Across both cohorts, *TP53* mutations (METABRIC: n = 238; TCGA: n = 153) were highly prevalent (~83%), with a significant subset (~23%) of these *TP53*-MUT tumours also carrying PI3K^{act} alterations (METABRIC: n = 55; TCGA: n = 35). PI3K^{act}-only tumours (METABRIC: n = 20; TCGA: n = 4) were relatively rare (~5%), while the "non-altered" category, comprising tumours WT for *TP53*, *PIK3CA*, and *AKT1* and lacking *PTEN* homozygous deletions (METABRIC: n = 41; TCGA: n = 14), accounted for ~11.5% of TNBC patients. Differences in TNBC definition may contribute to variation in subgroup distribution and downstream results; however, all analyses were performed separately, enabling reproducible patterns to be identified while accounting for cohort-specific characteristics.

Due to limited patient numbers in both cohorts, all non-synonymous coding variants were included in the analysis, regardless of mutation type (missense, inframe, splice, truncating, etc.). The majority of identified mutations were classified as putative drivers according to

annotations in cBioPortal, based on curated databases that predict functional relevance in cancer (e.g. OncoKB, CancerHotspots) (596). Moreover, the distribution of *TP53* mutation types was similar between *TP53*-PI3K^{act} and *TP53*-only tumours, indicating no overt enrichment of specific functional variant classes in the high-risk subgroup.

It should also be noted that the composition of *TP53*-PI3K^{act} tumours differs between cohorts (Figure 3-1). In METABRIC, *TP53*-PI3K^{act} tumours are *PIK3CA*-dominant (37 *PIK3CA*-MUT / 9 *AKT1*-MUT / 12 *PTEN*-deleted), whereas in TCGA, tumours are *PTEN*-deletion-dominant (10 *PIK3CA*-MUT / 26 *PTEN*-deleted). These differences may reflect technical factors, including variation in CN and structural variant detection sensitivity between the cohorts, and could contribute to some cohort-specific patterns observed in downstream molecular and clinical analyses of *TP53*-PI3K^{act} tumours.

Table 3-2: Prevalence of *TP53* and PI3K^{act} alterations and subgroup distribution in METABRIC and TCGA TNBC cohorts.

TNBC Cohort	Total	*TP53*	*PIK3CA*	*AKT1*	*PTEN*-del	*TP53*-PI3K^{act}	*TP53*-only	PI3K^{act}-only	Non-altered
METABRIC	299	238	53	10	15	55	183	20	41
TCGA	171	153	12	0	28	35	118	4	14

Data were derived from TCGA and METABRIC BC studies accessed via cBioPortal (www.cbioportal.org) (568,569,571).



Figure 3-1: Oncoprint of *TP53*, *PIK3CA*, *AKT1*, and *PTEN* alterations in METABRIC (n = 299) and TCGA (n = 171) TNBC cohorts. Tumours are ordered by alteration-defined subgroup: *TP53*-PI3K^{act}, *TP53*-only, PI3K^{act}-only, and non-altered. Genomic alteration types are indicated in the figure legend. Percentages indicate the frequency of alteration in each gene across the entire cohort. Alteration types are indicated in the figure. This oncoprint was generated using cBioPortal (https://www.cbioportal.org) (568,569,571).

3.3.1. Co-occurrence of *TP53* mutations and PI3K^{act} alterations in TNBC

As the first step in characterising the *TP53*-PI3K^{act} TNBC subgroup, we assessed whether *TP53* mutations and PI3K^{act} alterations co-occurred more frequently than expected. Using the METABRIC and TCGA cohorts, the observed number of *TP53*-PI3K^{act} tumours was generally in line with expectations under independence (METABRIC: observed = 55 vs. expected = 59.7; TCGA: observed = 35 vs. expected = 34.9; Table 3-3). Both Fisher's exact tests and permutation analyses indicated no statistically significant association between *TP53* and PI3K^{act} alterations in either cohort (METABRIC Fisher OR = 0.62, p = 0.137; perm p = 0.085; TCGA Fisher OR = 1.04, p = 1.00; perm p = 0.621).

Table 3-3: Co-occurrence and association of *TP53* mutations and PI3K^{act} alterations in TNBC cohorts.

Cohort	*TP53*-mut	PI3K^{act}	Observed *TP53*-PI3K^{act}	Expected *TP53*-PI3K^{act} †	Fisher OR (95% CI)	Fisher p-value	Expected *TP53*-PI3K^{act} (perm)	Perm p-value
METABRIC	238	75	55	59.70	0.62 (0.32-1.20)	0.137	59.67	0.085
TCGA	153	39	35	34.89	1.04 (0.30-4.61)	1.00	34.92	0.621

† Expected number of *TP53*-PI3K^{act} patients under the assumption of independent mutation events: (*TP53*-MUT x PI3K^{act}) / total patients.
Abbreviations: perm = permutation

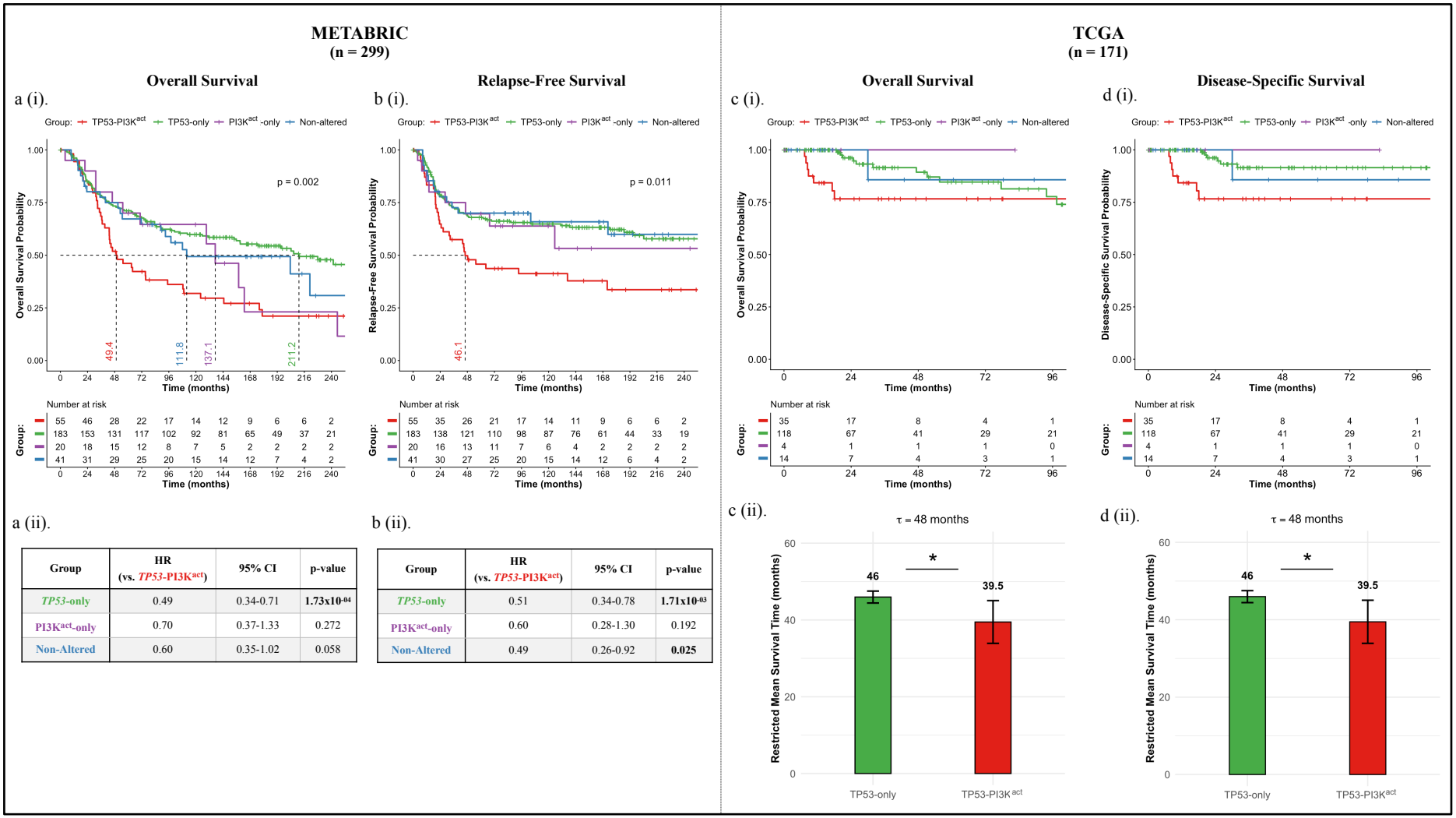
These findings suggest that *TP53* mutations and PI3K^{act} alterations largely arise independently in TNBC, suggesting that the *TP53*-PI3K^{act} subgroup captures a high-risk population defined by the convergence of separate oncogenic events, rather than a single co-dependent mechanism. It should be noted that the high prevalence of *TP53* mutations and relatively small number of PI3K^{act}-only tumours constrain the statistical power to detect co-occurrence or mutual exclusivity. Regardless, the majority of PI3K^{act} TNBC tumours also harbour *TP53* mutations, delineating a biologically distinct *TP53*-PI3K^{act} subgroup whose characterisation is essential for understanding tumour behaviour, signalling interactions, and potential impact on therapeutic response in TNBC.

3.3.2. Prognostic evaluation of *TP53*-PI3K^{act} in TNBC

Having defined *TP53*-PI3K^{act} as a high-risk subgroup in METABRIC, we next assessed whether this prognostic pattern was reproducible across TNBC cohorts. Survival outcomes were compared across *TP53*-PI3K^{act}, *TP53*-only, PI3K^{act}-only, and non-altered tumours in both the METABRIC and TCGA cohorts.

METABRIC cohort: Survival differences are illustrated in KM plots with accompanying risk tables for OS (Figure 3-2(a(i)) and RFS (Figure 3-2(b(i)), alongside the corresponding Cox HRs (Figure 3-2(a(ii), b(ii)). Cox PH models, which estimate HRs for differences in survival risk between groups, were used to evaluate both OS and RFS, with *TP53*-PI3K^{act} patients as the reference group. *TP53*-only patients exhibited significantly improved survival for OS (HR = 0.49, p = 1.73×10^{-04}) and RFS (HR = 0.51, p = 0.0017). These results correspond to the reciprocal of the HR reported in Table 3-1. Tumours in the non-altered subgroup demonstrated improved RFS (HR = 0.49, p = 0.025) and borderline improved OS (HR = 0.60, p = 0.058) relative to *TP53*-PI3K^{act} tumours. PI3K^{act}-only tumours showed trends toward better outcomes compared with *TP53*-PI3K^{act}, though these differences did not reach statistical significance.

TCGA cohort: Survival differences are visualised in KM plots for OS (Figure 3-2(c(i))) and DSS (Figure 3-2(d(i))), with RMST contrasts shown in bar charts (Figure 3-2(c(ii), d(ii))). PH assumptions were violated in TCGA, indicating that the relative hazard between groups was not constant over time, which violates a key assumption of Cox PH models (597). Therefore, survival was compared using RMST analysis, which estimates the average survival time up to a prespecified follow-up time without requiring PH (577). The truncation time was set to 48 months, reflecting the period during which sufficient patients remained at risk for robust estimation of RMST. Beyond this point, the small number of *TP53*-PI3K^{act} patients still at risk (n = 8) would limit the reliability of survival estimates. RMST, therefore, represents the average survival time up to 48 months. For both OS and DSS, *TP53*-PI3K^{act} patients had a significantly lower RMST of 39.5 months (CI = 33.9-45.0) versus 46 months (CI = 44.4-47.5) for *TP53*-only tumours, corresponding to a difference of -6.5 months (p = 0.03). The results are nearly identical for OS and DSS, with only minimal differences in the estimates (<0.02 months), because no non-cancer deaths occurred during the 48-month follow-up, resulting in nearly identical survival patterns across both outcomes.



Group	HR (vs. *TP53*-PI3K^{act})	95% CI	p-value
TP53-only	0.49	0.34-0.71	**1.73x10^{-04}**
PI3K^{act}-only	0.70	0.37-1.33	0.272
Non-Altered	0.60	0.35-1.02	0.058

Group	HR (vs. *TP53*-PI3K^{act})	95% CI	p-value
TP53-only	0.51	0.34-0.78	**1.71x10^{-03}**
PI3K^{act}-only	0.60	0.28-1.30	0.192
Non-Altered	0.49	0.26-0.92	**0.025**

Figure 3-2: Survival analysis of *TP53*-PI3K^{act} TNBC in METABRIC and TCGA cohorts. METABRIC: **(a)** OS and **(b)** RFS. **(i)** KM curves (0-240 months) for *TP53*-PI3K^{act}, *TP53*-only, PI3K^{act}-only, and non-altered patients, with medians, risk table, and global p-value. **(ii)** Corresponding unadjusted Cox HRs, 95% CIs, and p-values versus *TP53*-PI3K^{act}. TCGA: **(c)** OS and **(d)** DSS. (i) KM curves (0-96 months) for *TP53*-PI3K^{act} vs. *TP53*-only with risk table. **(ii)** RMST bar charts at 48 months showing mean survival with error bars and significance denoted.

To evaluate whether the high-risk status of *TP53*-PI3K^{act} tumours is independent of standard clinical covariates, we performed multivariable Cox PH analyses in METABRIC and TCGA, comparing *TP53*-PI3K^{act} to *TP53*-only TNBC. Clinical covariates were selected based on availability and relevance for each cohort: tumour size, age at diagnosis, nodal status, tumour size, and neoplastic histologic grade for METABRIC, and age, nodal status, and tumour stage for TCGA.

METABRIC cohort: For OS, the global PH assumption was violated, indicating that the relative effect of covariates on the hazard of death was not constant over time. To address this, the model was stratified by nodal status and histologic grade, and age at diagnosis was included as a time-dependent covariate; consequently, no overall HR is reported for age. In this stratified model, *TP53*-PI3K^{act} tumours remained significantly associated with poorer OS (HR = 1.68, p = 0.011). For RFS, PH assumptions were generally satisfied. Although histologic grade showed a minor violation of the PH assumption (p = 0.034), the global test assessing all covariates simultaneously was not significant. Therefore, the model was not stratified, as the overall PH assumption was considered acceptable. *TP53*-PI3K^{act} tumours also exhibited significantly worse outcomes (HR = 1.91, p = 3.85×10^{-03}), independent of age, nodal status, tumour size, and histologic grade. Nodal status was independently associated with worse RFS, while age at diagnosis was significantly associated with OS, indicating a non-proportional effect of age on survival (Table 3-4).

Table 3-4: Multivariable Cox PH analysis of OS and RFS in the TNBC METABRIC cohort.

Survival Group	Group / Covariate	HR	95% CI	p-value
OS†	*TP53*-PI3K^{act} vs. *TP53*-only (n = 55 vs. 183)	1.68	1.13-2.50	**0.011**
	Tumour size (mm)	1.01	1.00-1.02	0.064
	Age at diagnosis (time-dependent)	-	-	**2.07×10^{-04}**
RFS	*TP53*-PI3K^{act} vs. *TP53*-only	1.91	1.23-2.97	**3.85×10^{-03}**
	Age at diagnosis	1.00	0.99-1.02	0.965
	Nodal status (+ vs. -)	1.71	1.11-2.64	**0.016**
	Tumour size	1.01	1.00-1.02	0.111
	Neoplasm histologic grade (G3 vs. G1/2)	1.32	0.76-2.74	0.454

HR is reported for TP53-PI3K^{act} relative to the TP53-only reference group. Models are adjusted for clinical covariates. Nodal status was defined as ≥1 positive lymph node versus none; histologic grade was categorised as G1/2 versus G3.

† OS model stratified by nodal status and neoplasm histologic grade and age at diagnosis included as a time-dependent covariate

TCGA cohort: For both OS and DSS, the global PH assumption across all covariates was not violated, indicating that the overall model was acceptable. However, the *TP53*-PI3K^{act} group showed some evidence of non-proportional hazards, suggesting that its effect on survival may vary over time. Therefore, these results should be interpreted with caution. In multivariable models, *TP53*-PI3K^{act} tumours were associated with poorer OS (HR = 2.74, p = 0.044) and DSS (HR = 4.37, p = 0.013), after adjusting for age, nodal status, and tumour stage. Notably, CIs were wide, reflecting limited sample size and event numbers in the TCGA cohort. Nodal status and tumour stage were independently associated with worse survival outcomes (Table 3-5), indicating that patients with positive lymph nodes or more advanced tumours had a higher risk of death or disease-specific events, in addition to the elevated risk conferred by *TP53*-PI3K^{act} status.

Table 3-5: Multivariable Cox PH analysis of OS and DSS for *TP53*-PI3K^{act} versus *TP53*-only TNBC in the TCGA cohort.

Survival Group	Group / Covariate	HR	95% CI	p-value
OS	*TP53*-PI3K^{act} vs. *TP53*-only (n = 35 vs. 118)	2.74	1.03-7.34	**0.044**
	Age at diagnosis	1.02	0.98-1.05	0.365
	Nodal status (+ vs. -)	4.47	1.70-11.72	**2.36x10^{-03}**
	Tumour stage (T1/T2 vs. T3/T4)	2.32	0.82-6.56	0.112
DSS	*TP53*-PI3K^{act} vs. *TP53*-only	4.37	1.37-13.98	**0.013**
	Age at diagnosis	1.01	0.96-1.05	0.809
	Nodal status (+ vs. -)	4.95	1.31-18.66	**0.018**
	Tumour stage (T1/T2 vs. T3/T4)	3.88	1.11-13.52	**0.034**

Nodal status was derived from AJCC lymph node stage codes (N0 = negative; N1+ = positive), and tumour stage from AJCC T-stage codes (T1/T2 vs. T3/T4).

These analyses show that *TP53*-PI3K^{act} remains independently associated with poor survival in TNBC after adjustment for standard clinical factors. This association is robust in METABRIC, which benefits from a larger patient sample and longer, more complete survival follow-up. In TCGA, the cohort is somewhat smaller and follow-up is shorter, resulting in wider CIs and more limited but concordant evidence.

3.3.3. Clinical characterisation of *TP53*-PI3K^{act} TNBC

To characterise the clinical context of *TP53*-PI3K^{act} TNBC, clinical variables were extracted from cBioPortal and compared primarily between *TP53*-PI3K^{act} and *TP53*-only tumours within each cohort. All variables reported under the "clinical" section in cBioPortal – including patient-level features (age, tumour size, nodal status, etc.) as well as tumour annotations such as PAM50 subtype and *HER2* status – were included together in the clinical characterisation

of *TP53*-PI3K^{act} TNBC. *TP53*-only tumours were chosen as the reference group because TNBC is predominantly *TP53*-MUT, providing the largest and most robust comparison. Clinical features showing significant differences in this comparison were reported in Table 3-6 and then visualised across all four alteration-defined subgroups in Figure 3-3 to show the broader context of these differences. Percentages reported in Table 3-6 and throughout the results section were calculated from patient numbers in each subgroup.

Table 3-6: Clinical and tumour features associated with *TP53*-PI3K^{act} compared to *TP53*-only TNBC in METABRIC and TCGA cohorts.

Cohort	Variable	*TP53*-PI3K^{act} vs. *TP53*-only		
		p-value†	**q-value††**	**Main Observation**
METABRIC	Integrative Cluster	4.03×10^{-06}	1.16×10^{-04}	Cluster 10: 40% vs. 78%
	PAM50 + Claudin-low subtype	8.03×10^{-06}	1.16×10^{-04}	Basal: 40% vs. 62%; HER2: 27% vs. 5%
	Patient's Vital Status	1.96×10^{-03}	1.34×10^{-02}	Died of disease: 55% vs. 34%
	Age at diagnosis	2.32×10^{-03}	1.34×10^{-02}	Median: 60 vs. 53
	Tumour Histologic Subtype	5.66×10^{-03}	1.82×10^{-02}	Mostly ductal/NST; minimal differences in other subtypes (lobular: 9% vs. 2%; medullary: 0% vs. 8%)
	Types of Breast Surgery†††	1.01×10^{-02}	2.94×10^{-02}	Mastectomy: 66% vs. 47%
	HER2 Status (SNP6)	1.34×10^{-02}	3.00×10^{-02}	Gain: 18% vs. 7%;
	Inferred Menopausal State	1.52×10^{-02}	3.14×10^{-02}	Post: 78% vs. 59%
TCGA	Hypoxia Score††††	8.03×10^{-04}	-	Score: 21 vs. 12

† TP53-PI3K^{act} vs TP53-only comparisons used χ^2 tests for categorical variables and Wilcoxon rank-sum tests for continuous variables.

†† Q-values are FDR-adjusted using the BH method.

††† Data on type of breast surgery were unavailable for 3 TP53-PI3K^{act}, 3 TP53-only, and 1 PI3K^{act}-only patients; percentages are calculated based on available data

†††† Hypoxia Score for TCGA was calculated as the mean of three published hypoxia scores (Ragnum, Winter, Buffa), all of which were individually significant.

Note: All tumours in this analysis are clinically triple-negative (ER-, PR-, HER2-). Differences in PAM50 or Integrative Cluster reflect gene-expression–based subtypes, which can sometimes classify clinically TNBC tumours into subtypes typically associated with ER- or HER2-positive disease.

Patient-level data were obtained from cBioPortal and statistical analyses were generated in R.

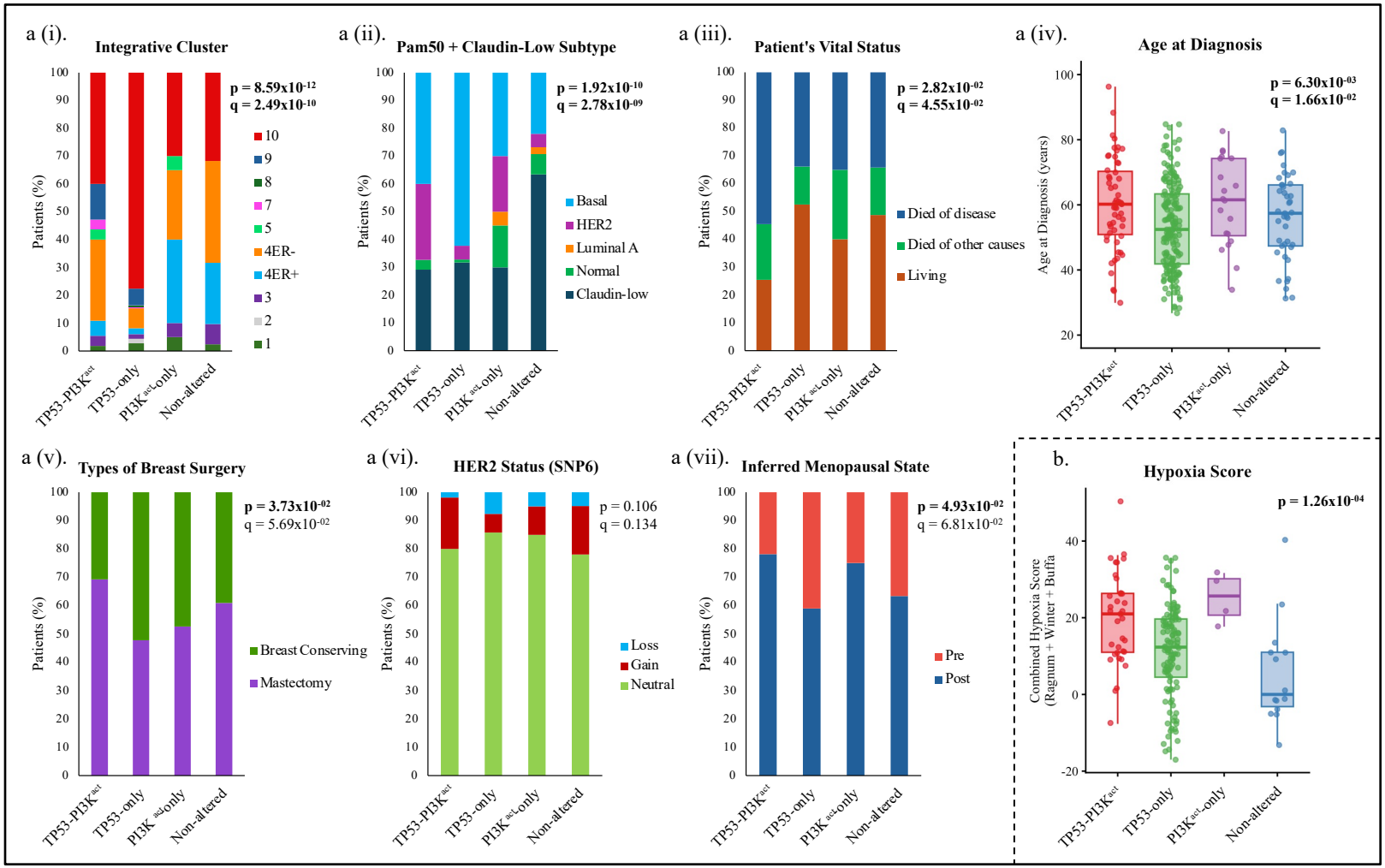


Figure 3-3: Clinical and tumour feature differences across alteration-defined TNBC subgroups. Bar charts (categorical) and box-and-whisker plots (continuous) show feature distributions across *TP53*-PI3K^{act}, *TP53*-only, PI3K^{act}-only, and non-altered TNBC subgroups. Panels **a(i-vii)**: significant features in METABRIC; panel **b**: significant combined hypoxia score in TCGA. Global p-values and FDR-adjusted q-values from χ^2 (categorical) or KW (continuous) tests are indicated on each plot with, significant p- and q-values shown in **bold**. For TCGA, three published hypoxia scores (Ragnum, Winter, Buffa) were individually significant and were combined into a single "Hypoxia Score" for plotting.

Subtype and molecular context: *TP53*-PI3K^{act} tumours were more frequently classified as cluster 4ER- (16/55: 29%) than *TP53*-only tumours (13/183: 7%). Cluster 4ER- primarily represents genomically quiet triple-negative tumours with high lymphocytic infiltration and immune activation, and is linked to favourable prognosis (598). *TP53*-PI3K^{act} tumours were less frequently classified as integrative cluster 10 (22/55: 40%) compared with *TP53*-only tumours (142/183: 78%). Cluster 10 primarily represents basal-like TNBC with *TP53* mutations.

The basal PAM50/Claudin-low subtype was less common in *TP53*-PI3K^{act} tumours (22/55: 40%) than in *TP53*-only tumours (114/183: 62%), while the HER2 subtype and *HER2* CN gain (measured by SNP6) were enriched in TP53-PI3K^{act} tumours (15/55: 28%; and 10/55: 18%, respectively) relative to *TP53*-only tumours (9/183: 5%; and 12/183: 7%;).

TP53-PI3K^{act} tumours displayed similar basal and HER2 frequencies to PI3K^{act}-only tumours, but still had unique distributions, including a higher frequency of cluster 9 (7/55: 13% in *TP53*-PI3K^{act}; 0% in PI3K^{act}-only). Cluster 9 represents mostly luminal B BC with high genomic instability, frequent *TP53* mutations, and intermediate prognosis.

Histologic subtype data are not shown in Figure 3-3 because most tumours in both groups were ductal/no special type (NST), and the differences in patient numbers across groups were very small, making these differences unlikely to meaningfully impact downstream analyses.

Patient outcomes and demographics: *TP53*-PI3K^{act} tumours were associated with the highest proportion of patients deceased due to disease (30/55: 55%) compared to *TP53*-only (62/183: 34%), PI3K^{act}-only (7/20: 35%), and non-altered (14/41: 34%), consistent with the poorer outcomes observed in the survival analyses. Age at diagnosis was higher in *TP53*-PI3K^{act} compared to *TP53*-only (median 60 vs. 53 years) and similar to PI3K^{act}-only (median 62 years). *TP53*-PI3K^{act} patients were also more frequently postmenopausal (43/55: 78%) compared to *TP53*-only (108/183: 59%), reflecting the higher proportion of older women in this subgroup. These age results were not reflected in the TCGA cohort, where no statistically significant difference was observed between *TP53*-PI3K^{act} and *TP53*-only. In terms of surgical treatment, *TP53*-PI3K^{act} patients were more frequently treated with mastectomy (36/55: 66%) than *TP53*-only patients (86/183: 47%). This may suggest presentation with more extensive local disease or reduced suitability for breast-conserving surgery; however, this may also reflect age distribution and treatment selection biases rather than differences in tumour burden alone.

Hypoxia: In TCGA, *TP53*-PI3K^{act} tumours exhibited higher combined hypoxia scores than *TP53*-only tumours (median 21 vs. 12), calculated as the mean of three published hypoxia signatures (Ragnum, Winter, Buffa (599–601)), each of which was individually significant. Scores in the small PI3K^{act}-only group (n = 4) were similar, consistent with a more hypoxic tumour microenvironment in PI3K-activated TNBC, though this comparison should be interpreted with caution due to the limited sample size (602).

Taken together, these results indicate that *TP53*-PI3K^{act} defines a distinct clinical TNBC subset. Compared with *TP53*-only tumours, *TP53*-PI3K^{act} tumours are less frequently basal and cluster 10, enriched in the more prognostically favourable cluster 4ER-, and show increased HER2 features. Despite this, TP53-PI3K^{act} tumours are associated with the poorest clinical outcomes across all groups, including the highest proportion of disease-related deaths. These tumours, similar to PI3K^{act}-only, tend to present at older ages, consistent with the idea that PI3K pathway activation occurs after *TP53* mutation, contributing additional growth or survival advantages. Importantly, these clinical and demographic patterns alone do not explain the high-risk behaviour of *TP53*-PI3K^{act} TNBC, highlighting the need for a deeper molecular characterisation to uncover the mechanisms driving their aggressive phenotype.

3.3.4. Molecular characterisation of *TP53*-PI3K^{act} TNBC

3.3.4.1. Co-occurring genomic alterations in *TP53*-PI3K^{act} TNBC

To begin the molecular characterisation of *TP53*-PI3K^{act} TNBC, we assessed whether recurrent somatic mutations, structural variants, and CNAs across all genes occurred at different frequencies in *TP53*-PI3K^{act} tumours compared with *TP53*-only tumours. This analysis was conducted in both the METABRIC and TCGA cohorts using cBioPortal.

Following multiple-testing correction, no additional mutations, structural variants, or gene fusions were significantly enriched in *TP53*-PI3K^{act} tumours. Several deletions reached significance (e.g. *RNLS*, *KLLN*, *ATAD1*, members of the *LIP* gene family) in both cohorts but these genes are all located in chromosome 10q23 and are co-deleted with *PTEN* (603), explaining their enrichment (results not shown).

Overall, these analyses indicate that *TP53*-PI3K^{act} tumours do not harbour recurrent mutations or CNAs beyond those associated with *PTEN* co-deletion, suggesting that the high-risk phenotype is unlikely to be explained by additional recurrent genomic events assessed in this study

3.3.4.2. TNBC subtype distribution in *TP53*-PI3K^{act}

We next sought to determine whether their aggressive clinical behaviour is reflected in, or potentially driven by, differences in intrinsic TNBC subtype composition. TNBC comprises multiple biologically distinct subtypes characterised by divergent signalling dependencies, immune states, and clinical outcomes, as described in established transcriptomic classifications such as the Lehmann and Burstein TNBC subtype frameworks (Section 1.4.1). These subtypes are not fully captured by broader BC classifications such as PAM50 or integrative clustering alone.

To assess whether *TP53*-PI3K^{act} tumours preferentially associate with specific TNBC transcriptional subtypes, we performed TNBC subtype classification using the TNBCtype subtyping tool (http://cbc.mc.vanderbilt.edu/tnbc/index.php). Subtyping was conducted independently in the METABRIC and TCGA cohorts to account for cohort-specific expression platforms and definitions, enabling evaluation of the reproducibility of subtype distributions across datasets. mRNA expression data were obtained from cBioPortal for both cohorts; TCGA RNA-seq data were used directly for TNBCtype input, whereas METABRIC microarray expression data were batch-corrected prior to subtype classification. Comparisons were made

between *TP53*-PI3K^{act} tumours and the other alteration-defined subgroups to determine whether enrichment of particular TNBC subtypes may contribute to the high-risk phenotype observed in this group.

TNBC subtypes were assigned using the TNBCtype-6 and TNBCtype-4 frameworks. TNBCtype-6 corresponds to the original six-subtype Lehmann classification, whereas TNBCtype-4 reflects the revised four-subtype model excluding the IM and MSL groups due to their stromal and immune origins (604). After removing samples flagged by the tool for potential ER expression (METABRIC: 4 samples; TCGA: 13 samples) and consolidating duplicate gene entries by highest variance, subtype classification was completed for the remaining tumours. The resulting subtype distributions for each alteration-defined subgroup are shown in Figure 3-4.



Figure 3-4: TNBC subtype distribution across alteration-defined TNBC subgroups. Stacked bar charts show the proportion of each TNBC subtype within *TP53*-PI3K^{act}, *TP53*-only, PI3K^{act}-only, and non-altered tumours. Data are presented for **(a)** METABRIC and **(b)** TCGA cohorts, with TNBC subtype assignment based on the **(i)** TNBCtype-6 framework and the refined **(ii)** TNBCtype-4 framework. Below each chart, tables indicate the number of tumours per subtype and subgroup.

Across both cohorts, TNBCtype-6 classification revealed differences in subtype composition between alteration-defined groups. In the METABRIC cohort (Figure 3-4a(i)), subtype distributions differed significantly (χ^2 test with simulated p-value = 1.0×10^{-04}), with increased representation of BL2 and LAR subtypes in *TP53*-PI3K^{act} tumours relative to *TP53*-only tumours. In the TCGA cohort (Figure 3-4b(i)), a similar trend of increased BL2 representation in *TP53*-PI3K^{act} tumours was observed; however, the overall subtype comparison did not reach statistical significance (χ^2 test with simulated p = 0.080).

Application of the refined TNBCtype-4 framework showed a consistent pattern of subtype associations across both cohorts (Figure 3-4a(ii), b(ii)). In METABRIC, subtype distributions again differed significantly between groups (χ^2 test with simulated p-value = 1.0×10^{-04}), with enrichment of BL2 and LAR in *TP53*-PI3K^{act} tumours. In TCGA, subtype distributions differed significantly under TNBCtype-4 classification (χ^2 test with simulated p-value = 0.010), with enrichment of BL2 observed in *TP53*-PI3K^{act} tumours. Overall, TNBCtype-4 reassignment increased the proportion of BL2 and LAR tumours within the *TP53*-PI3K^{act} group. While BL2 enrichment was consistent in both cohorts, LAR enrichment was stronger in METABRIC and attenuated in TCGA, likely reflecting the PAM50-based basal TNBC definition.

To assess the impact of removing the TNBCtype ambiguity filter, tumours with near-equal correlations to two subtype centroids (<0.05 difference) were examined within the *TP53*-PI3K^{act} subgroup (as described in Section 3.1.7.4). A small number of cases were identified in both cohorts (METABRIC n = 3; TCGA n = 4). These cases were rare, comprising three BL2/LAR, two BL1/M, one BL2/M, and one BL1/BL2 classifications, suggesting that the modified "best-hit" approach had minimal impact on overall subtype structure in *TP53*-PI3K^{act} tumours.

To determine whether the adverse prognosis associated with *TP53*-PI3K^{act} tumours could be explained by their altered TNBC subtype composition, we evaluated survival while accounting for TNBCType-4 subtype. Cox PH models were fitted in the METABRIC cohort including alteration-defined subgroup (*TP53*-PI3K^{act}, *TP53*-only, PI3K^{act}-only, non-altered) and standard clinical covariates, with TNBC subtype included as a stratification factor.

In these subtype-stratified multivariable models (Table 3-7), *TP53*-PI3K^{act} tumours remained associated with significantly poorer outcomes. For OS, *TP53*-only tumours showed substantially improved survival relative to *TP53*-PI3K^{act} tumours (HR = 0.42, p = 2.15×10^{-04}), corresponding to more than a two-fold increased risk of death for *TP53*-PI3K^{act} tumours independent of TNBC subtype and other clinical covariates. Similar findings were observed for RFS, where *TP53*-only tumours had significantly lower relapse risk than *TP53*-PI3K^{act} tumours (HR = 0.42, p = 4.85×10^{-04}).

Importantly, the adverse prognostic association of *TP53*-PI3K^{act} tumours remained broadly consistent when the model was re-specified to account for TNBC subtype (Table 3-7), compared with the unstratified analysis shown in Table 3-4. In both models, *TP53*-PI3K^{act} tumours showed significantly worse OS and RFS relative to *TP53*-only tumours. This suggests

that the enrichment of specific TNBC subtypes – including BL2 – does not fully explain their high-risk behaviour.

Table 3-7: Multivariable Cox PH analysis of OS and RFS in the TNBC METABRIC cohort, stratified by TNBC subtype.

Survival Group	Covariate	HR	95% CI	p-value
OS†	*TP53*-only vs. *TP53*-PI3K^{act} (n = 181 vs. 54)	0.42	0.26-0.66	**2.15x10^{-04}**
	PI3K^{act}-only vs. *TP53*-PI3K^{act} (n = 20 vs. 54)	0.75	0.35-1.60	0.458
	Non-altered vs. *TP53*-PI3K^{act} (n = 40 vs. 54)	0.56	0.31-1.05	0.069
	Tumour size (mm)	1.01	1.00-1.02	**5.21x10^{-03}**
	Age at diagnosis (time-dependent)	-	-	**4.36x10^{-05}**
RFS	*TP53*-only vs. *TP53*-PI3K^{act}	0.42	0.26-0.68	**4.85x10^{-04}**
	PI3K^{act}-only vs. *TP53*-PI3K^{act}	0.61	0.27-1.40	0.243
	Non-altered vs. *TP53*-PI3K^{act}	0.48	0.24-0.94	**0.032**
	Age at diagnosis	1.00	0.99-1.02	0.842
	Nodal status (+ vs. -)	2.11	1.40-3.18	**3.97x10^{-04}**
	Tumour size	1.01	1.00-1.02	0.055
	Neoplasm histologic grade (G3 vs. G1/2)	1.30	0.71-2.39	0.395

HR is reported for TP53-only relative to the TP53-PI3K^{act} reference group. Models are adjusted clinical covariates and stratified by TNBC subtype.
† OS model stratified by nodal status and neoplasm histologic grade and age at diagnosis included as a time-dependent covariate.

In a separate Cox regression analysis of TNBC subtype (not shown in Table 3-7), using BL2 as the reference group, no subtype was significantly associated with OS. For RFS, only the UNS subtype showed a significantly reduced risk of recurrence (HR = 0.41, p = 0.036). Overall, TNBC subtype provided limited prognostic information, whereas *TP53*-PI3K^{act} defined a high-risk state that was not restricted to any single subtype.

Overall, *TP53*-PI3K^{act} tumours occupy a transcriptionally distinct space relative to the other TNBC subgroups, most notably characterised by elevated BL2. Although BL2 has been associated with growth factor signalling and reduced chemotherapy sensitivity (115,605), survival analyses stratified by TNBC subtype show that *TP53*-PI3K^{act} tumours retain significantly higher risk of death and relapse regardless of subtype. This suggests that their aggressive phenotype is not merely due to enrichment in high-risk subtypes, but reflects a distinct molecular state driven by cooperative *TP53* loss and PI3K pathway activation, defining a cross-subtype high-risk TNBC subgroup whose poor prognosis cannot be fully explained by intrinsic subtype composition.

3.3.4.3. Transcriptional profiling of *TP53*-PI3K^{act} TNBC

The observed enrichment of BL2 and LAR transcriptional programmes in *TP53*-PI3K^{act} tumours indicates that their aggressive clinical behaviour may be underpinned by distinct gene expression patterns. To interrogate the molecular basis of this high-risk phenotype, we analysed mRNA expression profiles of *TP53*-PI3K^{act} tumours relative to *TP53*-only TNBC across two independent cohorts, METABRIC (n = 55 vs. 183) and TCGA (n = 35 vs. 118). This analysis was designed to identify DEGs and dysregulated pathways associated with *TP53*-PI3K^{act} tumours, determine which transcriptional features are consistently observed across independent cohorts, and uncover molecular mechanisms that may contribute to their aggressive clinical behaviour.

In METABRIC, 153 genes were significantly (L2FC $\geq$ 0.585; FDR $\leq$ 0.05) upregulated and 131 downregulated in *TP53*-PI3K^{act} tumours, as visualised in the volcano plot (Figure 3-5(a(i))), indicating widespread transcriptional changes. In contrast, TCGA showed a more limited set of DEGs, with 24 upregulated and 14 downregulated genes passing the same thresholds, shown in the volcano plot (Figure 3-5(b(i))).

In the METABRIC heatmap (Figure 3-5(a(ii))), which illustrates expression of the top 30 DEGs across all subgroups, *TP53*-PI3K^{act} tumours appeared to cluster together more clearly than in TCGA (Figure 3-5(b(ii))). Concordance between cohorts at the individual gene level for the top 30 DEGs was low, with only a single gene overlapping between the two cohorts. Chloride channel accessory 2 *(CLCA2)*, a calcium-activated chloride channel-associated gene, has previously been implicated in TNBC biology and is reported to have prognostic relevance, with higher expression linked to tumour progression and immune microenvironment features (606,607).

Several of the top upregulated genes in the METABRIC *TP53*-PI3K^{act} tumours, including *CLCA2, HGD, REEP6, SPDEF, ABCC11, SPINK8, and CRAT*, overlapped with a previously described TNBC co-expression module reported by Zhou et al. (2022), which was associated with the MC3 metabolic subtype. In that study, these genes were co-ordinately upregulated in a poor-prognosis metabolic subtype (607). In addition, luminal- and LAR-associated transcription factors, including *SPDEF*, *FOXA1*, and *TFAP2B*, were upregulated in *TP53*-PI3K^{act} tumours in METABRIC but not in TCGA (608,609). *FOXA1* is also a reported downstream target of PI3K/AKT signalling (610), whereas *INPP4B*, which was also upregulated in *TP53*-PI3K^{act} tumours, is a negative regulator of PI3K signalling (468).

In the TCGA cohort heatmap (Figure 3-5(b(ii))), *TP53*-PI3K^{act} tumours formed a distinct cluster characterised by downregulation of *PTEN* and *PTEN*-associated genes, including *PTENP1*, *ATAD1*, and *KLLN*, consistent with this subgroup being primarily defined by *PTEN* loss (Table 3-2; Figure 3-1).

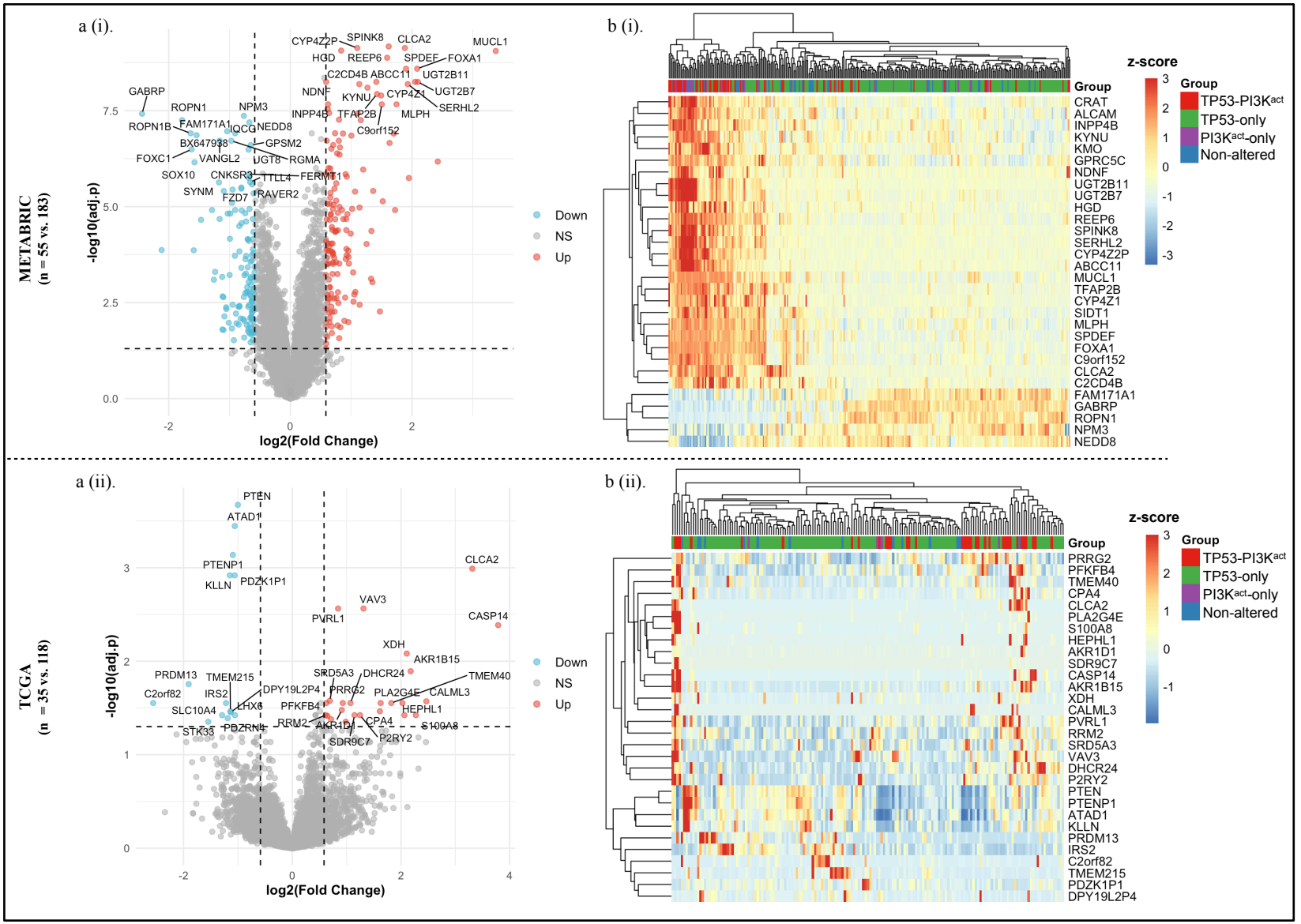
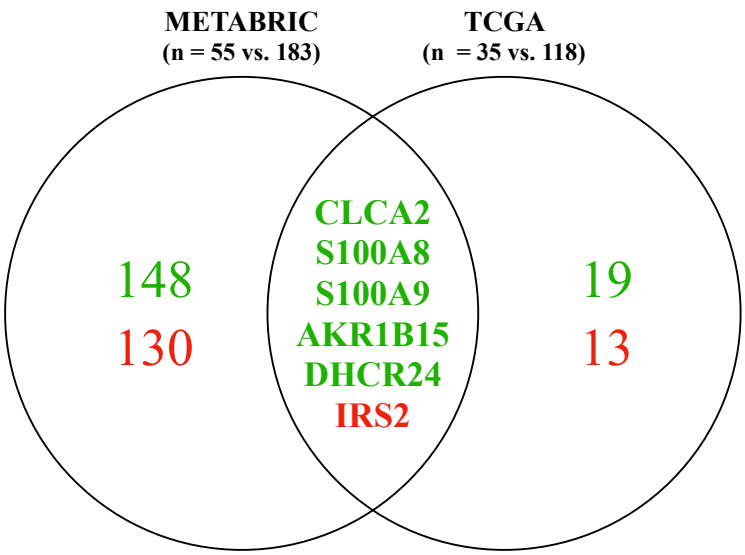


Figure 3-5: Differential gene expression in *TP53*-PI3K^{act} versus *TP53*-only TNBC. (a) METABRIC (n = 299) and **(b)** TCGA (n = 171) cohorts. **(i)** Volcano plots showing L2FC versus -log$_{10}$ FDR for all genes, with significantly up- (red) and downregulated (blue) genes highlighted (|L2FC| ≥ 0.585, FDR ≤ 0.05). **(ii)** Heatmaps of the top 30 DEGs, scaled by z-score, with hierarchical clustering of genes and samples. Z-scores were truncated at a maximum of +3 to prevent a small number of extreme values from compressing the colour scale. Samples are annotated by alteration-defined subgroup: *TP53*-PI3K^{act} (red), *TP53*-only (green), PI3K^{act}-only (purple), and non-altered (blue).

An overlap analysis of DEGs between the METABRIC and TCGA cohorts (Figure 3-6) identified five commonly upregulated genes and one commonly downregulated gene across the two datasets.

a.



b.

	METABRIC			TCGA		
	L2FC	**p-value**	**adj. p-value**	**L2FC**	**p-value**	**adj. p-value**
CLCA2	1.88	9.36×10^{-14}	7.36×10^{-10}	3.31	1.99×10^{-7}	1.02×10^{-3}
S100A8	1.33	1.99×10^{-5}	7.57×10^{-4}	2.27	6.99×10^{-5}	3.77×10^{-2}
S100A9	1.14	1.68×10^{-4}	3.60×10^{-3}	2.06	6.88×10^{-5}	3.77×10^{-2}
AKR1B15	0.91	3.92×10^{-6}	2.30×10^{-4}	2.18	6.86×10^{-6}	1.28×10^{-2}
DHCR24	0.70	5.81×10^{-6}	3.10×10^{-4}	1.07	3.13×10^{-5}	2.80×10^{-2}
IRS2	-0.73	2.06×10^{-6}	2.44×10^{-5}	-1.22	2.23×10^{-5}	2.80×10^{-2}

Figure 3-6. Overlap of DEGs between METABRIC and TCGA *TP53*-PI3K^{act} TNBC cohorts. (a) Venn diagram illustrating the overlap of significantly upregulated (green) and downregulated (red) genes between the METABRIC and TCGA datasets. **(b)** Table summarising the overlapping DEGs, including L2FC, p-values, and adjusted p-values for each gene in both cohorts

S100A8 and *S100A9*, among the overlapping upregulated genes, encode calcium-binding proteins previously implicated in tumour-associated inflammation, tumour microenvironment modulation, and TNBC progression, where they have also been proposed as predictive biomarkers of therapeutic response (611,612). *AKR1B15* and *DHCR24*, which were also upregulated in *TP53*-PI3K^{act} TNBC, are both involved in cellular metabolic processes (613,614), suggesting metabolic reprogramming in these tumours. In contrast, *IRS2*, the only overlapping downregulated gene, encodes an adaptor protein involved in insulin and insulin-like growth factor signalling upstream of the PI3K/AKT pathway (615).

3.3.4.3.1. Pathway-level enrichment and cross-cohort concordance in TP53-PI3K^{act} TNBC

To further investigate the biological programs underlying the high-risk *TP53*-PI3K^{act} group, we performed GSEA comparing *TP53*-PI3K^{act} and *TP53*-only TNBC in METABRIC and TCGA cohorts, using both Hallmark and Reactome gene sets. Hallmark gene sets provide a curated overview of core biological processes (616), while Reactome pathways capture more detailed signalling and metabolic networks (617). Genes were ranked by a composite score of L2FC x -$\log_{10}$(adj. p-value). Pathways significantly enriched or depleted in either cohort were visualised using dot plots (Figure 3-7(a,b)).

GSEA in the METABRIC cohort (Figure 3-7(a(i))) showed that *TP53*-PI3K^{act} tumours were primarily enriched for metabolic pathways, including xenobiotic and drug metabolism, lipid and fatty acid metabolism, glucuronidation, and biological oxidation processes. Additional enrichment was observed in androgen response and platelet activation signalling. In contrast, downregulated pathways were mainly associated with cell cycle progression and genome maintenance, including G2/M checkpoint regulation, mitotic processes, DNA repair, and proliferation-related programmes such as MYC targets.

In the TCGA cohort (Figure 3-7(a(ii))), *TP53*-PI3K^{act} tumours showed enrichment of epithelial differentiation and immune-related pathways, including keratinisation, cornified envelope formation, antimicrobial peptide activity, and innate immune system signalling. Additional enrichment was also observed in mTORC1 signalling, steroid metabolism, and p53 pathway gene sets. Notably, E2F targets and cell cycle gene sets were downregulated in *TP53*-PI3K^{act} in METABRIC relative to *TP53*-only tumours, but enriched in *TP53*-PI3K^{act} tumours in TCGA.

To assess whether other pathway-level changes in *TP53*-PI3K^{act} tumours were consistent across cohorts, we first identified all gene sets that were significantly enriched in at least one dataset (adjusted p-value threshold) and compared the direction of enrichment (NES) between METABRIC and TCGA. We then indicated which of these pathways were also nominally significant in the second cohort. These results are presented in Figure 3-7(b).

A substantial proportion of pathways showed directionally concordant enrichment across cohorts, with a subset also reaching nominal significance in both datasets. These included metabolic and detoxification programmes such as drug, xenobiotic, lipid metabolism, alongside immune-related pathways including antimicrobial peptides, innate immune system, and neutrophil degranulation.

Several pathways were directionally discordant, showing significant downregulation in METABRIC but nominal upregulation in TCGA. These included cell cycle and proliferation programmes (G2/M checkpoint, M phase, mitotic metaphase and anaphase, and cell cycle checkpoints). In addition, epithelial differentiation-associated gene sets, including keratinisation and formation of the cornified envelope, were significantly upregulated in TCGA but nominally downregulated in METABRIC. This may in part reflect differences in TNBC case definition between the TCGA and METABRIC cohorts.

We examined overlap of leading-edge genes for pathways that showed at least nominal significance ($p \leq 0.05$) in both METABRIC and TCGA (Figure 3-7(c)). Leading-edge genes represent the core subset of genes driving pathway enrichment in GSEA and therefore provide a more refined measure of biological concordance than pathway-level significance alone.

Across pathways, a moderate degree of overlap was observed between cohorts, with Jaccard indices (J) ranging from 0.10 to 0.34. The highest levels of concordance were observed in metabolic pathways, including phase II conjugation of compounds ($J = 0.34$), metabolism of steroids ($J = 0.33$), and xenobiotic metabolism ($J = 0.25$), indicating a relatively conserved set of genes underpinning metabolic reprogramming in *TP53*-PI3K^{act} tumours. Immune-related pathways showed intermediate concordance, with antimicrobial peptides ($J = 0.23$), neutrophil degranulation ($J = 0.22$), and innate immune system signalling ($J = 0.18$) displaying consistent, though less tightly overlapping, gene sets.

Cell cycle-related pathways exhibited greater heterogeneity. While two pathways – E2F targets and G2/M checkpoint ($J \approx 0.23$-0.28) – showed higher levels of overlap, most cell cycle pathways demonstrated lower overlap overall ($J \approx 0.10$-0.16). This suggests that cell cycle-associated transcriptional programmes are less consistently defined at the gene level and may be more context-dependent across datasets. Epithelial differentiation pathways, including keratinisation and formation of the cornified envelope, showed low overlap between METABRIC and TCGA ($J \approx 0.10$). Notably, within each cohort, these two pathways were driven by identical leading-edge gene sets, indicating that they capture the same underlying epithelial differentiation signal.

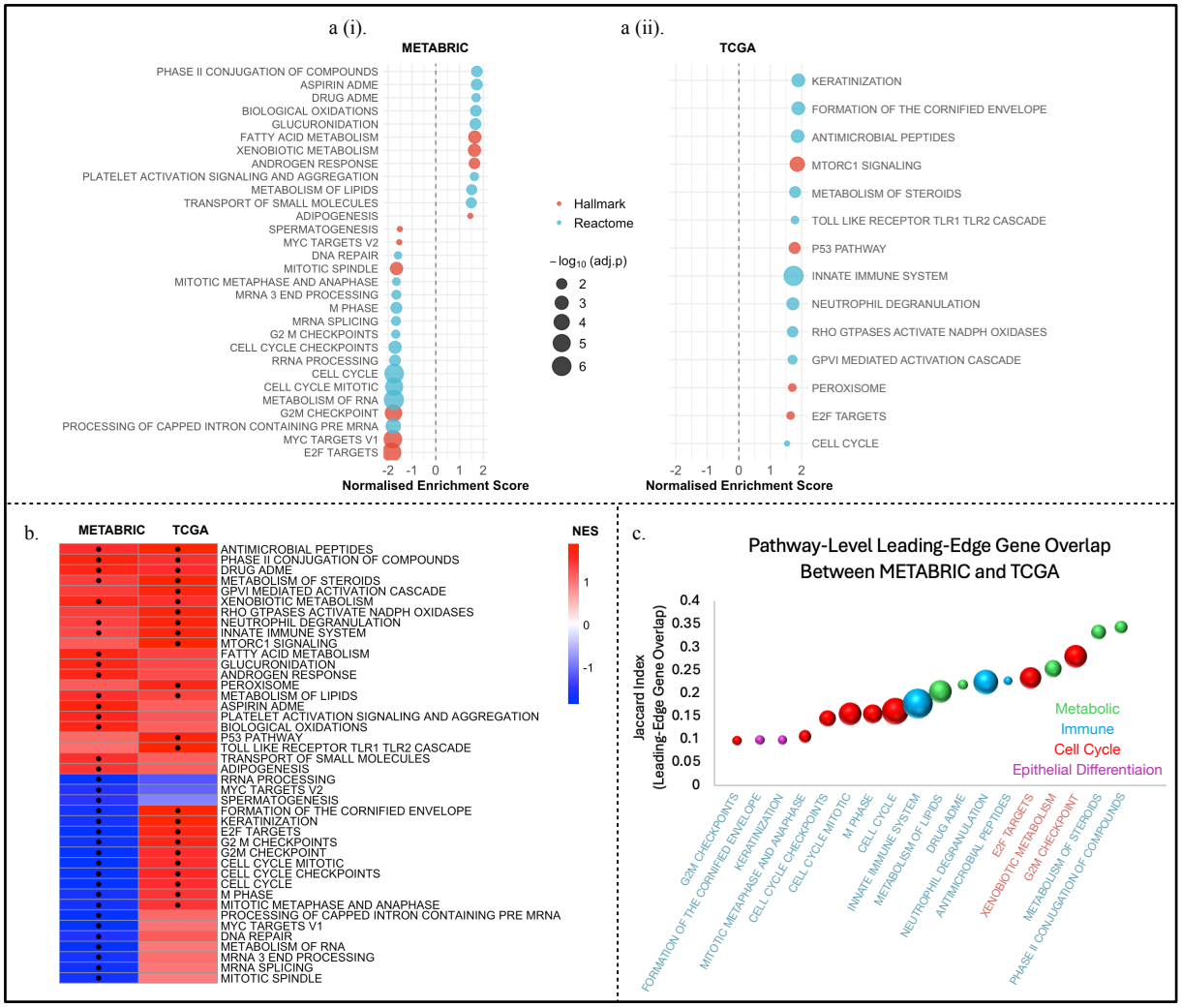


Figure 3-7: Pathway enrichment and cross-cohort concordance in *TP53*-PI3K^{act} versus *TP53*-only TNBC. (a) GSEA dotplots for **(i)** METABRIC and **(ii)** TCGA. Genes were ranked by L2FC x -$\log_{10}$(adj.p). The x-axis represents NES, dot size indicates -$\log_{10}$(adj.p), and colour indicates gene set category (Hallmark = red and Reactome = blue). **(b)** NES heatmap of pathways significant in at least one cohort, summarising directional concordance between cohorts. NES reflects enrichment or depletion and dots indicate nominal significance (p-value ≤ 0.05). **(c)** Bubble plot showing pathway-level concordance of leading-edge genes between METABRIC and TCGA. Each point represents a pathway, positioned by Jaccard index (x-axis), reflecting the proportion of shared leading-edge genes between cohorts. Bubble size corresponds to the number of overlapping leading-edge genes, and colour indicates functional category (metabolic = green, immune = blue, cell cycle = red, epithelial differentiation = purple).

Taken together, these results demonstrate that *TP53*-PI3K^{act} TNBC is characterised by a largely concordant pattern of metabolic and immune-associated transcriptional programmes across cohorts. In contrast, proliferation and differentiation-related pathways show greater cohort dependency, underscoring both the biological complexity and context-specific nature of this high-risk subtype.

3.3.4.3.2. Single-sample scoring of metabolic, immune, and cell cycle pathway activity in TP53-PI3K^{act} TNBC

To further contextualise the pathway-level differences identified by GSEA, we generated ssGSEA scores for the selected metabolic, immune, and cell cycle–related pathways that showed at least nominal significance in both the METABRIC and TCGA analyses. These pathway-level scores were calculated for each tumour individually and then summarised as mean scores for metabolic, immune, and cell cycle programmes. This approach enabled comparison of overall pathway activity across the four alteration-defined subgroups (*TP53*-PI3K^{act}, *TP53*-only, PI3K^{act}-only, and non-altered). Statistical comparisons were performed on both the aggregated programme scores and individual pathway scores, with all results presented in Table 3-8. Mean programme scores are additionally illustrated in Figure 3-8.

In the METABRIC cohort, metabolic pathway activity was significantly higher in *TP53*-PI3K^{act} tumours compared with *TP53*-only tumours, consistent with GSEA findings. However, no significant differences were observed when *TP53*-PI3K^{act} tumours were compared with PI3K^{act}-only tumours, indicating no evidence of further enhancement of metabolic activity in the combined *TP53*-PI3K^{act} state. In the TCGA cohort, metabolic pathway scores showed a similar pattern, with higher scores in *TP53*-PI3K^{act} tumours compared with *TP53*-only tumours, but no significant differences relative to PI3K^{act}-only or non-altered tumours. Overall, these findings suggest that while metabolic pathway activity is associated with *TP53*-PI3K^{act} tumours relative to *TP53*-only disease, there is no evidence of additional metabolic activation beyond that observed with PI3K pathway alteration alone.

Immune-related pathway activity was significantly higher in *TP53*-PI3K^{act} tumours compared with *TP53*-only tumours in METABRIC, and also compared with PI3K^{act}-only tumours, indicating a more pronounced immune-associated transcriptional state in the combined *TP53*-PI3K^{act} subgroup. No significant differences were observed when compared with non-altered tumours, although this group showed greater variability in immune scores, as reflected by wider dispersion in the boxplots (Figure 3-8(b)). This pattern was driven by multiple immune signatures, including antimicrobial peptide activity and innate immune system pathways. In the TCGA cohort, immune pathway differences were less consistent, with significant differences largely restricted to antimicrobial peptide activity in *TP53*-PI3K^{act} tumours compared with *TP53*-only tumours, and no significant differences observed for the overall immune programme score or other immune pathways. Overall, these findings suggest that immune

pathway activation associated with *TP53*-PI3K^{act} is most robust in METABRIC, with only partial and pathway-specific reproducibility in TCGA.

Cell cycle-related pathways showed the most discordant patterns between cohorts and analytical approaches. In METABRIC, ssGSEA-derived scores indicated significantly lower cell cycle activity in *TP53*-PI3K^{act} tumours compared with *TP53*-only tumours, consistent with the direction observed in GSEA. In contrast, *TP53*-PI3K^{act} tumours exhibited higher cell cycle activity relative to both PI3K^{act}-only and non-altered tumours, suggesting subgroup-dependent divergence in proliferative signalling within the cohort. In TCGA, despite GSEA evidence of increased cell cycle pathway enrichment in *TP53*-PI3K^{act} versus *TP53*-only tumours, this was not reflected in ssGSEA scores, which showed no statistically significant differences across alteration-defined subgroups or in the aggregated cell cycle programme score. This indicates that group-level enrichment signals in TCGA are not consistently captured at the single-sample pathway activity level.

Overall, metabolic activity emerged as the most robust feature, showing consistent elevation in *TP53*-PI3K^{act} tumours across cohorts, but without evidence of additional activity beyond PI3K^{act}-only disease. Immune activity showed a more *TP53*-PI3K^{act}-specific signal in METABRIC, distinguishing this group from both *TP53*-only and PI3K^{act}-only tumours, and was partially reproducible in TCGA. Cell cycle activity demonstrated more context-dependent differences. In METABRIC, *TP53*-PI3K^{act} tumours showed an intermediate level relative to *TP53*-only and PI3K^{act}-only groups, consistent with a moderate proliferative state. In TCGA, the group-level GSEA signal indicating cell cycle pathway enrichment in *TP53*-PI3K^{act} was not evident in ssGSEA, although this may reflect the greater sensitivity of GSEA to subtle, coordinated pathway-level shifts that are not always captured in single-sample analyses. This discrepancy may also be influenced by TCGA's TNBC definition based on PAM50 basal tumours, which have a higher baseline proliferative state and may reduce intergroup contrast.

Table 3-8: Single-sample pathway activity scores across *TP53*- and PI3K-defined TNBC subgroups in METABRIC and TCGA cohorts.

ssGSEA score	METABRIC				TCGA			
		TP53-PI3K^{act} vs.				*TP53*-PI3K^{act} vs.		
	Overall	*TP53*-only	PI3K^{act}-only	Non-altered	Overall	*TP53*-only	PI3K^{act}-only	Non-altered
Metabolic Activity	**$1.9x10^{-07}$**	**$3.7x10^{-07}$**	0.733	0.125	**0.013**	**0.014**	0.358	**0.048**
Phase II conjugation of compounds	**$1.1x10^{-04}$**	**$3.5x10^{-04}$**	0.788	0.229	0.268	0.450	0.950	0.400
Metabolism of steroids	**$2.1x10^{-04}$**	**$1.1x10^{-04}$**	0.586	0.099	**$1.3x10^{-03}$**	**$1.3x10^{-03}$**	0.491	**$8.5x10^{-03}$**
Xenobiotic metabolism	**$1.6x10^{-08}$**	**$6.4x10^{-08}$**	0.753	0.695	**0.029**	**0.014**	0.732	0.732
Drug ADME	**$1.4x10^{-06}$**	**$2.2x10^{-06}$**	0.679	0.106	0.133	0.170	0.690	0.170
Metabolism of lipids	**$9.7x10^{-07}$**	**$6.8x10^{-07}$**	0.995	0.095	0.185	0.330	0.120	0.730
Immune Activity	**$4.4x10^{-04}$**	**$2.1x10^{-03}$**	**0.019**	0.917	0.202	0.200	0.800	0.800
Antimicrobial peptides	**0.014**	**0.028**	**0.028**	0.454	**0.032**	**0.030**	0.880	0.520
Neutrophil degranulation	**$2.7x10^{-04}$**	**$5.1x10^{-04}$**	0.056	0.965	0.350	0.420	0.950	0.950
Innate immune system	**$4.4x10^{-04}$**	**$5.3x10^{-03}$**	0.073	0.449	0.353	0.410	0.410	0.780
Cell Cycle Activity	**$2.1x10^{-14}$**	**$1.4x10^{-04}$**	0.060	**$3.6x10^{-04}$**	0.235	0.240	1.000	0.970
G2M checkpoint (H)	**$2.9x10^{-15}$**	**$2.9x10^{-05}$**	**0.037**	**$6.0x10^{-04}$**	0.337	0.350	0.940	0.940
E2F targets	**$6.7x10^{-14}$**	**$4.5x10^{-05}$**	**0.039**	**0.002**	0.203	0.230	0.840	0.840
Cell cycle	**$2.6x10^{-14}$**	**$1.6x10^{-04}$**	0.090	**$2.3x10^{-04}$**	0.280	0.280	0.840	0.840
M phase	**$8.4x10^{-14}$**	**$4.8x10^{-04}$**	0.108	**$1.5x10^{-04}$**	0.358	0.420	0.860	0.860
Cell cycle mitotic	**$9.4x10^{-15}$**	**$1.2x10^{-04}$**	0.075	**$1.7x10^{-04}$**	0.314	0.330	0.880	0.880
Cell cycle checkpoints	**$4.2x10^{-14}$**	**$3.4x10^{-04}$**	0.088	**$9.7x10^{-05}$**	0.188	0.240	0.950	0.840
Mitotic metaphase and anaphase	**$1.5x10^{-12}$**	**$6.4x10^{-04}$**	**0.048**	**$4.4x10^{-04}$**	0.172	0.260	0.770	0.770
G2M checkpoints (R)	**$2.7x10^{-14}$**	**$6.0x10^{-04}$**	0.278	**$2.5x10^{-05}$**	0.053	0.056	0.911	0.449

H = Hallmark; R = Reactome

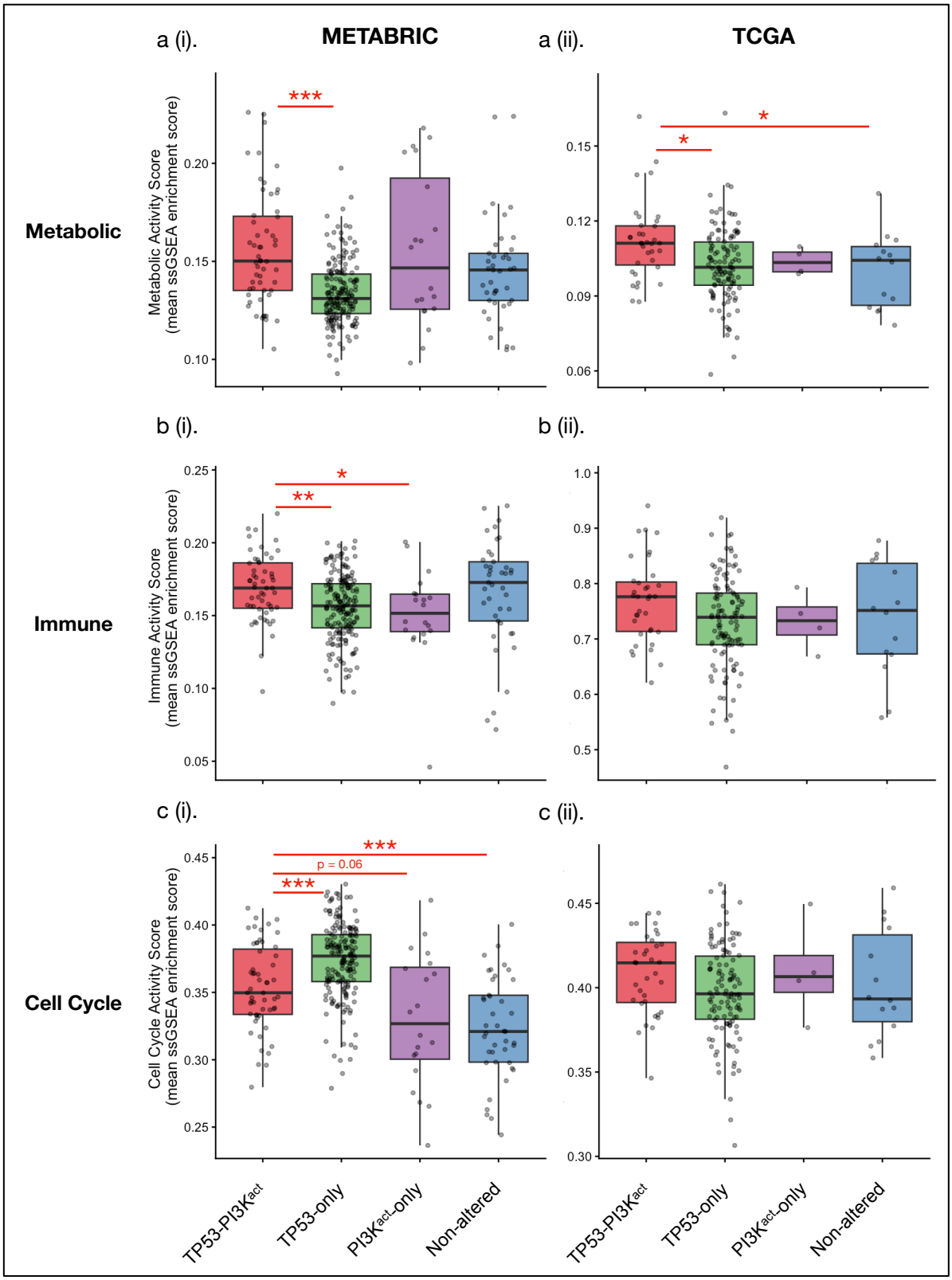


Figure 3-8: Pathway programme activity across alteration-defined TNBC subgroups. Box-and-whisker plots show z-score normalised (a) metabolic, (b) immune, and (c) cell cycle programme scores across *TP53*-PI3K^{act}, *TP53*-only, PI3K^{act}-only, and non-altered tumours. Programme scores were calculated as the mean ssGSEA-derived enrichment scores across gene sets within each functional category. Panels are shown for (i) METABRIC and (ii) TCGA cohorts. Statistical significance is indicated as * adj.p ≤ 0.05, ** adj.p ≤ 0.01, *** adj.p ≤ 0.001.

3.3.4.4. Differential protein expression in *TP53*-PI3K^{act} TNBC

To complement transcriptional analyses, we examined protein-level differences in *TP53*-PI3K^{act} versus *TP53*-only TNBC using TCGA RPPA data. RPPA measurements were available for 30 *TP53*-PI3K^{act} and 96 *TP53*-only, 4 PI3K^{act}-only, 13 non-altered tumours. Using linear modelling with empirical Bayes moderation, we identified proteins differentially expressed between *TP53*-PI3K^{act} and *TP53*-only tumours (L2FC $\geq$ 0.263, adjusted $p \leq 0.05$). Significant protein expression patterns were subsequently visualised across all alteration-defined subgroups to contextualise these differences (Figure 3-9).

Several proteins showed significant changes consistent with elevated PI3K-AKT pathway activity. AKT phosphorylation at S473 and T308 was increased, reflecting pathway activation, while GSK3α/β phosphorylation at S9 indicated downstream inhibition by AKT (618). NDRG1 phosphorylation at T346 was also elevated, consistent with PI3K-mediated stress and hypoxia signalling (619). Conversely, p27 (CDKN1B), a cyclin-dependent kinase inhibitor, was reduced, suggesting diminished cell cycle restraint (620). Finally, BCL2, an anti-apoptotic protein, was decreased, potentially reflecting compensatory survival signalling changes in response to sustained PI3K-AKT activation (621).

Together, these protein-level changes are consistent with canonical PI3K-AKT activation. Despite limited comparison with PI3K^{act}-only tumours, their concordance with established PI3K signalling indicates that they primarily reflect PI3K pathway activity, rather than a *TP53*-PI3K^{act}-specific effect.

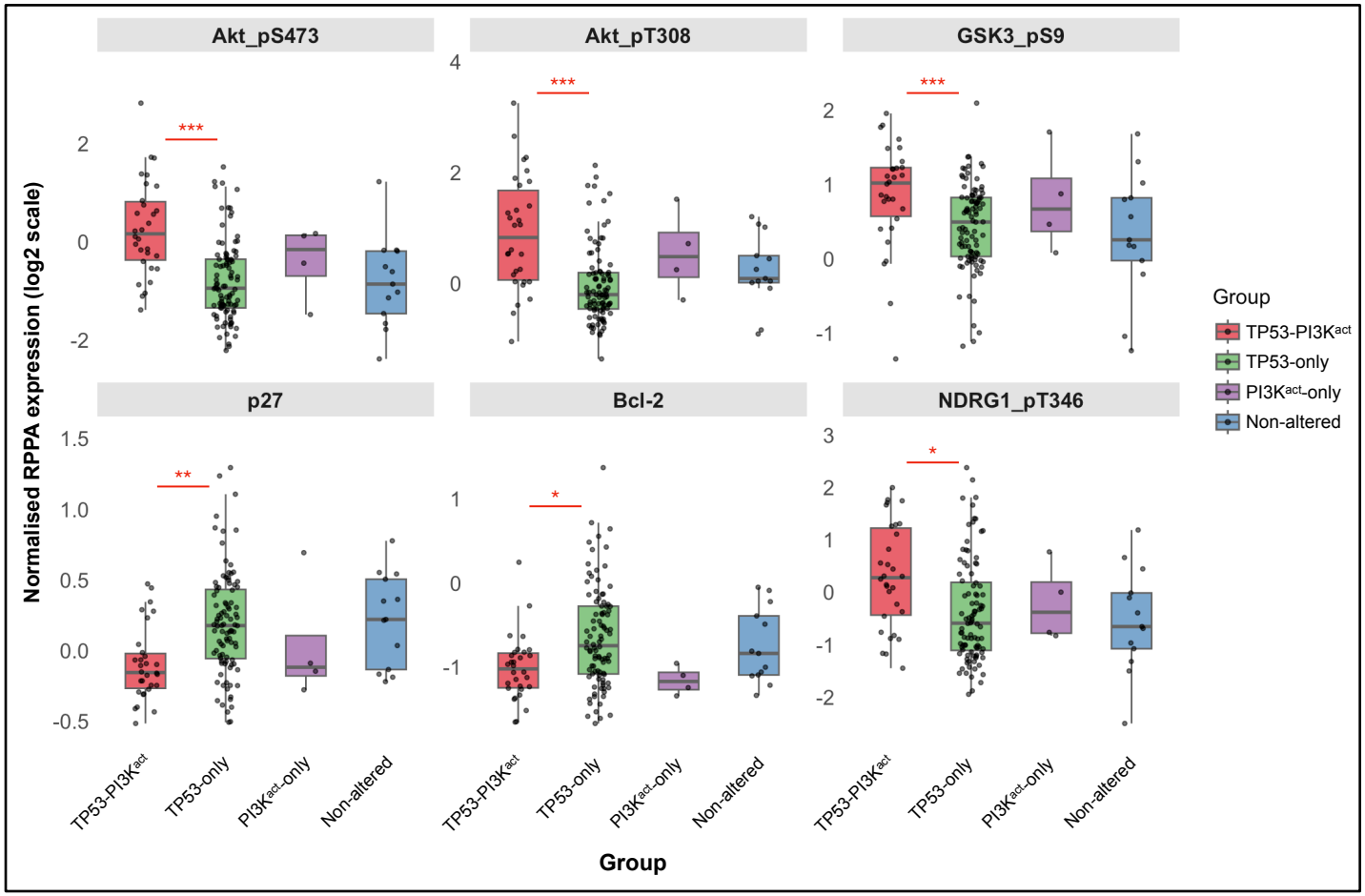


Figure 3-9: Differentially expressed proteins in *TP53*-PI3K^{act} versus *TP53*-only TNBC from TCGA RPPA analysis. Boxplots show $\log_2$ normalised RPPA protein expression levels for significantly differentially expressed proteins (L2FC $\geq$ 0.263, BH-adjusted $p \leq 0.05$) identified from differential analysis comparing *TP53*-PI3K^{act} and *TP53*-only tumours. Panels display AKT phosphorylation at S473 and T308, GSK3α/β phosphorylation at S9, NDRG1 phosphorylation at T346, and total protein levels of p27 (CDKN1B) and BCL-2. Statistical testing was performed only between *TP53*-PI3K^{act} (n = 30) and *TP53*-only (n = 96) tumours; PI3K^{act}-only (n = 4) and non-altered (n = 13) groups are shown for visual comparison but were not included in significance testing due to small sample size. BH-adjusted significance for the primary comparison is indicated in red with asterisks.

3.4. Summary

This chapter defines and characterises a TP53-PI3K pathway-activated (*TP53*-PI3K^{act}) subgroup of TNBC that is consistently associated with poor clinical outcomes across independent cohorts. By extending beyond *TP53-PIK3CA* co-mutation to include *AKT1* mutations and *PTEN* loss, a biologically coherent and clinically high-risk group is identified that captures additional aggressive tumours without diluting prognostic signal.

Across both METABRIC and TCGA cohorts, *TP53*-PI3K^{act} tumours show independently worse survival outcomes that persist after adjustment for standard clinical covariates and are not explained by differences in TNBC intrinsic subtype composition. While enriched for BL2 and LAR transcriptional programmes and displaying some cohort-specific differences in subtype distribution, their adverse prognosis remains robust when accounting for TNBC subtype, indicating that subtype enrichment does not fully account for their aggressive behaviour.

Molecularly, *TP53*-PI3K^{act} tumours are defined primarily by canonical PI3K/AKT pathway activation, alongside consistent metabolic reprogramming and partially reproducible immune-associated transcriptional changes. In contrast, proliferation- and differentiation-related programmes show greater heterogeneity between cohorts, reflecting both biological context and differences in cohort composition. Protein-level analyses further confirm activation of PI3K/AKT signalling and downstream effects on cell cycle and survival pathways.

Overall, *TP53*-PI3K^{act} represents a reproducible, cross-cohort high-risk TNBC subset characterised by convergent *TP53* loss and PI3K pathway activation, with distinct metabolic and signalling features that are not fully captured by existing clinical or intrinsic subtype classifications. These findings support its potential utility for refined prognostic stratification and highlight PI3K-associated biology as a key contributor to aggressive TNBC behaviour.

4.Targeting PI3K/AKT signalling in *TP53* and *PIK3CA* co-mutated TNBC: dual inhibition with alpelisib and RTK inhibitors

4.1. Introduction

The previous chapter identified *TP53*-PI3K^{act} as a clinically aggressive subgroup of TNBC defined by the co-occurrence of *TP53* mutation and genomic alterations predicted to activate PI3K signalling. This subgroup exhibited consistently poor clinical outcomes across independent cohorts and was characterised by transcriptional and proteomic features indicative of PI3K pathway activation, alongside metabolic and immune-associated programmes. Importantly, these features were not fully explained by intrinsic TNBC subtype composition, suggesting that the convergence of *TP53* dysfunction and PI3K pathway activation defines a key driver of tumour behaviour in this context.

PIK3CA mutations represent a well-defined and therapeutically actionable alteration within the PI3K pathway. Alpelisib, a PI3Kα-selective inhibitor approved for *PIK3CA*-MUT BC (as detailed in Section 1.6.1.2., Chapter 1), therefore provides a clinically relevant approach to test whether PI3K pathway activation in TNBC can be effectively targeted. To enable controlled functional investigation, this study focuses on TNBC models harbouring *TP53* mutation, *PIK3CA* mutation, or both, using *TP53/PIK3CA* co-mutant systems as an experimentally tractable proxy for the broader *TP53*-PI3K^{act} state.

However, clinical and preclinical studies have shown that PI3K inhibition alone is often insufficient to treat cancers, due to rapid adaptive resistance, frequently mediated through feedback reactivation of RTK signalling (622). This is particularly true in TNBC, where growth factor signalling in transcriptional subtypes such as BL2 (605), was enriched in *TP53*-PI3K^{act} tumours (Chapter 3). In addition, loss of functional p53 due to mutations, may further exacerbate RTK-driven signalling; as WT p53 has been implicated in constraining aberrant RTK activity (623–625). Together, these mechanisms suggest that PI3K inhibition in *TP53*-MUT TNBC may be accompanied by compensatory RTK activation, limiting PI3K inhibitor efficacy.

Based on this, we hypothesised that dual targeting of PI3K and RTK signalling may enhance therapeutic response in *TP53/PIK3CA* co-mutant TNBC. To test this, the PI3Kα inhibitor alpelisib was evaluated alone and in combination with RTK inhibitors, including crizotinib, capmatinib, and ceritinib, which target MET and related signalling pathways. These agents were selected based on their clinical availability and their potential to suppress compensatory signalling mechanisms associated with PI3K inhibition.

By comparing responses in *TP53*-MUT, *PIK3CA*-MUT, and *TP53/PIK3CA* co-mutant systems, this study aims to determine whether co-occurring *TP53* mutation modifies sensitivity to PI3K-targeted therapy and whether combination strategies can overcome resistance mechanisms in this high-risk TNBC subset.

4.2. Identification of *TP53*- and/or *PIK3CA*-MUT TNBC cell line models

The DepMap portal was used to identify cell lines of the ER-negative/HER2-negative molecular subtype (TNBC) harbouring *TP53* and/or *PIK3CA* mutations (see Table 4-1). The mutational status of *AKT1/2/3* was also determined via DepMap to assess the presence of activating mutations in the AKT family. *PTEN* CN was assessed using the Cancer Cell line Encyclopaedia (CCLE) dataset in cBioPortal. As previously discussed, both *PTEN* loss and *AKT* mutations can drive aberrant PI3K/AKT signalling, therefore, preference was given to cell lines that were *AKT*-WT and diploid for *PTEN* to minimise confounding effects. Where possible, cell lines harbouring hotspot mutations in *TP53* and *PIK3CA* were also prioritised. Each cell line was cross-referenced with the literature to confirm BC origin, TNBC subtype, and mutational and CN status.

Table 4-1: Panel of TNBC cell lines harbouring *TP53* and/or *PIK3CA* mutations, detailing TNBC subtype classification, specific gene mutations, and *PTEN* CN status (104,117).

Cell Line	TNBC Subtype Lehmann/Burstein	TP53	PIK3CA	PTEN	AKT
MDA-MB-468	BL1/BLIS	R273H	WT	Loss†††	WT
HDQ-P1	BL2/BLIS	R213*	WT	Diploid	WT
BT-20†	UNC	K132Q	H1047R; P539R	Low expression††††	WT
MFM-223	LAR/LAR	K132R	H1047R	Diploid	WT
MDA-MB-453††	LAR/LAR	WT	H1047R	Diploid	WT
CAL-51	M/MES	WT	E542K	Loss†††††	WT

† The BT-20 cell line is unclassified with regards to TNBC subtype due to its low correlation with defined TNBC subtypes or overlapping characteristics across multiple subtypes (626).
†† Despite some studies classifying the MDA-MB-453 cell line as HER2-amplified based on elevated HER2 mRNA expression, its HER2 protein levels remain relatively low (627).
††† Although cBioPortal reports a diploid PTEN CN for MDA-MB-468, literature evidence indicates that a specific PTEN mutation leads to functional loss in this cell line (628).
†††† Although cBioPortal reports a PTEN deep deletion in BT-20, literature evidence shows that PTEN is not deleted but rather expressed at low levels in this cell line (629).
††††† Although cBioPortal reports a diploid PTEN CN for CAL-51, literature evidence indicates that a specific PTEN mutation leads to functional loss in this cell line (630).

***TP53*-MUT / *PIK3CA*-WT**

The MDA-MB-468 and HDQ-P1 cell lines were selected to represent a *TP53*-MUT/*PIK3CA*-WT TNBC cohort. MDA-MB-468 harbours the *TP53* R273H hotspot mutation and HDQ-P1 carries the *TP53* R213* hotspot mutation (631). According to the Lehmann TNBC classification, MDA-MB-468 and HDQ-P1 belong to the BL1 and BL2 subtypes, respectively (104), both of which align with the BLIS subtype in the Burstein classification (117). It is worth noting that *EGFR* is amplified in MDA-MB-468 (315).

***TP53*-WT / *PIK3CA*-MUT**

The MDA-MB-453 and CAL-51 cell lines both harbour *PIK3CA* hotspot mutations – H1047R and E542K, respectively (632). According to the Lehmann classification, MDA-MB-453 is categorised as LAR (104), aligning with the LAR subtype in the Burstein classification (117). Notably, there is inconsistency in the literature regarding the BC subtype of MDA-MB-453, with some sources describing it as TNBC and others as HER2-overexpressing. This likely reflects high HER2 mRNA expression despite insufficient HER2 protein levels to classify the cells as HER2-positive (627). For the purposes of this study, MDA-MB-453 was classified as TNBC based on its HER2 protein expression. CAL-51 is classified as M by the Lehmann system (104), corresponding to the MES subtype in the Burstein classification (117). Although CAL-51 is diploid for *PTEN*, it harbours a *PTEN* LOF mutation. These cell lines were selected to represent a *TP53*-WT/*PIK3CA*-MUT TNBC cohort, based on the presence of specific *PIK3CA* hotspot mutations commonly found in TNBC (633).

***TP53*-MUT / *PIK3CA*-MUT**

The BT-20 and MFM-223 cell lines both harbour mutations in *TP53* and *PIK3CA*. Both cell lines carry *TP53* mutations at codon 132 (K132Q in BT-20 and K132R in MFM-223), which occur within the DNA-binding domain of the p53 protein (634). In addition, both cell lines possess the H1047R hotspot mutation in *PIK3CA*. BT-20 also carries the less common P539R mutation, which has been reported to co-occur with H1047R (635). According to the Lehmann classification, BT-20 is deemed as UNC, indicating it could not be assigned to a specific TNBC subtype (104). Furthermore, *EGFR* is amplified in this cell line (636). These cell lines were selected to represent a *TP53/PIK3CA* co-mutant TNBC cohort due to their availability in the laboratory. Alternative cell lines, such as SUM159PT and CAL-148, may be considered for future studies.

4.3. Effects of single-agent targeted therapies on TNBC cell lines harbouring *TP53* and/or *PIK3CA* mutations

4.3.1. Reduced sensitivity to alpelisib in *TP53/PIK3CA* co-mutant TNBC

As outlined in Section 1.6.1.2. (Chapter 1), alpelisib is the only FDA-approved PI3K inhibitor that selectively targets the p110α isoform of PI3K (637), receiving regulatory approval for the treatment of HR-positive/HER2-negative BC (458). This study seeks to repurpose alpelisib for the treatment of TNBC and to enhance therapeutic efficacy through the application of synergistic drug combinations. Alpelisib was selected for investigation due to its specificity for *PIK3CA*-MUT cancers and its prior approval in a distinct BC subtype.

Based on the SOLAR-1 trial, the maximum plasma concentration (C_{max}) of alpelisib at steady state (300 mg daily) is ~2480 ng/mL (638), which converts to ~5.62 µM, calculated as follows:

$$\frac{\text{alpelisib } C_{max}}{\text{alpelisib molecular weight}} = \frac{\text{2480 ng/mL}}{\text{441.47 g/mol}}$$

Sensitivity to alpelisib was assessed across a panel of TNBC cell lines with results illustrated in see Figure 4-1.

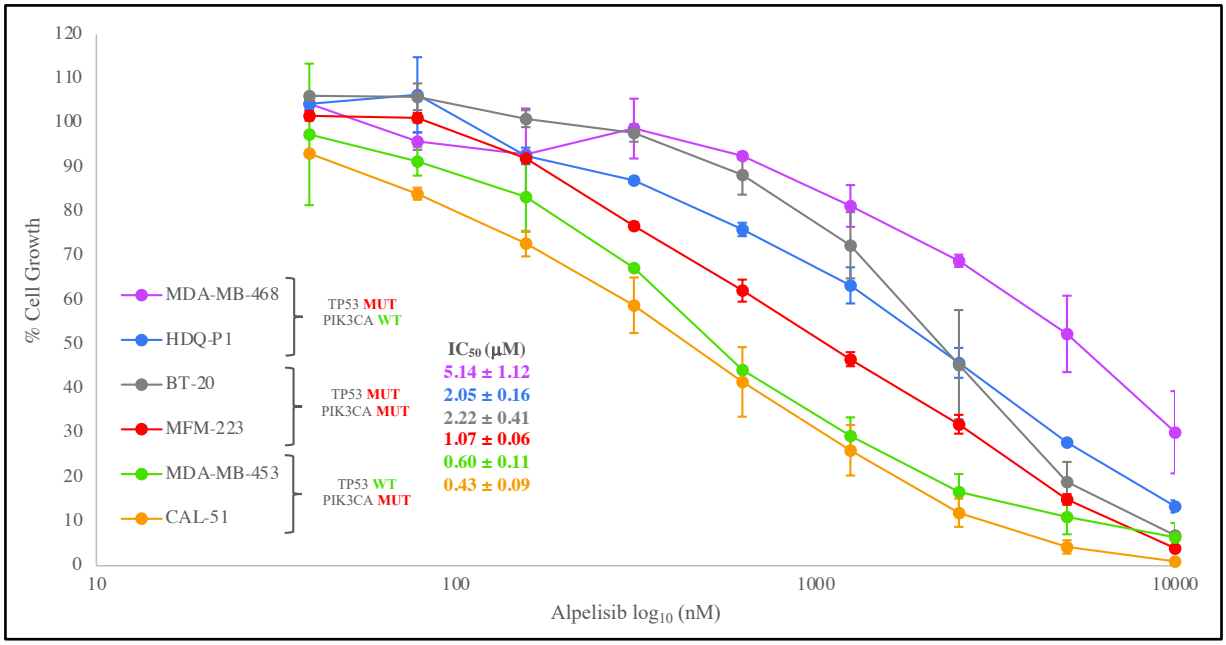


Figure 4-1: Antiproliferative effects of alpelisib on *TP53*- and/or *PIK3CA*-MUT TNBC cell lines. The proliferation of TNBC cell lines was assessed following 5 days of treatment with increasing concentrations of alpelisib (0-10 µM). Percentage growth was calculated relative to untreated control cells. Alpelisib concentrations (nM) were plotted on a $\log_{10}$ scale against percentage cell growth. Error bars indicate the SD of biological replicate experiments (n = 2). IC_{50} values (µM) were determined using CalcuSyn software.

The antiproliferative response to alpelisib varied according to the *TP53* and *PIK3CA* mutational status of the TNBC cell lines.

***TP53*-WT/*PIK3CA*-MUT**

The *TP53*-WT/*PIK3CA*-MUT cell lines, MDA-MB-453 and CAL-51, exhibited the greatest sensitivity, with IC_{50} values of 0.60 ± 0.11 µM and 0.43 ± 0.09 µM, respectively, falling below the C_{max}. This observation aligns with the known mechanism of action of alpelisib. Minimal variation in IC_{50} values between MDA-MB-453 and CAL-51 cell lines suggests that alpelisib effectively targets both the H1047R and E542K *PIK3CA* mutations with comparable potency.

***TP53*-MUT/*PIK3CA*-WT**

The *TP53*-MUT/*PIK3CA*-WT cell lines, MDA-MB-468 and HDQ-P1, exhibited markedly reduced sensitivity to alpelisib, as anticipated given the absence of activating *PIK3CA* mutations. Of these cell lines, MDA-MB-468 was the least responsive, with a significantly higher IC_{50} value of 5.14 ± 1.12 µM (at the C_{max}) compared to all other cell lines, including HDQ-P1. Although HDQ-P1 is *PIK3CA*-WT, its relatively lower IC_{50} value (2.05 ± 0.16 µM)

compared to MDA-MB-468 suggests a differential response to alpelisib among *TP53*-MUT cell lines.

***TP53*-MUT/*PIK3CA*-MUT**

The *TP53/PIK3CA* co-mutant cell lines, BT-20 and MFM-223, exhibited reduced sensitivity to alpelisib compared to the *PIK3CA*-MUT cell lines lacking *TP53* mutations, with IC_{50} values of 2.22 ± 0.41 μM and 1.07 ± 0.06 μM, respectively. Notably, BT-20, which harbours both the H1047R and P539R *PIK3CA* mutations, demonstrated lower sensitivity than both the *TP53/PIK3CA* co-mutant MFM-223 cell line and the *TP53*-MUT/*PIK3CA*-WT HDQ-P1.

These proliferation assay results indicate that *TP53* mutations may attenuate the sensitivity of *PIK3CA*-MUT TNBC cell lines to alpelisib.

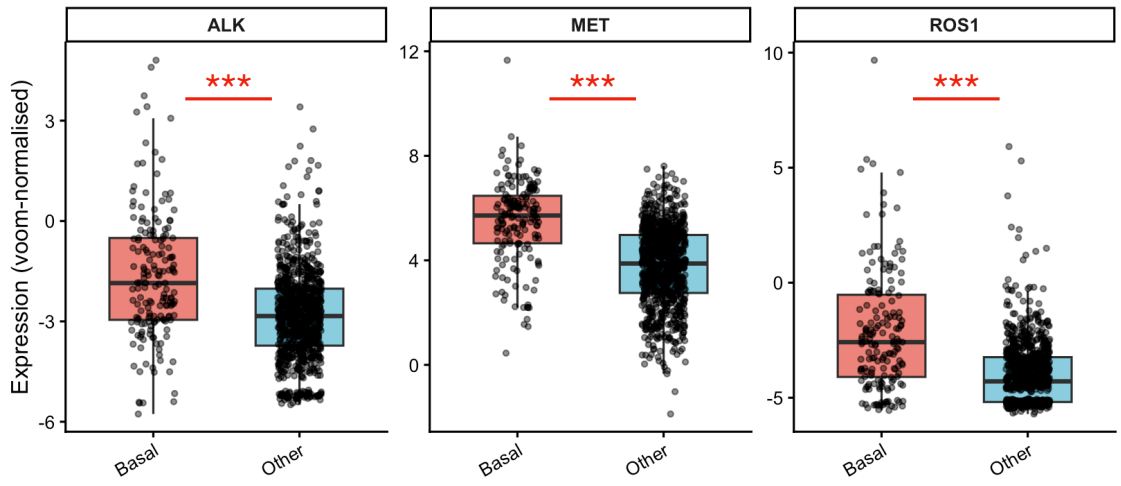
4.3.2. Targeting TNBC with RTK inhibitors

In this section, we sought to evaluate the efficacy of crizotinib as a single agent across our panel of TNBC cell lines before assessing its potential in combination with alpelisib.

4.3.2.1. RTK targets of crizotinib are upregulated in TNBC compared to other BC subtypes

DEA was performed on TCGA BC data, as described in Section 2.1.7.1. (Chapter 2), to assess the expression of genes encoding the primary targets of crizotinib (ALK, ROS, and MET). Expression in TNBC (basal) tumours was compared to other BC subtypes, with results summarised in Figure 4-2. All three RTK targets were significantly upregulated in basal relative to other BC subtypes. Specifically, ROS proto-oncogene 1 (*ROS1)*, *MET*, and *ALK* exhibited L2FCs of 1.84 (adj. $p = 1.01E^{-26}$), 1.71 (adj. $p = 8.74E^{-45}$), and 1.61 (adj. $p = 3.96E^{-16}$), respectively. These findings indicate that multiple crizotinib targets are transcriptionally enriched in basal/TNBC, supporting the rationale for targeting RTK signalling in this context.

a.



b.

		Basal vs. Other Subtypes		
Gene	**ENSEMBL ID**	**L2FC**	**p-val**	**adj.p**
ROS1	ENSG00000047936	**1.84**	**$1.78x10^{-27}$**	**$1.01x10^{-26}$**
MET	ENSG00000105976	**1.71**	**$7.53x10^{-46}$**	**$8.74x10^{-45}$**
ALK	ENSG00000171094	**1.61**	**$1.16x10^{-16}$**	**$3.96x10^{-16}$**

Figure 4-2: Differential expression of crizotinib target genes in basal versus other BC subtypes in TCGA. (a) Boxplots showing voom-normalised expression of *ROS1*, *MET*, and *ALK* across BC subtypes. Samples were grouped as basal (TNBC) or other BC subtypes. Points represent individual tumour samples; boxplots indicate median and IQR. **(b)** DEA results for *ROS1, MET, and ALK* comparing basal versus other BC subtypes.

Crizotinib (Xalkori) is a clinically approved multi-targeted RTK inhibitor primarily targeting MET, ALK, and ROS1. It was initially approved by the FDA in 2011 for *ALK*-positive NSCLC (639), with subsequent approvals extended to *ROS1*-rearranged NSCLC (640), *ALK*-positive systemic anaplastic large cell lymphoma (sALCL) (641), and *ALK*-positive inflammatory myofibroblastic tumours (642). Although previously evaluated in a phase II clinical trial in TNBC, no clinical responses were observed in the small cohort enrolled, highlighting the need for further investigation of its potential utility in this setting (643).

4.3.2.2.Differential sensitivity of TNBC cell lines to crizotinib treatment

Based on results from a Pfizer pharmacokinetic study, the C_{max} of crizotinib at steady state (250 mg twice daily) is ~368 ng/mL (644), which converts to ~0.82 µM, calculated as follows:

$$\frac{\text{crizotinib } C_{max}}{\text{crizotinib molecular weight}} = \frac{368 \text{ ng/mL}}{450.34 \text{ g/mol}}$$

Sensitivity to crizotinib was assessed across a panel of TNBC cell lines using 5-day acid phosphatase proliferation assays (see Figure 4-3)

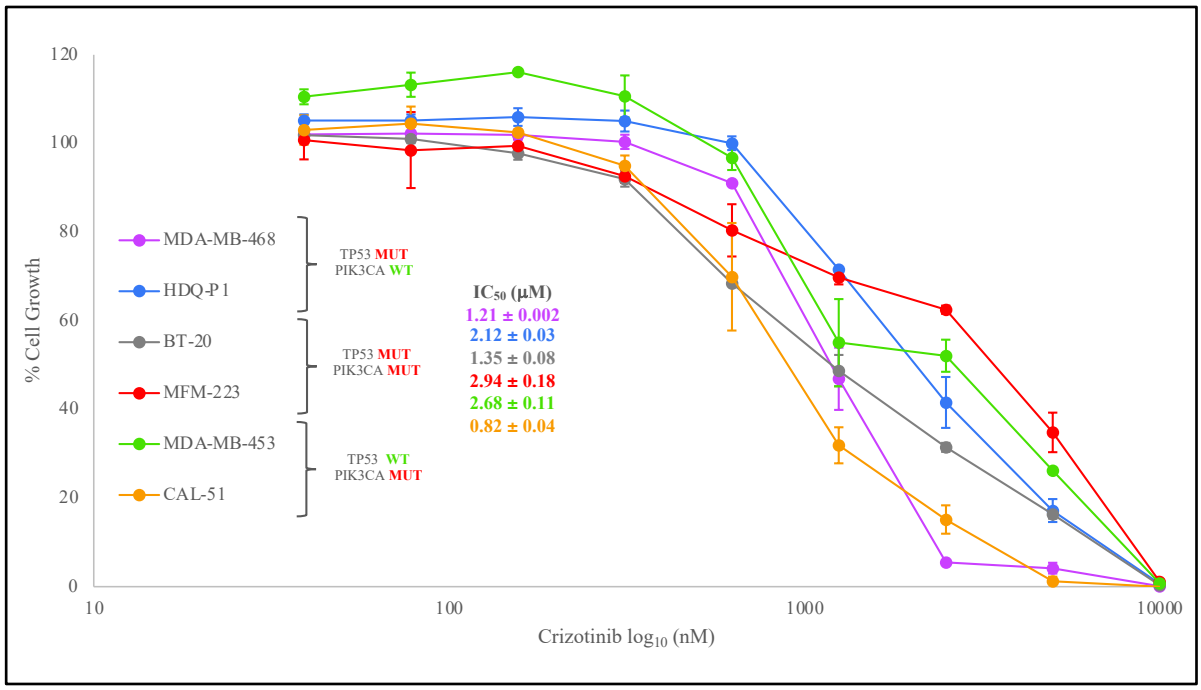


Figure 4-3: Antiproliferative effects of crizotinib on *TP53*- and/or *PIK3CA*-MUT TNBC cell lines. The proliferation of TNBC cell lines was assessed following 5 days of treatment with increasing concentrations of crizotinib (0-10 µM). Percentage growth was calculated relative to untreated control cells. Crizotinib concentrations (nM) were plotted on a $\log_{10}$ scale against percentage cell growth. Error bars indicate the SD of biological replicate experiments (n = 2). IC_{50} values (µM) were determined using CalcuSyn software.

The antiproliferative effects of crizotinib varied among the TNBC cell lines (as shown in Figure 4-3), however, no clear correlation was seen. Additionally, all of the IC_{50} values exceed crizotinib's C_{max} (0.82 µM) (i.e. TNBC is not responsive to crizotinib).

***TP53*-MUT/*PIK3CA*-WT**

Among the *TP53*-MUT/*PIK3CA*-WT cell lines, HDQ-P1 had a higher IC_{50} (2.12 ± 0.03 µM), while MDA-MB-468 had an IC_{50} (1.21 ± 0.002 µM) within the range observed for the *TP53/PIK3CA* co-mutant cell lines.

***TP53*-WT/*PIK3CA*-MUT**

Similar to the findings with alpelisib, the *TP53*-WT/*PIK3CA*-MUT CAL-51 cell line exhibited the greatest sensitivity to crizotinib, with an IC_{50} value of 0.82 ± 0.04 µM. In contrast, another cell line with the same mutational profile, MDA-MB-453, was one of the least sensitive, with an IC_{50} value of 2.68 ± 0.11 µM.

***TP53*-MUT/*PIK3CA*-MUT**

The *TP53/PIK3CA* co-mutant cell lines, BT-20 and MFM-223 demonstrated moderate sensitivity (relative to the other TNBC cell lines) to crizotinib, with IC_{50} values of 1.35 ± 0.08 μM and 2.94 ± 0.18 μM, respectively.

Taken together, despite transcriptional upregulation of crizotinib target genes in TCGA TNBC tumours (Figure 4-2), TNBC cell lines exhibited limited antiproliferative response, with all IC_{50} values exceeding the clinically achievable C_{max}. In addition, crizotinib response varied across TNBC cell lines with different *TP53* and *PIK3CA* mutational statuses, without a clear genotype-response relationship.

4.3.2.3.Sensitivity of *TP53/PIK3CA* co-mutant TNBC cell line to ALK inhibitor and resistance to MET inhibitor

Capmatinib is a selective MET inhibitor, while ceritinib is an ALK inhibitor with additional activity against ROS1 (645,646). These agents were selected to determine whether sensitivity to crizotinib in our model was driven by inhibition of a single dominant RTK (i.e. MET or ALK/ROS1 individually) or instead reflected broader multi-target RTK inhibition.

Based on results from a phase I clinical study, the C_{max} of capmatinib at steady state (400 mg twice daily) is ~4190 ng/mL (647), which converts to ~11.92 μM, calculated as follows:

$$\frac{\text{capmatinib } C_{max}}{\text{capmatinib molecular weight}} = \frac{\text{4910 ng/mL}}{\text{412.42 g/mol}}$$

Based on results from a pharmacokinetic study, the C_{max} of ceritinib at steady state (750 mg once daily) is ~1010 ng/mL, which converts to ~1.81 μM.

$$\frac{\text{ceritinib } C_{max}}{\text{ceritinib molecular weight}} = \frac{\text{1010 ng/mL}}{\text{558.14 g/mol}}$$

Both FDA-approved drugs were evaluated exclusively in the *TP53/PIK3CA* co-mutant MFM-223 cell line as potential alternatives to crizotinib for use in combination with alpelisib, as shown in Figure 4-4. For direct comparison of RTK sensitivity, results from MFM-223 cells treated with crizotinib (as shown in Figure 4-3) were also included.

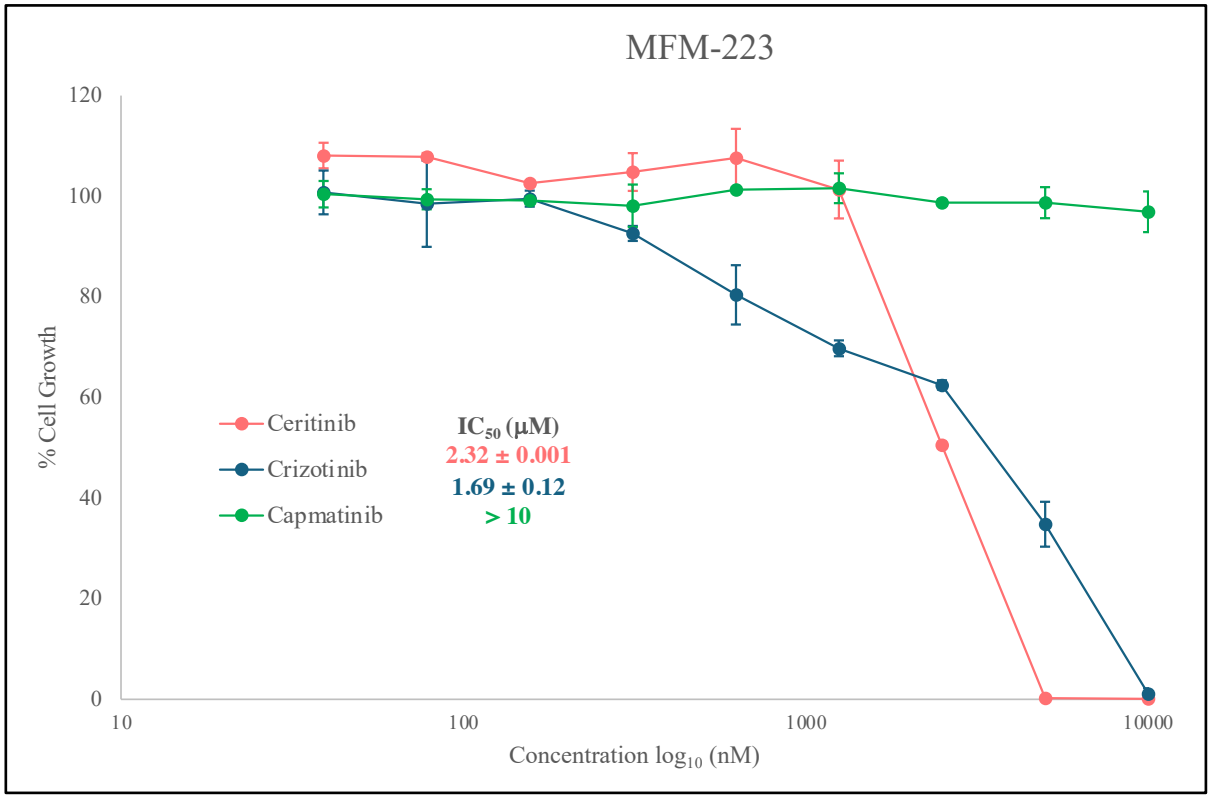


Figure 4-4: Antiproliferative effects of RTK inhibitors on *TP53/PIK3CA* co-mutant TNBC cell line with RTK target gene alterations. The proliferation of MFM-223 was assessed following 5 days of treatment with increasing concentrations of crizotinib, ceritinib, and capmatinib (0-10 µM). Percentage growth was calculated relative to untreated control cells. Drug concentrations (nM) were plotted on a $\log_{10}$ scale against percentage cell growth. Error bars indicate the SD of biological replicate experiments (n = 2).

The *TP53/PIK3CA* co-mutant MFM-223 cell line demonstrated some sensitivity to both crizotinib and ceritinib, particularly at higher drug concentrations, but showed no response to capmatinib, as illustrated in Figure 4-4. Ceritinib induced a response at 2.5 µM (IC_{50} = 2.32 ± 0.001 µM), which exceeds its clinically achievable C_{max}. Although MFM-223 harbours an *ALK* D1311N variant within the kinase domain, this mutation is reported to be non-transforming and does not affect ALK autophosphorylation, suggesting it is functionally inert (648). An IC_{50} value could not be calculated for capmatinib using CalcuSyn, as the MFM-223 cell line did not exhibit any inhibitory response to the drug. Notably, cell viability exceeded 100% at several concentrations, indicating a pro-proliferative response. These data indicate that selective MET inhibition with capmatinib, and ALK inhibition with ceritinib, both produce limited anti-proliferative effects, suggesting that neither RTK alone is a dominant single-agent therapeutic target in this *TP53/PIK3CA* co-mutant model

4.3.3. Summary

Table 4-2: IC_{50} values for alpelisib, crizotinib, ceritinib, and capmatinib across a panel of *TP53*- and/or *PIK3CA*-MUT TNBC cell lines.

		IC_{50} (μM)			
Cell Line	***TP53*/*PIK3CA***	**Alpelisib**	**Crizotinib**	**Ceritinib**	**Capmatinib**
MDA-MB-468	*TP53*-MUT/*PIK3CA*-WT	5.14 ± 1.12	1.21 ± 0.002	-	-
HDQ-P1	*TP53*-MUT/*PIK3CA*-WT	2.05 ± 0.16	2.12 ± 0.03	-	-
BT-20	*TP53*-MUT/*PIK3CA*-MUT	2.22 ± 0.41	1.35 ± 0.08	-	-
MFM-223	*TP53*-MUT/*PIK3CA*-MUT	1.07 ± 0.06	2.94 ± 0.18	2.32 ± 0.001	> 10
MDA-MB-453	*TP53*-WT/*PIK3CA*-MUT	0.60 ± 0.11	2.68 ± 0.11	-	-
CAL-51	*TP53*-WT/*PIK3CA*-MUT	0.43 ± 0.09	0.82 ± 0.04	-	-

The mutational status of *TP53* and *PIK3CA* appeared to influence the response to the PI3K inhibitor alpelisib, as reflected by the IC_{50} values presented in Table 4-2. Cell lines harbouring a *PIK3CA* mutation alone were the most sensitive, whereas those with a co-occurring *TP53* mutation exhibited increased resistance. Additionally, cell lines with *EGFR* amplification showed further resistance to alpelisib compared to a cell line with the same *TP53* and *PIK3CA* mutational background but without *EGFR* amplification (i.e. MDA-MB-468 vs. HDQ-P1 and BT-20 vs. MFM-223). These findings suggest that *TP53* mutations and *EGFR* amplification may independently contribute to reduced sensitivity to PI3K inhibition in *PIK3CA*-MUT TNBC.

No clear correlation was observed between *TP53* or *PIK3CA* mutational status and response to crizotinib, as cell lines exhibited variable sensitivity irrespective of genetic background. Although crizotinib targets (*MET*, *ALK*, and *ROS1*) were transcriptionally upregulated in TCGA TNBC tumours relative to other BC subtypes, all TNBC cell lines exhibited IC_{50} values exceeding the clinically achievable C_{max}, indicating limited single-agent activity *in vitro*. This may reflect a disconnect between tumour-level transcriptional enrichment and functional drug dependency in cell lines, potentially driven by pathway redundancy and compensatory signalling. However, crizotinib may retain utility in combination settings where RTK signalling is functionally engaged. Similarly, capmatinib and ceritinib may be more relevant as components of rational combination strategies rather than monotherapies in TNBC.

4.4. Effects of RTK-targeted therapies in combination with PI3K inhibitor alpelisib on TNBC cell lines harbouring *TP53* and/or *PIK3CA* mutations

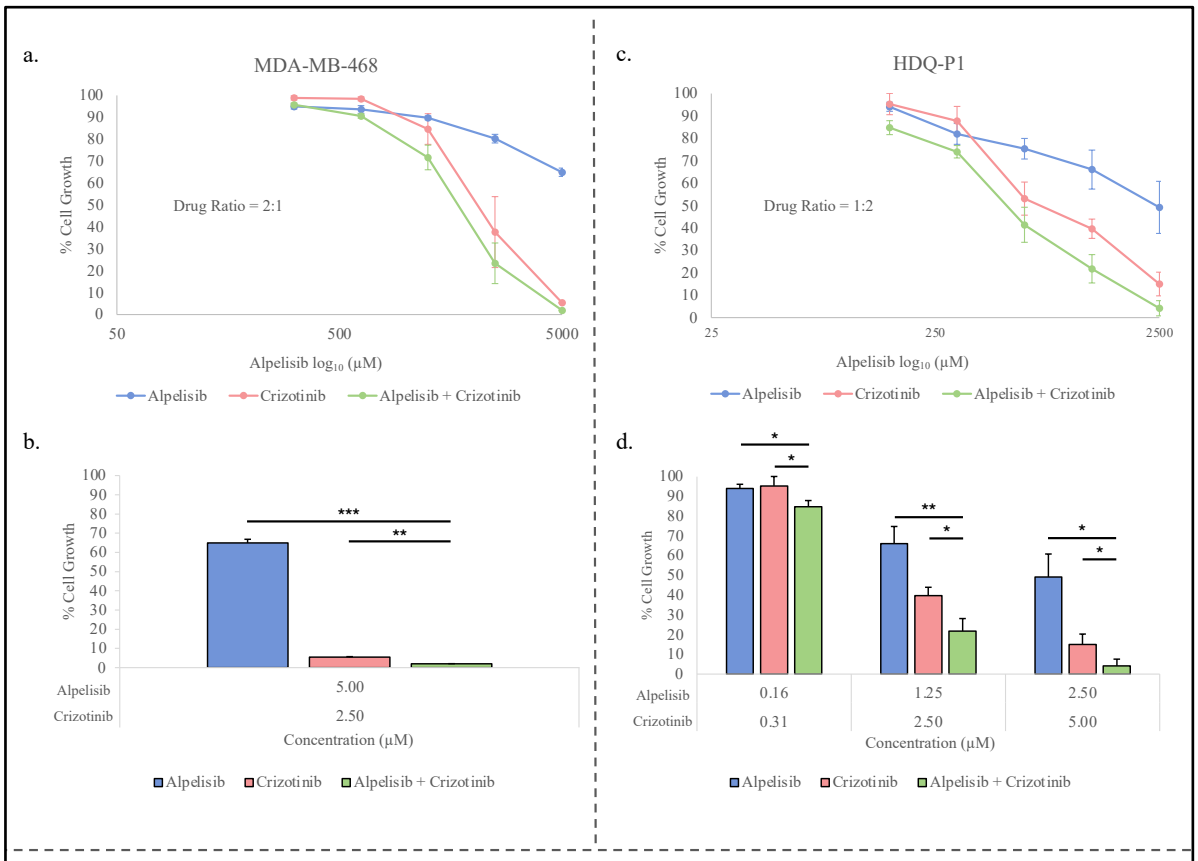
This section investigates the therapeutic potential of combining alpelisib with crizotinib, ceritinib, or capmatinib in TNBC. Given the limited efficacy of alpelisib as a single agent – particularly in *TP53/PIK3CA* co-mutant cell lines – we hypothesised that resistance to PI3K inhibition may, in part, be mediated by compensatory signalling. Although TNBC cell lines were not highly sensitive to RTK inhibition as single agents, RTK genes (*MET*, *ALK*, and *ROS1*) were transcriptionally upregulated in TCGA TNBC tumours relative to other BC subtypes (Figure 4-2). This suggests that these pathways may still contribute to TNBC biology and represent potential upstream signalling routes that could be therapeutically exploited through co-targeting strategies, consistent with previously described mechanisms of PI3K/AKT/mTOR inhibitor resistance involving RTK reactivation (Table 1-9, Chapter 1). Accordingly, combination strategies were evaluated to determine whether concurrent inhibition of PI3K and RTK signalling could enhance treatment efficacy.

Based on the single-agent IC_{50} results presented in Section 4.3 (Table 4-2), five serial concentrations of each drug were selected for treatment of the cell lines. The specific concentration ranges used are detailed in Table 2-6 (Chapter 2).

4.4.1. Crizotinib in combination with alpelisib

TNBC cell lines were treated with alpelisib, crizotinib, or a fixed-ratio combination of both agents to assess potential combinatorial effects between PI3K and RTK inhibition. Combination responses were evaluated using dose-response modelling to determine IC_{50} values, CI scores, and DRIs, allowing assessment of both synergy and potential for clinically relevant dose reduction relative to each drug's single-agent activity. Interpretation of CI values follows the Chou-Talalay classification framework (see Table 2-7, Chapter 2).

4.4.1.1. Moderately synergistic response to alpelisib and crizotinib combination in *TP53*-MUT/*PIK3CA*-WT TNBC cell lines



e.

Cell Line	Alpelisib IC_{50} (μM)	Crizotinib IC_{50} (μM)	Alpelisib + Crizotinib IC_{50} (μM)	CI at ED_{50}	CI at ED_{75}	CI at ED_{90}
MDA-MB-468	> 5.00 (9.75 ± 0.32)	1.07 ± 0.09	1.38 ± 0.09	0.88 ± 0.02 (+)	0.82 ± 0.04 (++)	0.80 ± 0.12 (++)
HDQ-P1	2.65 ± 1.06	1.76 ± 0.39	0.50 ± 0.33	0.91 ± 0.12 (±)	0.76 ± 0.01 (++)	0.70 ± 0.14 (++)

Figure 4-5: Antiproliferative effects of crizotinib, alpelisib, and their combination on *TP53*-MUT/*PIK3CA*-WT TNBC cell lines: (a) MDA-MB-468 and **(c)** HDQ-P1. Drug concentrations (nM) plotted on a $\log_{10}$ scale against percentage cell growth with the drug ratios for alpelisib plus crizotinib indicated (alpelisib:crizotinib). Error bars represent the SD from independent biological replicates (n = 3). Statistical significance of differences in cell growth between treatment conditions was assessed using Student's t-test, with significant results shown in bar charts for **(b)** MDA-MB-468 and **(d)** HDQ-P1 (drug concentrations shown in μM). **(e)** IC_{50} (μM) and CI values for *TP53*-MUT/*PIK3CA*-WT TNBC cell lines treated with alpelisib plus crizotinib. CI values at ED_{50}, ED_{75}, and ED_{90} were determined to assess the nature of the drug interactions. * = $p \leq 0.05$; ** = $p \leq 0.01$; *** = $p \leq 0.001$; **** = $p \leq 0.0001$.

As illustrated in Figure 4-5(e), *TP53*-MUT/*PIK3CA*-WT TNBC cell lines exhibited slight (+)/nearly additive (±) synergy at the ED_{50}, escalating to moderate synergy (++) at the ED_{75} and ED_{90} doses. Although synergy was evident across these metrics, statistically significant differences between the combination therapy and single-agent treatments were confined to the

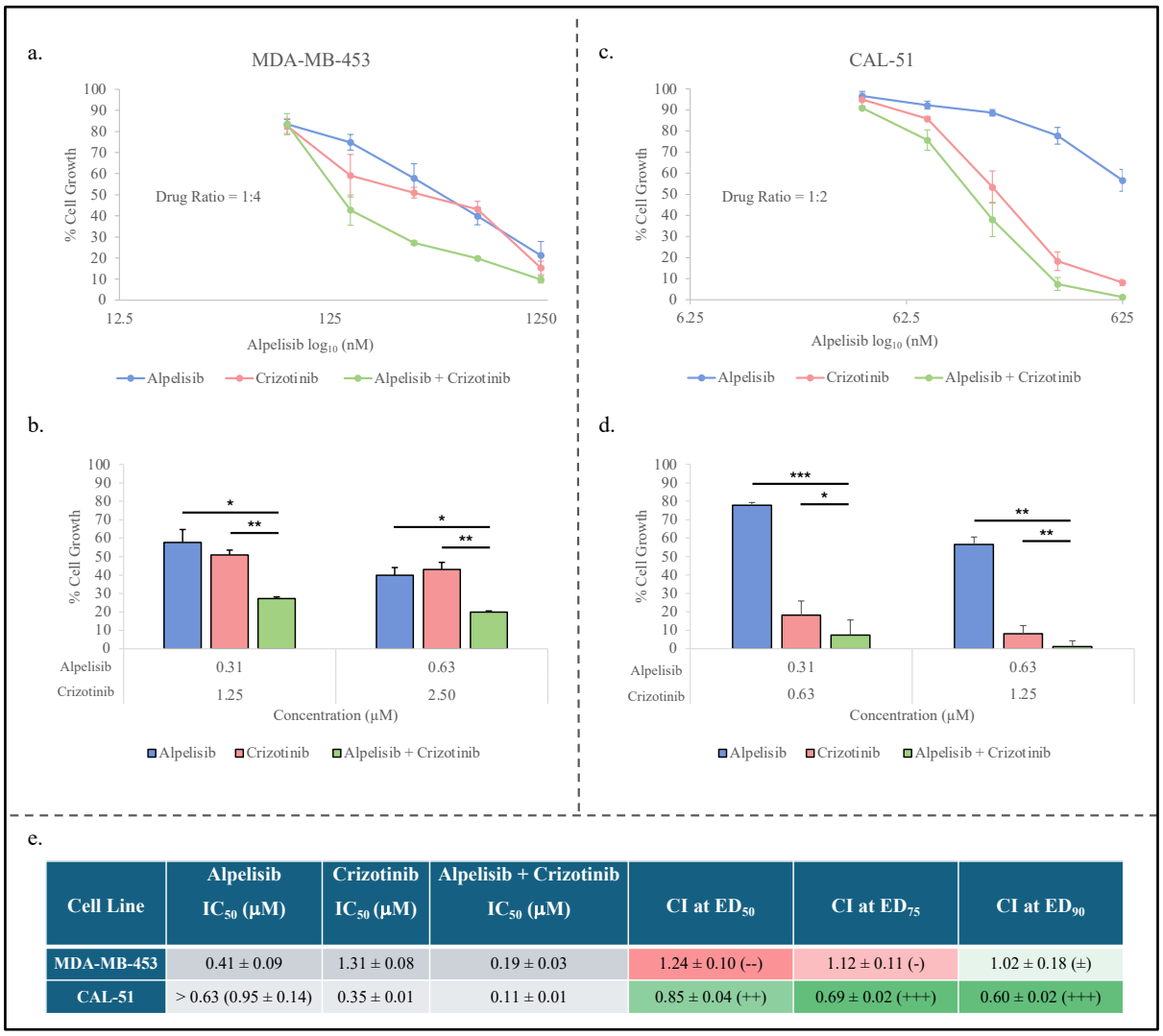
higher concentrations tested. Single drug concentrations in the combinations were assessed via Calcusyn-derived DRI values at ED_{50} to confirm achievability within therapeutic ranges (i.e. below C_{max}).

In MDA-MB-468 cells, for the combination only the highest concentrations of alpelisib (5.00 μM) and crizotinib (2.50 μM) yielded a significant reduction in growth (see Figure 4-5(b)), however this effect was modest relative to crizotinib treatment alone (2.76-fold decrease) and achieved significance primarily due to low inter-replicate variability. Alpelisib demonstrated a DRI of 7.09 ± 0.66 at ED_{50} (solo concentration: 9.54 μM), yielding a reduced combination concentration of 1.35 μM for equivalent efficacy – well below its C_{max} (~5.62 μM). In contrast, crizotinib showed a DRI of 1.55 ± 0.01 at ED_{50} (solo concentration: 10.12 μM), resulting in a reduced combination concentration of 6.54 μM, which greatly exceeded its C_{max} (~0.82 μM). Accordingly, while alpelisib exhibited synergistic dose reduction within a clinically achievable range, crizotinib required concentrations beyond its therapeutically achievable dose, suggesting that the observed interaction may have limited clinical applicability in MDA-MB-468 cells.

In contrast, HDQ-P1 cells showed significance at three combination concentrations (see Figure 4-5(d)), with the maximum fold-change (FC) reduction of 3.59 observed at the highest doses of alpelisib (2.50 μM) and crizotinib (5.00 μM) compared to crizotinib alone. Reductions in the remaining concentrations were minimal (< 2-fold). Alpelisib demonstrated a DRI of 5.17 ± 1.70 at ED_{50} (solo concentration: 3.19 μM), yielding a reduced combination concentration of 0.62 μM for equivalent efficacy – well below its C_{max} (~5.62 μM). Crizotinib showed a DRI of 1.75 ± 0.24 at ED_{50} (solo concentration: 1.43 μM), resulting in a reduced combination concentration of 0.82 μM, which matched its C_{max} (0.82 μM). Thus, the combination aligns with the therapeutic ranges for both drugs, affirming its potential clinical relevance at the ED_{50} level, though matching the reduced concentration to C_{max} for crizotinib leaves a narrow margin for variability in pharmacokinetics.

In summary, the combination of alpelisib and crizotinib exhibited modest to moderate synergy in *TP53*-MUT/*PIK3CA*-WT TNBC cell lines, although significant antiproliferative effects were confined to higher concentrations with small fold changes, and clinical relevance was limited as the therapeutic window for crizotinib was either exceeded or just matched in the tested models.

4.4.1.2. Differential response to alpelisib and crizotinib combination in *TP53*-WT/*PIK3CA*-MUT TNBC cell lines



e.

Cell Line	Alpelisib IC_{50} (µM)	Crizotinib IC_{50} (µM)	Alpelisib + Crizotinib IC_{50} (µM)	CI at ED_{50}	CI at ED_{75}	CI at ED_{90}
MDA-MB-453	0.41 ± 0.09	1.31 ± 0.08	0.19 ± 0.03	1.24 ± 0.10 (--)	1.12 ± 0.11 (-)	1.02 ± 0.18 (±)
CAL-51	> 0.63 (0.95 ± 0.14)	0.35 ± 0.01	0.11 ± 0.01	0.85 ± 0.04 (++)	0.69 ± 0.02 (+++)	0.60 ± 0.02 (+++)

Figure 4-6: Antiproliferative effects of crizotinib, alpelisib, and their combination on *TP53*-WT/*PIK3CA*-MUT TNBC cell lines: (a) MDA-MB-453 and **(c)** CAL-51. Drug concentrations (nM) plotted on a log_{10} scale against percentage cell growth, with the drug ratios for alpelisib plus crizotinib indicated (alpelisib:crizotinib). Error bars represent the SD from independent biological replicates (n = 3). Statistical significance of differences in cell growth between treatment conditions was assessed using Student's t-test, with significant results shown in bar charts for **(b)** MDA-MB-453 and **(d)** CAL-51 (drug concentrations shown in µM). **(e)** IC_{50} (µM) abd CI values for *TP53*-WT/*PIK3CA*-MUT TNBC cell lines treated with alpelisib plus crizotinib. CI values at ED_{50}, ED_{75}, and ED_{90} were determined to assess the nature of the drug interactions. * = $p \leq 0.05$; ** = $p \leq 0.01$; *** = $p \leq 0.001$; **** = $p \leq 0.0001$.

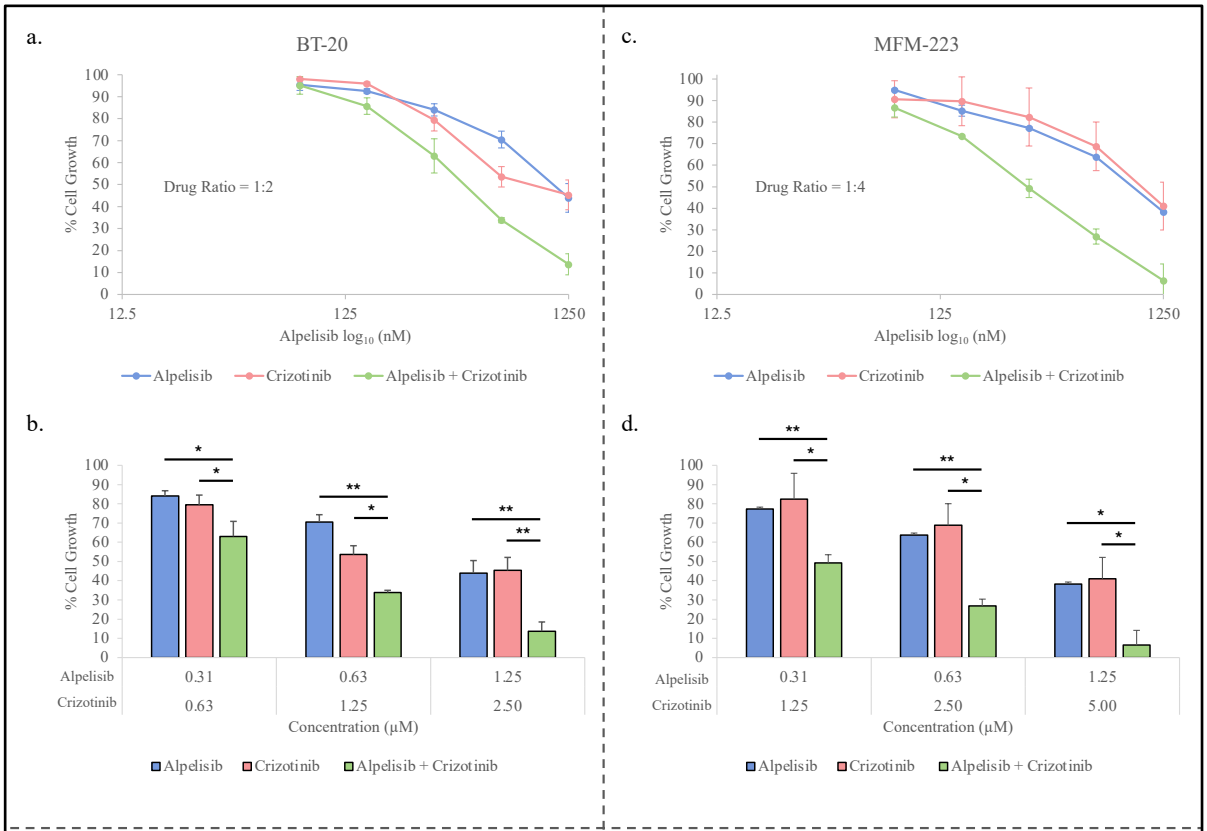
As illustrated in Figure 4-6(e), *TP53*-WT/*PIK3CA*-MUT TNBC cell lines exhibited heterogenous responses to the alpelisib plus crizotinib combination.

In MDA-MB-453 cells, slight (-)/moderate (--) antagonism was observed across the ED_{50} and ED_{75} doses, escalating to nearly additive (±) effects at the ED_{90} dose. Despite this antagonism, significant FCs were evident at two combination concentrations, with the greatest reductions (> 2-fold versus both single agents) occurring at 1.25 μM alpelisib and 0.31 μM crizotinib (see Figure 4-6(b)). The observed antagonism likely arises because the CI values are heavily influenced by the slope of the dose-response curves, and in this case, the combination curve did not appear to demonstrate a steeper slope than either single-agent curve at any of the doses, resulting in CI values exceeding 1. As the combination was not synergistic, the DRI values were not calculated for MDA-MB-453.

In contrast, CAL-51 cells demonstrated moderate (++) synergy at the ED_{50} dose, escalating to synergy (+++) at the ED_{75} and ED_{90} doses. Despite this synergy, only two concentrations showed significant FC differences between the combination and both single agents. Although the maximum FC versus crizotinib alone reached a 6.5-fold decrease, this appeared deceptively large, as the underlying differences in percentage cell growth were minimal (8.15% versus 1.25%). Alpelisib demonstrated a DRI of 8.35 ± 0.55 at ED_{50} (solo concentration: 8.13 μM), yielding a reduced combination concentration of 0.10 μM for equivalent efficacy – well below its C_{max} (~5.62 μM). Crizotinib showed a DRI of 1.54 ± 0.09 at ED_{50} (solo concentration: 0.94 μM), resulting in a reduced combination concentration of 0.61 μM, below its C_{max} (~0.82 μM). Thus, both drugs in this combination remain within their respective therapeutic windows at ED_{50}, supporting the potential clinical feasibility of this pairing in CAL-51 cells.

Overall, *TP53*-WT/*PIK3CA*-MUT TNBC cell lines showed heterogeneous responses to the alpelisib-crizotinib combination, with MDA-MB-453 exhibiting antagonism or near-additive effects, while CAL-51 displayed moderate to strong synergy within clinically achievable concentrations, highlighting cell line-specific differences in combination efficacy.

4.4.1.3.Synergistic response to alpelisib and crizotinib combination in *TP53/PIK3CA* co-mutant TNBC cell lines



e.

Cell Line	Alpelisib IC_{50} (μM)	Crizotinib IC_{50} (μM)	Alpelisib + Crizotinib IC_{50} (μM)	CI at ED_{50}	CI at ED_{75}	CI at ED_{90}
BT-20	1.14 ± 0.15	1.75 ± 0.20	0.43 ± 0.08	1.07 ± 0.16 (±)	0.85 ± 0.05 (+)	0.75 ± 0.0003 (++)
MFM-223	0.89 ± 0.01	3.84 ± 0.53	0.28 ± 0.06	0.74 ± 0.15 (++)	0.56 ± 0.02 (+++)	0.45 ± 0.06 (+++)

Figure 4-7: Antiproliferative effects of crizotinib, alpelisib, and their combination on *TP53/PIK3CA* co-mutant TNBC cell lines: (a) BT-20 and **(c)** MFM-223. Drug concentrations (nM) plotted on a $\log_{10}$ scale against percentage cell growth, with the drug ratios for alpelisib plus crizotinib indicated (alpelisib:crizotinib). Error bars represent the SD from independent biological replicates (n = 3). Statistical significance of differences in cell growth between treatment conditions was assessed using Student's t-test, with significant results shown in bar charts for **(b)** BT-20 and **(d)** MFM-223 (drug concentrations shown in μM). **(e)** IC_{50} (μM) and CI values for *TP53/PIK3CA* co-mutant TNBC cell lines treated with alpelisib plus crizotinib. CI values at ED_{50}, ED_{75}, and ED_{90} were determined to assess the nature of the drug interactions. * = $p \leq 0.05$; ** = $p \leq 0.01$; *** = $p \leq 0.001$; **** = $p \leq 0.0001$.

As illustrated in Figure 4-7(e), *TP53/PIK3CA* co-mutant TNBC cell lines exhibited synergistic responses to the alpelisib plus crizotinib combination, with escalating synergy across effective doses.

In BT-20 cells, nearly additive (±) effects were observed at the ED_{50} dose, progressing to slight (+) synergy at the ED_{75} and moderate (++) synergy at the ED_{90}. Significant FCs emerged at three combination concentrations, with the greatest reductions (> 3-fold versus either single agent) at the highest doses of alpelisib (1.25 μM) and crizotinib (2.50 μM) (see Figure 4-7(b)). Alpelisib demonstrated a DRI of 2.65 ± 0.14 at ED_{50} (solo concentration: 1.06 μM), yielding a reduced combination concentration of 0.40 μM for equivalent efficacy – well below its C_{max} (~5.62 μM). Crizotinib showed a DRI of 2.05 ± 0.42 at ED_{50} (solo concentration: 1.56 μM), resulting in a reduced combination concentration of 0.52 μM, falling below its C_{max} (~0.82 μM). However, the DRI values for ED_{75} and ED_{90} did not fall below the C_{max} for crizotinib, indicating that only the additive effects observed at ED_{50} occurred fully within the therapeutic window. Therefore, while higher-effect levels (ED_{75}-ED_{90}) extend beyond crizotinib's therapeutic range, the ED_{50} combination achieves effective inhibition at clinically attainable concentrations, supporting its potential translational relevance in BT-20 cells.

Similarly, MFM-223 cells demonstrated moderate (++) synergy at the ED_{50}, escalating to synergy (+++) at the ED_{75} and ED_{90} doses. Significant FCs were also noted at three concentrations, peaking at ~6-fold decreases versus either single agent at the highest doses of alpelisib (1.25 μM) and crizotinib (5.00 μM) (see Figure 4-7(d)). Alpelisib demonstrated a DRI of 3.24 ± 0.58 at ED_{50} (solo concentration: 0.88 μM), yielding a reduced combination concentration of 0.27 μM for equivalent efficacy – well below its C_{max} (~5.62 μM). Crizotinib showed a DRI of 3.47 ± 0.50 at ED_{50} (solo concentration: 0.90 μM), resulting in a reduced combination concentration of 0.26 μM, falling well below its C_{max} (~0.82 μM). Thus, the combination enables effective inhibition by both drugs at concentrations within their respective therapeutic windows, highlighting the potential clinical relevance of this pairing in MFM-223 cells.

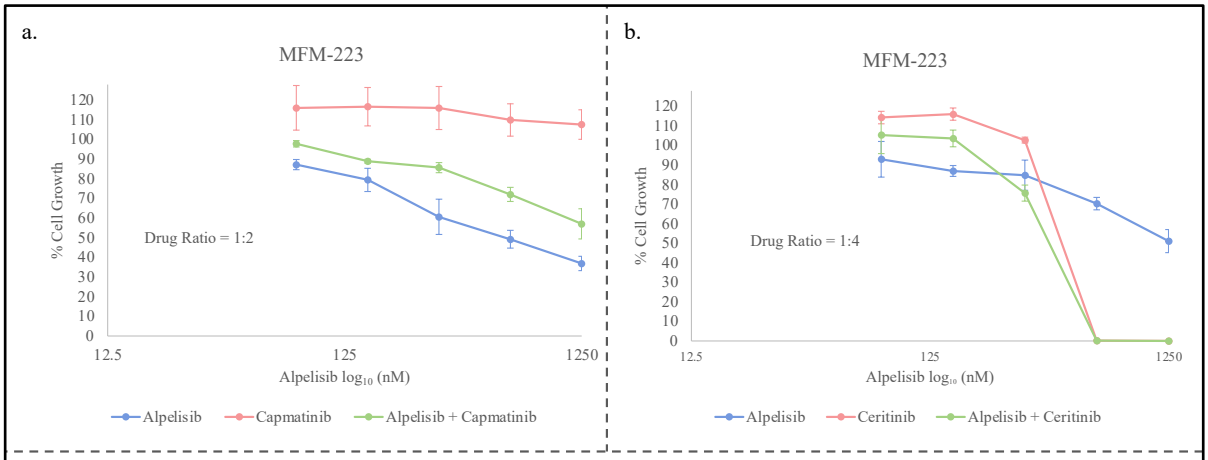
Overall, *TP53/PIK3CA* co-mutant TNBC cell lines exhibited dose-dependent synergy to the alpelisib-crizotinib combination, with both BT-20 and MFM-223 achieving effective inhibition within therapeutically achievable concentrations, underscoring the potential clinical relevance in *TP53/PIK3CA* co-mutant TNBC.

4.4.2. Other RTK inhibitors in combination with alpelisib

Given the synergistic effect observed with the alpelisib plus crizotinib combination in the *TP53/PIK3CA* co-mutant MFM-223 cell line (see Figure 4-7(c,d)), we extended our investigation to assess the effects of combining alpelisib with two additional RTK inhibitors: capmatinib and ceritinib. Ceritinib reduced proliferation in MFM-223 cells, whereas capmatinib alone did not (Figure 4-4). Despite this, we proceeded to test both in combination with alpelisib, hypothesising that the dual mechanism of action might enhance antiproliferation or help overcome potential resistance mechanisms.

The combination of ceritinib and alpelisib has demonstrated potent synergistic activity in a preclinical *in vivo* model of ALK-rearranged NSCLC (649). In contrast, there is no reported evidence of alpelisib being evaluated in combination with capmatinib.

The outcomes of the alpelisib plus capmatinib and alpelisib plus ceritinib combinations are presented in Figure 4-8.



c.

MFM-223 Combination	Alpelisib IC_{50} (μM)	Capmatinib / Ceritinib IC_{50} (μM)	Combination IC_{50} (μM)	CI at ED_{50}	CI at ED_{75}	CI at ED_{90}
Alpelisib + Capmatinib	1.36 ± 0.11	> 5.00	2.54 ± 0.35	1.98 ± 0.08 (---)	1.65 ± 0.02 (---)	1.38 ± 0..03 (--)
Alpelisib + Ceritinib	1.25 ± 0.39	1.77*	0.33 ± 0.01	1.20 ± 0.02 (-)	1.11 ± 0.04 (-)	1.20 ± 0.02 (-)

Figure 4-8: Antiproliferative effects of capmatinib, ceritinb, and their combination with alpelisib on *TP53/PIK3CA* co-mutant TNBC cell line MFM-223. Cell growth percentage is plotted against alpelisib concentration (nM) on a log_{10} scale, with the drug ratios for alpelisib and **(a)** capmatinib or **(b)** ceritinib indicated (alpelisib:capmatinib/ceritinib). Error bars represent the SD from independent biological replicates (n = 3). **(c)** IC_{50} and CI values (μM) for the MFM-223 cell line treated with alpelisib plus capmatinib or alpelisib plus ceritinib. CI values at ED_{50}, ED_{75}, and ED_{90} were determined to assess the nature of the drug interactions. * No SD value observed due to all cell growth % values falling outside the < 100% / > 0% range.

In both the alpelisib plus capmatinib and alpelisib plus ceritinib combination assays, cell growth percentages exceeded 100% (indicating stimulation) and reached 0% (indicating complete inhibition). Consequently, for CI calculations using CalcuSyn, negative fraction FA values (>100% growth) were substituted with 0.01, and FA values of 1.00 (0% growth) with 0.99, as the software cannot accommodate these extremes. Although this substitution may have influenced the resulting CI values, it was necessary to assess the nature of the drug interactions.

Treatment of MFM-223 cells with a combination of alpelisib plus capmatinib (see Figure 4-4(a)) appeared to diminish the antiproliferative effect of alpelisib rather than enhance it, as no reduction in cell growth was observed across any of the tested concentrations. This was reflected in the CI values (see Figure 4-8(c)) where the combination demonstrated antagonism (~3) across the ED_{50}, ED_{75}, and ED_{90} doses.

As illustrated in Figure 4-8(b), at lower concentrations (78-156 nM alpelisib concentration on the graph), ceritinib diminished the antiproliferative effect of alpelisib similarly to the alpelisib

plus capmatinib combination, with combination-induced cell growth rates falling between those of the individual single agents. Also, similarly to the alpelisib plus capmatinib pairing, both ceritinib monotherapy and the alpelisib plus ceritinib combination promoted cell growth, yielding percentages exceeding 100%. At higher concentrations where the combination elicited inhibition (~313 nM alpelisib concentration on the graph), the reduction in cell growth relative to ceritinib monotherapy was significant FC = 0.74, p = 0.004), however, it was not significant compared to alpelisib monotherapy, indicating no enhancement of antiproliferative activity over either single agent. These findings were reflected in the CI values (see Figure 4-8(c)) where the combination demonstrated slight antagonism (~1.1-1.2) across the ED_{50}, ED_{75}, and ED_{90} doses.

For the ceritinib single agent treatments, all replicate cell growth percentages either exceeded 100% or reached 0%, resulting in identical FA values across replicates for input into CalcuSyn. Consequently, this lack of variation between replicates produced a single IC_{50} value with no SD.

4.4.3. Summary

This section examined alpelisib combinations with crizotinib, ceritinib, or capmatinib to overcome TNBC resistance, hypothesising mitigation of compensatory PI3K/AKT activation, especially in alpelisib-resistant *TP53/PIK3CA* co-mutant TNBC cell lines.

- ***TP53*-MUT/*PIK3CA*-WT TNBC:** Alpelisib plus crizotinib showed modest-to-moderate synergy at high concentrations. Alpelisib doses could be reduced below C_{max}, but crizotinib either exceeded or just matched its C_{max}, limiting clinical applicability.
- ***TP53*-WT/*PIK3CA*-MUT TNBC:** Responses were heterogeneous. MDA-MB-453 showed antagonism or near-additive effects, while CAL-51 displayed moderate-to-strong synergy. In CAL-51, both drugs remained within therapeutic windows, supporting potential clinical feasibility.
- ***TP53*-MUT/*PIK3CA*-MUT TNBC:** BT-20 and MFM-223 exhibited robust, dose-dependent synergy. DRI calculations showed that the combination allowed both alpelisib and crizotinib to achieve effective inhibition at reduced concentrations well below their respective C_{max} values, highlighting strong translational potential for this genotype.

- **Alpelisib plus capmatinib or ceritinib (MFM-223):** Both combinations were largely antagonistic or ineffective. Capmatinib attenuated alpelisib activity, and ceritinib showed slight antagonism without enhancing antiproliferative effects. Effective concentrations could not be achieved within therapeutic windows, indicating low clinical relevance.

Overall: Alpelisib plus crizotinib demonstrates the most promising, genotype-specific efficacy, particularly in *TP53/PIK3CA* co-mutant TNBC, with effective concentrations achievable within the therapeutic window. Other RTK combinations are largely ineffective in TNBC models.

4.5. Combined treatment with alpelisib plus crizotinib induces apoptosis in *TP53/PIK3CA* co-mutant TNBC cell line

Due to the strong synergistic effect observed in MFM-223 cells following treatment with the combination of alpelisib plus crizotinib, this cell line was selected for further investigation. For the apoptosis experiments, cells were treated with 0.625 μM alpelisib and 2.5 μM crizotinib. While the crizotinib concentration exceeds the clinically achievable therapeutic window, the DRI analysis from Section 4.4.1.3. suggests that synergistic effects could be observed at lower, clinically relevant doses. The efficacy of the combination treatment was evaluated by monitoring apoptosis induction over five days (120 h), as described in Section 2.8. (Chapter 2).

Figure 4-9(a) presents the changes in cell confluence throughout this period and is consistent with the proliferation assay findings (see Figure 4-7(c)), demonstrating that the combination had a more pronounced inhibitory effect on cell growth compared to either drug alone, as well as the DMSO and untreated controls.

Figure 4-9(b) shows that apoptosis was significantly induced in cells treated with the drug combination. In contrast, apoptosis in the untreated, DMSO, and alpelisib-only groups was only observed at later timepoints. This delayed response may reflect apoptosis arising following prolonged PI3K inhibitor-induced cell-cycle arrest, rather than immediate drug-induced cell death. Notably, crizotinib-treated cells exhibited reduced confluence but did not undergo apoptosis, indicating a cytostatic rather than cytotoxic effect (650).

To account for variability between replicates, apoptosis levels were normalised to the untreated control, as shown in Figure 4-9(c). This analysis confirms that only the combination treatment

induced a clear apoptotic response relative to the baseline. A statistically significant increase in apoptosis in the combination-treated group compared to the DMSO control was observed at both the 24 h and 44 h timepoints.

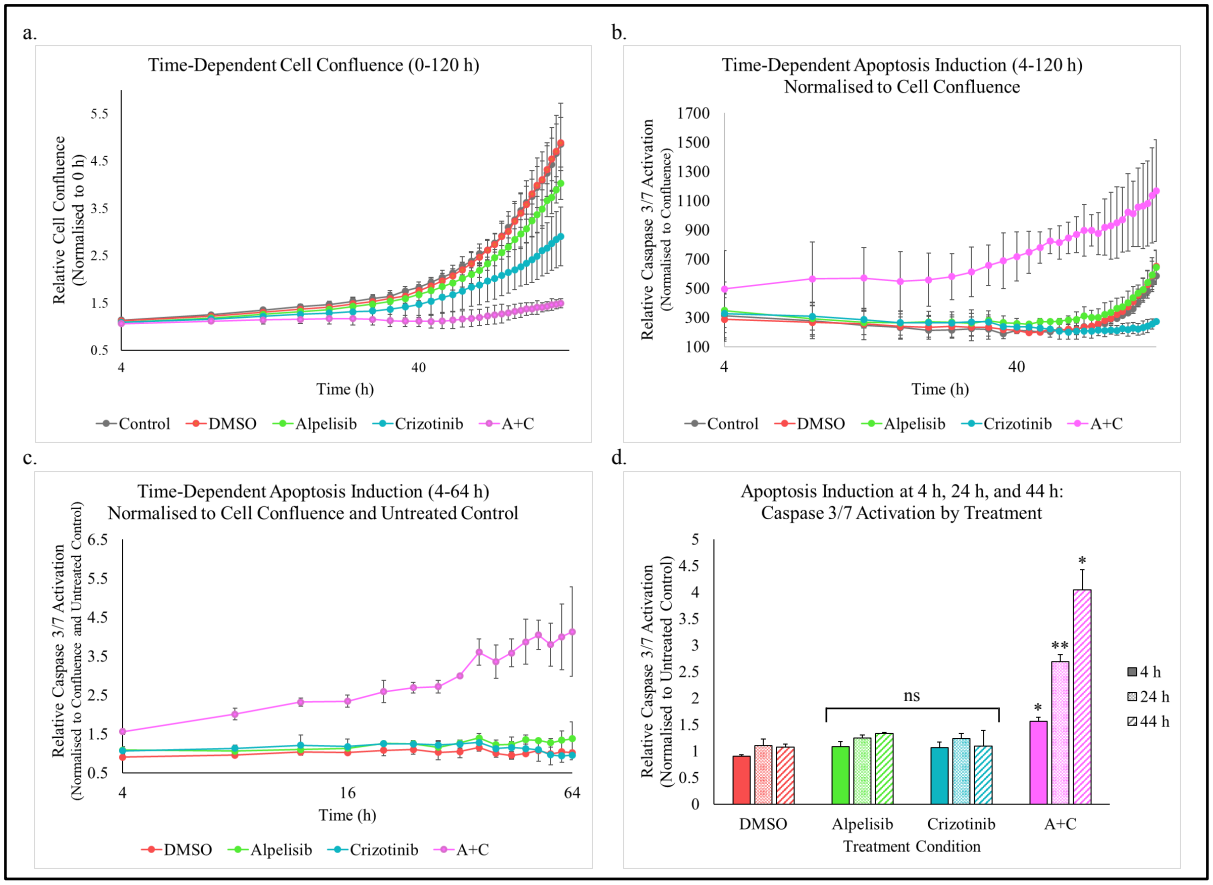


Figure 4-9: Induction of apoptosis (Caspase 3-7 activity) in MFM-223 cells following treatment with alpelisib, crizotinib, or a combination of both. MFM-223 cells were treated with 0.625 µM alpelisib, 2.5 µM crizotinib, or a combination of both. **(a)** Cell confluence (4-120 h) was determined from phase contrast images and normalised to the 0 h timepoint confluence. **(b)** Apoptosis was assessed by measuring Caspase 3/7 activity and normalised to the confluence. **(c)** Relative Caspase 3/7 activity was normalised to the untreated control for the 4-64 h timeframe. **(d)** Apoptosis induction at 4 h, 24 h, and 44 h timepoints are represented in a bar chart. Data are presented as mean ± SD from independent experiments (n = 2). Statistical significance between the treated cells versus the DMSO control at a specific timepoint was determined using Student's t-test; *p < 0.05, **p < 0.01.

4.6. Alpelisib plus crizotinib treatment induces significant protein dysregulation in *TP53/PIK3CA* co-mutant TNBC cells

To investigate the distinct effects and underlying mechanisms contributing to the enhanced antiproliferative and apoptotic activity of the alpelisib plus crizotinib combination compared to either agent alone, MFM-223 cells were treated with alpelisib and/or crizotinib for 24 h. This timepoint was selected to capture early signalling alterations preceding the onset of extensive apoptotic responses observed at later timepoints. Following treatment, protein lysates were prepared and submitted to the MD Anderson Cancer Center for RPPA analysis, as outlined in Section 2.11..

Drug concentrations were selected based on the lowest doses of each compound that demonstrated synergistic effects in MFM-223 cells – specifically, 0.3125 μM and 1.25 μM crizotinib – as demonstrated in Figure 4-7(d). Although 1.25 μM crizotinib exceeds its C_{max} (0.82 μM), the DRI values reported in Section 4.4.1.3. suggest that similar synergistic effects could be observed at lower, clinically relevant concentrations. The DMSO control was matched to the final DSMO concentration used in the combination treatment to ensure consistency across experimental conditions.

Three biological replicates per condition were initially generated and submitted for RPPA analysis. Following data acquisition, quality control assessment identified variability and occasional outliers within replicate measurements. To ensure robustness, outlier values were excluded, and a minimum of two consistent biological replicates ($n \geq 2$) were retained for downstream analysis.

Significant ($p \leq 0.05$) changes on the expression/phosphorylation profile of 108 proteins were identified in MFM-223 cells after treatment with either alpelisib or crizotinib as single agents or the combination of both. MFM-223 cells treated with alpelisib showed significantly altered levels of 55 proteins, whilst crizotinib altered levels of 31 proteins, and the combination of alpelisib plus crizotinib altered levels of 42 proteins. 52 of these proteins passed the 1.2-FC threshold set for significance (see Table 4-3).

An FC threshold of 1.2 (and 0.83 for downregulation, corresponding to the reciprocal of 1.2) was applied to identify potentially biologically meaningful changes in phosphorylation status. This threshold corresponds to a ~20% increase or decrease in protein level, respectively, and was used to capture relatively modest but functionally relevant shifts, recognising that even

small changes in phosphorylation can propagate through signalling networks to produce amplified downstream effects. This cutoff is widely employed in RPPA analyses to enhance sensitivity while maintaining statistical robustness (651,652).

Table 4-3: Number of proteins/phospho-proteins exhibiting statistically significant changes in expression in MFM-223 cells following 24 h treatment with alpelisib, crizotinib, or their combination, relative to DMSO control ($p \leq 0.05$; $n \geq 2$).

Treatment	Significantly ↑	Significantly ↓
Alpelisib	3	11
Crizotinib	10	7
Alpelisib + Crizotinib	12	9

Alpelisib treatment alone led to a significant upregulation of EMA, JNK2, and Tau protein expression. Concurrently, it downregulated the expression of A-Raf, C-Raf, POLG, ERRα, EZH2, GSK-3α-β, and RRM1. Additionally, a decrease in the phosphorylation levels of AKT (Thr308), HSP27 (Ser82), MAPK (Thr202 / Tyr204), and ULK1 (Ser757), was observed. These findings are summarised in Table 4-4 and illustrated in Figure 4-10(a).

Table 4-4: Proteins/phospho-proteins with significantly altered expression in MFM-223 cells following 24 h treatment with alpelisib ($p \leq 0.05$; $FC \geq 1.2$ or $FC \leq 0.83$; $n \geq 2$).

(Phospho-)protein	Abbreviation	FC	P-value
Epithelial membrane antigen	EMA	2.73	0.003
c-Jun N-terminal kinase 2	JNK2	1.37	0.014
Microtubule-associated protein	Tau	1.29	0.041
Phospho-protein kinase B (Threonine 308)	p-AKT (T308)	0.78	0.033
Rapidly accelerated fibrosarcoma, isoform A	A-Raf	0.79	0.027
Rapidly accelerated fibrosarcoma, isoform C	C-Raf	0.80	0.030
DNA polymerase subunit gamma	POLG	0.78	0.024
Estrogen-related receptor alpha	ERRα	0.57	0.012
Enhancer of Zeste Homolog 2	EZH2	0.69	0.022
Glycogen synthase kinase 3 alpha/beta	GSK-3α-β	0.81	0.019
Phospho-heat shock protein (Serine 82)	p-HSP27 (S82)	0.82	0.019
Phospho-mitogen-activated protein kinase (Threonine 202/Tyrosine 204)	p-MAPK (T202/Y204)	0.81	0.005
Ribonucleotide reductase M1	RRM1	0.65	0.003
Phospho-unc-51 like autophagy activating kinase 1 (Serine 757)	p-ULK1 (S757)	0.82	0.039

A STRING analysis was performed to investigate potential interactions between proteins significantly dysregulated following alpelisib treatment and components of the PI3K/AKT signalling pathway, as illustrated in Figure 4-10(b-c). 11 of the significantly dysregulated proteins exhibited high-confidence interactions either with the PI3K/AKT pathway members or among themselves. Notably, AKT phosphorylation at threonine 308 (Thr308) was significantly reduced. Under normal conditions, active (phosphorylated) AKT phosphorylates GSK-3α-β, leading to its enzymatic inactivation (653). However, RPPA analysis revealed a significant decrease in GSK-3α-β protein levels. As RPPA measures total protein abundance rather than enzymatic activity, this reduction is more consistent with broader pathway-level downregulation

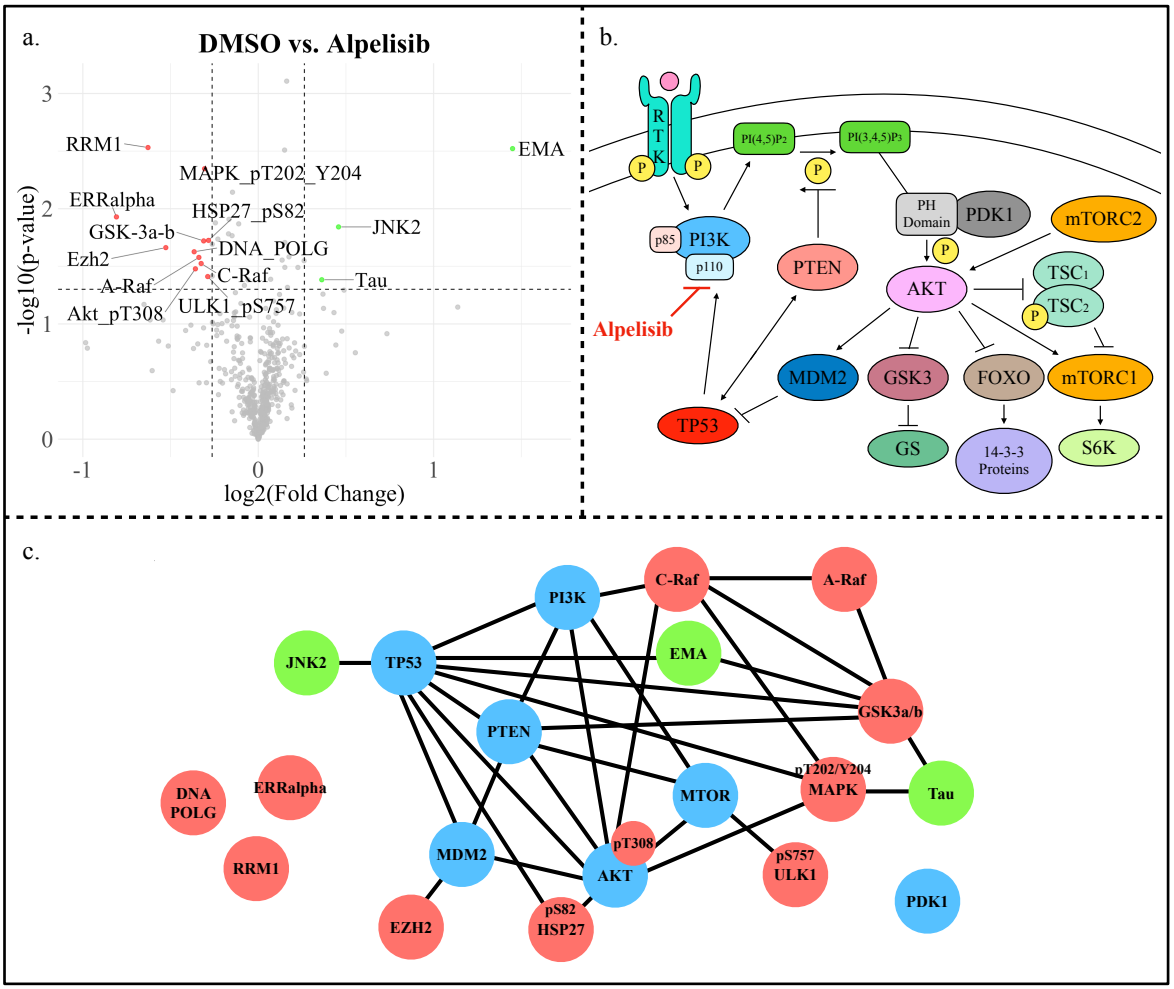


Figure 4-10. (a) Volcano plot illustrating DEA of total and phosphorylated proteins in MFM-223 cells treated with 0.3125 µM alpelisib versus DMSO control. Proteins shown in the volcano plot are based on L2FC, with significance defined using a FC threshold of ≥ 1.2 or ≤ 0.83. Significant proteins are highlighted (red = downregulated, green = upregulated) (n ≥ 2). **(b)** Schematic representation of the PI3K/AKT signalling pathway, the primary target of alpelisib. **(c)** STRING network illustrating high-confidence (>0.90) protein-protein interactions between members of the PI3K/AKT pathway (blue) and proteins significantly upregulated (green) or downregulated (red) following alpelisib treatment.

Treatment with crizotinib alone resulted in a significant upregulation of several proteins, including 53BP1, BCL2A1, CD171, Chk2, EMA, GRB7, HER3, PD-L1, and Sox2. In contrast, a marked downregulation was observed in the expression of A-Raf, Annexin-I, POLG, GSK-3α-β, RRM1, Stat5a, and Transglutaminase. These findings are summarised in Table 4-5 and illustrated in Figure 4-11(a).

Table 4-5: Proteins/phospho-proteins with significantly altered expression in MFM-223 cells following 24 h treatment with alpelisib ($p \leq 0.05$; FC ≥ 1.2 or FC ≤ 0.83; $n \geq 2$).

(Phospho-)protein	Abbreviation	FC	P-value
Tumour protein p53-binding protein 1	53BP1	1.38	0.001
B-cell lymphoma 2-related protein A1	BCL2A1	1.31	0.036
Cluster of differentiation 171	CD171	1.24	0.031
Checkpoint kinase 2	Chk2	1.23	0.043
C-terminal Src kinase	CSK	1.33	0.025
Epithelial membrane antigen	EMA	3.10	0.002
Growth factor receptor-bound protein 7	GRB7	1.24	0.010
Human epidermal growth factor receptor 3	HER3	1.98	0.003
Cyclin-dependent kinase inhibitor 1B	p27-Kip1	1.32	0.027
Programmed death ligand-1	PD-L1	1.71	0.020
SRY-box transcription factor 2	Sox2	1.34	0.016
V-raf murine sarcoma 3611 viral oncogene homolog A protein	A-Raf	0.75	0.042
Annexin-1	-	0.82	0.018
DNA polymerase subunit gamma	POLG	0.75	0.001
Glycogen synthase kinase 3 alpha/beta	GSK-3α-β	0.78	0.009
Ribonucleotide reductase regulatory subunit M1	RRM1	0.68	0.001
Signal transducer and activator of transcription 5a	Stat5a	0.44	0.010
Transglutaminase	-	0.40	0.043

A STRING analysis was conducted to assess potential interactions between proteins significantly dysregulated following crizotinib treatment and its primary kinase targets – MET, ALK, ROS1, and recepteur d'origine nantais (RON) – as shown in Figure 4-11(b-c). 5 of the dysregulated proteins demonstrated high-confidence interactions either with these primary targets or with each other.

Although no significant change was detected in p-MET (Y1234/Y1235), the sole crizotinib RTK target represented on the RPPA panel, a notable increase in HER3 expression was observed.

HER3, a known heterodimerisation partner of MET, is frequently upregulated as a compensatory response to MET inhibition. This mechanism, which has been previously

documented in preclinical studies (654–656), facilitates the maintenance of downstream signalling – particularly through the PI3K/AKT pathway – via alternative RTKs (657,658).

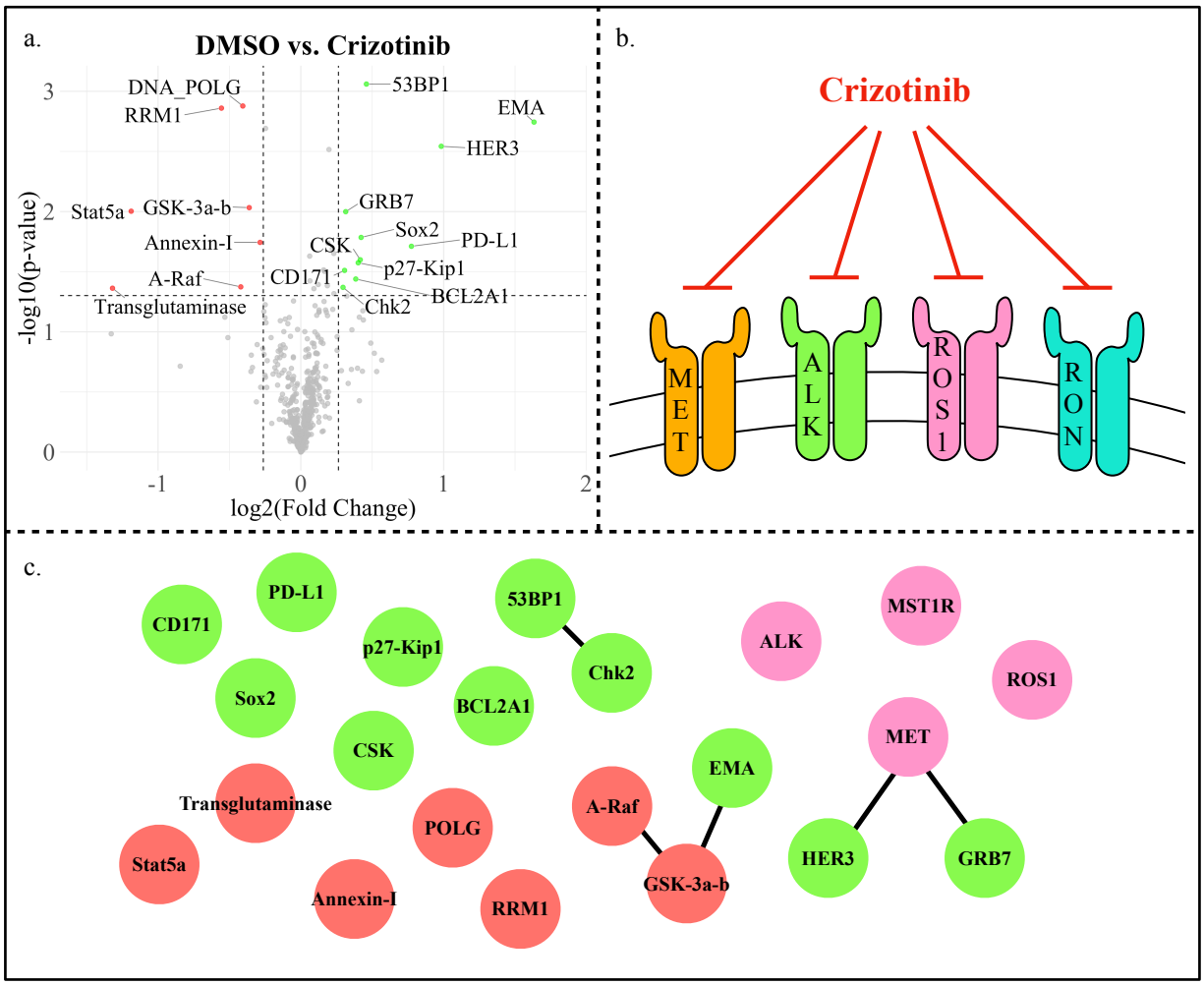


Figure 4-11. (a) Volcano plot illustrating DEA of total and phosphorylated proteins in MFM-223 cells treated with 1.25 µM crizotinib versus DMSO control. Proteins shown in the volcano plot are based on L2FC, with significance defined using a FC threshold of ≥ 1.2 or ≤ 0.83. Significant proteins are highlighted (red = downregulated, green = upregulated) (n ≥ 2). **(b)** Schematic representation of the primary RTK targets of crizotinib. **(c)** STRING network illustrating high-confidence (>0.90) protein-protein interactions between crizotinib's primary RTK targets (pink) and proteins significantly upregulated (green) or downregulated (red) following crizotinib treatment.

Treatment with the combination of alpelisib plus crizotinib led to significant upregulation of several proteins, including 53BP1, Bcl2, BCL2A1, Cyclophilin-F, HER3, p27-Kip1, PAR, Pdcd4, PLK1, and PTEN. Concurrently, expression levels of 4E-BP1, A-Raf, Cyclin-E1, POLG, GSK-3α-β, PRMT1, and Stat5a were significantly downregulated. Additionally, the combination treatment increased phosphorylation of ATM at Ser1981 and EGFR at Tyr1173, while reducing phosphorylation of AKT at Thr308 and B-Raf at Ser445. These findings are summarised in Table 4-6 and depicted in Figure 4-12(a).

Table 4-6: Proteins/phospho-proteins with significantly altered expression in MFM-223 cells following 24 h treatment with alpelisib plus crizotinib ($p \leq 0.05$; $FC \geq 1.2$ or $FC \leq 0.83$; $n \geq 2$).

(Phospho-)protein	Abbreviation	FC	P-value
Tumour protein p53 binding protein 1	53BP1	1.40	0.002
Phospho-ataxia telangiectasia mutated protein at serine 1981	p-ATM (S1981)	1.27	0.011
B-cell lymphoma 2	Bcl2	1.52	0.019
B-cell lymphoma 2-related protein A1	BCL2A1	1.29	0.047
Cyclophilin-F	-	1.22	0.026
Phospho-epidermal growth factor receptor at tyrosine 1173	p-EGFR (Y1173)	1.60	0.028
Human epidermal growth factor receptor 3	HER3	1.85	0.003
Cyclin-dependent kinase inhibitor 1B	p27-Kip1	1.26	0.022
Poly(Adenosine Diphosphate-ribose)	PAR	1.37	0.036
Programmed cell death protein 4	Pdcd4	1.73	0.001
Polo-like kinase 1	PLK1	1.21	0.013
Phosphatase and tensin homolog	PTEN	1.60	0.027
Eukaryotic translation initiation factor 4E-binding protein 1	4E-BP1	0.40	0.001
V-raf murine sarcoma 3611 viral oncogene homolog A protein	A-Raf	0.76	0.033
Phospho-protein kinase B (Threonine 308)	p-AKT (T308)	0.72	0.018
Phospho-V-raf murine sarcoma 3611 viral oncogene homolog A protein at serine 445	p-B-Raf (S445)	0.70	0.005
Cyclin-E1	-	0.68	0.009
DNA polymerase subunit gamma	POLG	0.72	0.032
Glycogen synthase kinase 3 alpha/beta	GSK-3α-β	0.76	0.004
Protein arginine methyltransferase 1	PRMT1	0.68	0.007
Signal transducer and activator of transcription 5a	Stat5a	0.59	0.018

A STRING analysis was performed to evaluate potential interactions between proteins significantly dysregulated following combined alpelisib plus crizotinib treatment, components of both the PI3K/AKT signalling pathway, and the primary RTK targets of crizotinib. As shown in Figure 4-12(b-c), 18 of the dysregulated proteins exhibited high-confidence interactions with PI3K/AKT pathway members, crizotinib's primary targets, or with one another. Notably, 12 of these proteins were uniquely dysregulated in response to the combination treatment, as opposed to either monotherapy. Additionally, two of crizotinib's usual targets – MET and ALK – demonstrated high-confidence interactions with PI3K, further supporting potential crosstalk between these pathways.

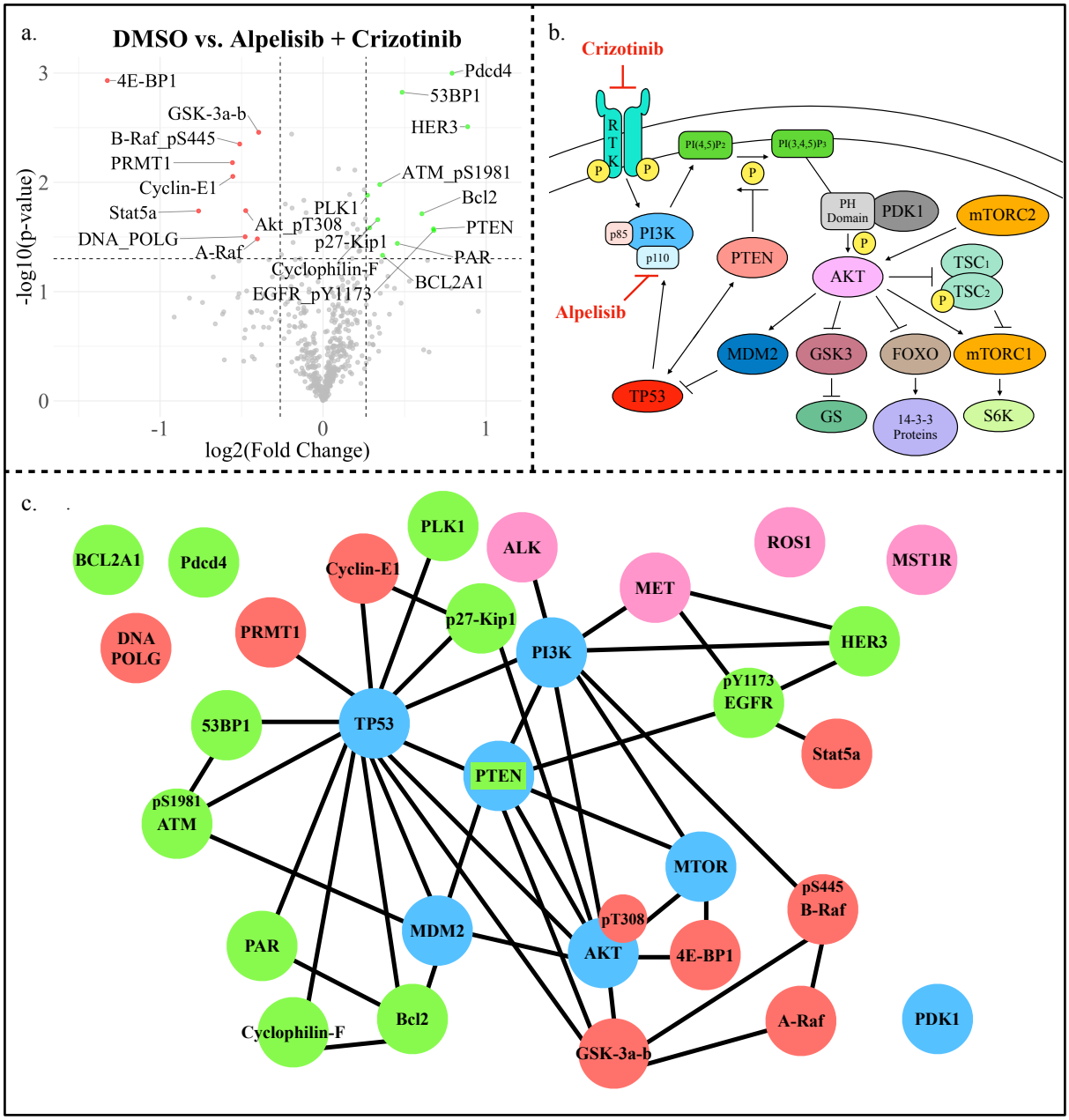


Figure 4-12. (a) Volcano plot illustrating DEA of total and phosphorylated proteins in MFM-223 cells treated with a combination of 0.3125 µM alpelisib and 1.25 µM crizotinib versus DMSO control. Proteins shown in the volcano plot are based on L2FC, with significance defined using a FC threshold of ≥ 1.2 or ≤ 0.83. Significant proteins are highlighted (red = downregulated, green = upregulated) (n ≥ 2). **(b)** Schematic representation of the PI3K/AKT signalling pathway, the primary target of alpelisib, and the RTK targets of crizotinib. **(c)** STRING network illustrating high-confidence (>0.90) protein-protein interactions between members of the PI3K/AKT pathway (blue), the primary RTK targets of crizotinib (pink), and proteins significantly upregulated (green) or downregulated (red) following alpelisib plus crizotinib treatment.

To assess whether the combination of alpelisib plus crizotinib elicited distinct changes in protein expression compared to either monotherapy, dysregulated proteins from each treatment condition were cross-analysed using a Venn diagram (Figure 4-13(a)). Expression values of dysregulated proteins which demonstrated high-confidence interactions with members of the PI3K/AKT pathway, primary RTK targets of crizotinib, or with each other were extracted and visualised using box-and-whisker plots (Figure 4-13(b)). These plots illustrate the protein response across four conditions: DMSO control, alpelisib alone, crizotinib alone, and the combination treatment. Statistical significance between treatment groups was determined using Student's t-test. Figure 4-13(c) presents a table summarising the FCs and p-values for each dysregulated protein across the different treatment groups.

Expression of 4E-BP1, Bcl2, and Cyclophpilin-F was uniquely dysregulated in response to the combination treatment, showing significant differences not only compared to the DMSO control but also relative to both single-agent treatments. A similar pattern was observed for phosphorylated (p-) B-Raf (Ser445), which was significantly downregulated in the combination group compared to DMSO and crizotinib alone. However, the difference compared to alpelisib did not reach statistical significance ($p = 0.0609$), despite surpassing the FC threshold.

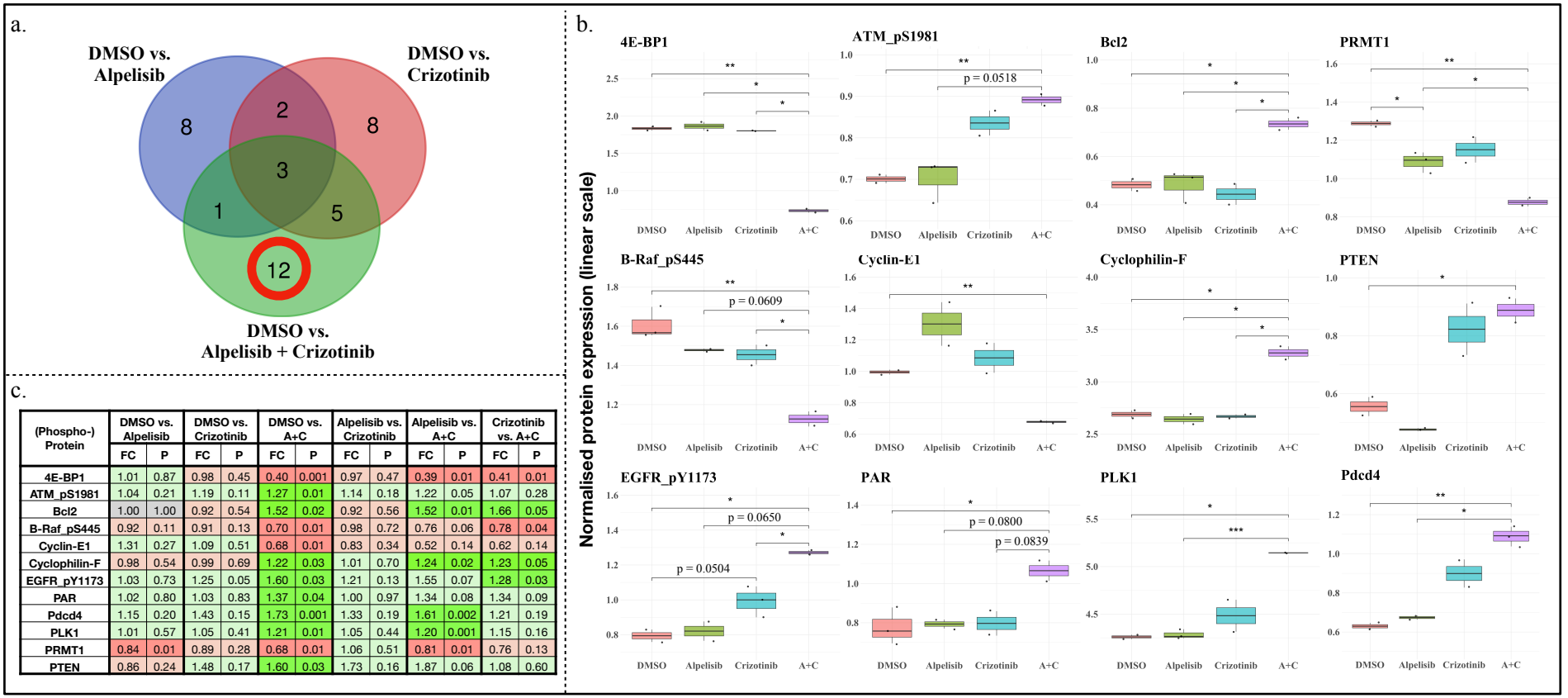
PAR also demonstrated a unique increase following combination treatment but narrowly missed statistical significance when compared to alpelisib ($p = 0.0800$) and crizotinib ($p = 0.0839$). A comparable trend was observed for p-EGFR (Tyr1173), which was significantly upregulated in the combination group versus DMSO and crizotinib, but did not meet the significance threshold when compared to alpelisib alone ($p = 0.065$). Interestingly, crizotinib treatment alone versus DMSO approached significance ($p = 0.0504$), suggesting that EGFR phosphorylation at Tyr1173 is enhanced by crizotinib and further elevated by the combination therapy.

Although statistical significance was not achieved, PRMT1 and PLK1 exhibited similar trends of increased dysregulation in the combination group relative to crizotinib. Cyclin-E1 also appeared to be uniquely downregulated by the combination treatment, although the comparison did not reach statistical significance versus either single agent. In contrast, the observed upregulation of PTEN expression and ATM phosphorylation at Ser1981 appears to be primarily driven by crizotinib treatment.

The combination of alpelisib and crizotinib induced unique proteomic changes that may enhance apoptotic and antiproliferative effects, potentially explaining the synergistic efficacy observed compared to single-agent treatments in this cancer model. Upregulation of ATM phosphorylation, a DNA damage sensor, appeared to be driven primarily by crizotinib, but the combination of alpelisib plus crizotinib increased it to statistical significance, potentially sustaining this pro-apoptotic response. Interestingly, Bcl2, an anti-apoptotic protein, showed unique dysregulation following alpelisib plus crizotinib treatment, which may represent a resistance mechanism in response to apoptosis induction.

Phosphorylated BRAF, a MAPK pathway driver (659), was significantly downregulated in cells treated with the combination versus DMSO and crizotinib alone, and showed near-significant downregulation compared to alpelisib alone, potentially attenuating survival signalling. Cyclin-E1, a key cell cycle regulator (660), was uniquely downregulated by the combination, supporting cell cycle arrest and sensitisation to apoptosis. Additionally, PAR, a marker of DNA damage-induced apoptosis (661), was increased, consistent with enhanced apoptosis. PTEN, a negative regulator of PI3K/AKT signalling (662), was upregulated, contributing to inhibition of survival pathways. Similarly, the tumour suppressor Pdcd4 – known to inhibit tumour progression and promote apoptosis – was also upregulated (663).

Together, these proteomic changes suggest that alpelisib plus crizotinib simultaneously promotes apoptosis and inhibits cell cycle progression, despite the compensatory upregulation of Bcl2, providing a mechanistic explanation for the observed synergistic efficacy in *TP53/PIK3CA* co-mutant TNBC cells.



c.

(Phospho-) Protein	DMSO vs. Alpelisib		DMSO vs. Crizotinib		DMSO vs. A+C		Alpelisib vs. Crizotinib		Alpelisib vs. A+C		Crizotinib vs. A+C	
	FC	P	FC	P	FC	P	FC	P	FC	P	FC	P
4E-BP1	1.01	0.87	0.98	0.45	0.40	0.001	0.97	0.47	0.39	0.01	0.41	0.01
ATM_pS1981	1.04	0.21	1.19	0.11	1.27	0.01	1.14	0.18	1.22	0.05	1.07	0.28
Bcl2	1.00	1.00	0.92	0.54	1.52	0.02	0.92	0.56	1.52	0.01	1.66	0.05
B-Raf_pS445	0.92	0.11	0.91	0.13	0.70	0.01	0.98	0.72	0.76	0.06	0.78	0.04
Cyclin-E1	1.31	0.27	1.09	0.51	0.68	0.01	0.83	0.34	0.52	0.14	0.62	0.14
Cyclophilin-F	0.98	0.54	0.99	0.69	1.22	0.03	1.01	0.70	1.24	0.02	1.23	0.05
EGFR_pY1173	1.03	0.73	1.25	0.05	1.60	0.03	1.21	0.13	1.55	0.07	1.28	0.03
PAR	1.02	0.80	1.03	0.83	1.37	0.04	1.00	0.97	1.34	0.08	1.34	0.09
Pdcd4	1.15	0.20	1.43	0.15	1.73	0.001	1.33	0.19	1.61	0.002	1.21	0.19
PLK1	1.01	0.57	1.05	0.41	1.21	0.01	1.05	0.44	1.20	0.001	1.15	0.16
PRMT1	0.84	0.01	0.89	0.28	0.68	0.01	1.06	0.51	0.81	0.01	0.76	0.13
PTEN	0.86	0.24	1.48	0.17	1.60	0.03	1.73	0.16	1.87	0.06	1.08	0.60

Figure 4-13: Proteins uniquely dysregulated by combined alpelisib plus crizotinib treatment. (a) Venn diagram showing the overlap of significantly dysregulated proteins ($p \leq 0.05$; $FC \geq 1.2$ for upregulation or ≤ 0.83 for downregulation) identified by RPPA analysis of MFM-223 cells treated with alpelisib, crizotinib, or their combination, each compared to DMSO control. **(b)** Box-and-whisker plots showing normalised RPPA protein expression levels (linear, back-transformed from $\log_2$ data) for proteins significantly dysregulated by combination treatment. **(c)** Table of proteins identified in (a) with FC and p-values for comparisons between each of the treatment conditions. Downregulated proteins are shown in red with significance indicated by a more intense red colour. Upregulated proteins are shown in green with significance indicated by a more intense green colour.

Due to the presence of outliers in the triplicate RPPA dataset, which reduced some measurements to duplicate replicates, selected targets identified in the RPPA analysis were validated using Western blotting followed by densitometric quantification. For the Western blot experiments, MFM-223 cells were treated with increased concentrations of alpelisib (1.25 μM) and crizotinib (5 μM) compared to the RPPA analysis to enhance the magnitude of detectable signalling changes.

The phosphorylation sites of AKT were investigated due to them being the primary downstream effectors of alpelisib. Both the Serine 473 (Ser473) and Thr308 sites, as well as total AKT levels were analysed. RPPA analysis of p-AKT at Ser473 (see Figure 4-14(a(i))) demonstrated significant downregulation following treatment with alpelisib or the combination versus crizotinib alone, with no significant difference between the combination and alpelisib alone. While none of the treatments resulted in a significant difference in expression versus the DMSO control, notable variability in DMSO-treated replicates may limit interpretation of differences relative to control. This was confirmed in the Western blot analysis, where p-AKT (Ser473) was significantly reduced following 24 treatment with alpelisib or the combination of alpelisib plus crizotinib versus both the DMSO control and crizotinib alone. Crizotinib did not have a significant effect on p-AKT (Ser 473) and the combination did not enhance inhibition versus the alpelisib alone (see Figure 4-14(b),(c(i))).

While RPPA analysis demonstrated a significant reduction of p-AKT (Thr308) following treatment with either alpelisib alone or the combination of alpelisib plus crizotinib (Figure 4-14(a(ii))), Western blot analysis of p-AKT (Thr308) revealed consistently faint bands across biological replicates (n = 3), indicating low detectable p-AKT (Thr308) signal under these experimental conditions (Figure 4-14(b)). This represents a limitation of the assay, as the low signal intensity may reduce sensitivity for detecting treatment-associated changes. Despite this, densitometric quantification of the Western blot bands indicated a reduction in p-AKT (Thr308) levels following alpelisib and crizotinib treatment (Figure 4-14(c(ii))).

Total protein levels of AKT demonstrated significant reduction across all treatment groups versus the DMSO control in the RPPA analysis, although the FC did not meet the threshold of 0.83 with very subtle changes in expression observed. The significant differences in expression are due to tight deviation between replicate results (see Figure 4-14(a(iii))). Western blot analysis revealed no significant reduction in total AKT expression following treatment with alpelisib, crizotinib, or the combination of both. Although, treatment with both of the single

agents alone resulted in a slight increase in AKT levels, with alpelisib treatment achieving significance and crizotinib reaching near significance (p = 0.069) (see Figure 4-14(b),(c(iii))).

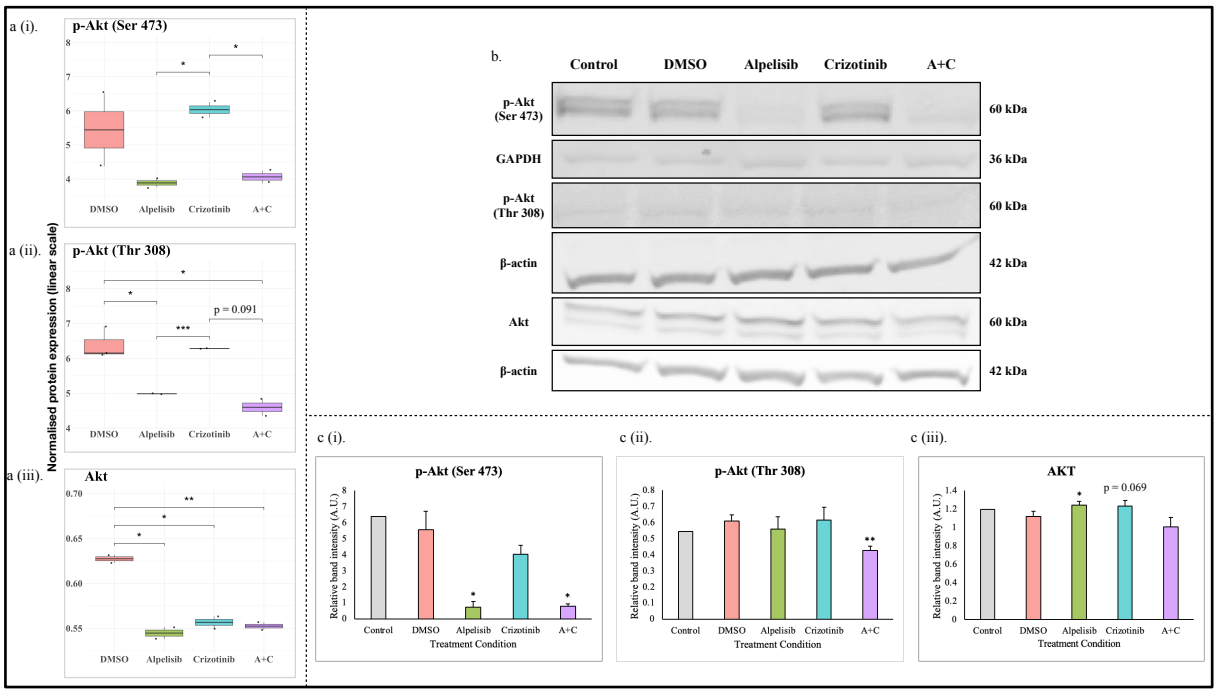


Figure 4-14: Inhibition of AKT signalling following combination treatment with alpelisib plus crizotinib. (a) RPPA analysis of MFM-223 cells treated for 24 h with DMSO control, alpelisib (0.3165 µM), crizotinib (1.25 µM), or their combination (A+C). Quantification of **(i)** p-AKT at Ser 473, **(ii)** p-AKT at Thr 308, and (iii) total AKT levels are shown as normalised log2 protein expression values. **(b)** Western blot validation following 24 h treatment with DMSO, alpelisib (1.25 µM), crizotinib (5 µM), or the combination (A+C). Blots show expression of p-AKT (Ser 473), p-AKT (Thr 308), and total AKT, with GAPDH or β-actin used as loading controls. Molecular weight is shown in kilodaltons (kDa). **(c)** Densitometric quantification of Western blot bands for **(i)** p-AKT (Ser 473), **(ii)** p-AKT (Thr 308), and **(iii)** total AKT. Band intensities were first normalised to their respective loading controls (GAPDH or β-actin) and subsequently normalised to the corresponding value from one representative replicate to allow comparison across replicates. Data are presented as relative band intensity (A.U.) and shown as mean ± SD from independent experiments (n = 3). Statistical significance was determined using Student's t-test; *p < 0.05, **p < 0.01.

The most pronounced and treatment-specific protein inhibition observed in the RPPA analysis in response to the combination of alpelisib plus crizotinib was seen in 4E-BP1 (FC = 0.40; p = 0.001) (Figure 4-15(a(iii))). This effect was unique to the combination and was not observed with either agent alone, suggesting a potential mechanistic link to the enhanced apoptotic response previously observed in MFM-223 cells.

Neither of the 4E-BP1 phosphorylation sites (Thr37/46 or Ser65) demonstrated significant changes upon treatment with alpelisib, crizotinib, or the combination of both, however, the deviation between replicates was high for p-4E-BP1 at Thr37/46, and all treatment groups achieved near significance (i.e. $p < 0.100$) for p-4E-BP1 at Ser64 (see Figure 4-15(a(ii),(iii))).

Western blot analysis was carried out to investigate the effect of the single and combination treatments on p-4E-BP1 at Thr37/46 due to the inconclusive results observed in the RPPA analysis. In addition to this, phosphorylation of 4E-BP1 occurs in a hierarchical manner, whereby Thr37/46 is phosphorylated first, acting as a priming event for further phosphorylation. In the event of subsequent phosphorylation events (e.g. phosphorylation at Ser65), the anti-Thr37/46 antibody will recognise these modified isoforms resulting in the detection of multiple bands. In short, the anti-Thr37/46 antibody detects all 4E-BP1 phosphorylation states when Thr37/46 are phosphorylated (664–666).

p-4E-BP1 at Th37/46 was significantly reduced following treatment with alpelisib (FC = 0.74; p = 0.03), and further reduced when treated with the alpelisib plus crizotinib combination (FC = 0.43; p = 0.01), when compared to the DMSO control, while treatment with crizotinib alone did not elicit a significant differential response (see Figure 4-15(b,c(i)).

Total 4E-BP1 expression was significantly reduced following treatment with alpelisib (FC = 0.86; p = 0.04) when compared to the DMSO control, while treatment with both the crizotinib single agent and combination did not elicit a significant differential response (see Figure 4-15(b,c(ii)). Notably, total protein expression of 4E-BP1 was significantly reduced in the DMSO treated group versus the non-treated control (FC = 0.65; p = 0.004), an effect which has previously been identified in the HL-60 leukaemia cell line (667).

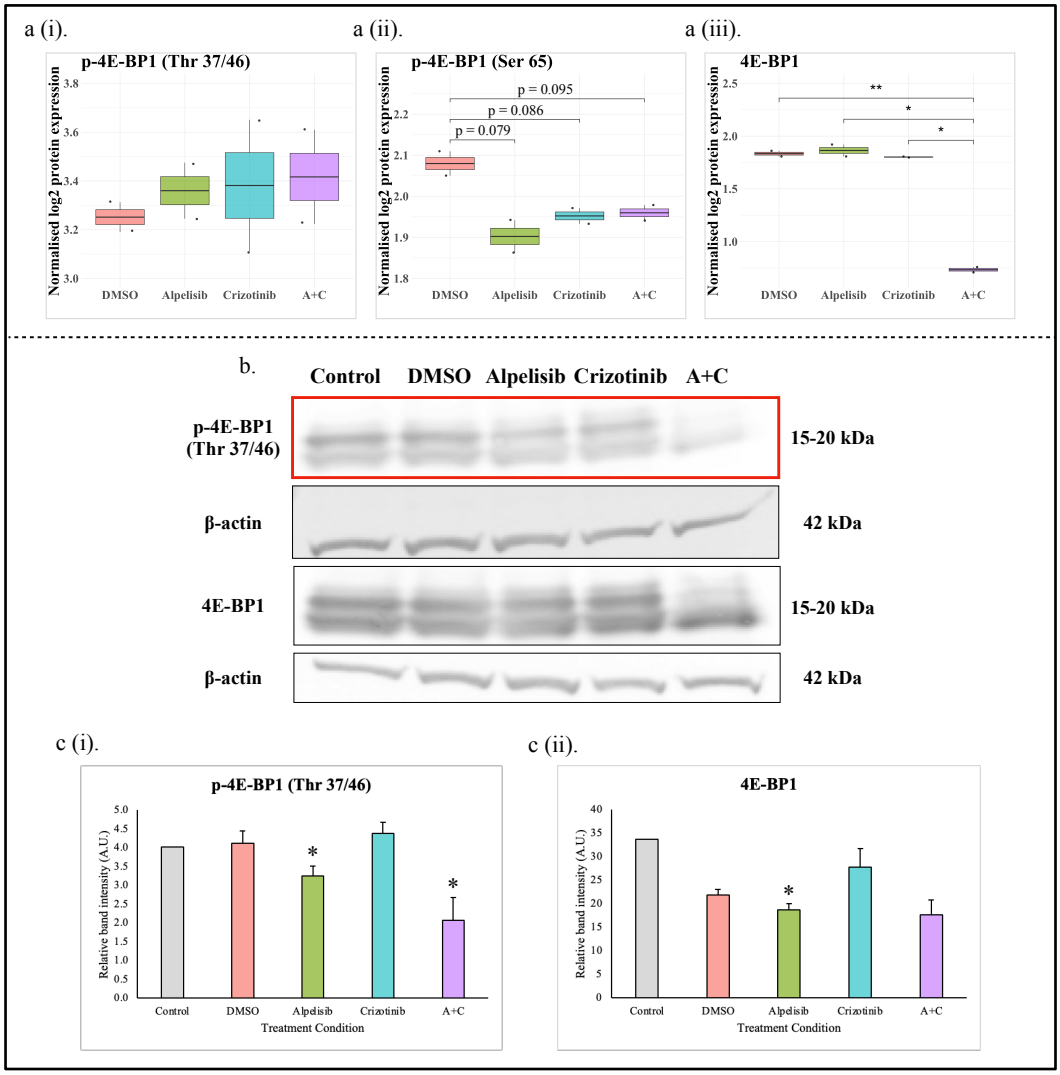


Figure 4-15: Inhibition of 4E-BP1 signalling following combination treatment with alpelisib plus crizotinib. (a) RPPA analysis of MFM-223 cells treated for 24 h with DMSO control, alpelisib (0.3165 µM), crizotinib (1.25 µM), or their combination (A+C). Quantification of **(i)** p-4E-BP1 at Thr 37/46, **(ii)** p-4E-BP1 at Ser 65, and (iii) total 4E-BP1 levels are shown as normalised log2 protein expression values. **(b)** Western blot validation following 24 h treatment with DMSO, alpelisib (1.25 µM), crizotinib (5 µM), or the combination (A+C). Blots show expression of p-4E-BP1 (Thr 37/46) and total 4E-BP1, with β-actin used as loading controls. Molecular weight is shown in kDa. **(c)** Densitometric quantification of Western blot bands for **(i)** p-4E-BP1 (Thr 37/46) and **(ii)** total 4E-BP1. Band intensities were first normalised to their respective loading controls (β-actin) and subsequently normalised to the corresponding value from one representative replicate to allow comparison across replicates. Data are presented as relative band intensity (A.U.) and shown as mean ± SD from independent experiments (n = 3). Statistical significance was determined using Student's t-test; *p < 0.05.

Given the p-4E-BP1 Thr37/46 antibody's recognition of multiple phosphorylation sites, we subsequently subdivided the analysis. Western blot analysis revealed three distinct bands (as shown in Figure 4-16(a)). Densitometric quantification was then performed on each band (top, middle, and bottom) to determine which phosphorylation sites were impacted by the treatment.

Figure 4-16(b(i–iii)) presents the results of the densitometric analysis for each band. The top band exhibited a significant reduction following alpelisib treatment (FC = 0.76; p = 0.04) and a further decrease with the combination treatment (FC = 0.56; p = 0.004), relative to the DMSO control. Notably, the DMSO control itself showed significant upregulation compared to the untreated control (FC = 1.37; p = 0.01).

Similarly, the middle band displayed a significant reduction in expression following alpelisib treatment (FC = 0.58; p = 0.002) and a more pronounced decrease with the combination treatment (FC = 0.25; p = 0.0005), relative to the DMSO control. As before, the DMSO control differed significantly from the untreated control, although in this case the expression was reduced by a negligible amount (FC = 0.94; p = 0.03).

For the bottom band, the only significant change relative to the DMSO control was an upregulation following crizotinib treatment (FC = 1.22; p = 0.02). The combination treatment approached but did not achieve statistical significance (FC = 0.83; p = 0.07). In this case, the DMSO control did not differ significantly from the untreated control.

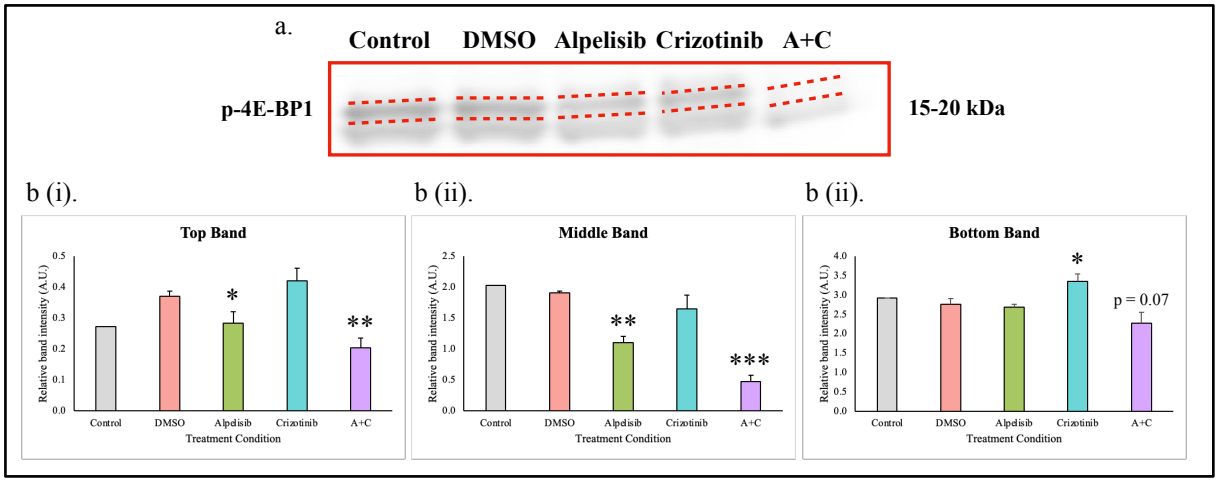


Figure 4-16: Inhibition of p-4E-BP1 following combination treatment with alpelisib plus crizotinib. (a) Resolution of p-4E-BP1 Western blot into three distinct bands separated by red dotted lines. **(b)** Densitometric quantification of Western blot bands for p-4E-BP1 **(i)** top band, **(ii)** middle band, and **(iii)** bottom band. Band intensities were first normalised to their respective loading controls (β-actin) and subsequently normalised to the corresponding value from one representative replicate to allow comparison across replicates. Data are presented as relative band intensity (A.U.) and shown as mean ± SD from independent experiments (n = 3). Statistical significance was determined using Student's t-test; *p < 0.05, **p < 0.01, ***p < 0.001.

4E-BP1 is a downstream effector of PI3K/AKT signalling (668) and its phosphorylation was differentially affected by the treatments. Alpelisib alone reduced p-4E-BP1 Thr37/46 and total 4E-BP1 levels, while crizotinib alone had minimal effect. The combination of alpelisib plus crizotinib resulted in a more pronounced reduction in p-4E-BP1 Thr37/46 compared to either single agent, indicating enhanced suppression of downstream translational signalling. These results suggest that inhibition of 4E-BP1 phosphorylation was most pronounced in the combination treatment, distinguishing it from the effects of the single agents, and may contribute to the enhanced apoptotic response observed previously in combination-treated cells.

4.7. Summary

This chapter investigated the therapeutic potential of targeting PI3K/AKT signalling in TNBC models stratified by *TP53* and *PIK3CA* mutational status, with particular emphasis on *TP53/PIK3CA* co-mutant systems as an experimentally tractable model of the clinically aggressive *TP53*-PI3K^{act} subgroup identified in Chapter 3.

Single-agent studies showed that *TP53*-WT TNBC cells harbouring a *PIK3CA* mutation were most sensitive to alpelisib, whereas co-occurring *TP53* mutation reduced sensitivity, suggesting that *TP53* dysfunction attenuates response to PI3Kα inhibition.

Combination studies demonstrated that alpelisib plus crizotinib produced the strongest and most clinically relevant synergy in *TP53/PIK3CA* co-mutant TNBC cell lines, with both BT-20 and MFM-223 showing dose-dependent synergistic inhibition at therapeutically achievable concentrations. In contrast, responses in other genotypic groups were more variable, and combinations of alpelisib with capmatinib or ceritinib were antagonistic or ineffective, suggesting that the benefit of crizotinib is not attributable to inhibition of a single RTK target alone.

Mechanistically, alpelisib plus crizotinib induced apoptosis in MFM-223 cells and elicited distinct proteomic changes not observed with either monotherapy, including enhanced inhibition of 4E-BP1 phosphorylation, and dysregulation of proteins involved in DNA damage signalling, apoptosis, and cell cycle control. These findings suggest that the combination enhances cytotoxicity through coordinated disruption of survival and translational signalling pathways.

Overall, these data identify *TP53/PIK3CA* co-mutant TNBC as a molecularly distinct and therapeutically targetable subset with enhanced sensitivity to dual PI3K/RTK inhibition. The alpelisib-crizotinib combination emerged as the most promising strategy tested, supporting further investigation of this approach as a targeted therapeutic strategy for *TP53*-PI3K^{act} TNBC.

5. The role of *TP53* alterations, alone and in combination with *PIK3CA* alteration, in modulating response to alpelisib and crizotinib in isogenic MCF10A models

5.1.Introduction

In Section 4.4.1.3., we observed that the two *PIK3CA*-MUT TNBC cell lines harbouring co-occurring *TP53* mutations exhibited higher alpelisib IC_{50} values than the two *PIK3CA*-MUT/*TP53*-WT TNBC cell lines tested, suggesting a potential association between *TP53* co-mutation and reduced alpelisib sensitivity. We further demonstrated that alpelisib in combination with crizotinib showed synergistic anti-proliferative effects in a *TP53/PIK3CA* co-mutant TNBC cell line and induced apoptosis in this model. However, emerging evidence indicates that not all *TP53* mutations confer identical functional consequences (231).

TP53 missense mutations can produce LOF, GOF, or dominant-negative (DN) effects (669). LOF mutations impair p53's canonical tumour suppressor activity, including cell cycle arrest and apoptosis induction (229). GOF mutations confer new oncogenic properties, such as promoting proliferation, metastasis, or drug resistance (670). DN mutations interfere with co-expressed WT p53, suppressing its tumour-suppressive activity (671). These functional consequences are often associated with the mutation class: DNA-contact mutants (e.g. R248Q, R273H) primarily impair direct DNA binding, whereas structural mutants (e.g. R175H, G245S) destabilise protein folding (672). However, the exact behaviour is allele- and context-dependent, so variant-level functional annotation is important for interpreting mutation-specific responses to therapy (673).

The primary aim of this chapter was to determine whether different *TP53* mutations lead to varying responses to alpelisib, and to identify baseline transcriptomic features that might explain these differences. We then sought to investigate the synergistic effects of alpelisib and crizotinib in a controlled genetic background, to assess how *TP53* and/or *PIK3CA* mutations influence therapeutic response.

To provide a controlled system for this analysis, we utilised the MCF10A *TP53*-altered cell line panel developed by Pal et al. (2023). In this study, the authors generated an isogenic panel of non-tumorigenic mammary epithelial MCF10A cell lines in which ten of the most common BC-associated *TP53* missense mutations were individually introduced into a uniform genetic background, alongside *TP53*-WT (p53WT), *TP53*-overexpression (p53OE), and *TP53*-knockdown (p53KD) controls. Using this platform, they performed multidimensional phenotypic and molecular characterisation, demonstrating that distinct *TP53* missense mutations confer heterogeneous and mutation-specific effects on cancer-relevant phenotypes including proliferation, survival, migration, invasion, anoikis resistance, and 3D mammosphere

morphology. They further assessed differential apoptotic responses following doxorubicin treatment, identifying *TP53* variants associated with relative apoptosis sensitivity or resistance. Importantly, this work showed that *TP53* missense mutations are not functionally equivalent and may exhibit mutation-specific neomorphic behaviours, thereby establishing a robust framework for investigating *TP53* mutation-specific biology in a controlled genetic context (585).

To investigate the impact of *TP53* mutation status on alpelisib sensitivity in a controlled genetic background, we utilised the MCF10A *TP53*-altered cell line panel developed by Pal et al. (2023) in the laboratory of Professor Joshua LaBaer at ASU, which was obtained during a research visit to this group. Using this isogenic model system, we assessed alpelisib sensitivity across the *TP53*-altered cell lines by proliferation assay and classified individual models as sensitive or resistant based on their drug response profiles. I then analysed baseline (untreated) RNA-seq data generated by LaBaer's group to identify pre-existing transcriptional differences associated with alpelisib sensitivity. Finally, selected *TP53*-altered lines were transduced with a *PIK3CA* mutation (H1047R) to generate double-mutant models, enabling evaluation of alpelisib-crizotinib combination responses and drug synergy within a controlled genetic context.

This chapter therefore comprises two components:

1. An analysis of alpelisib sensitivity and associated baseline transcriptomic differences in *TP53*-altered MCF10A models.
2. An evaluation of alpelisib and/or crizotinib responses in *TP53*- and/or *PIK3CA*-altered MCF10A models, assessing drug synergy within a controlled genetic context.

5.2. Distinct *TP53* alterations influence gene expression profiles, potentially enhancing sensitivity to the PI3K inhibitor alpelisib

In this section, we investigate whether distinct *TP53* alterations influence sensitivity to alpelisib within a controlled isogenic model system. Given the established interplay between *TP53* and PI3K/AKT pathway regulation, we hypothesised in Section 3.1 (Chapter 3) that *TP53* mutation status may influence response to alpelisib. This hypothesis was further motivated by observations in Chapter 4 suggesting a potential association between co-occurring *TP53* mutation and reduced alpelisib sensitivity in *PIK3CA*-MUT TNBC cell lines relative to *PIK3CA*-MUT/*TP53*-WT models (Figure 4-1).

5.2.1. Alpelisib sensitivity profiling in *TP53*-altered MCF10A cell lines revealed enhanced sensitivity in G245S and R273H mutants, consistent with baseline gene expression differences

The proliferation assay results, presented in Figure 5-1(a), show that the G245S (IC_{50} = 1.38 ± 0.23 μM) and R273H (IC_{50} = 2.30 ± 0.26 μM) cell lines exhibited heightened sensitivity to alpelisib compared to the p53WT (IC_{50} = 4.06 ± 0.96 μM) cell line, while the p53OE (IC_{50} = 4.57 ± 0.64 μM) and p53KD (IC_{50} > 5 μM) cell lines displayed decreased sensitivity. Meanwhile, the Y163C (IC_{50} = 2.53 ± 0.38 μM) cell line demonstrated increased sensitivity to alpelisib relative to the three WT controls (p53WT, p53OE, p53KD), yet it was less responsive than the two other *TP53*-MUT cell lines.

Based on the outcome of the alpelisib proliferation assay, the cell lines were categorised into three groups relative to alpelisib sensitivity, using the reported clinical C_{max} of approximately 5.62 μM (see Section 4.3.1., Chapter 4) as a reference for physiologically relevant exposure levels:

- IC_{50} > 4.5 μM: Resistant (p53OE and p53KD)
- IC_{50} > 2.5 μM: Intermediate (p53WT and Y163C)
- IC_{50} < 2.5 μM: Sensitive (G245S and R273H).

Although p53WT could alternatively be aligned with the resistant group and Y163C with the sensitive group, we opted to exclude these intermediate responders to ensure a robust contrast in differential expression between the sensitive and resistant categories.

Our next objective was to determine whether distinct *TP53* alterations influence the baseline gene expression profiles of the MCF10A cell lines (i.e. before treatment), potentially contributing to their varied responses to alpelisib. To address this, we analysed baseline untreated RNA-seq data generated by the LaBaer laboratory for the *TP53*-altered MCF10A cell line panel. An MDS plot of the normalised RNA-seq data, presented in Figure 5-1(b), revealed distinct clustering of cell lines corresponding to the alpelisib response groups, with the resistant (green) cell line samples on the bottom left, the intermediate (pink) clustered on the top left, and the sensitive (blue) clustered on the centre right. This suggests that *TP53*-induced gene expression differences at baseline may influence sensitivity to alpelisib.

To elucidate the specific transcriptomic impacts of *TP53* alterations on alpelisib-sensitive MCF10A cell lines, we performed a DEA comparing the sensitive group to the resistant group. The volcano plot in Figure 5-1(c) presents the DEA results, revealing 727 genes with significantly ($|L2FC| \geq 0.585$; $FDR \leq 0.05$) higher expression and 1020 genes with significantly lower expression in the sensitive group. Subsequent heatmap analysis of the significant DEGs from alpelisib-sensitive versus alpelisib-resistant DEA (shown in Figure 5-1(d)) highlighted the three distinct alpelisib sensitivity groups (sensitive = blue; intermediate = pink; resistant = green) via hierarchical clustering, with the intermediate group aligning more closely with the resistant group than the sensitive group.

The heatmap's colour intensity reveals that the intermediate group displays less intense reds (indicating high expression) and blues (indicating low expression) relative to the more intense colours in the sensitive and resistant groups, suggesting that many genes in the intermediate group have expression levels that lie between those of the sensitive and resistant groups.

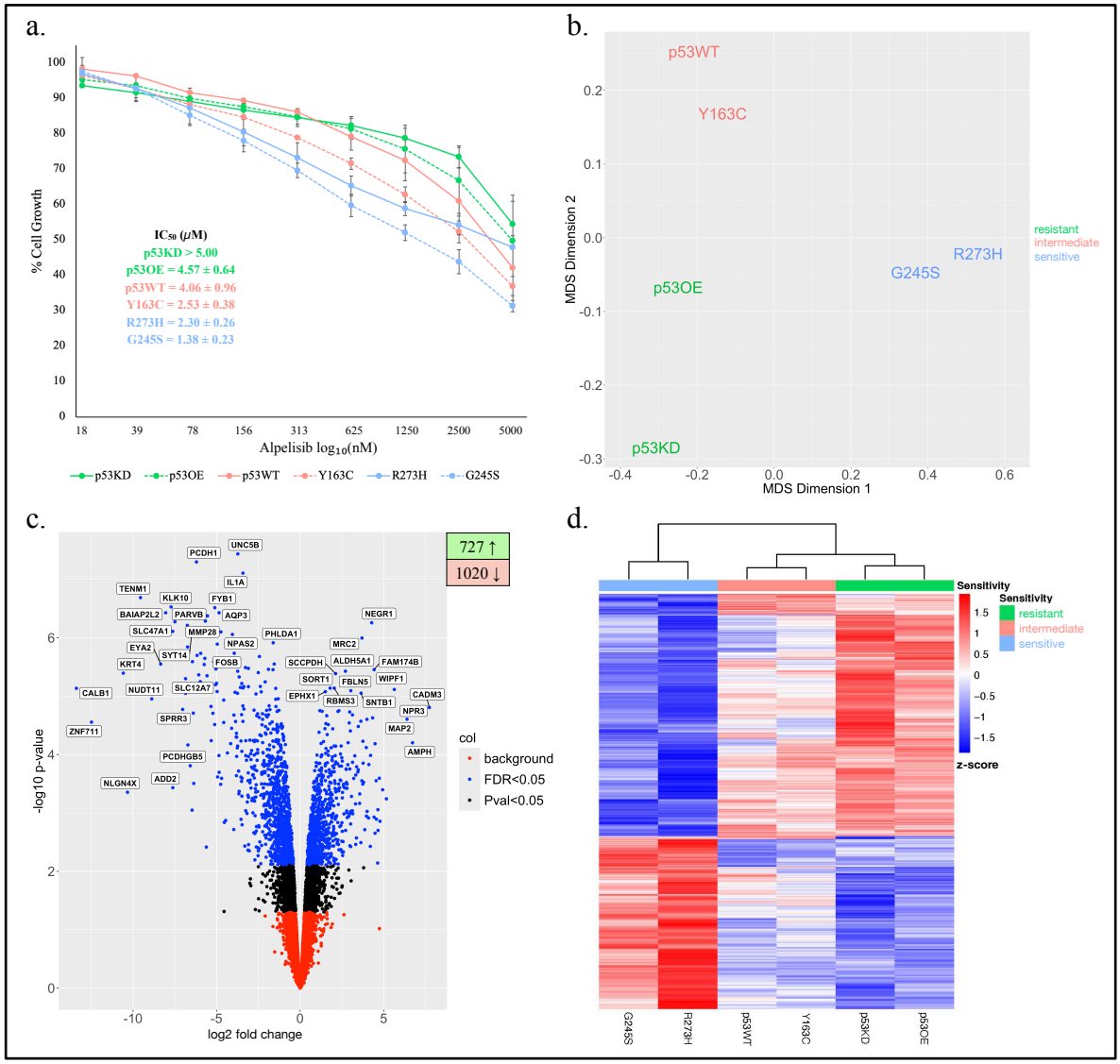


Figure 5-1. Alpelisib response and gene expression in MCF10A cells with *TP53* alterations, colour-coded by sensitivity: resistant (green: p53KD, p53OE), intermediate (pink: p53WT, Y163C), sensitive (blue: R273H, G245S). (a) Proliferation assay (18-5000 nM alpelisib; mean ± SD; n = 3). **(b)** MDS plot of baseline RNA-seq. **(c)** Volcano plot of DEA (alpelisib-sensitive versus alpelisib-resistant; L2FC, -log10(FDR)); blue: FDR ≤ 0.05; black: p ≤ 0.05; red: p > 0.05). DEGs (|L2FC| ≥ 0.585, FDR ≤ 0.05): green (upregulated), red (downregulated). **(d)** Heatmap of z-scored DEGs with hierarchical clustering by sensitivity.

GSEA was performed on the ranked gene list derived from the alpelisib-sensitive versus alpelisib-resistant DEA. Enrichment of Hallmark and Reactome pathways was assessed, with the top 15 pathways enriched in alpelisib-sensitive cells and the top 15 pathways enriched in alpelisib-resistant cells visualised in the dot plot in Figure 5-2(a).

The alpelisib-sensitive group was enriched for pathways associated with EMT and extracellular matrix remodelling, including EMT, extracellular matrix organisation, elastic fibre formation, and molecules associated with elastic fibres. These pathways were driven by leading-edge genes such as *VIM*, *FN1*, *CDH2*, *LOX*, and *POSTN*, indicating that the sensitive *TP53*-MUT

models exhibit a more mesenchymal-like baseline transcriptional profile relative to resistant cells. Additional enrichment of interferon alpha/gamma response and IL-6/JAK/STAT3 signalling suggested increased baseline inflammatory and cytokine-responsive signalling in the sensitive group. In contrast, the alpelisib-resistant group demonstrated enrichment of pathways related to epithelial differentiation and keratinocyte-associated programmes, including formation of the cornified envelope, keratinisation, and keratinocyte differentiation, with leading-edge genes including multiple keratins and epithelial structural markers such as *KRT14*, *KRT15*, *KRT17*, and *IVL*. In addition, resistant cells showed relative enrichment of gene sets associated with stress-response pathways – including p53 and TNFα/NFκB signalling – MYC signalling, and mitochondrial translation and protein import.

Given the enrichment of epithelial differentiation programmes in the resistant group, we next assessed whether these pathway-level differences were reflected in a focused basal epithelial gene set. This gene set comprised *TP63*, a master regulator of basal epithelial identity, the canonical basal keratins *KRT5* and *KRT14*, and the stress- and activation-associated keratins *KRT6A*, *KRT6B*, *KRT16*, and *KRT17*, which are often co-expressed in basal-like, proliferative, and stress-responsive epithelial states (674,675). Overall, a clear group-level trend was observed (shown in Figure 5-2(b)), with alpelisib-resistant cell lines (p53KD and p53OE) generally exhibiting the highest expression of the basal epithelial and stress-associated keratin programme, sensitive cell lines (G245S and R273H) showing the lowest expression, and intermediate lines (p53WT and Y163C) falling between these two extremes.

At the gene level, a clear contrast between R273H (alpelisib-sensitive) and p53KD (alpelisib-resistant) was observed for *TP63* and *KRT5*, both of which are markedly reduced in R273H. The reduced *TP63* expression in R273H is consistent with previous reports linking mutant p53 to *TP63* downregulation (676), suggesting mutation-specific effects in shaping basal epithelial programmes. Interestingly, p53OE clusters more closely with p53KD than with p53WT at the transcriptional level, indicating that both p53 loss and overexpression shift cells away from the WT-balanced state toward a shared rewired epithelial programme. While *TP63* and core basal keratins (*KRT5*, *KRT14*) remain broadly similar between p53OE and WT, p53OE shows increased expression of stress-associated keratins (e.g. *KRT6, KRT16, KRT17*), resembling p53KD. This suggests that p53OE does not simply recapitulate p53WT function, but instead perturbs epithelial differentiation and stress-response programmes in a manner partially convergent with p53 loss.

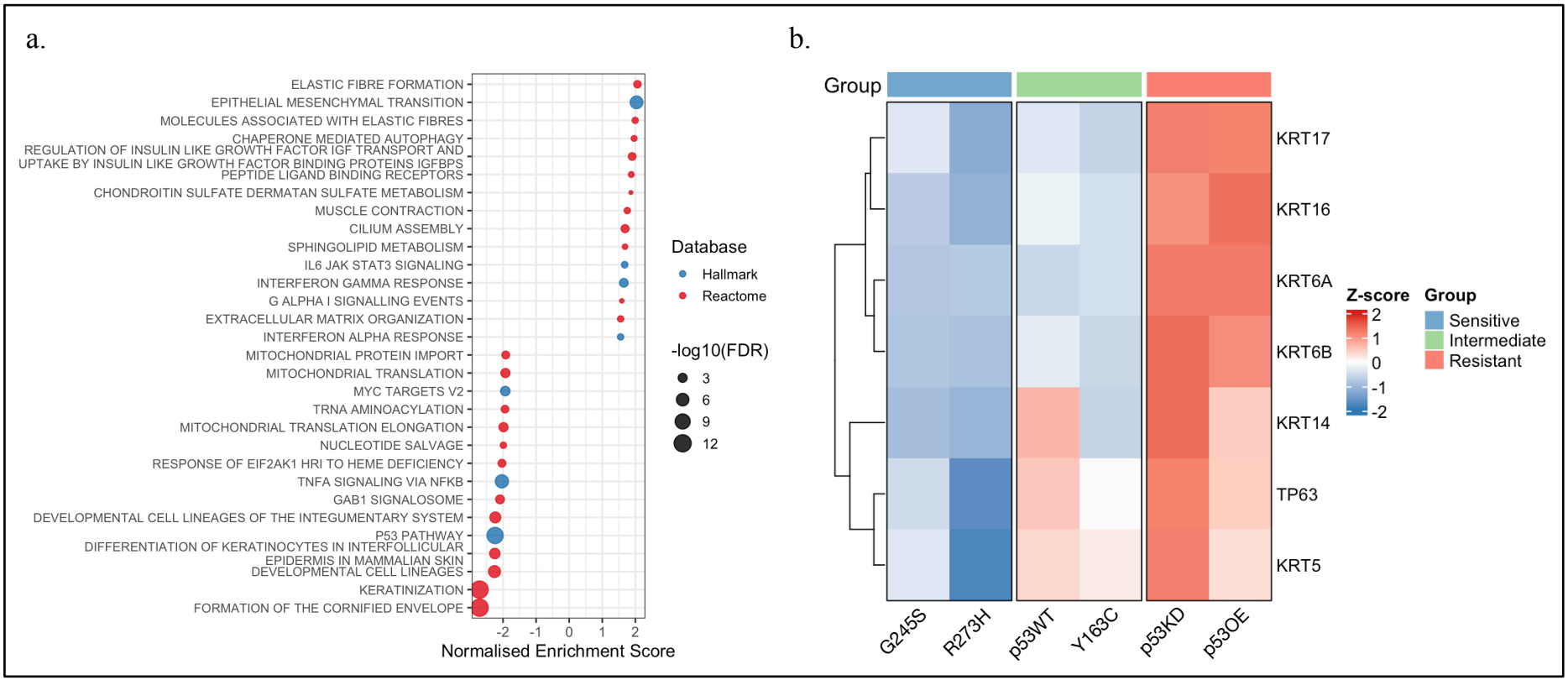


Figure 5-2. GSEA and basal gene signature differences between alpelisib-sensitive and alpelisib-resistant *TP53*-altered MCF10A cells. (a) GSEA was performed on ranked genes from DEA comparing sensitive versus resistant groups using Hallmark and Reactome gene sets (MSigDB). The plot shows the top 15 significantly enriched pathways in each direction (FDR < 0.05). Positive NES indicates enrichment in sensitive cells, and negative NES indicates enrichment in resistant cells. Bubble size represents statistical significance (-$\log_{10}$ adjusted p-value), and colour denotes gene set database (Hallmark or Reactome). **(b)** Heatmap of the basal gene expression signature across individual samples, scaled by row (z-score).

Overall, alpelisib-sensitive *TP53*-MUT models exhibit a mesenchymal and inflammatory baseline transcriptional state, whereas resistant models are characterised by epithelial differentiation and basal keratinocyte-associated programmes. These distinct *TP53*-driven baseline expression profiles may therefore contribute to differences in alpelisib sensitivity.

5.2.2. Analysis of the top ranked genes from the DEA of alpelisib-sensitive versus alpelisib-resistant MCF10A cell lines reveals potential drivers of alpelisib sensitivity

Our next analysis focused on examining the top ranked upregulated and downregulated genes from the alpelisib-sensitive versus alpelisib-resistant DEA to further identify baseline gene expression differences that might influence alpelisib response and serve as potential biomarkers of therapeutic sensitivity/resistance. Consistent with GSEA, genes were ranked using a composite score of the absolute L2FC and FDR, calculated as $|L2FC| \times -\log_{10}(FDR)$; the RANK function was then applied to each gene's score relative to the distribution of scores for all DEGs. The top 20 ranked up- and downregulated DEGs are presented in the tables in Figure 5-3(a(i),b(i)). We then extracted the normalised expression values of the DEGs and visualised them in bar charts, as shown in Figure 5-3(a(ii),b(ii)), to highlight expression variations across the three alpelisib sensitivity groups (sensitive, intermediate, resistant).

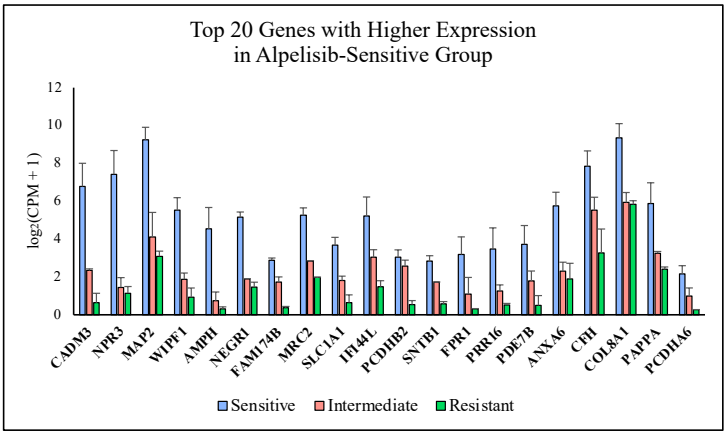
Across the top 20 genes upregulated in the alpelisib-sensitive group, several functional themes emerge, including genes involved in cell adhesion, cytoskeletal organisation, and plasticity-associated signalling. Strongly enriched genes such as *CADM3, AMPH, MAP2, NEGR1, PCDHB2,* and *PCDHA6* are classically associated with neuronal or synapse-related programmes, while *WIPF1, MRC2, COL8A1,* and CFH reflect cytoskeletal remodelling and extracellular matrix (ECM) interactions. In addition, immune- and stress-responsive genes such as *IFI44L, FPR1, PDE7B,* and *ANXA6* were also elevated in the sensitive group.

In contrast, genes upregulated in the alpelisib-resistant group were dominated by epithelial differentiation, keratinisation, and structural integrity programmes. The most strongly downregulated genes in the sensitive group included *CALB1, ZNF711, TENM1, KRT4, KLK10, SPRR1A, SPRR1B, SCEL,* and *CC2D2A*, alongside adhesion-related genes such as *PCDH1* and *PARVB*. Notably, multiple keratinisation-associated genes (e.g. SPRR family members) and epithelial structural regulators were enriched in resistant cells, consistent with the broader GSEA findings. The intermediate group exhibited intermediate expression levels between the sensitive and resistant groups, generally aligning more closely with the resistant group. This finding was consistent with the heatmap visualisation in Figure 5-1(d).

a (i).

Sensitive vs. Resistant			
Gene	ENSEMBL ID	LFC	FDR
CADM3	ENSG00000162706	7.73	2.42×10^{-03}
NPR3	ENSG00000113389	7.37	2.42×10^{-03}
MAP2	ENSG00000078018	6.40	2.77×10^{-03}
WIPF1	ENSG00000115935	5.63	1.53×10^{-03}
AMPH	ENSG00000078053	6.72	4.45×10^{-03}
NEGR1	ENSG00000172260	4.28	5.68×10^{-04}
FAM174B	ENSG00000185442	4.43	1.14×10^{-04}
MRC2	ENSG00000011028	3.70	6.57×10^{-04}
SLC1A1	ENSG00000106688	4.34	2.69×10^{-03}
IFI44L	ENSG00000137959	4.48	4.53×10^{-03}
PCDHB2	ENSG00000112852	4.00	2.77×10^{-03}
SNTB1	ENSG00000172164	3.65	1.57×10^{-03}
FPR1	ENSG00000171051	5.16	1.24×10^{-02}
PRR16	ENSG00000184838	4.74	8.55×10^{-03}
PDE7B	ENSG00000171408	4.94	1.04×10^{-02}
ANXA6	ENSG00000197043	4.21	5.80×10^{-03}
CFH	ENSG00000000971	4.55	8.89×10^{-03}
COL8A1	ENSG00000144810	3.63	2.94×10^{-03}
PAPPA	ENSG00000182752	3.96	4.92×10^{-03}
PCDHA6	ENSG00000081842	4.11	6.73×10^{-03}

a (ii).



b (i).

Sensitive vs. Resistant			
Gene	ENSEMBL ID	LFC	FDR
CALB1	ENSG00000104327	-13.39	1.49×10^{-03}
ZNF711	ENSG00000147180	-12.48	2.97×10^{-03}
TENM1	ENSG00000009694	-9.55	5.68×10^{-04}
KRT4	ENSG00000170477	-10.58	1.18×10^{-03}
BAIAP2L2	ENSG00000128298	-8.05	5.68×10^{-04}
KLK10	ENSG00000129451	-7.72	5.68×10^{-04}
EYA2	ENSG00000064655	-8.34	1.11×10^{-03}
SLC47A1	ENSG00000142494	-7.62	6.06×10^{-04}
PARVB	ENSG00000188677	-7.49	5.68×10^{-04}
NUDT11	ENSG00000196368	-8.88	1.88×10^{-03}
SPRR1B	ENSG00000169469	-6.75	5.82×10^{-04}
PCDH1	ENSG00000156453	-6.20	3.10×10^{-04}
SYT14	ENSG00000143469	-6.49	6.06×10^{-04}
ZNF485	ENSG00000198298	-6.73	8.05×10^{-04}
NLGN4X	ENSG00000146938	-10.33	1.09×10^{-02}
SPRR1A	ENSG00000169474	-6.85	1.32×10^{-03}
SLC12A7	ENSG00000113504	-6.85	1.57×10^{-03}
HCG11	ENSG00000228223	-6.44	1.10×10^{-03}
SCEL	ENSG00000136155	-6.17	9.89×10^{-04}
CC2D2A	ENSG00000048342	-5.67	5.69×10^{-04}

b (ii).

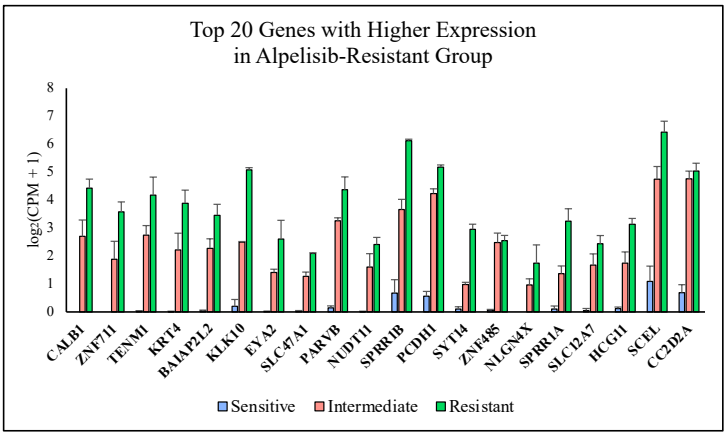


Figure 5-3: Analysis of baseline gene expression differences in MCF10A cell lines with varying *TP53* alterations based on alpelisib sensitivity: resistant (p53KD, p53OE), intermediate (p53WT, Y163C), sensitive (R273H, G245S). (a) Table of the top 20 ranked DEGs from the DEA comparing the most sensitive versus the least sensitive groups, ranked by L2FC and FDR. (b) Bar charts displaying the normalised expression levels (log2(CPM + 1)) of each of the top 20 ranked genes with higher expression in the (i) alpelisib-sensitive group or (ii) alpelisib-resistant group. Expression is visualised across the three sensitivity groups – blue = sensitive (G245S and R273H), pink = intermediate (Y163C and p53WT), and green = sensitive (p53KD and p53OE) – with error bars indicating SD from the mean.

Collectively, these findings extend the GSEA results by providing gene-level resolution of pathway differences between alpelisib-sensitive and -resistant models, supporting an association between *TP53* mutation-linked baseline transcriptional states and PI3K inhibitor response. Sensitive models show a more plastic, mesenchymal-like, ECM-interacting programme consistent with a more plastic cellular state and potentially reflecting differences in PI3K/AKT pathway engagement (677). In contrast, resistant models are enriched for epithelial differentiation pathways, suggesting reduced dependence on PI3K signalling. These differences appear to be driven by specific *TP53* missense variants rather than *TP53* status alone, indicating allele-specific effects on transcriptional reprogramming and drug sensitivity.

5.2.3. PI3K/AKT pathway KEGG analysis highlights dysregulated genes linked to alpelisib response in *TP53*-altered MCF10A cell lines

Consistent with the baseline transcriptional differences observed between alpelisib-sensitive and -resistant *TP53*-altered MCF10A cell lines, we next examined whether these differences extended to the PI3K/AKT signalling pathway, the direct molecular target of alpelisib. DEGs from the sensitive versus resistant comparison were mapped onto the KEGG PI3K/AKT pathway (hsa04151), revealing distinct baseline expression patterns of pathway-associated genes between the two groups (Figure 5-4).

DEA of alpelisib-sensitive versus alpelisib-resistant cell lines revealed 26 significantly upregulated and 31 significantly downregulated genes ($|L2FC| \geq 0.585$; FDR ≤ 0.05) in the PI3K/AKT pathway in sensitive cells, highlighting baseline pathway features that may confer drug responsiveness.

Within the PI3K/AKT pathway, alpelisib-sensitive cell lines exhibited higher expression of *PIK3R3* and *AKT3* and lower expression of *PIK3CD* and *AKT2*, indicating isoform-specific differences in PI3K/AKT pathway composition . Upstream of the pathway, RTKs including *EGFR, MET, FGFR3,* and *EPHA2* were broadly downregulated in sensitive cells, consistent with reduced expression of growth factor signalling inputs into PI3K/AKT activation (678).

At the level of downstream signalling, key effectors involved in translation and survival, including *EIF4EBP1*, *RPS6KB2*, *MYC*, and *BCL2L1*, were reduced in sensitive cells. This pattern indicates reduced engagement of proliferative and translational programmes downstream of AKT signalling in the sensitive group (621,679).

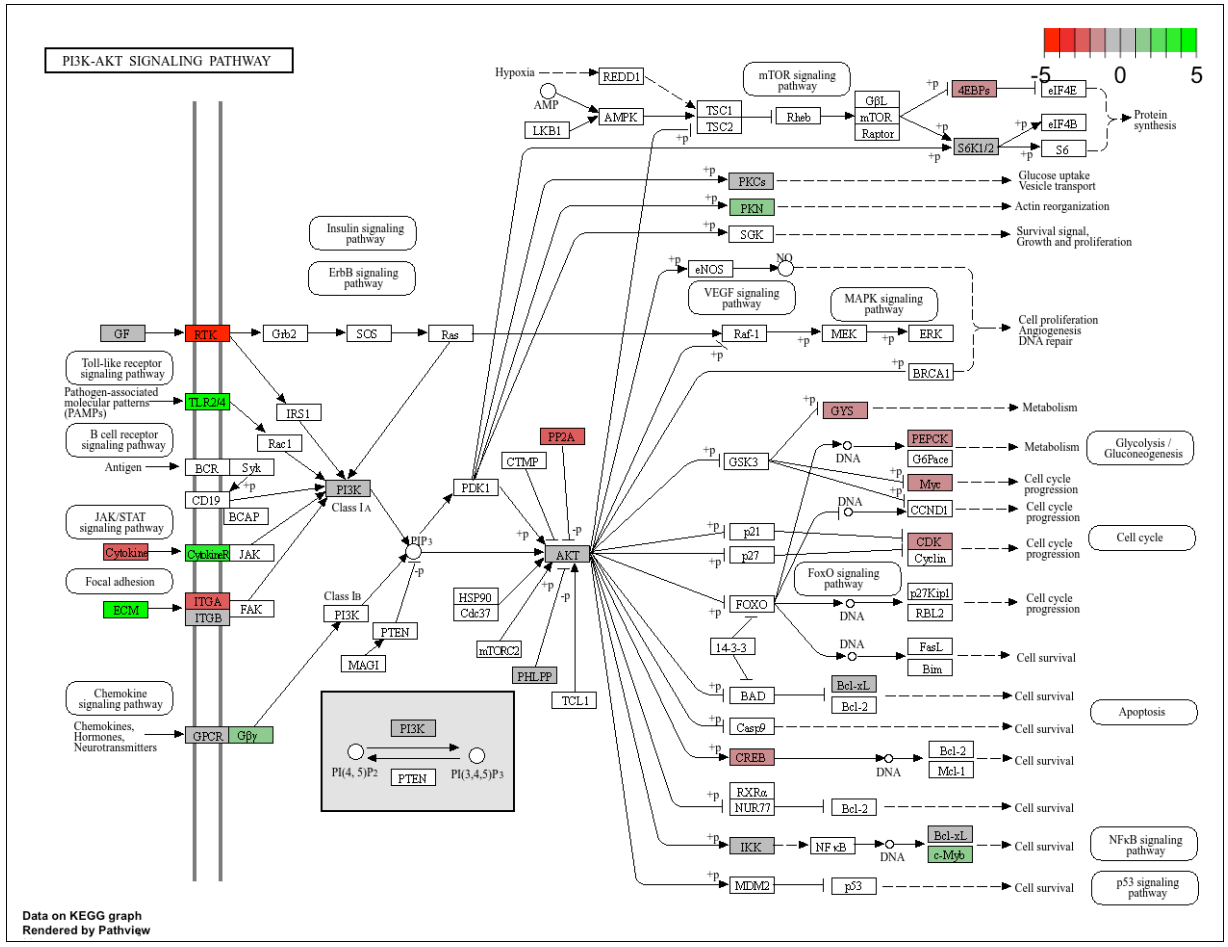
Negative regulators of PI3K/AKT signalling displayed mixed expression patterns, including *PHLPP2* and components of the PP2A complex (*PPP2R3A, PPP2R2C, PPP2CB*), suggesting altered feedback control of AKT activity in *TP53*-altered models (680–682). In parallel, ECM- and integrin-associated genes such as *ITGA1, ITGAV, LAMA1, LAMB2, ITGA3, ITGA6, ITGA10, LAMA3, and LAMB3* were differentially expressed, indicating broader remodelling of extracellular signalling inputs that converge on PI3K/AKT pathway activity (683).

Several of the genes altered within the PI3K/AKT pathway intersect with known p53-regulated signalling networks; however, most are not established direct *TP53* transcriptional targets. For example, *MYC* and *BCL2L1* are frequently modulated downstream of p53 activity in stress and survival contexts, but are generally regulated indirectly through *TP53*-dependent transcription

factor networks rather than direct p53 binding (684,685). This suggests that the observed differences are unlikely to reflect direct *TP53* target gene regulation alone. Instead, these findings are consistent with *TP53* mutation-associated differences in baseline transcriptional states that coincide with altered expression of growth factor and survival signalling components within the PI3K/AKT pathway.

Overall, the PI3K/AKT pathway analysis reveals coordinated differences in upstream signalling, downstream effector activity, and extracellular interaction genes between alpelisib-sensitive and -resistant *TP53*-altered MCF10A cell lines. These patterns align with the broader transcriptomic differences observed in earlier analyses and suggest that *TP53* mutation status is associated with distinct baseline configurations of PI3K/AKT pathway gene expression that may relate to differential drug response.

a.



b.

Upregulated			Downregulated		
Gene	**LFC**	**FDR**	**Gene**	**LFC**	**FDR**
ANGPT1	4.65	$1.57x10^{-02}$	**FGFR3**	-4.97	$1.57x10^{-03}$
TLR4	4.64	$4.82x10^{-02}$	**PGF**	-3.09	$1.21x10^{-02}$
FN1	2.56	$3.06x10^{-02}$	**PPP2R2C**	-2.68	$1.02x10^{-02}$
F2R	2.32	$1.06x10^{-02}$	**ITGA10**	-2.42	$3.08x10^{-02}$
COL6A3	2.27	$4.92x10^{-02}$	**LPAR5**	-2.41	$3.79x10^{-03}$
FGF2	1.76	$1.34x10^{-02}$	**NTF4**	-2.24	$2.51x10^{-02}$
GNG11	1.71	$3.51x10^{-02}$	**CSF3**	-2.12	$1.39x10^{-02}$
CSF1	1.58	$2.37x10^{-02}$	**PIK3CD**	-1.65	$4.26x10^{-02}$
MYB	1.35	$3.66x10^{-02}$	**CREB5**	-1.65	$7.29x10^{-03}$
PKN1	1.30	$5.80x10^{-03}$	**LAMB3**	-1.52	$8.67x10^{-03}$
OSMR	1.16	$3.48x10^{-02}$	**LAMA3**	-1.38	$3.05x10^{-03}$
EFNA1	1.13	$1.96x10^{-02}$	**TGFA**	-1.38	$3.19x10^{-03}$
IFNAR2	1.07	$2.12x10^{-02}$	**MYC**	-1.38	$2.42x10^{-03}$
PIK3R3	1.06	$2.50x10^{-02}$	**PCK2**	-1.37	$3.61x10^{-03}$
ITGA1	1.05	$2.91x10^{-02}$	**MET**	-1.34	$8.52x10^{-03}$
GHR	1.03	$4.13x10^{-02}$	**EIF4EBP1**	-1.28	$9.42x10^{-03}$
INSR	1.01	$5.80x10^{-03}$	**CDK6**	-1.22	$2.14x10^{-02}$
LAMA1	0.91	$3.57x10^{-02}$	**EPHA2**	-1.04	$1.05x10^{-02}$
PRKCA	0.90	$3.24x10^{-02}$	**GYS1**	-1.01	$8.63x10^{-03}$
AKT3	0.85	$1.39x10^{-02}$	**EGFR**	-1.00	$1.53x10^{-02}$
COL4A1	0.83	$4.07x10^{-02}$	**VEGFB**	-0.99	$2.87x10^{-02}$
PDGFC	0.76	$3.86x10^{-02}$	**ITGB4**	-0.98	$4.34x10^{-02}$
PHLPP2	0.75	$2.91x10^{-02}$	**PDGFD**	-0.89	$4.53x10^{-02}$
ITGAV	0.75	$3.13x10^{-02}$	**PDGFA**	-0.89	$2.06x10^{-02}$
LAMB2	0.72	$4.55x10^{-02}$	**ITGA6**	-0.83	$1.34x10^{-02}$
PPP2R3A	0.69	$4.99x10^{-02}$	**RPS6KB2**	-0.76	$2.87x10^{-02}$
			IKBKB	-0.69	$1.89x10^{-02}$
			PPP2CB	-0.68	$1.28x10^{-02}$
			BCL2L1	-0.67	$3.65x10^{-02}$
			AKT2	-0.64	$4.06x10^{-02}$
			ITGA3	-0.59	$4.13x10^{-02}$

Figure 5-4: Analysis of the PI3K/AKT KEGG pathway in the alpelisib-sensitive versus alpelisib-resistant DEA. (a) Overview of the KEGG PI3K/AKT pathway (hsa04151) with DEGs from the alpelisib-sensitive versus alpelisib-resistant DEA mapped onto it, where upregulated genes are marked in green and downregulated genes are in red. Colour scale represents L2FC (green = upregulated, red = downregulated). **(b)** DEA results (L2FCs and FDRs) for significant PI3K/AKT pathway DEGs, with upregulated genes in green and downregulated genes in red.

5.2.4. Crizotinib response profiling across *TP53*-altered MCF10A cell lines reveals mutation-specific differences in drug sensitivity

To determine whether *TP53* alterations influence sensitivity to receptor RTK inhibition, we next assessed the response of *TP53*-altered MCF10A cell lines to crizotinib, as summarised in Table 5-1. Overall, the *TP53*-MUT cell lines (R273H, G245S, Y163C) demonstrated a slight increase in sensitivity to crizotinib relative to the WT controls (p53WT, p53OE, p53KD) (mean $IC_{50} \approx 0.72$ µM vs. 0.91 µM, respectively). Among the *TP53* variants, the G245S mutant again emerged as the most sensitive ($IC_{50} = 0.65 \pm 0.03$ µM), whereas the p53KD line was the least sensitive ($IC_{50} = 1.06 \pm 0.05$ µM).

Relative to the reported clinical C_{max} of ~0.82 µM for crizotinib, all *TP53*-MUT cell lines fall within or just below the therapeutic window, while the WT control cells approach or slightly exceed it. Although the differences in sensitivity were subtler than for alpelisib, the consistently lower IC_{50} values in *TP53*-MUT cell lines indicate a potential vulnerability to RTK inhibition conferred by *TP53* mutation.

In the context of the transcriptomic data presented in Section 5.2.3, RTKs including *MET, EGFR, FGFR3* and *EPHA2* were differentially expressed between alpelisib-sensitive and -resistant cell lines. While these observations are based on RNA expression levels rather than protein activity, they indicate that differential RTK expression may contribute to the variation in crizotinib response observed across *TP53*-altered models.

Table 5-1. Crizotinib IC_{50} values in MCF10A cell lines with different TP53 alterations.

MCF10A Cell Line	Crizotinib IC_{50} (µM)
p53WT	0.86 ± 0.13
p53OE	0.81 ± 0.12
p53KD	1.06 ± 0.05
R273H	0.77 ± 0.05
Y163C	0.73 ± 0.07
G245S	0.65 ± 0.03

5.2.5. Summary

This section shows that *TP53* alterations are associated with distinct baseline transcriptional states in isogenic MCF10A models, which correlate with differential sensitivity to alpelisib. In particular, *TP53* missense mutants G245S and R273H are more sensitive to alpelisib, while p53KD and p53OE are relatively resistant. Baseline RNA-seq analysis indicates that alpelisib-sensitive models cluster together and are characterised by mesenchymal-like, ECM-remodelling and inflammatory programmes, whereas resistant models display epithelial differentiation and keratinisation signatures. Gene-level and pathway analyses further highlight differences in adhesion, stress-response, and PI3K/AKT signalling components that may underlie these responses. Crizotinib responses show only modest variation across *TP53*-altered lines, with a slight increase in sensitivity in *TP53*-MUT cells compared to controls, suggesting a weaker association between *TP53* status and RTK inhibitor response.

Overall, these findings indicate that *TP53* mutation-specific transcriptional rewiring influences baseline PI3K/AKT pathway activity and is associated with differential sensitivity to alpelisib, with more limited effects on crizotinib response

5.3.Investigating the impact of *TP53* alterations on alpelisib and crizotinib response in *PIK3CA*-MUT MCF10A models

In Chapter 4, we demonstrated that TNBC cell lines harbouring co-occurring *TP53* and *PIK3CA* mutations exhibited reduced sensitivity to alpelisib compared to cell lines with *PIK3CA* mutations alone (see Figure 4-1, Chapter 4). This observation led us to hypothesise that *TP53* mutations may promote compensatory signalling mechanisms that attenuate PI3Kα inhibitor sensitivity.

Supporting this, Croessmann et al. (2017) showed in isogenic MCF10A models that *TP53* and *PIK3CA* co-alterations influence targeted therapy response in a variant-specific manner. Although the PI3Kα inhibitor BYL719 (alpelisib) did not produce uniformly increased sensitivity across *PIK3CA*-MUT models, cells harbouring *TP53* alterations in combination with *PIK3CA* E545K appeared among the most sensitive to BYL719 relative to parental MCF10A controls. In contrast, co-occurring *TP53* alterations and *PIK3CA* H1047R – but not *PIK3CA* E545K – conferred relative resistance to the dual EGFR/HER2 inhibitor lapatinib compared with single *PIK3CA*-MUT counterparts (686). These findings suggest that the

therapeutic consequences of *TP53/PIK3CA* co-alteration depend on the specific mutational combination present and may involve differential engagement of RTK signalling pathways.

Consistent with this model, we observed that genes encoding crizotinib targets – *MET, ALK,* and *ROS1* – were more highly expressed in TNBC relative to other BC subtypes (see Figure 4-2, Chapter 4), supporting a potential role for RTK-mediated bypass signalling in this disease context. We therefore proposed that co-mutant models with reduced alpelisib sensitivity may be sensitised through dual PI3Kα/RTK inhibition using alpelisib in combination with crizotinib. In line with this hypothesis, combined alpelisib and crizotinib treatment was synergistic in *TP53/PIK3CA* co-mutant TNBC cell lines (see Figure 4-7, Chapter 4).

Separately, analysis of alpelisib response across our MCF10A *TP53* variant panel identified specific *TP53* alterations, particularly G245S and R273H, that enhanced alpelisib sensitivity relative to WT controls (p53WT, p53OE, and p53KD) (see Figure 5-1(a)). These variants represent distinct classes of *TP53* missense mutations, with G245S classified as a structural mutant and R273H as a DNA-contact mutant. Prior characterisation of this MCF10A panel by Pal *et al.* demonstrated that *TP53* missense mutations exhibit heterogeneous functional effects, with variability observed both between and within mutation classes, reflecting mutation-specific differences in DNA binding and transcriptional regulation.

The primary aim of this section was therefore to delineate the effects of *TP53* and *PIK3CA* alterations on sensitivity to alpelisib and crizotinib, both as single agents and in combination, within a genetically controlled, non-tumorigenic cellular model.

5.3.1. Expansion of MCF10A cell line panel to evaluate alpelisib sensitivity across diverse *TP53* alterations

In Section 5.3., we analysed alpelisib response in a selection of *TP53*-altered MCF10A cell lines (p53OE, p53KD, G245S, R273H, and Y163C) as well as the parental p53WT cell line. To build on this, we expanded our analysis to the full panel of 13 MCF10A cell lines from the Pal *et al*. study (see Figure 5-1), with the goal of assessing differential alpelisib sensitivity across diverse *TP53* alterations. This approach allowed us to investigate how distinct *TP53* alterations, which may have different functional consequences, influence alpelisib response. Additionally, we sought to identify the most and least alpelisib-sensitive cell lines within this panel, as these would be used in subsequent experiments involving the introduction of a *PIK3CA* mutation to assess responses to the alpelisib and crizotinib combination.

The table in Figure 5-5(a) presents the full MCF10A cell line panel, grouped based on mutation type (structural or DNA contact) or control. The antiproliferative effect of alpelisib was assessed in the remaining 7 MCF10A cell lines, as shown in Figure 5-5(b). Results for the entire cell line panel were included in this figure for visualisation of differential response. IC_{50} values from the proliferation assays are also presented in the figure (alpelisib C_{max} ~5.62 μM).

Alpelisib responses at 1.25 μM were statistically evaluated relative to the p53OE cell line (see Figure 5-5(c)), serving as controls for both *TP53*-WT expression and overexpression from transduction. The R248Q (1.61-fold decrease, $p = 1.29x10^{-03}$), G245S (1.45-fold decrease, $p = 3.38x10^{-03}$), and R273C (1.43-fold decrease, $p = 2.54x10^{-03}$) cell lines showed the greatest reductions in percentage cell growth. The R175H (1.32-fold decrease, $p = 1.13x10^{-02}$), R248W (1.31-fold decrease, $p = 7.89x10^{-03}$), R273H (1.29-fold decrease, $p = 1.15x10^{-02}$), and Y163C (FC 1.20-fold decrease, $p = 2.58x10^{-02}$) variants also demonstrated significant decreases in growth compared with p53OE. At 1.25 μM, p53OE exhibited no significant difference in percentage cell growth relative to the H179R, Y220C, and Y234C cell lines, as well as p53WT and p53KD.

To determine whether *TP53* mutation type broadly influences alpelisib sensitivity, we compared DNA contact versus structural mutants, assessing whether one class is generally more responsive to treatment than the other. The grouped bar chart in Figure 5-5(c) reveals that the structural mutant group (yellow) was significantly more sensitive to alpelisib than the control group (grey) (1.14-fold decrease, $p = 4.43x10^{-03}$), while the DNA contact mutant group (green) exhibited significantly greater sensitivity than both the structural mutant group (1.22-fold decrease, $p = 2.91x10^{-04}$) and the control group (1.39-fold decrease, $p = 1.36x10^{-08}$), indicating that DNA contact mutations may enhance drug efficacy to a greater extent than structural mutations.

a.

MCF10A Cell Line	Mutation Type
p53WT	Control
p53OE*	Control
p53KD	Control
R273H	DNA contact mutant
R273C	DNA contact mutant
R248W	DNA contact mutant
R248Q	DNA contact mutant
G245S	Structural mutant
Y234C	Structural mutant
Y220C	Structural mutant
H179R	Structural mutant
R175H	Structural mutant
Y163C	Structural mutant

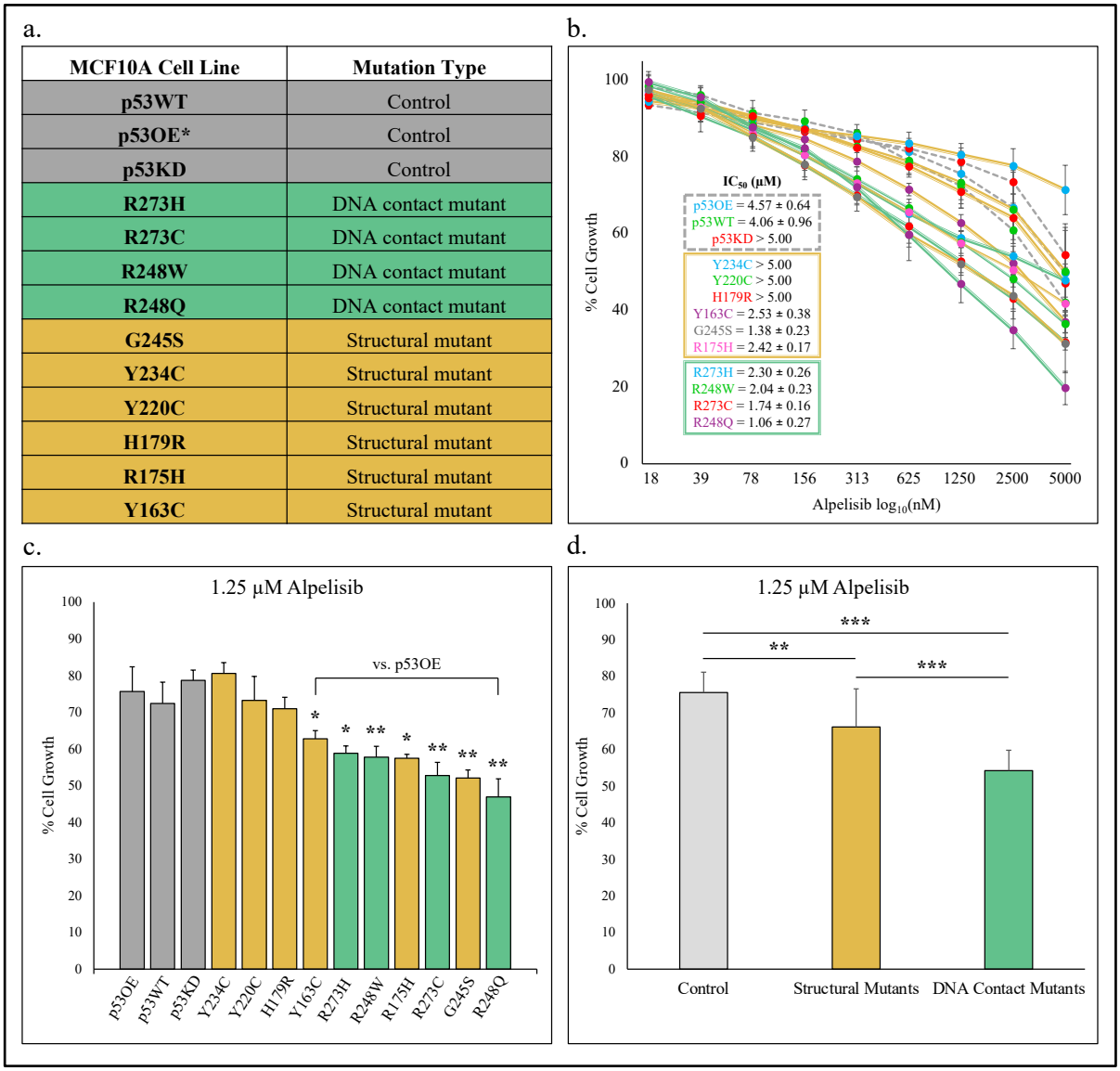


Figure 5-5: *TP53*-altered MCF10A cell line panel response to alpelisib treatment. Colours indicate the mutation type: grey = controls (p53OE, p53WT, p53KD), green = DNA contact mutants (R273H, R248W, R273C, R248Q), yellow = structural mutants (Y234C, Y220C, H179R, Y163C, G245S). (a) Panel of *TP53*-altered MCF10A cell lines and their mutation type. (b) Proliferation assay results from the *TP53*-altered MCF10A cell line panel, plotting percentage cell growth against $\log_{10}$ transformed alpelisib concentrations (18-5000 nM). Proliferation assay results at a fixed concentration of 1.25 μM alpelisib for *TP53*-altered MCF10A cell lines (c) individually and (d) grouped by mutation type, with error bars indicating SD from the mean and significance asterisks denoting Student's t-test results (* = $p \leq 0.05$; ** = $p \leq 0.01$).

These results support our earlier hypothesis that *TP53* mutations influence sensitivity to alpelisib in a mutation-specific manner, with DNA contact mutants exhibiting greater sensitivity than structural mutants, though outliers in the latter group suggest additional mutation-specific effects.

5.3.2. Confirmation of *PIK3CA*-WT and *PIK3CA*-MUT transduction by elevated PIK3CA protein expression in cell lines

To investigate the impact of co-occurring *TP53* and *PIK3CA* alterations on alpelisib sensitivity, we transduced selected *TP53*-altered MCF10A cell lines with a *PIK3CA* mutation (H1047R; the most prevalent *PIK3CA* mutation in both TNBC and cancer generally).

To explore potential differences in response, we chose *TP53*-altered cell lines exhibiting varied sensitivity to alpelisib for transduction. Additionally, we overexpressed *PIK3CA*-WT in these cell lines, mirroring the overexpression strategy employed in our prior analyses of *TP53*. However, given that *PIK3CA* overexpression may hyperactivate the PI3K pathway in a manner similar to the oncogenic mutation, a non-*PIK3CA*-transduced control was also incorporated to mitigate this potential confound. As the *PIK3CA* gene encodes the p110α protein, the cell lines were denoted based on this (e.g. p110αWT).

We selected two DNA contact *TP53*-MUT cell lines, R248Q and R273C, which exhibited heightened sensitivity to alpelisib relative to the p53OE control. To illustrate the reduced sensitivity typically observed among structural mutants, we included *Y234C*, which exhibited the lowest alpelisib sensitivity across the *TP53*-altered MCF10A panel. The p53OE line served as the principal control.

Each *TP53*-altered cell line was either non-*PIK3CA*-transduced (p110αWT), *PIK3CA*-WT-transduced (p110αOE), or *PIK3CA*-MUT-transduced (p110αMUT). To distinguish between the different *TP53* variants, these mutations were henceforth denoted with p53 (e.g. p53R273C). The table in Figure 5-6(a) presents the panel of MCF10A cell lines used for this analysis. Alpelisib sensitivity or resistance was indicated for the non-*PIK3CA*-transduced cell lines (i.e. *TP53*-altered only) based on results from Figure 5-5(b). Cell lines with an IC_{50} greater than 4.5 μM were considered to be alpelisib-resistant and cell lines with an IC_{50} less than 2.5 μM were considered to be sensitive.

Following the establishment of the transduced MCF10A cell lines, Western blot analysis was performed to quantify total PIK3CA protein levels, confirming successful transduction with the *PIK3CA* viral vectors. As shown in Figure 5-6(b), Western blot results revealed significantly elevated total PIK3CA protein levels in all *PIK3CA*-transduced cell lines (both p110αOE and p110αMUT) compared to the non-*PIK3CA*-transduced controls (p110αWT), with the exception of p53R248Q_p110αOE which displayed a smaller increase in PIK3CA

protein compared to other transduced cells. This modest elevation may suggest lower transduction efficiency or incomplete integration of the *PIK3CA*-WT viral vector in the p53R248Q cell line.

a.

Non-PIK3CA Transduced	Alpelisib	PIK3CA-WT Transduced	PIK3CA-MUT Transduced
p53OE_p110αWT	Resistant	p53OE_p110αOE	p53OE_p110αMUT
p53Y234C_p110αWT	Resistant	p53Y234C_p110αOE	p53Y234C_p110αMUT
p53R273C_p110αWT	Sensitive	p53R273C_p110αOE	p53R273C_p110αMUT
p53R248Q_p110αWT	Sensitive	p53R248Q_p110αOE	p53R248Q_p110αMUT

b.

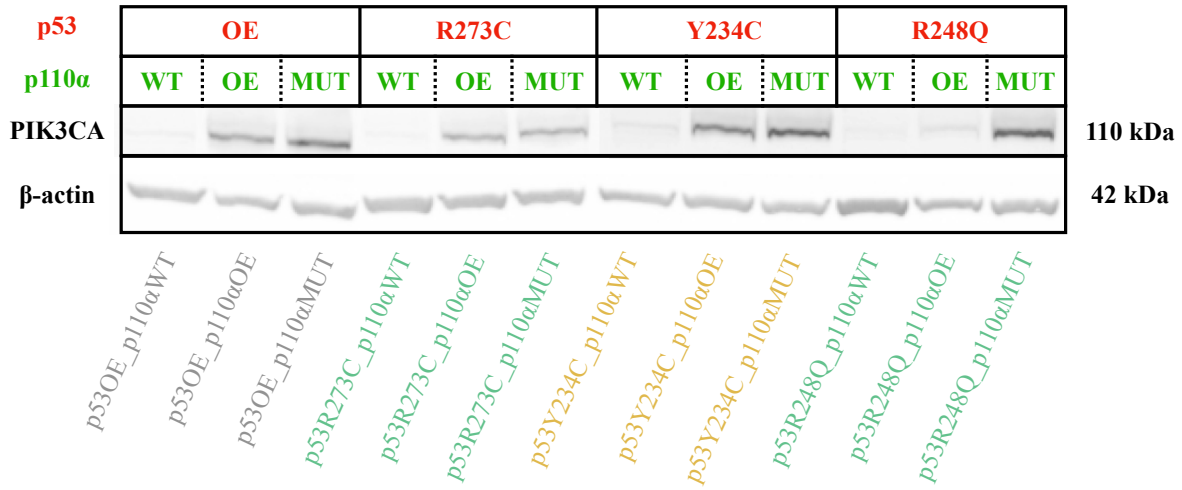


Figure 5-6: Western blot analysis of PIK3CA protein expression in transduced MCF10A cell lines. **(a)** Panel of *TP53*/*PIK3CA*-altered MCF10A cell lines coloured by *TP53* mutation type (grey = control, green = DNA contact mutant, yellow = structural mutant) with alpelisib sensitivity (green; $IC_{50} \leq 2.5$ µM) or resistance (red; $IC_{50} \geq 4.5$ µM) indicated for the non-*PIK3CA*-transduced cell lines. (b) Western blot analysis of total PIK3CA and β-actin protein levels in *TP53*-altered MCF10A cell lines (p53OE, p53R273C, p53Y234C, p53R248Q) non-*PIK3CA*-transduced (p110αWT), *PIK3CA*-WT-transduced (p110αOE), or *PIK3CA*-MUT-transdcued (p110αMUT). p53 status is indicated in red and p110α status is indicated in green, with full cell line descriptors labelled below the Western blot (coloured by mutation type or control). β-actin serves as the loading control. Molecular weight markers (kDa) are indicated on the right.

While total PIK3CA expression was confirmed by Western blot, direct assessment of downstream PI3K pathway activity (e.g. phosphorylation markers) was not performed in this study and would be an important extension in future work.

5.3.3. Alpelisib sensitivity in *TP53*/*PIK3CA*-altered MCF10A cell lines

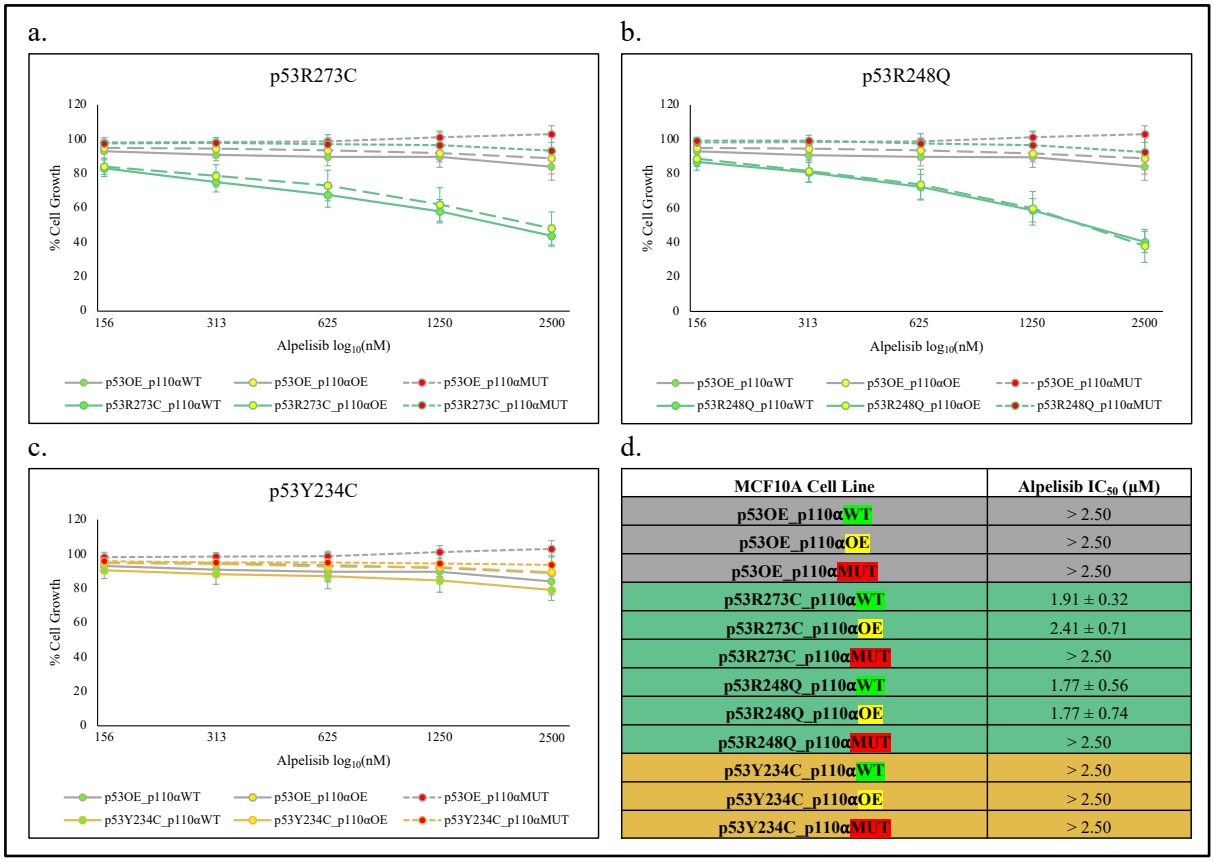
Alpelisib response was assessed across the panel of *TP53*/*PIK3CA*-altered MCF10A cell lines. Given the antiproliferative effects of alpelisib on TNBC cell lines observed in our study (see Figure 4-1, Chapter 4), we hypothesised that *TP53/PIK3CA* co-mutant MCF10A cell lines would exhibit reduced sensitivity compared *PIK3CA*-MUT-only cells and potentially increased sensitivity relative to *TP53*-MUT-only cells. As *PIK3CA* mutations drive hyperactivation of the PI3K pathway, we anticipated that overexpression of *PIK3CA* may yield responses to alpelisib comparable to those elicited by the *PIK3CA*-MUT transduced lines.

Alpelisib response was assessed across the panel of *TP53/PIK3CA*-altered MCF10A cell lines. Given the antiproliferative effects of alpelisib on TNBC cell lines observed in our study (see Figure 4-1, Chapter 4), we explored whether *TP53/PIK3CA* co-alteration would modulate sensitivity compared with single-gene alterations. While Crossman *et al.* reported increased alpelisib sensitivity in certain co-altered contexts, these effects are not consistent across genetic backgrounds (686).

Consistent with prior findings (see Figure 5-5(b)), non-*PIK3CA*-transduced (i.e. _p110αWT) p53R273C_p110αWT (Figure 5-7(a)) and p53R248Q_p110αWT (Figure 5-7(b)) were sensitive to alpelisib, while p53Y234C_p110αWT (Figure 5-7(c)) demonstrated resistance. The p53OE_p110αWT cell line, illustrated in each graph (Figure 5-7(a-c)) for comparison, also exhibited resistance.

Upon transduction with the *PIK3CA*-WT plasmid (i.e. _p110αOE), response to alpelisib in the p53R273C_p110αOE (Figure 5-7(a)) and p53R248Q_p110αOE (Figure 5-7(b)) remained similar to their non-*PIK3CA*-transduced counterparts. The same pattern was observed in the p53Y234C_p110αOE (5-7(c)) and p53OE_p110αOE (Figure 5-7(a-c)) cell lines.

Transduction with the *PIK3CA*-MUT plasmid (i.e. _p110αMUT) reduced sensitivity to alpelisib in both the p53R273C_p110αMUT (Figure 5-7(a)) and p53R248Q_p110αMUT (Figure 5-7(b)) cell lines, compared to their non-*PIK3CA*-transduced counterparts. A small reduction in cell growth inhibition at 2.5 μM alpelisib was also observed in the p53Y234C_p110αMUT (Figure 5-7(c)) and p53OE_p110αMUT (Figure 5-7(a-c)) cell lines compared to the non-*PIK3CA*-transduced cell lines (6% versus 21% and 0% versus 16%, respectively).



MCF10A Cell Line	Alpelisib IC_{50} (µM)
p53OE_p110αWT	> 2.50
p53OE_p110αOE	> 2.50
p53OE_p110αMUT	> 2.50
p53R273C_p110αWT	1.91 ± 0.32
p53R273C_p110αOE	2.41 ± 0.71
p53R273C_p110αMUT	> 2.50
p53R248Q_p110αWT	1.77 ± 0.56
p53R248Q_p110αOE	1.77 ± 0.74
p53R248Q_p110αMUT	> 2.50
p53Y234C_p110αWT	> 2.50
p53Y234C_p110αOE	> 2.50
p53Y234C_p110αMUT	> 2.50

Figure 5-7: Antiproliferative effects of alpelisib on *TP53*/*PIK3CA*-altered MCF10A cell lines. The proliferation of **(a)** p53R273C_p110αWT, p53R273C_p110αOE, p53R273C_p110αMUT, **(b)** p53R248Q_p110αWT, p53R248Q_p110αOE, p53R248Q_p110αMUT, **(c)** p53Y234C_p110αWT, p53Y234C_p110αOE, and p53Y234C_p110αMUT was assessed following 5 days of treatment with increasing concentrations of alpelisib (0-2.5 µM). Results for the control cell lines – p53OE_p110αWT, p53OE_p110αOE, and p53OE_p110αMUT – are also shown in each graph **(a-c)**. Percentage growth was calculated relative to untreated controls. Drug concentrations (nM) were $\log_{10}$ scaled and plotted against percentage cell growth. Error bars indicate the SD of biological replicate experiments (n = 3). **(d)** IC_{50} values (µM) for the panel of *TP53*/*PIK3CA*-altered MCF10A cell lines treated with alpelisib.

These results, in the context of the *TP53/PIK3CA*-altered MCF10A cell line model, suggest that alpelisib sensitivity is influenced by *TP53* and is not determined by *PIK3CA* mutation status alone. In *TP53*-MUT cells that were initially more sensitive to alpelisib, introduction of a *PIK3CA* mutation was associated with a reduction in sensitivity, partially offsetting the increased sensitivity observed with the p53R273C and p53R248Q backgrounds.

Despite *PIK3CA* being a known biomarker for alpelisib response (458), introduction of a *PIK3CA* mutation into p53OE cells did not sensitise them, instead, it slightly reduced sensitivity. A similar reduction in sensitivity was observed in the alpelisib-resistant p53Y234C cell line. Overexpression of *PIK3CA*-WT had no measurable effect on alpelisib response, contrary to our expectation that increased *PIK3CA*-WT expression might hyperactivate the PI3K pathway and mimic the impact of a *PIK3CA* mutation. In summary, these findings

confirm functional cross-talk between *PIK3CA* and *TP53* pathways and highlight a mechanism of intrinsic resistance that a PI3K inhibitor alone cannot overcome, which may explain the limited clinical responses observed in patients (687).

5.3.4. Crizotinib sensitivity in *TP53*/*PIK3CA*-altered MCF10A cell lines

Crizotinib response was assessed across the panel of *TP53*/*PIK3CA*-altered MCF10A cell lines. Based on our single-agent crizotinib results (Table 5-1), we expected at most a subtle difference in sensitivity attributable to *TP53* alterations.

Each of the non-*PIK3CA*-transduced p53R273C_p110αWT (Figure 5-8(a)), p53R248Q_p110αWT (Figure 5-8(b)), and p53Y234C_p110αWT (Figure 5-8(c)) cell lines, as well as the p53OE_p110αWT (Figure 5-8(a-c)), exhibited similar response to crizotinib.

Upon transduction with the *PIK3CA*-WT plasmid, response to crizotinib in the p53R273C_p110αOE (Figure 5-8(a)) and p53Y234C_p110αOE (Figure 5-8(c)) reduced, with the latter exhibiting a complete lack of response. The same pattern was observed in the p53OE_p110αOE (Figure 5-8(a-c)) cell line, while the p53R248Q_p110αOE (Figure 5-8(b)) cell line demonstrated similar response to its non-*PIK3CA*-transduced counterpart (as expected).

Transduction with the *PIK3CA*-MUT plasmid also reduced sensitivity to crizotinib in each of the p53R273C_p110αMUT (Figure 5-8(a)), p53R248Q_p110αMUT (Figure 5-8(b)), and p53Y234C_p110αMUT (Figure 5-8(c)) cell lines, as well as the p53OE_p110αMUT (Figure 5-8(a-c)) control, compared to their non-*PIK3CA*-transduced counterparts.

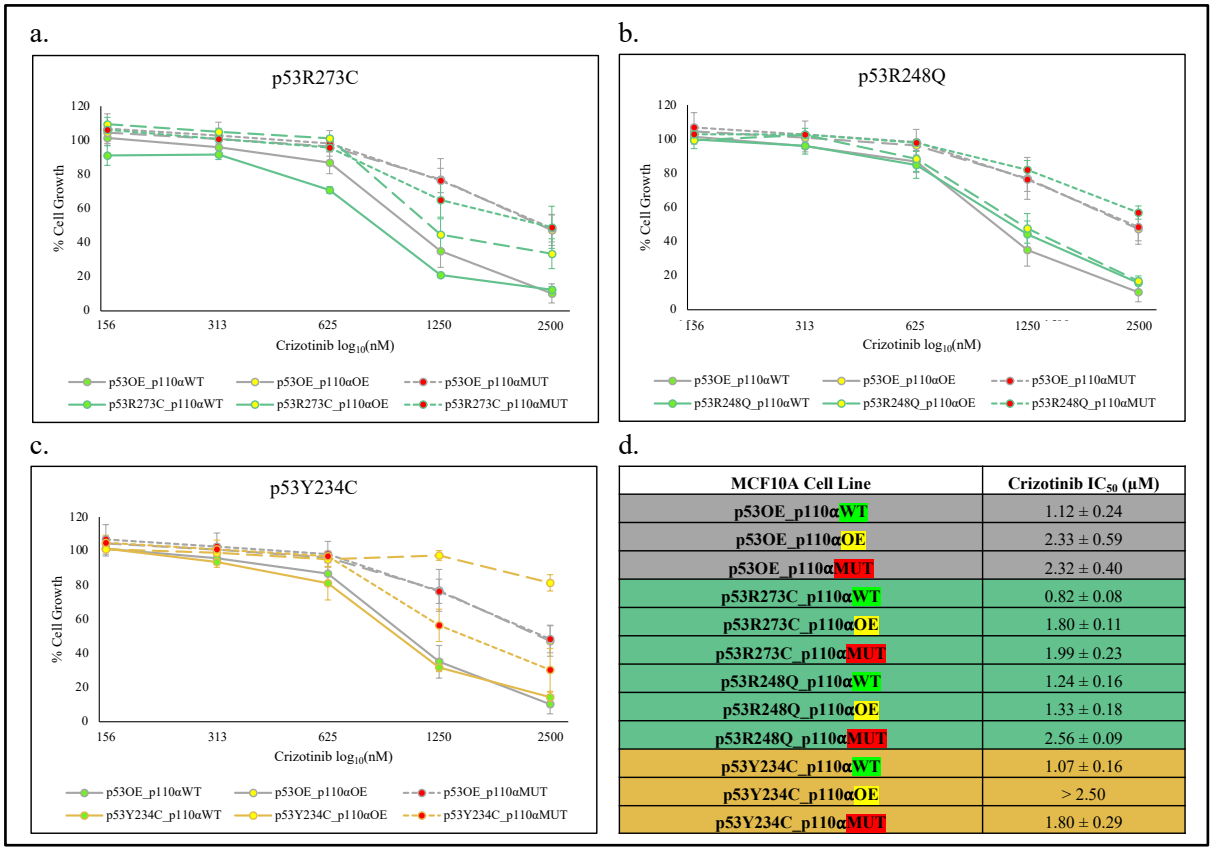
However, distinct patterns of crizotinib sensitivity were evident when comparing the individual cell lines to their *PIK3CA*-WT-transduced counterparts. Specifically, the p53R273C_p110αMUT (Figure 5-8(a)) and p53R248Q_p110αMUT (Figure 5-8(b)) cell lines exhibited reduced responsiveness to crizotinib relative to p53R273C_p110αOE and p53R248Q_p110αOE, respectively. In contrast, p53Y234C_p110αMUT (Figure 5-8(c)) demonstrated enhanced sensitivity compared to p53Y234C_p110αOE. The p53OE_p110αMUT cell line (Figure 5-8(a-c) exhibited equivalent responsiveness to crizotinib as p53OE_p110αMUT.

Overall, these results indicate that crizotinib sensitivity in *TP53*/*PIK3CA*-altered MCF10A cell lines is highly context-dependent. Most of the non-*PIK3CA*-transduced cell lines exhibited similar sensitivity to crizotinib (IC_{50} ~1 μM). p53R273C_p110αWT showed subtle

sensitisation similar to other *TP53* mutants (Table 5-1), whereas p53R248Q_p110αWT and p53Y234C_p110αWT exhibited sensitivity comparable to the p53OE_p110αWT control. These results suggest that while *TP53* mutations may modulate crizotinib sensitivity, the effect is small and variant-specific.

In contrast, transduction with both *PIK3CA*-MUT and *PIK3CA*-WT plasmids reduced response to crizotinib across all *TP53* backgrounds, with the exception of the p53R248Q_p110αOE cell line, where no change in response was observed – consistent with the lack of PIK3CA overexpression detected by Western blot. The magnitude of sensitivity reduction varied depending on *TP53* status: in p53R273C cells, the *PIK3CA* mutation reduced sensitivity more than *PIK3CA*-wildtpye, whereas in p53Y234C cells, overexpression of *PIK3CA* led to a greater reduction in response than *PIK3CA*-MUT. In p53OE cells, both *PIK3CA*-MUT and *PIK3CA*-WT transduction had a comparable effect in reducing crizotinib sensitivity.

These findings indicate that *PIK3CA* activation is the primary driver of altered crizotinib response, but its impact is modulated by *TP53* context, highlighting a nuanced interplay between these two genes in determining drug sensitivity.



d.

MCF10A Cell Line	Crizotinib IC_{50} (μM)
p53OE_p110αWT	1.12 ± 0.24
p53OE_p110αOE	2.33 ± 0.59
p53OE_p110αMUT	2.32 ± 0.40
p53R273C_p110αWT	0.82 ± 0.08
p53R273C_p110αOE	1.80 ± 0.11
p53R273C_p110αMUT	1.99 ± 0.23
p53R248Q_p110αWT	1.24 ± 0.16
p53R248Q_p110αOE	1.33 ± 0.18
p53R248Q_p110αMUT	2.56 ± 0.09
p53Y234C_p110αWT	1.07 ± 0.16
p53Y234C_p110αOE	> 2.50
p53Y234C_p110αMUT	1.80 ± 0.29

Figure 5-8: Antiproliferative effects of crizotinib on *TP53*/*PIK3CA*-altered MCF10A cell lines. The proliferation of **(a)** p53R273C_p110αWT, p53R273C_p110αOE, p53R273C_p110αMUT, **(b)** p53R248Q_p110αWT, p53R248Q_p110αOE, p53R248Q_p110αMUT, **(c)** p53Y234C_p110αWT, p53Y234C_p110αOE, and p53Y234C_p110αMUT was assessed following 5 days of treatment with increasing concentrations of crizotinib (0-2.5 μM). Results for the control cell lines – p53OE_p110αWT, p53OE_p110αOE, and p53OE_p110αMUT – are also shown in each graph **(a-c)**. Percentage growth was calculated relative to untreated controls. Drug concentrations (nM) were log_{10} scaled and plotted against percentage cell growth. Error bars indicate the SD of biological replicate experiments (n = 3). **(d)** IC_{50} values (μM) for the panel of *TP53*/*PIK3CA*-altered MCF10A cell lines treated with crizotinib.

5.3.5. Alpelisib plus crizotinib combination sensitivity in *TP53*/*PIK3CA*-altered MCF10A cell lines

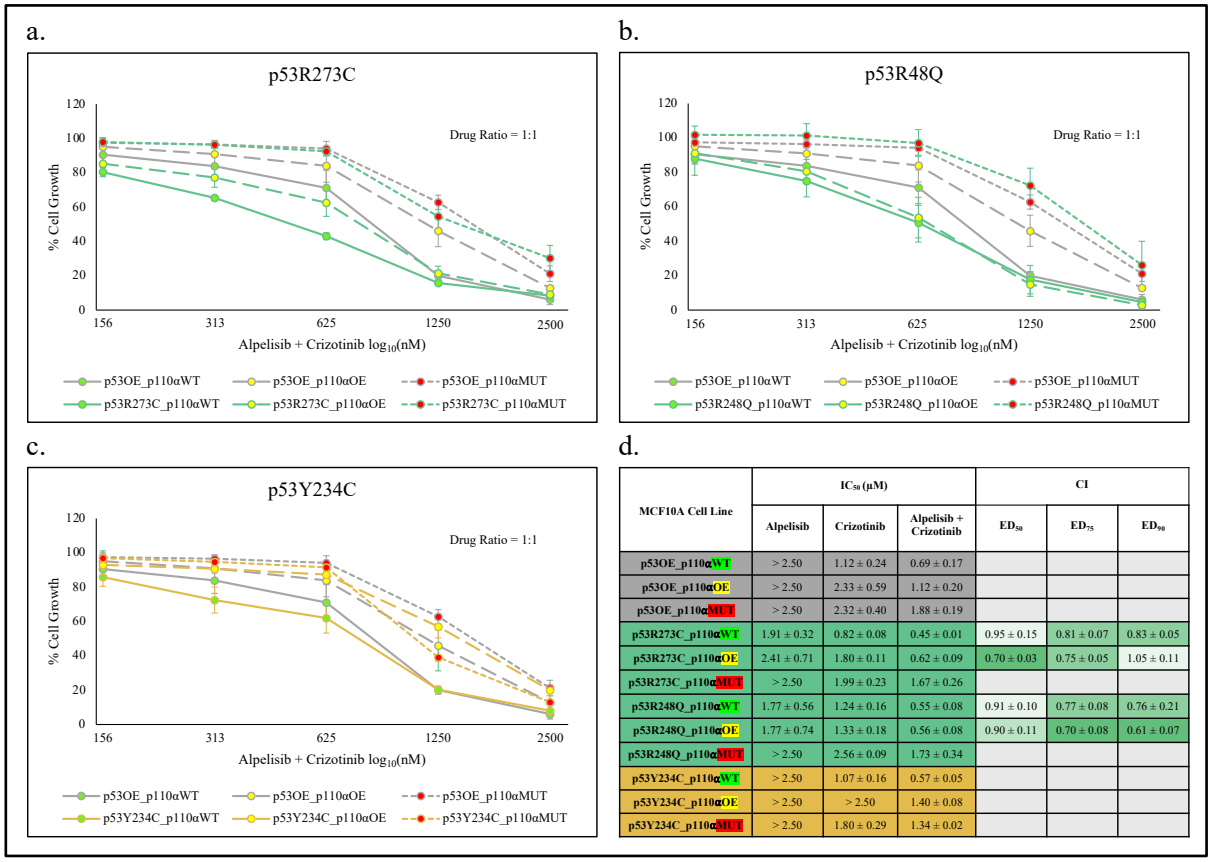
Response to the combination of alpelisib plus crizotinib was assessed across the panel of *TP53*/*PIK3CA*-altered MCF10A cell lines. Given the antiproliferative effects of this combination on TNBC cell lines observed in our study (see Figures 4-5 to 4-7, Chapter 4), we hypothesised that alpelisib plus crizotinib would enhance the antiproliferative effect relative to either drug alone, with the strongest synergy expected in the *TP53/PIK3CA* co-mutant MCF10A cell lines.

Each of the cell lines exhibited increased sensitivity to the combination relative to either single drug alone, as evidenced by the IC_{50} values in Figure 5-9(d). The general trend of response to the alpelisib plus crizotinib combination upon transduction with a *PIK3CA* mutation was a reduction in sensitivity, as evidenced by increasing IC_{50} values in Figure 5-9(d).

Transduction with *PIK3CA*-WT had little to no impact on response to the combination compared to non-*PIK3CA*-transduced cells in the p53R273C and p53R248Q cells. In contrast, *PIK3CA*-WT transduction reduced sensitivity to the combination in the p53OE and p53Y234C cells, similar to the effect observed with *PIK3CA*-MUT.

As 50% cell growth inhibition was not attained in the majority of cell lines upon single-agent alpelisib treatment (see Figure 5-7(d)), CI values could only be calculated for p53R273C_p110αWT, p53R273C_p110αOE, p53R248Q_p110αWT, and p53R248Q_p110αOE cell lines (see Figure 5-9(d)). Across these lines, the combination exhibited general synergy, with slightly enhanced synergy observed in the p53R273C_p110αOE relative to the p53R273C_p110αWT cell line.

In retrospect, the use of a higher alpelisib concentration range may have enabled more robust estimation of IC_{50} values and corresponding CI calculations across a greater proportion of cell lines. However, at the time of experimental design, we did not anticipate that introduction of *PIK3CA* alterations would reduce sensitivity in certain *TP53* backgrounds. In addition, for the least sensitive cell lines (p53Y234C and p53OE), IC_{50} values approached or exceeded 5 μM, which is close to the reported clinical Cmax (5.62 μM). Consequently, extending the concentration range substantially beyond this level would have provided limited additional clinically relevant information, as such exposures are unlikely to be achieved in patients. Furthermore, maintaining a single concentration range across all models was necessary to avoid excessively high dosing that would have resulted in near-complete growth inhibition in the more sensitive cell lines, limiting the ability to assess differential responses and potential synergy.



d.

MCF10A Cell Line	IC_{50} (μM)			CI		
	Alpelisib	Crizotinib	Alpelisib + Crizotinib	ED_{50}	ED_{75}	ED_{90}
p53OE_p110αWT	> 2.50	1.12 ± 0.24	0.69 ± 0.17			
p53OE_p110αOE	> 2.50	2.33 ± 0.59	1.12 ± 0.20			
p53OE_p110αMUT	> 2.50	2.32 ± 0.40	1.88 ± 0.19			
p53R273C_p110αWT	1.91 ± 0.32	0.82 ± 0.08	0.45 ± 0.01	0.95 ± 0.15	0.81 ± 0.07	0.83 ± 0.05
p53R273C_p110αOE	2.41 ± 0.71	1.80 ± 0.11	0.62 ± 0.09	0.70 ± 0.03	0.75 ± 0.05	1.05 ± 0.11
p53R273C_p110αMUT	> 2.50	1.99 ± 0.23	1.67 ± 0.26			
p53R248Q_p110αWT	1.77 ± 0.56	1.24 ± 0.16	0.55 ± 0.08	0.91 ± 0.10	0.77 ± 0.08	0.76 ± 0.21
p53R248Q_p110αOE	1.77 ± 0.74	1.33 ± 0.18	0.56 ± 0.08	0.90 ± 0.11	0.70 ± 0.08	0.61 ± 0.07
p53R248Q_p110αMUT	> 2.50	2.56 ± 0.09	1.73 ± 0.34			
p53Y234C_p110αWT	> 2.50	1.07 ± 0.16	0.57 ± 0.05			
p53Y234C_p110αOE	> 2.50	> 2.50	1.40 ± 0.08			
p53Y234C_p110αMUT	> 2.50	1.80 ± 0.29	1.34 ± 0.02			

Figure 5-9: Antiproliferative effects of alpelisib plus crizotinib on *TP53/PIK3CA*-altered MCF10A cell lines. The proliferation of **(a)** p53R273C_p110αWT, p53R273C_p110αOE, p53R273C_p110αMUT, **(b)** p53R248Q_p110αWT, p53R248Q_p110αOE, p53R248Q_p110αMUT, **(c)** p53Y234C_p110αWT, p53Y234C_p110αOE, and p53Y234C_p110αMUT was assessed following 5 days of treatment with increasing concentrations of alpelisib plus crizotinib (0-2.5 μM; drug ratio = 1:1). Results for the control cell lines – p53OE_p110αWT, p53OE_p110αOE, and p53OE_p110αMUT – are also shown in each graph **(a-c)**. Percentage growth was calculated relative to untreated controls. Drug concentrations (nM) were $\log_{10}$ scaled and plotted against percentage cell growth. Error bars indicate the SD of biological replicate experiments (n = 3). **(d)** IC_{50} values (μM) and CI values (μM; ED_{50}, ED_{75}, ED_{90}) for the panel of *TP53/PIK3CA*-altered MCF10A cell lines treated with alpelisib plus crizotinib.

Overall, the combination of alpelisib plus crizotinib exhibited enhanced antiproliferative effects across all *TP53/PIK3CA*-altered MCF10A cell lines relative to either single agent. Introduction of a *PIK3CA* mutation reduced sensitivity to the combination compared to cells harbouring only *TP53* alterations (either mutant or overexpressed). The effects of *PIK3CA*-WT overexpression were dependent on *TP53* background. In the DNA-contact mutants (p53R273C and p53R248Q), which were initially classified as alpelisib-sensitive, *PIK3CA*-WT overexpression produced little change in overall response; however, synergy appeared slightly greater in p53R273C, potentially reflecting more effective PIK3CA overexpression in this line, as suggested by Western blot analysis. In contrast, both the structural mutant p53Y234C and the p53OE control, which were initially classified as alpelisib-resistant, showed reduced

sensitivity to the combination following *PIK3CA*-WT overexpression, similar to the effect observed with the *PIK3CA*-MUT.

Notably, in both the p53OE and p53Y234C backgrounds – which were classified as alpelisib-resistant –, both *PIK3CA* mutation and *PIK3CA*-WT overexpression reduced sensitivity to crizotinib alone; however, this reduction was partially mitigated in the combination setting, where lower IC_{50} values were observed relative to either single agent.

Together, these findings indicate that the antiproliferative response to alpelisib plus crizotinib is modulated by both *TP53* mutation context and *PIK3CA* status, suggesting that the functional interplay between *TP53* and PI3K pathway alterations influences combination efficacy.

5.3.6. Summary

In summary, this section employed a genetically controlled MCF10A model to dissect the isolated contributions of *TP53* alterations – alone and in combination with *PIK3CA* alterations – on sensitivity to alpelisib, crizotinib, and their dual inhibition, building on observations from TNBC cell lines in Chapter 4 and extending findings reported by Crossman et al. (686).

Antiproliferative assessment of the *TP53*-altered MCF10A panel revealed mutation-specific effects on alpelisib response, with DNA contact mutants (e.g. R248Q, R273C) generally conferring greater sensitivity than structural mutants (e.g. Y234C, H179R), though outliers such as G245S highlighted intragroup heterogeneity. This supports the hypothesis that *TP53* mutations can impact PI3K/AKT signalling, but in a variant-dependent manner.

Successful transduction with *PIK3CA*-H1047R (p110αMUT) or *PIK3CA*-WT (p110αOE) was confirmed via elevated protein expression (except in the p53R248Q_p110αOE cell line), enabling assessment in selected *TP53* backgrounds (alpelisib-sensitive DNA contact mutants R273C and R248Q; alpelisib-resistant structural mutant Y234C; and p53OE control). Contrary to expectations, introduction of a *PIK3CA* mutation reduced alpelisib sensitivity in originally sensitive *TP53*-MUT cell lines. *PIK3CA*-WT overexpression had negligible impact, suggesting that oncogenic mutation, rather than overexpression alone, is required to meaningfully alter pathway output.

The alpelisib-crizotinib combination enhanced antiproliferative effects across all lines compared to monotherapy, consistent with synergistic dual pathway inhibition hypothesised from Chapter 4. However, *PIK3CA* mutations diminished overall sensitivity relative to *TP53*-altered-only cell lines, while the effects of *PIK3CA*-WT overexpression varied by *TP53* type –

minimal in alpelisib-sensitive DNA contact mutants but more pronounced in alpelisib-resistant backgrounds. Synergy was calculable in select lines, showing moderate to strong interactions.

Interestingly, in both the p53OE and Y234C cell lines – classified as alpelisib-resistant – *PIK3CA* mutation or overexpression reduced crizotinib sensitivity. Notably, this reduced sensitivity was partially overcome in the combination setting, with lower IC_{50} values observed for alpelisib plus crizotinib compared with either single agent, indicating that dual inhibition can mitigate *PIK3CA*-driven resistance in these backgrounds.

Collectively, despite enhancing therapeutic response relative to single agents, the alpelisib–crizotinib combination was less effective in the *TP53/PIK3CA* co-mutant context compared to single-mutant models. This contrasts with findings in Chapter 4, where the combination demonstrated synergy in *TP53/PIK3CA* co-mutant TNBC cell lines, and may reflect differences in genetic context and the non-tumorigenic nature of the MCF10A model. These results underscore mutation- and context-specific nuances that should inform personalised therapeutic strategies in *PIK3CA*-MUT TNBC, where *TP53* variant classification (e.g. DNA contact versus structural) could help predict response to PI3K-targeted and combination therapies.

6.Discussion

6.1. Introduction

TNBC remains one of the most aggressive and therapeutically challenging BC subtypes, representing approximately 10-15% of cases but contributing disproportionately to BC-related morbidity and mortality (406). Its clinical management is complicated by rapid progression, high recurrence rates, and limited targeted treatment options (98). Despite the introduction of new targeted therapies, standard treatment continues to rely predominantly on cytotoxic chemotherapy and ICIs, with only modest improvements in patient outcomes (688). ADCs, such as sacituzumab govitecan and T-DXd, provide a degree of molecular precision (689). However, their use is guided by antigen expression (TROP2 or HER2) rather than specific genomic alterations. The absence of targeted therapies directly addressing the most common TNBC genomic alterations underscores a critical need for variant-driven precision strategies capable of improving long-term outcomes.

TP53 mutation is the defining genomic feature of TNBC, occurring in approximately 80% of cases and contributing substantially to genomic instability, impaired DNA damage responses, and aggressive tumour behaviour (228,690). In parallel, aberrant activation of the PI3K/AKT/mTOR pathway represents one of the most common oncogenic signalling events in BC and can arise through multiple mechanisms, including *PIK3CA* mutation, *AKT1* activation, and *PTEN* loss (560). These alterations are biologically complementary. Under normal conditions, WT p53 constrains PI3K signalling through the transcriptional regulation of negative pathway regulators. Conversely, hyperactivation of the PI3K pathway overrides this suppression, ultimately promoting cellular proliferation, survival, metabolic adaptation, and therapeutic resistance (561,592). Consequently, concurrent *TP53* dysfunction and PI3K pathway activation may establish a particularly aggressive tumour state characterised by unchecked oncogenic signalling and impaired tumour suppressive control (686,691). Importantly, co-occurrence of *TP53* mutation and PI3K pathway-activating alterations is not rare in TNBC, observed in approximately 20% of cases across both the METABRIC and TCGA cohorts (568,571). This represents a substantial proportion of *TP53*-MUT TNBCs and defines a clinically relevant subgroup in which two major oncogenic axes converge.

Targeted inhibition of PI3K using isoform-specific agents such as alpelisib has demonstrated clinical efficacy in *PIK3CA*-mutant, HR-positive BC; however, adaptive resistance remains a major limitation to durable response (692). In TNBC, this challenge is further compounded by the high prevalence of *TP53* mutations, which may modulate cellular responses to PI3K

pathway inhibition through impaired apoptotic signalling and altered stress-response checkpoints (693,694). Loss of p53 function removes a key mediator of DNA damage-induced apoptosis and cell cycle arrest, potentially enabling tumour cells to better tolerate oncogenic stress that is induced by pathway-targeted therapies (695–697). In this context, PI3K pathway inhibition alone may be insufficient to induce sustained therapeutic responses in *TP53*-MUT, PI3K-activated TNBC.

This study was guided by four interrelated hypotheses. First, *TP53*-PI3K^{act} TNBC is a distinct, high-risk subgroup that drives tumour aggressiveness and poor patient outcomes. This clinical profile exists independently of established TNBC subtypes. Second, PI3K inhibitors show limited efficacy in TNBC due to resistance driven by *TP53* dysfunction; necessitating the use of combinatorial treatment strategies that target complementary pathways. Third, that distinct classes of *TP53* mutations differentially influence downstream signalling and therapeutic response, resulting in variable sensitivity to PI3K/AKT inhibition. Finally, while *PIK3CA*-MUT tumours are sensitive to PI3K inhibitors, co-occurring *TP53* mutations drive resistance by boosting survival signals and blocking cell death. However, combination therapies can partially overcome this resistance. Multi-omic profiling across patient cohorts, TNBC cell lines, and isogenic models was employed to test these hypotheses and validate mutation-specific vulnerabilities.

6.2. *TP53*-PI3K^{act} defines a high-risk state in TNBC

Concurrent alterations in *TP53* and the PI3K pathway have been consistently associated with adverse outcomes across multiple tumour types, including BC. Studies focusing on *TP53/PIK3CA* co-mutation have demonstrated significantly poorer survival compared with tumours harbouring either alteration alone, supporting a model in which loss of p53 tumour suppressor function cooperates with PI3K-driven oncogenic signalling to promote more aggressive disease biology (592,698).

In BC specifically, Lin *et al.* reported that *TP53/PIK3CA* co-mutant tumours exhibit adverse clinicopathological features, including higher grade, more advanced stage, and enrichment in HR-negative and HER2-positive disease in a cohort from Guangdong Provincial People's Hospital (GDPH). Consistent findings from the METABRIC cohort further showed that dual *TP53/PIK3CA* mutations are independently associated with worse OS and RFS, reinforcing the concept of a synergistically adverse prognostic interaction. However, these analyses were limited to *PIK3CA* mutations alone and did not evaluate TNBC specifically. In addition, they

did not capture the broader spectrum of PI3K pathway dysregulation, which extends beyond *PIK3CA* mutations to include multiple activating and LOF events across the pathway (592).

More recently, Zwimpfer *et al.* expanded the definition of PI3K/AKT pathway alteration using METABRIC and MSK cohorts by incorporating gene amplifications (*AKT1, AKT2, AKT3, PIK3CA,* rapamycin-insensitive companion of mTOR *(RICTOR))* and *PTEN* mutations. They demonstrated that combined *TP53* mutation and PI3K/AKT pathway alteration was associated with the worst OS across BC as a whole, with adverse effects persisting across molecular subtypes, including TNBC. However, the study did not specifically interrogate survival within TNBC as a primary focus, nor did it formally test whether PI3K/AKT alterations confer additional risk on top of a *TP53*-MUT background within this subgroup. Instead, the co-altered group was primarily compared against a *TP53*-WT/PI3K pathway-unaltered reference cohort, which limits interpretation of whether PI3K/AKT activation adds incremental prognostic information once *TP53* mutation is already present (594). This is particularly relevant given the near-ubiquity of *TP53* mutations in TNBC (699), which reduces its discriminatory power as a standalone stratifier and underscores the need for more refined, within-*TP53*-MUT risk stratification.

Methodologically, the Zwimpfer definition of PI3K activation – restricted to amplifications and *PTEN* mutations – may also underestimate clinically relevant pathway activation (594). There is substantial evidence that activating mutations in *PIK3CA* and *AKT* genes, as well as *PTEN* loss (including deletions), are key drivers of PI3K pathway hyperactivation (700,701) and are directly relevant to the mechanism of action of approved PI3K/AKT inhibitors (702). The exclusion of these mutation classes therefore represents a limitation in capturing the full biological and therapeutic landscape of PI3K signalling dysregulation.

In contrast, our study defined PI3K pathway activation using a mutation- and LOF-centric framework, incorporating activating mutations in *PIK3CA* and *AKT1*, as well as *PTEN* deletions, rather than relying on gene amplifications alone. This approach captures canonical drivers of PI3K pathway hyperactivation that are most directly aligned with established mechanisms of pathway signalling and therapeutic targeting. We also applied a stepwise analytical framework, sequentially assessing whether progressively expanded definitions of PI3K pathway activation either maintained or further exacerbated the adverse survival associated with the *TP53/PIK3CA* mutation. This approach allowed us to systematically define

a *TP53*-PI3K^{act} subset as a reproducible high-risk TNBC population, with direct relevance to PI3K-targeted therapeutic strategies.

Additionally, our study specifically evaluated the prognostic impact of PI3K pathway activation in a *TP53*-MUT background. In both the METABRIC and TCGA cohorts, TNBC patients with dual PI3K-activating and *TP53* alterations experienced significantly worse survival than those with *TP53* mutations alone or neither alterations. This effect was robust and reproducible across independent datasets, supporting the conclusion that PI3K pathway activation provides additional prognostic stratification within an already high-risk *TP53*-MUT TNBC population. Importantly, the adverse prognostic effect is not attributable to enrichment of a single clinical feature or TNBC subtype, indicating that *TP53*-PI3K^{act} represents an independent risk state rather than a surrogate for conventional clinicopathological stratification.

From a genomic perspective, no additional recurrent somatic mutations, structural variants, or CNAs were consistently enriched in the *TP53*-PI3K^{act} cohort, indicating that the high-risk phenotype is not driven by a distinct secondary genomic driver. Moreover, our study demonstrates that *TP53* mutations and PI3K^{act} alterations largely arise independently in TNBC. In contrast, Zwimpfer et al. reported a statistically significant interaction between *TP53* mutations and PI3K/AKT pathway alterations; however, their analysis was conducted at a pan-BC level and did not specifically assess interaction effects within TNBC (594). In the context of our TNBC-focused analysis, the absence of a significant interaction may reflect reduced variability in *TP53* status rather than a lack of biological cooperation between these pathways. In addition, differences in the definition of PI3K pathway activation may further contribute to discrepancies between studies.

Clinically, *TP53*-PI3K^{act} tumours showed a distinct and more aggressive phenotype across both cohorts. Patients presented at an older age with higher rates of post-menopausal status, resembling PI3K^{act}-only disease more than *TP53*-only tumours (see Figure 3-3). This observation is consistent with findings from Lin et al., who reported that patients with *TP53/PIK3CA* co-mutant BC in the GDPH cohort were significantly more likely to be diagnosed at an older age and to be post-menopausal compared with those harbouring *TP53* mutations alone (592). While their analysis was performed across BC as a whole and was enriched for HER2-positive disease, our findings demonstrate that this association persists within TNBC when PI3K pathway activation is defined more broadly.

This pattern is consistent with the evolutionary architecture described in TNBC, in which *TP53* mutations are highly prevalent and typically occur as early, clonal events that establish a background of genomic instability and enable subsequent clonal diversification. In contrast, PI3K signalling pathway alterations are less ubiquitous and are enriched in specific transcriptional subtypes such as LAR and apocrine tumours, where they appear to function more as lineage- or branch-defining events that shape tumour phenotype and fitness rather than initiating genomic instability (703). Accordingly, *TP53*-PI3K^{act} tumours may reflect evolutionary convergence of an early instability-driven clone with later or parallel acquisition of PI3K pathway activation, resulting in a biologically distinct disease state that combines early genomic permissiveness with growth and survival pathway dependency.

Importantly, *TP53*-PI3K^{act} tumours also exhibited higher rates of mastectomy and a greater proportion of disease-specific deaths compared with tumours harbouring either *TP53* or PI3K^{act} alterations alone, indicating a more aggressive clinical course and consistent with their worse survival. This is supported by findings from Croessmann *et al*. (as introduced in Chapter 5), who demonstrated in an isogenic MCF10A model that co-occurring *TP53* and *PIK3CA* alterations cooperate to enhance transformed phenotypes and increase genomic instability and tumour heterogeneity compared with either alteration alone (686).

We observed increased hypoxia in *TP53*-PI3K^{act} tumours compared with *TP53*-only disease, but levels were similar to PI3K^{act}-only tumours, indicating that the hypoxic phenotype is primarily PI3K-associated rather than specific to the co-altered state. Notably, *TP53*-only tumours did show increased hypoxia relative to non-altered TNBC. However, this effect appears modest compared with PI3K-driven hypoxic adaptation. This is consistent with evidence that PI3K/AKT/mTOR signalling promotes a hypoxia-adapted programme through HIF-1α stabilisation and enhanced translational capacity, driving angiogenesis, glycolytic reprogramming, and survival under low oxygen conditions (704). In contrast, *TP53* functions more as a modulator of hypoxic stress responses, regulating HIF-1 signalling and downstream survival or apoptotic outcomes in a context-dependent manner (705). In this co-altered context, PI3K pathway activation likely represents the dominant driver of hypoxia-associated transcriptional programmes, while *TP53* mutation removes a key regulatory checkpoint that would otherwise constrain hypoxia-induced survival and metabolic rewiring. The convergence of these alterations does not substantially increase hypoxia levels beyond PI3K-driven effects but is likely to amplify the biological consequences of hypoxia, promoting metabolic flexibility, hypoxia tolerance, and reduced apoptotic responsiveness (705,706). This may

contribute to the aggressive and therapeutically resistant phenotype observed in *TP53*-PI3K^{act} TNBC.

Across multiple molecular classification frameworks, *TP53*-PI3K^{act} tumours display a consistent shift away from a canonical basal-like TNBC phenotype towards a more receptor- and signalling-enriched state. Specifically, these tumours show reduced representation of basal-associated integrative Cluster 10. While cluster 10 is associated with early poor outcomes, its longer-term prognosis is more favourable, indicating a time-dependent risk pattern (598). This suggests *TP53*-PI3K^{act} disease is not merely a "basal-extreme" state, but a distinct biological phenotype with a different risk trajectory. This is supported by subtype-level analyses, where *TP53*-PI3K^{act} tumours show reduced PAM50 basal-like classification, alongside increased HER2-enriched calls. In parallel, SNP6 data demonstrate higher rates of HER2 gene CN gain, suggesting coordinated shifts in both transcriptional state and CN architecture towards a more receptor-signalling-driven biology (707). Notably, these tumours remain clinically HER2-negative by standard diagnostic criteria, indicating that HER2-enriched transcriptional states and low-level *ERBB2* CN increases can occur in the absence of overt HER2 amplification. This may reflect biology analogous to emerging HER2-low TNBC states, in which clinically HER2-negative tumours nevertheless demonstrate increased HER2 pathway activity, enrichment for non-basal phenotypes, and frequent PI3K pathway alteration (708).

In a study of TNBC cohorts (Life After Cancer Epidemiology and Pathways patient populations), Gulbahce et al. demonstrated that older patients with clinically defined TNBC show a clear shift in intrinsic biology, with a lower proportion of PAM50 basal-like tumours, reduced expression of proliferation-associated gene signatures, and higher *ERBB2* expression despite clinical HER2-negativity (709). This provides an important parallel to our findings in *TP53*-PI3K^{act} disease. While Gulbahce *et al.* described an age-associated transition towards a less basal and more HER2-associated TNBC phenotype, the molecular drivers underlying this shift remained unclear. Our findings raise the possibility that PI3K pathway activation in a *TP53*-MUT background may represent one genomic mechanism contributing to this biological transition. The enrichment of *TP53*-PI3K^{act} tumours among older and post-menopausal patients, together with their reduced basal-like identity and increased HER2-associated transcriptional features, suggests that this co-altered state may define a subset of TNBC responsible for some of the age-related heterogeneity observed within the disease.

Within TNBC-specific transcriptional classifications, a transition away from BL1-dominant biology (seen in *TP53*-only disease) towards relative enrichment of BL2- and LAR-like features in *TP53*-PI3K^{act} tumours was observed (see Figure 3-4). Characterised by elevated metabolic activity and enhanced growth factor/RTK signalling (710), the BL2 subtype represents a receptor-driven state primed by concurrent *TP53* loss and PI3K pathway activation. BL2 enrichment is much stronger in *TP53*-deficient/PI3K-activated tumours than in those with PI3K activation alone, which instead favour LAR features. This suggests that *TP53* loss allows PI3K signalling to drive a wider variety of growth factor-responsive states. This is consistent with evidence that *TP53* loss is associated with altered growth factor and RTK signalling dependencies (561). Despite these TNBC subtype shifts, survival associations remain independent of TNBC subtype, and *TP53*-PI3K^{act} tumours are distributed across all Lehmann/Burstein categories.

Unlike the Lehmann and Burstein TNBC classifications, which define tumours according to dominant transcriptional lineage and phenotypic programmes (117,584,626), *TP53*-PI3K^{act} represents a genomically and functionally unique oncogenic state driven by convergent *TP53* dysfunction and PI3K pathway activation. The distribution of *TP53*-PI3K^{act} tumours across diverse TNBC transcriptional subtypes indicates that this co-altered state operates independently of intrinsic identity, representing a distinct biological layer that co-exists with current molecular classifications. Consequently, *TP53*-PI3K^{act} may capture clinically relevant tumour biology and therapeutic dependencies not fully resolved by transcriptomic subtype classification alone, supporting the integration of genomic co-alteration states with existing TNBC subtype frameworks for improved biological stratification.

Our transcriptional analyses further support the concept that *TP53*-PI3K^{act} TNBC is characterised by substantial metabolic reprogramming. Across both METABRIC and TCGA cohorts, pathway-level analyses identified increased activity of pathways involved in xenobiotic metabolism, lipid and steroid metabolism, drug metabolism, and phase II conjugation (see Figure 3-7). While metabolic enrichment was more robust in METABRIC, many pathways retained nominal significance in TCGA, sharing significant leading-edge gene overlap. This indicates that despite differing enrichment magnitudes, the core genes driving these metabolic programs are conserved, reflecting reproducible biology rather than a cohort-specific artefact.

Importantly, ssGSEA demonstrated that this metabolic phenotype was reproducibly elevated in *TP53*-PI3K^{act} tumours relative to *TP53*-only disease across both cohorts (see Table 3-8). However, metabolic activity was not significantly different between *TP53*-PI3K^{act} and PI3K^{act}-only tumours. This is consistent with the central role of PI3K signalling in coordinating cancer metabolic reprogramming and supports the broader hypoxia-associated and HIF-linked transcriptional programme described previously (711). Together, these findings suggest that the metabolic phenotype observed in *TP53*-PI3K^{act} tumours reflects PI3K pathway activation, with *TP53* loss likely acting to modulate downstream cellular stress responses rather than directly driving metabolic output.

The DEAs further support this metabolically reprogrammed phenotype, particularly within the METABRIC cohort (see Figure 3-5). Several of the most highly expressed genes in *TP53*-PI3K^{act} tumours, including chloride channel accessory 2 *(CLCA2)*, homogentisate 1,2-dioxygenase *(HGD)*, receptor accessory protein 6 *(REEP6)*, SAM pointed domain containing ETS transcription factor *(SPDEF)*, ATP-binding cassette subfamily C member 11 *(ABCC11)*, serine peptidase inhibitor kazal type 8 *(SPINK8)*, and carnitine O-acetyltransferase *(CRAT)*, overlap with a previously described TNBC co-expression module associated with the MC3 metabolic subtype identified by Zhou et al.. In that study, the MC3 subtype was characterised by coordinated upregulation of metabolic and transport-related genes and was associated with poorer prognosis, consistent with the adverse clinical outcomes observed in *TP53*-PI3K^{act} tumours in our study (607). Many of these genes have putative roles in metabolic adaptation or secretory and transport processes that may support tumour fitness. For example, *CRAT* regulates mitochondrial fatty acid metabolism (712), *ABCC11* is involved in ATP-dependent transport of metabolites and xenobiotics (713), and *HGD* participates in tyrosine catabolism (714). The enrichment of this MC3-associated transcriptional programme therefore suggests that *TP53*-PI3K^{act} tumours adopt a metabolically adaptive state that may support survival under stress conditions and contribute to aggressive tumour behaviour.

In addition to metabolic rewiring, *TP53*-PI3K^{act} tumours also demonstrated altered immune-associated transcriptional programmes. Immune-related enrichment was prominent in the TCGA cohort, where *TP53*-PI3K^{act} tumours exhibited elevated activity in pathways linked to innate immune signalling, antimicrobial peptide responses, and neutrophil degranulation (Figure 3-7). ssGSEA subsequently demonstrated significantly increased immune pathway activity in METABRIC *TP53*-PI3K^{act} tumours relative to both *TP53*-only and PI3K^{act}-only disease, indicating that immune-associated activation is reproducible across cohorts (see Figure

3-8). Notably, these immune signatures exhibited strong directional concordance and shared leading-edge genes across datasets, demonstrating that these processes reflect a genuine underlying biology rather than cohort-specific artefacts.

These findings characterise the *TP53*-PI3K^{act} immune microenvironment as predominantly innate and inflammatory, suggesting a failure to mount an effective adaptive anti-tumour immune response (715). Increased neutrophil degranulation signalling may reflect recruitment or activation of myeloid-lineage immune cells, which are known to promote tumour progression, metastasis, and immune suppression in TNBC (716). This inflammatory phenotype may arise through combined effects of *TP53* dysfunction and PI3K pathway activation, as *TP53* loss promotes inflammatory signalling, immune evasion, and genomic instability (717), while PI3K/AKT signalling further modulates cytokine production and immune-cell recruitment within the TME (718,719). Consistent with this, a recent pan-cancer analysis demonstrated that *TP53*-MUT tumours are associated with broad modulation of the tumour immune microenvironment and enrichment of immune dysfunction signatures driven by hypoxia-linked metabolic reprogramming (706). The higher expression of S100 calcium binding protein A8 and A9 (*S100A8* and *S100A9*) across both cohorts further supports this interpretation (see Figure 3-6). These inflammatory mediators are associated with myeloid inflammation, neutrophil recruitment, and immunosuppressive signalling in BC, and have been linked to metastasis and therapeutic resistance (720). Together, these findings suggest that *TP53*-PI3K^{act} tumours are characterised by a chronic inflammatory state that may support tumour survival and treatment resistance rather than productive anti-tumour immunity. This is particularly relevant given emerging evidence that PI3K pathway activation contributes to immune evasion and altered immunotherapy responses in TNBC (721,567,722,723).

In contrast to the metabolic signatures, cell cycle pathways displayed context-dependent variation across cohorts. In METABRIC, *TP53*-PI3K^{act} tumours were characterised by the significant suppression of cell cycle hallmarks, such as E2F targets, G2/M checkpoint regulation, and mitotic progression (see Figure 3-7). This observation is consistent with the broader transcriptional departure from a BL1-dominant phenotype, which is classically hallmarked by robust proliferative activity and the upregulation of cell cycle and DNA replication machinery (626). In TCGA, however, cell cycle-related pathways showed apparent enrichment in *TP53*-PI3K^{act} tumours at the GSEA level, despite a concurrent shift in TNBC subtype composition away from BL1 and towards BL2 enrichment. This variance may relate to distinct classification methodologies. Unlike clinically derived cohorts based on

ER/PR/HER2 status, the TCGA TNBC cohort relies on PAM50 basal-like stratification, which could inherently influence the baseline proliferative and cell cycle profiles observed (724). Importantly, this apparent enrichment in TCGA was not significant at the ssGSEA level, in contrast to METABRIC where cell cycle pathways were significantly depleted. This suggests that the TCGA signal may reflect relative ranking effects within the cohort rather than a robust change in absolute pathway activity across tumours.

Notably, while cell cycle activity was diminished compared to *TP53*-only tumours in METABRIC, the *TP53*-PI3K^{act} cohort still displayed significantly elevated cell cycle ssGSEA scores relative to PI3K^{act}-only TNBC, with additional pathways trending toward significance (see Table 3-8). This suggests that *TP53*-PI3K^{act} tumours maintain an intermediate proliferative state, retaining greater cell cycle activity than PI3K^{act}-only tumours while remaining lower than *TP53*-driven proliferative programmes.

Similarly to the cell cycle programmes, keratinisation-related pathways showed a discordant pattern in *TP53*-PI3K^{act} TNBC across cohorts, with depletion in METABRIC but apparent enrichment in TCGA (see Figure 3-7). However, there was limited leading-edge gene overlap suggesting the signals are driven by different gene subsets. In TNBC, keratinisation signatures are closely linked to basal differentiation, and may therefore vary depending on the distribution of underlying transcriptional subtypes (725).

6.2.1. Conclusion

Overall, *TP53*-PI3K^{act} defines a reproducible, cross-subtype high-risk state in TNBC arising from the convergence of *TP53* loss and PI3K pathway activation. Across two independent cohorts, it is consistently associated with poorer outcomes independent of clinicopathological factors and intrinsic subtype, indicating a biological risk state not captured by existing classification systems. Molecularly, these tumours are characterised by metabolic reprogramming and hypoxia signalling, sustained proliferative capacity in a *TP53*-deficient context, and a distinct inflammatory phenotype with increased innate immune activity relative to both *TP53*-only and PI3K^{act}-only disease. In parallel, they show consistent enrichment of BL2 transcriptional features, reflecting a shift towards growth factor- and receptor-driven biology. Together, these features define a coherent convergence phenotype in which PI3K activation, *TP53* loss, and immune remodelling integrate to drive the aggressive clinical behaviour of this TNBC subset.

6.2.2. Limitations and future work

A key limitation of this study relates to survival analyses, particularly within TCGA, where follow-up time and clinical annotation are more limited compared with METABRIC (726). This reduces statistical power for long-term outcome assessment and may limit the sensitivity to detect more nuanced survival differences within stratified subgroups. In contrast, METABRIC provides more mature survival data, enabling more robust validation of the high-risk nature of *TP53*-PI3K^{act} disease. As such, survival associations in TCGA should be interpreted with appropriate caution and considered supportive rather than definitive.

Although analysis across two independent cohorts (METABRIC and TCGA) strengthens the robustness of the *TP53*-PI3K^{act} phenotype, differences in cohort composition and TNBC definition likely influenced specific transcriptional and pathway-level outputs. TCGA defines TNBC using PAM50 basal-like status, whereas METABRIC relies on clinical ER/PR/HER2 annotation, resulting in differences in baseline tumour composition and molecular subtype distribution. These factors may partially explain cohort-specific discrepancies observed in cell cycle and keratinisation-related pathways, despite overall concordance in core biological signals.

A further limitation relates to cohort composition and underlying biology of PI3K pathway activation. The *TP53*-PI3K^{act} subgroup was not biologically uniform across datasets: METABRIC was enriched for *PIK3CA*-mutant-driven PI3K activation, whereas TCGA was more heavily weighted towards *PTEN*-loss-driven cases. This distinction is important, as *PTEN* loss and *PIK3CA* activating mutations are known to exert both overlapping and distinct effects on PI3K pathway output and downstream signalling networks, despite converging on PIP3 accumulation. Prior experimental work has demonstrated that *PTEN*-deficient and *PIK3CA*-mutant tumours can exhibit differential activation of downstream signalling nodes, including divergence in RTK feedback (e.g. EGFR signalling enrichment in *PIK3CA*-driven models) and differences in pathway wiring and transcriptional output, despite broadly similar PI3K pathway induction (727). In this context, our findings likely reflect an integrated but compositionally heterogeneous PI3K-activated state rather than a single unified genetic driver, and future work should explicitly stratify *TP53*-PI3K^{act} tumours by the specific mechanism of PI3K activation to determine whether *PIK3CA*-mutant and *PTEN*-loss-driven disease exhibit distinct therapeutic vulnerabilities.

A related limitation is the operational definition of PI3K/AKT pathway activation used in this study. While our approach captured canonical activating mutations in *PIK3CA* and *AKT1* alongside LOF *PTEN* alterations, it did not include the full spectrum of PI3K/AKT events described in broader Zwimpfer et al. pan-BC framework (e.g. *AKT2* and *RICTOR* amplification) (594). Consequently, our PI3K-activated subgroup reflects a biologically focused but non-exhaustive representation of pathway dysregulation. This targeted approach prioritised well-established functional and therapeutic alterations but may limit direct comparability with broader classification schemes. Future studies should evaluate further expanded definitions of PI3K/AKT activation in TNBC to determine whether distinct genomic classes confer different prognostic or therapeutic implications.

While this study provides evidence of a reproducible immune-associated transcriptional phenotype in *TP53*-PI3K^{act} tumours, these findings are based on bulk transcriptomic data and do not allow definitive attribution of immune activity to specific cellular compartments. The observed enrichment of innate inflammatory signatures, including neutrophil-associated and myeloid-linked pathways, requires further validation using computational immune deconvolution methods such as CIBERSORT (728), alongside spatial profiling or flow cytometry-based immune cell quantification, to more precisely define the composition and functional state of the tumour immune microenvironment in *TP53*-PI3K^{act} TNBC (729). This will be essential to determine whether the inflammatory programme reflects immune exclusion, myeloid-driven immunosuppression, or a broader tumour-intrinsic inflammatory state.

An additional limitation is the restricted proteomic coverage available for TCGA and the absence of equivalent proteomic data for METABRIC. Within TCGA, only a limited subset of proteins showed significant differential expression, with many of the observed changes reflecting canonical PI3K pathway activation rather than revealing additional independent biology. Moreover, the very small number of PI3K^{act}-only samples at the proteomic level (n=4) substantially limited statistical power, preventing robust comparison between *TP53*-PI3K^{act} and PI3K^{act}-only tumours at the protein level and constraining conclusions regarding whether proteomic differences exist between these groups.

Despite these limitations, the consistent signal across independent cohorts and multi-omic analyses supports *TP53*-PI3K^{act} as a robust high-risk state in TNBC and a biologically meaningful framework for therapeutic targeting.

6.3. Therapeutic implications of *TP53* mutations and combination strategies in *TP53/PIK3CA* co-mutant TNBC

The identification of *TP53*-PI3K^{act} as a clinically aggressive TNBC subgroup supports therapeutic targeting of the PI3K pathway in this setting. Activating *PIK3CA* mutations occur in approximately 10-15% of TNBCs (239), driving constitutive PI3K/AKT/mTOR signalling. Consequently, inhibition of PI3Kα using alpelisib represents a biologically rational therapeutic strategy for this subgroup.

However, clinical translation of PI3K inhibition in TNBC has thus far produced only modest benefit. The phase III EPIK-B3 trial evaluating alpelisib in combination with nab-paclitaxel in advanced TNBC harbouring *PIK3CA* mutation or *PTEN* loss demonstrated only limited improvement in PFS compared with chemotherapy alone (7.2 vs. 5.6 months, respectively), despite biomarker selection. Although the study was ultimately terminated due to slow enrolment rather than safety concerns, the relatively modest efficacy observed highlights the challenge of achieving durable responses through PI3K pathway inhibition alone in TNBC (247).

The findings of the present study suggest that concurrent *TP53* dysfunction may contribute to this limited therapeutic efficacy. Loss of p53-mediated apoptotic and cell cycle checkpoint control may enable tumour cells to better tolerate PI3K inhibition, reducing dependence on PI3K signalling alone for survival and diminishing both the depth and durability of response. This interpretation is supported by preclinical evidence across multiple tumour contexts, indicating that *TP53* status can directly shape responsiveness to pathway-targeted therapies. In colorectal cancer models, *TP53* mutations impair apoptotic responses to combined MEK and PI3K/mTOR inhibition through failure to induce key downstream mediators such as p21 and BAX, resulting in reduced therapeutic efficacy in *TP53*-MUT compared with *TP53*-WT tumours (730). Similarly, CRISPR-engineered lung adenocarcinoma models with *TP53* deletion demonstrated altered sensitivity to multiple PI3K-pathway inhibitors and dysregulated expression of PI3K isoform genes, suggesting that loss of p53 promotes adaptive rewiring of PI3K signalling networks that may contribute to reduced inhibitor sensitivity (731).

Taken together, these mechanistic observations provide a coherent biological framework linking *TP53* co-mutation to resistance against PI3K-targeted strategies. In the context of TNBC, where *TP53* alterations are highly prevalent, such co-mutations may therefore represent

a key determinant of the limited responses observed in studies such as the phase III EPIK-B3 Trial evaluating alpelisib plus nab-paclitaxel, alongside other cooperating genomic alterations that further reduce dependence on PI3K pathway signalling.

Chapter 4's single-agent proliferation assays across mutation-stratified TNBC cell lines (Figure 4-1) demonstrate genotype-dependent responses to alpelisib, with *PIK3CA* mutations conferring sensitivity and *TP53* mutations promoting resistance. These *TP53/PIK3CA* co-mutant cell lines were more resistant than cell lines harbouring a *PIK3CA* mutation only, suggesting that *TP53* mutations drive this attenuated response. This pattern directly supports our hypothesis that *TP53* mutations confer resistance to PI3K inhibition in *PIK3CA*-mutant TNBC. *TP53* mutations could also act as potential predictive biomarkers of resistance to PI3K inhibition in *PIK3CA*-mutant in other cancers, including colorectal, in which these co-mutations correlate with worse patient outcomes (691). In clinical trials like EPIK-B3, genomic profiling for *TP53/PIK3CA* co-mutations can pinpoint high-risk TNBC patients. Prioritising these individuals for targeted combination regimens could reduce non-response rates and improve overall outcomes. Given the resistance to alpelisib observed in *TP53/PIK3CA* co-mutant TNBC, targeting compensatory pathways offers a rational approach to overcome this limitation.

The rationale for combining PI3K and RTK inhibition in this study is grounded in the broader biological characteristics of the *TP53*-PI3K^{act} high-risk TNBC cohort defined in Chapter 3. Specifically, the transcriptomic analyses demonstrated a shift from a BL1-dominant phenotype towards a BL2-like transcriptional state in *TP53*-PI3K^{act} tumours, suggesting increased growth factor and RTK signalling, consistent with the biology of BL2 TNBC. In parallel, RTK signalling is a well-established feature of TNBC biology more broadly, with frequent overexpression and activation of multiple RTKs contributing to tumour proliferation, survival, and metastatic potential (732). Within this context, *TP53* mutation may further enhance RTK pathway dependence, as loss of p53-mediated regulatory control can contribute to dysregulated RTK expression and sustained downstream signalling (561). In addition, RTK reactivation is a recognised adaptive response to PI3K inhibition, whereby compensatory upregulation of upstream receptor signalling can restore downstream pathway activity and limit therapeutic durability (463,733).

TCGA analysis demonstrated that the key crizotinib targets *MET*, *ALK*, and *ROS1* are significantly upregulated in basal-like BC compared with other molecular subtypes (see Figure

4-2), reinforcing the enrichment of RTK signalling within TNBC and providing a transcriptional basis for targeting this axis. Some evidence suggests that crizotinib may also promote proteasomal degradation of missense mutant p53, potentially attenuating GOF effects and sensitising *TP53*-MUT tumours to apoptosis (734). Preclinical studies indicate that this activity can restore chemotherapy sensitivity in p53-mutant cancers (735), although this mechanism was not directly explored in this study. While crizotinib has been assessed in a phase II clinical trial for TNBC (ClinicalTrials.gov Identifier: NCT03620643), recruitment was terminated after preliminary results showed no response in the six TNBC patients enrolled (643). This lack of response may be attributed to suboptimal stratification biomarkers in the trial and/or inefficacy as a monotherapy, necessitating improved patient stratification and combination therapy (736,737).

Consistent with these phase II trial findings, TNBC cell lines exhibited limited sensitivity to crizotinib and other RTK inhibitors as single agents, with all IC_{50} values exceeding clinically achievable C_{max} levels (see Figure 4-3), indicating monotherapy is unlikely to be effective. Accordingly, we next assessed whether concurrent inhibition of RTK and PI3K signalling using alpelisib in combination with crizotinib could overcome these limitations and enhance therapeutic response. Proliferation assays revealed genotype-dependent synergies, with the strongest effects in *TP53/PIK3CA* co-mutant models, supporting the hypothesis that dual mutations amplify resistance to PI3K inhibition alone, necessitating RTK co-targeting.

Cell lines harbouring a *TP53* mutation alone (i.e. *PIK3CA*-WT) did not respond within the therapeutic window (see Figure 4-5), indicating limited potential for clinical translatability of the combination. In *PIK3CA*-mutant-only MDA-MB-453 cells, there was an apparent increase in antiproliferative effect. However, formal analysis indicated that the combination was antagonistic. CAL-51 cells demonstrated dose-dependent synergy within clinically relevant concentrations, but the magnitude of growth inhibition remained modest.

In contrast, *TP53/PIK3CA* co-mutant models consistently exhibited synergistic interactions across the full range of effective doses (Figure 4-7). This response pattern reinforces our hypothesis: in *TP53/PIK3CA* co-mutant TNBC, alpelisib triggers RTK reactivation, which may be exacerbated in *TP53*-MUT cells due to the loss of p53-mediated regulation (561,738–740), thereby sustaining survival signalling. Crizotinib's multi-RTK blockade disrupts this feedback (178), while its reported p53-degrading activity may further attenuate GOF effects (734,735), restoring apoptotic sensitivity. The generally enhanced response in *TP53/PIK3CA* co-mutant

versus single-mutant cell lines underscores mutational synergy as a determinant of combination benefit.

In *TP53/PIK3CA* co-mutant cells, alternative RTK combinations were mostly antagonistic or ineffective: capmatinib reduced alpelisib's antiproliferative activity, while ceritinib showed slight antagonism. This highlights crizotinib's multi-target advantage in overcoming RTK compensation, which single-target inhibitors cannot achieve.

In *TP53/PIK3CA* co-mutant cells, the alpelisib-crizotinib combination uniquely induced sustained apoptosis, whereas monotherapies were largely cytostatic. Alpelisib showed minimal apoptotic effect, and crizotinib inhibited proliferation without inducing cell death.

RPPA and Western blot analyses confirmed that alpelisib monotherapy in *TP53/PIK3CA* co-mutant cells selectively suppressed PI3K/AKT signalling, including downstream targets such as GSK-3α/β and ULK1 (Ser757), which are associated with inhibition of survival, proliferation, and autophagy pathways (741,742). Reduced MAPK (Thr202/Tyr204) phosphorylation suggested PI3K-MAPK crosstalk (424,743,744), while decreased expression of EZH2, A-Raf, C-Raf, POLG, ERRα, and RRM1 reflected modulation of transcriptional, cell-cycle, and DNA-repair pathways (745–750). Conversely, EMA/MUC1, JNK2, and Tau were upregulated, likely representing compensatory or stress-responsive signalling that could facilitate RTK-mediated feedback and resistance (751–755).

Several proteins downstream of crizotinib targets involved in proliferation, DNA repair, and RTK-mediated signalling, including A-Raf, GSK-3α/β, POLG, and STAT5a, were modestly downregulated, suggesting partial suppression of RTK-driven pathways (746,747,749,756–759). However, p-MET was not reduced and other direct crizotinib targets were not included on the RPPA panel, limiting direct assessment of proximal RTK inhibition; this is consistent with prior work demonstrating that crizotinib does not suppress c-MET phosphorylation in pancreatic cancer cells despite its canonical activity against c-MET/ALK, with target engagement in this context occurring predominantly through ALK inhibition (760).

Notably, proteins associated with stress and compensatory signalling were upregulated, including HER3, EMA, GRB7, and 53BP1. HER3, EMA and GRB7 upregulation has been shown to upregulate or sustain oncogenic RTK expression (751–753,761,762).

A previous study has shown that 53BP1, a key mediator of cellular stress responses (763), can increase in response to crizotinib (764), reflecting activation of mitotic stress pathways (765).

TP53 mutations may impair 53BP1 recruitment, potentially altering the cellular response to mitotic stress (766,767).

The combination of alpelisib and crizotinib in *TP53/PIK3CA* co-mutant cells induced a unique proteomic signature which was distinct from either monotherapy, as evidenced by the Venn diagram analysis (Figure 4-13(a)), which identified 12 proteins exclusively or preferentially dysregulated by the combination. The STRING network analysis (Figure 4-12(c)) revealed high-confidence PPIs between the dysregulated proteins, key components of the PI3K/AKT pathway, and the primary RTK targets of crizotinib, indicating a coordinated, interconnected response to the combination. This supports our hypothesis that these drugs synergistically target compensatory signalling in *TP53/PIK3CA* co-mutant cells.

The enhanced efficacy of the alpelisib-crizotinib combination is best understood at the pathway and functional level.

Enhanced PI3K and MAPK inhibition

The combination of alpelisib and crizotinib effectively suppresses PI3K/AKT and MAPK signalling, disrupting compensatory survival pathways. PTEN, a tumour suppressor that antagonises PI3K/AKT signalling and promotes cell cycle arrest and apoptosis (768), showed a trend toward upregulation with crizotinib alone but reached significance with the combination, reflecting PI3K/AKT pathway inhibition. This may reflect crizotinib-mediated effects on upstream regulatory networks controlling PTEN expression and PI3K/AKT signalling.

4E-BP1, a translational repressor downstream of PI3K/AKT/mTOR (769), showed band-specific modulation (664–666,770). Phosphorylation of 4E-BP1 relieves its inhibition of eIF4E, allowing cap-dependent translation (771). Crizotinib alone increased the hypo-phosphorylated α form, indicating compensatory activation and resistance (772), while the combination reduced the β and γ bands, reflecting synergistic inhibition of translation and reinforcement of apoptotic priming (773). These data raise the possibility that translational control via 4E-BP1 represents a key downstream node contributing to the observed combinatorial effects, integrating PI3K and RTK signalling outputs at the level of protein synthesis. However, further work incorporating direct measures of translational activity and site-specific phosphorylation would help to better define this mechanism.

Single-agent treatments downregulated p-A-Raf and/or p-C-Raf, whereas the combination uniquely decreased p-B-Raf (S445) together with p-A-Raf, indicating a broader suppression of MAPK signalling (746,774). MAPK signalling has previously been reported as a mechanism of resistance to PI3K inhibition (775).

Together, these findings demonstrate that dual PI3K/RTK inhibition by alpelisib and crizotinib co-ordinately blocks PI3K/AKT and MAPK signalling, overcomes compensatory survival mechanisms, and enhances apoptotic susceptibility.

Mitotic stress

p-ATM (S1981) was upregulated, indicating activation of stress response pathways. ATM autophosphorylation at Ser1981 has been reported not only in response to DNA damage but also under conditions of mitotic stress, where it contributes to checkpoint activation and apoptosis (776–778). Notably, 53BP1 was also increased, consistent with the effect observed following crizotinib monotherapy. The study discussed previously, which demonstrated that crizotinib increases 53BP1 expression, also reported concomitant induction of ATM autophosphorylation (764). In our study, p-ATM appeared to be primarily driven by crizotinib but reached statistical significance only in the combination setting, suggesting that dual PI3K and RTK inhibition may amplify mitotic stress signalling beyond that induced by RTK inhibition alone. This increased stress signalling may help explain why apoptosis was observed with the combination but not with either single agent. Although mutant p53 impairs canonical checkpoint control (779,780), ATM has been reported to promote p53-independent apoptosis through CHK2 and related pathways (781,782), suggesting that stress signalling can be activated even in the absence of functional p53. While we observed increased CHK2 protein levels following crizotinib monotherapy, a significant increase was not observed following combination treatment, and future studies should further explore the dynamics of CHK2 activation and its downstream effectors in the context of dual PI3K and RTK inhibition.

PLK1 was also upregulated following the combination, consistent with a compensatory mitotic response. As a key regulator of centrosome maturation, spindle formation, and G2/M transition, PLK1 upregulation likely reflects an adaptive attempt to sustain proliferation under stress (783,784). Prior reports show that PLK1 inhibition enhances alpelisib efficacy (785), suggesting that targeting this compensatory axis could further potentiate apoptosis. Conversely, Cyclin-E1, a G1/S transition driver (786), was significantly downregulated in the combination, implying G1 arrest and reduced proliferative capacity (787).

Together, these changes indicate that dual PI3K/RTK inhibition induces mitotic stress, engaging ATM and compensatory PLK1 signalling, and suppresses cell cycle progression, collectively reinforcing apoptotic priming.

Programmed cell death

PAR was upregulated following alpelisib-crizotinib treatment. Excessive PARP activation generates PAR polymers that translocate to mitochondria, promote apoptosis-inducing factor (AIF) release, and trigger caspase-independent cell death (parthanatos) (788,789). While not the main apoptotic driver, this pathway likely contributes to the enhanced antiproliferative effect observed with the combination treatment.

BCL2, an anti-apoptotic protein, was also upregulated, likely reflecting a compensatory resistance mechanism counteracting increased apoptotic signalling and potentially indicating emerging adaptive survival responses (790).

Cyclophilin-F or cyclophilin-D (CypD), a regulator of the mitochondrial permeability transition pore (791), was uniquely upregulated by the combination, suggesting mitochondrial stress and enhanced apoptotic priming through mPTP opening and cytochrome c release (792). Thus, dual pathway inhibition appears to engage both DNA damage- and mitochondria-mediated apoptosis.

PRMT1, a methyltransferase involved in transcriptional regulation, signal transduction, and DNA damage repair (793), was downregulated by the combination treatment. Reduced PRMT1 expression may compromise DNA repair processes and attenuate oncogenic transcriptional programmes that support tumour cell survival (794,795). In addition, studies suggest that PRMT1 inhibition can promote anti-tumour stress responses, including activation of interferon-associated viral mimicry pathways, and may reduce adaptive mechanisms that contribute to therapeutic resistance. Collectively, these effects could increase cellular susceptibility to apoptosis (796,797). Notably, alpelisib alone partially decreased PRMT1 expression, whereas the combination produced a greater reduction, suggesting that PRMT1 suppression may contribute to the enhanced efficacy observed with combined PI3K/RTK blockade.

PDCD4, a tumour suppressor gene, inhibits tumour promotion, proliferation, invasion, and metastasis, in part through suppression of protein translation and modulation of oncogenic signalling pathways (798–800). PDCD4 expression is frequently reduced in cancer and its loss

has been associated with tumour progression and poor clinical outcomes. Therefore, its upregulation following combination treatment may contribute to the enhanced anti-tumour response by limiting the translation of proteins that support tumour growth and survival, while promoting apoptotic signalling. Given that PDCD4 is negatively regulated by the PI3K/AKT/mTOR pathway, its increased expression is also consistent with effective pathway inhibition by the combination treatment (801).

While alpelisib or crizotinib alone partially inhibit PI3K/AKT and MAPK signalling, they do not trigger apoptosis. Only the combination sufficiently suppresses these pathways, induces mitotic and DNA damage stress, and engages both mitochondrial- and DNA damage-mediated apoptotic pathways, priming cells for programmed cell death.

RTK dysregulation

p-EGFR (Y1173) was upregulated by crizotinib alone at near-significant levels, suggesting a compensatory response to RTK inhibition as previously reported (802). Although this feedback reflects a resistance mechanism, it nonetheless supports that RTKs are being effectively targeted. The upregulation was greater and significant with the alpelisib-crizotinib combination, indicating amplified compensatory signalling under dual PI3K/RTK blockade.

In summary, the alpelisib-crizotinib combination uniquely induces apoptosis in *TP53/PIK3CA* co-mutant TNBC by simultaneously suppressing PI3K/AKT and MAPK signalling, triggering DNA damage and mitotic stress, and engaging both mitochondrial- and DNA damage-mediated apoptotic pathways. This dual inhibition overcomes compensatory survival mechanisms observed with single agents, creating a distinct proteomic and signalling signature that primes cells for programmed cell death and highlights the mechanistic basis for the observed synergy.

6.3.1. Conclusion

Based on our evidence, we propose a mechanistic model (Figure 6-1) in which mutant *PIK3CA* drives constitutive activation of PI3K signalling in *TP53/PIK3CA* co-mutant TNBC cells. Alpelisib inhibits PI3Kα, resulting in suppression of downstream PI3K/AKT signalling; however, this is accompanied by compensatory RTK reactivation, consistent with adaptive feedback mechanisms that limit pathway inhibition (463).

In addition, *TP53* mutation may contribute to this signalling environment not only through loss of WT tumour suppressor function, including regulation of RTKs, but also through reported

GOF activities that can enhance oncogenic signalling pathways, including PI3K/AKT and RTK-associated networks (561,803). Together, these alterations may reinforce survival signalling and increase reliance on compensatory feedback loops following PI3K inhibition.

Crizotinib is proposed to counteract this adaptive response through inhibition of multiple RTKs, thereby reducing compensatory signalling and enhancing suppression of downstream PI3K/AKT and MAPK pathways when combined with alpelisib. Previous studies have also suggested that crizotinib may promote degradation or destabilisation of mutant p53 (734,804); however, this was not directly assessed in the present study and remains speculative.

Collectively, this model integrates mutant *PIK3CA*-driven PI3K activation, *TP53*-associated dysregulation of RTK and PI3K signalling, and adaptive RTK feedback following PI3K inhibition to explain the observed synergistic effect of the combination treatment. Enhanced pathway suppression is consistent with disruption of these interconnected survival networks and increased apoptotic response. These findings provide a proposed framework to explain the observed synergy between alpelisib and crizotinib; however, the mechanisms described remain hypothetical and require further experimental validation, including time-resolved analyses to confirm RTK reactivation dynamics and additional studies to assess the potential role of mutant p53 regulation.

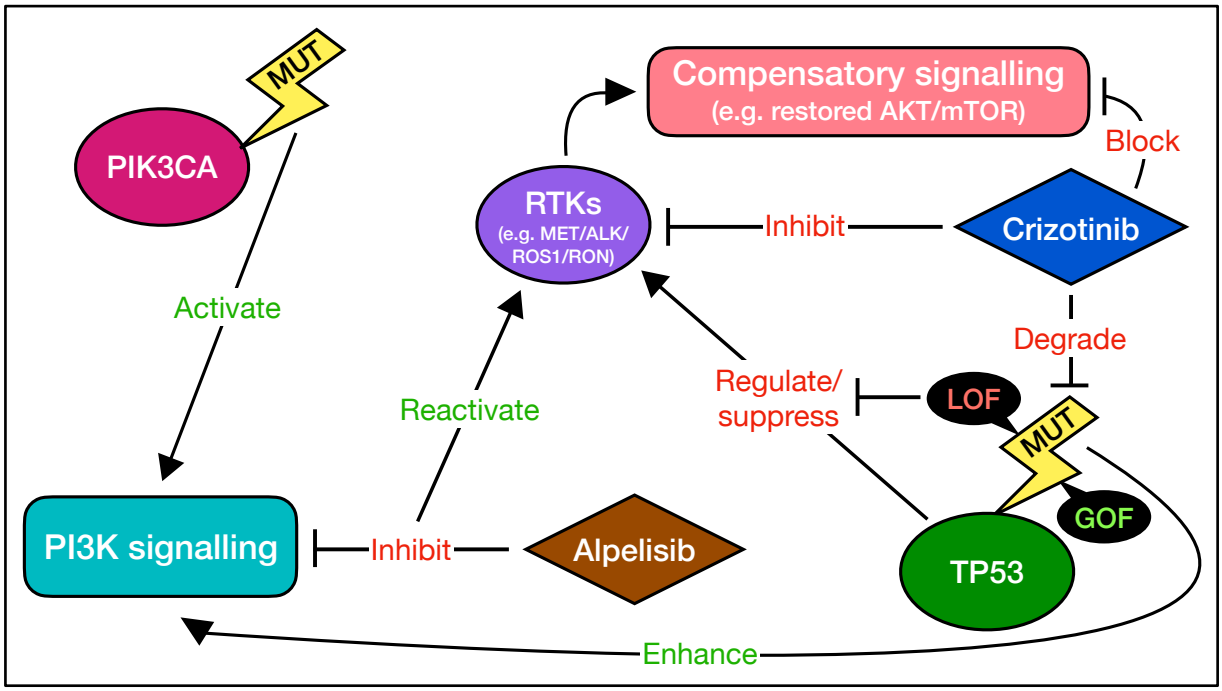


Figure 6-1: Proposed model of alpelisib and crizotinib synergy in *TP53/PIK3CA* co-mutant TNBC. Proposed mechanism of alpelisib-induced PI3K inhibition leading to unchecked RTK reactivation in *TP53/PIK3CA* co-mutant TNBC cells and its mitigation by crizotinib-mediated RTK inhibition and mutant p53 degradation.

6.3.2. Limitations and future work

While this study provides novel insights into the therapeutic implications of *TP53* and *PIK3CA* co-mutations in TNBC, several limitations must be acknowledged to contextualise the findings. These constraints highlight opportunities for future research to validate and extend the proposed mechanisms, particularly through expanded models, direct mechanistic assays, and clinical translation.

First, while the study relied on *in vitro* TNBC cell lines stratified by mutational status, these models lack the complex TME – including immune, stromal, and extracellular matrix interactions – that influence drug response *in vivo* (805,806). Factors such as hypoxia, nutrient gradients, and paracrine signalling may further modulate compensatory RTK activity and resistance in patient tumours (756,178,807). Consequently, clinical translation remains limited by the absence of *in vivo* efficacy and patient-derived data. Although IC_{50} and synergy metrics were benchmarked against clinical C_{max} values, pharmacokinetic parameters (e.g. tissue penetration, metabolism (808)) and toxicities (e.g. alpelisib-induced hyperglycaemia, crizotinib-related hepatotoxicity (809,810)) were not assessed. Future studies should employ PDXs, organoids, or syngeneic models (811,812) to validate the alpelisib-crizotinib synergy under physiologically relevant conditions – an effort already initiated through my Health Products Regulatory Authority (HPRA) application for *in vivo* testing. Retrospective analyses of trials such as EPIK-B3 (which assessed alpelisib in TNBC) (813), incorporating *TP53*/*PIK3CA* co-mutation, could support biomarker-driven patient selection. Moreover, artificial intelligence (AI)-based modelling of genomic, proteomic, and pharmacologic data could help predict drug responses, optimise combination strategies, and identify patient subgroups most likely to benefit from dual PI3K-RTK inhibition – thereby reducing reliance on extensive *in vivo* experimentation (814,815).

Second, the number of cell lines per genotype was limited, restricting generalisability, as each line harbours distinct co-alterations (e.g. *EGFR* amplification in BT-20 and MDA-MB-468, *PTEN* loss in CAL-51 and MDA-MB-468) that may confound mutation-specific effects. The greater alpelisib resistance in *EGFR*-amplified BT-20 and MDA-MB-468 – compared to MFM-223 and HDQ-P1 – suggests *EGFR*-driven bypass signalling as a resistance mechanism (816,817), potentially explaining BT-20's weaker synergy with the alpelisib-crizotinib combination. Expanding the panel to include additional *TP53/PIK3CA* co-mutant models, such as CRISPR-engineered isogenic lines (818) or patient-derived cells with defined *EGFR* status,

would help disentangle the effects of dual mutations and co-alterations. The lack of *TP53/PIK3CA*-WT TNBC cell line models also limits baseline comparisons. Although DU4475 fits this genotype and has been used in prior studies (819), its suspension growth prevented application of the same adherent-based proliferation assays used for our other cell lines. This *TP53/PIK3CA*-WT genotype scarcity reflects the rarity of *TP53*-WT TNBC, as *TP53* mutations occur in ~80% of cases (699).

Third, while RPPA and Western blot analyses yielded valuable proteomic insights, both methods have inherent limitations. RPPA is semi-quantitative and restricted to pre-selected analytes (820), potentially missing relevant resistance mediators (e.g. unassessed crizotinib targets such as ALK or ROS1). Western blots, though confirmatory, covered only a subset of markers and may not reflect temporal signalling dynamics (821). Notably, there is no direct evidence that crizotinib engaged its target RTKs, as p-MET was not downregulated and other targets were absent from the RPPA panel. The observed p-EGFR upregulation and downstream MAPK modulation are indirect and could arise from PI3K inhibition or off-target effects rather than specific RTK blockade (775,822). Likewise, evidence for alpelisib-induced RTK reactivation or crizotinib-mediated mutant p53 degradation remains circumstantial. Future studies should use phosphoproteomic or mass spectrometry-based profiling to capture global RTK and signalling dynamics (823), complemented by targeted validation (e.g. Western blot for p-ALK, p-ROS1) and time-course assays to track compensatory feedback (824,825). For p53 degradation, immunoprecipitation, ubiquitination, or proteasome inhibition assays could provide direct mechanistic confirmation (826).

Fourth, the study assessed only short-term transcriptional and proteomic changes, without examining long-term adaptive responses such as clonal selection or epigenetic reprogramming (827,828). The upregulation of BCL2 and compensatory p-EGFR under combination treatment suggests emerging resistance mechanisms (829,830), consistent with the *EGFR* amplification observed in the *TP53/PIK3CA* co-mutant BT-20 cell line that exhibited reduced synergy. Such feedback may enable bypass signalling and diminish long-term efficacy. Longitudinal studies – such as drug holiday experiments, repeated dosing assays, or single-cell sequencing – are needed to track these adaptive dynamics and guide strategies to prevent relapse (831–833). Future work should directly test *EGFR's* role using EGFR inhibitors (e.g. erlotinib) or siRNA knockdown in *EGFR*-amplified models (834,835). Although EGFR inhibitors demonstrate toxicity in patients due to healthy cell targeting (836,837), lower-dose combinations with alpelisib and crizotinib may help counteract *EGFR*-mediated resistance.

In conclusion, these limitations underscore the preliminary nature of our findings and emphasise the need for rigorous validation. By addressing these through advanced models, direct mechanistic assays, and clinical studies, future work can refine the therapeutic rationale for targeting *TP53/PIK3CA* co-mutant TNBC, potentially leading to personalised combination strategies that improve outcomes in this challenging subtype.

6.4. Modelling mutation-specific therapeutic responses in isogenic cell models

While the preceding analyses support *TP53/PIK3CA* co-mutation as a determinant of reduced sensitivity to PI3K inhibition and identify dual PI3K/RTK blockade as a potential strategy to overcome this resistance, *TP53* mutation itself represents a highly heterogeneous biological entity. *TP53* mutations differ markedly in their effects on protein function, ranging from complete loss of tumour suppressor activity to DN and GOF phenotypes that can differentially influence oncogenic signalling networks (838,839). Consequently, the extent to which individual *TP53* variants influence PI3K pathway dependence and therapeutic response remains incompletely understood.

The rationale for this study arose from previous work demonstrating that interactions between *TP53* and *PIK3CA* alterations can influence PI3K inhibitor response in a mutation-specific manner. In an isogenic MCF10A model, Croessmann et al. generated cell lines harbouring either *PIK3CA* hotspot mutations (E545K or H1047R), *TP53* alterations (R248W knock-in or TP53 knockout), or combinations of these alterations, and evaluated their responses to a panel of targeted therapies. Notably, neither *PIK3CA* mutation alone nor *TP53* alteration alone consistently sensitised cells to the PI3Kα inhibitor alpelisib (BYL719). However, enhanced sensitivity to alpelisib was observed in cells harbouring combined *TP53* alteration and *PIK3CA* E545K mutation, whereas co-alteration with the *PIK3CA* H1047R mutation did not produce the same effect. Specifically, both *TP53* R248W/*PIK3CA* E545K and *TP53* knockout/*PIK3CA* E545K models appeared among the most sensitive to alpelisib relative to parental MCF10A cells, while *TP53* R248W/*PIK3CA* H1047R and *TP53* knockout/*PIK3CA* H1047R models showed no comparable sensitisation (686). These findings suggested that the influence of *TP53* on PI3K inhibitor response is highly dependent on the specific mutational context and raised the possibility that different *TP53* variants may differentially modulate PI3K pathway dependence.

Importantly, these observations contrast with the resistance phenotype observed in *TP53/PIK3CA* co-mutant TNBC cell lines in Chapter 4, highlighting the complexity of *TP53*-PI3K interactions and suggesting that therapeutic responses may depend not only on *TP53* and *PIK3CA* status, but also on the specific *TP53* variant present and the broader cellular context. However, the study examined only a single *TP53* missense mutation (R248W) and one *TP53* LOF model, leaving unresolved whether other clinically relevant *TP53* mutations exert similar or distinct effects on PI3K inhibitor sensitivity. Our study was therefore undertaken to address this knowledge gap by systematically evaluating alpelisib response across a broader panel of *TP53*-altered MCF10A models and by investigating how selected *TP53* variants interact with *PIK3CA* H1047R to influence sensitivity to alpelisib, crizotinib, and their combination.

In *TP53*-altered MCF10A models, mutations generally enhanced alpelisib sensitivity compared to WT controls, supporting our hypothesis from Chapter 4 that *TP53* alterations modulate PI3K inhibitor response. Alpelisib-sensitive mutants (G245S, R273H) displayed distinct baseline gene expression profiles relative to resistant cell lines (p53OE, p53KD) (Figure 5-1). Pathway analysis of the MCF10A models (Figure 5-4) reveals isoform-specific PI3K/AKT "rewiring" (840,841). In alpelisib-sensitive cells *PIK3CD* and *AKT2* are downregulated while *PIK3R3* and *AKT3* are upregulated. *PIK3R3* (p55γ) is a regulatory subunit that can reconfigure which catalytic PI3K complexes are engaged and has been linked to migration and aggressive behaviour in TNBC datasets, supporting its role as an alternative PI3K regulator (55,842). *AKT3*, in turn, has a TNBC-specific role in promoting spheroid growth, stemness and treatment resistance, such that many TNBCs preferentially depend on *AKT3* rather than *AKT1/2* (490,843,844). Mechanistically, loss of *PIK3CD* and *AKT2* may funnel signalling through a p55γ-AKT3 axis, creating a single vulnerable survival pathway. Taken together, (i) the *TP53*-altered MCF10A transcriptional state mirrors key PI3K/AKT features of TNBC (*PIK3R3/AKT3* enrichment), and (ii) the *PIK3R3*-high/*AKT3*-high with *PIK3CD*-low/*AKT2*-low identifies a pattern of potential PI3K dependence, which could support this signature as a baseline predictor of PI3K inhibitor response.

RTKs (e.g. *EGFR*, *MET*, *FGFR3*) were broadly downregulated in alpelisib-sensitive *TP53*-MUT cells. This observation is consistent with previous reports suggesting that baseline RTK expression influences PI3K inhibitor sensitivity. Reduced baseline RTK levels limit alternative signalling routes, heightening dependence on the PI3K/AKT axis and rendering cells vulnerable to alpelisib, whereas resistant cells may retain higher RTK expression to enable

bypass mechanisms under PI3K blockade (845–847). Although literature evidence suggests *TP53* mutations often upregulate RTKs – leading to aberrant activation by relieving p53-mediated suppression –, the mutation-specific downregulation observed here may reflect variant-dependent effects.

Resistant cell lines showed higher expression of basal and stress-associated epithelial programmes, suggesting that alpelisib resistance is linked to a more basal-like, stress-adapted state. In p53KD cells, increased *TP63* - a transcription factor that regulates basal epithelial cell identity and differentiation – alongside elevated basal keratins (*KRT5*, *KRT14*) is consistent with activation of a *TP63*-driven basal programme (848). By contrast, p53OE cells maintained *TP63* and basal keratin levels similar to p53WT, yet both p53KD and p53OE converged on increased stress-associated keratins (*KRT6A/B, KRT16, KRT17*), indicating a shared injury- or stress-like epithelial state (849). This suggests that p53 loss or overexpression disrupts epithelial homeostasis via distinct mechanisms but converge on a common stress-adapted programme. In contrast, alpelisib-sensitive mutants (G245S, R273H) showed lower baseline *TP63* and basal keratin expression than p53WT, indicating reduced basal programme activity. Collectively, p53 mutant cells appear more dependent on PI3K-AKT signalling in a less stress-adapted epithelial state, whereas p53KD and p53OE cells engage robust basal and injury-associated programmes that may protect against pathway inhibition and reduce alpelisib sensitivity.

Interestingly, alpelisib sensitivity in *TP53*-altered MCF10A cells generally paralleled with doxorubicin sensitivity from the Pal *et al*. study (585), with sensitive variants (G245S, R273H) showing enhanced responses to both. We also observed that Crizotinib responses followed a similar trend but the effects were less striking. This similarity indicates that *TP53* variants disrupt common target pathways, i.e. apoptosis, PI3K/AKT, and RTK signalling. Thus, the observed response patterns are not drug-specific but instead reflect the broader impact of *TP53* alterations on common signalling pathways, highlighting how these alterations shape drug sensitivity.

Our expanded MCF10A panel showed that *TP53* mutations modulate alpelisib response in a variant-specific manner (see Figure 5-5): DNA-contact mutants (R248Q, R273C) were generally more sensitive than structural mutants (Y234C, H179R). DNA-contact mutants (e.g. R273H) disrupt DNA binding, causing a loss of normal transcriptional activity. Unlike structural mutants, they maintain their stable shape, allowing them to still interact with

cofactors and signalling partners even though they cannot bind DNA. In contrast, structural mutants (e.g. Y220C) misfold the protein, causing instability and preventing DNA binding. This misfolding broadly impairs protein-protein interactions, and can lead to a complete loss of function (850,851). We propose that DNA-contact mutants, rely heavily on PI3K/AKT signalling for survival. In the absence of canonical p53 transcriptional programmes, PI3K inhibition removes their main survival route. By contrast, structural mutants are misfolded, disrupting many interaction surfaces and activating multiple alternative pathways, reducing dependence on PI3K and making them less sensitive to its inhibition. Further analysis however would be required to validate this hypothesis. In particular, immunoprecipitation of p53MUT proteins followed by mass spectrometry could be used to characterise differences in protein-protein interactions between structural and DNA-contact mutants, providing mechanistic insight into how distinct binding partners may contribute to differential PI3K dependency and alpelisib sensitivity (852).

The structural versus contact classification provides a useful framework but does not fully capture the heterogeneity among structural mutants, which likely arises from mutation-specific effects on folding and functional outcomes. In general, structural mutants disrupting the β-sandwich core or zinc-binding region tend to cause more pronounced destabilisation, including partial or extensive loss of fold (853,854). By contrast, mutants such as G245S induce only moderate destabilisation and local structural changes, leading to more limited disruption of function (850,855). However, these trends are not absolute: for example, the structural mutant R175H, despite significant destabilisation (854), responded to alpelisib similarly to the R273H contact mutant, illustrating allele-specific variation. These observations suggest that the effects of individual *TP53* mutations on protein stability and interaction networks shape variant-specific responses to PI3K inhibition. Collectively, our data show that loss of DNA binding by *TP53* contact mutants reliably sensitises cells to PI3K inhibition, providing a potential biomarker for patient stratification. Conversely, structural mutants exhibit allele-specific responses, highlighting the limitations of broad contact-versus-structural classifications and the need for mutation-specific consideration.

Our findings demonstrate that alpelisib sensitivity in MCF10A cells is highly dependent on the interplay between *TP53* and *PIK3CA* status. Introduction of *PIK3CA*-MUT into *TP53*-MUT cells reduced sensitivity to alpelisib (Figure 5-7). This supports the concept that *TP53* and *PIK3CA* mutations interact to modulate PI3K inhibitor response, consistent with previous

reports indicating that co-occurring mutations can alter cancer cell phenotypes drug sensitivity in a context-dependent manner (237,487,686,696,698). Interestingly, *TP53*-MUT-only TNBC cells exhibited greater resistance to alpelisib compared with *TP53/PIK3CA* co-mutant cells (Figure 4-1), which disagrees with the above finding. This suggests greater PI3K pathway dependence in the MCF10A models, likely due to the absence of additional oncogenic drivers which are present in TNBC. Despite these differences, the data support a functional interplay between *TP53* and *PIK3CA* in mediating resistance to PI3K inhibition.

We must also consider whether *PIK3CA*-MUT or *PIK3CA*-OE results in differential PI3K inhibitor sensitivity. In TNBC models, Hu *et al*. have previously shown that *PIK3CA*-OE led to activation of the PI3K/AKT pathway (indicated by p-AKT expression), but the level of signalling was significantly lower than that observed with activating *PIK3CA*-H1047R (240). Similarly, in endometrial carcinoma, *PIK3CA* amplification increased mRNA and protein levels but produced less PI3K/AKT activation than activating mutations (856). In the MCF10A *TP53*-MUT models *PIK3CA*-OE had minimal impact on alpelisib response, indicating in our model that *PIK3CA*-OE alone is insufficient to drive robust PI3K pathway activation and confer substantial resistance to alpelisib. This is further supported by our findings in Chapter 1 (Table 3-1), where inclusion of *PIK3CA* amplification within the $PI3K^{act}$ definition reduced the observed worse survival effect compared with *PIK3CA*-MUT-only stratification, suggesting that CN-driven *PIK3CA* gains may represent a weaker or less functionally dominant form of PI3K pathway activation in TNBC.

Interestingly, Croessmann *et al*. reported that specific *TP53/PIK3CA* combinations, such as *PIK3CA*-E545K with *TP53*-R248W or *TP53*-knockout, actually sensitised MCF10A cells to alpelisib, whereas knock-in of either alteration alone did not. In contrast, our observations show that MCF10A cells expressing the *TP53/PIK3CA* co-mutation were more resistant. The discrepancy with Croessmann *et al*. likely reflects two factors. First, the specific mutations differed: Croessmann *et al*. observed sensitisation with *PIK3CA*-E545K combined with *TP53*-R248W or *TP53*-knockout, whereas we used *PIK3CA*-H1047R with different *TP53* alterations, which may contribute to the differing drug responses. Second, the methodology differed: they used precise targeted knock-in/knockout MCF10A models, while our lentiviral transduction approach can lead to variable mutation levels and non-physiological expression, potentially altering downstream signalling (686,857,858).

Overall, our findings demonstrate that alpelisib response is shaped by the specific interplay between *TP53* and *PIK3CA* alterations rather than by *PIK3CA* status alone. This emphasises the need to consider co-occurring mutations and cellular context when predicting PI3K inhibitor sensitivity and interpreting clinical efficacy.

TP53 allele-specific effects influenced crizotinib response in MCF10A models (Figure 5-8), whereby the impact of the *PIK3CA* status was linked to the specific *TP53* background. In the DNA-contact mutant (*TP53*-R273C), *PIK3CA*-MUT conferred greater crizotinib resistance than PIK3CA-OE. In contrast, the structural mutant (*TP53*-Y234C) was more crizotinib resistant when expressing *PIK3CA*-OE rather than *PIK3CA*-MUT. In p53OE cells, both *PIK3CA*-OE and -MUT increased resistance relative to *PIK3CA*-WT.

These findings highlight that crizotinib sensitivity is shaped by the interplay of *TP53* allele type, PI3K perturbation, and downstream signalling architecture. Notably, the modest increase in crizotinib sensitivity observed in MCF10A cells expressing different *TP53* mutants (Table 5-1) may reflect mutation-specific effects beyond transcriptional regulation, such as *TP53's* non-transcriptional roles in apoptosis and mitotic stress responses (779). This suggests that integrating mutation-specific context could improve prediction of RTK inhibitor sensitivity across diverse cancer settings.

In TNBC models, we proposed that *TP53/PIK3CA* co-mutations drive compensatory RTK reactivation in response to alpelisib, that can be overcome with dual targeted treatment using PI3K and an RTK inhibitors (Figure 6-1). However, the MCF10A *TP53/PIK3CA* co-mutant cell lines demonstrated reduced single drug sensitivity relative to the p53OE/*PIK3CA*-MUT or p53MUT/*PIK3CA*-WT models (see Figure 5-9). This differential drug sensitivity provides further evidence of the complex interplay between *TP53* and *PIK3CA* mutations in modulating the response to alpelisib and crizotinib.

The combination of alpelisib and crizotinib had a stronger antiproliferative effect in the *TP53/PIK3CA* co-mutant MCF10As relative to either single agent. ED_{50} values could not be calculated for these models due to reduced alpelisib sensitivity upon the introduction of the *PIK3CA*-MUT, meaning it was not possible for Calcusyn to determine CIs and DRIs. This raises the question of whether the combination of drugs can achieve anti-proliferative efficacy at clinically relevant concentrations (i.e. below Cmax).

A notable finding was observed in the structural Y234C p53MUT, which was already resistant to alpelisib. In this background, both *PIK3CA*-MUT and *PIK3CA*-OE reduced sensitivity to crizotinib (Figure 5-8(c)). This suggests that conformational changes in structurally altered p53 (859) cooperate with co-occurring PI3K-AKT activation to sustain downstream survival signalling, thereby reducing the efficacy of crizotinib-mediated RTK inhibition. Importantly, this resistance was largely reversed by combined alpelisib and crizotinib treatment (Figure 5-9(c)), which restored sensitivity to levels comparable with *PIK3CA*-MUT cells. Consequently, dual inhibition is required to bypass this resistance phenotype, suggesting that combining alpelisib and crizotinib can overcome single-agent resistance in structural *TP53* mutants co-harbouring *PIK3CA* alterations. Future studies will be required to determine whether this effect is consistent across other structural *TP53* mutants and to elucidate the precise molecular mechanisms underlying the observed phenotype.

Overall, *PIK3CA*-MUT or -OE consistently attenuated the alpelisib plus crizotinib combination response, with the magnitude and nature of this effect modulated by *TP53* alteration type. Additionally, the lack of other oncogenic drivers and adaptive signalling networks in MCF10A cells, such as constitutive RTK activation and complex feedback loops present in TNBC (860–862), may further impact the response to these targeted drugs and their combination, highlighting the context-dependent nature of *TP53*-*PIK3CA* interactions.

6.4.1. Conclusion

TP53 mutations drive mutation- and allele-specific effects on therapeutic response by reshaping transcriptional programmes, signalling networks, and translational control. DNA-contact mutants are generally PI3K-dependent and sensitive to alpelisib, while structural mutants show heterogeneous responses due to broader pathway rewiring. Co-occurring *TP53* and *PIK3CA* alterations modulate these effects, promoting resistance to PI3K and RTK inhibitors in a *TP53*-mutation dependent manner. Combination therapy can partially overcome *PIK3CA*-driven resistance, but efficacy is context-dependent, highlighting the role of additional oncogenic circuitry. Overall, therapeutic response is determined by the specific interplay of *TP53* and *PIK3CA* mutations, underscoring the need for mutation-informed, context-specific precision strategies.

6.4.2. Limitations and future work

This study provides insights into the mutation-specific effects of *TP53* alterations on therapeutic responses in isogenic models, however, several limitations in methodology and model choice warrant consideration and suggest directions for future research on *TP53*-*PIK3CA* interplay in TNBC.

A primary limitation is the reliance on baseline transcriptomic analysis to infer therapeutic response. While RNA-seq profiling in MCF10A cells identified baseline gene expression differences associated with alpelisib sensitivity, such as dysregulation of epithelial integrity genes and PI3K/AKT components, transcriptomic data capture only steady-state mRNA levels. They do not reflect protein abundance, PTMs, or dynamic pathway activity, all of which are critical for drug response (863–865). For example, *TP53/PIK3CA* co-mutant TNBC tumours showed no significant ($|L2FC| \geq 0.585$; $adj.p \leq 0.05$) PI3K/AKT (i.e. *PIK3CA*, *AKT*) dysregulation transcriptomically relative to *TP53*-only, yet *TP53/PIK3CA* co-mutant TNBC cell lines responded synergistically to dual PI3K/RTK inhibition, highlighting how transcriptomics may overlook functional signalling adaptations.

Another limitation lies in the use of MCF10A cells as a TNBC model. While this non-tumourigenic, basal-like, immortalised mammary epithelial line provides a controlled isogenic background, it lacks the full oncogenic transformation, heterogeneity, and microenvironmental interactions characteristic of TNBC (862,866–869). *TP53/PIK3CA* co-mutant MCF10A cells have previously been shown to display enhanced proliferation and morphologic abnormalities but fail to form tumours *in vivo* (686), in contrast to primary TNBC cell lines that retain tumourigenic potential (870). This discrepancy implies a lack of oncogenic drivers that may have contributed to differences in observed drug synergy between models.

The lentiviral transduction method for introducing *TP53* and *PIK3CA* mutations also has drawbacks. It can produce variable expression levels, non-physiological integration sites, and off-target effects (857,871–873). In our study, PIK3CA protein expression was elevated in most transduced lines, but variability remained, potentially explaining differences in drug sensitivity compared with targeted HRc knock-in/knockout models or more modern CRISPR-Cas9 systems, which better preserve native regulation and allele-specific effects (686,874).

Some of the conclusions drawn are correlative rather than mechanistic. For instance, the suggestion that DNA-contact *TP53* mutants are more alpelisib-sensitive than structural mutants

is based on IC_{50} trends without direct validation. Proposed mechanisms – such as isoform-specific PI3K/AKT rewiring or differential effects of *PIK3CA*-OE versus -MUT – remain speculative without functional assays to measure pathway flux, isoform interactions, or AKT-independent effectors (55,875–877). While the study supports an interplay between *TP53* and *PIK3CA* in modulating drug responses, the precise nature of this interaction remains unresolved.

Future work should address these gaps through mechanistic studies and more physiologically relevant models. To delineate structural versus DNA-contact *TP53* mutant effects, techniques like immunoprecipitation and mass spectrometry could map differential protein-protein interactions (878,879), identifying how contact mutants preserve cofactor binding while structural ones disrupt broader networks. Proteomic and phosphoproteomic profiling could validate pathway activation beyond transcriptomics (880–882). CRISPR-based knock-in models in TNBC-relevant lines or patient-derived organoids could isolate endogenous effects (883,884), complemented by functional assays such as kinase activity measurements or synthetic lethality screens (885,886). *In vivo* models would incorporate TME influences (887), while expanding the *TP53* variant panel and conducting high-throughput drug screens (888) could systematically assess allele-specific vulnerabilities. Integrating multi-omics data with machine learning could ultimately predict mutation-contextual therapeutic sensitivities, guiding precision strategies for *PIK3CA*-mutant TNBC (889,890).

6.5. Final conclusion

In conclusion, *TP53*-PI3K^{act} represents a convergent oncogenic state in TNBC arising from the interaction between *TP53* loss and PI3K pathway activation. This co-altered state defines a distinct, clinically aggressive phenotype characterised by metabolic reprogramming, hypoxia-associated and inflammatory signalling, and a shift towards receptor- and growth factor-driven transcriptional programmes. It is consistently associated with poor outcomes independent of established TNBC subtype classifications, indicating a higher-order layer of tumour biology not captured by current stratification approaches. Functionally, *TP53*-PI3K^{act} tumours show reduced sensitivity to PI3K inhibition, consistent with *TP53* dysfunction and adaptive RTK-mediated compensatory signalling, which together may contribute to therapeutic resistance. However, dual targeting of PI3K and RTKs disrupts these feedback networks, suppresses downstream signalling, and restores apoptotic susceptibility, overcoming resistance in co-mutant contexts. Importantly, therapeutic response is not uniform but is strongly shaped by mutation-specific *TP53* effects and modulated by co-occurring *PIK3CA* alterations, highlighting substantial biological heterogeneity within this subgroup.

Clinically, these findings support *TP53*-PI3K^{act} as a high-risk, targetable TNBC subset that could improve patient stratification beyond current subtype-based frameworks. They also provide a rationale for integrating *TP53* and PI3K pathway status into trial design and for prioritising combined PI3K and RTK inhibition strategies in appropriately selected TNBC patients, with the ultimate goal of improving outcomes in this otherwise poor-prognosis population.

References

1. Brown JS, Amend SR, Austin RH, Gatenby RA, Hammarlund EU, Pienta KJ. Updating the Definition of Cancer. Mol Cancer Res. 2023 Nov 1;21(11):1142–7. doi:10.1158/1541-7786.MCR-23-0411

2. Types of cancer | Cancer Research UK [Internet]. [cited 2025 Dec 29]. Available from: https://cancerresearchuk.org/about-cancer/what-is-cancer/how-cancer-start-grow-spread/types-of-cancer

3. Arnold M, Morgan E, Rumgay H, Mafra A, Singh D, Laversanne M, et al. Current and future burden of breast cancer: Global statistics for 2020 and 2040. Breast. 2022 Dec;66:15–23. doi:10.1016/j.breast.2022.08.010 PubMed PMID: 36084384; PubMed Central PMCID: PMC9465273.

4. Breast Cancer Statistics | How Common Is Breast Cancer? [Internet]. [cited 2025 Dec 29]. Available from: https://www.cancer.org/cancer/types/breast-cancer/about/how-common-is-breast-cancer.html

5. Cancer in Ireland 1994-2022: Annual statistical report of the National Cancer Registry (2024) | National Cancer Registry Ireland [Internet]. 2024 [cited 2025 Dec 29]. Available from: https://www.ncri.ie/en/reports-publications/reports/cancer-in-ireland-1994-2022-annual-statistical-report-of-the-national

6. ResearchGate [Internet]. [cited 2025 Dec 29]. (PDF) The Financial Impact of a Cancer Diagnosis. Available from: https://www.researchgate.net/publication/265121882_The_Financial_Impact_of_a_Cancer_Diagnosis

7. Kitaw TA, Tilahun BD, Zemariam AB, Getie A, Bizuayehu MA, Haile RN. The financial toxicity of cancer: unveiling global burden and risk factors – a systematic review and meta-analysis. BMJ Glob Health. 2025 Feb 10;10(2):e017133. doi:10.1136/bmjgh-2024-017133 PubMed PMID: 39929536; PubMed Central PMCID: PMC11815433.

8. De Silva F, Alcorn J. A Tale of Two Cancers: A Current Concise Overview of Breast and Prostate Cancer. Cancers (Basel). 2022 Jun 15;14(12):2954. doi:10.3390/cancers14122954 PubMed PMID: 35740617; PubMed Central PMCID: PMC9220807.

9. Feng Y, Spezia M, Huang S, Yuan C, Zeng Z, Zhang L, et al. Breast cancer development and progression: Risk factors, cancer stem cells, signaling pathways, genomics, and molecular pathogenesis. Genes & Diseases. 2018 Jun 1;5(2):77–106. doi:10.1016/j.gendis.2018.05.001

10. Metastatic Breast Cancer - Symptoms, Diagnosis & More [Internet]. [cited 2025 Dec 29]. Available from: https://www.breastcancer.org/types/metastatic

11. Piñeiro R. Introduction - Biology of Breast Cancer Metastasis and Importance of the Analysis of CTCs. Adv Exp Med Biol. 2020;1220:1–10. doi:10.1007/978-3-030-35805-1_1 PubMed PMID: 32304076.

12. Park M, Kim D, Ko S, Kim A, Mo K, Yoon H. Breast Cancer Metastasis: Mechanisms and Therapeutic Implications. Int J Mol Sci. 2022 Jun 18;23(12):6806.

doi:10.3390/ijms23126806 PubMed PMID: 35743249; PubMed Central PMCID: PMC9224686.

13. Ginsburg O, Yip CH, Brooks A, Cabanes A, Caleffi M, Dunstan Yataco JA, et al. Breast cancer early detection: A phased approach to implementation. Cancer. 2020 May 15;126 Suppl 10(Suppl 10):2379–93. doi:10.1002/cncr.32887 PubMed PMID: 32348566; PubMed Central PMCID: PMC7237065.

14. Giaquinto AN, Sung H, Miller KD, Kramer JL, Newman LA, Minihan A, et al. Breast Cancer Statistics, 2022. CA: A Cancer Journal for Clinicians. 2022;72(6):524–41. doi:10.3322/caac.21754

15. Siegel RL, Miller KD, Wagle NS, Jemal A. Cancer statistics, 2023. CA Cancer J Clin. 2023 Jan;73(1):17–48. doi:10.3322/caac.21763 PubMed PMID: 36633525.

16. Shao F, Sun H, Deng CX. Potential therapeutic targets of triple-negative breast cancer based on its intrinsic subtype. Oncotarget. 2017 Aug 16;8(42):73329–44. doi:10.18632/oncotarget.20274

17. Luque-Bolivar A, Pérez-Mora E, Villegas VE, Rondón-Lagos M. Resistance and Overcoming Resistance in Breast Cancer. Breast Cancer (Dove Med Press). 2020;12:211–29. doi:10.2147/BCTT.S270799 PubMed PMID: 33204149; PubMed Central PMCID: PMC7666993.

18. Hanahan D, Weinberg RA. The hallmarks of cancer. Cell. 2000 Jan 7;100(1):57–70. doi:10.1016/s0092-8674(00)81683-9 PubMed PMID: 10647931.

19. Hanahan D, Weinberg RA. Hallmarks of Cancer: The Next Generation. Cell. 2011 Mar 4;144(5):646–74. doi:10.1016/j.cell.2011.02.013 PubMed PMID: 21376230.

20. Hanahan D. Hallmarks of Cancer: New Dimensions. Cancer Discov. 2022 Jan;12(1):31–46. doi:10.1158/2159-8290.CD-21-1059 PubMed PMID: 35022204.

21. Feitelson MA, Arzumanyan A, Kulathinal RJ, Blain SW, Holcombe RF, Mahajna J, et al. Sustained proliferation in cancer: Mechanisms and novel therapeutic targets. Seminars in Cancer Biology. 2015 Dec;35:S25–54. doi:10.1016/j.semcancer.2015.02.006

22. Amin ARMR, Karpowicz PA, Carey TE, Arbiser J, Nahta R, Chen ZG, et al. Evasion of anti-growth signaling: A key step in tumorigenesis and potential target for treatment and prophylaxis by natural compounds. Seminars in Cancer Biology. 2015 Dec 1;A broad-spectrum integrative design for cancer prevention and therapy35:S55–77. doi:10.1016/j.semcancer.2015.02.005

23. Mortezaee K. Immune escape: A critical hallmark in solid tumors. Life Sciences. 2020 Oct 1;258:118110. doi:10.1016/j.lfs.2020.118110

24. Yaswen P, MacKenzie KL, Keith WN, Hentosh P, Rodier F, Zhu J, et al. Therapeutic targeting of replicative immortality. Seminars in Cancer Biology. 2015 Dec 1;A broad-spectrum integrative design for cancer prevention and therapy35:S104–28. doi:10.1016/j.semcancer.2015.03.007

25. Guterres AN, Villanueva J. Targeting telomerase for cancer therapy. Oncogene. 2020 Sep;39(36):5811–24. doi:10.1038/s41388-020-01405-w

26. Khusnurrokhman G, Wati FF. Tumor-promoting inflammation in lung cancer: A literature review. Ann Med Surg (Lond). 2022 Jul;79:104022. doi:10.1016/j.amsu.2022.104022 PubMed PMID: 35860063; PubMed Central PMCID: PMC9289429.

27. Greten FR, Grivennikov SI. Inflammation and Cancer: Triggers, Mechanisms, and Consequences. Immunity. 2019 Jul 16;51(1):27–41. doi:10.1016/j.immuni.2019.06.025 PubMed PMID: 31315034; PubMed Central PMCID: PMC6831096.

28. Fares J, Fares MY, Khachfe HH, Salhab HA, Fares Y. Molecular principles of metastasis: a hallmark of cancer revisited. Sig Transduct Target Ther. 2020 Mar 12;5(1):28. doi:10.1038/s41392-020-0134-x

29. Majidpoor J, Mortezaee K. Angiogenesis as a hallmark of solid tumors - clinical perspectives. Cell Oncol (Dordr). 2021 Aug;44(4):715–37. doi:10.1007/s13402-021-00602-3 PubMed PMID: 33835425.

30. Li H, Zimmerman SE, Weyemi U. Genomic instability and metabolism in cancer. Int Rev Cell Mol Biol. 2021;364:241–65. doi:10.1016/bs.ircmb.2021.05.004 PubMed PMID: 34507785.

31. Chen M, Linstra R, van Vugt MATM. Genomic instability, inflammatory signaling and response to cancer immunotherapy. Biochimica et Biophysica Acta (BBA) - Reviews on Cancer. 2022 Jan 1;1877(1):188661. doi:10.1016/j.bbcan.2021.188661

32. Zhu Y, Yang R, Law JH, Khan M, Yip KW, Sun Q. Editorial: Hallmark of cancer: Resisting cell death. Front Oncol. 2022 Nov 7;12. doi:10.3389/fonc.2022.1069947

33. Ravi S, Alencar AM, Arakelyan J, Xu W, Stauber R, Wang CCI, et al. An Update to Hallmarks of Cancer. Cureus. 2022 May;14(5):e24803. doi:10.7759/cureus.24803 PubMed PMID: 35686268; PubMed Central PMCID: PMC9169686.

34. Hartman ML. Non-Apoptotic Cell Death Signaling Pathways in Melanoma. Int J Mol Sci. 2020 Apr 23;21(8):2980. doi:10.3390/ijms21082980 PubMed PMID: 32340261; PubMed Central PMCID: PMC7215321.

35. Adekola K, Rosen ST, Shanmugam M. Glucose transporters in cancer metabolism. Curr Opin Oncol. 2012 Nov;24(6):650–4. doi:10.1097/CCO.0b013e328356da72 PubMed PMID: 22913968; PubMed Central PMCID: PMC6392426.

36. Burkhardt DB, San Juan BP, Lock JG, Krishnaswamy S, Chaffer CL. Mapping Phenotypic Plasticity upon the Cancer Cell State Landscape Using Manifold Learning. Cancer Discov. 2022 Aug 5;12(8):1847–59. doi:10.1158/2159-8290.CD-21-0282

37. Costa PM da S, Sales SLA, Pinheiro DP, Pontes LQ, Maranhão SS, Pessoa C do Ó, et al. Epigenetic reprogramming in cancer: From diagnosis to treatment. Front Cell Dev Biol. 2023 Feb 14;11. doi:10.3389/fcell.2023.1116805

38. Lythgoe MP, Mullish BH, Frampton AE, Krell J. Polymorphic microbes: a new emerging hallmark of cancer. Trends Microbiol. 2022 Dec;30(12):1131–4. doi:10.1016/j.tim.2022.08.004 PubMed PMID: 36058787.

39. Takasugi M, Yoshida Y, Ohtani N. Cellular senescence and the tumour microenvironment. Molecular Oncology. 2022;16(18):3333–51. doi:10.1002/1878-0261.13268

40. Hinck L, Näthke I. Changes in cell and tissue organization in cancer of the breast and colon. Current Opinion in Cell Biology. 2014 Feb;26:87–95. doi:10.1016/j.ceb.2013.11.003

41. Méndez-García LA, Nava-Castro KE, Ochoa-Mercado TDL, Palacios-Arreola MI, Ruiz-Manzano RA, Segovia-Mendoza M, et al. Breast Cancer Metastasis: Are Cytokines Important Players During Its Development and Progression? Journal of Interferon & Cytokine Research. 2019 Jan;39(1):39–55. doi:10.1089/jir.2018.0024

42. Arendt LM, Rudnick JA, Keller PJ, Kuperwasser C. Stroma in breast development and disease. Seminars in Cell & Developmental Biology. 2010 Feb;21(1):11–8. doi:10.1016/j.semcdb.2009.10.003

43. Khan YS, Fakoya AO, Sajjad H. Anatomy, Thorax: Mammary Gland. In: StatPearls [Internet]. Treasure Island (FL): StatPearls Publishing; 2025 [cited 2025 Dec 29]. Available from: http://www.ncbi.nlm.nih.gov/books/NBK547666/ PubMed PMID: 31613446.

44. Atlas of breast cancer early detection [Internet]. [cited 2025 Dec 29]. Available from: https://screening.iarc.fr/atlasbreastdetail.php?Index=005&e=

45. Natale G, Stouthandel MEJ, Van Hoof T, Bocci G. The Lymphatic System in Breast Cancer: Anatomical and Molecular Approaches. Medicina. 2021 Nov 19;57(11):1272. doi:10.3390/medicina57111272

46. Sharma GN, Dave R, Sanadya J, Sharma P, Sharma KK. VARIOUS TYPES AND MANAGEMENT OF BREAST CANCER: AN OVERVIEW. Journal of Advanced Pharmaceutical Technology & Research. 2010 Jun;1(2):109.

47. Kim R, Kawai A, Wakisaka M, Shimoyama M, Yasuda N, Ito M, et al. Outcomes in patients with non-invasive breast carcinoma. Cancer Reports. 2023 Apr;6(4):e1768. doi:10.1002/cnr2.1768

48. Posner MC, Wolmark N. Non-invasive breast carcinoma. Breast Cancer Res Tr. 1992 Oct;21(3):155–64. doi:10.1007/BF01974998

49. Timbres J, Kohut K, Caneppele M, Troy M, Schmidt MK, Roylance R, et al. DCIS and LCIS: Are the Risk Factors for Developing In Situ Breast Cancer Different? Cancers. 2023 Sep 1;15(17). doi:10.3390/cancers15174397

50. Types of Breast Cancer Archives. Breast Cancer Research Foundation [Internet]. [cited 2026 May 23]. Available from: https://www.bcrf.org/about-breast-cancer/types-of-breast-cancer/

51. Shea EKH, Koh VCY, Tan PH. Invasive breast cancer: Current perspectives and emerging views. Pathology International. 2020 May;70(5):242–52. doi:10.1111/pin.12910

52. Makki J. Diversity of Breast Carcinoma: Histological Subtypes and Clinical Relevance. Clin Med Insights Pathol. 2015 Jan;8:CPath.S31563. doi:10.4137/CPath.S31563

53. Invasive Breast Cancer (IDC/ILC) | American Cancer Society [Internet]. [cited 2026 May 23]. Available from: https://www.cancer.org/cancer/types/breast-cancer/about/types-of-breast-cancer/invasive-breast-cancer.html

54. Sakibuzzaman M, Mahmud S, Afroze T, Fathma S, Zakia UB, Afroz S, et al. Pathology of breast cancer metastasis and a view of metastasis to the brain. International Journal of Neuroscience. 2023 May 4;133(5):544–54. doi:10.1080/00207454.2021.1935929

55. He S, Ding L, Yuan H, Zhao G, Yang X, Wu Y. A review of sensors for classification and subtype discrimination of cancer: Insights into circulating tumor cells and tumor-derived extracellular vesicles. Analytica Chimica Acta. 2023 Mar;1244:340703. doi:10.1016/j.aca.2022.340703

56. Siegel RL, Kratzer TB, Giaquinto AN, Sung H, Jemal A. Cancer statistics, 2025. CA A Cancer J Clinicians. 2025 Jan;75(1):10–45. doi:10.3322/caac.21871

57. Breast cancer cases and deaths are projected to rise globally [Internet]. [cited 2026 May 23]. Available from: https://www.iarc.who.int/news-events/breast-cancer-cases-and-deaths-are-projected-to-rise-globally

58. Kim J, Harper A, McCormack V, Sung H, Houssami N, Morgan E, et al. Global patterns and trends in breast cancer incidence and mortality across 185 countries. Nat Med. 2025 Apr;31(4):1154–62. doi:10.1038/s41591-025-03502-3

59. da Costa Vieira RA, Biller G, Uemura G, Ruiz CA, Curado MP. Breast cancer screening in developing countries. Clinics (Sao Paulo). 2017 Apr;72(4):244–53. doi:10.6061/clinics/2017(04)09 PubMed PMID: 28492725; PubMed Central PMCID: PMC5401614.

60. Kamińska M, Ciszewski T, Łopacka-Szatan K, Miotła P, Starosławska E. Breast cancer risk factors. Prz Menopauzalny. 2015 Sep;14(3):196–202. doi:10.5114/pm.2015.54346 PubMed PMID: 26528110; PubMed Central PMCID: PMC4612558.

61. Arthur RS, Dannenberg AJ, Kim M, Rohan TE. The association of body fat composition with risk of breast, endometrial, ovarian and colorectal cancers among normal weight participants in the UK Biobank. Br J Cancer. 2021 Apr 27;124(9):1592–605. doi:10.1038/s41416-020-01210-y

62. Gopinath A, Cheema AH, Chaludiya K, Khalid M, Nwosu M, Agyeman WY, et al. The Impact of Dietary Fat on Breast Cancer Incidence and Survival: A Systematic Review. Cureus. 2022 Oct 6. doi:10.7759/cureus.30003

63. Gonçalves AK, Florêncio GLD, De Atayde Silva MJM, Cobucci RN, Giraldo PC, Cote NM. Effects of Physical Activity on Breast Cancer Prevention: A Systematic Review.

Journal of Physical Activity and Health. 2014 Feb;11(2):445–54. doi:10.1123/jpah.2011-0316

64. Coronado GD, Beasley J, Livaudais J. Alcohol consumption and the risk of breast cancer. Salud Publica Mex. 2011;53(5):440–7. PubMed PMID: 22218798.

65. Scala M, Bosetti C, Bagnardi V, Possenti I, Specchia C, Gallus S, et al. Dose-response Relationships Between Cigarette Smoking and Breast Cancer Risk: A Systematic Review and Meta-analysis. Journal of Epidemiology. 2023 Dec 5;33(12):640–8. doi:10.2188/jea.JE20220206

66. Travis RC, Key TJ. Oestrogen exposure and breast cancer risk. Breast Cancer Res. 2003 Oct;5(5):239. doi:10.1186/bcr628

67. Does the contraceptive pill increase risk of cancer? | Cancer Research UK [Internet]. [cited 2025 Dec 29]. Available from: https://cancerresearchuk.org/about-cancer/causes-of-cancer/hormones-and-cancer/does-the-contraceptive-pill-increase-cancer-risk

68. Burchardt NA, Eliassen AH, Shafrir AL, Rosner B, Tamimi RM, Kaaks R, et al. Oral contraceptive use by formulation and breast cancer risk by subtype in the Nurses' Health Study II: a prospective cohort study. Am J Obstet Gynecol. 2022 Jun;226(6):821.e1-821.e26. doi:10.1016/j.ajog.2021.12.022 PubMed PMID: 34921803.

69. Nasrazadani A, Marti JLG, Kip KE, Marroquin OC, Lemon L, Shapiro SD, et al. Breast cancer mortality as a function of age. Aging. 2022 Feb 15;14(3):1186–99. doi:10.18632/aging.203881

70. Anderson WF, Jatoi I, Tse J, Rosenberg PS. Male Breast Cancer: A Population-Based Comparison With Female Breast Cancer. JCO. 2010 Jan 10;28(2):232–9. doi:10.1200/JCO.2009.23.8162

71. Tian JM, Ran B, Zhang CL, Yan DM, Li XH. Estrogen and progesterone promote breast cancer cell proliferation by inducing cyclin G1 expression. Braz J Med Biol Res. 2018;51(3):e5612. doi:10.1590/1414-431x20175612

72. Arthur RS, Wang T, Xue X, Kamensky V, Rohan TE. Genetic Factors, Adherence to Healthy Lifestyle Behavior, and Risk of Invasive Breast Cancer Among Women in the UK Biobank. JNCI: Journal of the National Cancer Institute. 2020 Sep 1;112(9):893–901. doi:10.1093/jnci/djz241

73. Narod SA, Tung N, Lubinski J, Huzarski T, Robson M, Lynch HT, et al. A Prior Diagnosis of Breast Cancer is a Risk Factor for Breast Cancer in Brca1 and Brca2 Carriers. Current Oncology. 2014 Apr 1;21(2):64–8. doi:10.3747/co.21.1656

74. Yedjou CG, Sims JN, Miele L, Noubissi F, Lowe L, Fonseca DD, et al. Health and Racial Disparity in Breast Cancer. In: Ahmad A, editor. Breast Cancer Metastasis and Drug Resistance [Internet]. Cham: Springer International Publishing; 2019 [cited 2025 Dec 29]. p. 31–49. (Advances in Experimental Medicine and Biology). Available from: http://link.springer.com/10.1007/978-3-030-20301-6_3 doi:10.1007/978-3-030-20301-6_3

75. Moskowitz CS, Chou JF, Wolden SL, Bernstein JL, Malhotra J, Novetsky Friedman D, et al. Breast Cancer After Chest Radiation Therapy for Childhood Cancer. JCO. 2014 Jul 20;32(21):2217–23. doi:10.1200/JCO.2013.54.4601

76. Hartmann LC, Degnim AC, Santen RJ, Dupont WD, Ghosh K. Atypical Hyperplasia of the Breast — Risk Assessment and Management Options. N Engl J Med. 2015 Jan 1;372(1):78–89. doi:10.1056/NEJMsr1407164

77. Dall GV, Britt KL. Estrogen Effects on the Mammary Gland in Early and Late Life and Breast Cancer Risk. Front Oncol. 2017;7:110. doi:10.3389/fonc.2017.00110 PubMed PMID: 28603694; PubMed Central PMCID: PMC5445118.

78. Yedjou CG, Sims JN, Miele L, Noubissi F, Lowe L, Fonseca DD, et al. Health and Racial Disparity in Breast Cancer. Adv Exp Med Biol. 2019;1152:31–49. doi:10.1007/978-3-030-20301-6_3 PubMed PMID: 31456178; PubMed Central PMCID: PMC6941147.

79. Malhotra GK, Zhao X, Band H, Band V. Histological, molecular and functional subtypes of breast cancers. Cancer Biology & Therapy. 2010 Nov 15;10(10):955–60. doi:10.4161/cbt.10.10.13879

80. Pescia C, Guerini-Rocco E, Viale G, Fusco N. Advances in Early Breast Cancer Risk Profiling: From Histopathology to Molecular Technologies. Cancers. 2023 Nov 15;15(22):5430. doi:10.3390/cancers15225430

81. Fragomeni SM, Sciallis A, Jeruss JS. Molecular Subtypes and Local-Regional Control of Breast Cancer. Surgical Oncology Clinics of North America. 2018 Jan;27(1):95–120. doi:10.1016/j.soc.2017.08.005

82. Kensler KH, Sankar VN, Wang J, Zhang X, Rubadue CA, Baker GM, et al. PAM50 Molecular Intrinsic Subtypes in the Nurses' Health Study Cohorts. Cancer Epidemiol Biomarkers Prev. 2019 Apr;28(4):798–806. doi:10.1158/1055-9965.EPI-18-0863 PubMed PMID: 30591591; PubMed Central PMCID: PMC6449178.

83. Dix-Peek T, Phakathi BP, Van Den Berg EJ, Dickens C, Augustine TN, Cubasch H, et al. Discordance between PAM50 intrinsic subtyping and immunohistochemistry in South African women with breast cancer. Breast Cancer Res Treat. 2023 May;199(1):1–12. doi:10.1007/s10549-023-06886-3

84. Dai X, Li T, Bai Z, Yang Y, Liu X, Zhan J, et al. Breast cancer intrinsic subtype classification, clinical use and future trends. Am J Cancer Res. 2015 Sep 15;5(10):2929–43. PubMed PMID: 26693050; PubMed Central PMCID: PMC4656721.

85. Orrantia-Borunda E, Anchondo-Nuñez P, Acuña-Aguilar LE, Gómez-Valles FO, Ramírez-Valdespino CA. Subtypes of Breast Cancer. In: Mayrovitz HN, editor. Breast Cancer [Internet]. Brisbane (AU): Exon Publications; 2022 [cited 2026 May 23]. Available from: http://www.ncbi.nlm.nih.gov/books/NBK583808/ PubMed PMID: 36122153.

86. Swain SM, Shastry M, Hamilton E. Targeting HER2-positive breast cancer: advances and future directions. Nat Rev Drug Discov. 2023 Feb;22(2):101–26. doi:10.1038/s41573-022-00579-0

87. Female Breast Cancer Subtypes — Cancer Stat Facts [Internet]. [cited 2026 May 23]. Available from: https://seer.cancer.gov/statfacts/html/breast-subtypes.html

88. Impact of breast cancer subtypes on prognosis of women with operable invasive breast cancer: a population-based study using SEER database | Clinical Cancer Research | American Association for Cancer Research [Internet]. [cited 2025 Dec 29]. Available from: https://aacrjournals.org/clincancerres/article/doi/10.1158/1078-0432.CCR-18-2782/74282/am/Impact-of-breast-cancer-subtypes-on-prognosis-of

89. Anderson DH. Luminal A breast cancer resistance mechanisms and emerging treatments. In: Biological Mechanisms and the Advancing Approaches to Overcoming Cancer Drug Resistance [Internet]. Elsevier; 2021 [cited 2025 Dec 29]. p. 1–22. Available from: https://linkinghub.elsevier.com/retrieve/pii/B9780128213100000103 doi:10.1016/B978-0-12-821310-0.00010-3

90. Guliyev M, Güren AK, Özge E, Çolak R, Majidova N, Alkan Şen G, et al. The Impact of Progesterone Receptor Status on Survival Outcomes in Metastatic Breast Cancer Patients Treated with First-Line CDK4/6 Inhibitors. Cancers. 2025 Feb 18;17(4):693. doi:10.3390/cancers17040693

91. Nishimukai A, Yagi T, Yanai A, Miyagawa Y, Enomoto Y, Murase K, et al. High Ki-67 Expression and Low Progesterone Receptor Expression Could Independently Lead to a Worse Prognosis for Postmenopausal Patients With Estrogen Receptor-Positive and HER2-Negative Breast Cancer. Clinical Breast Cancer. 2015 Jun;15(3):204–11. doi:10.1016/j.clbc.2014.12.007

92. Li Y, Ma L. Efficacy of chemotherapy for lymph node-positive luminal A subtype breast cancer patients: an updated meta-analysis. World J Surg Onc. 2020 Dec 2;18(1):316. doi:10.1186/s12957-020-02089-y

93. Tran B, Bedard PL. Luminal-B breast cancer and novel therapeutic targets. Breast Cancer Res. 2011 Nov 30;13(6):221. doi:10.1186/bcr2904

94. McGuire A, Kalinina O, Holian E, Curran C, Malone CA, McLaughlin R, et al. Differential impact of hormone receptor status on survival and recurrence for HER2 receptor-positive breast cancers treated with Trastuzumab. Breast Cancer Res Treat. 2017 Jul;164(1):221–9. doi:10.1007/s10549-017-4225-5

95. Martínez-Sáez O, Prat A. Current and Future Management of HER2-Positive Metastatic Breast Cancer. JCO Oncology Practice. 2021 Oct;17(10):594–604. doi:10.1200/OP.21.00172

96. Almansour NM. Triple-Negative Breast Cancer: A Brief Review About Epidemiology, Risk Factors, Signaling Pathways, Treatment and Role of Artificial Intelligence. Front Mol Biosci. 2022 Jan 25;9. doi:10.3389/fmolb.2022.836417

97. Giaquinto AN, Sung H, Newman LA, Freedman RA, Smith RA, Star J, et al. Breast cancer statistics 2024. CA A Cancer J Clinicians. 2024 Nov;74(6):477–95. doi:10.3322/caac.21863

98. Yin L, Duan JJ, Bian XW, Yu S cang. Triple-negative breast cancer molecular subtyping and treatment progress. Breast Cancer Res. 2020 Dec;22(1):61. doi:10.1186/s13058-020-01296-5

99. Pogoda K, Niwińska A, Sarnowska E, Nowakowska D, Jagiełło-Gruszfeld A, Siedlecki J, et al. Effects of *BRCA* Germline Mutations on Triple-Negative Breast Cancer Prognosis. Journal of Oncology. 2020 Jan 27;2020:1–10. doi:10.1155/2020/8545643

100. Akshata Desai KA. Triple Negative Breast Cancer – An Overview. Hereditary Genetics. 2012. doi:10.4172/2161-1041.S2-001

101. Park WK, Chung SY, Jung YJ, Ha C, Kim JW, Nam SJ, et al. Long-term oncologic outcomes of unselected triple-negative breast cancer patients according to BRCA1/2 mutations. npj Precis Onc. 2024 Apr 30;8(1):96. doi:10.1038/s41698-024-00559-0

102. Da Silva JL, Cardoso Nunes NC, Izetti P, De Mesquita GG, De Melo AC. Triple negative breast cancer: A thorough review of biomarkers. Critical Reviews in Oncology/Hematology. 2020 Jan;145:102855. doi:10.1016/j.critrevonc.2019.102855

103. Marra A, Trapani D, Viale G, Criscitiello C, Curigliano G. Practical classification of triple-negative breast cancer: intratumoral heterogeneity, mechanisms of drug resistance, and novel therapies. npj Breast Cancer. 2020 Oct 16;6(1):54. doi:10.1038/s41523-020-00197-2

104. Lehmann BD, Bauer JA, Chen X, Sanders ME, Chakravarthy AB, Shyr Y, et al. Identification of human triple-negative breast cancer subtypes and preclinical models for selection of targeted therapies. J Clin Invest. 2011 Jul;121(7):2750–67. doi:10.1172/JCI45014 PubMed PMID: 21633166; PubMed Central PMCID: PMC3127435.

105. Santonja A, Sánchez-Muñoz A, Lluch A, Chica-Parrado MR, Albanell J, Chacón JI, et al. Triple negative breast cancer subtypes and pathologic complete response rate to neoadjuvant chemotherapy. Oncotarget. 2018 May 29;9(41):26406–16. doi:10.18632/oncotarget.25413

106. Wang T, Heng YJ, Baker GM, Bret-Mounet VC, Quintana LM, Frueh L, et al. Loss of PTEN Expression, *PIK3CA* Mutations, and Breast Cancer Survival in the Nurses' Health Studies. Cancer Epidemiology, Biomarkers & Prevention. 2022 Oct 4;31(10):1926–34. doi:10.1158/1055-9965.EPI-22-0672

107. Prvanović M, Nedeljković M, Tanić N, Tomić T, Terzić T, Milovanović Z, et al. Role of PTEN, PI3K, and mTOR in Triple-Negative Breast Cancer. Life. 2021 Nov 16;11(11). doi:10.3390/life11111247

108. Sporikova Z, Koudelakova V, Trojanec R, Hajduch M. Genetic Markers in Triple-Negative Breast Cancer. Clinical Breast Cancer. 2018 Oct;18(5):e841–50. doi:10.1016/j.clbc.2018.07.023

109. Pascual J, Turner NC. Targeting the PI3-kinase pathway in triple-negative breast cancer. Annals of Oncology. 2019 Jul 1;30(7):1051–60. doi:10.1093/annonc/mdz133 PubMed PMID: 31050709.

110. Massihnia D, Galvano A, Fanale D, Perez A, Castiglia M, Incorvaia L, et al. Triple negative breast cancer: shedding light onto the role of pi3k/akt/mtor pathway. Oncotarget. 2016 Sep 13;7(37):60712–22. doi:10.18632/oncotarget.10858

111. Chan JJ, Tan TJY, Dent RA. Novel therapeutic avenues in triple-negative breast cancer: PI3K/AKT inhibition, androgen receptor blockade, and beyond. Ther Adv Med Oncol. 2019 Jan;11:1758835919880429. doi:10.1177/1758835919880429

112. Dewi C, Fristiohady A, Amalia R, Khairul Ikram NK, Ibrahim S, Muchtaridi M. Signaling Pathways and Natural Compounds in Triple-Negative Breast Cancer Cell Line. Molecules. 2022 Jun 7;27(12):3661. doi:10.3390/molecules27123661

113. Haque M, Shyanti RK, Mishra MK. Targeted therapy approaches for epithelial-mesenchymal transition in triple negative breast cancer. Front Oncol. 2024 Oct 10;14:1431418. doi:10.3389/fonc.2024.1431418

114. Emara HM, Allam NK, Youness RA. A comprehensive review on targeted therapies for triple negative breast cancer: an evidence-based treatment guideline. Discov Onc. 2025 Apr 17;16(1):547. doi:10.1007/s12672-025-02227-6

115. Limsakul P, Choochuen P, Jungrungrueang T, Charupanit K, Limsakul P, Choochuen P, et al. Prognostic Markers in Tyrosine Kinases Specific to Basal-like 2 Subtype of Triple-Negative Breast Cancer. International Journal of Molecular Sciences. 2024 Jan 23;25(3). doi:10.3390/ijms25031405

116. Chen Z, Liu Y, Lyu M, Chan CH, Sun M, Yang X, et al. Classifications of triple-negative breast cancer: insights and current therapeutic approaches. Cell Biosci. 2025 Feb 1;15(1):13. doi:10.1186/s13578-025-01359-0

117. Burstein MD, Tsimelzon A, Poage GM, Covington KR, Contreras A, Fuqua SAW, et al. Comprehensive Genomic Analysis Identifies Novel Subtypes and Targets of Triple-Negative Breast Cancer. Clinical Cancer Research. 2015 Apr 1;21(7):1688–98. doi:10.1158/1078-0432.CCR-14-0432

118. Jiang YZ, Ma D, Suo C, Shi J, Xue M, Hu X, et al. Genomic and Transcriptomic Landscape of Triple-Negative Breast Cancers: Subtypes and Treatment Strategies. Cancer Cell. 2019 Mar;35(3):428-440.e5. doi:10.1016/j.ccell.2019.02.001

119. Liu YR, Jiang YZ, Xu XE, Yu KD, Jin X, Hu X, et al. Comprehensive transcriptome analysis identifies novel molecular subtypes and subtype-specific RNAs of triple-negative breast cancer. Breast Cancer Res. 2016 Dec;18(1):33. doi:10.1186/s13058-016-0690-8

120. Lee YM, Oh MH, Go JH, Han K, Choi SY. Molecular subtypes of triple-negative breast cancer: understanding of subtype categories and clinical implication. Genes Genom. 2020 Dec;42(12):1381–7. doi:10.1007/s13258-020-01014-7

121. Cocco S, Piezzo M, Calabrese A, Cianniello D, Caputo R, Di Lauro V, et al. Biomarkers in Triple-Negative Breast Cancer: State-of-the-Art and Future Perspectives. IJMS. 2020 Jun 27;21(13):4579. doi:10.3390/ijms21134579

122. Ganatra H, Tan JK, Simmons A, Bigogno CM, Khurana V, Ghose A, et al. Applying whole-genome and whole-exome sequencing in breast cancer: a review of the landscape. Breast Cancer. 2024 Nov;31(6):999–1009. doi:10.1007/s12282-024-01628-9

123. Di Cosimo S, Appierto V, Silvestri M, Pruneri G, Vingiani A, Perrone F, et al. Targeted-Gene Sequencing to Catch Triple Negative Breast Cancer Heterogeneity before and after Neoadjuvant Chemotherapy. Cancers. 2019 Nov 8;11(11):1753. doi:10.3390/cancers11111753

124. Vora H, Desai M, Patel G, Patel N, Patel P. Comparative genomic hybridisation and transcriptome microarray analysis in triple negative breast cancer: An INDIAN study. Advances in Cancer Biology - Metastasis. 2023 Dec;9:100109. doi:10.1016/j.adcanc.2023.100109

125. Fei H, Chen S, Xu C. RNA-sequencing and microarray data mining revealing: the aberrantly expressed mRNAs were related with a poor outcome in the triple negative breast cancer patients. Ann Transl Med. 2020 Mar;8(6):363–363. doi:10.21037/atm.2020.02.51

126. Shome R, Sen P, Sarkar S, Ghosh SS. Single-cell transcriptomics reveals the intra-tumoral heterogeneity and SQSTM1/P62 and Wnt/β-catenin mediated epithelial to mesenchymal transition and stemness of triple-negative breast cancer. Experimental Cell Research. 2024 May;438(1):114032. doi:10.1016/j.yexcr.2024.114032

127. Wang N, Zhu Y, Wang L, Dai W, Hu T, Song Z, et al. Parallel Analyses by Mass Spectrometry (MS) and Reverse Phase Protein Array (RPPA) Reveal Complementary Proteomic Profiles in Triple-Negative Breast Cancer (TNBC) Patient Tissues and Cell Cultures. Proteomics. 2025 Feb;25(4):e202400107. doi:10.1002/pmic.202400107 PubMed PMID: 39548956.

128. Yadav BS. Biomarkers in triple negative breast cancer: A review. WJCO. 2015;6(6):252. doi:10.5306/wjco.v6.i6.252

129. Aine M, Nacer DF, Arbajian E, Veerla S, Karlsson A, Häkkinen J, et al. The DNA methylation landscape of primary triple-negative breast cancer. Nat Commun. 2025 Mar 28;16(1):3041. doi:10.1038/s41467-025-58158-x

130. Yan G, Dai M, Poulet S, Wang N, Boudreault J, Daliah G, et al. Combined in vitro/in vivo genome-wide CRISPR screens in triple negative breast cancer identify cancer stemness regulators in paclitaxel resistance. Oncogenesis. 2023 Nov 6;12(1):51. doi:10.1038/s41389-023-00497-9

131. Xie G, Yang H, Ma D, Sun Y, Chen H, Hu X, et al. Integration of whole-genome sequencing and functional screening identifies a prognostic signature for lung metastasis in triple-negative breast cancer. Int J Cancer. 2019 Nov 15;145(10):2850–60. doi:10.1002/ijc.32329 PubMed PMID: 30977117.

132. He X, Gu J, Zou D, Yang H, Zhang Y, Ding Y, et al. NMR-Based Metabolomics Analysis Predicts Response to Neoadjuvant Chemotherapy for Triple-Negative Breast Cancer. Front Mol Biosci. 2021 Nov 2;8:708052. doi:10.3389/fmolb.2021.708052

133. Huang X, Ali A, Yachioui DEI, Le Dévédec SE, Hankemeier T. Lipid dysregulation in triple negative breast cancer: Insights from mass spectrometry-based approaches. Progress in Lipid Research. 2025 Apr;98:101330. doi:10.1016/j.plipres.2025.101330

134. Wang G, Yao Y, Huang H, Zhou J, Ni C. Multiomics technologies for comprehensive tumor microenvironment analysis in triple-negative breast cancer under neoadjuvant chemotherapy. Front Oncol. 2023 May 22;13:1131259. doi:10.3389/fonc.2023.1131259

135. Zhang F, Li H, Lin X, Zhu X, Chen X, Wang B, et al. In vivo flow cytometry reveals an anti-metastatic effect of Rujifang in triple-negative breast cancer. Cytometry A. 2023 Sep;103(9):723–31. doi:10.1002/cyto.a.24768 PubMed PMID: 37276218.

136. Wang X, Venet D, Lifrange F, Larsimont D, Rediti M, Stenbeck L, et al. Spatial transcriptomics reveals substantial heterogeneity in triple-negative breast cancer with potential clinical implications. Nat Commun. 2024 Nov 26;15(1):10232. doi:10.1038/s41467-024-54145-w

137. Lin L, Li H, Wang X, Wang Z, Su G, Zhou J, et al. Components of the tumor immune microenvironment based on m-IHC correlate with prognosis and subtype of triple-negative breast cancer. Cancer Med. 2023 Dec;12(24):21639–50. doi:10.1002/cam4.6718 PubMed PMID: 38059408; PubMed Central PMCID: PMC10757132.

138. Yi Y, Zhong Y, Xie L, Lu S, Zhang Y. The analysis of gene co-expression network and immune infiltration revealed biomarkers between triple-negative and non-triple negative breast cancer. Front Genet. 2025 Jan 6;15:1505011. doi:10.3389/fgene.2024.1505011

139. Cai Y, Li Y, Wang W, Zhou Y, Wang J, Zhang L, et al. A Machine-Learning Model for the Prediction of Triple-Negative Breast Cancer Based on Multiparameter MRI. BCTT. 2025 Jul;Volume 17:611–25. doi:10.2147/BCTT.S513779

140. Li L, Huang H, Zhu M, Wu J. Identification of Hub Genes and Pathways of Triple Negative Breast Cancer by Expression Profiles Analysis. CMAR. 2021 Mar;Volume 13:2095–104. doi:10.2147/CMAR.S295951

141. Schmid P, Cortes J, Dent R, McArthur H, Pusztai L, Kümmel S, et al. Overall Survival with Pembrolizumab in Early-Stage Triple-Negative Breast Cancer. N Engl J Med. 2024 Nov 28;391(21):1981–91. doi:10.1056/NEJMoa2409932

142. Bittman-Soto XS, Thomas ES, Ganshert ME, Mendez-Santacruz LL, Harrell JC. The Transformative Role of 3D Culture Models in Triple-Negative Breast Cancer Research. Cancers. 2024 May 13;16(10):1859. doi:10.3390/cancers16101859

143. Guillen KP, Fujita M, Butterfield AJ, Scherer SD, Bailey MH, Chu Z, et al. A human breast cancer-derived xenograft and organoid platform for drug discovery and precision oncology. Nat Cancer. 2022 Feb 24;3(2):232–50. doi:10.1038/s43018-022-00337-6

144. Mazzeo R, Sears J, Palmero L, Bolzonello S, Davis AA, Gerratana L, et al. Liquid biopsy in triple-negative breast cancer: unlocking the potential of precision oncology. ESMO Open. 2024 Oct;9(10):103700. doi:10.1016/j.esmoop.2024.103700

145. Cui S, Liu W, Wang W, Miao K, Guan X. Advances in the diagnosis and prognosis of minimal residual lesions of breast cancer. Pathology - Research and Practice. 2023 May;245:154428. doi:10.1016/j.prp.2023.154428

146. Pastena P, Perera H, Martinino A, Kartsonis W, Giovinazzo F. Unraveling Biomarker Signatures in Triple-Negative Breast Cancer: A Systematic Review for Targeted Approaches. IJMS. 2024 Feb 22;25(5):2559. doi:10.3390/ijms25052559

147. Sajjad F, Jalal A, Jalal A, Gul Z, Mubeen H, Rizvi SZ, et al. Multi-omic analysis of dysregulated pathways in triple negative breast cancer. Asia Pac J Clin Oncol. 2024 Jun 20. doi:10.1111/ajco.14095 PubMed PMID: 38899578.

148. El Hejjioui B, Lamrabet S, Amrani Joutei S, Senhaji N, Bouhafa T, Malhouf MA, et al. New Biomarkers and Treatment Advances in Triple-Negative Breast Cancer. Diagnostics. 2023 Jun 2;13(11):1949. doi:10.3390/diagnostics13111949

149. Ma L, Liang Z, Zhou H, Qu L. Applications of RNA Indexes for Precision Oncology in Breast Cancer. Genomics, Proteomics & Bioinformatics. 2018 Apr 1;16(2):108–19. doi:10.1016/j.gpb.2018.03.002

150. Vasseur D, Arbab A, Giudici F, Marzac C, Michiels S, Tagliamento M, et al. Genomic landscape of liquid biopsy mutations in TP53 and DNA damage genes in cancer patients. npj Precis Onc. 2024 Feb 26;8(1):51. doi:10.1038/s41698-024-00544-7

151. Zong B, Sun L, Peng Y, Wang Y, Yu Y, Lei J, et al. HORMAD1 promotes docetaxel resistance in triple negative breast cancer by enhancing DNA damage tolerance. Oncol Rep. 2021 May 21;46(1):138. doi:10.3892/or.2021.8089

152. Wee P, Wang Z. Epidermal Growth Factor Receptor Cell Proliferation Signaling Pathways. Cancers. 2017 May 17;9(5):52. doi:10.3390/cancers9050052

153. Shetty SR, Kar T, Das A. Epidermal growth factor receptor mutations in breast Cancer: Therapeutic challenges and way forward. Bioorganic Chemistry. 2025 Jan;154:108037. doi:10.1016/j.bioorg.2024.108037

154. Ogden A, Bhattarai S, Sahoo B, Mongan NP, Alsaleem M, Green AR, et al. Combined HER3-EGFR score in triple-negative breast cancer provides prognostic and predictive significance superior to individual biomarkers. Sci Rep. 2020 Feb 20;10(1):3009. doi:10.1038/s41598-020-59514-1

155. Park HS, Jang MH, Kim EJ, Kim HJ, Lee HJ, Kim YJ, et al. High EGFR gene copy number predicts poor outcome in triple-negative breast cancer. Modern Pathology. 2014 Sep;27(9):1212–22. doi:10.1038/modpathol.2013.251

156. Secq V, Villeret J, Fina F, Carmassi M, Carcopino X, Garcia S, et al. Triple negative breast carcinoma EGFR amplification is not associated with EGFR, Kras or ALK mutations. Br J Cancer. 2014 Feb;110(4):1045–52. doi:10.1038/bjc.2013.794

157. You KS, Yi YW, Cho J, Park JS, Seong YS. Potentiating Therapeutic Effects of Epidermal Growth Factor Receptor Inhibition in Triple-Negative Breast Cancer. Pharmaceuticals. 2021 Jun 18;14(6):589. doi:10.3390/ph14060589

158. Ribatti D, Nico B, Ruggieri S, Tamma R, Simone G, Mangia A. Angiogenesis and Antiangiogenesis in Triple-Negative Breast cancer. Translational Oncology. 2016 Oct;9(5):453–7. doi:10.1016/j.tranon.2016.07.002

159. Nilsson M, Heymach JV. Vascular Endothelial Growth Factor (VEGF) Pathway. Journal of Thoracic Oncology. 2006 Oct;1(8):768–70. doi:10.1016/S1556-0864(15)30404-4

160. Sukumar J, Gast K, Quiroga D, Lustberg M, Williams N. Triple-negative breast cancer: promising prognostic biomarkers currently in development. Expert Review of Anticancer Therapy. 2021 Feb 1;21(2):135–48. doi:10.1080/14737140.2021.1840984

161. Bell R, Brown J, Parmar M, Toi M, Suter T, Steger GG, et al. Final efficacy and updated safety results of the randomized phase III BEATRICE trial evaluating adjuvant bevacizumab-containing therapy in triple-negative early breast cancer. Annals of Oncology. 2017 Apr;28(4):754–60. doi:10.1093/annonc/mdw665

162. Riaz F, Gruber JJ, Telli ML. New Treatment Approaches for Triple-Negative Breast Cancer. Am Soc Clin Oncol Educ Book. 2025 Jun;45(3):e481154. doi:10.1200/EDBK-25-481154

163. Gion M, Blancas I, Cortez-Castedo P, Cortés-Salgado A, Marmé F, Blanch S, et al. Atezolizumab plus paclitaxel and bevacizumab as first-line treatment of advanced triple-negative breast cancer: the ATRACTIB phase 2 trial. Nat Med. 2025 Aug;31(8):2746–54. doi:10.1038/s41591-025-03734-3

164. Li T, Zhao M, Cao J, Wang J, Tao Z, Wang B, et al. A phase II trial combining SHR-1316, bevacizumab, and cisplatin/carboplatin in patients with TNBC with active brain metastases. JCO. 2024 Jun 1;42(16_suppl):e13133–e13133. doi:10.1200/JCO.2024.42.16_suppl.e13133

165. Wang BC. Bevacizumab combined with chemotherapy and anti-PD-1 therapy for the first-line treatment of previously untreated metastatic triple-negative breast cancer. J Immunother Cancer. 2025 Apr;13(4):e012312. doi:10.1136/jitc-2025-012312

166. Ferguson HR, Smith MP, Francavilla C. Fibroblast Growth Factor Receptors (FGFRs) and Noncanonical Partners in Cancer Signaling. Cells. 2021 May 14;10(5):1201. doi:10.3390/cells10051201

167. Santolla MF, Maggiolini M. The FGF/FGFR System in Breast Cancer: Oncogenic Features and Therapeutic Perspectives. Cancers. 2020 Oct 18;12(10):3029. doi:10.3390/cancers12103029

168. Chen J, Wang Q, Wu H, Huang X, Cao C. Therapies targeting triple-negative breast cancer: a perspective on anti-FGFR. Front Oncol. 2025 Mar 11;14:1415820. doi:10.3389/fonc.2024.1415820

169. Chew NJ, Lim Kam Sian TCC, Nguyen EV, Shin SY, Yang J, Hui MN, et al. Evaluation of FGFR targeting in breast cancer through interrogation of patient-derived models. Breast Cancer Res. 2021 Aug 3;23(1):82. doi:10.1186/s13058-021-01461-4

170. Levine KM, Priedigkeit N, Basudan A, Tasdemir N, Sikora MJ, Sokol ES, et al. FGFR4 overexpression and hotspot mutations in metastatic ER+ breast cancer are enriched in the

lobular subtype. npj Breast Cancer. 2019 Jun 27;5(1):19. doi:10.1038/s41523-019-0114-x

171. Turner N, Lambros MB, Horlings HM, Pearson A, Sharpe R, Natrajan R, et al. Integrative molecular profiling of triple negative breast cancers identifies amplicon drivers and potential therapeutic targets. Oncogene. 2010 Apr 8;29(14):2013–23. doi:10.1038/onc.2009.489

172. Liao M, Zhou J, Wride K, Lepley D, Cameron T, Sale M, et al. Population Pharmacokinetic Modeling of Lucitanib in Patients with Advanced Cancer. Eur J Drug Metab Pharmacokinet. 2022 Sep;47(5):711–23. doi:10.1007/s13318-022-00773-w

173. Wu Y, Yi Z, Li J, Wei Y, Feng R, Liu J, et al. FGFR blockade boosts T cell infiltration into triple-negative breast cancer by regulating cancer-associated fibroblasts. Theranostics. 2022;12(10):4564–80. doi:10.7150/thno.68972

174. Luo Q, Zhang L, Hao Y, Xu C, Wang X, Jia Z, et al. Erdafitinib inhibits the tumorigenicity of MDA-MB-231 triple-negative breast cancer cells by inducing TRIM25/ubiquitin-dependent degradation of FGFR4. Breast Cancer Res. 2025 Jul 9;27(1):128. doi:10.1186/s13058-025-02086-7

175. Gaudio G, Martino E, Pellizzari G, Cavallone M, Castellano G, Omar A, et al. Developing combination therapies with biologics in triple-negative breast cancer. Expert Opinion on Biological Therapy. 2024 Oct 2;24(10):1075–94. doi:10.1080/14712598.2024.2408756

176. Servetto A, Formisano L, Arteaga CL. FGFR signaling and endocrine resistance in breast cancer: Challenges for the clinical development of FGFR inhibitors. Biochim Biophys Acta Rev Cancer. 2021 Dec;1876(2):188595. doi:10.1016/j.bbcan.2021.188595 PubMed PMID: 34303787; PubMed Central PMCID: PMC10537726.

177. Zhou Y, Wu C, Lu G, Hu Z, Chen Q, Du X. FGF/FGFR signaling pathway involved resistance in various cancer types. J Cancer. 2020;11(8):2000–7. doi:10.7150/jca.40531

178. Tomuleasa C, Tigu AB, Munteanu R, Moldovan CS, Kegyes D, Onaciu A, et al. Therapeutic advances of targeting receptor tyrosine kinases in cancer. Sig Transduct Target Ther. 2024 Aug 14;9(1):201. doi:10.1038/s41392-024-01899-w

179. Bar Y, Fell G, Dedeoglu A, Moffett N, Vidula N, Spring L, et al. Dynamic HER2-low status among patients with triple negative breast cancer (TNBC) and the impact of repeat biopsies. npj Breast Cancer. 2025 Mar 11;11(1):27. doi:10.1038/s41523-025-00741-y

180. Yi Z, Feng K, Lv D, Guan Y, Shao Y, Ma F, et al. Genomic landscape of circulating tumor DNA in HER2-low metastatic breast cancer. Sig Transduct Target Ther. 2024 Dec 9;9(1):345. doi:10.1038/s41392-024-02047-0

181. Gampenrieder SP, Dezentjé V, Lambertini M, De Nonneville A, Marhold M, Le Du F, et al. Influence of HER2 expression on prognosis in metastatic triple-negative breast cancer—results from an international, multicenter analysis coordinated by the AGMT Study Group. ESMO Open. 2023 Feb;8(1):100747. doi:10.1016/j.esmoop.2022.100747

182. Fares M, Gart M, Blanc S, Zheng J, Saunders W, Smith R, et al. Abstract P5-02-43: Incidence of HER2-low Expression in HR-positive/HER2-negative and Triple-Negative

Breast Cancers in the Integra Connect Database. Cancer Research. 2023 Mar 1;83(5_Supplement):P5-02-43-P5-02–43. doi:10.1158/1538-7445.SABCS22-P5-02-43

183. Bedoya-López AF, Ahn S, Ensenyat-Mendez M, Orozco JIJ, Iñiguez-Muñoz S, Llinàs-Arias P, et al. Epigenetic determinants of an immune-evasive phenotype in HER2-low triple-negative breast cancer. npj Precis Onc. 2025 Aug 16;9(1):287. doi:10.1038/s41698-025-01023-3

184. Raghavendra AS, Zakon DB, Jin Q, Strahan A, Grimm M, Hughes ME, et al. Clinical outcomes of early-stage triple-negative breast cancer after neoadjuvant chemotherapy according to HER2-low status☆. ESMO Open. 2024 Nov;9(11):103973. doi:10.1016/j.esmoop.2024.103973

185. Park WK, Nam SJ, Kim SW, Lee JE, Yu J, Lee SK, et al. The Prognostic Impact of HER2-Low and Menopausal Status in Triple-Negative Breast Cancer. Cancers. 2024 Jul 17;16(14):2566. doi:10.3390/cancers16142566

186. Iwai M, Horimoto Y, Wu R, Amaya K, Yamada A, Narui K, et al. Clinical Significance of HER2-low Expression in Triple-negative Breast Cancer: A Retrospective Multicenter Study. Cancer Diagn Progn. 2025;5(4):492–8. doi:10.21873/cdp.10463 PubMed PMID: 40600223; PubMed Central PMCID: PMC12208201.

187. FDA approves fam-trastuzumab deruxtecan-nxki for unresectable or metastatic HR-positive, HER2-low or HER2-ultralow breast cancer | FDA [Internet]. [cited 2025 Dec 29]. Available from: https://www.fda.gov/drugs/resources-information-approved-drugs/fda-approves-fam-trastuzumab-deruxtecan-nxki-unresectable-or-metastatic-hr-positive-her2-low-or-her2

188. Sheikh E, Tran T, Vranic S, Levy A, Bonfil RD. Role and Significance of c-KIT Receptor Tyrosine Kinase in Cancer: A Review. Bosn J of Basic Med Sci. 2022 Apr 27. doi:10.17305/bjbms.2021.7399

189. Jansson S, Bendahl PO, Grabau DA, Falck AK, Fernö M, Aaltonen K, et al. The Three Receptor Tyrosine Kinases c-KIT, VEGFR2 and PDGFRα, Closely Spaced at 4q12, Show Increased Protein Expression in Triple-Negative Breast Cancer. Petronini PG, editor. PLoS ONE. 2014 Jul 15;9(7):e102176. doi:10.1371/journal.pone.0102176

190. López-Mejía JA, Tallabs-Utrilla LF, Salazar-Sojo P, Mantilla-Ollarves JC, Sánchez-Carballido MA, Rocha-Zavaleta L, et al. c-Kit Induces Migration of Triple-Negative Breast Cancer Cells and Is a Promising Target for Tyrosine Kinase Inhibitor Treatment. International Journal of Molecular Sciences. 2022 Aug 4;23(15). doi:10.3390/ijms23158702

191. Zhu Y, Wang Y, Guan B, Rao Q, Wang J, Ma H, et al. C-kit and PDGFRA gene mutations in triple negative breast cancer. Int J Clin Exp Pathol. 2014 Jun 15;7(7):4280–5. PubMed PMID: 25120810; PubMed Central PMCID: PMC4129045.

192. Gaule P, Mukherjee N, Corkery B, Eustace A, Gately K, Roche S, et al. Dasatinib Treatment Increases Sensitivity to c-Met Inhibition in Triple-Negative Breast Cancer Cells. Cancers. 2019 Apr 17;11(4):548. doi:10.3390/cancers11040548

193. Finn RS, Bengala C, Ibrahim N, Roché H, Sparano J, Strauss LC, et al. Dasatinib as a single agent in triple-negative breast cancer: results of an open-label phase 2 study. Clin Cancer Res. 2011 Nov 1;17(21):6905–13. doi:10.1158/1078-0432.CCR-11-0288 PubMed PMID: 22028489.

194. Tian J, Raffa FA, Dai M, Moamer A, Khadang B, Hachim IY, et al. Dasatinib sensitises triple negative breast cancer cells to chemotherapy by targeting breast cancer stem cells. Br J Cancer. 2018 Dec;119(12):1495–507. doi:10.1038/s41416-018-0287-3

195. Bahadoran E, Moghbelinejad S, Mohammadi G, Shahbazmohammadi H, Abdolvahabi Z, Jalilvand M, et al. Cytokeratin expression in breast cancer: from mechanisms, progression, diagnosis, and prognosis to therapeutic implications. Molecular & Cellular Oncology. 2025 Dec 31;12(1):2526230. doi:10.1080/23723556.2025.2526230

196. Zhu Y, Li K, Zhang J, Wang L, Sheng L, Yan L. The prognostic and predictive significance of cytokeratin 5/6 and epidermal growth factor receptor in metastatic triple-negative breast cancer treated with maintenance capecitabine. Transl Cancer Res TCR. 2021 Mar;10(3):1193–203. doi:10.21037/tcr-20-1760

197. Wang Z, Liu L, Li Y, Song Z, Jing Y, Fan Z, et al. Analysis of CK5/6 and EGFR and Its Effect on Prognosis of Triple Negative Breast Cancer. Front Oncol. 2021 Jan 20;10:575317. doi:10.3389/fonc.2020.575317

198. Yamashita N, Tokunaga E, Kitao H, Hisamatsu Y, Taketani K, Akiyoshi S, et al. Vimentin as a poor prognostic factor for triple-negative breast cancer. J Cancer Res Clin Oncol. 2013 May;139(5):739–46. doi:10.1007/s00432-013-1376-6

199. Yasin R, Zafar G, Rooman Ali Syed F, Afzal S, Fatima M, Rathore Z, et al. CK5/6 Expression in Molecular Subtypes of Invasive Ductal Carcinoma. Cureus. 2024 Oct 29. doi:10.7759/cureus.72608

200. Sood N, Nigam JS. Correlation of CK5 and EGFR with Clinicopathological Profile of Triple-Negative Breast Cancer. Pathology Research International. 2014 Oct 23;2014:1–6. doi:10.1155/2014/141864

201. Abdelrahman AE, Rashed HE, Abdelgawad M, Abdelhamid MI. Prognostic impact of EGFR and cytokeratin 5/6 immunohistochemical expression in triple-negative breast cancer. Annals of Diagnostic Pathology. 2017 Jun;28:43–53. doi:10.1016/j.anndiagpath.2017.01.009

202. Choccalingam C, Rao L, Rao S. Clinico-Pathological Characteristics of Triple Negative and Non Triple Negative High Grade Breast Carcinomas with and without Basal Marker (CK5/6 and EGFR) Expression at a Rural Tertiary Hospital in India. Breast Cancer (Auckl). 2012 Jan;6:BCBCR.S8611. doi:10.4137/BCBCR.S8611

203. Davey RA, Grossmann M. Androgen Receptor Structure, Function and Biology: From Bench to Bedside. Clin Biochem Rev. 2016 Feb;37(1):3–15. PubMed PMID: 27057074; PubMed Central PMCID: PMC4810760.

204. Mina A, Yoder R, Sharma P. Targeting the androgen receptor in triple-negative breast cancer: current perspectives. OTT. 2017 Sep;Volume 10:4675–85. doi:10.2147/OTT.S126051

205. Vtorushin S, Dulesova A, Krakhmal N. Luminal androgen receptor (LAR) subtype of triple-negative breast cancer: molecular, morphological, and clinical features. J Zhejiang Univ Sci B. 2022 Aug;23(8):617–24. doi:10.1631/jzus.B2200113

206. Haruna M, Daramola AO, Awolola NA, Badr NM, Fehintola Banjo AA, Shaaban A. Clinicopathological features and androgen receptor expression in triple negative breast cancer at Lagos, Nigeria. ecancer. 2022 Oct 3;16. doi:10.3332/ecancer.2022.1452

207. Astvatsaturyan K, Yue Y, Walts AE, Bose S. Androgen receptor positive triple negative breast cancer: Clinicopathologic, prognostic, and predictive features. Ahmad A, editor. PLoS ONE. 2018 Jun 8;13(6):e0197827. doi:10.1371/journal.pone.0197827

208. Lyalkin SA, Verevkina NO, Alekseyenko OO, Syvak LA. Prognostic role of androgen receptor expression in patients with metastatic triple negative breast cancer. Exp oncol. 2023 Jun 1;42(2):140–3. doi:10.32471/exp-oncology.2312-8852.vol-42-no-2.14579

209. Bhattarai S, Klimov S, Mittal K, Krishnamurti U, Li X, Oprea-Ilies G, et al. Prognostic Role of Androgen Receptor in Triple Negative Breast Cancer: A Multi-Institutional Study. Cancers. 2019 Jul 17;11(7):995. doi:10.3390/cancers11070995

210. Sridhar N, Glisch C, Jawa Z, Chaudhary LN, Kamaraju S, Burfeind J, et al. Androgen receptor expression in patients with triple negative breast cancer treated with neoadjuvant chemotherapy: a single institution study. J Cancer. 2022;13(8):2472–6. doi:10.7150/jca.67536

211. Barton VN, Gordon MA, Richer JK, Elias A. Anti-androgen therapy in triple-negative breast cancer. Ther Adv Med Oncol. 2016 Jul;8(4):305–8. doi:10.1177/1758834016646735

212. Xiong N, Wu H, Yu Z. Advancements and challenges in triple-negative breast cancer: a comprehensive review of therapeutic and diagnostic strategies. Front Oncol. 2024 May 28;14:1405491. doi:10.3389/fonc.2024.1405491

213. Gorodetska I, Kozeretska I, Dubrovska A. *BRCA* Genes: The Role in Genome Stability, Cancer Stemness and Therapy Resistance. J Cancer. 2019;10(9):2109–27. doi:10.7150/jca.30410

214. Garrido-Castro AC, Lin NU, Polyak K. Insights into Molecular Classifications of Triple-Negative Breast Cancer: Improving Patient Selection for Treatment. Cancer Discovery. 2019 Feb 1;9(2):176–98. doi:10.1158/2159-8290.CD-18-1177

215. Hahnen E, Hauke J, Engel C, Neidhardt G, Rhiem K, Schmutzler RK. Germline Mutations in Triple-Negative Breast Cancer. Breast Care. 2017;12(1):15–9. doi:10.1159/000455999

216. Huang L, Lang GT, Liu Q, Shi JX, Shao ZM, Cao AY. A predictor of pathological complete response to neoadjuvant chemotherapy in triple-negative breast cancer patients with the DNA repair genes. Ann Transl Med. 2021 Feb;9(4):301–301. doi:10.21037/atm-20-4852

217. Jia X, Wang K, Xu L, Li N, Zhao Z, Li M. A systematic review and meta-analysis of BRCA1/2 mutation for predicting the effect of platinum-based chemotherapy in triple-negative breast cancer. The Breast. 2022 Dec;66:31–9. doi:10.1016/j.breast.2022.08.012

218. Arun B, Couch FJ, Abraham J, Tung N, Fasching PA. BRCA-mutated breast cancer: the unmet need, challenges and therapeutic benefits of genetic testing. Br J Cancer. 2024 Nov 16;131(9):1400–14. doi:10.1038/s41416-024-02827-z

219. Zhou T, Zhang J. Therapeutic advances and application of PARP inhibitors in breast cancer. Translational Oncology. 2025 Jul;57:102410. doi:10.1016/j.tranon.2025.102410

220. Gupta T, Vinayak S, Telli M. Emerging strategies: PARP inhibitors in combination with immune checkpoint blockade in BRCA1 and BRCA2 mutation-associated and triple-negative breast cancer. Breast Cancer Res Treat. 2023 Jan;197(1):51–6. doi:10.1007/s10549-022-06780-4

221. Xiao F, Wang Z, Qiao L, Zhang X, Wu N, Wang J, et al. Application of PARP inhibitors combined with immune checkpoint inhibitors in ovarian cancer. J Transl Med. 2024 Aug 21;22(1):778. doi:10.1186/s12967-024-05583-z

222. Feng C, Zhang Y, Wu F, Li J, Liu M, Lv W, et al. Relationship between homologous recombination deficiency and clinical features of breast cancer based on genomic scar score. The Breast. 2023 Jun;69:392–400. doi:10.1016/j.breast.2023.04.002

223. Moore GM, Powell SN, Higginson DS, Khan AJ. Examining the prevalence of homologous recombination repair defects in ER+ breast cancers. Breast Cancer Res Treat. 2022 Apr;192(3):649–53. doi:10.1007/s10549-022-06529-z

224. Clark CA, Yang ES. Harnessing DNA Repair Defects to Augment Immune-Based Therapies in Triple-Negative Breast Cancer. Front Oncol. 2021 Sep 24;11:703802. doi:10.3389/fonc.2021.703802

225. Temaj G, Chichiarelli S, Telkoparan-Akillilar P, Saha S, Nuhii N, Hadziselimovic R, et al. P53: A key player in diverse cellular processes including nuclear stress and ribosome biogenesis, highlighting potential therapeutic compounds. Biochemical Pharmacology. 2024 Aug;226:116332. doi:10.1016/j.bcp.2024.116332

226. Qayoom H, Haq BU, Sofi S, Jan N, Jan A, Mir MA. Targeting mutant p53: a key player in breast cancer pathogenesis and beyond. Cell Commun Signal. 2024 Oct 10;22(1):484. doi:10.1186/s12964-024-01863-9

227. Mitri ZI, Abuhadra N, Goodyear SM, Hobbs EA, Kaempf A, Thompson AM, et al. Impact of TP53 mutations in Triple Negative Breast Cancer. npj Precis Onc. 2022 Sep 9;6(1):64. doi:10.1038/s41698-022-00303-6

228. Rabab KE, Buchanan PJ, Colley G, White A, Murphy A, McCormack C, et al. TP53 Mutation-Specific Dysregulation of Store-Operated Calcium Entry and Apoptotic Sensitivity in Triple-Negative Breast Cancer. Cancers. 2025 May 10;17(10):1614. doi:10.3390/cancers17101614

229. Baliakas P, Soussi T. The TP53 tumor suppressor gene: From molecular biology to clinical investigations. J Intern Med. 2025 Aug;298(2):78–96. doi:10.1111/joim.20106

230. Hwang SH, Baek SH, Lee MJ, Kook Y, Bae SJ, Ahn SG, et al. Clinical Relevance of TP53 Mutation and Its Characteristics in Breast Cancer with Long-Term Follow-Up Date. Cancers. 2024 Nov 21;16(23):3899. doi:10.3390/cancers16233899

231. Kennedy MC, Lowe SW. Mutant p53: it's not all one and the same. Cell Death Differ. 2022 May;29(5):983–7. doi:10.1038/s41418-022-00989-y

232. Audeh MW. Novel treatment strategies in triple-negative breast cancer: specific role of poly(adenosine diphosphate-ribose) polymerase inhibition. Pharmgenomics Pers Med. 2014;7:307–16. doi:10.2147/PGPM.S39765 PubMed PMID: 25342917; PubMed Central PMCID: PMC4205934.

233. Sizemore ST, Mohammad R, Sizemore GM, Nowsheen S, Yu H, Ostrowski MC, et al. Synthetic Lethality of PARP Inhibition and Ionizing Radiation is p53-dependent. Mol Cancer Res. 2018 Jul;16(7):1092–102. doi:10.1158/1541-7786.MCR-18-0106 PubMed PMID: 29592899; PubMed Central PMCID: PMC6713455.

234. Nishikawa S, Iwakuma T. Drugs Targeting p53 Mutations with FDA Approval and in Clinical Trials. Cancers. 2023 Jan 9;15(2):429. doi:10.3390/cancers15020429

235. Wang Y, Rozen V, Zhao Y, Wang Z. Oncogenic activation of PIK3CA in cancers: Emerging targeted therapies in precision oncology. Genes & Diseases. 2025 Mar;12(2):101430. doi:10.1016/j.gendis.2024.101430

236. Ascione L, Zagami P, Nicolò E, Crimini E, Curigliano G, Criscitiello C. PIK3CAMutations in Breast Cancer Subtypes Other Than HR-Positive/HER2-Negative. JPM. 2022 Oct 31;12(11):1793. doi:10.3390/jpm12111793

237. Lin XY, Guo L, Lin X, Wang Y, Zhang G. Concomitant *PIK3CA* and *TP53* Mutations in Breast Cancer: An Analysis of Clinicopathologic and Mutational Features, Neoadjuvant Therapeutic Response, and Prognosis. J Breast Cancer. 2023;26(4):363. doi:10.4048/jbc.2023.26.e30

238. Lehmann BD, Bauer JA, Schafer JM, Pendleton CS, Tang L, Johnson KC, et al. PIK3CA mutations in androgen receptor-positive triple negative breast cancer confer sensitivity to the combination of PI3K and androgen receptor inhibitors. Breast Cancer Res. 2014;16:406. doi:10.1186/s13058-014-0406-x PubMed PMID: 25103565; PubMed Central PMCID: PMC4187324.

239. Amato O, Buisseret L, Gebhart G, Plouznikoff N, Larsimont D, Awada A, et al. *PIK3CA* copy-number gain and inhibitors of the PI3K/AKT/mTOR pathway in triple-negative breast cancer. Cold Spring Harb Mol Case Stud. 2023 Apr;9(2):a006255. doi:10.1101/mcs.a006255

240. Hu H, Zhu J, Zhong Y, Geng R, Ji Y, Guan Q, et al. PIK3CA mutation confers resistance to chemotherapy in triple-negative breast cancer by inhibiting apoptosis and activating the PI3K/AKT/mTOR signaling pathway. Ann Transl Med. 2021 Mar;9(5):410–410. doi:10.21037/atm-21-698

241. Mosele F, Stefanovska B, Lusque A, Tran Dien A, Garberis I, Droin N, et al. Outcome and molecular landscape of patients with PIK3CA-mutated metastatic breast cancer. Annals of Oncology. 2020 Mar;31(3):377–86. doi:10.1016/j.annonc.2019.11.006

242. Gordon V, Banerji S. Molecular Pathways: PI3K Pathway Targets in Triple-Negative Breast Cancers. Clin Cancer Res. 2013 Jul 15;19(14):3738–44. doi:10.1158/1078-0432.CCR-12-0274

243. Altundag K. Clinical research on triple-negative breast cancer that targets the PIK3CA pathway. Med Oncol. 2024 Oct 14;41(11):268. doi:10.1007/s12032-024-02493-4

244. Andrikopoulou A, Chatzinikolaou S, Panourgias E, Kaparelou M, Liontos M, Dimopoulos MA, et al. "The emerging role of capivasertib in breast cancer". The Breast. 2022 Jun;63:157–67. doi:10.1016/j.breast.2022.03.018

245. Fuso P, Muratore M, D'Angelo T, Paris I, Carbognin L, Tiberi G, et al. PI3K Inhibitors in Advanced Breast Cancer: The Past, The Present, New Challenges and Future Perspectives. Cancers. 2022 Apr 26;14(9):2161. doi:10.3390/cancers14092161

246. Sharma P, Abramson VG, O'Dea A, Nye L, Mayer I, Pathak HB, et al. Clinical and Biomarker Results from Phase I/II Study of PI3K Inhibitor Alpelisib plus Nab-paclitaxel in HER2-Negative Metastatic Breast Cancer. Clinical Cancer Research. 2021 Jul 15;27(14):3896–904. doi:10.1158/1078-0432.CCR-20-4879

247. Novartis Pharmaceuticals. A Phase III, Multicenter, Randomized, Double-blind, Placebo-controlled Study to Assess the Efficacy and Safety of Alpelisib (BYL719) in Combination With Nab-paclitaxel in Patients With Advanced Triple Negative Breast Cancer With Either Phosphoinositide-3-kinase Catalytic Subunit Alpha (PIK3CA) Mutation or Phosphatase and Tensin Homolog Protein (PTEN) Loss Without PIK3CA Mutation [Clinical trial registration] [Internet]. clinicaltrials.gov; 2026 May [cited 2026 May 28]. Clinical trial registration no.: NCT04251533. Available from: https://clinicaltrials.gov/study/NCT04251533

248. The Cancer Genome Atlas Network. Comprehensive molecular portraits of human breast tumours. Nature. 2012 Oct;490(7418):61–70. doi:10.1038/nature11412

249. Eustace AJ, Lee MJ, Colley G, Roban J, Downing T, Buchanan PJ. Aberrant calcium signalling downstream of mutations in TP53 and the PI3K/AKT pathway genes promotes disease progression and therapy resistance in triple negative breast cancer. Cancer Drug Resist. 2022;5(3):560–76. doi:10.20517/cdr.2022.41

250. Xu J, Wu K jing, Jia Q jun, Ding X feng. Roles of miRNA and lncRNA in triple-negative breast cancer. J Zhejiang Univ Sci B. 2020 Sep;21(9):673–89. doi:10.1631/jzus.B1900709 PubMed PMID: 32893525; PubMed Central PMCID: PMC7519626.

251. Piasecka D, Braun M, Kordek R, Sadej R, Romanska H. MicroRNAs in regulation of triple-negative breast cancer progression. J Cancer Res Clin Oncol. 2018 Aug;144(8):1401–11. doi:10.1007/s00432-018-2689-2

252. Ghosh A, Ranjan N, Jiang L, Ansari AH, Degyatoreva N, Ahluwalia S, et al. Fine-tuning miR-21 expression and inhibition of EMT in breast cancer cells using aromatic-neomycin derivatives. Molecular Therapy Nucleic Acids. 2022 Mar;27:685–98. doi:10.1016/j.omtn.2021.12.027

253. Santana TABDS, De Oliveira Passamai L, De Miranda FS, Borin TF, Borges GF, Luiz WB, et al. The Role of miRNAs in the Prognosis of Triple-Negative Breast Cancer: A Systematic Review and Meta-Analysis. Diagnostics. 2022 Dec 30;13(1):127. doi:10.3390/diagnostics13010127

254. Qian H, Maghsoudloo M, Kaboli PJ, Babaeizad A, Cui Y, Fu J, et al. Decoding the Promise and Challenges of miRNA-Based Cancer Therapies: An Essential Update on miR-21, miR-34, and miR-155. Int J Med Sci. 2024 Oct 28;21(14):2781–98. doi:10.7150/ijms.102123

255. Kumar V, Gautam M, Chaudhary A, Chaurasia B. Impact of three miRNA signature as potential diagnostic marker for triple negative breast cancer patients. Sci Rep. 2023 Dec 8;13(1):21643. doi:10.1038/s41598-023-48896-7

256. Chakkaravarthi K, Ramesh R, Palaniyandi T, Baskar G, Viswanathan S, Wahab MRA, et al. Prospectives of mirna gene signaling pathway in triple-negative breast cancer. Pathology - Research and Practice. 2023 Aug;248:154658. doi:10.1016/j.prp.2023.154658

257. Volovat SR, Volovat C, Hordila I, Hordila DA, Mirestean CC, Miron OT, et al. MiRNA and LncRNA as Potential Biomarkers in Triple-Negative Breast Cancer: A Review. Front Oncol. 2020 Nov 20;10:526850. doi:10.3389/fonc.2020.526850

258. Cahill HF, Brown JM, Leslie-Toogood M, Venkatesh J, Wasson MCD, Arun RP, et al. LncRNA NRAD1 regulates the triple-negative breast cancer transcriptome by miRNA biogenesis, localization, and predominately non-ceRNA interactions. Sci Rep. 2025 Jul 23;15(1):26708. doi:10.1038/s41598-025-12415-7

259. Li R, Cao L. The role of tumor-infiltrating lymphocytes in triple-negative breast cancer and the research progress of adoptive cell therapy. Front Immunol. 2023 May 18;14:1194020. doi:10.3389/fimmu.2023.1194020

260. Chaudhuri S, Thomas S, Munster P. Immunotherapy in breast cancer: A clinician's perspective. J Natl Cancer Cent. 2021 Jun;1(2):47–57. doi:10.1016/j.jncc.2021.01.001 PubMed PMID: 39035768; PubMed Central PMCID: PMC11256727.

261. Leon-Ferre RA, Jonas SF, Salgado R, Loi S, De Jong V, Carter JM, et al. Tumor-Infiltrating Lymphocytes in Triple-Negative Breast Cancer. JAMA. 2024 Apr 2;331(13):1135. doi:10.1001/jama.2024.3056

262. Coleman C, Selvakumar T, Thurlapati A, Graf K, Pavuluri S, Mehrotra S, et al. Harnessing Tumor-Infiltrating Lymphocytes in Triple-Negative Breast Cancer: Opportunities and Barriers to Clinical Integration. IJMS. 2025 May 1;26(9):4292. doi:10.3390/ijms26094292

263. Li M, Panet F, Barberi V, Salgado R, Oliveira M, Loi S. Biomarkers of response and resistance to immune checkpoint inhibitors in breast cancer. The Breast. 2025 Oct;83:104545. doi:10.1016/j.breast.2025.104545

264. Jin M, Fang J, Peng J, Wang X, Xing P, Jia K, et al. PD-1/PD-L1 immune checkpoint blockade in breast cancer: research insights and sensitization strategies. Mol Cancer. 2024 Nov 29;23(1):266. doi:10.1186/s12943-024-02176-8

265. Nakhjavani M, Shigdar S. Future of PD-1/PD-L1 axis modulation for the treatment of triple-negative breast cancer. Pharmacological Research. 2022 Jan;175:106019. doi:10.1016/j.phrs.2021.106019

266. Stanowska O, Kuczkiewicz-Siemion O, Dębowska M, Olszewski WP, Jagiełło-Gruszfeld A, Tysarowski A, et al. PD-L1-Positive High-Grade Triple-Negative Breast Cancer Patients Respond Better to Standard Neoadjuvant Treatment—A Retrospective Study of PD-L1 Expression in Relation to Different Clinicopathological Parameters. JCM. 2022 Sep 21;11(19):5524. doi:10.3390/jcm11195524

267. Shah M, Hubbard RA, Mamtani R, Marmarelis ME, Hennessy S. Very high PD-L1 expression as a prognostic indicator of overall survival among patients with advanced non-small cell lung cancer receiving anti-PD-(L)1 monotherapies in routine practice. Pharmacoepidemiol Drug Saf. 2022 Oct;31(10):1121–6. doi:10.1002/pds.5487 PubMed PMID: 35670103; PubMed Central PMCID: PMC9464674.

268. Porta FM, Sajjadi E, Venetis K, Frascarelli C, Cursano G, Guerini-Rocco E, et al. Immune Biomarkers in Triple-Negative Breast Cancer: Improving the Predictivity of Current Testing Methods. JPM. 2023 Jul 23;13(7):1176. doi:10.3390/jpm13071176

269. Bagegni NA, Davis AA, Clifton KK, Ademuyiwa FO. Targeted Treatment for High-Risk Early-Stage Triple-Negative Breast Cancer: Spotlight on Pembrolizumab. BCTT. 2022 Apr;Volume 14:113–23. doi:10.2147/BCTT.S293597

270. Ryspayeva D, Seyhan AA, MacDonald WJ, Purcell C, Roady TJ, Ghandali M, et al. Signaling pathway dysregulation in breast cancer. Oncotarget. 2025 Mar 13;16:168–201. doi:10.18632/oncotarget.28701 PubMed PMID: 40080721; PubMed Central PMCID: PMC11906143.

271. Rocca A, Braga L, Volpe MC, Maiocchi S, Generali D. The Predictive and Prognostic Role of RAS–RAF–MEK–ERK Pathway Alterations in Breast Cancer: Revision of the Literature and Comparison with the Analysis of Cancer Genomic Datasets. Cancers. 2022 Oct 28;14(21):5306. doi:10.3390/cancers14215306

272. Jiang W, Wang X, Zhang C, Xue L, Yang L. Expression and clinical significance of MAPK and EGFR in triple-negative breast cancer. Oncol Lett. 2020 Mar;19(3):1842–8. doi:10.3892/ol.2020.11274 PubMed PMID: 32194678; PubMed Central PMCID: PMC7038935.

273. Wu X, Que H, Li Q, Wei X. Wnt/β-catenin mediated signaling pathways in cancer: recent advances, and applications in cancer therapy. Mol Cancer. 2025 Jun 10;24(1):171. doi:10.1186/s12943-025-02363-1

274. Dey N, Young B, Abramovitz M, Bouzyk M, Barwick B, De P, et al. Differential Activation of Wnt-β-Catenin Pathway in Triple Negative Breast Cancer Increases MMP7 in a PTEN Dependent Manner. Burchell JM, editor. PLoS ONE. 2013 Oct 15;8(10):e77425. doi:10.1371/journal.pone.0077425

275. Pavitra E, Kancharla J, Gupta VK, Prasad K, Sung JY, Kim J, et al. The role of NF-κB in breast cancer initiation, growth, metastasis, and resistance to chemotherapy. Biomedicine & Pharmacotherapy. 2023 Jul;163:114822. doi:10.1016/j.biopha.2023.114822

276. De La Cruz P, McAdams J, Morales Aquino M, Fernandez AI, Elliott A, Lustberg M, et al. NF-κB associated markers of prognosis in early and metastatic triple negative breast cancer. Breast Cancer Res. 2024 Dec 2;26(1):175. doi:10.1186/s13058-024-01925-3

277. Devanaboyina M, Kaur J, Whiteley E, Lin L, Einloth K, Morand S, et al. NF-κB Signaling in Tumor Pathways Focusing on Breast and Ovarian Cancer. Oncol Rev. 2022 Oct 3;16:10568. doi:10.3389/or.2022.10568

278. Vecchi L, Mota STS, Zóia MAP, Martins IC, De Souza JB, Santos TG, et al. Interleukin-6 Signaling in Triple Negative Breast Cancer Cells Elicits the Annexin A1/Formyl Peptide Receptor 1 Axis and Affects the Tumor Microenvironment. Cells. 2022 May 20;11(10):1705. doi:10.3390/cells11101705

279. Balko JM, Schwarz LJ, Luo N, Estrada MV, Giltnane JM, Dávila-González D, et al. Triple-negative breast cancers with amplification of JAK2 at the 9p24 locus demonstrate JAK2-specific dependence. Sci Transl Med. 2016 Apr 13;8(334):334ra53. doi:10.1126/scitranslmed.aad3001 PubMed PMID: 27075627; PubMed Central PMCID: PMC5256931.

280. Qin JJ, Yan L, Zhang J, Zhang WD. STAT3 as a potential therapeutic target in triple negative breast cancer: a systematic review. J Exp Clin Cancer Res. 2019 Dec;38(1):195. doi:10.1186/s13046-019-1206-z

281. Arzi L, Mollaei H, Hoshyar R. Countering Triple Negative Breast Cancer via Impeding Wnt/β-Catenin Signaling, a Phytotherapeutic Approach. Plants. 2022 Aug 24;11(17):2191. doi:10.3390/plants11172191

282. Wang W, Nag SA, Zhang R. Targeting the NFκB signaling pathways for breast cancer prevention and therapy. Curr Med Chem. 2015;22(2):264–89. doi:10.2174/0929867321666141106124315 PubMed PMID: 25386819; PubMed Central PMCID: PMC6690202.

283. Balanis N, Carlin CR. Stress-induced EGF receptor signaling through STAT3 and tumor progression in triple-negative breast cancer. Molecular and Cellular Endocrinology. 2017 Aug;451:24–30. doi:10.1016/j.mce.2017.01.013

284. Masuda H, Zhang D, Bartholomeusz C, Doihara H, Hortobagyi GN, Ueno NT. Role of epidermal growth factor receptor in breast cancer. Breast Cancer Res Treat. 2012 Nov;136(2):331–45. doi:10.1007/s10549-012-2289-9

285. Song X, Liu Z, Yu Z. EGFR Promotes the Development of Triple Negative Breast Cancer Through JAK/STAT3 Signaling. CMAR. 2020 Jan;Volume 12:703–17. doi:10.2147/CMAR.S225376

286. Edwards A, Brennan K. Notch Signalling in Breast Development and Cancer. Front Cell Dev Biol. 2021 Jul 6;9:692173. doi:10.3389/fcell.2021.692173

287. Giuli MV, Giuliani E, Screpanti I, Bellavia D, Checquolo S. Notch Signaling Activation as a Hallmark for Triple-Negative Breast Cancer Subtype. Journal of Oncology. 2019 Jul 11;2019:1–15. doi:10.1155/2019/8707053

288. He L, Wick N, Germans SK, Peng Y. The Role of Breast Cancer Stem Cells in Chemoresistance and Metastasis in Triple-Negative Breast Cancer. Cancers. 2021 Dec 9;13(24):6209. doi:10.3390/cancers13246209

289. Habib JG, O'Shaughnessy JA. The hedgehog pathway in triple-negative breast cancer. Cancer Medicine. 2016 Oct;5(10):2989–3006. doi:10.1002/cam4.833

290. Liu R, Yu Y, Wang Q, Zhao Q, Yao Y, Sun M, et al. Interactions between hedgehog signaling pathway and the complex tumor microenvironment in breast cancer: current knowledge and therapeutic promises. Cell Commun Signal. 2024 Sep 9;22(1):432. doi:10.1186/s12964-024-01812-6

291. Chen Y, Sang Y, Li S, Xue J, Chen M, Hong S, et al. The ERK inhibitor GDC-0994 selectively inhibits growth of BRAF mutant cancer cells. Translational Oncology. 2024 Jul;45:101991. doi:10.1016/j.tranon.2024.101991

292. Grogan L, Shapiro P. Progress in the development of ERK1/2 inhibitors for treating cancer and other diseases. Adv Pharmacol. 2024;100:181–207. doi:10.1016/bs.apha.2024.04.001 PubMed PMID: 39034052.

293. Han H, Yang M, Wen Z, Mei F, Chen Q, Ma Y, et al. Trametinib and M17, a novel small molecule inhibitor of AKT, display a synergistic antitumor effect in triple negative breast cancer cells through the AKT/mTOR and MEK/ERK pathways. Bioorganic Chemistry. 2025 Jan;154:107981. doi:10.1016/j.bioorg.2024.107981

294. Zhou Y, Lin S, Tseng KF, Han K, Wang Y, Gan Z hua, et al. Selumetinib suppresses cell proliferation, migration and trigger apoptosis, G1 arrest in triple-negative breast cancer cells. BMC Cancer. 2016 Dec;16(1):818. doi:10.1186/s12885-016-2773-4

295. Maqbool M, Bekele F, Fekadu G. Treatment Strategies Against Triple-Negative Breast Cancer: An Updated Review. BCTT. 2022 Jan;Volume 14:15–24. doi:10.2147/BCTT.S348060

296. Zhao X, Ma Y, Luo J, Xu K, Tian P, Lu C, et al. Blocking the WNT/β-catenin pathway in cancer treatment:pharmacological targets and drug therapeutic potential. Heliyon. 2024 Aug;10(16):e35989. doi:10.1016/j.heliyon.2024.e35989

297. De Pellegars-Malhortie A, Picque Lasorsa L, Mazard T, Granier F, Prévostel C. Why Is Wnt/β-Catenin Not Yet Targeted in Routine Cancer Care? Pharmaceuticals. 2024 Jul 16;17(7):949. doi:10.3390/ph17070949

298. Berdan CA, Ho R, Lehtola HS, To M, Hu X, Huffman TR, et al. Parthenolide Covalently Targets and Inhibits Focal Adhesion Kinase in Breast Cancer Cells. Cell Chemical Biology. 2019 Jul;26(7):1027-1035.e22. doi:10.1016/j.chembiol.2019.03.016

299. Larsson P, Pettersson D, Olsson M, Sarathchandra S, Abramsson A, Zetterberg H, et al. Repurposing proteasome inhibitors for improved treatment of triple-negative breast cancer. Cell Death Discov. 2024 Jan 29;10(1):57. doi:10.1038/s41420-024-01819-5

300. Awasthee N, Rai V, Chava S, Nallasamy P, Kunnumakkara AB, Bishayee A, et al. Targeting IκappaB kinases for cancer therapy. Seminars in Cancer Biology. 2019 Jun;56:12–24. doi:10.1016/j.semcancer.2018.02.007

301. Shetti D, Zhang B, Fan C, Mo C, Lee BH, Wei K. Low Dose of Paclitaxel Combined with XAV939 Attenuates Metastasis, Angiogenesis and Growth in Breast Cancer by Suppressing Wnt Signaling. Cells. 2019 Aug 14;8(8):892. doi:10.3390/cells8080892

302. Stover DG, Gil Del Alcazar CR, Brock J, Guo H, Overmoyer B, Balko J, et al. Phase II study of ruxolitinib, a selective JAK1/2 inhibitor, in patients with metastatic triple-negative breast cancer. npj Breast Cancer. 2018 May 4;4(1):10. doi:10.1038/s41523-018-0060-z

303. Wang R, Li LP, Zhao C, Yang YD, Li X, Yang BB, et al. Discovery of potent and selective STAT3 inhibitors against triple-negative breast cancer. European Journal of Medicinal Chemistry. 2025 Nov;298:118020. doi:10.1016/j.ejmech.2025.118020

304. Mansilla-Polo M, Morgado-Carrasco D. Biologics Versus JAK Inhibitors. Part I: Cancer Risk. A Narrative Review. Dermatol Ther (Heidelb). 2024 Jun;14(6):1389–442. doi:10.1007/s13555-024-01166-4

305. Ball DP, Lewis AM, Williams D, Resetca D, Wilson DJ, Gunning PT. Signal transducer and activator of transcription 3 (STAT3) inhibitor, S3I-201, acts as a potent and non-selective alkylating agent. Oncotarget. 2016 Apr 12;7(15):20669–79. doi:10.18632/oncotarget.7838

306. Nedeljković M, Vuletić A, Mirjačić Martinović K. Divide and Conquer—Targeted Therapy for Triple-Negative Breast Cancer. IJMS. 2025 Feb 7;26(4):1396. doi:10.3390/ijms26041396

307. Ramos EK, Hoffmann AD, Gerson SL, Liu H. New Opportunities and Challenges to Defeat Cancer Stem Cells. Trends in Cancer. 2017 Nov;3(11):780–96. doi:10.1016/j.trecan.2017.08.007

308. Schott AF, Landis MD, Dontu G, Griffith KA, Layman RM, Krop I, et al. Preclinical and Clinical Studies of Gamma Secretase Inhibitors with Docetaxel on Human Breast Tumors. Clinical Cancer Research. 2013 Mar 15;19(6):1512–24. doi:10.1158/1078-0432.CCR-11-3326

309. You KS, Kim TS, Back SM, Park JS, Liu K, Seong YS, et al. JAK2 Inhibition Augments the Anti-Proliferation Effects by AKT and MEK Inhibition in Triple-Negative Breast Cancer Cells. IJMS. 2025 Jun 26;26(13):6139. doi:10.3390/ijms26136139

310. Rao X, Qiao Z, Yang Y, Deng Y, Zhang Z, Yu X, et al. Unveiling Epigenetic Vulnerabilities in Triple-Negative Breast Cancer through 3D Organoid Drug Screening. Pharmaceuticals. 2024 Feb 8;17(2):225. doi:10.3390/ph17020225

311. Mehta K, Hegde M, Girisa S, Vishwa R, Alqahtani MS, Abbas M, et al. Targeting RTKs/nRTKs as promising therapeutic strategies for the treatment of triple-negative breast cancer: evidence from clinical trials. Military Med Res. 2024 Dec 12;11(1):76. doi:10.1186/s40779-024-00582-z

312. Mullooly M, Conklin D, McGowan PM, O'Brien NA, O'Donovan N, Slamon DJ, et al. Neratinib to inhibit the growth of triple-negative breast cancer cells. JCO. 2015 May 20;33(15_suppl):1099–1099. doi:10.1200/jco.2015.33.15_suppl.1099

313. Bhateja P, Cherian M, Majumder S, Ramaswamy B. The Hedgehog Signaling Pathway: A Viable Target in Breast Cancer? Cancers. 2019 Aug 7;11(8):1126. doi:10.3390/cancers11081126

314. Jing J, Wu Z, Wang J, Luo G, Lin H, Fan Y, et al. Hedgehog signaling in tissue homeostasis, cancers and targeted therapies. Sig Transduct Target Ther. 2023 Aug 18;8(1):315. doi:10.1038/s41392-023-01559-5

315. Nakai K, Hung MC, Yamaguchi H. A perspective on anti-EGFR therapies targeting triple-negative breast cancer. Am J Cancer Res. 2016 Aug 1;6(8):1609–23. PubMed PMID: 27648353; PubMed Central PMCID: PMC5004067.

316. Mahmoud R, Ordóñez-Morán P, Allegrucci C. Challenges for Triple Negative Breast Cancer Treatment: Defeating Heterogeneity and Cancer Stemness. Cancers. 2022 Sep 1;14(17):4280. doi:10.3390/cancers14174280

317. Manjunath M, Choudhary B. Triple-negative breast cancer: A run-through of features, classification and current therapies (Review). Oncol Lett. 2021 May 5;22(1):512. doi:10.3892/ol.2021.12773

318. Obidiro O, Battogtokh G, Akala EO. Triple Negative Breast Cancer Treatment Options and Limitations: Future Outlook. Pharmaceutics. 2023 Jun 23;15(7):1796. doi:10.3390/pharmaceutics15071796

319. Traina TA, Miller K, Yardley DA, Eakle J, Schwartzberg LS, O'Shaughnessy J, et al. Enzalutamide for the Treatment of Androgen Receptor-Expressing Triple-Negative Breast Cancer. J Clin Oncol. 2018 Mar 20;36(9):884–90. doi:10.1200/JCO.2016.71.3495 PubMed PMID: 29373071; PubMed Central PMCID: PMC5858523.

320. Badve SS, Penault-Llorca F, Reis-Filho JS, Deurloo R, Siziopikou KP, D'Arrigo C, et al. Determining PD-L1 Status in Patients With Triple-Negative Breast Cancer: Lessons Learned From IMpassion130. JNCI: Journal of the National Cancer Institute. 2022 May 9;114(5):664–75. doi:10.1093/jnci/djab121

321. Barchiesi G, Roberto M, Verrico M, Vici P, Tomao S, Tomao F. Emerging Role of PARP Inhibitors in Metastatic Triple Negative Breast Cancer. Current Scenario and Future Perspectives. Front Oncol. 2021 Nov 25;11:769280. doi:10.3389/fonc.2021.769280

322. Chew HK. Adjuvant therapy for breast cancer: who should get what? Western Journal of Medicine. 2001 Apr 1;174(4):284–7. doi:10.1136/ewjm.174.4.284

323. Oikawa M. The history, present situation, and future directions of neoadjuvant chemotherapy for HER2-negative breast cancer. Chin Clin Oncol. 2020 Jun;9(3):29–29. doi:10.21037/cco-20-12

324. Flores JAS, Pineda JC. Radiation Therapy. In: Pak SC, Ooi SL, Micalos PS, Ghoneum MH, editors. Modified Rice Bran Arabinoxylan [Internet]. Singapore: Springer Nature Singapore; 2023 [cited 2025 Dec 29]. p. 81–6. Available from: https://link.springer.com/10.1007/978-981-19-5735-2_7 doi:10.1007/978-981-19-5735-2_7

325. Haussmann J, Corradini S, Nestle-Kraemling C, Bölke E, Njanang FJD, Tamaskovics B, et al. Recent advances in radiotherapy of breast cancer. Radiat Oncol. 2020 Dec;15(1):71. doi:10.1186/s13014-020-01501-x

326. Bessa JDF, Marta GN. Triple-negative breast cancer and radiation therapy. Rep Pract Oncol Radiother. 2022 Mar 9;VM/OJS/J/88873. doi:10.5603/RPOR.a2022.0025

327. Pashtan IM, Recht A, Ancukiewicz M, Brachtel E, Abi-Raad RF, D'Alessandro HA, et al. External Beam Accelerated Partial-Breast Irradiation Using 32 Gy in 8 Twice-Daily Fractions: 5-Year Results of a Prospective Study. International Journal of Radiation Oncology*Biology*Physics. 2012 Nov;84(3):e271–7. doi:10.1016/j.ijrobp.2012.04.019

328. Senkus-Konefka E, Jassem J. Complications of Breast-cancer Radiotherapy. Clinical Oncology. 2006 Apr;18(3):229–35. doi:10.1016/j.clon.2005.11.004

329. Nakamura H, Maeda H. Cancer Chemotherapy. In: Uchegbu IF, Schätzlein AG, Cheng WP, Lalatsa A, editors. Fundamentals of Pharmaceutical Nanoscience [Internet]. New York, NY: Springer New York; 2013 [cited 2025 Dec 29]. p. 401–27. Available from: https://link.springer.com/10.1007/978-1-4614-9164-4_15 doi:10.1007/978-1-4614-9164-4_15

330. Behranvand N, Nasri F, Zolfaghari Emameh R, Khani P, Hosseini A, Garssen J, et al. Chemotherapy: a double-edged sword in cancer treatment. Cancer Immunol Immunother. 2022 Mar;71(3):507–26. doi:10.1007/s00262-021-03013-3

331. Zhang X, Li H, Wu F, Sun D, Zhang H, Jin L, et al. Neoadjuvant Chemotherapy Combined with Breast-Conserving Surgery in the Treatment of Triple-Negative Breast Cancer. Wu X, editor. Journal of Oncology. 2022 May 26;2022:1–6. doi:10.1155/2022/7847889

332. Li S, Ma D, Shi HH, Yu KD, Zhang Q. The effect of delayed adjuvant chemotherapy on relapse of triple-negative breast cancer. J Thorac Dis. 2018 May;10(5):2837–41. doi:10.21037/jtd.2018.04.94

333. Nakatsukasa K, Koyama H, Oouchi Y, Imanishi S, Mizuta N, Sakaguchi K, et al. Docetaxel and cyclophosphamide as neoadjuvant chemotherapy in HER2-negative primary breast cancer. Breast Cancer. 2017 Jan;24(1):63–8. doi:10.1007/s12282-016-0666-7

334. Mai N, Myers S, Shen S, Downs-Canner S, Robson M, Norton L, et al. Dose dense doxorubicin plus cyclophosphamide in a modified KEYNOTE522 regimen for triple negative breast cancer. npj Breast Cancer. 2024 Jun 4;10(1):39. doi:10.1038/s41523-024-00643-5

335. Yagata H, Kajiura Y, Yamauchi H. Current strategy for triple-negative breast cancer: appropriate combination of surgery, radiation, and chemotherapy. Breast Cancer. 2011 Jul;18(3):165–73. doi:10.1007/s12282-011-0254-9

336. Ge J, Zuo W, Chen Y, Shao Z, Yu K. The advance of adjuvant treatment for triple-negative breast cancer. Cancer Biol Med. 2021;18:0–0. doi:10.20892/j.issn.2095-3941.2020.0752

337. Han HS, Vikas P, Costa RLB, Jahan N, Taye A, Stringer-Reasor EM. Early-Stage Triple-Negative Breast Cancer Journey: Beginning, End, and Everything in Between. American Society of Clinical Oncology Educational Book. 2023 Jun;(43):e390464. doi:10.1200/EDBK_390464

338. Schmid P, Cortes J, Dent R, Pusztai L, McArthur H, Kümmel S, et al. Event-free Survival with Pembrolizumab in Early Triple-Negative Breast Cancer. N Engl J Med. 2022 Feb 10;386(6):556–67. doi:10.1056/NEJMoa2112651

339. Rayner DM, Cutts SM. Anthracyclines. In: Side Effects of Drugs Annual [Internet]. Elsevier; 2014 [cited 2025 Dec 29]. p. 683–94. Available from: https://linkinghub.elsevier.com/retrieve/pii/B9780444634078000459 doi:10.1016/B978-0-444-63407-8.00045-9

340. da Costa R, Passos GF, Quintão NLM, Fernandes ES, Maia JRLCB, Campos MM, et al. Taxane-induced neurotoxicity: Pathophysiology and therapeutic perspectives. Br J Pharmacol. 2020 Jul;177(14):3127–46. doi:10.1111/bph.15086 PubMed PMID: 32352155; PubMed Central PMCID: PMC7312267.

341. Stork CM, Schreffler SM. Cyclophosphamide. In: Encyclopedia of Toxicology [Internet]. Elsevier; 2014 [cited 2025 Dec 29]. p. 1111–3. Available from: https://linkinghub.elsevier.com/retrieve/pii/B978012386454300720X doi:10.1016/B978-0-12-386454-3.00720-X

342. Bardal SK, Waechter JE, Martin DS. Neoplasia. In: Applied Pharmacology [Internet]. Elsevier; 2011 [cited 2025 Dec 29]. p. 305–24. Available from: https://linkinghub.elsevier.com/retrieve/pii/B9781437703108000208 doi:10.1016/B978-1-4377-0310-8.00020-8

343. Cardinale D, Iacopo F, Cipolla CM. Cardiotoxicity of Anthracyclines. Front Cardiovasc Med. 2020 Mar 18;7:26. doi:10.3389/fcvm.2020.00026

344. Martins-Teixeira MB, Carvalho I. Antitumour Anthracyclines: Progress and Perspectives. ChemMedChem. 2020 Jun 4;15(11):933–48. doi:10.1002/cmdc.202000131

345. Ismail U, Killeen RB. Taxane Toxicity. In: StatPearls [Internet]. Treasure Island (FL): StatPearls Publishing; 2025 [cited 2025 Dec 29]. Available from: http://www.ncbi.nlm.nih.gov/books/NBK589655/ PubMed PMID: 36943973.

346. Oun R, Moussa YE, Wheate NJ. The side effects of platinum-based chemotherapy drugs: a review for chemists. Dalton Trans. 2018;47(19):6645–53. doi:10.1039/C8DT00838H

347. Ahmed AR, Hombal SM. Cyclophosphamide (Cytoxan). A review on relevant pharmacology and clinical uses. J Am Acad Dermatol. 1984 Dec;11(6):1115–26. doi:10.1016/s0190-9622(84)80193-0 PubMed PMID: 6392368.

348. Chen RJ, Arora RD, Menezes RG. Vinca Alkaloid Toxicity. In: StatPearls [Internet]. Treasure Island (FL): StatPearls Publishing; 2025 [cited 2025 Dec 29]. Available from: http://www.ncbi.nlm.nih.gov/books/NBK557842/ PubMed PMID: 32491774.

349. Townsend D. Vinorelbine. In: xPharm: The Comprehensive Pharmacology Reference [Internet]. Elsevier; 2007 [cited 2025 Dec 29]. p. 1–4. Available from:

https://linkinghub.elsevier.com/retrieve/pii/B9780080552323628557 doi:10.1016/B978-008055232-3.62855-7

350. Maggiore U, Palmisano A, Buti S, Claire Giudice G, Cattaneo D, Giuliani N, et al. Chemotherapy, targeted therapy and immunotherapy: Which drugs can be safely used in the solid organ transplant recipients? Transplant International. 2021 Dec;34(12):2442–58. doi:10.1111/tri.14115

351. Boussios S, Pentheroudakis G, Katsanos K, Pavlidis N. Systemic treatment-induced gastrointestinal toxicity: incidence, clinical presentation and management. Ann Gastroenterol. 2012;25(2):106–18. PubMed PMID: 24713845; PubMed Central PMCID: PMC3959393.

352. Wang Y. Clinical effectiveness and safety of gemcitabine plus capecitabine in the treatment of advanced triple-negative breast cancer. Am J Transl Res. 2024;16(5):1945–52. doi:10.62347/QOWN3646

353. Pizzuti L, Krasniqi E, Barchiesi G, Mazzotta M, Barba M, Amodio A, et al. Eribulin in Triple Negative Metastatic Breast Cancer: Critic Interpretation of Current Evidence and Projection for Future Scenarios. J Cancer. 2019;10(24):5903–14. doi:10.7150/jca.35109

354. Al Sukhun S, Temin S, Barrios CH, Antone NZ, Guerra YC, Chavez-MacGregor M, et al. Systemic Treatment of Patients With Metastatic Breast Cancer: ASCO Resource–Stratified Guideline. JCO Glob Oncol. 2024 Sep;(10):e2300285. doi:10.1200/GO.23.00285

355. Treatment of Triple-negative Breast Cancer | Treatment of TNBC [Internet]. [cited 2026 Jun 1]. Available from: https://www.cancer.org/cancer/types/breast-cancer/treatment/treatment-of-triple-negative.html

356. García-Saenz JÁ, Rodríguez-Lescure Á, Cruz J, Albanell J, Alba E, Llombart A. Second-Line Treatment Options for Patients with Metastatic Triple-Negative Breast Cancer: A Review of the Clinical Evidence. Targ Oncol. 2025 Mar;20(2):191–213. doi:10.1007/s11523-024-01125-1

357. Alaklabi S, Roy AM, Chaudhary LN, Gandhi S. Facing the conundrum: which first-line therapy should be used for patients with metastatic triple-negative breast cancer carrying germline BRCA mutation? Exploration of Targeted Anti-tumor Therapy. 2023 Dec 27;4(6):1301–9. doi:10.37349/etat.2023.00198

358. Ma T, Hao X meng, Chen H dan, Zheng M hui, Chen X geng, Cai SL, et al. Predictive markers of rapid disease progression and chemotherapy resistance in triple-negative breast cancer patients following postoperative adjuvant therapy. Sci Rep. 2025 Jan 2;15(1):386. doi:10.1038/s41598-024-84785-3

359. Li Y, Zhang H, Merkher Y, Chen L, Liu N, Leonov S, et al. Recent advances in therapeutic strategies for triple-negative breast cancer. J Hematol Oncol. 2022 Aug 29;15(1):121. doi:10.1186/s13045-022-01341-0

360. Zheng YZ, Ying JQ, Wu TT, Su YH, Wang OC. Comparative survival outcomes of neoadjuvant and adjuvant therapy in patients with T1c, node-negative, triple-negative

breast cancer: A population-based analysis. The Breast. 2025 Feb;79:103877. doi:10.1016/j.breast.2025.103877

361. Li Q, Lei X, Zhu J, Zhong Y, Yang J, Wang J, et al. Radiotherapy/Chemotherapy-Immunotherapy for Cancer Management: From Mechanisms to Clinical Implications. Tong Q, editor. Oxidative Medicine and Cellular Longevity. 2023 Feb 2;2023:1–9. doi:10.1155/2023/7530794

362. Chan WY, Brown LJ, Reid L, Joshua AM. PARP Inhibitors in Melanoma—An Expanding Therapeutic Option? Cancers. 2021 Sep 8;13(18):4520. doi:10.3390/cancers13184520

363. Rose M, Burgess JT, O'Byrne K, Richard DJ, Bolderson E. PARP Inhibitors: Clinical Relevance, Mechanisms of Action and Tumor Resistance. Front Cell Dev Biol. 2020 Sep 9;8:564601. doi:10.3389/fcell.2020.564601

364. Demir Cetinkaya B, Biray Avci C. Molecular perspective on targeted therapy in breast cancer: a review of current status. Med Oncol. 2022 Jul 14;39(10):149. doi:10.1007/s12032-022-01749-1

365. Xu Y, Song G, Xie S, Jiang W, Chen X, Chu M, et al. The roles of PD-1/PD-L1 in the prognosis and immunotherapy of prostate cancer. Molecular Therapy. 2021 Jun;29(6):1958–69. doi:10.1016/j.ymthe.2021.04.029

366. Yu J, Guo Z, Wang L. Progress and Challenges of Immunotherapy Predictive Biomarkers for Triple Negative Breast Cancer in the Era of Single-Cell Multi-Omics. Life. 2023 May 16;13(5):1189. doi:10.3390/life13051189

367. Pavone G, Motta L, Martorana F, Motta G, Vigneri P. A New Kid on the Block: Sacituzumab Govitecan for the Treatment of Breast Cancer and Other Solid Tumors. Molecules. 2021 Dec 1;26(23):7294. doi:10.3390/molecules26237294

368. Kim D, Nam HJ. PARP Inhibitors: Clinical Limitations and Recent Attempts to Overcome Them. IJMS. 2022 Jul 29;23(15):8412. doi:10.3390/ijms23158412

369. Sachdev E, Tabatabai R, Roy V, Rimel BJ, Mita MM. PARP Inhibition in Cancer: An Update on Clinical Development. Targ Oncol. 2019 Dec;14(6):657–79. doi:10.1007/s11523-019-00680-2

370. Konecny GE, Kristeleit RS. PARP inhibitors for BRCA1/2-mutated and sporadic ovarian cancer: current practice and future directions. Br J Cancer. 2016 Nov;115(10):1157–73. doi:10.1038/bjc.2016.311

371. Ai L, Xu A, Xu J. Roles of PD-1/PD-L1 Pathway: Signaling, Cancer, and Beyond. In: Xu J, editor. Regulation of Cancer Immune Checkpoints [Internet]. Singapore: Springer Singapore; 2020 [cited 2025 Dec 29]. p. 33–59. (Advances in Experimental Medicine and Biology). Available from: http://link.springer.com/10.1007/978-981-15-3266-5_3 doi:10.1007/978-981-15-3266-5_3

372. Shen Y, Rehman FL, Feng Y, Boshuizen J, Bajrami I, Elliott R, et al. BMN 673, a novel and highly potent PARP1/2 inhibitor for the treatment of human cancers with DNA repair

deficiency. Clin Cancer Res. 2013 Sep 15;19(18):5003–15. doi:10.1158/1078-0432.CCR-13-1391 PubMed PMID: 23881923; PubMed Central PMCID: PMC6485449.

373. Litton JK, Rugo HS, Ettl J, Hurvitz SA, Gonçalves A, Lee KH, et al. Talazoparib in Patients with Advanced Breast Cancer and a Germline *BRCA* Mutation. N Engl J Med. 2018 Aug 23;379(8):753–63. doi:10.1056/NEJMoa1802905

374. Robson M, Im SA, Senkus E, Xu B, Domchek SM, Masuda N, et al. Olaparib for Metastatic Breast Cancer in Patients with a Germline *BRCA* Mutation. N Engl J Med. 2017 Aug 10;377(6):523–33. doi:10.1056/NEJMoa1706450

375. Tutt ANJ, Garber JE, Kaufman B, Viale G, Fumagalli D, Rastogi P, et al. Adjuvant Olaparib for Patients with *BRCA1* - or *BRCA2* -Mutated Breast Cancer. N Engl J Med. 2021 Jun 24;384(25):2394–405. doi:10.1056/NEJMoa2105215

376. Litton JK, Hurvitz SA, Mina LA, Rugo HS, Lee KH, Gonçalves A, et al. Talazoparib versus chemotherapy in patients with germline BRCA1/2-mutated HER2-negative advanced breast cancer: final overall survival results from the EMBRACA trial. Annals of Oncology. 2020 Nov;31(11):1526–35. doi:10.1016/j.annonc.2020.08.2098

377. Gruber JJ, Afghahi A, Timms K, DeWees A, Gross W, Aushev VN, et al. A phase II study of talazoparib monotherapy in patients with wild-type BRCA1 and BRCA2 with a mutation in other homologous recombination genes. Nat Cancer. 2022 Oct 17;3(10):1181–91. doi:10.1038/s43018-022-00439-1

378. Lee KH, Sohn J, Goodwin A, Usari T, Lanzalone S, Im SA, et al. Talazoparib Versus Chemotherapy in Patients with HER2-negative Advanced Breast Cancer and a Germline BRCA1/2 Mutation Enrolled in Asian Countries: Exploratory Subgroup Analysis of the Phase III EMBRACA Trial. Cancer Res Treat. 2021 Oct 15;53(4):1084–95. doi:10.4143/crt.2020.1381

379. Senkus E, Delaloge S, Domchek SM, Conte P, Im SA, Xu B, et al. Olaparib efficacy in patients with germline BRCA-mutated, HER2-negative metastatic breast cancer: Subgroup analyses from the phase III OlympiAD trial. Int J Cancer. 2023 Aug 15;153(4):803–14. doi:10.1002/ijc.34525 PubMed PMID: 36971103.

380. Joris S, Denys H, Collignon J, Rasschaert M, T'Kint De Roodenbeke D, Duhoux FP, et al. Efficacy of olaparib in advanced cancers with germline or somatic mutations in BRCA1, BRCA2, CHEK2 and ATM, a Belgian Precision tumor-agnostic phase II study. ESMO Open. 2023 Dec;8(6):102041. doi:10.1016/j.esmoop.2023.102041

381. Szentmartoni G, Mühl D, Csanda R, Szasz AM, Herold Z, Dank M. Predictive Value and Therapeutic Significance of Somatic BRCA Mutation in Solid Tumors. Biomedicines. 2024 Mar 6;12(3):593. doi:10.3390/biomedicines12030593

382. Simon S, Labarriere N. PD-1 expression on tumor-specific T cells: Friend or foe for immunotherapy? OncoImmunology. 2018 Jan 2;7(1):e1364828. doi:10.1080/2162402X.2017.1364828

383. Zheng Y, Fang YC, Li J. PD-L1 expression levels on tumor cells affect their immunosuppressive activity. Oncol Lett. 2019 Nov;18(5):5399–407.

doi:10.3892/ol.2019.10903 PubMed PMID: 31612048; PubMed Central PMCID: PMC6781757.

384. Dong Y, Sun Q, Zhang X. PD-1 and its ligands are important immune checkpoints in cancer. Oncotarget. 2017 Jan 10;8(2):2171–86. doi:10.18632/oncotarget.13895

385. Yang T, Li W, Huang T, Zhou J. Immunotherapy Targeting PD-1/PD-L1 in Early-Stage Triple-Negative Breast Cancer. JPM. 2023 Mar 15;13(3):526. doi:10.3390/jpm13030526

386. Alečković M, Li Z, Zhou N, Qiu X, Lulseged B, Foidart P, et al. Combination Therapies to Improve the Efficacy of Immunotherapy in Triple-negative Breast Cancer. Molecular Cancer Therapeutics. 2023 Nov 1;22(11):1304–18. doi:10.1158/1535-7163.MCT-23-0303

387. Merck's KEYTRUDA® (pembrolizumab) Plus Chemotherapy Showed Statistically Significant Increase in Pathological Complete Response Versus Chemotherapy as Neoadjuvant Therapy in Early-Stage Triple-Negative Breast Cancer (TNBC). Merck.com [Internet]. [cited 2026 Jun 1]. Available from: https://www.merck.com/news/mercks-keytruda-pembrolizumab-plus-chemotherapy-showed-statistically-significant-increase-in-pathological-complete-response-versus-chemotherapy-as-neoadjuvant-therapy-in-early-stage-t/

388. Pelosci A. Event-Free Survival Improvement Noted in KEYNOTE-522 Study for Patients With Triple-Negative Breast Cancer | CancerNetwork [Internet]. 2025 [cited 2025 Dec 29]. Available from: https://www.cancernetwork.com/view/event-free-survival-improvement-noted-in-keynote-522-study-for-patients-with-triple-negative-breast-cancer

389. Staff TAP. FDA Grants Accelerated Approval to Pembrolizumab for Locally Recurrent Unresectable or Metastatic Triple-Negative Breast Cancer [Internet]. [cited 2026 Jun 1]. Available from: https://ascopost.com/news/november-2020/fda-grants-accelerated-approval-to-pembrolizumab-for-locally-recurrent-unresectable-or-metastatic-triple-negative-breast-cancer/

390. Helwick C. KEYNOTE-355 Final Analysis Reveals Survival Benefit With Pembrolizumab in Triple-Negative Breast Cancer [Internet]. [cited 2025 Dec 29]. Available from: https://ascopost.com/issues/december-10-2021/keynote-355-final-analysis-reveals-survival-benefit-with-pembrolizumab-in-triple-negative-breast-cancer/

391. Seymour C. European Commission Approves Pembrolizumab Plus Chemotherapy for High-Risk Early-Stage TNBC | OncLive [Internet]. 2025 [cited 2025 Dec 29]. Available from: https://www.onclive.com/view/european-commission-approves-pembrolizumab-plus-chemotherapy-for-high-risk-early-stage-tnbc

392. Schmid P, Cortés J, Dent R, Pusztai L, McArthur HL, Kuemmel S, et al. KEYNOTE-522: Phase III study of pembrolizumab (pembro) + chemotherapy (chemo) vs placebo (pbo) + chemo as neoadjuvant treatment, followed by pembro vs pbo as adjuvant treatment for early triple-negative breast cancer (TNBC). Annals of Oncology. 2019 Oct;30:v853–4. doi:10.1093/annonc/mdz394.003

393. FDA Approves Merck's KEYTRUDA® (pembrolizumab) in Combination With Chemotherapy for Patients With Locally Recurrent Unresectable or Metastatic Triple-Negative Breast Cancer Whose Tumors Express PD-L1 (CPS ≥10). Merck.com [Internet]. [cited 2026 Jun 1]. Available from: https://www.merck.com/news/fda-approves-mercks-keytruda-pembrolizumab-in-combination-with-chemotherapy-for-patients-with-locally-recurrent-unresectable-or-metastatic-triple-negative-breast-cancer-whose/

394. Immunotherapy Success in TNBC: Key Trial Insights [Internet]. 2025 [cited 2025 Dec 29]. Available from: https://oncodaily.com/oncolibrary/immunotherapy-tnbc-key-trials-overview

395. Franzoi MA, De Azambuja E. Atezolizumab in metastatic triple-negative breast cancer: IMpassion130 and 131 trials - how to explain different results? ESMO Open. 2020;5(6):e001112. doi:10.1136/esmoopen-2020-001112

396. Miles D, Gligorov J, André F, Cameron D, Schneeweiss A, Barrios C, et al. Primary results from IMpassion131, a double-blind, placebo-controlled, randomised phase III trial of first-line paclitaxel with or without atezolizumab for unresectable locally advanced/metastatic triple-negative breast cancer. Annals of Oncology. 2021 Aug;32(8):994–1004. doi:10.1016/j.annonc.2021.05.801

397. Shastry M, Jacob S, Rugo HS, Hamilton E. Antibody-drug conjugates targeting TROP-2: Clinical development in metastatic breast cancer. The Breast. 2022 Dec;66:169–77. doi:10.1016/j.breast.2022.10.007

398. Vidula N, Yau C, Rugo H. Trophoblast Cell Surface Antigen 2 gene (TACSTD2) expression in primary breast cancer. Breast Cancer Res Treat. 2022 Aug;194(3):569–75. doi:10.1007/s10549-022-06660-x

399. Sakach E, Sacks R, Kalinsky K. Trop-2 as a Therapeutic Target in Breast Cancer. Cancers. 2022 Nov 30;14(23):5936. doi:10.3390/cancers14235936

400. Rossi V, Turati A, Rosato A, Carpanese D. Sacituzumab govitecan in triple-negative breast cancer: from bench to bedside, and back. Front Immunol. 2024 Aug 15;15:1447280. doi:10.3389/fimmu.2024.1447280

401. Bardia A, Hurvitz SA, Tolaney SM, Loirat D, Punie K, Oliveira M, et al. Sacituzumab Govitecan in Metastatic Triple-Negative Breast Cancer. N Engl J Med. 2021 Apr 22;384(16):1529–41. doi:10.1056/NEJMoa2028485

402. Bardia A, Rugo HS, Tolaney SM, Loirat D, Punie K, Oliveira M, et al. Final Results From the Randomized Phase III ASCENT Clinical Trial in Metastatic Triple-Negative Breast Cancer and Association of Outcomes by Human Epidermal Growth Factor Receptor 2 and Trophoblast Cell Surface Antigen 2 Expression. JCO. 2024 May 20;42(15):1738–44. doi:10.1200/JCO.23.01409

403. Schreiber AR, O'Bryant CL, Kabos P, Diamond JR. The emergence of targeted therapy for HER2-low triple-negative breast cancer: a review of fam-trastuzumab deruxtecan. Expert Review of Anticancer Therapy. 2023 Oct 3;23(10):1061–9. doi:10.1080/14737140.2023.2257885

404. Kabraji S, Ni J, Sammons S, Li T, Van Swearingen AED, Wang Y, et al. Preclinical and Clinical Efficacy of Trastuzumab Deruxtecan in Breast Cancer Brain Metastases. Clinical Cancer Research. 2023 Jan 4;29(1):174–82. doi:10.1158/1078-0432.CCR-22-1138

405. Yamashita T, Sohn JH, Tokunaga E, Niikura N, Park YH, Lee KS, et al. Trastuzumab deruxtecan versus treatment of physician's choice in previously treated Asian patients with HER2-low unresectable/metastatic breast cancer: subgroup analysis of the DESTINY-Breast04 study. Breast Cancer. 2024 Sep;31(5):858–68. doi:10.1007/s12282-024-01600-7

406. Agelidis A, Ter-Zakarian A, Jaloudi M. Triple-Negative Breast Cancer on the Rise: Breakthroughs and Beyond. BCTT. 2025 Jun;Volume 17:523–9. doi:10.2147/BCTT.S516125

407. Lin CC, Garralda E, Schöffski P, Hong DS, Siu LL, Martin M, et al. A phase 2, multicenter, open-label study of anti-LAG-3 ieramilimab in combination with anti-PD-1 spartalizumab in patients with advanced solid malignancies. Oncoimmunology. 13(1):2290787. doi:10.1080/2162402X.2023.2290787 PubMed PMID: 38170160; PubMed Central PMCID: PMC10761073.

408. Garber HR, Basu S, Jindal S, He Z, Chu K, Raghavendra AS, et al. Durvalumab and tremelimumab before surgery in patients with hormone receptor positive, HER2-negative stage II–III breast cancer. Oncotarget. 2024 Mar 19;15:238–47. doi:10.18632/oncotarget.28567 PubMed PMID: 38502947; PubMed Central PMCID: PMC10950364.

409. Bai X, Ni J, Beretov J, Graham P, Li Y. Immunotherapy for triple-negative breast cancer: A molecular insight into the microenvironment, treatment, and resistance. J Natl Cancer Cent. 2021 Jul 6;1(3):75–87. doi:10.1016/j.jncc.2021.06.001 PubMed PMID: 39036372; PubMed Central PMCID: PMC11256541.

410. Emara HM, Allam NK, Youness RA. A comprehensive review on targeted therapies for triple negative breast cancer: an evidence-based treatment guideline. Discov Oncol. 2025 Apr 17;16(1):547. doi:10.1007/s12672-025-02227-6 PubMed PMID: 40244488; PubMed Central PMCID: PMC12006628.

411. Damodaran C, Cho JY, Güngör C. Therapeutic resistance and combination therapy for cancer: recent developments and future directions. Sci Rep. 2025 Jul 24;15(1):26881, s41598-025-12725-w. doi:10.1038/s41598-025-12725-w

412. Hassan A, Aubel C. The PI3K/Akt/mTOR Signaling Pathway in Triple-Negative Breast Cancer: A Resistance Pathway and a Prime Target for Targeted Therapies. Cancers. 2025 Jul 2;17(13). doi:10.3390/cancers17132232

413. He J, McLaughlin RP, Van Der Noord V, Foekens JA, Martens JWM, Van Westen G, et al. Multi-targeted kinase inhibition alleviates mTOR inhibitor resistance in triple-negative breast cancer. Breast Cancer Res Treat. 2019 Nov;178(2):263–74. doi:10.1007/s10549-019-05380-z

414. Xiao H, Wang A, Shuai W, Qian Y, Wu C, Wang X, et al. A first-in-class selective inhibitor of ERK1/2 and ERK5 overcomes drug resistance with a single-molecule

strategy. Sig Transduct Target Ther. 2025 Feb 20;10(1):70. doi:10.1038/s41392-025-02169-z

415. De Nonneville A, Goncalves A, Mamessier E, Bertucci F. Sacituzumab govitecan in triple-negative breast cancer. Ann Transl Med. 2022 Jun;10(11):647–647. doi:10.21037/atm-22-813

416. Chen Y, Xu Y, Shao Z, Yu K. Resistance to antibody-drug conjugates in breast cancer: mechanisms and solutions. Cancer Communications. 2023 Mar;43(3):297–337. doi:10.1002/cac2.12387

417. Sabit H, Adel A, Abdelfattah MM, Ramadan RM, Nazih M, Abdel-Ghany S, et al. The role of tumor microenvironment and immune cell crosstalk in triple-negative breast cancer (TNBC): Emerging therapeutic opportunities. Cancer Lett. 2025 Sep 28;628:217865. doi:10.1016/j.canlet.2025.217865 PubMed PMID: 40516902.

418. Yi H, Li Y, Tan Y, Fu S, Tang F, Deng X. Immune Checkpoint Inhibition for Triple-Negative Breast Cancer: Current Landscape and Future Perspectives. Front Oncol. 2021 May 19;11:648139. doi:10.3389/fonc.2021.648139

419. Zheng Y, Li S, Tang H, Meng X, Zheng Q. Molecular mechanisms of immunotherapy resistance in triple-negative breast cancer. Front Immunol. 2023 Jun 23;14:1153990. doi:10.3389/fimmu.2023.1153990

420. Mahendran G, Shangaradas AD, Romero-Moreno R, Wickramarachchige Dona N, Sarasija SHGS, Perera S, et al. Unlocking the epigenetic code: new insights into triple-negative breast cancer. Front Oncol. 2024 Dec 18;14:1499950. doi:10.3389/fonc.2024.1499950

421. Singh DD, Parveen A, Yadav DK. Role of PARP in TNBC: Mechanism of Inhibition, Clinical Applications, and Resistance. Biomedicines. 2021 Oct 21;9(11):1512. doi:10.3390/biomedicines9111512

422. Garg P, Malhotra J, Kulkarni P, Horne D, Salgia R, Singhal SS. Emerging Therapeutic Strategies to Overcome Drug Resistance in Cancer Cells. Cancers. 2024 Jul 7;16(13):2478. doi:10.3390/cancers16132478

423. Jain A, Barge A, Parris CN. Combination strategies with PARP inhibitors in BRCA-mutated triple-negative breast cancer: overcoming resistance mechanisms. Oncogene. 2025 Feb 10;44(4):193–207. doi:10.1038/s41388-024-03227-6

424. He Y, Sun MM, Zhang GG, Yang J, Chen KS, Xu WW, et al. Targeting PI3K/Akt signal transduction for cancer therapy. Sig Transduct Target Ther. 2021 Dec 16;6(1):425. doi:10.1038/s41392-021-00828-5

425. Sun K, Luo J, Guo J, Yao X, Jing X, Guo F. The PI3K/AKT/mTOR signaling pathway in osteoarthritis: a narrative review. Osteoarthritis and Cartilage. 2020 Apr;28(4):400–9. doi:10.1016/j.joca.2020.02.027

426. Shi X, Wang J, Lei Y, Cong C, Tan D, Zhou X. Research progress on the PI3K/AKT signaling pathway in gynecological cancer (Review). Mol Med Report. 2019 Apr 3. doi:10.3892/mmr.2019.10121

427. Yang J, Nie J, Ma X, Wei Y, Peng Y, Wei X. Targeting PI3K in cancer: mechanisms and advances in clinical trials. Mol Cancer. 2019 Dec;18(1):26. doi:10.1186/s12943-019-0954-x

428. Vidal S, Bouzaher YH, El Motiam A, Seoane R, Rivas C. Overview of the regulation of the class IA PI3K/AKT pathway by SUMO. Seminars in Cell & Developmental Biology. 2022 Dec;132:51–61. doi:10.1016/j.semcdb.2021.10.012

429. Shymanets A, Prajwal, Bucher K, Beer-Hammer S, Harteneck C, Nürnberg B. p87 and p101 Subunits Are Distinct Regulators Determining Class IB Phosphoinositide 3-Kinase (PI3K) Specificity. Journal of Biological Chemistry. 2013 Oct;288(43):31059–68. doi:10.1074/jbc.M113.508234

430. Desale SE, Chidambaram H, Chinnathambi S. G-protein coupled receptor, PI3K and Rho signaling pathways regulate the cascades of Tau and amyloid-β in Alzheimer's disease. Mol Biomed. 2021 Dec;2(1):17. doi:10.1186/s43556-021-00036-1

431. Asati V, Mahapatra DK, Bharti SK. PI3K/Akt/mTOR and Ras/Raf/MEK/ERK signaling pathways inhibitors as anticancer agents: Structural and pharmacological perspectives. European Journal of Medicinal Chemistry. 2016 Feb;109:314–41. doi:10.1016/j.ejmech.2016.01.012

432. Campa CC, Ciraolo E, Ghigo A, Germena G, Hirsch E. Crossroads of PI3K and Rac pathways. Small GTPases. 2015 Apr 3;6(2):71–80. doi:10.4161/21541248.2014.989789

433. Krygowska AA, Castellano E. PI3K: A Crucial Piece in the RAS Signaling Puzzle. Cold Spring Harb Perspect Med. 2018 Jun;8(6):a031450. doi:10.1101/cshperspect.a031450

434. Chalhoub N, Baker SJ. PTEN and the PI3-Kinase Pathway in Cancer. Annu Rev Pathol Mech Dis. 2009 Feb 1;4(1):127–50. doi:10.1146/annurev.pathol.4.110807.092311

435. Lien EC, Dibble CC, Toker A. PI3K signaling in cancer: beyond AKT. Current Opinion in Cell Biology. 2017 Apr;45:62–71. doi:10.1016/j.ceb.2017.02.007

436. Gao X, Lowry PR, Zhou X, Depry C, Wei Z, Wong GW, et al. PI3K/Akt signaling requires spatial compartmentalization in plasma membrane microdomains. Proc Natl Acad Sci USA. 2011 Aug 30;108(35):14509–14. doi:10.1073/pnas.1019386108

437. Chadha R, Meador-Woodruff JH. Downregulated AKT-mTOR signaling pathway proteins in dorsolateral prefrontal cortex in Schizophrenia. Neuropsychopharmacol. 2020 May;45(6):1059–67. doi:10.1038/s41386-020-0614-2

438. Lin J, Fang Y, Zhang M, Wang X, Li L, He M, et al. Phosphorylation of PRAS40 contributes to the activation of the PI3K/AKT/mTOR signaling pathway and the inhibition of autophagy following status epilepticus in rats. Exp Ther Med. 2020 Jul 31. doi:10.3892/etm.2020.9085

439. Porta C, Paglino C, Mosca A. Targeting PI3K/Akt/mTOR Signaling in Cancer. Front Oncol. 2014 Apr 14;4. doi:10.3389/fonc.2014.00064

440. Huang J, Manning BD. A complex interplay between Akt, TSC2 and the two mTOR complexes. Biochemical Society Transactions. 2009 Feb 1;37(1):217–22. doi:10.1042/BST0370217

441. Mendoza MC, Er EE, Blenis J. The Ras-ERK and PI3K-mTOR pathways: cross-talk and compensation. Trends in Biochemical Sciences. 2011 Jun;36(6):320–8. doi:10.1016/j.tibs.2011.03.006

442. Fu W, Hall MN. Regulation of mTORC2 Signaling. Genes. 2020 Sep 4;11(9):1045. doi:10.3390/genes11091045

443. Nitulescu G, Van De Venter M, Nitulescu G, Ungurianu A, Juzenas P, Peng Q, et al. The Akt pathway in oncology therapy and beyond (Review). Int J Oncol. 2018 Oct 16. doi:10.3892/ijo.2018.4597

444. Chibaya L, Karim B, Zhang H, Jones SN. Mdm2 phosphorylation by Akt regulates the p53 response to oxidative stress to promote cell proliferation and tumorigenesis. Proc Natl Acad Sci USA. 2021 Jan 26;118(4):e2003193118. doi:10.1073/pnas.2003193118

445. Wang L, Li J, Di L. Glycogen synthesis and beyond, a comprehensive review of GSK3 as a key regulator of metabolic pathways and a therapeutic target for treating metabolic diseases. Medicinal Research Reviews. 2022 Mar;42(2):946–82. doi:10.1002/med.21867

446. Li J, Cho YY, Langfald A, Carper A, Lubet RA, Grubbs CJ, et al. Lapatinib, a Preventive/Therapeutic Agent against Mammary Cancer, Suppresses RTK-Mediated Signaling through Multiple Signaling Pathways. Cancer Prevention Research. 2011 Aug 1;4(8):1190–7. doi:10.1158/1940-6207.CAPR-10-0330

447. Kazi A, Xiang S, Yang H, Delitto D, Trevino J, Jiang RHY, et al. GSK3 suppression upregulates β-catenin and c-Myc to abrogate KRas-dependent tumors. Nat Commun. 2018 Dec 4;9(1):5154. doi:10.1038/s41467-018-07644-6

448. Kim AH, Khursigara G, Sun X, Franke TF, Chao MV. Akt Phosphorylates and Negatively Regulates Apoptosis Signal-Regulating Kinase 1. Mol Cell Biol. 2001 Feb;21(3):893–901. doi:10.1128/MCB.21.3.893-901.2001

449. Brown AK, Webb AE. Regulation of FOXO Factors in Mammalian Cells. In: Current Topics in Developmental Biology [Internet]. Elsevier; 2018 [cited 2025 Dec 29]. p. 165–92. Available from: https://linkinghub.elsevier.com/retrieve/pii/S0070215317300558 doi:10.1016/bs.ctdb.2017.10.006

450. Fruman DA, Chiu H, Hopkins BD, Bagrodia S, Cantley LC, Abraham RT. The PI3K Pathway in Human Disease. Cell. 2017 Aug;170(4):605–35. doi:10.1016/j.cell.2017.07.029

451. Jiang W, Ji M. Receptor tyrosine kinases in PI3K signaling: The therapeutic targets in cancer. Seminars in Cancer Biology. 2019 Dec;59:3–22. doi:10.1016/j.semcancer.2019.03.006

452. Mukohara T. PI3K mutations in breast cancer: prognostic and therapeutic implications. BCTT. 2015 May;111. doi:10.2147/BCTT.S60696

453. Reinhardt K, Stückrath K, Hartung C, Kaufhold S, Uleer C, Hanf V, et al. PIK3CA-mutations in breast cancer. Breast Cancer Res Treat. 2022 Dec;196(3):483–93. doi:10.1007/s10549-022-06637-w

454. Wilhoit, PharmD T, M. Patrick, PharmD, Bcop J, B. May, PharmD, Bcop M. Alpelisib: A Novel Therapy for Patients With PIK3CA-Mutated Metastatic Breast Cancer. JADPRO. 2020 Sep 1;11(7). doi:10.6004/jadpro.2020.11.7.9

455. Ligresti G, Militello L, Steelman LS, Cavallaro A, Basile F, Nicoletti F, et al. PIK3CA mutations in human solid tumors: Role in sensitivity to various therapeutic approaches. Cell Cycle. 2009 May;8(9):1352–8. doi:10.4161/cc.8.9.8255

456. Shimoi T, Hamada A, Yamagishi M, Hirai M, Yoshida M, Nishikawa T, et al. PIK3CA mutation profiling in patients with breast cancer, using a highly sensitive detection system. Cancer Sci. 2018 Aug;109(8):2558–66. doi:10.1111/cas.13696 PubMed PMID: 29906308; PubMed Central PMCID: PMC6113507.

457. De Mattos-Arruda L. PIK3CA mutation inhibition in hormone receptor-positive breast cancer: time has come. ESMO Open. 2020;5(4):e000890. doi:10.1136/esmoopen-2020-000890

458. André F, Ciruelos E, Rubovszky G, Campone M, Loibl S, Rugo HS, et al. Alpelisib for *PIK3CA* -Mutated, Hormone Receptor–Positive Advanced Breast Cancer. N Engl J Med. 2019 May 16;380(20):1929–40. doi:10.1056/NEJMoa1813904

459. Savas P, Lo LL, Luen SJ, Blackley EF, Callahan J, Moodie K, et al. Alpelisib Monotherapy for PI3K-Altered, Pretreated Advanced Breast Cancer: A Phase II Study. Cancer Discovery. 2022 Sep 2;12(9):2058–73. doi:10.1158/2159-8290.CD-21-1696

460. Batalini F, Xiong N, Tayob N, Polak M, Eismann J, Cantley LC, et al. Phase 1b Clinical Trial with Alpelisib plus Olaparib for Patients with Advanced Triple-Negative Breast Cancer. Clinical Cancer Research. 2022 Apr 14;28(8):1493–9. doi:10.1158/1078-0432.CCR-21-3045

461. Tao JJ, Sisoudiya SD, Tukachinsky H, Schrock A, Sivakumar S, Sokol ES, et al. Clinicogenomic landscape and function of *PIK3CA* , *AKT1* , and *PTEN* mutations in breast cancer [Internet]. Oncology; 2025 [cited 2025 Dec 29]. Available from: http://medrxiv.org/lookup/doi/10.1101/2025.06.18.25329632 doi:10.1101/2025.06.18.25329632

462. Gremke N, Besong I, Stroh A, Von Wichert L, Witt M, Elmshäuser S, et al. Targeting PI3K inhibitor resistance in breast cancer with metabolic drugs. Sig Transduct Target Ther. 2025 Mar 21;10(1):92. doi:10.1038/s41392-025-02180-4

463. Wright SCE, Vasilevski N, Serra V, Rodon J, Eichhorn PJA. Mechanisms of Resistance to PI3K Inhibitors in Cancer: Adaptive Responses, Drug Tolerance and Cellular Plasticity. Cancers. 2021 Mar 26;13(7):1538. doi:10.3390/cancers13071538

464. Yang JM, Nguyen HN, Sesaki H, Devreotes PN, Iijima M. Engineering PTEN function: Membrane association and activity. Methods. 2015 May;77–78:119–24. doi:10.1016/j.ymeth.2014.10.018

465. Vo TTT, Fruman DA. INPP4B Is a Tumor Suppressor in the Context of PTEN Deficiency. Cancer Discovery. 2015 Jul 1;5(7):697–700. doi:10.1158/2159-8290.CD-15-0609

466. Yehia L, Keel E, Eng C. The Clinical Spectrum of *PTEN* Mutations. Annu Rev Med. 2020 Jan 27;71(1):103–16. doi:10.1146/annurev-med-052218-125823

467. Stjernström A, Karlsson C, Fernandez OJ, Söderkvist P, Karlsson MG, Thunell LK. Alterations of INPP4B, PIK3CA and pAkt of the PI3K pathway are associated with squamous cell carcinoma of the lung. Cancer Medicine. 2014 Apr;3(2):337–48. doi:10.1002/cam4.191

468. Rodgers SJ, Ooms LM, Oorschot VMJ, Schittenhelm RB, Nguyen EV, Hamila SA, et al. INPP4B promotes PI3Kα-dependent late endosome formation and Wnt/β-catenin signaling in breast cancer. Nat Commun. 2021 May 25;12(1):3140. doi:10.1038/s41467-021-23241-6

469. Recher C. INPP4B, a new player in the chemoresistance of AML. Blood. 2015 Apr 30;125(18):2738–9. doi:10.1182/blood-2015-03-633669

470. Dzneladze I, He R, Woolley JF, Son MH, Sharobim MH, Greenberg SA, et al. INPP4B overexpression is associated with poor clinical outcome and therapy resistance in acute myeloid leukemia. Leukemia. 2015 Jul;29(7):1485–95. doi:10.1038/leu.2015.51

471. Tserga A, Chatziandreou I, Michalopoulos NV, Patsouris E, Saetta AA. Mutation of genes of the PI3K/AKT pathway in breast cancer supports their potential importance as biomarker for breast cancer aggressiveness. Virchows Arch. 2016 Jul;469(1):35–43. doi:10.1007/s00428-016-1938-5

472. Liu H, Paddock MN, Wang H, Murphy CJ, Geck RC, Navarro AJ, et al. The INPP4B Tumor Suppressor Modulates EGFR Trafficking and Promotes Triple-Negative Breast Cancer. Cancer Discovery. 2020 Aug 1;10(8):1226–39. doi:10.1158/2159-8290.CD-19-1262

473. Bae H, Viennet T, Park E, Chu N, Salguero A, Eck MJ, et al. PH domain-mediated autoinhibition and oncogenic activation of Akt. Elife. 2022 Aug 15;11:e80148. doi:10.7554/eLife.80148 PubMed PMID: 35968932; PubMed Central PMCID: PMC9417420.

474. Turner NC, Oliveira M, Howell SJ, Dalenc F, Cortes J, Gomez Moreno HL, et al. Capivasertib in Hormone Receptor–Positive Advanced Breast Cancer. N Engl J Med. 2023 Jun;388(22):2058–70. doi:10.1056/NEJMoa2214131

475. Feroz W, Sheikh AMA. Exploring the multiple roles of guardian of the genome: P53. Egypt J Med Hum Genet. 2020 Dec;21(1):49. doi:10.1186/s43042-020-00089-x

476. Kato S, Han SY, Liu W, Otsuka K, Shibata H, Kanamaru R, et al. Understanding the function–structure and function–mutation relationships of p53 tumor suppressor protein by high-resolution missense mutation analysis. Proc Natl Acad Sci USA. 2003 Jul 8;100(14):8424–9. doi:10.1073/pnas.1431692100

477. Zhang Y, Wang J, Yuan Y, Zhang W, Guan W, Wu Z, et al. Negative regulation of HDM2 to attenuate p53 degradation by ribosomal protein L26. Nucleic Acids Research. 2010 Oct 1;38(19):6544–54. doi:10.1093/nar/gkq536

478. Stambolic V, MacPherson D, Sas D, Lin Y, Snow B, Jang Y, et al. Regulation of PTEN transcription by p53. Mol Cell. 2001 Aug;8(2):317–25. doi:10.1016/s1097-2765(01)00323-9 PubMed PMID: 11545734.

479. Mayo LD, Dixon JE, Durden DL, Tonks NK, Donner DB. PTEN Protects p53 from Mdm2 and Sensitizes Cancer Cells to Chemotherapy. Journal of Biological Chemistry. 2002 Feb;277(7):5484–9. doi:10.1074/jbc.M108302200

480. Zhao K, Zhou Y, Qiao C, Ni T, Li Z, Wang X, et al. Oroxylin A promotes PTEN-mediated negative regulation of MDM2 transcription via SIRT3-mediated deacetylation to stabilize p53 and inhibit glycolysis in wt-p53 cancer cells. J Hematol Oncol. 2015 Dec;8(1):41. doi:10.1186/s13045-015-0137-1

481. Lee C, Kim JS, Waldman T. Activated PI3K Signaling as an Endogenous Inducer of p53 in Human Cancer. Cell Cycle. 2007 Feb 15;6(4):394–6. doi:10.4161/cc.6.4.3810

482. Singh B, Reddy PG, Goberdhan A, Walsh C, Dao S, Ngai I, et al. p53 regulates cell survival by inhibiting PIK3CA in squamous cell carcinomas. Genes Dev. 2002 Apr 15;16(8):984–93. doi:10.1101/gad.973602

483. Shahbandi A, Nguyen HD, Jackson JG. TP53 Mutations and Outcomes in Breast Cancer: Reading beyond the Headlines. Trends in Cancer. 2020 Feb;6(2):98–110. doi:10.1016/j.trecan.2020.01.007

484. Astanehe A, Arenillas D, Wasserman WW, Leung PCK, Dunn SE, Davies BR, et al. Mechanisms underlying p53 regulation of PIK3CA transcription in ovarian surface epithelium and in ovarian cancer. Journal of Cell Science. 2008 Mar 1;121(5):664–74. doi:10.1242/jcs.013029

485. Astanehe A, Arenillas D, Wasserman WW, Leung PCK, Dunn SE, Davies BR, et al. Expression of Concern: Mechanisms underlying p53 regulation of PIK3CA transcription in ovarian surface epithelium and in ovarian cancer. J Cell Sci. 2020 Sep 11;133(17):jcs253260. doi:10.1242/jcs.253260 PubMed PMID: 32917731.

486. Chen SMY, Li B, Nicklawsky AG, Krinsky AL, Brunetti T, Woolaver RA, et al. Deletion of p53 and Hyper-Activation of PIK3CA in Keratin-15+ Stem Cells Lead to the Development of Spontaneous Squamous Cell Carcinoma. IJMS. 2020 Sep 9;21(18):6585. doi:10.3390/ijms21186585

487. Kook Y, Kim K, Jang JS, Baek SH, BAe SJ, Jeong J, et al. Abstract 1412: Co-existence of *TP53* mutation confers endocrine resistance in *PIK3CA* -mutated ER+HER2- breast cancer. Cancer Research. 2023 Apr 4;83(7_Supplement):1412–1412. doi:10.1158/1538-7445.AM2023-1412

488. Li G, Guo X, Chen M, Tang L, Jiang H, Day JX, et al. Prevalence and spectrum of AKT1, PIK3CA, PTEN and TP53 somatic mutations in Chinese breast cancer patients. Galli A, editor. PLoS ONE. 2018 Sep 13;13(9):e0203495. doi:10.1371/journal.pone.0203495

489. Zhang Z, Richmond A. The Role of PI3K Inhibition in the Treatment of Breast Cancer, Alone or Combined With Immune Checkpoint Inhibitors. Front Mol Biosci. 2021 May 7;8:648663. doi:10.3389/fmolb.2021.648663

490. Zhang H ping, Jiang R yuan, Zhu J yu, Sun K na, Huang Y, Zhou H huan, et al. PI3K/AKT/mTOR signaling pathway: an important driver and therapeutic target in triple-negative breast cancer. Breast Cancer. 2024 Jul;31(4):539–51. doi:10.1007/s12282-024-01567-5

491. Kim M, Lee M, Lee A, Choi BO, Park WC, Kim SH, et al. Correlating p53 immunostaining patterns with somatic TP53 mutation and functional properties of mutant p53 in triple-negative breast cancer. Histopathology. 2025 Aug;87(2):299–309. doi:10.1111/his.15453 PubMed PMID: 40162573; PubMed Central PMCID: PMC12232215.

492. Chen H, Ding Q, Khazai L, Zhao L, Damodaran S, Litton JK, et al. PTEN in triple-negative breast carcinoma: protein expression and genomic alteration in pretreatment and posttreatment specimens. Ther Adv Med Oncol. 2023 Jan;15:17588359231189422. doi:10.1177/17588359231189422

493. Kumar S, Bal A, Das A, Loriya I, Khare S, Bhattacharya S, et al. Spectrum of PIK3CA/AKT mutations across molecular subtypes of triple-negative breast cancer. Breast Cancer Res Treat. 2021 Jun;187(3):625–33. doi:10.1007/s10549-021-06242-3

494. Cobleigh MA, Layng KV, Mauer E, Mahon B, Hockenberry AJ, Abukhdeir AM. Comparative genomic analysis of PIK3R1-mutated and wild-type breast cancers. Breast Cancer Res Treat. 2024 Apr;204(2):407–14. doi:10.1007/s10549-023-07196-4

495. Tsay A, Wang JC. The Role of PIK3R1 in Metabolic Function and Insulin Sensitivity. IJMS. 2023 Aug 11;24(16):12665. doi:10.3390/ijms241612665

496. Yu M, Chen J, Xu Z, Yang B, He Q, Luo P, et al. Development and safety of PI3K inhibitors in cancer. Arch Toxicol. 2023 Mar;97(3):635–50. doi:10.1007/s00204-023-03440-4

497. Tarantelli C, Lange M, Gaudio E, Cascione L, Spriano F, Kwee I, et al. Copanlisib synergizes with conventional and targeted agents including venetoclax in B- and T-cell lymphoma models. Blood Advances. 2020 Mar 10;4(5):819–29. doi:10.1182/bloodadvances.2019000844

498. Mishra R, Patel H, Alanazi S, Kilroy MK, Garrett JT. PI3K Inhibitors in Cancer: Clinical Implications and Adverse Effects. IJMS. 2021 Mar 27;22(7):3464. doi:10.3390/ijms22073464

499. Vangapandu HV, Jain N, Gandhi V. Duvelisib: a phosphoinositide-3 kinase δ/γ inhibitor for chronic lymphocytic leukemia. Expert Opinion on Investigational Drugs. 2017 May 4;26(5):625–32. doi:10.1080/13543784.2017.1312338

500. De Vera AA, Reznik SE. Combining PI3K/Akt/mTOR Inhibition With Chemotherapy. In: Protein Kinase Inhibitors as Sensitizing Agents for Chemotherapy [Internet]. Elsevier; 2019 [cited 2025 Dec 29]. p. 229–42. Available from:

https://linkinghub.elsevier.com/retrieve/pii/B9780128164358000146 doi:10.1016/B978-0-12-816435-8.00014-6

501. Mensah F, Blaize JP, Bryan L. Spotlight on copanlisib and its potential in the treatment of relapsed/refractory follicular lymphoma: evidence to date. OTT. 2018 Aug;Volume 11:4817–27. doi:10.2147/OTT.S142264

502. Zinzani PL, Wang H, Feng J, Kim TM, Tao R, Zhang H, et al. CHRONOS-4: phase 3 study of copanlisib plus rituximab-based immunochemotherapy in relapsed indolent B-cell lymphoma. Blood Advances. 2024 Sep 24;8(18):4866–76. doi:10.1182/bloodadvances.2024013236

503. Keegan NM, Furney SJ, Walshe JM, Gullo G, Kennedy MJ, Smith D, et al. Phase Ib Trial of Copanlisib, A Phosphoinositide-3 Kinase (PI3K) Inhibitor, with Trastuzumab in Advanced Pre-Treated HER2-Positive Breast Cancer 'PantHER'. Cancers (Basel). 2021 Mar 11;13(6):1225. doi:10.3390/cancers13061225 PubMed PMID: 33799597; PubMed Central PMCID: PMC7999809.

504. Damodaran S, Zhao F, Deming DA, Mitchell EP, Wright JJ, Gray RJ, et al. Phase II Study of Copanlisib in Patients With Tumors With *PIK3CA* Mutations: Results From the NCI-MATCH ECOG-ACRIN Trial (EAY131) Subprotocol Z1F. JCO. 2022 May 10;40(14):1552–61. doi:10.1200/JCO.21.01648

505. Guo Z, Luo J, Mashl RJ, Hoog J, Maiti P, Fettig N, et al. Evaluation of Copanlisib in Combination with Eribulin in Triple-negative Breast Cancer Patient-derived Xenograft Models. Cancer Research Communications. 2024 Jun 5;4(6):1430–40. doi:10.1158/2767-9764.CRC-24-0047

506. Burguin A, Diorio C, Durocher F. Breast Cancer Treatments: Updates and New Challenges. JPM. 2021 Aug 19;11(8):808. doi:10.3390/jpm11080808

507. Ma CX, Luo J, Naughton M, Ademuyiwa F, Suresh R, Griffith M, et al. A Phase I Trial of BKM120 (Buparlisib) in Combination with Fulvestrant in Postmenopausal Women with Estrogen Receptor–Positive Metastatic Breast Cancer. Clinical Cancer Research. 2016 Apr 1;22(7):1583–91. doi:10.1158/1078-0432.CCR-15-1745

508. Di Leo A, Johnston S, Lee KS, Ciruelos E, Lønning PE, Janni W, et al. Buparlisib plus fulvestrant in postmenopausal women with hormone-receptor-positive, HER2-negative, advanced breast cancer progressing on or after mTOR inhibition (BELLE-3): a randomised, double-blind, placebo-controlled, phase 3 trial. Lancet Oncol. 2018 Jan;19(1):87–100. doi:10.1016/S1470-2045(17)30688-5 PubMed PMID: 29223745.

509. Martín M, Chan A, Dirix L, O'Shaughnessy J, Hegg R, Manikhas A, et al. A randomized adaptive phase II/III study of buparlisib, a pan-class I PI3K inhibitor, combined with paclitaxel for the treatment of HER2- advanced breast cancer (BELLE-4). Ann Oncol. 2017 Feb 1;28(2):313–20. doi:10.1093/annonc/mdw562 PubMed PMID: 27803006.

510. Garrido-Castro AC, Saura C, Barroso-Sousa R, Guo H, Ciruelos E, Bermejo B, et al. Phase 2 study of buparlisib (BKM120), a pan-class I PI3K inhibitor, in patients with metastatic triple-negative breast cancer. Breast Cancer Res. 2020 Dec;22(1):120. doi:10.1186/s13058-020-01354-y

511. Nunnery SE, Mayer IA. Management of toxicity to isoform α-specific PI3K inhibitors. Annals of Oncology. 2019 Dec;30:x21–6. doi:10.1093/annonc/mdz440

512. Nair KS, Cheson B. The role of idelalisib in the treatment of relapsed and refractory chronic lymphocytic leukemia. Therapeutic Advances in Hematology. 2016 Apr;7(2):69–84. doi:10.1177/2040620715625966

513. Danilov AV, Flinn IW, Davids MS, Gregory B, Bentur O, Sidransky D, et al. The phase III DUO trial of PI3K inhibitor duvelisib *versus* ofatumumab in relapsed/refractory chronic lymphocytic leukemia/small lymphocytic lymphoma: final analysis including overall survival. haematol. 2024 May 30;109(10):3379–82. doi:10.3324/haematol.2024.285043

514. Davids MS, Kuss BJ, Hillmen P, Montillo M, Moreno C, Essell J, et al. Efficacy and Safety of Duvelisib Following Disease Progression on Ofatumumab in Patients with Relapsed/Refractory CLL or SLL in the DUO Crossover Extension Study. Clinical Cancer Research. 2020 May 1;26(9):2096–103. doi:10.1158/1078-0432.CCR-19-3061

515. Rosa K. Secura Bio Withdraws Duvelisib Relapsed/Refractory Follicular Lymphoma Indication in the United States | OncLive [Internet]. 2025 [cited 2025 Dec 29]. Available from: https://www.onclive.com/view/secura-bio-withdraws-duvelisib-relapsed-refractory-follicular-lymphoma-indication-in-the-united-states

516. Flinn IW, Miller CB, Ardeshna KM, Tetreault S, Assouline SE, Mayer J, et al. DYNAMO: A Phase II Study of Duvelisib (IPI-145) in Patients With Refractory Indolent Non-Hodgkin Lymphoma. JCO. 2019 Apr 10;37(11):912–22. doi:10.1200/JCO.18.00915

517. Mehta-Shah N, Zinzani PL, Jacobsen ED, Zain J, Mead M, Casulo C, et al. Duvelisib in Patients with Relapsed/Refractory Peripheral T-Cell Lymphoma: Final Results from the Phase 2 PRIMO Trial. Blood. 2024 Nov 5;144(Supplement 1):3061–3061. doi:10.1182/blood-2024-203577

518. Cwynarski K, Domingo Domenech E, Sidransky D, Bentur OS, Zinzani PL. A Multicenter, Open-Label, Phase 3, Randomized Controlled Trial of Duvelisib Versus Investigator's Choice of Gemcitabine or Bendamustine in Patients with Relapsed/Refractory Nodal T Cell Lymphoma with T Follicular Helper Phenotype. Blood. 2024 Nov 5;144(Supplement 1):3074.1. doi:10.1182/blood-2024-203290

519. S. Popovic L, Matovina-Brko G, Popovic M, Punie K, Cvetanovic A, Lambertini M. Targeting triple-negative breast cancer: A clinical perspective. Oncology Research. 2023;31(3):221–38. doi:10.32604/or.2023.028525

520. Hanan EJ, Braun MG, Heald RA, MacLeod C, Chan C, Clausen S, et al. Discovery of GDC-0077 (Inavolisib), a Highly Selective Inhibitor and Degrader of Mutant PI3Kα. J Med Chem. 2022 Dec 22;65(24):16589–621. doi:10.1021/acs.jmedchem.2c01422

521. Gambardella V, Accordino MK, Bedard PL, Cervantes A, Hamilton E, Italiano A, et al. Safety overview and management of inavolisib alone and in combination therapies in PIK3CA-mutated, HR-positive, HER2-negative advanced breast cancer (GO39374). ESMO Open. 2025 Jul;10(7):105303. doi:10.1016/j.esmoop.2025.105303

522. Turner NC, Im SA, Saura C, Juric D, Loibl S, Kalinsky K, et al. Inavolisib-Based Therapy in *PIK3CA* -Mutated Advanced Breast Cancer. N Engl J Med. 2024 Oct 31;391(17):1584–96. doi:10.1056/NEJMoa2404625

523. Blair HA. Inavolisib: First Approval. Drugs. 2025 Feb;85(2):271–8. doi:10.1007/s40265-024-02136-y

524. Dent S, Cortés J, Im YH, Diéras V, Harbeck N, Krop IE, et al. Phase III randomized study of taselisib or placebo with fulvestrant in estrogen receptor-positive, PIK3CA-mutant, HER2-negative, advanced breast cancer: the SANDPIPER trial. Annals of Oncology. 2021 Feb;32(2):197–207. doi:10.1016/j.annonc.2020.10.596

525. Abramson VG, Oliveira M, Cervantes A, Wildiers H, Patel MR, Bauer TM, et al. A phase Ib, open-label, dose-escalation study of the safety and pharmacology of taselisib (GDC-0032) in combination with either docetaxel or paclitaxel in patients with HER2-negative, locally advanced, or metastatic breast cancer. Breast Cancer Res Treat. 2019 Nov;178(1):121–33. doi:10.1007/s10549-019-05360-3

526. Wu X, Xu Y, Liang Q, Yang X, Huang J, Wang J, et al. Recent Advances in Dual PI3K/mTOR Inhibitors for Tumour Treatment. Front Pharmacol. 2022 May 9;13:875372. doi:10.3389/fphar.2022.875372

527. Gedatolisib Doublet, Triplet Regimens Improve PFS in Patients With PIK3CA Wild-Type HR+/HER2– Breast Cancer | Pharmacy Times [Internet]. [cited 2025 Dec 29]. Available from: https://www.pharmacytimes.com/view/gedatolisib-doublet-triplet-regimens-improve-progression-free-survival-in-patients-with-pik3ca-wild-type-hr-her2-breast-cancer

528. Celcuity to Initiate NDA Submission of Gedatolisib in PIK3CA Wild-Type Cohort in HR+/HER2- Advanced Breast Cancer Under FDA's Real-Time Oncology Review Program | FirstWord Pharma [Internet]. [cited 2025 Dec 29]. Available from: https://firstwordpharma.com/story/5992681

529. Capivasertib & Paclitaxel Research Shows Varied Results for mTNBC | FocusOn Oncology [Internet]. [cited 2025 Dec 29]. Available from: https://focusononcology.com/esmo2024/capivasertib-paclitaxel-research-shows-varied-results-for-mtnbc

530. Panwar V, Singh A, Bhatt M, Tonk RK, Azizov S, Raza AS, et al. Multifaceted role of mTOR (mammalian target of rapamycin) signaling pathway in human health and disease. Sig Transduct Target Ther. 2023 Oct 2;8(1):375. doi:10.1038/s41392-023-01608-z

531. Yardley DA, Noguchi S, Pritchard KI, Burris HA, Baselga J, Gnant M, et al. Everolimus Plus Exemestane in Postmenopausal Patients with HR+ Breast Cancer: BOLERO-2 Final Progression-Free Survival Analysis. Adv Ther. 2013 Oct;30(10):870–84. doi:10.1007/s12325-013-0060-1

532. Dong C, Wu J, Chen Y, Nie J, Chen C. Activation of PI3K/AKT/mTOR Pathway Causes Drug Resistance in Breast Cancer. Front Pharmacol. 2021 Mar 15;12:628690. doi:10.3389/fphar.2021.628690

533. Everolimus Plus Adjuvant ET in Shows No Significant iDFS or OS Advantage in HR+/HER2- Breast Cancer | Targeted Oncology - Immunotherapy, Biomarkers, and Cancer Pathways [Internet]. [cited 2025 Dec 29]. Available from: https://www.targetedonc.com/view/everolimus-plus-adjuvant-et-in-shows-no-significant-idfs-or-os-advantage-in-hr-her2--breast-cancer

534. Rugo HS, Tolaney SM, Chan N, Hamilton EP, Sharifi MN, Rinn K, et al. Elacestrant (Ela) combinations with ribociclib (Ribo) and everolimus (Eve) in patients (pts) with ER+/HER2- locally advanced or metastatic breast cancer (mBC): Update from ELEVATE, a phase (Ph) 1b/2, open-label, umbrella study. JCO. 2025 Jun;43(16_suppl):1070–1070. doi:10.1200/JCO.2025.43.16_suppl.1070

535. Jovanović B, Mayer IA, Mayer EL, Abramson VG, Bardia A, Sanders ME, et al. A Randomized Phase II Neoadjuvant Study of Cisplatin, Paclitaxel With or Without Everolimus in Patients with Stage II/III Triple-Negative Breast Cancer (TNBC): Responses and Long-term Outcome Correlated with Increased Frequency of DNA Damage Response Gene Mutations, TNBC Subtype, AR Status, and Ki67. Clin Cancer Res. 2017 Aug 1;23(15):4035–45. doi:10.1158/1078-0432.CCR-16-3055 PubMed PMID: 28270498; PubMed Central PMCID: PMC5540799.

536. Chan S, Scheulen ME, Johnston S, Mross K, Cardoso F, Dittrich C, et al. Phase II Study of Temsirolimus (CCI-779), a Novel Inhibitor of mTOR, in Heavily Pretreated Patients With Locally Advanced or Metastatic Breast Cancer. JCO. 2005 Aug 10;23(23):5314–22. doi:10.1200/JCO.2005.66.130

537. Wolff AC, Lazar AA, Bondarenko I, Garin AM, Brincat S, Chow L, et al. Randomized Phase III Placebo-Controlled Trial of Letrozole Plus Oral Temsirolimus As First-Line Endocrine Therapy in Postmenopausal Women With Locally Advanced or Metastatic Breast Cancer. JCO. 2013 Jan 10;31(2):195–202. doi:10.1200/JCO.2011.38.3331

538. Gandhi L, Bahleda R, Tolaney SM, Kwak EL, Cleary JM, Pandya SS, et al. Phase I study of neratinib in combination with temsirolimus in patients with human epidermal growth factor receptor 2-dependent and other solid tumors. J Clin Oncol. 2014 Jan 10;32(2):68–75. doi:10.1200/JCO.2012.47.2787 PubMed PMID: 24323026.

539. Abuhadra N, Sun R, Bassett RL, Huo L, Chang JT, Teshome M, et al. Targeting chemotherapy resistance in mesenchymal triple-negative breast cancer: a phase II trial of neoadjuvant angiogenic and mTOR inhibition with chemotherapy. Invest New Drugs. 2023 Jun;41(3):391–401. doi:10.1007/s10637-023-01357-4

540. Acevedo-Gadea C, Hatzis C, Chung G, Fishbach N, Lezon-Geyda K, Zelterman D, et al. Sirolimus and trastuzumab combination therapy for HER2-positive metastatic breast cancer after progression on prior trastuzumab therapy. Breast Cancer Res Treat. 2015 Feb;150(1):157–67. doi:10.1007/s10549-015-3292-8

541. Yi Z, Liu B, Sun X, Rong G, Wang W, Li H, et al. Safety and efficacy of sirolimus combined with endocrine therapy in patients with advanced hormone receptor-positive breast cancer and the exploration of biomarkers. The Breast. 2020 Aug;52:17–22. doi:10.1016/j.breast.2020.04.004

542. Zeng Q, Yang Z, Gao YJ, Yuan H, Cui K, Shi Y, et al. Treating triple-negative breast cancer by a combination of rapamycin and cyclophosphamide: An in vivo bioluminescence imaging study. European Journal of Cancer. 2010 Apr;46(6):1132–43. doi:10.1016/j.ejca.2010.01.014

543. Juric D, Castel P, Griffith M, Griffith OL, Won HH, Ellis H, et al. Convergent loss of PTEN leads to clinical resistance to a PI(3)Kα inhibitor. Nature. 2015 Feb 12;518(7538):240–4. doi:10.1038/nature13948

544. Castellano E, Downward J. RAS Interaction with PI3K: More Than Just Another Effector Pathway. Genes & Cancer. 2011 Mar 1;2(3):261–74. doi:10.1177/1947601911408079

545. Hopkins BD, Pauli C, Du X, Wang DG, Li X, Wu D, et al. Suppression of insulin feedback enhances the efficacy of PI3K inhibitors. Nature. 2018 Aug 23;560(7719):499–503. doi:10.1038/s41586-018-0343-4

546. Song KW, Edgar KA, Hanan EJ, Hafner M, Oeh J, Merchant M, et al. RTK-Dependent Inducible Degradation of Mutant PI3Kα Drives GDC-0077 (Inavolisib) Efficacy. Cancer Discovery. 2022 Jan 1;12(1):204–19. doi:10.1158/2159-8290.CD-21-0072

547. Dibble CC, Cantley LC. Regulation of mTORC1 by PI3K signaling. Trends in Cell Biology. 2015 Sep;25(9):545–55. doi:10.1016/j.tcb.2015.06.002

548. Toska E, Castel P, Chhangawala S, Arruabarrena-Aristorena A, Chan C, Hristidis VC, et al. PI3K Inhibition Activates SGK1 via a Feedback Loop to Promote Chromatin-Based Regulation of ER-Dependent Gene Expression. Cell Reports. 2019 Apr;27(1):294-306.e5. doi:10.1016/j.celrep.2019.02.111

549. Zhou J, Du T, Li B, Rong Y, Verkhratsky A, Peng L. Crosstalk Between MAPK/ERK and PI3K/AKT Signal Pathways During Brain Ischemia/Reperfusion. ASN Neuro. 2015 Sep;7(5):1759091415602463. doi:10.1177/1759091415602463

550. Ibanez KR, Huang TT, Lee JM. Combination Therapy Approach to Overcome the Resistance to PI3K Pathway Inhibitors in Gynecological Cancers. Cells. 2024 Jun 19;13(12):1064. doi:10.3390/cells13121064

551. Vitale SR, Martorana F, Stella S, Motta G, Inzerilli N, Massimino M, et al. PI3K inhibition in breast cancer: Identifying and overcoming different flavors of resistance. Critical Reviews in Oncology/Hematology. 2021 Jun;162:103334. doi:10.1016/j.critrevonc.2021.103334

552. Nakanishi Y, Walter K, Spoerke JM, O'Brien C, Huw LY, Hampton GM, et al. Activating Mutations in *PIK3CB* Confer Resistance to PI3K Inhibition and Define a Novel Oncogenic Role for p110β. Cancer Research. 2016 Mar 1;76(5):1193–203. doi:10.1158/0008-5472.CAN-15-2201

553. Coleman N, Subbiah V, Pant S, Patel K, Roy-Chowdhuri S, Yedururi S, et al. Emergence of mTOR mutation as an acquired resistance mechanism to AKT inhibition, and subsequent response to mTORC1/2 inhibition. npj Precis Onc. 2021 Dec 1;5(1):99. doi:10.1038/s41698-021-00240-w

554. Stottrup C, Tsang T, Chin YR. Upregulation of AKT3 Confers Resistance to the AKT Inhibitor MK2206 in Breast Cancer. Molecular Cancer Therapeutics. 2016 Aug 1;15(8):1964–74. doi:10.1158/1535-7163.MCT-15-0748

555. Mele L, Del Vecchio V, Liccardo D, Prisco C, Schwerdtfeger M, Robinson N, et al. The role of autophagy in resistance to targeted therapies. Cancer Treatment Reviews. 2020 Aug;88:102043. doi:10.1016/j.ctrv.2020.102043

556. Locasale JW. Metabolic rewiring drives resistance to targeted cancer therapy. Molecular Systems Biology. 2012 Jan;8(1):597. doi:10.1038/msb.2012.30

557. Polo ML, Riggio M, May M, Rodríguez MJ, Perrone MC, Stallings-Mann M, et al. Activation of PI3K/Akt/mTOR signaling in the tumor stroma drives endocrine therapy-dependent breast tumor regression. Oncotarget. 2015 Sep 9;6(26):22081–97. doi:10.18632/oncotarget.4203

558. Stamatkin C, Ratermann KL, Overley CW, Black EP. Inhibition of class IA PI3K enzymes in non-small cell lung cancer cells uncovers functional compensation among isoforms. Cancer Biology & Therapy. 2015 Sep 2;16(9):1341–52. doi:10.1080/15384047.2015.1070986

559. Marvalim C, Datta A, Lee SC. Role of p53 in breast cancer progression: An insight into p53 targeted therapy. Theranostics. 2023 Feb 27;13(4):1421–42. doi:10.7150/thno.81847 PubMed PMID: 36923534; PubMed Central PMCID: PMC10008729.

560. Papa A, Pandolfi PP. The PTEN–PI3K Axis in Cancer. Biomolecules. 2019 Apr 17;9(4):153. doi:10.3390/biom9040153 PubMed PMID: 30999672; PubMed Central PMCID: PMC6523724.

561. Tang Q, Su Z, Gu W, Rustgi AK. Mutant p53 on the Path to Metastasis. Trends in Cancer. 2020 Jan 1;6(1):62–73. doi:10.1016/j.trecan.2019.11.004

562. Grit JL, McGee LE, Tovar EA, Essenburg CJ, Wolfrum E, Beddows I, et al. p53 modulates kinase inhibitor resistance and lineage plasticity in NF1-related MPNSTs. Oncogene. 2024 May;43(19):1411–30. doi:10.1038/s41388-024-03000-9

563. Bhardwaj PV, Wang Y, Brunk E, Spanheimer PM, Abdou YG. Advances in the Management of Early-Stage Triple-Negative Breast Cancer. International Journal of Molecular Sciences. 2023 Aug 4;24(15). doi:10.3390/ijms241512478

564. Martínez-Sáez O, Chic N, Pascual T, Adamo B, Vidal M, González-Farré B, et al. Frequency and spectrum of PIK3CA somatic mutations in breast cancer. Breast Cancer Res. 2020 May 13;22(1):45. doi:10.1186/s13058-020-01284-9

565. Jiang W, Ji M. Receptor tyrosine kinases in PI3K signaling: The therapeutic targets in cancer. Semin Cancer Biol. 2019 Dec;59:3–22. doi:10.1016/j.semcancer.2019.03.006 PubMed PMID: 30943434.

566. Georgescu MM. PTEN Tumor Suppressor Network in PI3K-Akt Pathway Control. Genes Cancer. 2010 Dec;1(12):1170–7. doi:10.1177/1947601911407325 PubMed PMID: 21779440; PubMed Central PMCID: PMC3092286.

567. Hassan A, Aubel C. The PI3K/Akt/mTOR Signaling Pathway in Triple-Negative Breast Cancer: A Resistance Pathway and a Prime Target for Targeted Therapies. Cancers (Basel). 2025 Jul 3;17(13):2232. doi:10.3390/cancers17132232 PubMed PMID: 40647529; PubMed Central PMCID: PMC12248877.

568. Curtis C, Shah SP, Chin SF, Turashvili G, Rueda OM, Dunning MJ, et al. The genomic and transcriptomic architecture of 2,000 breast tumours reveals novel subgroups. Nature. 2012 Apr 18;486(7403):346–52. doi:10.1038/nature10983 PubMed PMID: 22522925; PubMed Central PMCID: PMC3440846.

569. Pereira B, Chin SF, Rueda OM, Vollan HKM, Provenzano E, Bardwell HA, et al. The somatic mutation profiles of 2,433 breast cancers refines their genomic and transcriptomic landscapes. Nat Commun. 2016 May 10;7:11479. doi:10.1038/ncomms11479 PubMed PMID: 27161491; PubMed Central PMCID: PMC4866047.

570. Yoon S, Won HS, Kang K, Qiu K, Park WJ, Ko YH. Hormone Receptor-Status Prediction in Breast Cancer Using Gene Expression Profiles and Their Macroscopic Landscape. Cancers (Basel). 2020 May 5;12(5):1165. doi:10.3390/cancers12051165 PubMed PMID: 32380759; PubMed Central PMCID: PMC7281553.

571. Weinstein JN, Collisson EA, Mills GB, Shaw KRM, Ozenberger BA, Ellrott K, et al. The Cancer Genome Atlas Pan-Cancer analysis project. Nat Genet. 2013 Oct;45(10):1113–20. doi:10.1038/ng.2764

572. Ellrott K, Bailey MH, Saksena G, Covington KR, Kandoth C, Stewart C, et al. Scalable Open Science Approach for Mutation Calling of Tumor Exomes Using Multiple Genomic Pipelines. Cell Syst. 2018 Mar 28;6(3):271-281.e7. doi:10.1016/j.cels.2018.03.002 PubMed PMID: 29596782; PubMed Central PMCID: PMC6075717.

573. Upton GJG. Fisher's Exact Test. Journal of the Royal Statistical Society Series A (Statistics in Society). 1992;155(3):395–402. doi:10.2307/2982890

574. Efron B, Tibshirani RJ. An Introduction to the Bootstrap. New York: Chapman and Hall/CRC; 1994. 456 p. doi:10.1201/9780429246593

575. Chen SY, Feng Z, Yi X. A general introduction to adjustment for multiple comparisons. J Thorac Dis. 2017 Jun;9(6):1725–9. doi:10.21037/jtd.2017.05.34 PubMed PMID: 28740688; PubMed Central PMCID: PMC5506159.

576. Abeysekera WWM, Sooriyarachchi MR. Use of Schoenfeld's global test to test the proportional hazards assumption in the Cox proportional hazards model: an application to a clinical study. Journal of the National Science Foundation of Sri Lanka. 2009 Mar 29;37(1). doi:10.4038/jnsfsr.v37i1.456

577. Royston P, Parmar MKB. Restricted mean survival time: an alternative to the hazard ratio for the design and analysis of randomized trials with a time-to-event outcome. BMC Med Res Methodol. 2013 Dec 7;13:152. doi:10.1186/1471-2288-13-152 PubMed PMID: 24314264; PubMed Central PMCID: PMC3922847.

578. Wu H, Yuan H, Yang Z, Hou Y, Chen Z. Implementation of an Alternative Method for Assessing Competing Risks: Restricted Mean Time Lost. Am J Epidemiol. 2022 Jan 1;191(1):163–72. doi:10.1093/aje/kwab235 PubMed PMID: 34550319.

579. Ritchie ME, Phipson B, Wu D, Hu Y, Law CW, Shi W, et al. limma powers differential expression analyses for RNA-sequencing and microarray studies. Nucleic Acids Res. 2015 Apr 20;43(7):e47. doi:10.1093/nar/gkv007 PubMed PMID: 25605792; PubMed Central PMCID: PMC4402510.

580. Korotkevich G, Sukhov V, Budin N, Shpak B, Artyomov MN, Sergushichev A. Fast gene set enrichment analysis [Internet]. bioRxiv; 2021 [cited 2026 Mar 7]. p. 060012. Available from: https://www.biorxiv.org/content/10.1101/060012v3 doi:10.1101/060012

581. Reimand J, Isser R, Voisin V, Kucera M, Tannus-Lopes C, Rostamianfar A, et al. Pathway enrichment analysis and visualization of omics data using g:Profiler, GSEA, Cytoscape and EnrichmentMap. Nat Protoc. 2019 Feb;14(2):482–517. doi:10.1038/s41596-018-0103-9 PubMed PMID: 30664679; PubMed Central PMCID: PMC6607905.

582. Candia J, Ferrucci L. Assessment of Gene Set Enrichment Analysis using curated RNA-seq-based benchmarks. PLoS One. 2024 May 16;19(5):e0302696. doi:10.1371/journal.pone.0302696 PubMed PMID: 38753612; PubMed Central PMCID: PMC11098418.

583. Chen X, Li J, Gray WH, Lehmann BD, Bauer JA, Shyr Y, et al. TNBCtype: A Subtyping Tool for Triple-Negative Breast Cancer. Cancer Inform. 2012 Jul 24;11:147–56. doi:10.4137/CIN.S9983 PubMed PMID: 22872785; PubMed Central PMCID: PMC3412597.

584. Lehmann BD, Jovanović B, Chen X, Estrada MV, Johnson KN, Shyr Y, et al. Refinement of Triple-Negative Breast Cancer Molecular Subtypes: Implications for Neoadjuvant Chemotherapy Selection. PLoS One. 2016;11(6):e0157368. doi:10.1371/journal.pone.0157368 PubMed PMID: 27310713; PubMed Central PMCID: PMC4911051.

585. Pal A, Gonzalez-Malerva L, Eaton S, Xu C, Zhang Y, Grief D, et al. Multidimensional quantitative phenotypic and molecular analysis reveals neomorphic behaviors of p53 missense mutants. npj Breast Cancer. 2023 Sep 29;9(1):78. doi:10.1038/s41523-023-00582-7

586. Engelman JA, Luo J, Cantley LC. The evolution of phosphatidylinositol 3-kinases as regulators of growth and metabolism. Nat Rev Genet. 2006 Aug;7(8):606–19. doi:10.1038/nrg1879 PubMed PMID: 16847462.

587. Pfisterer U, Kirkeby A, Torper O, Wood J, Nelander J, Dufour A, et al. Direct conversion of human fibroblasts to dopaminergic neurons. Proc Natl Acad Sci USA. 2011 Jun 21;108(25):10343–8. doi:10.1073/pnas.1105135108

588. Stewart SA, Dykxhoorn DM, Palliser D, Mizuno H, Yu EY, An DS, et al. Lentivirus-delivered stable gene silencing by RNAi in primary cells. RNA. 2003 Apr;9(4):493–501. doi:10.1261/rna.2192803

589. Ng PKS, Li J, Jeong KJ, Shao S, Chen H, Tsang YH, et al. Systematic Functional Annotation of Somatic Mutations in Cancer. Cancer Cell. 2018 Mar;33(3):450-462.e10. doi:10.1016/j.ccell.2018.01.021

590. Chou TC. Theoretical Basis, Experimental Design, and Computerized Simulation of Synergism and Antagonism in Drug Combination Studies. Pharmacological Reviews. 2006 Sep;58(3):621–81. doi:10.1124/pr.58.3.10

591. Chou TC. Drug Combination Studies and Their Synergy Quantification Using the Chou-Talalay Method. Cancer Research. 2010 Jan 15;70(2):440–6. doi:10.1158/0008-5472.CAN-09-1947

592. Lin XY, Guo L, Lin X, Wang Y, Zhang G. Concomitant PIK3CA and TP53 Mutations in Breast Cancer: An Analysis of Clinicopathologic and Mutational Features, Neoadjuvant Therapeutic Response, and Prognosis. J Breast Cancer. 2023 Jul 12;26(4):363–77. doi:10.4048/jbc.2023.26.e30 PubMed PMID: 37565929; PubMed Central PMCID: PMC10475711.

593. Chai C, Wu HH, Abuetabh Y, Sergi C, Leng R. Regulation of the tumor suppressor PTEN in triple-negative breast cancer. Cancer Letters. 2022 Feb 28;527:41–8. doi:10.1016/j.canlet.2021.12.003

594. Zwimpfer TA, Heidinger M, Coelho R, Stiegeler N, Schwab FD, Montavon C, et al. TP53 Mutations and Phosphatidylinositol 3-Kinase/AKT Pathway Alterations Are Key Determinants of Breast Cancer Outcome Independent of Subtype and Stage. JCO Precis Oncol. 2025 May;(9):e2400767. doi:10.1200/PO-24-00767

595. Ensenyat-Mendez M, Llinàs-Arias P, Orozco JIJ, Íñiguez-Muñoz S, Salomon MP, Sesé B, et al. Current Triple-Negative Breast Cancer Subtypes: Dissecting the Most Aggressive Form of Breast Cancer. Front Oncol. 2021 Jun 16;11:681476. doi:10.3389/fonc.2021.681476 PubMed PMID: 34221999; PubMed Central PMCID: PMC8242253.

596. Onco Query Language (OQL) [Internet]. [cited 2026 Mar 15]. Available from: https://docs.cbioportal.org/user-guide/oql/

597. Austin PC, Giardiello D. The Impact of Violation of the Proportional Hazards Assumption on the Calibration of the Cox Proportional Hazards Model. Stat Med. 2025 Jun;44(13–14):e70161. doi:10.1002/sim.70161 PubMed PMID: 40492822; PubMed Central PMCID: PMC12150894.

598. Dawson SJ, Rueda OM, Aparicio S, Caldas C. A new genome-driven integrated classification of breast cancer and its implications. EMBO J. 2013 Mar 6;32(5):617–28. doi:10.1038/emboj.2013.19 PubMed PMID: 23395906; PubMed Central PMCID: PMC3590990.

599. Buffa FM, Harris AL, West CM, Miller CJ. Large meta-analysis of multiple cancers reveals a common, compact and highly prognostic hypoxia metagene. Br J Cancer. 2010 Jan 19;102(2):428–35. doi:10.1038/sj.bjc.6605450 PubMed PMID: 20087356; PubMed Central PMCID: PMC2816644.

600. Winter SC, Buffa FM, Silva P, Miller C, Valentine HR, Turley H, et al. Relation of a hypoxia metagene derived from head and neck cancer to prognosis of multiple cancers. Cancer Res. 2007 Apr 1;67(7):3441–9. doi:10.1158/0008-5472.CAN-06-3322 PubMed PMID: 17409455.

601. Ragnum HB, Vlatkovic L, Lie AK, Axcrona K, Julin CH, Frikstad KM, et al. The tumour hypoxia marker pimonidazole reflects a transcriptional programme associated with aggressive prostate cancer. Br J Cancer. 2015 Jan 20;112(2):382–90. doi:10.1038/bjc.2014.604 PubMed PMID: 25461803; PubMed Central PMCID: PMC4453458.

602. Chen Z, Han F, Du Y, Shi H, Zhou W. Hypoxic microenvironment in cancer: molecular mechanisms and therapeutic interventions. Sig Transduct Target Ther. 2023 Feb 17;8(1):70. doi:10.1038/s41392-023-01332-8

603. Poluri RTK, Audet-Walsh É. Genomic Deletion at 10q23 in Prostate Cancer: More Than PTEN Loss? Front Oncol. 2018 Jun 29;8:246. doi:10.3389/fonc.2018.00246 PubMed PMID: 30009155; PubMed Central PMCID: PMC6033966.

604. Current Triple-Negative Breast Cancer Subtypes: Dissecting the Most Aggressive Form of Breast Cancer - PMC [Internet]. [cited 2026 Mar 15]. Available from: https://pmc.ncbi.nlm.nih.gov/articles/PMC8242253/

605. Hubalek M, Czech T, Müller H. Biological Subtypes of Triple-Negative Breast Cancer. Breast Care (Basel). 2017 Mar;12(1):8–14. doi:10.1159/000455820 PubMed PMID: 28611535; PubMed Central PMCID: PMC5465739.

606. Purrington KS, Knight J, Dyson G, Ali-Fehmi R, Schwartz AG, Boerner JL, et al. CLCA2 expression is associated with survival among African American women with triple negative breast cancer. PLoS One. 2020 Apr 16;15(4):e0231712. doi:10.1371/journal.pone.0231712 PubMed PMID: 32298355; PubMed Central PMCID: PMC7161959.

607. Zhou Y, Che Y, Fu Z, Zhang H, Wu H. Triple-Negative Breast Cancer Analysis Based on Metabolic Gene Classification and Immunotherapy. Front Public Health. 2022 Jul 6;10. doi:10.3389/fpubh.2022.902378

608. Lehmann BD, Colaprico A, Silva TC, Chen J, An H, Ban Y, et al. Multi-omics analysis identifies therapeutic vulnerabilities in triple-negative breast cancer subtypes. Nat Commun. 2021 Nov 1;12(1):6276. doi:10.1038/s41467-021-26502-6

609. Mustafa E, Laven-Law G, Winter J, Kikhtyak Z, Bergeron A, MacGrogan G, et al. The transcription factor AP-2β defines active enhancers conferring molecular apocrine cell identity in breast cancer [Internet]. bioRxiv; 2025 [cited 2026 Jun 16]. p. 2025.07.05.663274. Available from: https://www.biorxiv.org/content/10.1101/2025.07.05.663274v1 doi:10.1101/2025.07.05.663274

610. Liu Y, Marin A, Ejlerskov P, Rasmussen LM, Prinz M, Issazadeh-Navikas S. Neuronal IFN-beta–induced PI3K/Akt-FoxA1 signalling is essential for generation of FoxA1+Treg cells. Nat Commun. 2017 Apr 24;8(1):14709. doi:10.1038/ncomms14709

611. Chen Y, Ouyang Y, Li Z, Wang X, Ma J. S100A8 and S100A9 in Cancer. Biochimica et Biophysica Acta (BBA) - Reviews on Cancer. 2023 May 1;1878(3):188891. doi:10.1016/j.bbcan.2023.188891

612. Begg LR, Orriols AM, Zannikou M, Yeh C, Vadlamani P, Kanojia D, et al. S100A8/A9 predicts response to PIM kinase and PD-1/PD-L1 inhibition in triple-negative breast cancer mouse models. Commun Med. 2024 Feb 20;4(1):22. doi:10.1038/s43856-024-00444-8

613. Weber S, Salabei JK, Möller G, Kremmer E, Bhatnagar A, Adamski J, et al. Aldo-keto Reductase 1B15 (AKR1B15). J Biol Chem. 2015 Mar 6;290(10):6531–45. doi:10.1074/jbc.M114.610121 PubMed PMID: 25577493; PubMed Central PMCID: PMC4358287.

614. Cheng L, Xu Y, Li Z, Sun D, Xu Y, He J, et al. DHCR24 overexpression is involved in lipid metabolic reprogramming to drive cervical cancer malignant progression and is associated with immune microenvironment. BMC Cancer. 2025 Aug 9;25(1):1291. doi:10.1186/s12885-025-14663-2

615. Landis J, Shaw LM. Insulin Receptor Substrate 2-mediated Phosphatidylinositol 3-kinase Signaling Selectively Inhibits Glycogen Synthase Kinase 3β to Regulate Aerobic Glycolysis. J Biol Chem. 2014 Jun 27;289(26):18603–13. doi:10.1074/jbc.M114.564070 PubMed PMID: 24811175; PubMed Central PMCID: PMC4140254.

616. Liberzon A, Birger C, Thorvaldsdóttir H, Ghandi M, Mesirov JP, Tamayo P. The Molecular Signatures Database (MSigDB) hallmark gene set collection. Cell Syst. 2015 Dec 23;1(6):417–25. doi:10.1016/j.cels.2015.12.004 PubMed PMID: 26771021; PubMed Central PMCID: PMC4707969.

617. Croft D, O'Kelly G, Wu G, Haw R, Gillespie M, Matthews L, et al. Reactome: a database of reactions, pathways and biological processes. Nucleic Acids Res. 2011 Jan;39(Database issue):D691–7. doi:10.1093/nar/gkq1018 PubMed PMID: 21067998; PubMed Central PMCID: PMC3013646.

618. Meng F, Li H, Wang Y, Zheng Z, Chen Y. The mechanism of AKT activation in cancer. Cell Investigation. 2025 Dec 1;1(4):100046. doi:10.1016/j.clnves.2025.100046

619. Azad MG, Russell TM, Gu X, Zhao X, Richardson V, Wijesinghe TP, et al. NDRG1 and its family members: More than just metastasis suppressor proteins and targets of thiosemicarbazones. Journal of Biological Chemistry. 2025 Jul 1;301(7):110230. doi:10.1016/j.jbc.2025.110230

620. Prasad SB, Yadav SS, Das M, Modi A, Kumari S, Pandey LK, et al. PI3K/AKT pathway-mediated regulation of p27(Kip1) is associated with cell cycle arrest and apoptosis in cervical cancer. Cell Oncol (Dordr). 2015 Jun;38(3):215–25. doi:10.1007/s13402-015-0224-x PubMed PMID: 25821107.

621. Vogler M, Braun Y, Smith VM, Westhoff MA, Pereira RS, Pieper NM, et al. The BCL2 family: from apoptosis mechanisms to new advances in targeted therapy. Sig Transduct Target Ther. 2025 Mar 21;10(1):91. doi:10.1038/s41392-025-02176-0

622. Wright SCE, Vasilevski N, Serra V, Rodon J, Eichhorn PJA. Mechanisms of Resistance to PI3K Inhibitors in Cancer: Adaptive Responses, Drug Tolerance and Cellular Plasticity. Cancers (Basel). 2021 Mar 26;13(7):1538. doi:10.3390/cancers13071538 PubMed PMID: 33810522; PubMed Central PMCID: PMC8037590.

623. Tang Q, Su Z, Gu W, Rustgi AK. Mutant p53 on the Path to Metastasis. Trends Cancer. 2020 Jan;6(1):62–73. doi:10.1016/j.trecan.2019.11.004 PubMed PMID: 31952783; PubMed Central PMCID: PMC7485681.

624. Seol DW, Chen Q, Smith ML, Zarnegar R. Regulation of the c-met proto-oncogene promoter by p53. J Biol Chem. 1999 Feb 5;274(6):3565–72. doi:10.1074/jbc.274.6.3565 PubMed PMID: 9920903.

625. Hwang CI, Matoso A, Corney DC, Flesken-Nikitin A, Körner S, Wang W, et al. Wild-type p53 controls cell motility and invasion by dual regulation of MET expression. Proceedings of the National Academy of Sciences. 2011 Aug 23;108(34):14240–5. doi:10.1073/pnas.1017536108

626. Lehmann BD, Bauer JA, Chen X, Sanders ME, Chakravarthy AB, Shyr Y, et al. Identification of human triple-negative breast cancer subtypes and preclinical models for selection of targeted therapies. J Clin Invest. 2011 Jul 1;121(7):2750–67. doi:10.1172/JCI45014

627. Smith SE, Mellor P, Ward AK, Kendall S, McDonald M, Vizeacoumar FS, et al. Molecular characterization of breast cancer cell lines through multiple omic approaches. Breast Cancer Res. 2017 Dec;19(1):65. doi:10.1186/s13058-017-0855-0

628. Wieland A, Strissel PL, Schorle H, Bakirci E, Janzen D, Beckmann MW, et al. Brain and Breast Cancer Cells with PTEN Loss of Function Reveal Enhanced Durotaxis and RHOB Dependent Amoeboid Migration Utilizing 3D Scaffolds and Aligned Microfiber Tracts. Cancers. 2021 Oct 14;13(20):5144. doi:10.3390/cancers13205144

629. Pappas K, Martin TC, Wolfe AL, Nguyen CB, Su T, Jin J, et al. NOTCH and EZH2 collaborate to repress PTEN expression in breast cancer. Commun Biol. 2021 Mar 9;4(1):312. doi:10.1038/s42003-021-01825-8

630. El Guerrab A, Bamdad M, Bignon YJ, Penault-Llorca F, Aubel C. Co-targeting EGFR and mTOR with gefitinib and everolimus in triple-negative breast cancer cells. Sci Rep. 2020 Apr 14;10(1):6367. doi:10.1038/s41598-020-63310-2

631. Patil MR, Bihari A. Cancer Classification Through p53 Hotspot Mutations: An Ensemble Learning Approach. Cell Biology International. 2025;49(9):1115–27. doi:10.1002/cbin.70041

632. Jönsson C, Alkashaf Z, Sandström J, Johansson A, Fornander T, Lindström LS, et al. Abstract B027: *PIK3CA* hotspot mutations as biomarkers for prognosis and treatment prediction in low-risk postmenopausal breast cancer patients. Cancer Research. 2023 Jan 15;83(2_Supplement_2):B027–B027. doi:10.1158/1538-7445.METASTASIS22-B027

633. Guo S, Loibl S, Von Minckwitz G, Darb-Esfahani S, Lederer B, Denkert C. PIK3CA H1047R Mutation Associated with a Lower Pathological Complete Response Rate in Triple-Negative Breast Cancer Patients Treated with Anthracycline-Taxane–Based Neoadjuvant Chemotherapy. Cancer Res Treat. 2020 Jul 15;52(3):689–96. doi:10.4143/crt.2019.497

634. Lu Q, Tan YH, Luo R. Molecular Dynamics Simulations of p53 DNA-Binding Domain. J Phys Chem B. 2007 Oct 4;111(39):11538–45. doi:10.1021/jp0742261 PubMed PMID: 17824689; PubMed Central PMCID: PMC2522240.

635. Rasti AR, Guimaraes-Young A, Datko F, Borges VF, Aisner DL, Shagisultanova E. *PIK3CA* Mutations Drive Therapeutic Resistance in Human Epidermal Growth Factor Receptor 2–Positive Breast Cancer. JCO Precision Oncology. 2022 May;(6):e2100370. doi:10.1200/PO.21.00370

636. Simon N, Antignani A, Sarnovsky R, Hewitt SM, FitzGerald D. Targeting a Cancer-Specific Epitope of the Epidermal Growth Factor Receptor in Triple-Negative Breast Cancer. JNCI J Natl Cancer Inst. 2016 Aug;108(8):djw028. doi:10.1093/jnci/djw028

637. Jamieson S, Flanagan JU, Kolekar S, Buchanan C, Kendall JD, Lee WJ, et al. A drug targeting only p110α can block phosphoinositide 3-kinase signalling and tumour growth in certain cell types. Biochemical Journal. 2011 Aug 15;438(1):53–62. doi:10.1042/BJ20110502

638. Jin G, Zheng K, Liu S, Yi H, Wei W, Xu C, et al. In Vivo PK-PD and Drug–Drug Interaction Study of Dorzagliatin for the Management of PI3Kα Inhibitor-Induced Hyperglycemia. Pharmaceuticals. 2025 Jun 19;18(6):927. doi:10.3390/ph18060927

639. Kazandjian D, Blumenthal GM, Chen HY, He K, Patel M, Justice R, et al. FDA Approval Summary: Crizotinib for the Treatment of Metastatic Non-Small Cell Lung Cancer With Anaplastic Lymphoma Kinase Rearrangements. The Oncologist. 2014 Oct 1;19(10):e5–11. doi:10.1634/theoncologist.2014-0241

640. Kazandjian D, Blumenthal GM, Luo L, He K, Fran I, Lemery S, et al. Benefit-Risk Summary of Crizotinib for the Treatment of Patients With ROS1 Alteration-Positive, Metastatic Non-Small Cell Lung Cancer. The Oncologist. 2016 Aug 1;21(8):974–80. doi:10.1634/theoncologist.2016-0101

641. Merino M, Kasamon Y, Li H, Ma L, Leong R, Zhou J, et al. FDA approval summary: Crizotinib for pediatric and young adult patients with relapsed or refractory systemic anaplastic large cell lymphoma. Pediatric Blood & Cancer. 2022 Aug;69(8):e29602. doi:10.1002/pbc.29602

642. Aschenbrenner DS. New Indication for Cancer Drug Crizotinib. AJN, American Journal of Nursing. 2022 Nov;122(11):20–20. doi:10.1097/01.NAJ.0000897112.29413.1a

643. Okines A, Sawyer E, Roylance R, Armstrong A, Johnston S, Ring A, et al. Abstract P2-07-24: Results from the Phase II Study of ROS1 Targeting with Crizotinib in Advanced E-cadherin Negative Lobular Breast Cancer (ROLo). Clinical Cancer Research. 2025 Jun 13;31(12_Supplement):P2-07-24-P2-07–24. doi:10.1158/1557-3265.SABCS24-P2-07-24

644. Wang E, Nickens DJ, Bello A, Khosravan R, Amantea M, Wilner KD, et al. Clinical Implications of the Pharmacokinetics of Crizotinib in Populations of Patients with Non-Small Cell Lung Cancer. Clin Cancer Res. 2016 Dec 1;22(23):5722–8. doi:10.1158/1078-0432.CCR-16-0536 PubMed PMID: 27281559.

645. Fraser M, Seetharamu N, Diamond M, Lee CS. Profile of Capmatinib for the Treatment of Metastatic Non-Small Cell Lung Cancer (NSCLC): Patient Selection and Perspectives. Cancer Manag Res. 2023 Nov 3;15:1233–43. doi:10.2147/CMAR.S386799 PubMed PMID: 37941971; PubMed Central PMCID: PMC10629434.

646. Zhang H, Li X, Zhang Z, Huang S, Guo Q, Yan N. Activity of ceritinib in crizotinib-resistant ROS1-rearranged non-small-cell lung cancer patients. Medicine (Baltimore). 2023 Jul 21;102(29):e33543. doi:10.1097/MD.0000000000033543 PubMed PMID: 37478263; PubMed Central PMCID: PMC10662874.

647. Bang Y, Su W, Schuler M, Nam D, Lim WT, Bauer TM, et al. Phase 1 study of capmatinib in MET-positive solid tumor patients: Dose escalation and expansion of selected cohorts. Cancer Science. 2020 Feb;111(2):536–47. doi:10.1111/cas.14254

648. McDuff FKE, Lim SV, Dalbay M, Turner SD. Assessment of the transforming potential of novel anaplastic lymphoma kinase point mutants. Mol Carcinog. 2013 Jan;52(1):79–83. doi:10.1002/mc.21836 PubMed PMID: 22086496.

649. Di Tomaso E, Linnartz R, Li F, Massacesi C, Hirawat S. Abstract 4698: Combination of ceritinib (LDK378) with PI3K inhibitors (buparlisib [BKM120] and alpelisib [BYL719]) demonstrates synergistic preclinical antitumor activity in ALK-rearranged non-small cell lung cancer (NSCLC). Cancer Research. 2015 Aug 1;75(15_Supplement):4698–4698. doi:10.1158/1538-7445.AM2015-4698

650. Sazonova EV, Chesnokov MS, Zhivotovsky B, Kopeina GS. Drug toxicity assessment: cell proliferation versus cell death. Cell Death Discov. 2022 Oct 14;8(1):417. doi:10.1038/s41420-022-01207-x

651. Finnerty BM, Moore MD, Verma A, Aronova A, Huang S, Edwards DP, et al. UCHL1 loss alters the cell cycle in metastatic pancreatic neuroendocrine tumors. Endocrine-Related Cancer. 2019 Apr;26(4):411–23. doi:10.1530/ERC-18-0507

652. Zhang Y, Ou M, Lin H, Lai L, Chen H, Chen J, et al. Proteomic analysis of differentially expressed proteins in the serum of patients with acute renal allograft rejection using iTRAQ labelling technology. Mol Med Rep. 2020 Jul 6;22(3):2329–41. doi:10.3892/mmr.2020.11299

653. Limantoro J, De Liyis BG, Sutedja JC. Akt signaling pathway: a potential therapy for Alzheimer's disease through glycogen synthase kinase 3 beta inhibition. Egypt J Neurol Psychiatry Neurosurg. 2023 Nov 7;59(1):147. doi:10.1186/s41983-023-00751-2

654. Jenke R, Holzhäuser-Rein M, Mueller-Wilke S, Lordick F, Aigner A, Büch T. SATB1-Mediated Upregulation of the Oncogenic Receptor Tyrosine Kinase HER3 Antagonizes MET Inhibition in Gastric Cancer Cells. IJMS. 2020 Dec 23;22(1):82. doi:10.3390/ijms22010082

655. Stern YE, Al-Ghabkari A, Monast A, Fiset B, Aboualizadeh F, Yao Z, et al. Met–HER3 crosstalk supports proliferation via MPZL3 in MET-amplified cancer cells. Cell Mol Life Sci. 2022 Mar;79(3):178. doi:10.1007/s00018-022-04149-w

656. Novoplansky O, Fury M, Prasad M, Yegodayev K, Zorea J, Cohen L, et al. MET activation confers resistance to cetuximab, and prevents HER2 and HER3 upregulation

in head and neck cancer. Intl Journal of Cancer. 2019 Aug;145(3):748–62. doi:10.1002/ijc.32170

657. Jamme P, Fernandes M, Copin MC, Descarpentries C, Escande F, Morabito A, et al. Alterations in the PI3K Pathway Drive Resistance to MET Inhibitors in NSCLC Harboring MET Exon 14 Skipping Mutations. Journal of Thoracic Oncology. 2020 May;15(5):741–51. doi:10.1016/j.jtho.2020.01.027

658. Hervieu A, Kermorgant S. The Role of PI3K in Met Driven Cancer: A Recap. Front Mol Biosci. 2018 Oct 24;5:86. doi:10.3389/fmolb.2018.00086

659. Roa P, Bremer NV, Foglizzo V, Cocco E. Mutations in the Serine/Threonine Kinase BRAF: Oncogenic Drivers in Solid Tumors. Cancers. 2024 Mar 20;16(6):1215. doi:10.3390/cancers16061215

660. Xi Q, Kunita A, Ogawa M, Ka M, Tanimoto S, Tsuchimochi S, et al. Cyclin E1 overexpression sensitizes ovarian cancer cells to WEE1 and PLK1 inhibition. Oncogene. 2025 May 26;44(19):1375–86. doi:10.1038/s41388-025-03312-4

661. Malanga M, Althaus FR. DNA Damage Signaling through Poly(ADP-Ribose). In: Poly(ADP-Ribosyl)ation [Internet]. Boston, MA: Springer US; 2006 [cited 2026 Apr 22]. p. 41–50. (Molecular Biology Intelligence Unit). Available from: http://link.springer.com/10.1007/0-387-36005-0_4 doi:10.1007/0-387-36005-0_4

662. Georgescu MM. PTEN Tumor Suppressor Network in PI3K-Akt Pathway Control. Genes & Cancer. 2010 Dec 1;1(12):1170–7. doi:10.1177/1947601911407325

663. Matsuhashi S, Manirujjaman M, Hamajima H, Ozaki I. Control Mechanisms of the Tumor Suppressor PDCD4: Expression and Functions. IJMS. 2019 May 9;20(9):2304. doi:10.3390/ijms20092304

664. Ayuso MI, Hernández-Jiménez M, Martín ME, Salinas M, Alcázar A. New Hierarchical Phosphorylation Pathway of the Translational Repressor eIF4E-binding Protein 1 (4E-BP1) in Ischemia-Reperfusion Stress. Journal of Biological Chemistry. 2010 Nov;285(45):34355–63. doi:10.1074/jbc.M110.135103

665. Livingstone M, Bidinosti M. Rapamycin-insensitive mTORC1 activity controls eIF4E:4E-BP1 binding. F1000Res. 2012 Jul 18;1:4. doi:10.12688/f1000research.1-4.v1

666. Gingras AC, Raught B, Gygi SP, Niedzwiecka A, Miron M, Burley SK, et al. Hierarchical phosphorylation of the translation inhibitor 4E-BP1. Genes Dev. 2001 Nov 1;15(21):2852–64. doi:10.1101/gad.912401

667. Grolleau A, Sonenberg N, Wietzerbin J, Beretta L. Differential Regulation of 4E-BP1 and 4E-BP2, Two Repressors of Translation Initiation, During Human Myeloid Cell Differentiation. The Journal of Immunology. 1999 Mar 15;162(6):3491–7. doi:10.4049/jimmunol.162.6.3491

668. She QB, Halilovic E, Ye Q, Zhen W, Shirasawa S, Sasazuki T, et al. 4E-BP1 Is a Key Effector of the Oncogenic Activation of the AKT and ERK Signaling Pathways that Integrates Their Function in Tumors. Cancer Cell. 2010 Jul;18(1):39–51. doi:10.1016/j.ccr.2010.05.023

669. Hertel A, Storchová Z. The Role of p53 Mutations in Early and Late Response to Mitotic Aberrations. Biomolecules. 2025 Feb 8;15(2):244. doi:10.3390/biom15020244

670. Alvarado-Ortiz E, De La Cruz-López KG, Becerril-Rico J, Sarabia-Sánchez MA, Ortiz-Sánchez E, García-Carrancá A. Mutant p53 Gain-of-Function: Role in Cancer Development, Progression, and Therapeutic Approaches. Front Cell Dev Biol. 2021 Feb 11;8:607670. doi:10.3389/fcell.2020.607670

671. Wang H, Guo M, Wei H, Chen Y. Targeting p53 pathways: mechanisms, structures and advances in therapy. Sig Transduct Target Ther. 2023 Mar 1;8(1):92. doi:10.1038/s41392-023-01347-1

672. Joerger AC, Fersht AR. The p53 Pathway: Origins, Inactivation in Cancer, and Emerging Therapeutic Approaches. Annu Rev Biochem. 2016 Jun 2;85(1):375–404. doi:10.1146/annurev-biochem-060815-014710

673. Funk JS, Klimovich M, Drangenstein D, Pielhoop O, Hunold P, Borowek A, et al. Deep CRISPR mutagenesis characterizes the functional diversity of TP53 mutations. Nat Genet. 2025 Jan;57(1):140–53. doi:10.1038/s41588-024-02039-4

674. Romano RA, Ortt K, Birkaya B, Smalley K, Sinha S. An Active Role of the ΔN Isoform of p63 in Regulating Basal Keratin Genes K5 and K14 and Directing Epidermal Cell Fate. PLOS ONE. 2009 May 20;4(5):e5623. doi:10.1371/journal.pone.0005623

675. Zhang X, Yin M, Zhang L juan. Keratin 6, 16 and 17—Critical Barrier Alarmin Molecules in Skin Wounds and Psoriasis. Cells. 2019 Aug 1;8(8):807. doi:10.3390/cells8080807 PubMed PMID: 31374826; PubMed Central PMCID: PMC6721482.

676. Tan E, Morton J, Timpson P, Tucci P, Melino G, Flores E, et al. Functions of TAp63 and p53 in restraining the development of metastatic cancer. Oncogene. 2014 Jun 19;33(25):3325–33. doi:10.1038/onc.2013.287 PubMed PMID: 23873029; PubMed Central PMCID: PMC4181588.

677. Poltavets V, Kochetkova M, Pitson SM, Samuel MS. The Role of the Extracellular Matrix and Its Molecular and Cellular Regulators in Cancer Cell Plasticity. Front Oncol. 2018 Oct 9;8. doi:10.3389/fonc.2018.00431

678. Wang T, Wei L, Lu Q, Shao Y, You S, Yin JC, et al. Landscape of potentially targetable receptor tyrosine kinase fusions in diverse cancers by DNA-based profiling. npj Precis Onc. 2022 Nov 11;6(1):84. doi:10.1038/s41698-022-00325-0

679. Karlsson E, Pérez-Tenorio G, Amin R, Bostner J, Skoog L, Fornander T, et al. The mTOR effectors 4EBP1 and S6K2 are frequently coexpressed, and associated with a poor prognosis and endocrine resistance in breast cancer: a retrospective study including patients from the randomised Stockholm tamoxifen trials. Breast Cancer Res. 2013 Oct 17;15(5):R96. doi:10.1186/bcr3557

680. Brognard J, Niederst M, Reyes G, Warfel N, Newton AC. Common Polymorphism in the Phosphatase PHLPP2 Results in Reduced Regulation of Akt and Protein Kinase C. Journal of Biological Chemistry. 2009 May;284(22):15215–23. doi:10.1074/jbc.M901468200

681. Gao R, Li X, Gao H, Zhao K, Liu X, Liu J, et al. Protein phosphatase 2A catalytic subunit β suppresses PMA/ionomycin-induced T-cell activation by negatively regulating PI3K/Akt signaling. FEBS J. 2022 Aug;289(15):4518–35. doi:10.1111/febs.16370 PubMed PMID: 35068054.

682. Fan Y ling, Chen L, Wang J, Yao Q, Wan J qing. Over expression of PPP2R2C inhibits human glioma cells growth through the suppression of mTOR pathway. FEBS Letters. 2013 Dec 11;587(24):3892–7. doi:10.1016/j.febslet.2013.09.029

683. Dzobo K, Dandara C. The Extracellular Matrix: Its Composition, Function, Remodeling, and Role in Tumorigenesis. Biomimetics. 2023 Apr 5;8(2):146. doi:10.3390/biomimetics8020146

684. Porter JR, Fisher BE, Baranello L, Liu JC, Kambach DM, Nie Z, et al. Global inhibition with specific activation: how p53 and MYC redistribute the transcriptome in the DNA double-strand break response. Mol Cell. 2017 Sep 21;67(6):1013-1025.e9. doi:10.1016/j.molcel.2017.07.028 PubMed PMID: 28867293; PubMed Central PMCID: PMC5657607.

685. Zhang N, Wang F, Zhu L, Chang R, Mok SRS, Peixoto RD, et al. Molecular mechanism of the miR-7/BCL2L1/P53 signaling axis regulating the progression of hepatocellular carcinoma. Ann Transl Med. 2023 Jan 15;11(1):12. doi:10.21037/atm-22-5929 PubMed PMID: 36760243; PubMed Central PMCID: PMC9906214.

686. Croessmann S, Wong HY, Zabransky DJ, Chu D, Rosen DM, Cidado J, et al. PIK3CA mutations and TP53 alterations cooperate to increase cancerous phenotypes and tumor heterogeneity. Breast Cancer Res Treat. 2017 Apr;162(3):451–64. doi:10.1007/s10549-017-4147-2

687. Lim AR, Kim B, Kim JH, Hyun MH, Park KH, Kim YH, et al. Phase Ib and pharmacokinetics study of alpelisib, a PIK3CA inhibitor, and capecitabine in patients with advanced solid tumors. Front Oncol. 2024 Jul 12;14:1390452. doi:10.3389/fonc.2024.1390452

688. Zagami P, Carey LA. Triple negative breast cancer: Pitfalls and progress. npj Breast Cancer. 2022 Aug 20;8(1):95. doi:10.1038/s41523-022-00468-0

689. Liang Y, Zhang P, Li F, Lai H, Qi T, Wang Y. Advances in the study of marketed antibody-drug Conjugates (ADCs) for the treatment of breast cancer. Front Pharmacol. 2024 Jan 30;14:1332539. doi:10.3389/fphar.2023.1332539

690. Darb-Esfahani S, Denkert C, Stenzinger A, Salat C, Sinn B, Schem C, et al. Role of *TP53* mutations in triple negative and HER2-positive breast cancer treated with neoadjuvant anthracycline/taxane-based chemotherapy. Oncotarget. 2016 Oct 12;7(42):67686–98. doi:10.18632/oncotarget.11891

691. Li AJ, Li HG, Tang EJ, Wu W, Chen Y, Jiang HH, et al. *PIK3CA* and *TP53* mutations predict overall survival of stage II/III colorectal cancer patients. WJG. 2018 Feb 7;24(5):631–40. doi:10.3748/wjg.v24.i5.631

692. Gremke N, Besong I, Stroh A, von Wichert L, Witt M, Elmshäuser S, et al. Targeting PI3K inhibitor resistance in breast cancer with metabolic drugs. Signal Transduct Target

Ther. 2025 Mar 21;10:92. doi:10.1038/s41392-025-02180-4 PubMed PMID: 40113784; PubMed Central PMCID: PMC11926384.

693. Ekshyyan O, Anandharaj A, Nathan CAO. Dual PI3K/mTOR Inhibitors: Does p53 Modulate Response? Clin Cancer Res. 2013 Jul 15;19(14):3719–21. doi:10.1158/1078-0432.CCR-13-1291

694. Shen J, Wang Q, Mao Y, Gao W, Duan S. Targeting the p53 signaling pathway in cancers: Molecular mechanisms and clinical studies. MedComm. 2023 Jun;4(3):e288. doi:10.1002/mco2.288

695. Yao S, Wei L, Hu Q, Liu S, Manojlovic Z, Fiorica PN, et al. Mutational landscape of triple-negative breast cancer in African American women. Nat Genet. 2025 Sep;57(9):2166–76. doi:10.1038/s41588-025-02322-y

696. Choi JH, Yu J, Jung M, Jekal J, Kim KS, Jung SU. Prognostic significance of TP53 and PIK3CA mutations analyzed by next-generation sequencing in breast cancer. Medicine. 2023 Sep 22;102(38):e35267. doi:10.1097/MD.0000000000035267

697. Chen J. The Cell-Cycle Arrest and Apoptotic Functions of p53 in Tumor Initiation and Progression. Cold Spring Harb Perspect Med. 2016 Mar;6(3):a026104. doi:10.1101/cshperspect.a026104 PubMed PMID: 26931810; PubMed Central PMCID: PMC4772082.

698. Wang H, Zhao X, He X, Wang M, Zhang H, Cheng J, et al. PIK3CA - TP53 co-mutation as a biomarker of overall survival in malignant tumor. JCO. 2021 May 20;39(15_suppl):e15001–e15001. doi:10.1200/JCO.2021.39.15_suppl.e15001

699. Li J ping, Zhang X mei, Zhang Z, Zheng L hua, Jindal S, Liu Y jiang. Association of p53 expression with poor prognosis in patients with triple-negative breast invasive ductal carcinoma. Medicine. 2019 May;98(18):e15449. doi:10.1097/MD.0000000000015449

700. Tao JJ, Sisoudiya SD, Tukachinsky H, Schrock AB, Ebot EM, Sivakumar S, et al. Clinicogenomic Landscape and Function of PIK3CA, AKT1, and PTEN Mutations in Breast Cancer. JCO Precis Oncol. 2026 Apr;10(4):e2500609. doi:10.1200/PO-25-00609

701. Meric-Bernstam F, Akcakanat A, Chen H, Do KA, Sangai T, Adkins F, et al. PIK3CA/PTEN Mutations and Akt Activation as Markers of Sensitivity to Allosteric mTOR inhibitors. Clin Cancer Res. 2012 Mar 15;18(6):1777–89. doi:10.1158/1078-0432.CCR-11-2123 PubMed PMID: 22422409; PubMed Central PMCID: PMC3307149.

702. Liu L, Graff SL, Wang Y. New Emerging Therapies Targeting PI3K/AKT/mTOR/PTEN Pathway in Hormonal Receptor-Positive and HER2-Negative Breast Cancer—Current State and Molecular Pathology Perspective. Cancers (Basel). 2024 Dec 24;17(1):16. doi:10.3390/cancers17010016 PubMed PMID: 39796647; PubMed Central PMCID: PMC11718791.

703. Derakhshan F, Reis-Filho JS. Pathogenesis of Triple-Negative Breast Cancer. Annu Rev Pathol. 2022 Jan 24;17:181–204. doi:10.1146/annurev-pathol-042420-093238 PubMed PMID: 35073169; PubMed Central PMCID: PMC9231507.

704. Srivastava N, Usmani SS, Subbarayan R, Saini R, Pandey PK. Hypoxia: syndicating triple negative breast cancer against various therapeutic regimens. Front Oncol. 2023 Jul 10;13:1199105. doi:10.3389/fonc.2023.1199105 PubMed PMID: 37492478; PubMed Central PMCID: PMC10363988.

705. Zhang C, Liu J, Wang J, Zhang T, Xu D, Hu W, et al. The Interplay Between Tumor Suppressor p53 and Hypoxia Signaling Pathways in Cancer. Front Cell Dev Biol. 2021 Feb 18;9:648808. doi:10.3389/fcell.2021.648808 PubMed PMID: 33681231; PubMed Central PMCID: PMC7930565.

706. Luo K, Qian Z, Jiang Y, Lv D, Zhu K, Shao J, et al. Characterization of the metabolic alteration-modulated tumor microenvironment mediated by *TP53* mutation and hypoxia. Computers in Biology and Medicine. 2023 Sep 1;163:107078. doi:10.1016/j.compbiomed.2023.107078

707. Pan L, Li J, Xu Q, Gao Z, Yang M, Wu X, et al. HER2/PI3K/AKT pathway in HER2-positive breast cancer: A review. Medicine (Baltimore). 2024 Jun 14;103(24):e38508. doi:10.1097/MD.0000000000038508 PubMed PMID: 38875362; PubMed Central PMCID: PMC11175886.

708. Yang Y, Pan L, Zhou W, Shao Z. Clinical and molecular characteristics of HER2-low triple-negative breast cancer: insights from multi-omics analysis. Breast. 2025 Sep 21;84:104584. doi:10.1016/j.breast.2025.104584 PubMed PMID: 40991980; PubMed Central PMCID: PMC12495238.

709. Gulbahce HE, Bernard PS, Weltzien EK, Factor RE, Kushi LH, Caan BJ, et al. Differences in Molecular Features of Triple Negative Breast Cancers Based on Age at Diagnosis. Cancer. 2018 Dec 15;124(24):4676–84. doi:10.1002/cncr.31776 PubMed PMID: 30311638; PubMed Central PMCID: PMC6294689.

710. Li CJ, Tzeng YDT, Chiu YH, Lin HY, Hou MF, Chu PY. Pathogenesis and Potential Therapeutic Targets for Triple-Negative Breast Cancer. Cancers (Basel). 2021 Jun 14;13(12):2978. doi:10.3390/cancers13122978 PubMed PMID: 34198652; PubMed Central PMCID: PMC8232221.

711. Garg P, Singhal G, Horne D, Salgia R, Singhal SS. Metabolic reprogramming in breast cancer: Pathways driving progression, drug resistance, and emerging therapeutics. Biochimica et Biophysica Acta (BBA) - Reviews on Cancer. 2025 Oct 1;1880(5):189396. doi:10.1016/j.bbcan.2025.189396

712. Volpicella M, Sgobba MN, Laera L, Francavilla AL, De Luca DI, Guerra L, et al. Carnitine O-Acetyltransferase as a Central Player in Lipid and Branched-Chain Amino Acid Metabolism, Epigenetics, Cell Plasticity, and Organelle Function. Biomolecules. 2025 Feb 2;15(2):216. doi:10.3390/biom15020216 PubMed PMID: 40001519; PubMed Central PMCID: PMC11852590.

713. Ishikawa T, Toyoda Y, Yoshiura K ichiro, Niikawa N. Pharmacogenetics of human ABC transporter ABCC11: new insights into apocrine gland growth and metabolite secretion. Front Genet. 2013 Jan 2;3:306. doi:10.3389/fgene.2012.00306 PubMed PMID: 23316210; PubMed Central PMCID: PMC3539816.

714. Homogentisate 1,2-dioxygenase - an overview | ScienceDirect Topics [Internet]. [cited 2026 May 24]. Available from: https://www.sciencedirect.com/topics/neuroscience/homogentisate-1-2-dioxygenase

715. Leng S, Ren Y, Tian Y, Zhao W, Mou Y, Chen X, et al. Innate immunity in tumors: roles and therapeutic targets. Front Immunol. 2025 Oct 22;16:1689714. doi:10.3389/fimmu.2025.1689714 PubMed PMID: 41200171; PubMed Central PMCID: PMC12585967.

716. Zheng C, Xu X, Wu M, Xue L, Zhu J, Xia H, et al. Neutrophils in triple-negative breast cancer: an underestimated player with increasingly recognized importance. Breast Cancer Res. 2023;25:88. doi:10.1186/s13058-023-01676-7 PubMed PMID: 37496019; PubMed Central PMCID: PMC10373263.

717. Liang L, Wang W. The impact of p53 mutation on tumor immune evasion: mechanistic insights and clinical implications. Front Immunol. 17:1753215. doi:10.3389/fimmu.2026.1753215 PubMed PMID: 41727427; PubMed Central PMCID: PMC12920560.

718. Xie S, Chen M, Yan B, He X, Chen X, Li D. Identification of a Role for the PI3K/AKT/mTOR Signaling Pathway in Innate Immune Cells. PLoS One. 2014 Apr 9;9(4):e94496. doi:10.1371/journal.pone.0094496 PubMed PMID: 24718556; PubMed Central PMCID: PMC3981814.

719. Collins NB, Abosy RA, Miller BC, Bi K, Zhao Q, Quigley M, et al. PI3K activation allows immune evasion by promoting an inhibitory myeloid tumor microenvironment. J Immunother Cancer. 2022 Mar 9;10(3). doi:10.1136/jitc-2021-003402 PubMed PMID: 10.1136/jitc-2021-003402.

720. Zhou H, Zhao C, Shao R, Xu Y, Zhao W. The functions and regulatory pathways of S100A8/A9 and its receptors in cancers. Front Pharmacol. 2023 Aug 28;14:1187741. doi:10.3389/fphar.2023.1187741 PubMed PMID: 37701037; PubMed Central PMCID: PMC10493297.

721. Peng W, Chen JQ, Liu C, Malu S, Creasy C, Tetzlaff MT, et al. Loss of PTEN Promotes Resistance to T Cell-Mediated Immunotherapy. Cancer Discov. 2016 Feb;6(2):202–16. doi:10.1158/2159-8290.CD-15-0283 PubMed PMID: 26645196; PubMed Central PMCID: PMC4744499.

722. Zhang Z, Richmond A, Yan C. Immunomodulatory Properties of PI3K/AKT/mTOR and MAPK/MEK/ERK Inhibition Augment Response to Immune Checkpoint Blockade in Melanoma and Triple-Negative Breast Cancer. Int J Mol Sci. 2022 Jul 1;23(13):7353. doi:10.3390/ijms23137353 PubMed PMID: 35806358; PubMed Central PMCID: PMC9266842.

723. Yang Y, Wang W. Recent progress in immune evasion mechanisms of triple-negative breast cancer. J Transl Med. 2025 Nov 18;23:1314. doi:10.1186/s12967-025-07370-w PubMed PMID: 41254706; PubMed Central PMCID: PMC12624998.

724. Alexandrou S, George SM, Ormandy CJ, Lim E, Oakes SR, Caldon CE. The Proliferative and Apoptotic Landscape of Basal-like Breast Cancer. Int J Mol Sci. 2019 Feb

4;20(3):667. doi:10.3390/ijms20030667 PubMed PMID: 30720718; PubMed Central PMCID: PMC6387372.

725. Lee MK, Joo H, Bae M, Lee Y, Noh JK, Lee YC, et al. Keratinization-related gene signature predicting survival and response to radiation in patients with HPV-negative head and neck squamous cell carcinoma via regulation of cornification and integrin signaling. Cell Mol Biol Lett. 2026 Jan 29;31:26. doi:10.1186/s11658-025-00855-y PubMed PMID: 41612193; PubMed Central PMCID: PMC12924225.

726. Felsheim BM, Fernandez-Martinez A, Fan C, Pfefferle AD, Hayward MC, Hoadley KA, et al. Prognostic and molecular multi-platform analysis of CALGB 40603 (Alliance) and public triple-negative breast cancer datasets. NPJ Breast Cancer. 2025 Mar 8;11:24. doi:10.1038/s41523-025-00740-z PubMed PMID: 40057511; PubMed Central PMCID: PMC11890565.

727. Liu JC, Wang DY, Egan SE, Zacksenhaus E. Common and distinct features of mammary tumors driven by Ptendeletion or activating Pik3ca mutation. Oncotarget. 2016 Jan 22;7(8):9060–8. doi:10.18632/oncotarget.6985

728. White BS, de Reyniès A, Newman AM, Waterfall JJ, Lamb A, Petitprez F, et al. Community assessment of methods to deconvolve cellular composition from bulk gene expression. Nat Commun. 2024 Aug 27;15(1):7362. doi:10.1038/s41467-024-50618-0

729. Hu B, Sajid M, Lv R, Liu L, Sun C. A review of spatial profiling technologies for characterizing the tumor microenvironment in immuno-oncology. Front Immunol. 2022 Oct 31;13:996721. doi:10.3389/fimmu.2022.996721 PubMed PMID: 36389765; PubMed Central PMCID: PMC9659855.

730. García-García C, Rivas MA, Ibrahim YH, Calvo MT, Gris-Oliver A, Rodríguez O, et al. MEK plus PI3K/mTORC1/2 therapeutic efficacy is impacted by TP53 mutation in preclinical models of colorectal cancer. Clin Cancer Res. 2015 Dec 15;21(24):5499–510. doi:10.1158/1078-0432.CCR-14-3091 PubMed PMID: 26272063; PubMed Central PMCID: PMC5087596.

731. Hou J, Cao X, Cheng Y, Wang X. Roles of TP53 gene in the development of resistance to PI3K inhibitor resistances in CRISPR-Cas9-edited lung adenocarcinoma cells. Cell Biol Toxicol. 2020 Oct;36(5):481–92. doi:10.1007/s10565-020-09523-7 PubMed PMID: 32239370.

732. Mehta K, Hegde M, Girisa S, Vishwa R, Alqahtani MS, Abbas M, et al. Targeting RTKs/nRTKs as promising therapeutic strategies for the treatment of triple-negative breast cancer: evidence from clinical trials. Mil Med Res. 2024 Dec 12;11:76. doi:10.1186/s40779-024-00582-z PubMed PMID: 39668367; PubMed Central PMCID: PMC11636053.

733. Jaradat SK, Ayoub NM, Al Sharie AH, Aldaod JM. Targeting Receptor Tyrosine Kinases as a Novel Strategy for the Treatment of Triple-Negative Breast Cancer. Technol Cancer Res Treat. 2024 Jan;23:15330338241234780. doi:10.1177/15330338241234780

734. Yi T, Qian J, Ye Y, Zhang H, Jin X, Wang M, et al. Crizotinib Nanomicelles Synergize with Chemotherapy through Inducing Proteasomal Degradation of Mutp53 Proteins. ACS Appl Mater Interfaces. 2023 Jan 11;15(1):511–23. doi:10.1021/acsami.2c18020

735. Musa S, Amara N, Selawi A, Wang J, Marchini C, Agbarya A, et al. Overcoming Chemoresistance in Cancer: The Promise of Crizotinib. Cancers. 2024 Jul 7;16(13):2479. doi:10.3390/cancers16132479

736. Wang Y, Tian P, Xia L, Li L, Han R, Zhu M, et al. The clinical efficacy of combinatorial therapy of EGFR-TKI and crizotinib in overcoming MET amplification-mediated resistance from prior EGFR-TKI therapy. Lung Cancer. 2020 Aug;146:165–73. doi:10.1016/j.lungcan.2020.06.003

737. Zhang C, Stockwell SR, Elbanna M, Ketteler R, Freeman J, Al-Lazikani B, et al. Signalling involving MET and FAK supports cell division independent of the activity of the cell cycle-regulating CDK4/6 kinases. Oncogene. 2019 Jul 25;38(30):5905–20. doi:10.1038/s41388-019-0850-2

738. Muller PAJ, Trinidad AG, Timpson P, Morton JP, Zanivan S, Van Den Berghe PVE, et al. Mutant p53 enhances MET trafficking and signalling to drive cell scattering and invasion. Oncogene. 2013 Mar;32(10):1252–65. doi:10.1038/onc.2012.148

739. Bheda A, Creek KE, Pirisi L. Loss of p53 induces epidermal growth factor receptor promoter activity in normal human keratinocytes. Oncogene. 2008 Jul 17;27(31):4315–23. doi:10.1038/onc.2008.65

740. Pfister NT, Fomin V, Regunath K, Zhou JY, Zhou W, Silwal-Pandit L, et al. Mutant p53 cooperates with the SWI/SNF chromatin remodeling complex to regulate *VEGFR2* in breast cancer cells. Genes Dev. 2015 Jun 15;29(12):1298–315. doi:10.1101/gad.263202.115

741. Ryu HY, Kim LE, Jeong H, Yeo BK, Lee JW, Nam H, et al. GSK3B induces autophagy by phosphorylating ULK1. Exp Mol Med. 2021 Mar;53(3):369–83. doi:10.1038/s12276-021-00570-6

742. Shirono Y, Bilim V, Anraku T, Kuroki H, Kazama A, Murata M, et al. Targeting Pro-Survival Autophagy Enhanced GSK-3β Inhibition-Induced Apoptosis and Retarded Proliferation in Bladder Cancer Cells. Current Oncology. 2023 May 28;30(6):5350–65. doi:10.3390/curroncol30060406

743. Aksamitiene E, Kiyatkin A, Kholodenko BN. Cross-talk between mitogenic Ras/MAPK and survival PI3K/Akt pathways: a fine balance. Biochemical Society Transactions. 2012 Feb 1;40(1):139–46. doi:10.1042/BST20110609

744. Aditi Roy. Crosstalk Between MAPK and PI3K/AKT Signaling Pathways in Cellular Responses: Implications for Cancer Therapy. URR. 2024 Jul 22;11(4):30–45. doi:10.36676/urr.v11.i4.1304

745. Liu Y, Yang Q. The roles of EZH2 in cancer and its inhibitors. Med Oncol. 2023 May 6;40(6):167. doi:10.1007/s12032-023-02025-6

746. Bahar ME, Kim HJ, Kim DR. Targeting the RAS/RAF/MAPK pathway for cancer therapy: from mechanism to clinical studies. Sig Transduct Target Ther. 2023 Dec 18;8(1):455. doi:10.1038/s41392-023-01705-z

747. King DE, Copeland WC. DNA repair pathways in the mitochondria. DNA Repair. 2025 Feb;146:103814. doi:10.1016/j.dnarep.2025.103814

748. Ma T, Xie W, Xu Z, Gao W, Zhou J, Wang Y, et al. Estrogen-related receptor alpha (ERRα) controls the stemness and cellular energetics of prostate cancer cells via its direct regulation of citrate metabolism and zinc transportation. Cell Death Dis. 2025 Mar 5;16(1):154. doi:10.1038/s41419-025-07460-z

749. Yang S, Wang R, Liu L, Xu F, Zhao X, Yao Z, et al. RRM1 promotes homologous recombination and radio/chemo-sensitivity via enhancing USP11 and E2F1-mediated RAD51AP1 transcription. Cell Death Discov. 2024 Dec 18;10(1):496. doi:10.1038/s41420-024-02267-x

750. Nasrazadani A, Van Den Berg CL. c-Jun N-terminal Kinase 2 Regulates Multiple Receptor Tyrosine Kinase Pathways in Mouse Mammary Tumor Growth and Metastasis. Genes & Cancer. 2011 Jan 1;2(1):31–45. doi:10.1177/1947601911400901

751. Qing L, Li Q, Dong Z. MUC1: An emerging target in cancer treatment and diagnosis. Bulletin du Cancer. 2022 Nov;109(11):1202–16. doi:10.1016/j.bulcan.2022.08.001

752. Kharbanda A, Rajabi H, Jin C, Tchaicha J, Kikuchi E, Wong KK, et al. Targeting the oncogenic MUC1-C protein inhibits mutant EGFR-mediated signaling and survival in non-small cell lung cancer cells. Clin Cancer Res. 2014 Nov 1;20(21):5423–34. doi:10.1158/1078-0432.CCR-13-3168 PubMed PMID: 25189483; PubMed Central PMCID: PMC4219601.

753. Bitler BG, Goverdhan A, Schroeder JA. MUC1 regulates nuclear localization and function of the epidermal growth factor receptor. Journal of Cell Science. 2010 May 15;123(10):1716–23. doi:10.1242/jcs.062661

754. Manole S, Richards EJ, Meyer AS. JNK Pathway Activation Modulates Acquired Resistance to EGFR/HER2-Targeted Therapies. Cancer Res. 2016 Sep 15;76(18):5219–28. doi:10.1158/0008-5472.CAN-16-0123 PubMed PMID: 27450453; PubMed Central PMCID: PMC5026573.

755. Mercado-Gómez O, Hernández-Fonseca K, Villavicencio-Queijeiro A, Massieu L, Chimal-Monroy J, Arias C. Inhibition of Wnt and PI3K Signaling Modulates GSK-3β Activity and Induces Morphological Changes in Cortical Neurons: Role of Tau Phosphorylation. Neurochem Res. 2008 Aug;33(8):1599–609. doi:10.1007/s11064-008-9714-9

756. Sudhesh Dev S, Zainal Abidin SA, Farghadani R, Othman I, Naidu R. Receptor Tyrosine Kinases and Their Signaling Pathways as Therapeutic Targets of Curcumin in Cancer. Front Pharmacol. 2021 Nov 15;12:772510. doi:10.3389/fphar.2021.772510

757. Moreli JB, Santos MRD, Calderon IDMP, Hebeda CB, Farsky SHP, Bevilacqua E, et al. The Role of Annexin A1 in DNA Damage Response in Placental Cells: Impact on

Gestational Diabetes Mellitus. IJMS. 2023 Jun 15;24(12):10155. doi:10.3390/ijms241210155

758. Vaparanta K, Jokilammi A, Tamirat M, Merilahti JAM, Salokas K, Varjosalo M, et al. An extracellular receptor tyrosine kinase motif orchestrating intracellular STAT activation. Nat Commun. 2022 Nov 14;13(1):6953. doi:10.1038/s41467-022-34539-4

759. Sivaramakrishnan M, Shooter GK, Upton Z, Croll TI. Transglutaminases and receptor tyrosine kinases. Amino Acids. 2013 Jan;44(1):19–24. doi:10.1007/s00726-011-1113-x

760. Yan HH, Jung KH, Son MK, Fang Z, Kim SJ, Ryu YL, et al. Crizotinib Exhibits Antitumor Activity by Targeting ALK Signaling not c-MET in Pancreatic Cancer. Oncotarget. 2014 Aug 23;5(19):9150–68. doi:10.18632/oncotarget.2363 PubMed PMID: 25193856; PubMed Central PMCID: PMC4253425.

761. Dagogo-Jack I, Shaw AT. Crizotinib resistance: implications for therapeutic strategies. Annals of Oncology. 2016 Sep;27:iii42–50. doi:10.1093/annonc/mdw305

762. Yu C, Luo D, Yu J, Zhang M, Zheng X, Xu G, et al. Genome-wide CRISPR-cas9 knockout screening identifies GRB7 as a driver for MEK inhibitor resistance in KRAS mutant colon cancer. Oncogene. 2022 Jan 5;41(2):191–203. doi:10.1038/s41388-021-02077-w

763. Gupta A, Hunt CR, Chakraborty S, Pandita RK, Yordy J, Ramnarain DB, et al. Role of 53BP1 in the Regulation of DNA Double-Strand Break Repair Pathway Choice. Radiation Research. 2014 Jan;181(1):1–8. doi:10.1667/RR13572.1

764. Huber KVM, Salah E, Radic B, Gridling M, Elkins JM, Stukalov A, et al. Stereospecific targeting of MTH1 by (S)-crizotinib as anticancer strategy. Nature. 2014 Apr 10;508(7495):222–7. doi:10.1038/nature13194 PubMed PMID: 24695225; PubMed Central PMCID: PMC4150021.

765. Belal H, Ying Ng EF, Meitinger F. 53BP1-mediated activation of the tumor suppressor p53. Current Opinion in Cell Biology. 2024 Dec 1;91:102424. doi:10.1016/j.ceb.2024.102424

766. Kumari K, Rai GP, Shriya S, Khan N, Ola MS, Shanker A, et al. Coevolutionary dynamics of 53BP1 and its impact on TP53 interaction for DNA damage repair. Computational Biology and Chemistry. 2025 Oct;118:108508. doi:10.1016/j.compbiolchem.2025.108508

767. Fagherazzi P, Stixová L, Bartova E. Specific TP53 mutations impair the recruitment of 53BP1 to DNA double-strand breaks underlying the mechanism of radioresistance. Eur Biophys J. 2025 Nov;54(8):601–12. doi:10.1007/s00249-025-01774-8

768. Luongo F, Colonna F, Calapà F, Vitale S, Fiori ME, De Maria R. PTEN Tumor-Suppressor: The Dam of Stemness in Cancer. Cancers. 2019 Jul 30;11(8):1076. doi:10.3390/cancers11081076

769. Woodcock HV, Eley JD, Guillotin D, Platé M, Nanthakumar CB, Martufi M, et al. The mTORC1/4E-BP1 axis represents a critical signaling node during fibrogenesis. Nat Commun. 2019 Jan 2;10(1):6. doi:10.1038/s41467-018-07858-8

770. Lum MA, Jonas KA, Parmar S, Black AR, O'Connor CM, Dobersch S, et al. Small-molecule modulators of B56-PP2A restore 4E-BP function to suppress eIF4E-dependent translation in cancer cells. Journal of Clinical Investigation. 2025 Feb 17;135(4):e176093. doi:10.1172/JCI176093

771. Böhm R, Imseng S, Jakob RP, Hall MN, Maier T, Hiller S. The dynamic mechanism of 4E-BP1 recognition and phosphorylation by mTORC1. Molecular Cell. 2021 Jun;81(11):2403-2416.e5. doi:10.1016/j.molcel.2021.03.031

772. Xu W, Kim JW, Jung WJ, Koh Y, Yoon SS. Crizotinib in Combination with Everolimus Synergistically Inhibits Proliferation of Anaplastic Lymphoma Kinase–Positive Anaplastic Large Cell Lymphoma. Cancer Res Treat. 2018 Apr;50(2):599–613. doi:10.4143/crt.2016.357 PubMed PMID: 28675026; PubMed Central PMCID: PMC5912135.

773. Bi C, Zhang X, Lu T, Zhang X, Wang X, Meng B, et al. Inhibition of 4EBP phosphorylation mediates the cytotoxic effect of mechanistic target of rapamycin kinase inhibitors in aggressive B-cell lymphomas. Haematologica. 2017 Apr;102(4):755–64. doi:10.3324/haematol.2016.159160

774. McGrail K, Granado-Martínez P, Esteve-Puig R, García-Ortega S, Ding Y, Sánchez-Redondo S, et al. BRAF activation by metabolic stress promotes glycolysis sensitizing NRASQ61-mutated melanomas to targeted therapy. Nat Commun. 2022 Nov 19;13(1):7113. doi:10.1038/s41467-022-34907-0

775. Carr A, Coulter JA, Workman J, Fay J, Farrelly A, Eustace AJ, et al. Targeting the phosphatidylinositol-3-kinase (PI3K) and mitogen activated protein kinase (MAPK) signalling pathways to enhance chemoradiotherapy in locally advanced rectal cancer. Cancer Treatment and Research Communications. 2025;43:100926. doi:10.1016/j.ctarc.2025.100926

776. Aki T, Uemura K. Cell Death and Survival Pathways Involving ATM Protein Kinase. Genes. 2021 Oct 7;12(10):1581. doi:10.3390/genes12101581

777. Lee JH. Targeting the ATM pathway in cancer: Opportunities, challenges and personalized therapeutic strategies. Cancer Treatment Reviews. 2024 Sep;129:102808. doi:10.1016/j.ctrv.2024.102808

778. Yang C, Tang X, Guo X, Niikura Y, Kitagawa K, Cui K, et al. Aurora-B Mediated ATM Serine 1403 Phosphorylation Is Required for Mitotic ATM Activation and the Spindle Checkpoint. Molecular Cell. 2011 Nov;44(4):597–608. doi:10.1016/j.molcel.2011.09.016

779. Hernández Borrero LJ, El-Deiry WS. Tumor suppressor p53: Biology, signaling pathways, and therapeutic targeting. Biochimica et Biophysica Acta (BBA) - Reviews on Cancer. 2021 Aug;1876(1):188556. doi:10.1016/j.bbcan.2021.188556

780. Mahat DB, Kumra H, Castro SA, Metcalf E, Nguyen K, Morisue R, et al. Mutant p53 exploits enhancers to elevate immunosuppressive chemokine expression and impair immune checkpoint inhibitors in pancreatic cancer. Immunity. 2025 Jul;58(7):1688-1705.e9. doi:10.1016/j.immuni.2025.06.005

781. Hirao A, Cheung A, Duncan G, Girard PM, Elia AJ, Wakeham A, et al. Chk2 is a tumor suppressor that regulates apoptosis in both an ataxia telangiectasia mutated (ATM)-dependent and an ATM-independent manner. Mol Cell Biol. 2002 Sep;22(18):6521–32. doi:10.1128/MCB.22.18.6521-6532.2002 PubMed PMID: 12192050; PubMed Central PMCID: PMC135625.

782. McNamee LM, Brodsky MH. p53-Independent Apoptosis Limits DNA Damage-Induced Aneuploidy. Genetics. 2009 Jun 1;182(2):423–35. doi:10.1534/genetics.109.102327

783. Liu Z, Sun Q, Wang X. PLK1, A Potential Target for Cancer Therapy. Translational Oncology. 2017 Feb;10(1):22–32. doi:10.1016/j.tranon.2016.10.003

784. Lee SY, Jang C, Lee KA. Polo-Like Kinases (Plks), a Key Regulator of Cell Cycle and New Potential Target for Cancer Therapy. Development & Reproduciton. 2014 Mar;18(1):65–71. doi:10.12717/DR.2014.18.1.065

785. Sreekumar S, Montaudon E, Klein D, Gonzalez ME, Painsec P, Derrien H, et al. PLK1 Inhibitor Onvansertib Enhances the Efficacy of Alpelisib in PIK3CA-Mutated HR-Positive Breast Cancer Resistant to Palbociclib and Endocrine Therapy: Preclinical Insights. Cancers. 2024 Sep 25;16(19):3259. doi:10.3390/cancers16193259

786. Gourguechon S, Savich JM, Wang CC. The Multiple Roles of cyclin E1 in Controlling Cell Cycle Progression and Cellular Morphology of Trypanosoma brucei. Journal of Molecular Biology. 2007 May;368(4):939–50. doi:10.1016/j.jmb.2007.02.050

787. Fagundes R, Teixeira LK. Cyclin E/CDK2: DNA Replication, Replication Stress and Genomic Instability. Front Cell Dev Biol. 2021 Nov 24;9:774845. doi:10.3389/fcell.2021.774845

788. Fatokun AA, Dawson VL, Dawson TM. Parthanatos: mitochondrial-linked mechanisms and therapeutic opportunities. Br J Pharmacol. 2014 Apr;171(8):2000–16. doi:10.1111/bph.12416 PubMed PMID: 24684389; PubMed Central PMCID: PMC3976618.

789. Hong SJ, Dawson TM, Dawson VL. PARP and the Release of Apoptosis-Inducing Factor from Mitochondria. In: Madame Curie Bioscience Database [Internet] [Internet]. Landes Bioscience; 2013 [cited 2025 Dec 29]. Available from: https://www.ncbi.nlm.nih.gov/books/NBK6179/

790. Qian S, Wei Z, Yang W, Huang J, Yang Y, Wang J. The role of BCL-2 family proteins in regulating apoptosis and cancer therapy. Front Oncol. 2022 Oct 12;12:985363. doi:10.3389/fonc.2022.985363

791. Zhou S, Yu Q, Zhang L, Jiang Z. Cyclophilin D-mediated Mitochondrial Permeability Transition Regulates MitochondrialFunction. CPD. 2023 Mar;29(8):620–9. doi:10.2174/1381612829666230313111314

792. Coluccino G, Muraca VP, Corazza A, Lippe G. Cyclophilin D in Mitochondrial Dysfunction: A Key Player in Neurodegeneration? Biomolecules. 2023 Aug 18;13(8):1265. doi:10.3390/biom13081265

793. Wei H, Mundade R, Lange K, Lu T. Protein arginine methylation of non-histone proteins and its role in diseases. Cell Cycle. 2014 Jan;13(1):32–41. doi:10.4161/cc.27353

794. Lee YJ, Chang WW, Chang CP, Liu TY, Chuang CY, Qian K, et al. Downregulation of PRMT1 promotes the senescence and migration of a non-MYCN amplified neuroblastoma SK-N-SH cells. Sci Rep. 2019 Feb 11;9(1):1771. doi:10.1038/s41598-018-38394-6

795. Li Z, Meng D, Liu Y, Bi F, Tian K, Xu J, et al. Knockdown of PRMT1 suppresses the malignant biological behavior of osteosarcoma cells and increases cisplatin sensitivity via c-Myc-mediated BCAT1 downregulation. J Biochem Mol Toxicol. 2024 Jan;38(1):e23537. doi:10.1002/jbt.23537 PubMed PMID: 37700640.

796. Wu Q, Nie DY, Ba-alawi W, Ji Y, Zhang Z, Cruickshank J, et al. PRMT inhibition induces a viral mimicry response in triple-negative breast cancer. Nat Chem Biol. 2022 Aug;18(8):821–30. doi:10.1038/s41589-022-01024-4

797. Yamamoto T, Hayashida T, Masugi Y, Oshikawa K, Hayakawa N, Itoh M, et al. PRMT1 Sustains De Novo Fatty Acid Synthesis by Methylating PHGDH to Drive Chemoresistance in Triple-Negative Breast Cancer. Cancer Res. 2024 Apr 1;84(7):1065–83. doi:10.1158/0008-5472.CAN-23-2266 PubMed PMID: 38383964; PubMed Central PMCID: PMC10982647.

798. Jiang Y, Jia Y, Zhang L. Role of programmed cell death 4 in diseases: a double-edged sword. Cell Mol Immunol. 2017 Nov;14(11):884–6. doi:10.1038/cmi.2017.84

799. Pin G, Huanting L, Chengzhan Z, Xinjuan K, Yugong F, Wei L, et al. Down-Regulation of PDCD4 Promotes Proliferation, Angiogenesis and Tumorigenesis in Glioma Cells. Front Cell Dev Biol. 2020 Nov 12;8:593685. doi:10.3389/fcell.2020.593685

800. Wang Q, Yang H. The role of Pdcd4 in tumour suppression and protein translation. Biology of the Cell. 2018 Aug;110(8):169–77. doi:10.1111/boc.201800014

801. Cai Q, Yang HS, Li YC, Zhu J. Dissecting the Roles of PDCD4 in Breast Cancer. Front Oncol. 2022 Jun 20;12. doi:10.3389/fonc.2022.855807

802. Yamaguchi N, Lucena-Araujo AR, Nakayama S, De Figueiredo-Pontes LL, Gonzalez DA, Yasuda H, et al. Dual ALK and EGFR inhibition targets a mechanism of acquired resistance to the tyrosine kinase inhibitor crizotinib in ALK rearranged lung cancer. Lung Cancer. 2014 Jan;83(1):37–43. doi:10.1016/j.lungcan.2013.09.019

803. Wang W, Liu X, Liu H, Abolhassani H, Yan H, Zhang H, et al. p53: from understanding its structure to advances in therapeutic targeting. Sig Transduct Target Ther. 2026 Apr 6;11(1):121. doi:10.1038/s41392-025-02549-5

804. Song B, Kim D, Ho JN, Le VH, Lee S. Crizotinib Inhibits Viability, Migration, and Invasion by Suppressing the c-Met/PI3K/Akt Pathway in the Three-Dimensional Bladder Cancer Spheroid Model. Current Oncology. 2025 Apr 17;32(4):236. doi:10.3390/curroncol32040236

805. Zhang C, Sui Y, Liu S, Yang M. In vitro and in vivo experimental models for cancer immunotherapy study. Current Research in Biotechnology. 2024;7:100210. doi:10.1016/j.crbiot.2024.100210

806. Kozlova N, Grossman JE, Iwanicki MP, Muranen T. The Interplay of the Extracellular Matrix and Stromal Cells as a Drug Target in Stroma-Rich Cancers. Trends in Pharmacological Sciences. 2020 Mar;41(3):183–98. doi:10.1016/j.tips.2020.01.001

807. Neben CL, Lo M, Jura N, Klein OD. Feedback regulation of RTK signaling in development. Developmental Biology. 2019 Mar;447(1):71–89. doi:10.1016/j.ydbio.2017.10.017

808. Garattini S. Pharmacokinetics in cancer chemotherapy. European Journal of Cancer. 2007 Jan;43(2):271–82. doi:10.1016/j.ejca.2006.10.015

809. Zhang X, Ni K, Chen H. Successful Retreatment with Crizotinib After Crizotinib-Induced Liver Failure in ALK-Positive Advanced Lung Adenocarcinoma: A Case Report. OTT. 2023 Jan;Volume 16:87–90. doi:10.2147/OTT.S393165

810. Tankova T, Senkus E, Beloyartseva M, Borštnar S, Catrinoiu D, Frolova M, et al. Management Strategies for Hyperglycemia Associated with the α-Selective PI3K Inhibitor Alpelisib for the Treatment of Breast Cancer. Cancers. 2022 Mar 22;14(7):1598. doi:10.3390/cancers14071598

811. Fang Z, Li P, Du F, Shang L, Li L. The role of organoids in cancer research. Exp Hematol Oncol. 2023 Aug 3;12(1):69. doi:10.1186/s40164-023-00433-y

812. Liu Y, Wu W, Cai C, Zhang H, Shen H, Han Y. Patient-derived xenograft models in cancer therapy: technologies and applications. Sig Transduct Target Ther. 2023 Apr 12;8(1):160. doi:10.1038/s41392-023-01419-2

813. Sharma P, Farooki A, Fasching PA, Loi S, Peterson K, Prat A, et al. 349TiP EPIK-B3: A phase III, randomised, double-blind (DB), placebo (PBO)-controlled study of alpelisib (ALP) + nab-paclitaxel (nab-PTX) in advanced triple-negative breast cancer (TNBC) with either PIK3CA mutation or phosphatase and tensin homolog (PTEN) loss without PIK3CA mutation. Annals of Oncology. 2020 Sep 1;31:S387–8. doi:10.1016/j.annonc.2020.08.451

814. Sobhani N, Kugeratski FG, Venturini S, Roudi R, Nguyen T, D'Angelo A, et al. AI-Based Cancer Models in Oncology: From Diagnosis to ADC Drug Prediction. Cancers. 2025 Oct 24;17(21):3419. doi:10.3390/cancers17213419

815. Long X, Sun K, Lai S, Liu Y, Su J, Chen W, et al. Artificial intelligence and anti-cancer drugs' response. Acta Pharmaceutica Sinica B. 2025 Jul 1;15(7):3355–71. doi:10.1016/j.apsb.2025.05.009

816. Niederst MJ, Engelman JA. Bypass Mechanisms of Resistance to Receptor Tyrosine Kinase Inhibition in Lung Cancer. Sci Signal. 2013 Sep 24;6(294). doi:10.1126/scisignal.2004652

817. Michaux L, Perrier A, Mehlman C, Alshehhi H, Dubois A, Lacave R, et al. Therapeutic strategies to overcome EGFR mutations as acquired resistance mechanism in ALK-

rearranged non-small-cell lung cancer: Case Reports. Front Oncol. 2023 Jun 28;13:1182558. doi:10.3389/fonc.2023.1182558

818. Cook AL, Wyhs N, Sur S, Ptak B, Popoli M, Dobbyn L, et al. An isogenic cell line panel for sequence-based screening of targeted anticancer drugs. iScience. 2022 Jun;25(6):104437. doi:10.1016/j.isci.2022.104437

819. Gautam P, Karhinen L, Szwajda A, Jha SK, Yadav B, Aittokallio T, et al. Identification of selective cytotoxic and synthetic lethal drug responses in triple negative breast cancer cells. Mol Cancer. 2016 Dec;15(1):34. doi:10.1186/s12943-016-0517-3

820. Akbani R, Becker KF, Carragher N, Goldstein T, de Koning L, Korf U, et al. Realizing the Promise of Reverse Phase Protein Arrays for Clinical, Translational, and Basic Research: A Workshop Report: The RPPA (Reverse Phase Protein Array) Society. Molecular & Cellular Proteomics. 2014 Jul 1;13(7):1625–43. doi:10.1074/mcp.O113.034918

821. Wang S, Zhang Y, Zhang L, Huang Y, Zhang J, Zhang K, et al. Unraveling the complex dynamics of signaling molecules in cellular signal transduction. Abramov A, editor. PNAS Nexus. 2023 Dec 21;3(1):pgae020. doi:10.1093/pnasnexus/pgae020

822. Serra V, Scaltriti M, Prudkin L, Eichhorn PJA, Ibrahim YH, Chandarlapaty S, et al. PI3K inhibition results in enhanced HER signaling and acquired ERK dependency in HER2-overexpressing breast cancer. Oncogene. 2011 Jun;30(22):2547–57. doi:10.1038/onc.2010.626

823. Muneer G, Chen C, Chen Y. Advancements in Global Phosphoproteomics Profiling: Overcoming Challenges in Sensitivity and Quantification. Proteomics. 2025 Jan;25(1–2):e202400087. doi:10.1002/pmic.202400087

824. Alasiri G, Jiramongkol Y, Trakansuebkul S, Ke HL, Mahmud Z, Intuyod K, et al. Reciprocal regulation between GCN2 (eIF2AK4) and PERK (eIF2AK3) through the JNK-FOXO3 axis to modulate cancer drug resistance and clonal survival. Molecular and Cellular Endocrinology. 2020 Sep;515:110932. doi:10.1016/j.mce.2020.110932

825. Chakrabarty A, Sánchez V, Kuba MG, Rinehart C, Arteaga CL. Feedback upregulation of HER3 (ErbB3) expression and activity attenuates antitumor effect of PI3K inhibitors. Proc Natl Acad Sci USA. 2012 Feb 21;109(8):2718–23. doi:10.1073/pnas.1018001108

826. Herranz-Montoya I, Angulo-Aguado M, Perna C, Zagorac S, García-Jimeno L, Park S, et al. p53 protein degradation redefines the initiation mechanisms and drives transitional mutations in colorectal cancer. Nat Commun. 2025 Apr 26;16(1):3934. doi:10.1038/s41467-025-59282-4

827. Karlsson J, Briggs M, Vedi A, Gisselsson D. Clonal evolution and therapy resistance in the era of precision cancer medicine: evolutionary trajectories in pediatric cancer. Seminars in Cancer Biology. 2025 Nov;116:121–34. doi:10.1016/j.semcancer.2025.10.001

828. Dai W, Qiao X, Fang Y, Guo R, Bai P, Liu S, et al. Epigenetics-targeted drugs: current paradigms and future challenges. Sig Transduct Target Ther. 2024 Nov 26;9(1):332. doi:10.1038/s41392-024-02039-0

829. Jiang Z, Gu Z, Yu X, Cheng T, Liu B. Research progress on the role of bypass activation mechanisms in resistance to tyrosine kinase inhibitors in non-small cell lung cancer. Front Oncol. 2024 Nov 8;14:1447678. doi:10.3389/fonc.2024.1447678

830. Cheong HT, Xu F, Choy CT, Hui CWC, Mok TSK, Wong CH. Upregulation of Bcl2 in NSCLC with acquired resistance to EGFR-TKI. Oncol Lett. 2018 Jan;15(1):901–7. doi:10.3892/ol.2017.7377 PubMed PMID: 29422965; PubMed Central PMCID: PMC5772989.

831. Lal-Nag M, McGee L, Titus SA, Brimacombe K, Michael S, Sittampalam G, et al. Exploring Drug Dosing Regimens In Vitro Using Real-Time 3D Spheroid Tumor Growth Assays. SLAS Discovery. 2017 Jun;22(5):537–46. doi:10.1177/2472555217698818

832. Kabeer F, Tran H, Andronescu M, Singh G, Lee H, Salehi S, et al. Single-cell decoding of drug induced transcriptomic reprogramming in triple negative breast cancers. Genome Biol. 2024 Jul 18;25(1):191. doi:10.1186/s13059-024-03318-3

833. Aissa AF, Islam ABMMK, Ariss MM, Go CC, Rader AE, Conrardy RD, et al. Single-cell transcriptional changes associated with drug tolerance and response to combination therapies in cancer. Nat Commun. 2021 Mar 12;12(1):1628. doi:10.1038/s41467-021-21884-z

834. Zhen Y, Guanghui L, Xiefu Z. Knockdown of EGFR inhibits growth and invasion of gastric cancer cells. Cancer Gene Ther. 2014 Nov;21(11):491–7. doi:10.1038/cgt.2014.55

835. Lee HK, Noh MH, Hong SW, Kim SM, Kim SH, Kim YS, et al. Erlotinib Activates Different Cell Death Pathways in EGFR-mutant Lung Cancer Cells Grown in 3D *Versus* 2D Culture Systems. Anticancer Res. 2021 Mar;41(3):1261–9. doi:10.21873/anticanres.14883

836. Harandi A, Zaidi AS, Stocker AM, Laber DA. Clinical Efficacy and Toxicity of Anti-EGFR Therapy in Common Cancers. Journal of Oncology. 2009;2009:1–14. doi:10.1155/2009/567486

837. Wheeler DL, Dunn EF, Harari PM. Understanding resistance to EGFR inhibitors—impact on future treatment strategies. Nat Rev Clin Oncol. 2010 Sep;7(9):493–507. doi:10.1038/nrclinonc.2010.97

838. Lozano G, Prives C, Sabapathy K. Mutant p53 Gain of Function: Why Many See It, Why some Don't. Cancer Discov. 2025 Jun 3;15(6):1099–104. doi:10.1158/2159-8290.CD-24-1638 PubMed PMID: 40287981; PubMed Central PMCID: PMC12133405.

839. Sasaki K, Takahashi S, Ouchi K, Otsuki Y, Wakayama S, Ishioka C. Different impacts of TP53 mutations on cell cycle-related gene expression among cancer types. Sci Rep. 2023 Mar 24;13:4868. doi:10.1038/s41598-023-32092-8 PubMed PMID: 36964217; PubMed Central PMCID: PMC10039000.

840. Thorpe LM, Yuzugullu H, Zhao JJ. PI3K in cancer: divergent roles of isoforms, modes of activation and therapeutic targeting. Nat Rev Cancer. 2015 Jan;15(1):7–24. doi:10.1038/nrc3860

841. Cescon DW, Gorrini C, Mak TW. Breaking up Is Hard to Do: PI3K Isoforms on the Rebound. Cancer Cell. 2015 Jan;27(1):5–7. doi:10.1016/j.ccell.2014.12.003

842. Sohn EJ. PIK3R3, a regulatory subunit of PI3K, modulates ovarian cancer stem cells and ovarian cancer development and progression by integrative analysis. BMC Cancer. 2022 Dec;22(1):708. doi:10.1186/s12885-022-09807-7

843. Tian Y, Li J, Cheung TC, Tam V, Lau CG, Wang X, et al. Akt3 promotes cancer stemness in triple-negative breast cancer through YB1-Snail/Slug signaling axis. Genes & Diseases. 2023 Mar;10(2):301–6. doi:10.1016/j.gendis.2022.08.006

844. Chin YR, Yoshida T, Marusyk A, Beck AH, Polyak K, Toker A. Targeting Akt3 Signaling in Triple-Negative Breast Cancer. Cancer Research. 2014 Feb 1;74(3):964–73. doi:10.1158/0008-5472.CAN-13-2175

845. Guo Z, Primeau T, Luo J, Zhang C, Sun H, Hoog J, et al. Proteomic Resistance Biomarkers for PI3K Inhibitor in Triple Negative Breast Cancer Patient-Derived Xenograft Models. Cancers. 2020 Dec 21;12(12):3857. doi:10.3390/cancers12123857

846. Xu Y chao, Wang X, Chen Y, Chen S meng, Yang X ying, Sun Y ming, et al. Integration of Receptor Tyrosine Kinases Determines Sensitivity to PI3Kα-selective Inhibitors in Breast Cancer. Theranostics. 2017;7(4):974–86. doi:10.7150/thno.17830

847. Isoyama S, Kajiwara G, Tamaki N, Okamura M, Yoshimi H, Nakamura N, et al. Basal expression of insulin-like growth factor 1 receptor determines intrinsic resistance of cancer cells to a phosphatidylinositol 3-kinase inhibitor ZSTK474. Cancer Sci. 2015 Feb;106(2):171–8. doi:10.1111/cas.12582 PubMed PMID: 25483727; PubMed Central PMCID: PMC4399020.

848. Palmbos PL, Wang Y, Bankhead A, Kelleher AJ, Wang L, Yang H, et al. ATDC Mediates a TP63-Regulated Basal Cancer Invasive Program. Oncogene. 2019 May;38(18):3340–54. doi:10.1038/s41388-018-0646-9 PubMed PMID: 30643195; PubMed Central PMCID: PMC6499660.

849. Romashin DD, Tolstova TV, Varshaver AM, Kozhin PM, Rusanov AL, Luzgina NG. Keratins 6, 16, and 17 in Health and Disease: A Summary of Recent Findings. Curr Issues Mol Biol. 2024 Aug 6;46(8):8627–41. doi:10.3390/cimb46080508 PubMed PMID: 39194725; PubMed Central PMCID: PMC11352355.

850. Tan YS, Mhoumadi Y, Verma CS. Roles of computational modelling in understanding p53 structure, biology, and its therapeutic targeting. Lane DP, editor. Journal of Molecular Cell Biology. 2019 Apr 1;11(4):306–16. doi:10.1093/jmcb/mjz009

851. Tan Y, Luo R. Structural and functional implications of p53 missense cancer mutations. PMC Biophys. 2009 Dec;2(1):5. doi:10.1186/1757-5036-2-5

852. Deb S, Graves PR. Identification of novel mutant p53 interacting proteins by proteomic analysis. Methods Mol Biol. 2013;962:85–94. doi:10.1007/978-1-62703-236-0_7 PubMed PMID: 23150439.

853. Lepre M, Omar S, Grasso G, Morbiducci U, Deriu M, Tuszynski J. Insights into the Effect of the G245S Single Point Mutation on the Structure of p53 and the Binding of the Protein to DNA. Molecules. 2017 Aug 16;22(8):1358. doi:10.3390/molecules22081358

854. Alsulami AF. Mutational Disruption of TP53: A Structural Approach to Understanding Chemoresistance. IJMS. 2025 Sep 18;26(18):9135. doi:10.3390/ijms26189135

855. Kogan S, Carpizo D. Pharmacological targeting of mutant p53. Transl Cancer Res. 2016 Dec;5(6):698–706. doi:10.21037/tcr.2016.11.74

856. Holst F, Werner HMJ, Mjøs S, Hoivik EA, Kusonmano K, Wik E, et al. *PIK3CA* Amplification Associates with Aggressive Phenotype but Not Markers of AKT-MTOR Signaling in Endometrial Carcinoma. Clinical Cancer Research. 2019 Jan 1;25(1):334–45. doi:10.1158/1078-0432.CCR-18-0452

857. Shearer RF, Saunders DN. Experimental design for stable genetic manipulation in mammalian cell lines: lentivirus and alternatives. Genes to Cells. 2015 Jan;20(1):1–10. doi:10.1111/gtc.12183

858. Page A, Fusil F, Cosset FL. Toward Tightly Tuned Gene Expression Following Lentiviral Vector Transduction. Viruses. 2020 Dec 11;12(12):1427. doi:10.3390/v12121427

859. Butera A, Amelio I. Deciphering the significance of p53 mutant proteins. Trends in Cell Biology. 2025 Mar 1;35(3):258–68. doi:10.1016/j.tcb.2024.06.003

860. Imbalzano KM, Tatarkova I, Imbalzano AN, Nickerson JA. Increasingly transformed MCF-10A cells have a progressively tumor-like phenotype in three-dimensional basement membrane culture. Cancer Cell Int. 2009;9(1):7. doi:10.1186/1475-2867-9-7

861. Kilinc S, Paisner R, Camarda R, Gupta S, Momcilovic O, Kohnz RA, et al. Oncogene-regulated release of extracellular vesicles. Developmental Cell. 2021 Jul;56(13):1989-2006.e6. doi:10.1016/j.devcel.2021.05.014

862. Qu Y, Han B, Yu Y, Yao W, Bose S, Karlan BY, et al. Evaluation of MCF10A as a Reliable Model for Normal Human Mammary Epithelial Cells. Liu X, editor. PLoS ONE. 2015 Jul 6;10(7):e0131285. doi:10.1371/journal.pone.0131285

863. Zecha J, Bayer FP, Wiechmann S, Woortman J, Berner N, Müller J, et al. Decrypting drug actions and protein modifications by dose- and time-resolved proteomics. Science. 2023 Apr 7;380(6640):93–101. doi:10.1126/science.ade3925

864. Edfors F, Danielsson F, Hallström BM, Käll L, Lundberg E, Pontén F, et al. Gene-specific correlation of RNA and protein levels in human cells and tissues. Mol Syst Biol. 2016 Oct 20;12(10):883. doi:10.15252/msb.20167144 PubMed PMID: 27951527; PubMed Central PMCID: PMC5081484.

865. Perl K, Ushakov K, Pozniak Y, Yizhar-Barnea O, Bhonker Y, Shivatzki S, et al. Reduced changes in protein compared to mRNA levels across non-proliferating tissues. BMC Genomics. 2017 Dec;18(1):305. doi:10.1186/s12864-017-3683-9

866. Witt BL, Tollefsbol TO. Molecular, Cellular, and Technical Aspects of Breast Cancer Cell Lines as a Foundational Tool in Cancer Research. Life. 2023 Dec 8;13(12):2311. doi:10.3390/life13122311

867. Pellacani D, Tan S, Lefort S, Eaves CJ. Transcriptional regulation of normal human mammary cell heterogeneity and its perturbation in breast cancer. The EMBO Journal. 2019 Jul 15;38(14):e100330. doi:10.15252/embj.2018100330

868. Vincent KM, Findlay SD, Postovit LM. Assessing breast cancer cell lines as tumour models by comparison of mRNA expression profiles. Breast Cancer Res. 2015 Dec;17(1):114. doi:10.1186/s13058-015-0613-0

869. Almahdi YA, Schwark ER, Mclaughlin AJ, Xhabija B. Dissecting Morphological and Functional Dynamics of Non-Tumorigenic and Triple-Negative Breast Cancer Cell Lines Using PCA and t-SNE Analysis. Cancer Rep (Hoboken). 2025 Jul;8(7):e70257. doi:10.1002/cnr2.70257 PubMed PMID: 40576474; PubMed Central PMCID: PMC12203836.

870. Thorek DLJ, Ku AT, Mitsiades N, Veach D, Watson PA, Metha D, et al. Harnessing Androgen Receptor Pathway Activation for Targeted Alpha Particle Radioimmunotherapy of Breast Cancer. Clinical Cancer Research. 2019 Jan 15;25(2):881–91. doi:10.1158/1078-0432.CCR-18-1521

871. Chong ZX, Yeap SK, Ho WY. Transfection types, methods and strategies: a technical review. PeerJ. 2021 Apr 21;9:e11165. doi:10.7717/peerj.11165

872. Napoleone A, Sebastian IR, De Marco F, Molin A, Hussein M, Kramer L, et al. Overcoming lentiviral delivery limitations in hard-to-transduce suspension cells for genome-wide CRISPR screening. Molecular Therapy Advances. 2026 Mar 12;34(1):201678. doi:10.1016/j.omta.2026.201678

873. Franz K, Singh A, Weinberger LS. Lentiviral Vectors to Study Stochastic Noise in Gene Expression. In: Methods in Enzymology [Internet]. Elsevier; 2011 [cited 2025 Dec 29]. p. 603–22. Available from: https://linkinghub.elsevier.com/retrieve/pii/B9780123850751000263 doi:10.1016/B978-0-12-385075-1.00026-3

874. Yang J, Guo F, Chin HS, Chen GB, Zhang Z, Williams L, et al. Rapid and Robust Generation of Homozygous Fluorescent Reporter Knock-In Cell Pools by CRISPR-Cas9. Cells. 2025 Jul 29;14(15):1165. doi:10.3390/cells14151165

875. Vasudevan KM, Barbie DA, Davies MA, Rabinovsky R, McNear CJ, Kim JJ, et al. AKT-Independent Signaling Downstream of Oncogenic PIK3CA Mutations in Human Cancer. Cancer Cell. 2009 Jul;16(1):21–32. doi:10.1016/j.ccr.2009.04.012

876. Orlacchio A, Ranieri M, Brave M, Arciuch VA, Forde T, De Martino D, et al. SGK1 Is a Critical Component of an AKT-Independent Pathway Essential for PI3K-Mediated Tumor Development and Maintenance. Cancer Research. 2017 Dec 15;77(24):6914–26. doi:10.1158/0008-5472.CAN-17-2105

877. Martin NE, Gerke T, Sinnott JA, Stack EC, Andrén O, Andersson SO, et al. Measuring PI3K Activation: Clinicopathologic, Immunohistochemical, and RNA Expression

Analysis in Prostate Cancer. Molecular Cancer Research. 2015 Oct 1;13(10):1431–40. doi:10.1158/1541-7786.MCR-14-0569

878. Galhuber M, Michenthaler H, Heininger C, Reinisch I, Nössing C, Krstic J, et al. Complementary omics strategies to dissect p53 signaling networks under nutrient stress. Cell Mol Life Sci. 2022 Jun;79(6):326. doi:10.1007/s00018-022-04345-8

879. Deb S, Graves PR. Identification of Novel Mutant p53 Interacting Proteins by Proteomic Analysis. In: Deb S, Deb SP, editors. p53 Protocols [Internet]. Totowa, NJ: Humana Press; 2013 [cited 2026 Jun 16]. p. 85–94. Available from: https://doi.org/10.1007/978-1-62703-236-0_7 doi:10.1007/978-1-62703-236-0_7

880. Gao Q, Wu H, Duan L, Lv G, Quan D. Multi-omics analysis of the tumor microenvironment after metastasis: advancing toward personalized immunotherapy and molecular targeted strategies. Front Immunol. 2025 Sep 23;16:1648987. doi:10.3389/fimmu.2025.1648987

881. Tasdemir N, Ding K, Savariau L, Levine KM, Du T, Elangovan A, et al. Proteomic and transcriptomic profiling identifies mediators of anchorage-independent growth and roles of inhibitor of differentiation proteins in invasive lobular carcinoma. Sci Rep. 2020 Jul 13;10(1):11487. doi:10.1038/s41598-020-68141-9

882. Creighton CJ, Fu X, Hennessy BT, Casa AJ, Zhang Y, Gonzalez-Angulo AM, et al. Proteomic and transcriptomic profiling reveals a link between the PI3K pathway and lower estrogen-receptor (ER) levels and activity in ER+ breast cancer. Breast Cancer Res. 2010 Jun 22;12(3):R40. doi:10.1186/bcr2594

883. Tong L, Cui W, Zhang B, Fonseca P, Zhao Q, Zhang P, et al. Patient-derived organoids in precision cancer medicine. Med. 2024 Nov;5(11):1351–77. doi:10.1016/j.medj.2024.08.010

884. Chakravarty L, Ahmad SI, Khatun A, Khan SA. Exploring the potential of CRISPR in triple-negative breast cancer treatment. Innovative Practice in Breast Health. 2025;7:100028. doi:10.1016/j.ibreh.2024.100028

885. Van De Stolpe A. Quantitative Measurement of Functional Activity of the PI3K Signaling Pathway in Cancer. Cancers. 2019 Mar 1;11(3):293. doi:10.3390/cancers11030293

886. Shao S, Li S, Huo Y, Tang S, Gökbağ B, Fan K, et al. CRISPR-Cas9 Genome and Double-Knockout Screening to Identify Novel Therapeutic Targets for Chemoresistance in Triple-Negative Breast Cancer. Cancers (Basel). 2025 Dec 3;17(23):3876. doi:10.3390/cancers17233876 PubMed PMID: 41375077; PubMed Central PMCID: PMC12691371.

887. Reyes-Aldasoro CC. Modelling the Tumour Microenvironment, but What Exactly Do We Mean by “Model”? Cancers (Basel). 2023 Jul 26;15(15):3796. doi:10.3390/cancers15153796 PubMed PMID: 37568612; PubMed Central PMCID: PMC10416922.

888. Vulin M, Jehanno C, Sethi A, Correia AL, Obradović MMS, Couto JP, et al. A high-throughput drug screen reveals means to differentiate triple-negative breast cancer. Oncogene. 2022 Sep 23;41(39):4459–73. doi:10.1038/s41388-022-02429-0

889. Jia K, Wang Y, Cao Q, Wang Y. Extensive prediction of drug response in mutation-subtype-specific LUAD with machine learning approach. OR. 2024;32(2):409–19. doi:10.32604/or.2023.042863

890. Zou Y, Xie J, Zheng S, Liu W, Tang Y, Tian W, et al. Leveraging diverse cell-death patterns to predict the prognosis and drug sensitivity of triple-negative breast cancer patients after surgery. International Journal of Surgery. 2022 Nov;107:106936. doi:10.1016/j.ijsu.2022.106936